TIP5 is a Critical Epigenetic Regulator of Aggressive Prostate Cancer

Dissertation

zur
Erlangung der naturwissenschaftlichen Doktorwürde
(Dr. sc. nat.)

vorgelegt der
Mathematischen-naturwissenschaftlichen Fakultät

der
Universität Zürich

von

Sandra Carina Frommel

aus Deutschland

Promotionskomitee
Prof. Dr. Dr. Michael O. Hottiger (Vorsitz)
PD Dr. Raffaella Santoro (Leitung der Dissertation)
Prof. Dr. Mark D. Robinson
PD Dr. Lubor Borsig
PD Dr. Maurizio Provenzano

Zürich, 2015

To my dear Mum

Acknowledgements

First, I would like to express my sincere gratitude to my thesis adviser PD Dr. Raffaella Santoro for offering me this attractive project in the emerging field of cancer epigenetics. Raffaella, thank you very much for constant support and excellent guidance throughout this work. Moreover, I would like to thank you for making me become a researcher and for the possibility to enter the scientific community by sending me to numerous conferences and meetings.

Next, would like to thank Prof. Dr. Dr. Michael O. Hottiger for being the chairman of my doctoral thesis committee and for the outstanding infrastructure and scientific community of our institute.

I am very grateful to my committee members Prof. Dr. Dr. Michael O. Hottiger, Prof. Dr. Mark D. Robinson, PD Dr. Lubor Borsig and PD Dr. Maurizio Provenzano for their help and support at any moments as well as inspiring discussions and constructive advises during our committee meetings.

I would also like to thank Susanna Bachmann from the Life Science Zurich Graduate School for terrific organization of the MLS PhD program.

I am especially grateful to Peter Müller for his fellowship supporting my first PhD year. Our meetings have been always truly refreshing in the daily lab routine. In addition, I would like to give my sincere thank to the Sassella Foundation for providing me a fellowship during the last year of my PhD studies.

Now, I want to thank the IVBMB and CABMM members for a great working environment, their help and support whenever needed. Countless (institute) parties and trips have made my time as a PhD student extremely enjoyable and absolutely unforgettable. At this point I would like to give a special thank to my group including Eva Vollenweider, Sergio Leone, Dominik Bär, Dr. Sarah Wyck, Damian Dalcher, Karolina Pietrzak, Rodrigo Pena-Hernandez and Julia Kuhn but also to the former group members Dr. Claudio Guetg, Dr. Cristina Gerig, Dr. Natasa Savic and Anita Steiner for their help and scientific input, and of course many funny lunch/coffee breaks and memorable evenings.

My boyfriend, Dr. Hans Scheuren, has always stood by my side throughout the past years. Hans, I am deeply grateful for your unlimited support and encouragement and the one or other weekend you went along with me to the lab.

Last but not least, I would like to deeply thank my mother, my brother, and my stepfather who have always given me immeasurable support throughout my whole education.

Summary

Cancer has traditionally been viewed as a set of diseases that are driven by the accumulation of genetic mutations that have been considered the major causes of neoplasia. However, this paradigm has now been expanded to incorporate the disruption of epigenetic regulatory mechanisms that are prevalent in a wide variety of human cancers. The reversible nature of epigenetic modifications provides exciting new avenues for cancer research. Particularly, the reactivation of tumor suppressor genes has made them attractive targets for cancer treatment. A recent outcome of whole exome sequencing of thousands of human cancers has been the unexpected discovery of many inactivating mutations in genes that control the epigenome. These mutations have the potential to disrupt DNA methylation patterns, histone modifications, and nucleosome positioning which in turn deregulate genes critical to cancer pathogenesis. These alterations are now recognized as key events governing the tumor cell phenotype. However, prostate cancer is characterized by a low frequency of somatic mutations, making it unclear how its aberrant epigenetic signature is established. Understanding this process has not only the potential to establish new approaches for prostate cancer therapy but also to shed light on the most vital question in the current treatment paradigm of prostate cancer: how to distinguish indolent and aggressive tumors?

Prostate cancer is the most common non-cutaneous malignancy in men over the age of 50. Prediction of clinical behavior remains challenging using the currently available histopathological and biochemical (prostate-specific antigen; PSA) markers. Thus, novel molecular-based approaches will likely improve prognostic accuracy in this disease. Particularly, the absence of early prognostic markers able to distinguish between indolent tumors and those that will become truly aggressive, as well as the lack of efficient therapies for advanced prostate cancer, remain a major health problem.

Previous studies have shown that elevated expression of the epigenetic regulator EZH2 (Enhancer of zeste homolog 2) is highly correlated with prostate cancer progression and poor outcome. EZH2 is a subunit of the Polycomb repressive complex 2 (PRC2) that catalyzes a repressive histone mark, the trimethylation of lysine 27 on histone H3 (H3K27me3). However, how EZH2 is aberrantly recruited to specific genes during the neoplastic process is yet to be elucidated.

This work has investigated the function of TIP5 in cancer. TIP5 is the largest subunit of the nucleolar complex NoRC (nucleolar remodeling complex), known to establish epigenetic silencing and transcriptional repression at the ribosomal (rRNA) genes through the association with DNA methyltransferases and histone modifier complexes. Analysis of expression profiles of benign, clinically localized and metastatic prostate cancer revealed that TIP5 is upregulated in metastatic prostate cancer. TIP5 is paradoxically involved in maintaining prostate cancer cell growth, a feature that is specific to cancer cells. Moreover, TIP5 is required for migration, invasion and stem cell-like features of prostate cancer cells, which are important properties in metastasis formation and cancer recurrence. Transcriptomic profiling has demonstrated a significant overlap (30%) of TIP5- and EZH2-regulated genes in metastatic prostate cancer. A combination of epigenomic and transcriptomic analyses has revealed that TIP5 cooperates with the Polycomb group protein EZH2. TIP5 and EZH2 together establish repressive epigenetic signatures such as H3K27me3 and repress the transcription of developmental and tumor suppressor genes, which are frequently silenced in metastatic prostate cancer. Interestingly, depletion of TIP5 impairs EZH2 recruitment and decreases H3K27me3 levels, suggesting a role for TIP5 in guiding EZH2 to genes that are critical for prostate cancer aggressiveness. Importantly, TIP5 overexpression is tightly associated with a prostate cancer subtype displaying a CpG island methylator phenotype (CIMP). Finally, high TIP5 levels serve as an independent predictor of biochemical recurrence in a cohort of 7,682 individuals with prostate cancer. This work defines a mechanistic and functional crosstalk between TIP5 and Polycomb-mediated epigenetic silencing in prostate cancer. Thus, these data indicate a novel aberrant role for the epigenetic regulator TIP5, which can also serve as a useful biomarker to determine aggressive/metastatic potential in prostate cancer.

Zusammenfassung

Krebs wurde traditionell als eine Reihe von Krankheiten gesehen, die durch die Anhäufung von genetischen Mutationen entstehen, welche bislang als Hauptursache einer Neoplasie betrachtet wurden. Dieses Paradigma wurde erweitert und umfasst nun auch Störungen in epigenetischen regulatorischen Mechanismen, welche weit verbreitet in verschiedenen humanen Krebserkrankungen sind. Epigenetische Modifizierungen können rückgängig gemacht werden, eine Eigenschaft, die neue Wege in der Krebsforschung eröffnet. Insbesondere die Re-Aktivierung von Tumorsuppressor-Genen macht sie zu einem attraktiven Angriffspunkt in der Krebsbehandlung. Kürzlich durchgeführte Studien von vollständigen Exom-Sequenzierungen von tausenden humanen Tumoren machten die unerwartete Entdeckung, dass es viele inaktivierende Mutationen in Genen gibt, welche das Epigenom kontrollieren. Diese Mutationen können potenzielle Störungen in DNA-Methylierungsmustern, Histonmodifikationen, und Nukleosom-Positionierung verursachen, welche im Gegenzug zur Deregulierung von Genen führen, die kritisch in der Pathogenese von Krebs sind. Diese Veränderungen werden nun als Schlüsselereignis für die Ausprägung des Phänotyps einer Krebszelle betrachtet. Prostatakrebs ist jedoch durch eine geringe somatische Mutationsrate charakterisiert, es ist daher unklar, wie die veränderte epigenetische Signatur hier etabliert wird. Das Verständnis dieses Prozesses hat nicht nur das Potenzial neue Ansätze in der Krebstherapie zu finden, sondern gibt auch Aufschluss über die entscheidende Frage im derzeitigen Behandlungsparadigma von Prostatakrebs: wie kann man indolente von aggressiven Tumoren unterscheiden?

Prostatakrebs ist die häufigste, nicht-dermatologische Erkrankung unter Männern im Alter über 50 Jahren. Die Vorhersage des klinischen Verlaufs mit der Verwendung der derzeitigen histopathologischen und biochemischen (Prostataspezifisches Antigen; PSA) Markern bleibt eine Herausforderung. Daher werden neue molekular-basierte Ansätze die prognostische Genauigkeit für diese Erkrankung wahrscheinlich verbessern. Besonders das Fehlen von frühen prognostischen Markern, die in der Lage sind zwischen indolenten Tumoren und Tumoren, die wirklich aggressiv werden, zu unterscheiden, sowie das Nichtvorhandensein von effizienten Therapien für Patienten mit fortgeschrittenem Prostatakrebs stellen ein bedeutendes Gesundheitsproblem dar.

Vergangene Studien haben gezeigt, dass die verstärkte Expression des epigenetischen Regulators EZH2 (Enhancer of zeste homolog 2) mit der Progression von Prostatakrebs und ei-

ner schlechten Diagnose korreliert ist. EZH2 ist eine Untereinheit des Polycomb repressive complex 2 (PRC2) welche die Trimethylierung von Lysin 27 des Histons H3 (H3K27me3), eine repressive Histonmodifikation, katalysiert. Jedoch ist bislang unklar, wie die anormale Rekrutierung von EZH2 zu den spezifischen Genen während des neoplastischen Prozesses stattfindet.

Diese Arbeit untersuchte die Funktion von TIP5 in Krebs. TIP5 ist die grösste Untereinheit des nukleolaren Komplexes NoRC (nucleolar remodeling complex), welcher durch die Assoziation mit DNA-Methyltransferasen und Histon-Modifizierungs-Komplexen die Etablierung von epigenetischem Inaktivierungen und transkriptionelle Repression an den ribosomalen (rRNA) Genen ausführt. Die Analyse von Expressionsprofilen von gutartigen, klinisch lokalisierten und metastatischen Prostatakrebs zeigte, dass TIP5 in metastatischem Prostatakrebs stark erhöht ist. Paradoxerweise ist TIP5 in der Aufrechterhaltung des Wachstums von Prostatakrebszellen involviert und diese Eigenschaft ist spezifisch für Krebszellen. Zudem wird TIP5 für die Migration, Invasion und stammzell-ähnliche Eigenschaften von Prostatakrebszellen benötigt, allesamt Eigenschaften welche bedeutend für die Bildung von Metastasen und das erneute Auftreten von Krebs sind. Transkriptomische Analysen deckten eine signifikante Überlappung (30%) von TIP5- und EZH2-regulierten Genen in metastatischem Prostatakrebs auf. Eine Kombination von epigenomischen und transkriptomischen Analysen zeigte auf, dass TIP5 mit dem Polycomb Group Protein EZH2 kooperiert. TIP5 und EZH2 etablieren zusammen epigenetische Signaturen wie z. B. H3K27me3 und hemmen die Transkription von Entwicklungs-Genen und Tumorsuppressor-Genen, welche in metastatischem Prostatakrebs häufig ausgeschaltet sind. Interessanterweise beeinträchtigt das Ausschalten von TIP5 die Rekrutierung von EZH2 und reduziert die Werte von H3K27me3. Diese Ergebnisse weisen auf eine Funktion von TIP5 bei der Rekrutierung von EZH2 zu Genen hin, die kritisch für die Aggressivität von Prostatakrebs sind. Von grosser Bedeutung ist die Beobachtung, dass die verstärkte Expression von TIP5 stark mit einem Subtyp von Prostatakrebs, der einen Phänotypen mit der Bezeichnung „CpG Island Methylator Phenotype“ (CIMP) zeigt, assoziiert ist. Schliesslich konnte in einer Kohorte von 7'682 Prostatakrebspatienten gezeigt werden, dass hohe Mengen von TIP5 zur unabhängigen Vorhersage des biochemischen Wiederauftreten des Tumors verwendet werden können. Die vorliegende Arbeit beschreibt ein funktionales Zusammenspiel zwischen TIP5 und einer Polycomb-vermittelten epigenetischen Inaktivierung in Prostatakrebs. Diese Ergebnisse weisen somit auf eine neue anormale Rolle

des epigenetischen Regulators TIP5 hin, welcher als nützlicher Biomarker zur Bestimmung des aggressiven/metastatischen Potenzials von Prostatakrebs verwendet werden kann.

Abbreviations

5caC	5-carboxycytosine
5fC	5-formylcytosine
5hmC	5-hydroxymethylcytosine
5mC	5-methylcytosine
ALL	acute lymphoblastic leukemia
AML	acute-myeloid leukemia
AR	androgen receptor
ATP	adenosine triphosphate
BAZ2A	bromodomain adjacent to zinc finger 2A
BET	bromodomain and extraterminal
bp	base pairs
CGI	CpG island
CIMP	CpG island methylator phenotype
CpG	C-phosphate-G
CTCL	cutaneous T cell lymphoma
DMR	differentially methylated region
DNA	deoxyribonucleic acid
DNMT	DNA methyltransferase
ESC	embryonic stem cell
EZH2	Enhancer of zeste 2
HATs	histone acetyltransferase
HDAC	histone deacetylase
HDM	histone demethylase
HMT	histone methyltransferase
HP1	heterochromatin protein 1
LOI	loss of imprinting
MBT	malignant brain tumor
ncRNA	non-coding ribonucleic acid
NoRC	nucleolar remodeling complex

O-Glc-NAc	β-N-acetylglucosamine
Pc	Polycomb
PcG	Polycomb group
PGC	primordial germ cell
PHD	plant homeodomain
PhoRC	PHO-repressive complex
PR-DUB	polycomb repressive deubiquitinase
PRC1	polycomb repressive complex 1
PRC2	polycomb repressive complex 2
PRE	polycomb response element
PSA	prostate-specific antigen
PTM	posttranslational modification
RB	retinoblastoma protein
RNA	ribonucleic acid
rRNA	ribosomal RNA
SAM	*S*-Adenosyl methionine
SWI/SNF	SWItch/Sucrose NonFermentable
TDG	thymine-DNA glycosylase
TET	ten-eleven translocation
TIP5	TTF1-interacting protein 5
TrxG	Trithorax group
α-KG	α-ketoglutarate

Table of Contents

1 Introduction

The human body consists of approximately 3×10^{13} cells which all carry a compete copy of the genome within the cell nucleus. In humans, each cell normally contains 23 pairs of chromosomes, for a total of 46. Twenty-two of these pairs, called autosomes, look the same in both males and females. The 23rd pair, the sex chromosomes, differs between males and females (one X chromosome in males, two in females; in males only, one Y chromosome). The stretched linear double helix consists of about three billion nucleotide base pairs (bp) and would measure 1.8 m (Ball, 2003). In order to fit a fully extended DNA molecule within the nucleus, DNA has to be compacted 100,000 times (Razin et al., 2007). To achieve this enormous compartmentalization and compaction, DNA is associated with proteins forming a complex called chromatin. Around 1880, Walther Flemming proposed the term chromatin (from the Greek χρῶμα, *chroma* = color) based on his work using aniline dyes to visualize the threadlike structures in the cell nucleus. The overall structure of chromatin depends on the stage of the cell cycle. During cell division chromatin can be seen as individual compact chromosomes; whereas in non-dividing (interphase) cells it is distributed throughout the nucleus and organized into highly condensed (heterochromatin) and the more open regions (euchromatin) (Felsenfeld and Groudine, 2003). Chromatin is a dynamic structure and exerts profound control on DNA-related metabolic processes including transcription, recombination, DNA repair, replication, kinetochore and centrosome formation and other fundamental cellular processes.

The DNA molecule as “the instruction manual of life” directs how a fertilized egg turns into the specific cells, tissues and organs (Marx, 2012). How does each cell type interpret this common manual to achieve specific identity? Although the human genome project was completed in 2001, yet the primary DNA sequence is only a basis for our understanding how the genome is read. Superimposed upon primary DNA sequence is a second layer of heritable “epigenetic” information.

1.1 Epigenetics

Epigenetics has been defined as ‘the study of mitotically and/or meiotically heritable changes in gene function that cannot be explained by changes in DNA sequence’ (Russo et al., 1996). In other words, epigenetic inheritance involves the transmission of information not encoded in DNA sequences from mother to daughter cells or from generation to generation (‘epi-’ is de-

rived from the Greek for ‘above’; hence, ‘above genetics’). This mechanism involves modifications to either DNA or histones that control the transcriptional program of each cell by regulating the chromatin structure (**Figure 1**). For example, modifications promoting chromatin compaction do not allow access by the transcription machinery, whereas others acts as signals that modulate gene expression.

The functional subunit of chromatin is the nucleosome that consists of 147 bp of DNA wrapped in two super-helical turns around an octamer of core histones (two each of histones H2A, H2B, H3 and H4 (Kornberg, 1974; Luger et al., 1997; Van Holde et al., 1980). Each nucleosome is connected to its neighbors by a variable length of linker DNA (about 10-80 bp in length) forming the so-called “beads on a string”-like structure. Further compaction is achieved by incorporation of the linker histone H1, which binds to each nucleosome and to its adjacent linker giving rise to a 30 nm chromatin fiber (Felsenfeld and Groudine, 2003).

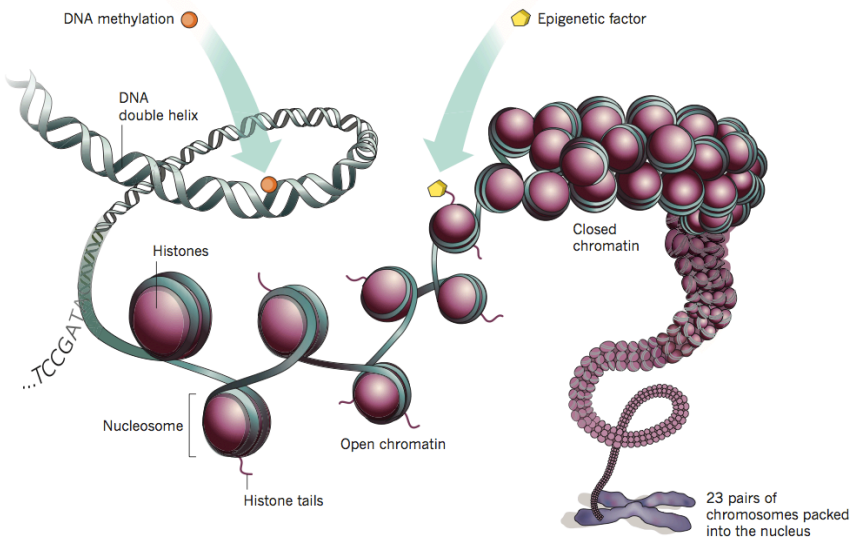

Figure 1. Structure of chromatin. DNA molecule wrapped around nucleosomes gives rise to a higher order structure allowing for compaction into the characteristic chromatin fibre and chromosomes. DNA methylation influences which genes are expressed, and other epigenetic factors (e.g. histone modifications) determine the compaction status of Chromatin. Hence, both epigenetic marks control the transcriptional and compaction state of DNA without changing the underlying DNA sequence. From (Marx, 2012).

Besides the canonical core histones H2A, H2B, H3 and H4, several histones variants have evolved for diverse cellular functions like transcriptional activation/repression, kinetochore assembly, DNA repair and recombination, gene expression, chromosome segregation and X chromosome inactivation (Malik and Henikoff, 2003; Sarma and Reinberg, 2005).

1.1.1 Histone modifications

Modifications or epigenetic marks are found on both histones and DNA. However, DNA can be primarily methylated, whereas histones are subject to a wide array of post-translational modifications (PTMs), which were discovered by Allfrey and coworkers more than 50 years ago (Allfrey et al., 1964).

The core histones are predominantly globular except for their highly basic amino-terminal extensions (histone "tails") which are unstructured (Kouzarides, 2007). The histone tails are highly conserved across species and protrude from the surface of the chromatin polymer, thus providing an exposed surface for PTMs and potential interactions with other proteins (Strahl and Allis, 2000). The tails of histone H3 and H4 as well as sites within the globular domains of all four core histones and the linker histone H1 are subject to various PTMs (**Figure 2**). There are at least eight distinct modifications such as methylation (me) of lysine (K) and arginine (R); acetylation (ac), ubiquitylation (ub) and sumoylation (su) of lysine (K) residues; phosphorylation (ph) of serine (S), theronine (T) and tyrosine (Y) (Basnet et al., 2014); and mono- and poly-ADP ribosylation of glutamate (E) and arginine (R) residues (Kouzarides, 2007). The methylation of lysine and arginine occurs in the fashion of mono- and dimethylation, whereas trimethylation is only found on lysine residues. Other modifications involve the deimination by conversion of arginine to citrulline and the isomerization of proline residues (Bannister and Kouzarides, 2011). Recently, histones H2A, H2B and H4 have been shown to be modified by β-N-acetylglucosamine (O-GlcNAc) sugar residues (Sakabe et al., 2010). Based on the diversity and biological specificity associated with distinct patterns of covalent histone marks, histone modifications have been proposed to function as a 'histone code' to coordinate the recruitment of proteins that trigger selective effects on transcription, replication and other chromatin-related processes (Jenuwein and Allis, 2001; Strahl and Allis, 2000; Taverna et al., 2007).

The histone PTMs can be found in the promoter region as well as in gene bodies. Histone modifications promoting transcription, so-called 'active' marks, include marks such as H3K4me1/3, H3K9me1, H3K9ac, H3K14ac, H3K27me1, H3K27ac and H3K79me1/2, H3K36me3, H4K20me, H2BK5me1, whereas 'repressive' marks such as H3K9me2/3, H3K27me2/3, H3K79me3, H2BK5me3 are correlating with transcriptional repression. The large number of modifications gives an enormous potential for functional responses, but not all these modifications will be located on the same histone at the same time. The appearance of histone PTMs will depend on the signaling conditions within a cell. A special case was

found in embryonic stem cells (ESCs) (and other stem cells) where many promoters carry both active H3K4me3 and repressive H3K27me3 marks. These 'bivalent promoters' are considered to poise the transcription of developmental genes. Upon differentiation these 'bivalent promoters' allow a rapid resolution to either an active or repressive state depending on the chosen lineage.

Histone PTMs are mediated and regulated by a variety of enzymes that modify ('writers') or revert a modification ('erasers'). Epigenetic 'writers' include enzymes such as histone methyltransferases (HMTs), histone acetyltransferases (HATs) and kinases; whereas histone demethylases (HDMs), histone deacetylases (HDACs) and phosphatases are examples for 'eraser' enzymes. Most of these enzymes act in protein complexes such as Trithorax group (TrxG) and Polycomb group (PcG) complexes (see 1.1.1.1) that are required for maintenance of gene expression patters. The histone modifications serve as a platform for the recruitment of proteins or protein complexes ('readers'), which influence chromatin dynamics and function. Recruitment of 'reader' proteins to the side of modifications is based on their binding via specific domains. Readers of methylation include proteins that contain specific methyl histone-binding domains, such as chromodomains, PHD (plant homeodomain) domains, or Tudor domains (Kouzarides, 2007). Acetylation is read by proteins containing a bromodomain, and phosphorylation is recognized by a domain within 14-3-3 proteins (Kouzarides, 2007).

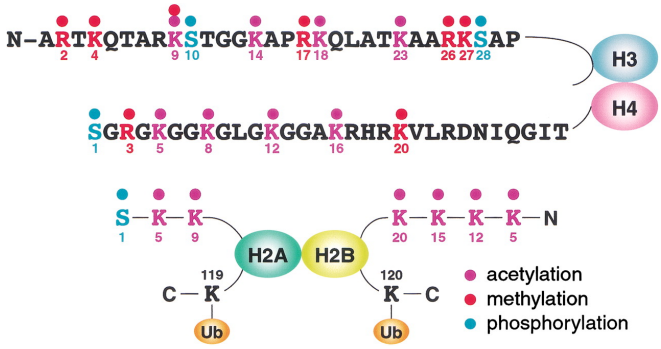

Figure 2. Sites of post-transcriptional modifications on the histone tails. Modifications shown include acetylation (purple), methylation (red), phosphorylation (cyan), and ubiquitination (orange). From (Zhang and Reinberg, 2001).

Besides PTMs of histones, other factors – including DNA methylation (see 1.1.2), histone variants, nucleosome positioning, noncoding RNAs and histone chaperones - are responsible for fine-tuning chromatin structure and function, and together they constitute the powerful and dynamic epigenetic machinery (Musselman et al., 2012). Changes in epigenetic modifica-

tions can be linked to cancer initiation and progression involving aberrant histone modifications or the dysregulation of the associated epigenetic enzymes (see 1.2).

1.1.1.1 Polycomb group proteins

Polycomb group proteins were first discovered in *Drosophila melanogaster*, where the term *Polycomb* (*Pc*) initially referred to a *Drosophila* mutant that displayed improper body segmentation (Lewis, 1949). Later, *Polycomb* was proposed to encode a negative regulator of the homeotic (*Hox*) genes that are required for segmentation (Lewis, 1978). More genes characterized by mutations that result in similar phenotypes to those of *Polycomb* were found in the 1980s suggesting that these genes belong to a group of repressors, the Polycomb group (PcG), which are required to prevent inappropriate activation of *Hox* genes (Duncan, 1982; Jürgens, 1985; Struhl, 1981). The PcG proteins are essential regulators of epigenetic gene silencing (Schwartz and Pirrotta, 2007; Simon and Kingston, 2009; Sparmann and van Lohuizen, 2006) having key roles in developmental pattering, X chromosome inactivation and stem cell maintenance (Lee et al., 2006; Plath et al., 2003; Shen et al., 2009). PcG proteins regulate epigenetically mediated transcriptional silencing of hundreds of genes encoding crucial developmental regulators in organisms ranging from plants to humans (Simon and Kingston, 2009). Polycomb-mediated silencing is based on the formation of chromatin-modifying complexes implicated in the regulation of chromatin structure in part through PTM of histones. The essential role of PcG proteins during development is highlighted by early embryonic lethality in mice upon deletion of *Eed*, *Ezh2*, *Suz12* and *Ring1B* (*Rnf2*) (Faust et al., 1995; O'Carroll et al., 2001; Pasini et al., 2004; Voncken et al., 2003). Loss of Eed, Ezh2, or Suz12 has been shown to be associated with severe defects during gastrulation, consistent with the role of PRC2 in the repression of genes involved in lineage specification (Bracken and Helin, 2009).

In mammals, two main PcG complexes exist: Polycomb repressive complex 1 (PRC1) and Polycomb repressive complex 2 (PRC2). PRC1 catalyzes monoubiquitylation of histone H2A K119 (H2AK119ub1) via the ubiquitin ligases RING1A and RING1B (**Figure 3a**) leading to chromatin compaction (Cao et al., 2005; Wang et al., 2004a). PRC2 is responsible for the di- and trimethylation of histone H3K27 (H3K27me2/3) through its subunits EZH1/2 having a catalytic SET domain (**Figure 3b**).

The core of PRC2 consists of four components: EZH1/2, SUZ12, EED and RbAp46/48 (also known as RBBP7/4) and is conserved from *Drosophila* to mammals (**Figure 3b**). Several other polypeptides were shown to be associated with PRC2 such as AEBP2, PCLs and JARID2 (**Figure 3b**). AEBP2, a zinc-finger protein was reported to enhance PRC2 enzymatic activity (Cao and Zhang, 2004) and to co-localize with PRC2 at some target genes (Kim et al., 2009). PCL1, 2 and 3, the mammalian orthologues of *Drosophila* Polycomb-like (PCL), have a tudor domain and two PHD finger domains. They were shown to interact with EZH2, SUZ12 and the histone chaperone RbAp46/48 (Nekrasov et al., 2007) and have been suggested to regulate PRC2 enzymatic activity (Nekrasov et al., 2007; Sarma et al., 2008) and recruitment (Savla et al., 2008; Walker et al., 2010). JARID2 is a member of the Jumonji protein family catalyzing the demethylation of histones but JARID2 lacks enzymatic activity. It was demonstrated to interact with EZH2 and the recruitment of JARID2 and PRC2 seems to be partially interdependent (Landeira et al., 2010; Li et al., 2010; Pasini et al., 2010; Peng et al., 2009; Shen et al., 2009).

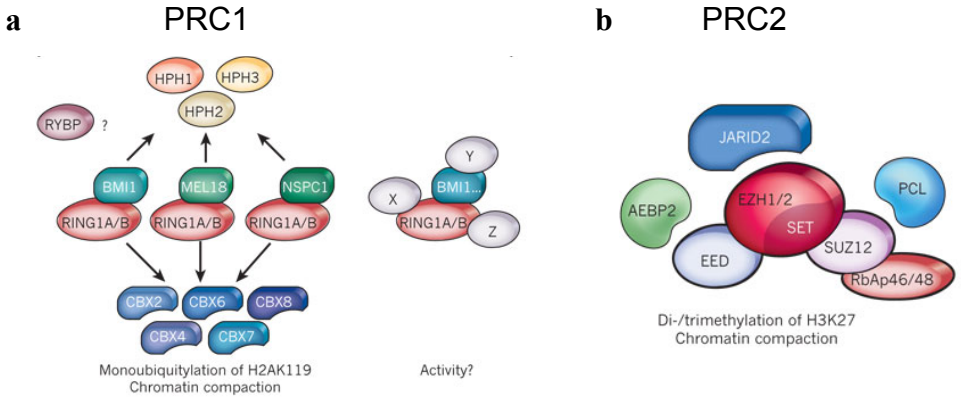

Figure 3. Polycomb complexes PRC1 and PRC2. Graphics showing the composition of PRC1 and PRC2. **a.** In PRC1, the classical PRC1 complex is depicted on the left, while those on the right correspond to the so-called PRC1-like complexes. Based on their homogly with Drosophila PSC protein, BMI1, MEL18 and NSPC1-containing PRC1 complexes are assumed to compact chromatin. CBX proteins specifically recognize H3K9/27me3 as represented by the 'pocket' shape. HPH1, 2, and 3 indicate human polyhomeotic homolog 1, 2, and 3. X, Y and Z denominate various proteins such as SCMH1/2, FBXL10, E2F6 and JARID1D, which are supposed to contribute to the formation of PRC1-like complexes. **b.** PRC2 with the core subunits EZH1/2, EED, SUZ12 and RbAp46/48 and the associated polypeptides AEBP2, PCL and JARID2. Modified from (Margueron and Reinberg, 2011).

Compared to PRC2, the composition of PRC1 is more variable, with only two core components: RING1A/B together with BMI1, MEL18 (PCGF2) or NSPC1 (PCGF1) (**Figure 3a**) (Margueron and Reinberg, 2011). In *Drosophila* two other PcG complexes were described, PHO-repressive complex (PhoRC) and Polycomb repressive deubiquitinase (PR-DUB). How-

ever, the conservation of their function in mammalian orthologues has not yet been studied. PRC1 was shown to specifically bind to H3K27me3 via its subunit Pc (known as CBX in mammals) leading to the hypothesis that PRC1 might function downstream of PRC2. However, this mechanism is equivocal since there are genes that are targeted by PRC1 without PRC2 and *vice versa* (see 1.1.1.1.2) (Margueron and Reinberg, 2011). PRC2-EZH1 complexes were reported to have a lower methyltransferase activity when compared to PRC2-EZH2 complexes indicating that the latter is involved in establishing H3K27me2/3 levels through EZH2 and that PRC2-EZH1 is implicated in the restoration of H3K27me2/3 that has been lost after histone exchange or through demethylase activity (Margueron et al., 2008). Shen and coworkers have reported that non-canonical EZH1-mediated PRC2 coexists with the classic EZH2-mediated PRC2 in catalyzing H3K27me3 at overlapping genes in mouse ESCs (Shen et al., 2008b).

1.1.1.1.1 Evolution of PRC2

Compared to mammals, PRC2 evolved to a greater complexity in plants, e.g. in *Arabidopsis thaliana* up to 12 homologues of PRC2 components were identified (Margueron and Reinberg, 2011). Interestingly, a mammalian homologue of Heterochromatin Protein 1 (HP1) that binds to H3K9me3 was found in *Arabidopsis thaliana*, named LH1, and was shown to bind H3K27me3 and to interact with the RING1 homologues AtRING1A and AtRING1B. These results suggest the existence of a PRC1-like complex in plants (Hennig and Derkacheva, 2009). Hence, it was proposed that PRC2 might have evolved from a function, partially redundant with gene silencing though H3K9me3 pathway, yielding in a more specific role for the acquisition of diverse cell lineages in higher organisms (Margueron and Reinberg, 2011).

1.1.1.1.2 Transcriptional repression by PRCs

Polycomb-mediated gene silencing is thought to rely mostly on regulation of chromatin structure, in part through post-translational modification (PTM) of histones. Hence, the PRC2 complex is responsible for the methylation (di- and tri-) of lysine 27 of histone H3 (H3K27me2/3) via its enzymatic subunits EZH1 and EZH2, whereas the PRC1 complex mono-ubiquitylates lysine 119 of histone H2A (H2AK119ub) via the ubiquitin ligases RING1A or RING1B. In addition, some PRC1 complexes can regulate gene expression by compacting chromatin in a manner independent of enzymatic activity (Eskeland et al., 2010).

The PRC1 component Pc (CBX in mammals), binds specifically to the product of PRC2 catalysis, H3K27me3, leading to the hypothesis that PRC1 functions downstream of PRC2. Although this logical premise is still cited in the literature, its operational status is equivocal as there are genes targeted by PRC2 that lack H2AK119ub (Ku et al., 2008) an genes targeted by PRC1 in the absence of PRC2 (Schoeftner et al., 2006; Sing et al., 2009). Notwithstanding, PRC2 and PRC1 are often both required to maintain gene repression.

In general, histone PTMs regulate biological processes either by altering chromatin structure (*i.e.* by loosening DNA/histone interaction) or by contributing to the recruitment of additional regulatory factors. Thus far, H3K27me3 has been implicated only in the latter mechanism of action suggesting that additional factors such as PRC1 are required to maintain gene repression (Margueron and Reinberg, 2011). Yet, H3K27me3 might also indirectly regulate transcription by sterically preventing proteins from binding to chromatin. Enrichment of H3K27me3 correlates with gene silencing (Barski et al., 2007), and this observation is supported by the finding that H3K27me3 and H3K36me3, a mark that is linked to transcription elongation, exhibit distinct localizations (Mikkelsen et al., 2007). Yet, RNA polymerase II (RNA PolII) that is phosphorylated at Ser-5 of its C-terminal domain is present at a substantial fraction of H3K27me3 enriched promoters (Stock et al., 2007) and low levels of transcripts are detected (Zhao et al., 2007), leading to the suggestion that RNA PolII could be paused at PcG targeted genes (Margueron and Reinberg, 2011). Indeed, a number of PcG-regulated genes in *Drosophila* and mammals can recruit the RNA PolII transcription complex to their respective promoters and engage in early transcription, yet these polymerases encounter an early block to elongation. A recent report has proposed that short transcripts that are generated upon transcription and remain bound to a paused RNA PolII could recruit PRC2 (Kanhere et al., 2010). This result suggests that PRC2 and H3K27me3 might affect gene expression by controlling an engaged RNA PolII during promoter escape or elongation, rather than by regulating the initiation phase of transcription. Taken together, these different PRC2-mediated repression mechanisms strongly suggest that PRC2 can repress transcription by different ways and this may be gene-specific (Margueron and Reinberg, 2011).

DNA methylation (see also 1.1.2) and H3K27me3 are both involved in the establishment and maintenance of epigenetic gene silencing. There are data showing coordinate regulation between these marks. Some evidence points toward a cooperative relationship. For example, EZH2 has been shown to positively regulate DNA methylation (Vire et al., 2006). In these studies, EZH2 was observed to interact with DNA methyltransferases (DNMTs) and was re-

quired for DNA methylation of EZH2-target promoters. Alternatively, several lines of evidence suggest the coordination between DNA methylation and H3K27me3 may be antagonistic. A proteomic analysis has shown that the PRC2 components EED and SUZ12 are excluded from methylated DNA (Bartke et al., 2010), and in neural stem cells Dnmt3a deficiency leads to increased H3K27me3 (Wu et al., 2010). Finally, additional studies suggest that an important relationship between DNA methylation and H3K27me3 is disrupted in cancer cells. Polycomb group targets are more likely to have cancer-specific promoter DNA hypermethylation than non-targets (Gal-Yam et al., 2008; Schlesinger et al., 2007; Widschwendter et al., 2007). However, embryonic carcinoma cells lack DNA hypermethylation at PRC targets (Ohm et al., 2007), and knockdown of EZH2 in cancer cells may lead to hypomethylation (McGarvey et al., 2007). Thus, the evidence of interaction is conflicting, but it is clear that the relationship between these marks is important in both normal and cancerous cells.

1.1.1.1.3 Targeting of PRC to genomic loci

In *Drosophila*, Polycomb complexes are recruited to Polycomb response elements (PREs), that contain several hundreds of base pairs (Ringrose and Paro, 2007) and often contain clusters of GAGAG motifs (Schwartz and Pirrotta, 2007). PREs can be bound by sequence-specific DNA-binding factors such as GAGA factor (GAF), Pipsqueak (PSQ), both BTP/POZ proteins, Pleiohomeotic (PHO) and the related PHO-like (PHOL) (Ringrose and Paro, 2004; Schwartz and Pirrotta, 2007).

Besides the critical implication of PcG proteins in development and cell fate specification (Schuettengruber et al., 2007), PRC2 has gained much of attention since aberrant human PRC2 expression was shown to be linked to cancer and disease (Bernardi and Pandolfi, 2007; Rajasekhar and Begemann, 2007; Simon and Lange, 2008; Sparmann and van Lohuizen, 2006). In contrast to *Drosophila*, the recruitment of mammalian PRC2 remains poorly understood. As described earlier, JARID2 has been proposed to have a potential function in PRC2 recruitment. JARID2 binds to DNA with a slight bias towards CG-rich sequences (Li et al., 2010), which were reported to represent a sequence composition of PRC2 target genes (Ku et al., 2008). Therefore, it has been suggested that PRC2 recruitment in mammals involves genome-wide CpG islands (Deaton and Bird, 2011; Ku et al., 2008; Riising et al., 2014). Interestingly, the histone variant H2AZ, usually associated with active genes, was shown to co-localize with PRC2 in ESCs (Creyghton et al., 2008). Furthermore, the authors demonstrated

that H2AZ and PcG protein occupancy is interdependent at promoters, and that H2AZ is necessary for ES cell differentiation.

PcG recruitment via PREs does not seem to be generally conserved in mammals. So far, very few DNA binding factors have been described to have the ability to recruit PcG proteins to specific chromatin sites in mammals and Yin and yang 1 (YY1), the mammalian orthologue of PHO, is one of the best candidates (Bracken and Helin, 2009). Similar to PcG proteins, YY1 activity is required for mammalian development, as YY1-null embryos die at the peri-implantation stages of embryogenesis (Donohoe et al., 1999). Two studies have identified a PRE in mammalian cells and have suggested an important role for YY1 (Sing et al., 2009; Woo et al., 2010). Along this line, the RYBP protein was shown to interact with both YY1 and PRC1, and is suggested to be required for PRC1 and PRC2 recruitment (Woo et al., 2010). YY1 was shown to directly interact with EED in Burkitt's lymphoma cells (Satijn et al., 2001), to mediate EZH2 recruitment during myoblasts differentiation (Caretti et al., 2004) and during muscles regeneration from satellite stem cells (Palacios et al., 2010), and to act as a DNA–RNA binding factor during X chromosome inactivation, that links PcG-Xist to the inactive X chromosome (Jeon and Lee, 2011). However, several reports suggest that YY1 has PcG-independent functions (Cai et al., 2007; Gordon et al., 2006; He et al., 2011a; Sui et al., 2004; Wu et al., 2007). In addition, a recent study has shown that YY1 does not share physical and functional properties with PcG proteins in ESCs; it preferentially associates with the CG-rich promoters of actively transcribed genes (Vella et al., 2012). Nevertheless, genome-wide analysis did not confirm a significant overlap between YY1 and Polycomb target genes (Xi et al., 2007). PRC2 was even shown to be under-represented at YY1-response elements (Ku et al., 2008). Although, YY1 binding sites contribute to the repression of some loci, there is no strong evidence that transcription factors are involved in PRC2 recruitment in mammals suggesting that other factors might be involved in the regulation of these loci (Margueron and Reinberg, 2011).

Recently, long noncoding RNAs (long ncRNAs) have emerged as important players in epigenetic regulation and in PRC2 function. Several PRC2 subunits have RNA-binding motifs that could mediate functional interactions between RNAs and PRC2 (Bernstein and Allis, 2005; Bernstein et al., 2006; Denisenko et al., 1998). Suz12 contains a zinc finger domain that can bind to RNA (Hall, 2005), and EZH2 and EED both have been shown to have *in vitro* RNA binding activity (Denisenko et al., 1998). For example, the human *HOX-D* locus is regulated *in trans* by HOTAIR RNA, which arises from the unlinked *HOX-C* locus (Rinn et

al., 2007). Tsix, RepA, and Xist RNAs have been shown to target PRC2 *in cis* during X chromosome inactivation (Zhao et al., 2008). Similarly, KCNQ1OT1 RNA mediates spreading of PRC2 *in cis* in order to maintain the imprinted expression of the KCNQ1 domain (Pandey et al., 2008). Kanhere and colleagues have identified several short candidate RNAs of 50-200 nt in length that regulate PRC2 via Suz12 (Kanhere et al., 2010). Another study by Zhao and co-workers, which aimed to identify genome-wide Polycomb-associated RNAs, proposed a PRC2-RNA interaction to occur most likely via the EZH2 subunit (Zhao et al., 2010). It was also suggested that PRC1 regulation is based on RNA (Yap et al., 2010). In summary, these studies support the idea that long ncRNAs represent a platform for the targeting of PcG complexes to specific sites in the genome but the molecular mechanisms remain yet unclear. On basis of these observations, a model was proposed, in which the sum of weak interactions by the subunits of the PRC2 holoenzyme complex function together to accomplish the necessary energy to guide PRC2 to its target genes (Margueron and Reinberg, 2011).

1.1.2 DNA methylation

DNA methylation belongs to the most studied epigenetic modification and has a profound impact on mammalian development, transcription and genome stability. Methylation at the carbon 5-position of cytosine (5mC) is well conserved among most plants, animals and fungi (Feng et al., 2010) and affects gene activity directly by inhibiting the binding of transcription factors and indirectly by recruiting repressive chromatin-associated proteins (Bell et al., 2011). 5mC mediates long-term gene silencing and is involved in cell-lineage specification, genomic imprinting, X chromosome inactivation and the suppression of mobile genetic elements (Bestor and Bourc'his, 2004; Jaenisch and Bird, 2003; Wu and Zhang, 2010). Although it is an ubiquitous mechanism in multicellular organisms, DNA methylation is undetectable in *Saccharomyces cerevisiae* and adult *Drosophila melanogaster* (Issa, 2004). In mammals, DNA methylation is mainly restricted to symmetrical CpG dinucleotides (Ramsahoye et al., 2000; Ziller et al., 2011) and deposited by DNA methyltransferase (DNMT) enzymes, which use S-adenosyl methionine (SAM) as the methyl donor (Goll and Bestor, 2005). DNA methylation is catalyzed either by the maintenance methyltransferase DNMT1, which methylates hemimethylated CpGs during replication, or by the *de novo* methyltransferases DNMT3A and DNMT3B, making it a long-term and potentially heritable mark (Goll and Bestor, 2005) (**Figure 4**). The importance of DNA methylation is reflected by the fact that all three enzymes

are essential for normal development (Kaneda et al., 2004; Li et al., 1992; Okano et al., 1999), for example, mouse DNMT1 null embryos die at day 11-12 of gestation (Li et al., 1992).

The mammalian genome is globally CpG-depleted, and in humans about 60-80% of the roughly 28 million CpGs are methylated (Smith and Meissner, 2013). CpGs can be located in CpG-dense regions, termed CpG islands (CGIs). However, this only accounts for less than 10% of CpGs sites. CGI are located at transcription start sites of housekeeping and developmental genes where they are largely resistant to methylation (Deaton and Bird, 2011). In contrast to methylation in promoter regions, methylation of CpG sites within gene bodies, most of them are not CGIs, was shown to be a feature of transcribed genes (Wolf et al., 1984). Thus, methylation in gene promoters is inversely correlated with gene expression, while methylation in gene bodies is positively correlated with expression (Jones, 1999).

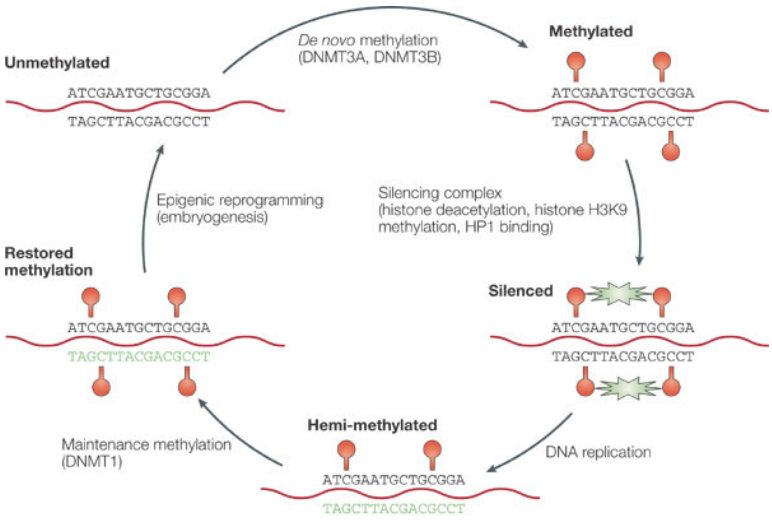

Figure 4. DNA methylation and gene silencing. DNA is largely unmethylated in early embryogenesis (top left). After implantation, *de novo* methylation starts (red circles), primarily mediated by DNMT3A and DNMT3B (top). At CpG islands, methyl-binding proteins trigger a silencing cascade (activity illustrated by green stars) whereby histone H3K9 is sequentially deaceylated and then methylated, allowing binding of heterochromatin protein 1 (HP1); eventually resulting in a closed chromatin structure (bottom right). After DNA replication, newly synthesized DNA (in green) is unmethylated. DNMT1 scans DNA and deposits methyl groups on newly synthesized DNA, according to the hemi-methylated pattern present on the old strand. This ensures faithful replication of methylation patterns (bottom left) and the maintenance of silencing. Adult methylation patterns are erased by epigenetic reprogramming in early embryogenesis (top left). From (Issa, 2004).

Methylation occurs in a highly specific manner as evident by differentially methylated regions (DMRs), which are regions in the genome where multiple adjacent CpG sites show differential methylation patterns compared to other samples. This does not apply to CGIs, as most of them are unmethylated. There are several types of DMRs: imprinting-specific (iDMR), tissue-specific (tDMR), reprogramming-specific (rDMR), cancer-specific (cDMR)

and ageing-specific differentially methylated region (aDMR) (Rakyan et al., 2011). Methylated DNA can be recognized by proteins harboring a methyl-CpG-binding domain (MBD) such as MeCP2, MBD1, MBD2, MBD4. These proteins in turn recruit further chromatin modifiers such as HDACs or methyltransferases (Bird and Wolffe, 1999). On the other hand, transcriptional activators like TrxG proteins can bind to unmethylated CpGs with high affinity via their zinc-finger CXXC (zf-CXXC) domain (Voo et al., 2000).

DNA methylation represents a relatively stable mark when compared with most histone modifications. However, methylation can be removed from DNA by a process named DNA demethylation, which is involved in different biological processes. Recently, the discovery of the ten-eleven translocation (TET) family enzymes has shed light on a potential mechanism of DNA demethylation. TET enzymes catalyze the iterative oxidation of 5mC to 5-hydroxymethylcytosine (5hmC), 5-formylcytosine (5fC) and 5-carboxylcytosine (5caC) (Ito et al., 2011), whereby 5hmC was suggested to be the key intermediate in the active demethylation pathway (Ito et al., 2010; Ito et al., 2011; Kriaucionis and Heintz, 2009; Tahiliani et al., 2009). By using molecular oxygen as a substrate to catalyze oxidative decarboxylation of α-ketoglutarate (α-KG), TET enzymes generate a reactive high-valent enzyme-bound Fe(IV)-oxo intermediate that converts 5mC to 5hmC (Kohli and Zhang, 2013). 5hmC can either be actively removed by its reversion to cytosine through iterative oxidation followed by base excision repair by thymine-DNA glycosylase (TDG) (He et al., 2011b), or passively depleted in consecutive rounds of replication in the absence of the DNA methylation maintenance machinery (Kohli and Zhang, 2013). Like DNMTs, TDG, in contrast to other DNA glycosylases, is also required for embryonic development (Cortazar et al., 2011; Cortellino et al., 2011). DNA demethylation plays a crucial role in early embryonic development. During fertilization of the egg, before paternal and maternal genomes merge, the paternal genome undergoes complex remodeling processes including deposition of histone H3.3 and reshaping of DNA methylation patterns by a rapid erasure of 5mC (Jenkins and Carrell, 2012). The loss of 5mC is specific to the paternal genome as it does not take place in the maternal genome, and was therefore suggested to reflect an active 5mC editing mechanism (Mayer et al., 2000; Oswald et al., 2000). After implantation of the embryo, a fraction of posterior epiblast cells become primordial germ cells (PGCs) that go through an erasure of genome-wide DNA methylation patterns (Hackett et al., 2012) to prime them for germ-cell-specific processes, like meiosis. DNA demethylation is relevant not only in zygotes and PGCs, it was also reported at specific loci in response to environmental stimuli or in post-mitotic cells, even in the absence of repli-

cation (Kangaspeska et al., 2008; Metivier et al., 2008; Thillainadesan et al., 2012). These observations allow the postulation of a model compromising methylation, oxidation and repair that seems to be of great significance for biological processes known to involve active DNA demethylation (Kohli and Zhang, 2013).

Aberrant DNA methylation patterns are a prevalent feature of cancer cells (Baylin and Jones, 2011), suggesting that methylation/demethylation pathways may contribute to cancer development (Cimmino et al., 2011) (see 1.2.2).

1.2 Epigenetics in Cancer

Cancer evolution at all stages is driven by both epigenetic abnormalities as well as genetic alterations. Dysregulation of epigenetic control events may lead to abnormal patterns of DNA methylation and chromatin configurations, both of which are critical contributors to the pathogenesis of cancer. There is evidence that this can occur via at least two mechanisms; (i) by the alteration of gene expression programs, including aberrant regulation of oncogenes and/or tumor suppressor genes, and (ii) on a more global level, histone modifications may affect genome integrity and/or chromosome segregation (Bannister and Kouzarides, 2011). Recently, cancer genome sequencing studies have revealed an abundance of somatic mutations in genes encoding chromatin-modifying proteins, suggesting a crucial role of epigenetic gene regulation. The mechanisms by which these mutations could contribute to tumor fitness have thus become a major challenge in cancer research (Ryan and Bernstein, 2012). Undoubtedly, most chromatin modifying proteins bind to thousands of loci within the genome thereby influencing (directly or indirectly) the gene expression of various genes and pathways. Hence, the reversible nature of epigenetic marks, such as aberrant DNA methylation and histone modification patterns, has made them attractive targets for therapeutic intervention in cancer (Kelly et al., 2010).

1.2.1 Histone modifications and cancer

Several studies provide evidence that aberrant histone modification profiles are intimately linked to the initiation stage of cancer development. A work by Huntly and co-workers has investigated the MOZ-TIF2 fusion, which is associated with acute myeloid leukemia (AML) (Carapeti et al., 1998; Liang et al., 1998). MOZ was identified as a HAT, and TIF2 is a nuclear receptor coactivator that is able to bind to another HAT, CBP (Torchia et al., 1997). The

transduction of the MOZ-TIF2 fusion protein into normal committed murine hematopoietic progenitor cells lacking self-renewal capacity was sufficient to confer self-renewal *in vitro* and to develop AML *in vivo* (Huntly et al., 2004). Another example is given by studies showing that JAK2-mediated phosphorylation of H3Y41, preventing HP1α-binding to H3, relieves *lmo2* gene expression (Dawson et al., 2009), a key oncogene in hematopoietic cancers (McCormack and Rabbitts, 2004; Yamada et al., 1998). JAK2 has been reported to be frequently activated in hematological malignancies by chromosomal translocations or point mutations (Dawson et al., 2009).

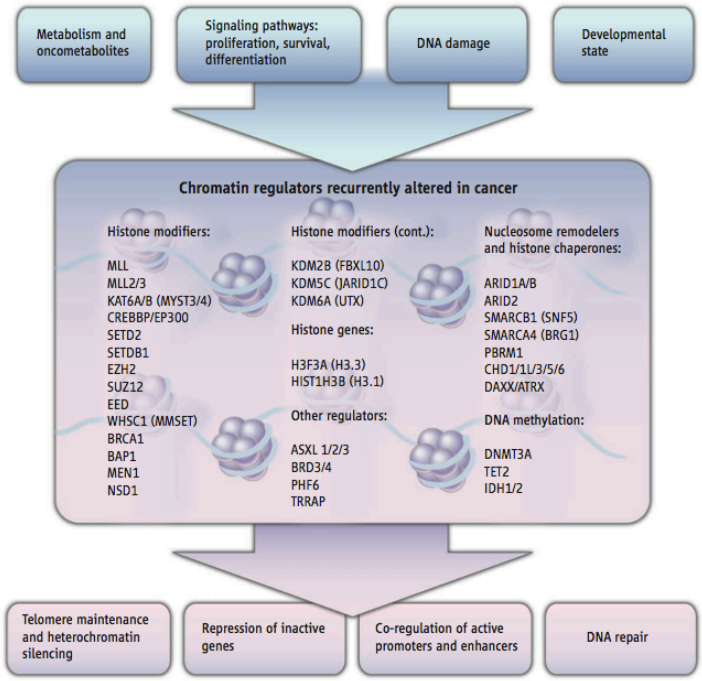

Figure 5. Alteration of epigenetic regulators in cancer. List of epigenetic regulators frequently mutated, up- or downregulated in cancers that affect transcriptional regulation, genome stability, telomere maintenance, and other aspects of cell physiology. From (Ryan and Bernstein, 2012).

A prominent alteration in histone modifications in tumor cells is the global loss of H4K16 monoacetylation (Fraga et al., 2005). HDACs are responsible for the removal of acetylation marks and are frequently mutated (Ropero et al., 2006) or overexpressed (Zhu et al., 2004) in several tumor types. For example, SirT1, a HDAC, is upregulated in various cancer types and was shown to interact with DNMT1, thus influencing DNA methylation patterns (Espada et al., 2007). Noonan and colleagues have demonstrated that HDAC expression can be regulated by miRNAs. Interestingly, *miR-449a* is downregulated in prostate cancer tissues compared to normal control tissue (Noonan et al., 2009). The authors have identified HDAC1 as a direct

target of *miR-449a*, which represses HDAC1 expression in prostate tumor cells, thereby regulating cell growth and survival (Noonan et al., 2009). Besides alterations in HDAC expression and function, the global imbalance in histone acetylation has been shown in other cancer types to be caused by mutations, deletions or translocations in HATs and HAT-related genes (Bryan et al., 2002; Moore et al., 2004) (**Figure 5**).

In addition to the global loss of H4K16ac, tumors cells endure a global loss of the repressive mark H4K20me3 (Fraga et al., 2005) and a gain in the active mark H3K4me3 (Hamamoto et al., 2004) and the repressive marks H3K9me (Ellinger et al., 2014; Kondo et al., 2007) and H3K27me3 (Vire et al., 2006). Like alterations in histone acetylation, thechanges in histone methylation patterns in cancer are mainly caused by aberrant expression of both, HMTs and HDMs (Chi et al., 2010). A recent study by Dalgliesh and co-workers has identified inactivating mutations in SETD2, a histone methyltransferase, and in the histone demethylases UTX and JARID1C in renal carcinomas (Dalgliesh et al., 2010). Inactivating mutations in UTX have been also reported in multiple myeloma and esophageal squamous cell carcinomas (van Haaften et al., 2009). Remarkably, the histone methyltransferase EZH2 has been demonstrated to induce extensive gene silencing and its overexpression has been linked to progression of multiple solid tumors, including melanoma, breast, bladder and prostate cancer (Bachmann et al., 2006; Kleer et al., 2003; Varambally et al., 2002; Weikert et al., 2005). This process also involves widespread elevated levels of H3K27me3, the mark deposited by EZH2. Interestingly, upregulation of the lincRNA *HOTAIR* has been demonstrated to contribute to cancer metastasis and poor survival in breast and esophageal squamous cell carcinoma by retargeting EZH2 leading to alterations in the H3K27me3 landscape (Chen et al., 2013; Gupta et al., 2010). Furthermore, upregulation of EZH2 in many cancer types has been shown to depend on the genomic loss of *miR-101* (Varambally et al., 2008). Nevertheless, several studies have reported inactivating mutations in different myeloid malignancies, proposing EZH2 to act as a tumor suppressor protein (Ernst et al., 2010; Nikoloski et al., 2010). Clearly, this is contrary to the situation in solid tumors, where EZH2 functions as an oncogene. Therefore, it is assumed that changes in H3K27me3 levels (in both directions) are critical for cellular homeostasis and may are involved in tumor development (Bannister and Kouzarides, 2011). EZH2 overexpression and inactivating mutations in HDMs have been reported to occur in many cancer types supporting an important role of the H3K27me3 mark in carcinogenesis. Besides EZH2, also SUZ12 has been found to be overexpressed in both colon and breast cancer (Kirmizis et al., 2003).

Also other HMTs are deregulated in cancers. For example, NSD1 has been reported to undergo epigenetic silencing by promoter CpG hypermethylation in neuroblastoma and glioma (Berdasco et al., 2009). For the *MLL* (mixed lineage leukemia) gene, which encodes a H3K4 histone methyltransferase, more than different 50 translocations or partial tandem duplications on chromosome 11q13 have been discovered and found to be associated with poor survival in leukemia (Caligiuri et al., 1997; Dohner et al., 2002; Krivtsov and Armstrong, 2007; Zeminvan der Poel et al., 1991). Recently, DOT1L, the major H3K79 methyltransferase has been implicated in the development of MLL-rearranged leukemia, where MLL fusion oncoproteins result in inappropriate recruitment of DOT1L causing aberrant H3K79 and H3K4 methylation patterns (Dohner et al., 2002; Krivtsov and Armstrong, 2007; Krivtsov et al., 2008; Okada et al., 2005; Wang et al., 2009).

Upregulation of HDMs has been shown to occur in some cancers (Shi, 2007). For example the H3K4 and H3K9 demethylase LSD1 is overexpressed in prostate cancer, where it was shown to be involved in AR (androgen receptor)-mediated transcription by acting as an H3K9 demethylase (Kahl et al., 2006; Metzger et al., 2005). Moreover, the three tudor domain-containing KDM4/JMJD2 (A, B and C) proteins have been reported to be overexpressed in lung, breast, colorectal and prostate cancer and in esophageal squamous carcinoma (Berry and Janknecht, 2013; Yang et al., 2000).

Alterations of histone modifications are not only linked to cellular identity but also to genomic instability and chromosome segregation defects, both prominent features of cancer cells. In this regard, it was shown that homozygous null mutant mice for *PR-Set7*, an H4K20me1 histone methyltransferase, die at an early embryonic state as a result of enormous DNA damage, cell cycle defects and improper chromosome condensation (Oda et al., 2009). H4K20me1 is read by L3MBTL1 via its malignant brain tumor (MBT) domain leading to local chromatin compaction and transcriptional repression (Kalakonda et al., 2008; Trojer et al., 2007; Trojer and Reinberg, 2008). H4K20me3 is enriched in pericentromeric heterochromatin (Schotta et al., 2004) and global changes in H4K20me3 levels have been implicated in carcinogenesis. In this regard, Fraga and colleagues have reported a loss of H4K16ac and H4K20me3 in cancer cells in association with hypomethylation of DNA repetitive sequences, a hallmark that is frequently observed in human cancers (Fraga et al., 2005). Interestingly, using a mouse model of multistage skin carcinogenesis, Fraga and co-workers have demonstrated that these changes in histone modification patterns occur early and accumulate during the tumorigenic process (Fraga et al., 2004) supporting an intimate link of aberrant histone

modification profiles with cancer progression. Another histone methyltransferase SUV39, responsible for H3K9 methylation, is also required for genomic stability. *Suv39h*-deficient mice display reduced H3K9me2/3 levels, impaired viability and chromosomal instabilities associated with an increased risk of tumor development (Peters et al., 2001).

1.2.2 DNA methylation and cancer

Aberrant DNA methylation is a hallmark of cancer cells (Baylin and Jones, 2011; Esteller, 2007a). The cancer epigenome is characterized by a loss of global methylation (Goelz et al., 1985) along with a gain of methylation at the promoters of selected CpG islands (CGIs) of tumor suppressor genes (Baylin et al., 2001). Global hypomethylation is predominantly found at repetitive sequences and is linked to chromosomal instability, translocations, gene disruption and reactivation of endoparasitic sequences (Gaudet et al., 2003; Goelz et al., 1985). For example L1, a LINE family member, has been shown to be hypomethylated in a variety of cancers such as breast, lung, bladder and liver tumors (Wilson et al., 2007). Hypomethylation at specific promoters is thought to be responsible for the aberrant expression of oncogenes and the induction of loss of imprinting (LOI) in some regions (Portela and Esteller, 2010). For example, the tumor suppressor *MASPIN* (also known as *SERPINB5*) is hypermethylated in breast and prostate epithelial cells (Futscher et al., 2004) and seems to be hypomethylated in other cancers. *MASPIN* hypomethylation and its expression have been demonstrated to increase with the dedifferentiation of some cancer cells (Bettstetter et al., 2005; Futscher et al., 2002). Other well-studied examples of hypomethylated genes in cancer include *SNCG* in breast and ovarian cancer, *S100P* in pancreatic cancer and *MAGE* and *DPP6* in melanomas (Irizarry et al., 2009; Portela and Esteller, 2010; Wilson et al., 2007). The most frequently observed LOI event based on hypomethylation is the insulin-like growth factor 2 (*IGF2*) that has been reported in several tumors such as breast, liver, lung and colon cancer (Ito et al., 2008).

In contrast to global DNA hypomethylation, hypermethylation is found at particular CGIs. Transcriptional silencing due to promoter hypermethylation occurs early in tumor progression and mediates abnormalities in important cellular pathways such as loss of cell cycle control, altered receptor function, disruption of cell-cell/cell-substratum interaction, inactivation of signal transduction pathways, loss of apoptotic signals and genetic instability (Baylin et al., 2001) (see 1.2.5). It has been proposed that these hypermethylated promoters constitute a new

generation of biomarkers which possess diagnostic and prognostic features in the clinic (Kelly et al., 2010). Aberrant CGI methylation in tumors was first described almost three decades ago (Baylin et al., 1986). Later, as more and more genes affected by this process were identified, it was observed that in some tumors the consistent increase in methylation occurs at particular groups of genes. The methylation of two separate genes was shown to be correlated in a given tumor type. These multiple concordant methylation evens was named CpG island methylator phenotype (CIMP) and was first described in colon cancer (Toyota et al., 1999) (see 1.2.6).

CGIs of promoter regions have been in the focus of most studies but recent findings propose that most of the aberrant DNA methylation in cancer occurs in CpG island shores, for example in *HOXA2* and *GATA2* (Portela and Esteller, 2010). About half of the changes in CpG island shores are assumed to occur at regions that become hypermethylated during normal tissue differentiation (Portela and Esteller, 2010), for example *TGFB1* and *PAX5* (Doi et al., 2009; Irizarry et al., 2009). Therefore, differential DNA methylation has been suggested to correlate with gene expression at CpG island shores like it does with CGI (Ji et al., 2010).

DNMTs have been reported to be upregulated in several cancers such colon (el-Deiry et al., 1991), prostate (Patra et al., 2002), breast (Girault et al., 2003) and liver cancer (Oh et al., 2007) and in leukemia (Melki et al., 1998). Besides alterations in the expression levels of DNMTs also mutations have been found. For example, DNMT3A mutations have been reported in leukemia (Ley et al., 2010) leading to either a reduction in catalytic activity and subsequent activation of more than 800 genes including *HOX* genes and *IDH1*, or aberrant binding affinity of DNMT3A to histone H3 (Yan et al., 2011). In addition to leukemia, further mutations have been also reported in lung, ovarian, kidney, liver and uterus cancer (Plass et al., 2013). Recently, the gain-of-function mutation in the isocitrate dehydrogenase 1 (IDH1) Arg132His (R132H) (also equivalent mutations in IDH2) has been described to also exert a massive effect on chromatin structure in glioblastoma and leukemia by production of the oncometabolite 2-hydroxyglutarate (2-HG) (Xu et al., 2011). Several reports have demonstrated that 2-HG inhibits TET family hydroxylases and JmjC family of histone demethylases leading to DNA hypermethylation and an increase in H3K9me3, H3K27me3, H3K4me3 and H3K36me3 (Figueroa et al., 2010; Lu et al., 2012). Mutations in IDH1/2 have been also reported in leukemia (Figueroa et al., 2010).

1.2.3 Chromatin remodeling and cancer

Chromatin remodelers function in complexes in an ATP-dependent manner to disrupt the DNA-nucleosome interaction in order to move, replace or remove nucleosome from chromatin (Hargreaves and Crabtree, 2011). All four classes of chromatin remodelers, SWI/SNF, chromodomain helicase DNA-binding proteins (CHDs), ISWI and INO80, have been reported to contribute to cancer progression (Portela and Esteller, 2010). Genome-wide sequencing of human cancers has revealed that genes involved in establishing chromatin structure are also frequently mutated (Shain and Pollack, 2013). Yet, the mechanisms by which mutations in chromatin remodeler complexes drive tumorigenesis remain unclear. Clearly, chromatin remodeler complexes act on large proportions of the genome. Therefore, it is assumed that mutations in their components can cause serious aberrations in chromatin structure thereby influencing cancer progression (Plass et al., 2013). Several chromatin modifiers have been proposed to be tumor suppressors but mutations in these complexes might also lead to a change of function rather than to a loss of function (Wilson and Roberts, 2011). SWI/SNF chromatin remodelers play a central role during lineage specification and in the maintenance of pluripotency by regulating and coordinating the gene expression program. Inactivating mutations in subunits of the SWI/SNF complexes including SNF5 (also known as SMARCB1), ARID1A, BAF180, BRM, and BRG1 are frequently found in various cancer types (Wilson and Roberts, 2011). ARID1A has been found to be amongst genes showing the highest mutation rates across multiple cancers (Lawrence et al., 2014) and *ARID1A* is mutated in ~57% of ovarian clear cell carcinomas (Jones et al., 2010; Wiegand et al., 2010). Recently, Bitler and coworkers have identified a synthetic lethality in *ARID1A*-mutated cancers upon EZH2 inhibition representing a novel treatment strategy in these cancers (Bitler et al., 2015). A bi-allelic inactivation of SNF5 has been identified to be the only recurrent mutation in malignant rhabdoid tumors, which usually have a low frequency of mutations (Versteege et al., 1998). These data demonstrate the importance of proper chromatin remodeling. It has been proposed that SWI/SNF complexes contribute to tumor suppression by influencing gene expression of key pathways, including Rb, p53, Polycomb, Sonic hedgehog, MYC, nuclear hormone receptor signaling and stem cell programs (Shain and Pollack, 2013) but also by affecting overall chromatin structure and genome packaging for mitosis. Interestingly, CHD5, a member of the CHD family, has been found to gain DNA hypermethylation in the promoter region resulting in transcriptional silencing in colon and breast cancers and gliomas (Mulero-Navarro and Esteller, 2008).

In addition to nucleosome positioning, histone variants have been linked to cancer. For example, in lung cancer, cells expressing macroH2A isoforms have been shown to undergoing cellular senescence. Moreover, patients with elevated expression of histone macroH2A1.1 and macroH2A2 have slower tumor proliferation rates and a better prognosis (Sporn et al., 2009).

Recently, recurrent gain-of-function mutations in the histone H3 genes have been identified in pediatric glioblastoma with major implications on chromatin structure and gene expression (Schwartzentruber et al., 2012; Wu et al., 2012). Of particular interest are the mutations found in the *H3F3A* gene, encoding the histone variant H3.3, with important consequences for chromatin remodeling. These H3.3 mutations result in Lys27Met (K27M) and Gly34Arg or Gly34Val (G34R/V) substitutions leading to global changes in histone modifications, involving H3K27me3 and H3K36me3 (Sturm et al., 2012). The K27M mutation has been reported to inhibit EZH2 within PRC2, resulting in a prominent global loss in H3K27me3 and upregulation of PRC2-target genes. The other mutation G34R/V has been shown to induce a redistribution of H3K36me3 and might affect the distribution of its corresponding enzyme SETD2, leading to upregulation of *MYCN* (Bjerke et al., 2013). Tumors carrying these mutations also display a DNA hypomethylation phenotype, suggesting a relationship between histone modifications and DNA methylation (Bender et al., 2013).

1.2.4 Epigenetic therapies

As epigenetic alterations are potentially reversible, unlike DNA mutations, the pharmacological inhibition of oncogenically activated chromatin modifying enzymes or the modulation of other chromatin modifiers to ‘correct’ aberrant modifications may have important therapeutic implications in cancer as well as in other diseases with an altered epigenome. The identification of downstream ‘driver pathways’ which are responsible for the oncogenic effects of these mutations may prove efficacious and provide opportunities for synthetic lethal strategies. For example, as described above, a synthetic lethality was identified in *ARID1A*-mutated ovarian cancers upon inhibition of EZH2 using the small-molecule inhibitor GSK126 (Bitler et al., 2015).

In general, two classes of drugs can be distinguished, on the one hand drugs targeting epigenetic regulators (such as DMNTs and HDACs) and on the other hand drugs specifically

targeting mutations in epigenetic regulators (such as IDH1 R132H). The latter one may are less toxic but they can be only used in a subset of patients with that particular mutation.

So far, the US Food and Drug Administration (FDA) has approved four epigenetic drugs based on their considerable clinical benefit. These are the two DNMT inhibitors azacytidine and 5-aza-2´deoxycytidine (also known as Vidaza and Dacogen/Decitabin, respectively) and the two HDAC inhibitors SAHA and romidepsin (also known as Vorinostat and Istodax, respectively). Inhibitors of DNA methylation are cytosine analogues, which after being incorporated into the DNA during replication, trap DNMT via covalent binding. Both inhibitors for DNMTs have been shown to induce significant response rates and a survival benefit in patients with acute myeloid leukemia (Kantarjian et al., 2012) and myelodysplastic syndrome (Fenaux, 2005; Lubbert et al., 2011). HDAC inhibitors promote the acetylation of histones and facilitate an open form of chromatin structure resulting in gene activation. In 2006, the first HDAC inhibitor Vorinostat has been approved by the FDA for treatment of patients with cutaneous T cell lymphoma (CTCL) (Kelly et al., 2005; O'Connor et al., 2006). Also the second HDAC inhibitor romidepsin was approved for CTCL. During the last years, second-generation HDAC inhibitors have been developed to achieve a more selective targeting of particular HDACs (the family of HDACs comprises 18 members) (Arrowsmith et al., 2012). For example, in preliminary studies the potent HDAC inhibitor Panobinostat has proven efficacy in CTCL (Ellis et al., 2008) and promising results in clinical trials have been reported in Hodgkins`s lymphoma and prostate cancer (Dickinson et al., 2009; Rathkopf et al., 2010).

Both classes of DNMT and HDAC inhibitors aim to reactivate genes which have underwent epigenetic silencing in cancer. In preclinical studies it has been demonstrated that transcriptional derepression is associated with chromatin remodeling and anti-tumor activity (both *in vitro* and *in vivo*). As depicted in **Figure 6**, epigenetic drugs induce several anti-tumor effects. The reactivation of hypermethylated genes by DNMT inhibitors has been shown to inhibit cell growth (e.g. by upregulation of the cell cycle regulator p16), increase chemosensitivity (e.g. by upregulation of the repair gene *MLH1*) and increase cell adhesion (e.g. by upregulation of *E-Cadherin*) (**Figure 6a**). The potential activation of transposons and tumor antigens might be beneficial as it could induce the interferon response and increase immunogenicity (Yoo and Jones, 2006) (**Figure 6a**). The inhibition of HDACs prevents hypomethylation of histones resulting in chromatin remodeling, transcriptional activation, and restoration of malignant cells to a more normal state (Yoo and Jones, 2006). Most HDAC inhibitors induce $p21^{WAF1/CIP1}$ gene expression, which leads to the inhibition of complexes of cyclin D with

CDK4 (cyclin D kinase-4) and promotes cell cycle arrest as well as differentiation (Rocchi et al., 2005) (**Figure 6b**). HDAC inhibitors have been found to cause an anti-angiogenic effect (Michaelis et al., 2004; Zgouras et al., 2004) and to promote apoptosis (Dai et al., 2005) (**Figure 6b**). Particularly for the treatment of solid cancers, it might be beneficial to combine both HDAC and DNMT inhibitors (Rudek et al., 2005) since the administration of DNA methylation inhibitors alone in solid tumors has not been successful to date (Yoo and Jones, 2006).

So far, targeting of histone acetyltransferases has proven to be difficult, therefore clinical studies have not been undertaken. However, some potent inhibitors have been identified for histone methyltransferases. For example, AZ505 targets the oncogenic protein SMYD2, which represses p53 and Rb (Ferguson et al., 2011). Potent inhibitors have been found to target DOT1L, such as EPZ004777 and EPZ-5676, which both show activity in MLL-fusion proteins causing aberrant DOT1L localization (Daigle et al., 2013; Daigle et al., 2011). In 2012, EPZ-5676 has entered phase 1 clinical trials in patients with acute myeloid leukemia (AML) and acute lymphoblastic leukemia (ALL) (Basavapathruni et al., 2014). Furthermore, the highly selective EZH2 inhibitor GSK126 has been recently shown *in vivo* and *in vitro* to reduce global H3K27me3 levels and to reactive PRC2-target genes in lymphomas with activating EZH2 mutations (McCabe et al., 2012).

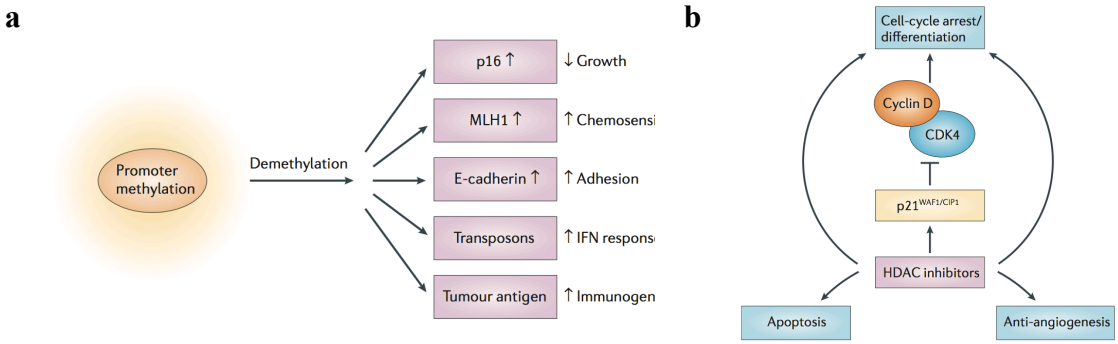

Figure 6. Effects of DNMT and HDAC inhibitors in human cancer. a. DNMT inhibitors such as azacytidine induce genome-wide demethylation resulting in the reactivation of methylation-silenced genes. Upregulation of cell-cycle regulators such as p16 leads to inhibition of growth. Chemosensitivity is increased with the activation of repair genes such as *MLH1*, and cell adhesion can be increased due to E-cadherin reactivation. The potential activation of transposons might be beneficial, as it would increase interferon response. Activation of tumor antigens can lead to increased immunogenicity, which might be helpful when considering combining immunotherapy with epigenetic drugs. **b.** HDAC inhibitors prevent hypomethylation of histones resulting in chromatin remodeling, transcriptional activation, and restoration of malignant cells to a more normal state. Almost all HDAC inhibitors induce gene expression of $p21^{WAF1/CIP1}$, which leads to inhibition of cyclin D-CDK4 complexes and cell cycle arrest and differentiation. HDAC inhibitors are also known to have anti-angiogenic effects and to promote apoptosis. Many pathways are assumed to be involved in this process and promote growth inhibition, differentiation, apoptosis and anti-angiogenesis. IFN, interferon; CDK4, cyclin D kinase-4; MLH1, mutL homologue-1. From (Yoo and Jones, 2006).

The pharmacological inhibition of epigenetic modifiers is not only restricted to inhibition of enzymatic activity and a novel concept aims to disrupt protein-protein interactions of epigenetic reader proteins. A prominent example is the targeting of the bromodomain and extra-terminal (BET) family proteins of transcriptional regulators, which can recognize acetylated lysine residues via their bromodomain. Specific small-molecule inhibitors such as JQ1 and PFI-1 have been demonstrated to inhibit recruitment of BET proteins to chromatin and to be potent in both *in vitro* and *in vivo* models of solid tumors (Asangani et al., 2014; Filippakopoulos et al., 2010) and hematological malignancies. Importantly, inhibition of BET proteins suppresses transcription of *MYC*, which plays an essential role in progression of AML, MLL and Burkitt`s lymphoma (Dawson et al., 2011; Delmore et al., 2011; Mertz et al., 2011).

Many more epigenetic drugs are currently in preclinical or clinical trials (also in combination with other epigenetic drugs or with therapies such as immunotherapy) (Arrowsmith et al., 2012; Plass et al., 2013). Thus, targeting the epigenome of cancer cells represents a new frontier in drug discovery, which has an enormous potential for the development of future cancer therapeutics.

1.2.5 Epigenetic silencing of tumor suppressor genes

Disruption of gene function in cancer cells can occur through genetic alterations, by gene mutation or deletion, or through epigenetic alterations that alter the heritable state of gene expression (Baylin et al., 2001). Epigenetic silencing of tumor suppressor genes is generally thought to involve DNA methylation, histone modifications, and the compaction of chromatin (**Figure 7**). The most studied epigenetic alteration in carcinogenesis is transcriptional silencing associated with a gain in DNA methylation (in a normally unmethylated gene promoter) and, recently, the establishment of repressive histone marks at site of tumor suppressor genes has been increasingly investigated in numerous studies.

Transcriptional silencing of tumor suppressor genes by CGI promoter hypermethylation plays a key role in the tumorigenic process and contributes to all of the hallmarks of cancer cells as a result of tumor suppressor inactivation (Hanahan and Weinberg, 2000). This process involves methyl-CpG-binding proteins and DNMTs, which are associated with HDACs and HMTs (Dobosy and Selker, 2001; Fuks, 2005; Wade, 2001; Wang et al., 2004b). The affected genes are involved in all cellular pathways and confer characteristic features to tumor cells

once they undergo transcriptional silencing. The list of hypermethylated genes in various tumor types is constantly growing and this epigenetic aberration is now considered to be a common feature of human cancers (Esteller, 2007a). Genes with key roles in cancer biology such as the negative cell cycle regulators $p16^{INK4a}$ and *Rb*, and the DNA repair genes *BRCA1* and *MHL1* have been shown to undergo silencing by DNA methylation in tumor cells (Egger et al., 2004; Esteller, 2005; Feinberg and Tycko, 2004; Herman and Baylin, 2003). Importantly, the pattern of CGI hypermethylation has been shown to vary with the cancer type (Costello et al., 2000; Esteller et al., 2001a; Paz et al., 2003). Each cancer shows a specific DNA hypermethylome, which almost completely defines that particular tumor type, similar than cytogenetic and cancer-specific genetic markers (Esteller, 2007b; Schuebel et al., 2007). Thus, these features have a significant value for diagnostic and prognostic usage in cancer treatment (Esteller, 2007a).

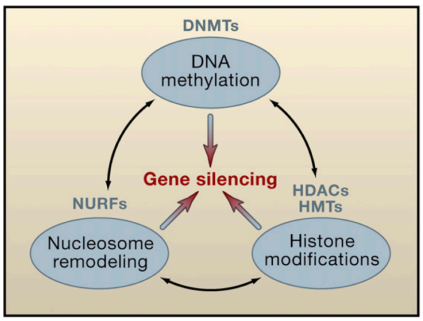

Figure 7. Heritable gene silencing. The interplay between DNA methylation, histone modifications and nucleosome remodeling contributes to gene silencing. Several epigenetic enzymes including DNMTs, HDACs and HMTs, as well as chromatin remodeler factors such as NURFs contribute to the establishment of a heritable repressive state at genes leading to transcriptional silencing. The process of gene silencing is crucial for development and differentiation; however, aberrant silencing at tumor suppressor genes contributes to cancer development. DNMT, DNA methyltransferase; HDAC, histone deacetylase; HMT, histone methyltransferase; NURF, nucleosomal remodeling factor. From (Jones and Baylin, 2007).

The association of PcG proteins with cancer development was first shown by identifying BMI1 a proto-oncogene, which together with MYC promotes generation of B- and T-cell lymphomas (Haupt et al., 1991; van Lohuizen et al., 1991). It has been proposed that BMI1 inhibits MYC-induced apoptosis through repression of the *CDKN2A* locus (Jacobs et al., 1999a; Jacobs et al., 1999b). The tumor suppressor gene *CDKN2A* encodes two distinct proteins, INK4A and ARF, both restricting cellular proliferation in response to aberrant mitogenic signaling (Sparmann and van Lohuizen, 2006). The cyclin-dependent kinase inhibitor INK4A is responsible for the activation of the retinoblastoma (RB) pathway, whereas ARF induces p53 though inhibition of MDM2 (Sherr, 2001). The *CDKN2A* gene is frequently hit

by mutations, deletions and methylation-associated epigenetic silencing in a variety of human tumors (Lowe and Sherr, 2003) highlighting the importance of these pathways.

Hypermethylation of CGIs often affects promoters of miRNAs (Saito et al., 2006) leading to an overall downregulation of miRNAs in human cancers (Melo et al., 2009). It has been demonstrated that miRNAs have a tumor suppressor function. For example, repression of *miR-124a* by hypermethylation has been found to mediate *CDK6* activation and phosphorylation of *Rb* (Lujambio et al., 2007). However, hypermethylation of miRNA and subsequent repression of miRNA expression has been not only described in cancer but also in metastasis development. Inactivation of *miR-148*, *miR-34b/c* and *miR-9* by promoter hypermethylation has been shown to promote tumor dissemination from the primary tumor site (Lujambio et al., 2008).

It is still poorly understood why some genes become hypermethylated in a given tumor type whereas others with similar function remain methylation-free in others. In this context, Keshet and colleagues have performed a genome-wide investigation of DNA methylation in prostate and colon cancer cells and have suggested that there might be a common sequence motif in promoters, that acquire CGI methylation (Keshet et al., 2006). Alternatively, the precise locations of *de novo* methylation in cancer may be determined by a pre-programmed targeting mechanism (Cedar and Bergman, 2009). In respect thereof, genes targeted by transcriptional repressor complexes, for example by PcG proteins, early in development might mark these genes, which are more prone to gain hypermethylation later in the tumor cells. Indeed, several studies have demonstrated that a significant proportion of *de novo* methylated CGIs are target sites for PcG proteins such as EZH2. (Ohm et al., 2007; Schlesinger et al., 2007; Widschwendter et al., 2007). Apart from that, aberrant methylation could also result from genetic alterations leading to selective targeting of the DNA methylation machinery. Fusion proteins such as promyelocytic leukemia-retinoic acid receptor-α (PML-RARA) might lead to aberrant CGI methylation patterns in leukemia though recruitment of DNMTs and HDACs to several novel target genes (Di Croce et al., 2002). Another example is given by the oncogenic Myc protein that has been demonstrated to bind Dnmt3a and to associate with DNA methyltransferase activity *in vivo* (Brenner et al., 2005). Similar as suggested for genetic mutations, it is also possible that hypermethylated genes and their subsequent inactivation confers a selective clonal advantage to tumor cells (Esteller, 2007a). Therefore, it might be that the selection for targeting and hypermethylation does not occur exclusively, and both

events presumably arise during generation and maintenance of hypermethylated CGIs at tumor suppressor genes (Esteller, 2007a).

Similar to changes in histone modification patterns, which have been shown to arise early in carcinogenesis (Fraga et al., 2005), it has been demonstrated that also CGI hypermethylation of tumor suppressor genes occurs early in tumorigenesis. For example, CGI hypermethylation occurs in genes such as $p16^{INK4a}$, $p14^{ARF}$ and *MGMT* in colorectal adenomas and aberrant methylation in *MLH1* has been found in atypical endometrial hyperplasia (Esteller, 2005). Furthermore, CGI hypermethylation has been observed to precede mutations in *KRAS* in small colorectal adenomas (Esteller and Herman, 2004) suggesting that that epigenetic changes might be crucial steps during the neoplastic transformation process (Esteller, 2007a). In this context, Baylin and Ohm have proposed that epigenetic changes might commit cancer cells to altered signal-transduction pathways during the early stages of tumor development (Baylin and Ohm, 2006).

It has been also observed that the number of genes acquiring promoter CGI hypermethylation increases during tumorigenic progression (Fraga et al., 2004; Gallagher et al., 2005), which might be meaningful in early detection screenings in cases of sporadic cancers but particularly in patients with high familial risk of cancer development (Esteller et al., 2001b). In support of that, epigenetic silencing of tumor suppressors via promoter CGI hypermethylation could provide a powerful tool for the prediction of tumor prognosis. For example, hypermethylation of the tumor suppressors such as DAPK (death-associated protein kinase), $p16^{INK4a}$ and EMP3 (epithelial membrane protein 3) have been correlated with tumor aggressiveness in lung, colorectal and brain cancers patients (Esteller, 2005).

The hypermethylation of promoter CGI sites in cancer cells is accompanied by specific histone marks including deacetylation of histone H3 and H4, loss of H3K4me3, and gain of H3K9me3 and H3K27me3 (Ballestar et al., 2003; Fahrner et al., 2002; Vire et al., 2006). A key link between histone modifications and DNA methylation was demonstrated by pioneering studies showing that 5mC could attract methyl-CpG-binding proteins and HDACs in methylated CGIs in the process of chromatin compaction and gene repression (Jones et al., 1998; Nan et al., 1998). In addition to histone modifications and DNA methylation, nucleosome remodeling is also involved in the process of gene silencing at tumor suppressor genes (**Figure 7**). Zhang and co-workers have shown that MBD2 interacts with the nucleosomal remodeling complex (NuRD), thus directing the complex to methylated DNA (Zhang et al., 1999). Another example is given by Brahma (Brm), the catalytic subunit of the SWI/SNF

chromatin-remodeling complex, which has been shown to associate with MeCP2 and to participate in MeCP2-dependent transcriptional silencing (Harikrishnan et al., 2005). Lin and colleagues have found that changes in the nucleosomal occupancy contribute to the epigenetic silencing of the CGI in the *MLH1* gene (Lin et al., 2007). The authors suggest that heritable changes in nucleosome occupancy enabled by DNA methylation may contribute to epigenetic silencing of tumor suppressor genes. Moreover, also histone modifications are involved in the chromatin-remodeling process. For example, NURF (nucleosome remodeling factor), a member of the ISWI family of chromatin remodeling complexes, has been demonstrated to couple H3K4me3 with chromatin remodeling (Li et al., 2006; Wysocka et al., 2006). These findings highlight that all three processes of DNA methylation, histone modifications and nucleosome remodeling are intimately linked (**Figure 7**) and that alterations in these processes lead to the permanent silencing of cancer-relevant genes (Jones and Baylin, 2007).

1.2.6 CpG island methylator phenotype

In cancer cells CpG island promoters are commonly hypermethylated, and this methylation is associated with transcriptional repression and gain of histone repressive marks (Jones and Baylin, 2007). The changes in CpG island methylation in a given tumor can involve a group of loci and has been hypothesized to constitute a distinct phenotype. Toyota and co-workers reported methylation profiling data that indicated a dichotomous classification of human colon carcinomas into frequent promoter methylation and infrequent methylation groups (Toyota et al., 1999). The authors have then proposed to term this observation a ‘CpG island methylator phenotype’ or ‘CIMP’ (Toyota et al., 1999). Although, the CIMP existence has been challenged (Yamashita et al., 2002), several studies have succeeded to show that a subset of CpG islands are coordinately methylated in various tumors types. Weisenberger and colleagues have reported that CIMP-positive colorectal cancers represent a distinct subset, encompassing tumors that frequently have a BRAF mutation and display a mismatch repair deficiency as a consequence of CIMP-associated methylation of *MLH1* (Weisenberger et al., 2006). Remarkably, studies in gliomas, have identified that IDH1 mutations correlate with tumors displaying a CpG island methylator phenotype (Noushmehr et al., 2010). These findings constitute an important concept that might also occur in other tumor types. Recently, Mack and colleagues have identified that poor-prognosis hindbrain ependymomas exhibit a CpG island methylator phenotype (Mack et al., 2014). Remarkably, many CIMP loci have

been identified as targets of PcG proteins (Mack et al., 2014; Widschwendter et al., 2007), for example, transcriptional silencing at these loci in ependymomas has been found to largely overlap with PRC2 target sites and its catalyzed H3K27me3 mark (Mack et al., 2014). These findings have implications for cancer therapy, as CIMP-positive hindbrain ependymomas were responsive to clinical drugs that target either DNA or H3K27 methylation both *in vitro* and *in vivo* (Mack et al., 2014).

In addition to CIMP, some studies have reported that epigenetic inactivation is not limited to single genes but can also encompass large stretches of DNA across the genome during tumorigenesis which can become aberrantly methylated through long-range epigenetic silencing (LRES) (Coolen et al., 2010; Frigola et al., 2006; Hsu et al., 2010). The characteristics of LRES are an increase in CpG island hypermethylation and gain or reinforcement of the repressive histone modifications H3K9me2 and H3K27me3 (Coolen et al., 2010).

1.3 Prostate Cancer

Prostate cancer is the most common male malignancy and one of the leading causes of death in western countries. Clinically advanced prostate cancer causes over 250,000 deaths worldwide annually (Jemal et al., 2011). If detected at early stages, when still locally confined, prostate cancer is eradicated in 70-80% of the patients by radical prostatectomy (surgical excision of the prostate) or radiation therapy. However, around five years after primary treatment, the remaining 20-30% of patients develop metastasis (Cooperberg et al., 2007).

An important tool in prostate cancer diagnosis is the measurement of the prostate-specific antigen (PSA). PSA, a kallikrein-related serine protease, is produced in normal prostate tissues, but is released into the blood upon disruption of normal prostate architecture during tumorigenesis (Lilja et al., 2008). Patients with elevated PSA levels usually undergo biopsy to determine the presence of prostate cancer. After biopsy, histological grading is performed using the Gleason scoring system. The Gleason scoring classifies tumors from 1 to 5 (from most to least differentiated) based on the most abundant differentiation status by assigning a combined score (the sum of the two most common patterns) (Epstein, 2010; Mellinger et al., 1967). Patients with a Gleason score of less than 5 (low risk prostate cancer), 3+3 and 3+4 (low-intermediate risk prostate cancer) and 4+3 (intermediate risk prostate cancer) are considered to have indolent tumors, which are not causing symptoms and are expected to grow slowly. Therefore, this group of patients is managed conservatively by ‘active surveillance’

through monitoring of their PSA levels. Nonetheless, a small fraction of these tumors will progress rapidly and require immediate treatment (Albertsen et al., 2005; Eggener et al., 2007). Therefore, a major clinical challenge is the current inability to distinguish indolent from aggressive tumors in patients displaying a low Gleason score in the biopsy (Sartor et al., 2008). The lack of this prognostic information has led to an enormous 'overtreatment' of patients who would instead require only conservative treatment (Shen and Abate-Shen, 2010). Patients with a Gleason score of 4+4 or higher (high risk prostate cancer) are considered to have aggressive tumors and therefore undergo immediate treatment by surgery, radiation therapy or hormonal therapy targeting the androgen receptor (AR) pathway depending of type, size and location of the tumor.

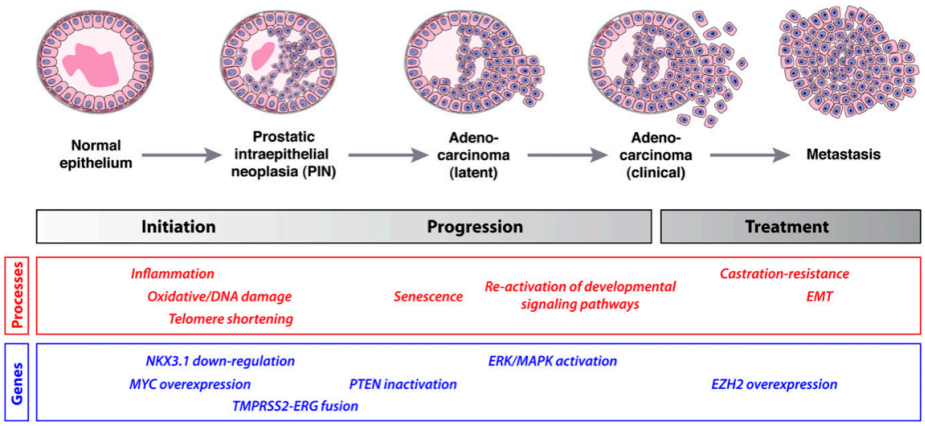

Figure 8. Disease progression of human prostate cancer. Stages of tumor progression are depicted, together with molecular processes (red) and genes (blue), which are likely to significantly contribute at each stage. From (Shen and Abate-Shen, 2010).

Androgens are crucial for the development and function of the prostate gland and for the maintenance of prostate cancer cells, which arise from the secretory epithelium of the prostate. Therefore, treatment of advanced prostate cancer is based on blocking or reducing the production of androgens or antagonizing the AR and its target genes (Chen et al., 2008). However, prostate cancer relapse can be managed efficiently by androgen-deprivation therapy (ADT) only for a limited time period by targeting the AR axis under which the majority of cancer cells die, producing a tumor remission and a reduction in circulating PSA levels (Denmeade and Isaacs, 2002). Thus far, these treatments are not curative, the most effective standard chemotherapies result only in a mean increase in survival time of two months (Petrylak et al., 2004; Tannock et al., 2004), and castration-resistance inevitably follows within a period of months to years, resulting in relapse and metastasis. Prostate cancer metastatic

sites are lung, liver, pleura and bones, where osteoblastic lesions are formed (Bubendorf et al., 2000; Logothetis and Lin, 2005). Hence, the second major challenge in prostate cancer management is the durable control of advanced prostate cancer and the understanding of pathways of castration-resistance and the identification of novel therapeutic approaches (Shen and Abate-Shen, 2010).

Prostate cancer is considered as a heterogeneous, multifocal disease as primary tumors often contain multiple independent histologic cancer foci, which are often genetically distinct (Shen and Abate-Shen, 2010). Remarkably, major tumor subtypes are not present on the histopathological level. Gene expression analyses of prostate cancer have not been able to strictly define molecular signatures associated with distinct tumor subtypes that correlate with disease outcome (Lapointe et al., 2004; Singh et al., 2002; Tomlins et al., 2007b). Recently, genomic analyses have provided evidence for defined molecular subtypes (Palanisamy et al., 2010; Taylor et al., 2010; Tomlins et al., 2008). For example, genomic profiling of prostate cancer has identified numerous recurrent DNA alterations that lead to the dysregulation of genes involved in prostate development, chromatin modification, cell cycle regulation, and androgen signaling (Baca and Garraway, 2012). Early in tumorigenesis, prostate cancer cells undergo chromosomal deletions resulting in the inactivation of tumor suppressor genes including *PTEN*, *TP53* and *CDKN1B* (Shen and Abate-Shen, 2010). Comparative genomic hybridization arrays have identified a number of chromosomal alterations including gains at 8q and losses at 3p, 8p, 10q, 13q and 17p (Dong, 2001; Lapointe et al., 2007; Taylor et al., 2010). Several key regulatory genes are located within these chromosomal regions and undergo copy number alterations such as *NKX3.1* at 8p21, *MYC* at 8q24 and *PTEN* at 10q23 (Shen and Abate-Shen, 2010). These events result in *NKX3.1* downregulation, *PTEN* inactivation and *MYC* overexpression **(Figure 8)**. Loss of PTEN is a frequent event in prostate cancer progression - up to 70% of late stage tumors exhibit loss of *PTEN* function or activation of the PI3K pathway (Taylor et al., 2010) **(Figure 8)**. Both events result in enhanced cell proliferation, migration and survival (Stiles et al., 2004; Vivanco and Sawyers, 2002) but also lead to castration-resistant growth (Gao et al., 2006; Jiao et al., 2007; Wang et al., 2003). About half of prostatic adenocarcinomas overexpress an oncogenic *ETS* transcription factor gene, mostly *ERG*, due to a somatic fusion with a constitutively active or androgen-regulated promoter (Tomlins et al., 2007a; Tomlins et al., 2005). The most common rearrangement results in the generation of a *TMPRSS2-ERG* fusion gene (**Figure 8**). In this regard, Berger and colleagues have reported complex ‘chains’ of rearrangements in prostate cancer genomes that may arise

from the shuffling and re-ligation of broken DNA fragments to one another resulting in a novel configuration (Berger et al., 2011). These shuffling events may simultaneously deregulate numerous cancer-related genes.

Recent studies have performed exome sequencing of localized and castration-resistant prostate cancer and have discovered base pair mutations in genes such as *SPOP*, *FOXA1* and *KDM6A*, which are implicated in deregulated cellular process during prostate carcinogenesis (Barbieri et al., 2012; Grasso et al., 2012; Kumar et al., 2011). However, compared to other cancers, the prostate cancer genome displays a low frequency of mutations (Barbieri et al., 2012; Grasso et al., 2012; Kumar et al., 2011). Thus, the perturbation of epigenetic pathways is likely to essentially contribute to the tumorigenic process (see 1.3.1).

In order to develop more effective therapies, a concerted effort is underway to characterize and target the critical cell population resistant to conventional treatment regimens, particularly upon AR withdrawal. Unfortunately, the identification of such cells has been hampered by the fact that, unlike other cancer types, prostate cancer has proven remarkably resilient to classification into molecular subtypes associated with distinct disease outcomes (Taylor et al., 2010). Up to now, available molecular biomarkers do not provide greater prognostic significance than the usage of the Gleason score system (True et al., 2006). In addition, an inherent lack of understanding of the biological processes that distinguish indolence from aggressiveness is a considerable limitation for the identification of early prognostic biomarkers, which could aid in preoperative therapy decision making for low and intermediate risk cases, and the identification of therapeutic targets.

Tumor cells may be divided into well-differentiated mature or immature precursor cells according to different sources. The latter are considered to be cancer stem cells (CSCs) (Dean et al., 2005). They possess unlimited proliferative differentiation potential, self-renewal, potential tumorigenic capacity and permanency (Collins et al., 2005). Importantly, CSCs where shown to be resistant to conventional treatment regimens, particularly chemotherapy (Abdullah and Chow, 2013) and radiotherapy (Rich, 2007). Prostate cancer stem cells are an enticing explanation for cancer relapse, metastasis formation, therapy failure, and, thus are the object in current cancer research. However, the molecular pathways regulating generation and propagation of stem-like prostate cancer cells are poorly understood. The population of prostate cancer stem cells may constitute an important target for therapeutic intervention in aggressive prostate cancer.

1.3.1 Epigenetics in prostate cancer

Since prostate cancer is characterized by a low frequency of mutations (Grasso et al., 2012), aberrant gene activity contributing to prostate cancer is likely based on alterations in gene expression levels, which can be driven by copy number alterations and/or translocations (such as *PTEN*, *TP53* loss and *ERG* fusions) or by alterations in transcriptional or post-transcriptional regulation. In addition, recent studies provide strong evidence that alterations in epigenetic pathways play an important role in prostate cancer initation and progression. DNA methylation and histone modifications, have been demonstrated to play critical roles in prostate cancer growth and metastasis (Albany et al., 2011). The best-studied epigenetic alteration in prostate cancer is aberrant DNA methylation (hypo- and hypermethylation) leading to genomic instability and inappropriate gene expression patterns. Hypermethylation frequently silences DNA repair genes (*GSTP1*, *MGMT*), hormone-receptor genes (*AR*, *ESR*), cell adhesion genes (*CDH1*, *CD44*), cell cycle control genes (*CCND2*, *CDKN1B*, *SFN*), apoptotic genes (*PYCARD*, *RPRM*, *GLIPR1*) and the well-characterized tumor suppressor genes *APC*, *RARB* and *RASSF1* (Jeronimo et al., 2004; Kang et al., 2004; Maruyama et al., 2002; Sasaki et al., 2002; Yegnasubramanian et al., 2004). For example, *GSTP1*, encoding the intracellular detoxification enzyme glutathione S-transferase P, has been shown to undergo promoter hypermethylation in early tumorigenesis (Brooks et al., 1998; Kang et al., 2004; Perry et al., 2007). Hypermethylation and subsequent silencing of *GSTP1* was detected in >90% of prostate tumors and in about 75% of preinvasive high-grade PIN (Brooks et al., 1998; Kang et al., 2004; Lee et al., 1994). Loss of GSTP1 is thought to sensitize cells to DNA damage by electrophilic compounds (Jeronimo et al., 2004; Yegnasubramanian et al., 2004).

Genome-wide hypomethylation is found in both primary tumors but to a higher extend in metastatic prostate cancer (Brothman et al., 2005; Yegnasubramanian et al., 2008). It has been demonstrated that global hypomethylation is associated with increased tumor stage, Gleason grade ≥ 7 and hypermethylation of particular loci, such as *GSTP1*, *RARB*, *APC*, *PYCARD*, *PTGS2*, *ABCB1* and *RASSF1* (Florl et al., 2004; Kang et al., 2004).

Specific histone modification patterns were identified to be altered in prostate cancer and may serve as prognostic markers of the disease. Seligson and colleagues have reported a marked reduction of H3K4me1, H3K9me2, H3K9me3 and H3 and H4 acetylation in prostate cancer when compared to normal prostate tissue (Seligson et al., 2005). This histone modification pattern was shown be predictive of clinical outcome independently of tumor stage, preoperative PSA levels, and capsule invasion (Seligson et al., 2005). Another study has reported

a substantial increase of H3K4me1, H3K4me2 and H3K4me3 in tissue of patients with castration-resistant prostate cancer (Ellinger et al., 2010).

Gene expression levels of epigenetic regulators are frequently altered in cancer (see 1.2). Overexpression of histone-modifying enzymes have been linked to prostate cancer progression and many of which are reported to be independent prognostic markers. The lysine-specific demethylase KDM1A (also known as LSD1) interacts with the AR and promotes AR-dependent transcription of target genes through demethylation of H3K9me1 and H3K9me2 (Metzger et al., 2005). Overexpression of the AR coactivators KDM1A and four and a half LIM domain protein 2 (FHL2) have been demonstrated to correlate with an increased risk of cancer relapse after radial prostatectomy (Kahl et al., 2006). UHRF1, which together with PCNA recruits DNMT1 to replication foci, has been reported to be involved in epigenetic silencing of tumor suppressor genes (Babbio et al., 2012). UHRF1 overexpression has been associated with reduced survival rates in prostate cancer (Babbio et al., 2012). As mentioned earlier, a prominent example is EZH2 that is frequently amplified (Saramaki et al., 2006) and overexpressed in prostate cancer with a moderate increase in localized tumors and higher expression in metastatic prostate cancers (Bachmann et al., 2006; Varambally et al., 2002; Xiao, 2011). Strong expression of EZH2 is associated with increased tumor cell proliferation and aggressive tumors, and clinically localized prostate cancer tumors with high EZH2 levels are associated with a poorer prognosis (Bachmann et al., 2006; Varambally et al., 2002). EZH2 target genes in prostate cancer include genes that are associated with metastasis such as *E-Cadherin* (Cao et al., 2008) and *DAB2IP* (Chen et al., 2005). Loss of these genes promotes metastasis formation through activation of NF-κB and Ras pathways (Min et al., 2010).

Another example of aberrant expression of an epigenetic modifier in prostate cancer is given by the SWI/SNF ATPase BRM, whose expression, both on mRNA and protein levels, has been found downregulated in prostate cancer compared to non-neoplastic tissue (Shen et al., 2008a).

Expression profiling studies in prostate cancer has unveiled a widespread dysregulation of miRNAs contributing to important clinical and pathological features, for example extraprostatic extension (Ambs et al., 2008; Ozen et al., 2008). Mounting evidence suggests that miRNAs have key roles in the tumorigenic process by modulating the cancer epigenome for example by posttranslational gene silencing of components of the DNA methylation machinery (DNMTs), histone-modifying enzymes (HDACs, HATs, HMTs) or nucleosome remodel-

ing factors (NURFs) (Perry et al., 2010). For example, miR-101 has been identified to negatively regulate EZH2. During prostate tumor progression miR-101 levels decrease due to somatic loss of one or both of the two genomic loci encoding miR-101 resulting in the upregulation of EZH2 (Varambally et al., 2008). Expression of miR-101 was significantly decreased in metastatic prostate cancer compared to that in clinically localized disease or benign adjacent prostate tissue and genomic loss of miRNA-101 was found in about one-third of tumors (Varambally et al., 2008). Downregulation of miR-101 has been also reported in other cancers including breast, ovarian, lung and colorectal cancers (Iorio et al., 2005; Schepeler et al., 2008; Varambally et al., 2008; Yanaihara et al., 2006) suggesting that miR-101 might be part of a solid tumor signature. In addition, miRNAs with tumor suppressor functions can be subject to promoter hypermethylation, which is now considered as a common hallmark of human cancers including prostate cancer.

1.4 The epigenetic regulator TIP5

TIP5 is an epigenetic factor identified as a transcription termination factor 1 (TTF1) interacting protein in a yeast-two hybrid screen (Strohner et al., 2001). The novel gene was named *TIP5* (TTF1-interacting protein 5), also known as *BAZ2A,* and encodes a 205 kDa protein. Together with the ATPase SNF2h, the mammalian homolog of ISWI, TIP5 forms a macromolecular complex. This novel chromatin remodeling complex was termed NoRC (nucleolar remodeling complex) and induces nucleosome sliding in an ATP- and histone 4 tail-dependent manner (Strohner et al., 2001). NoRC is responsible for the establishment of heterochromatic structures at the rDNA locus after cell division (**Figure 9**) (Guetg et al., 2010; Li et al., 2005; Santoro and Grummt, 2005; Santoro et al., 2002; Zhou et al., 2002). TIP5 contains several domains including a TAM/MBD domain, several AT-hook domains, a DDT domain, a BAZ1 and a BAZ2 motif, a WAKZ motif, a bromodomain, and a PHD finger (Strohner et al., 2001). In order to establish the heterochromatic structure of the rDNA locus, TIP5 recruits several histone-modifying enzymes (HMTs, HDACs, PARP1/ARTD1), DNMTs and non-coding RNAs (pRNA) to the rDNA promoter (Guetg et al., 2010; Guetg and Santoro, 2012; Guetg et al., 2012; Mayer et al., 2006; Santoro and Grummt, 2005; Santoro et al., 2002).

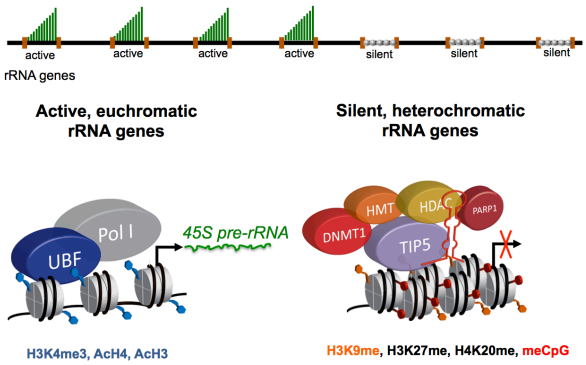

Figure 9. Active and silent ribosomal RNA genes. Association of TIP5 and its interacting factors (chromatin enzymes and non-coding RNA) with silent rRNA genes. In contrast, active rRNA genes are bound by Polymerase I (Pol I) and the Pol I transcription factor UBF.

Recently, TIP5 has been implicated in the epigenetic silencing of other genes than rRNA (ribosomal RNA) genes. A screen aimed to discover factors (RESEs) required for Ras-mediated epigenetic silencing of the pro-apoptotic *Fas* gene in *K-ras*-transformed NIH3T3 cells, identified several polycomb proteins, and proteins involved in chromatin modification and chromatin remodeling, including EZH2 and TIP5 (Gazin et al., 2007). This study has shown that knockdown of TIP5 or EZH2 in *K-ras*-transformed NIH3T3 cells impairs DNA methylation of the *Fas* gene promoter and inhibits anchorage-independent growth of transformed cells and tumor growth in nude mice. Interestingly, *K-ras*-transformed NIH3T3 cells displayed upregulated *TIP5* mRNA expression levels when compared to NIH3T3 cells (Gazin et al., 2007). The positive correlation between TIP5 levels and cancer has also been suggested by several other studies. For example, TIP5 was proposed as an eventual biomarker for early diagnosis of osteosarcoma, since the expression levels of TIP5 were higher in three osteosarcoma cell lines (U2OS, MG-63, Saos-2) than in the osteoblastic cell line hFOB1.19 (Li et al., 2009). Furthermore, TIP5 was found abundantly expressed in ovarian cancer cell lines including OVCAR3, A2780, ES2, and MPSC1, whereas its expression levels were relatively low in the OSE4 cell line, which was derived from normal ovarian surface epithelium (Sheu et al., 2008). Recently, a study by Leite and co-workers have suggested a role for miR-let7c, miR-100, and miR-218 in prostate cancer since they were less expressed in metastatic prostate cancer (Leite et al., 2011). The authors propose a possible involvement of these miRNAs in the metastasation of prostate cancer though controlling the expression of RAS, c-Myc, Laminin-5-β3, THAP2, SMARCA5, and TIP5. Finally, a putative *TIP5* deregulation has been reported in a pediatric case of pre-B acute lymphoblastic leukemia (ALL) in which a cryptic rearrangement between 12p13 and 12q13 generated a fusion of *ETV6* with an intronic se-

quence of *TIP5* (Panagopoulos et al., 2006). Taken together, these studies suggest that TIP5 might play a role in tumor initiation and progression in various cancer types.

2 Aim of the work

As prostate cancer is characterized by a low frequency of somatic mutations, disruption of epigenetic pathways is likely to have an important role in the disease. Aberrant DNA methylation patterns are universally found in prostate cancer and are known to frequently affect genes involved in cancer-related processes. The aim of this work was to identify alterations to epigenetic regulators that contribute to poor prognosis in prostate cancer. For this purpose we initially analyzed expression profiles of prostate tumors and determined that the expression of the epigenetic regulator TIP5 is upregulated in prostate cancer.

In this work we aimed to determine the role of TIP5 in prostate cancer by:

1. Analyzing the function of TIP5 in cancer-specific properties such as cell migration, invasion and stem cell-like features (self-renewal).
2. Analyzing the molecular mechanisms of epigenetic silencing mediated by TIP5 in metastatic prostate cancer cells.
3. Identifying genes regulated by TIP5 in metastatic prostate cancer cells and the associated biological pathways.
4. Investigating the suitability of TIP5 as a potential early biomarker in prostate cancer.

3 Results

3.1 BAZ2A (TIP5) is involved in epigenetic alterations in prostate cancer and its overexpression predicts disease recurrence

Authors: Lei Gu, Sandra C. Frommel, Christopher C. Oakes, Ronald Simon, Katharina Grupp, Cristina Y. Gerig, Dominik Bär, Mark D. Robinson, Constance Baer, Melanie Weiss, Zuguang Gu, Matthieu Schapira, Ruprecht Kuner, Holger Sültmann, Maurizio Provenzano, ICGC Project on Early Onset Prostate Cancer, Marie-Laure Yaspo, Benedikt Brors, Jan Korbel, Thorsten Schlomm, Guido Sauter, Roland Eils, Christoph Plass & Raffaella Santoro
Journal: Nature Genetics
DOI: 10.1038/ng.3165
Link: http://www.nature.com/ng/journal/v47/n1/full/ng.3165.html (03.04.2015)
Contributions: L.G., S.C.F., C.C.O., R. Simon, K.G., C.Y.G., D.B., M.P., C.B., M.W. and R.K. designed the experiments and performed experimental work. L.G., S.C.F., C.C.O., R. Simon, C.P., G.S., R.E. and R. Santoro prepared the manuscript and figures. G.S., R.E., C.P. and R. Santoro jointly supervised this work. L.G., S.C.F., C.C.O., R. Simon contributed equally to this work.
Detailed contribution of Sandra C. Frommel: Designing, performance and analysis of experiments of the following figures: Fig. 1b, Fig.1e, Fig. 2, Fig. 3, Fig. 4, Suppl. Fig. 1a, Suppl. Fig. 1d-g, Suppl. Fig. 3, Suppl. Fig. 4, Suppl. Fig. 6, Suppl. Fig. 7, Suppl. Fig. 8.

3.2 lncRNA maturation to initiate heterochromatin formation in the nucleolus is required for exit from pluripotency in ESCs

Authors: Nataša Savić, Dominik Bär, Sergio Leone, Sandra C. Frommel, Fabienne A. Weber, Eva Vollenweider, Elena Ferrari, Urs Ziegler, Andres Kaech, Olga Shakhova, Paolo Cinelli & Raffaella Santoro
Journal: Cell Stem Cell
DOI: 10.1016/j.stem.2014.10.005
Link: http://www.cell.com/cell-stem-cell/abstract/S1934-5909(14)00456-1 (03.04.2015)
Detailed contribution of Sandra C. Frommel: Performance and analysis of experiment of following figures: Fig. 6e and Suppl. Fig. 6a.

3.3 The epigenetic modifier EZH2 controls melanoma growth and metastasis through silencing of distinct tumour suppressors

Authors: Daniel Zingg, Julien Debbache, Simon M. Schaefer, Eylul Tuncer, Sandra C. Frommel, Phil Cheng, Natalia Arenas-Ramirez, Jessica Haeusel, Yudong Zhang, Mario Bonalli, Michael T. McCabe, Caretha L. Creasy, Mitchell P. Levesque, Onur Boyman, Raffaella Santoro, Olga Shakhova, Reinhard Dummer & Lukas Sommer
Journal: Nature Communications
DOI: 10.1038/ncomms7051
Link: http://www.nature.com/ncomms/2015/150122/ncomms7051/abs/ncomms7051.html (03.04.2015)
Detailed contribution of Sandra C. Frommel: Designing, performance and analysis of experiments of following figures: Fig. 8e, Fig. 8h.

3.4 Methylation-dependent *SOX9* expression mediates invasion in human melanoma cells and is a negative prognostic factor in advanced melanoma

Authors: Phil F. Cheng, Olga Shakhova, Daniel S. Widmer, Ossia M. Eichhoff, Daniel Zingg, Sandra C. Frommel, Benedetta Belloni, Marieke I.G. Raaijmakers, Simone M. Goldinger, Raffaella Santoro, Silvio Hemmi, Lukas Sommer, Reinhard Dummer & Mitchell P. Levesque

Journal: Genome Biology

DOI: 10.1186/s13059-015-0594-4

Link: http://genomebiology.com/2015/16/1/42/comments (03.04.2015)

Detailed contribution of Sandra C. Frommel: Designing, performance and analysis of experiments of figure 7e.

3.5 DTX3L and ARTD9 inhibit IRF1 expression and mediate in cooperation with ARTD8 survival and proliferation of metastatic prostate cancer cells

Authors: Samia B. Bachmann, Sandra C. Frommel, Rosalba Camicia, Hans C. Winkler, Raffaella Santoro & Paul O. Hassa

Journal: Molecular Cancer

DOI: 10.1186/1476-4598-13-125

Link: http://www.molecular-cancer.com/content/13/1/125/#ins1 (03.04.2015)

Detailed contribution of Sandra C. Frommel: Designing, performance and analysis of experiments of the following figures: Fig. 5g, Suppl. Fig. 2b, Suppl. Fig. 8d. P.O.H. and S.C.F. prepared the manuscript.

BAZ2A (TIP5) is involved in epigenetic alterations in prostate cancer and its overexpression predicts disease recurrence

Lei Gu[1,2,16,17], Sandra C Frommel[3,4,17], Christopher C Oakes[2,17], Ronald Simon[5,17], Katharina Grupp[5], Cristina Y Gerig[3], Dominik Bär[3], Mark D Robinson[6,7], Constance Baer[2], Melanie Weiss[2], Zuguang Gu[1], Matthieu Schapira[8], Ruprecht Kuner[9], Holger Sültmann[9], Maurizio Provenzano[10], ICGC Project on Early Onset Prostate Cancer[11], Marie-Laure Yaspo[12], Benedikt Brors[1], Jan Korbel[13], Thorsten Schlomm[14], Guido Sauter[5,18], Roland Eils[1,15,18], Christoph Plass[2,18] & Raffaella Santoro[3,18]

Prostate cancer is driven by a combination of genetic and/or epigenetic alterations. Epigenetic alterations are frequently observed in all human cancers, yet how aberrant epigenetic signatures are established is poorly understood. Here we show that the gene encoding BAZ2A (TIP5), a factor previously implicated in epigenetic rRNA gene silencing, is overexpressed in prostate cancer and is paradoxically involved in maintaining prostate cancer cell growth, a feature specific to cancer cells. BAZ2A regulates numerous protein-coding genes and directly interacts with EZH2 to maintain epigenetic silencing at genes repressed in metastasis. *BAZ2A* overexpression is tightly associated with a molecular subtype displaying a CpG island methylator phenotype (CIMP). Finally, high BAZ2A levels serve as an independent predictor of biochemical recurrence in a cohort of 7,682 individuals with prostate cancer. This work identifies a new aberrant role for the epigenetic regulator BAZ2A, which can also serve as a useful marker for metastatic potential in prostate cancer.

Prostate cancer is the most common non-cutaneous malignancy in men. Despite intensive research, prediction of clinical behavior remains challenging using the currently available histopathological and biochemical (prostate-specific antigen; PSA) markers; thus, novel molecular-based approaches will likely improve prognostic accuracy in this disease.

Cancer evolution is driven by a combination of genetic and epigenetic abnormalities; the crucial role of epigenetic gene regulation is indicated by the high frequency of mutations in key regulators of epigenetic marks, including DNA methylation[1–3]. As prostate cancer is characterized by a low frequency of somatic mutations[1], disruption of epigenetic pathways is likely to have an important role in the disease. Aberrant DNA methylation patterns are universally found in prostate cancer and are known to frequently affect genes involved in cancer-related processes[4–6]. An important contributor to altered epigenetic patterns in prostate cancer is enhancer of zeste homolog 2 (EZH2), whose altered expression is linked to malignancy and poor prognosis[7–11]. As the catalytic subunit of the Polycomb repressive complex (PRC2), EZH2 controls gene silencing by mediating trimethylation of histone H3 at lysine 27 (H3K27me3). Overexpression contributes to tumor development in part by leading to chromatin condensation and transcriptional repression of a broad range of genes involved in proliferation, invasion and angiogenesis[12–14].

In this work, we aimed to identify additional alterations to epigenetic regulators that contribute to poor prognosis in prostate cancer. We found that the epigenetic factor BAZ2A (also known as TIP5) is broadly overexpressed in prostate cancer. Alteration in BAZ2A levels is not caused by somatic structural or sequence variations but rather is likely due to post-transcriptional regulation involving loss of miR-133a. Interestingly, we found that BAZ2A cooperates with EZH2 to induce aberrant gene silencing in prostate cancer cell lines. BAZ2A overexpression is tightly associated with a prostate cancer subtype displaying CIMP in tumors and with prostate cancer recurrence in patients. Our results demonstrate that BAZ2A is a new biomarker that

[1]Division of Theoretical Bioinformatics, German Cancer Research Center (DKFZ), Heidelberg, Germany. [2]Division of Epigenomics and Cancer Risk Factors, German Cancer Research Center (DKFZ), Heidelberg, Germany. [3]Institute of Veterinary Biochemistry and Molecular Biology, University of Zurich, Zurich, Switzerland. [4]Molecular Life Science Program, Life Science Zurich Graduate School, University of Zurich, Zurich, Switzerland. [5]Institute of Pathology, University Medical Center Hamburg-Eppendorf, Hamburg, Germany. [6]Institute of Molecular Life Sciences, University of Zurich, Zurich, Switzerland. [7]Swiss Institute of Bioinformatics (SIB), University of Zurich, Zurich, Switzerland. [8]Department of Pharmacology and Toxicology, University of Toronto, Toronto, Ontario, Canada. [9]Unit of Cancer Genome Research, German Cancer Research Center (DKFZ) and National Center of Tumour Diseases, Heidelberg, Germany. [10]Oncology Research Unit, Division of Urology, University Hospital of Zurich, Zurich, Switzerland. [11]A list of contributing members and affiliations appears in the **Supplementary Note**. [12]Max Planck Institute for Molecular Genetics, Berlin, Germany. [13]Genome Biology Unit, European Molecular Biology Laboratory (EMBL), Heidelberg, Germany. [14]Martini Clinic, Prostate Cancer Center, University Medical Center Hamburg-Eppendorf, Hamburg, Germany. [15]Department for Bioinformatics and Functional Genomics, Institute for Pharmacy and Molecular Biotechnology (IPMB) and BioQuant, Heidelberg University, Heidelberg, Germany. [16]Present addresses: Department of Cell Biology, Harvard Medical School, Boston, Massachusetts, USA and Division of Newborn Medicine, Boston Children's Hospital, Boston, Massachusetts, USA. [17]These authors contributed equally to this work. [18]These authors jointly supervised this work. Correspondence should be addressed to R. Santoro (raffaella.santoro@vetbio.uzh.ch), C.P. (c.plass@dkfz-heidelberg.de), R.E. (r.eils@dkfz-heidelberg.de) or G.S. (g.sauter@uke.de).

Received 25 September; accepted 17 November; published online 8 December 2014; doi:10.1038/ng.3165

distinguishes aggressive disease and suggest a role for BAZ2A in the establishment of epigenetic alterations in aggressive prostate cancer.

RESULTS

BAZ2A is upregulated in prostate cancer

The low frequency of somatic mutations in prostate cancer prompted us to perform a focused search for epigenetic regulatory genes displaying altered expression in prostate cancer tumors. A recently defined list of 709 genes associated with epigenetic regulation[3] was interrogated in patient-matched tumor-normal expression data available from The Cancer Genome Atlas (TCGA) database[15] and in a second large data set containing 51 tumors and 48 normal samples (Brase data set)[16] (Supplementary Table 1). Genes showing altered expression (false discovery rate (FDR) $q < 0.05$) were ranked according to the degree of expression difference in each data set. This analysis identified consistent, high-ranking (within the top ten genes) overexpression of *BAZ2A* alongside other known epigenetic regulators with described roles in cancer, such as *PHF12*, *CHD6* and *EZH2*. Analysis of early-onset prostate cancer (EOPC) samples[2] provided further support for the overexpression of *BAZ2A* and *EZH2* (Fig. 1a and Supplementary Table 1b). BAZ2A (TIP5) is the largest subunit of the nucleolar remodeling complex NoRC, known to establish epigenetic silencing and transcriptional repression at rRNA genes (rDNA) through association with DNA methyltransferases and histone modifier complexes[17–19]. As upregulation of rRNA transcription is considered to contribute to malignant transformation and tumor cell proliferation[20,21], the upregulation of BAZ2A, a repressor of rDNA, is contradictory and peaked our further interest. *BAZ2A* levels were also increased in prostate cancer metastatic samples, whereas the expression of the polymerase I transcription factor *UBF* was not affected (Fig. 1b and Supplementary Fig. 1a). *BAZ2A* expression was again similar to that of *EZH2*, which was also increased in metastatic tumors[7] (Fig. 1b).

Analysis of genomic and DNA methylation data from 12 EOPC samples[2] did not demonstrate a genetic or epigenetic explanation for *BAZ2A* upregulation, with a lack of copy number alterations (CNAs), loss of heterozygosity, single-nucleotide variations, structural variations and promoter demethylation at the *BAZ2A* locus. The lack of mutations and CNAs was also verified in TCGA data (Supplementary Fig. 2), suggesting a post-transcriptional cause for aberrant *BAZ2A* expression in prostate cancer. *In silico* prediction of microRNAs (miRNAs) for *BAZ2A*[22] indicated that there was a high potential that miR-133a targets the 3′ UTR of this gene (Supplementary Table 2). miR-133a is known to function as a tumor suppressor in several cancer types[23–25] and has recently been reported to suppress cell proliferation, migration and invasion when expressed in prostate cancer cells[26,27]. We found that miR-133a levels were downregulated in the EOPC samples as well as in the TCGA and Brase data sets (Fig. 1c). In analysis of luciferase reporter constructs containing the *BAZ2A* 3′ UTR sequence, miR-133a expression mediated reduced luciferase levels (Supplementary Fig. 1b), whereas a reporter construct with a mutated miR-133a binding site in the *BAZ2A* 3′ UTR did not show reduced luciferase levels with miR-133a expression (Fig. 1d). Furthermore, miR-133a caused robust decreases in BAZ2A mRNA and protein levels, similar to those found using small interfering RNA (siRNA) targeting *BAZ2A* (Fig. 1e and Supplementary Fig. 1c). These data indicate that *BAZ2A* overexpression is typically not caused by somatic structural or sequence variations in prostate cancer but is rather likely due to post-transcriptional regulation involving loss of miR-133a.

BAZ2A paradoxically contributes to the proliferation and viability of metastatic prostate cancer cell lines

BAZ2A and its role in rDNA repression via the establishment of silent epigenetic marks has been studied so far only in non-malignant cells[17,19,28]; depletion of BAZ2A in NIH3T3 and COS cells caused

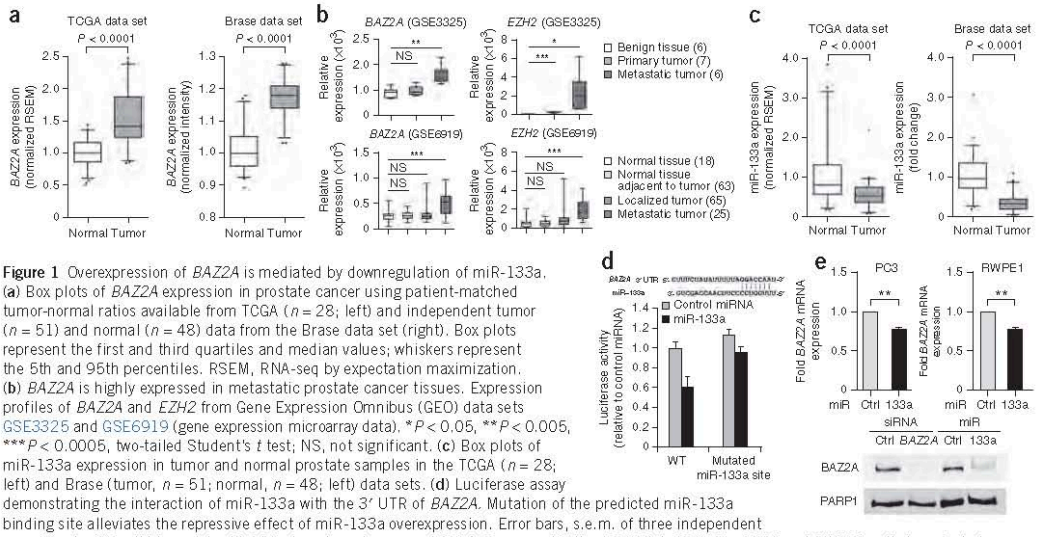

Figure 1 Overexpression of *BAZ2A* is mediated by downregulation of miR-133a. (**a**) Box plots of *BAZ2A* expression in prostate cancer using patient-matched tumor-normal ratios available from TCGA ($n = 28$; left) and independent tumor ($n = 51$) and normal ($n = 48$) data from the Brase data set (right). Box plots represent the first and third quartiles and median values; whiskers represent the 5th and 95th percentiles. RSEM, RNA-seq by expectation maximization. (**b**) *BAZ2A* is highly expressed in metastatic prostate cancer tissues. Expression profiles of *BAZ2A* and *EZH2* from Gene Expression Omnibus (GEO) data sets GSE3325 and GSE6919 (gene expression microarray data). $^*P < 0.05$, $^{**}P < 0.005$, $^{***}P < 0.0005$, two-tailed Student's *t* test; NS, not significant. (**c**) Box plots of miR-133a expression in tumor and normal prostate samples in the TCGA ($n = 28$; left) and Brase (tumor, $n = 51$; normal, $n = 48$; left) data sets. (**d**) Luciferase assay demonstrating the interaction of miR-133a with the 3′ UTR of *BAZ2A*. Mutation of the predicted miR-133a binding site alleviates the repressive effect of miR-133a overexpression. Error bars, s.e.m. of three independent experiments. WT, wild type. (**e**) miR-133a targets endogenous *BAZ2A*. Top, quantitative RT-PCR (qRT-PCR) of PC3 and RWPE1 cells transfected with miRNA-133a or control (Ctrl) miRNA. Data were normalized to *ACTB* mRNA levels. Bottom, BAZ2A immunoblot of nuclear extracts of PC3 cells transfected with the indicated siRNA or miRNA. $^{**}P < 0.005$, two-tailed Student's *t* test. Error bars, s.e.m. from three independent experiments.

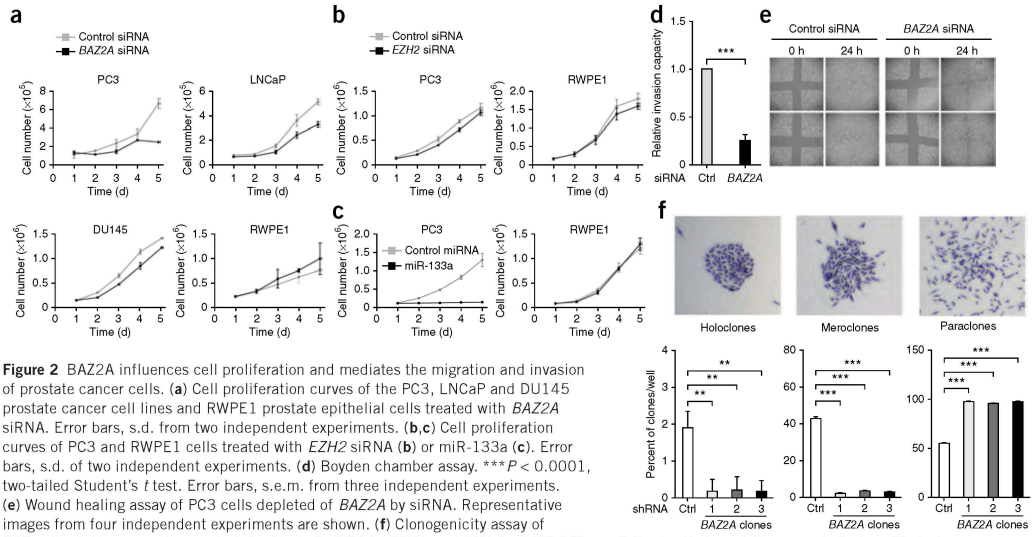

Figure 2 BAZ2A influences cell proliferation and mediates the migration and invasion of prostate cancer cells. (**a**) Cell proliferation curves of the PC3, LNCaP and DU145 prostate cancer cell lines and RWPE1 prostate epithelial cells treated with *BAZ2A* siRNA. Error bars, s.d. from two independent experiments. (**b**,**c**) Cell proliferation curves of PC3 and RWPE1 cells treated with *EZH2* siRNA (**b**) or miR-133a (**c**). Error bars, s.d. of two independent experiments. (**d**) Boyden chamber assay. $***P < 0.0001$, two-tailed Student's *t* test. Error bars, s.e.m. from three independent experiments. (**e**) Wound healing assay of PC3 cells depleted of *BAZ2A* by siRNA. Representative images from four independent experiments are shown. (**f**) Clonogenicity assay of PC3 cells stably expressing control short hairpin RNA (shRNA) or shRNA to *BAZ2A* (three distinct cell clones). Top, morphologies of holoclones, meroclones and paraclones isolated from PC3 cells. Bottom, frequency of each type of cell clone. $**P < 0.01$, $***P < 0.0001$, two-tailed Student's *t* test. Error bars, s.e.m. from three independent experiments.

loss of silencing epigenetic marks at rDNA, upregulation of rDNA transcription and an increase in ribosome production and cell proliferation, underscoring the intimate link between rRNA synthesis and cell proliferation[29,30]. Consistent with these previous findings, knockdown of *BAZ2A* by siRNA in normal prostate epithelial RWPE1 cells increased rDNA transcription and slightly enhanced cell proliferation (**Fig. 2a** and **Supplementary Fig. 1d–f**). *BAZ2A* depletion instead slowed proliferation rates and reduced rDNA transcription in all tested metastatic prostate cancer cell lines, including PC3, DU145 and LNCaP cells, although BAZ2A maintained its role in the epigenetic regulation of rDNA in PC3 cells. The unexpected downregulation of rDNA transcription upon *BAZ2A* knockdown might reflect the defective cell proliferation known to affect and modulate the activity of the rDNA transcription machinery[31]. The unusual phenotypes observed upon *BAZ2A* knockdown in metastatic prostate cancer cells suggest that the role of BAZ2A in prostate cancer cells extends beyond the epigenetic control of the rDNA locus. Similarly to *BAZ2A* knockdown, depletion of *EZH2* reduced the proliferation and viability of PC3 cells, underscoring the recognized oncogenic role of EZH2 in prostate cancer cells[7] (**Fig. 2b** and **Supplementary Fig. 1g**). Remarkably, addition of miR-133a drastically impaired the proliferation of PC3 cells, whereas RWPE1 cells remained unaffected (**Fig. 2c**).

No obvious changes in apoptosis and senescence were evident with *BAZ2A* knockdown in PC3 cells and in the non-malignant RWPE1 cell line (**Supplementary Fig. 3a**,**b**). However, cell cycle analysis showed an accumulation of PC3 cells in G1 phase after *BAZ2A* depletion, whereas no detectable changes were observed in RWPE1 cells (**Supplementary Fig. 3c**). In analysis of progression to S phase after the release of G1/S-synchronized PC3 cells, *BAZ2A* depletion induced a delay in progression in comparison to control PC3 cells and RWPE1 cells (**Supplementary Fig. 3d**). Consistent with these results, only PC3 cells with *BAZ2A* knockdown increased the expression of negative cell cycle regulators such as CDKN1A (**Supplementary Fig. 3e** and **Supplementary Tables 3** and **4**). Analysis of the invasion and migration of metastatic PC3 prostate cancer cells showed that these features of metastatic and aggressive prostate cancer were drastically impaired upon *BAZ2A* knockdown (**Fig. 2d**,**e**). Previous studies demonstrated that the PC3 cell line retains a small fraction of cells (~1%) that can initiate serially transplantable tumors[32,33] and can be distinguished by their ability to form holoclones, which are small, dense colonies with a high capacity for self-renewal[34,35]. Remarkably, unlike control knockdown cells, PC3 cells stably depleted of *BAZ2A* were unable to form holoclones and meroclones (an intermediate phenotype of holoclones) and generated only paraclones, which retain no self-renewal capacity (**Fig. 2f** and **Supplementary Fig. 3f**,**g**).

Taken together, these results indicate that, in contrast to its role in non-malignant cells, BAZ2A paradoxically contributes to the proliferation and viability of metastatic prostate cancer cell lines and is implicated in a cancer cell–specific phenotype involving migration, invasion and stem cell–like features of prostate cancer, which are important in metastasis and disease recurrence[36].

BAZ2A and EZH2 coordinate epigenetic silencing in prostate cancer cells

As the phenotypic analysis in prostate cancer cells suggested additional roles for BAZ2A that are rDNA independent, we reasoned that BAZ2A might regulate a class of non-rRNA genes that are critical for prostate cancer. Because of the various similarities between EZH2 and BAZ2A, we investigated global gene expression in PC3 prostate cancer cells depleted of *BAZ2A* or *EZH2* using microarrays. In this analysis, the transcription of 1,921 genes was significantly up- or downregulated after *BAZ2A* knockdown ($\log_2$ fold difference = 0.58; $P < 0.05$), whereas depletion of *EZH2* affected the expression of 1,793 genes (**Fig. 3a**,**b** and **Supplementary Table 3**). Remarkably, about one-third of the genes regulated by BAZ2A were also

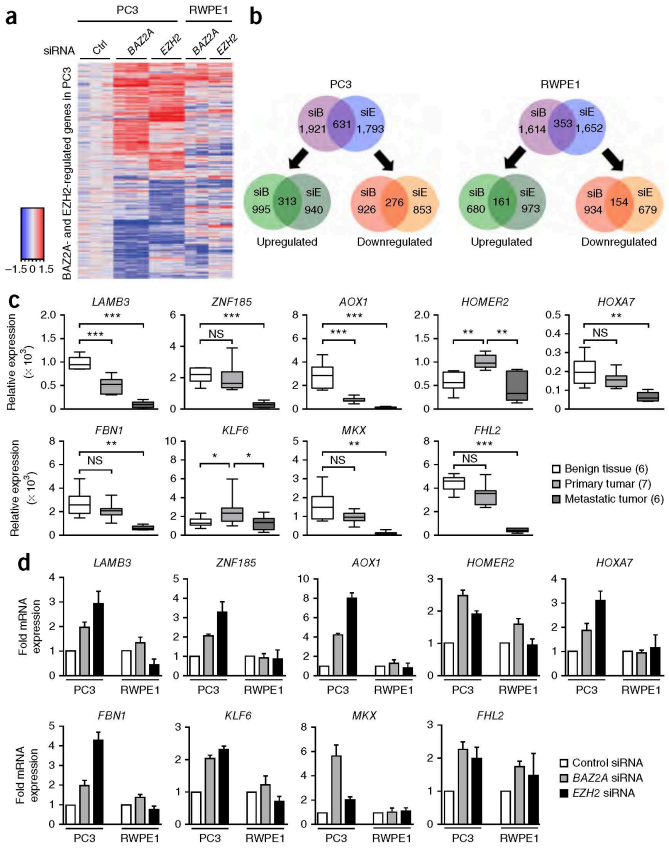

Figure 3 BAZ2A and EZH2 coordinate the repression of genes frequently silenced in metastatic prostate cancer. (**a**) Heat map of the expression levels of BAZ2A- and EZH2-regulated genes in PC3 and RWPE1 cells treated with the corresponding siRNAs. The heat map shows the $\log_2$ ratio relative to the average of the siRNA control samples.(**b**) Venn diagrams of BAZ2A- and EZH2-regulated genes in PC3 and RWPE1 cells treated with the corresponding siRNAs (siB, siRNA to *BAZ2A*; siE, siRNA to *EZH2*). The top diagram represents all genes regulated by BAZ2A or EZH2. The bottom diagrams refer to genes up- or downregulated in cells depleted of *BAZ2A* or *EZH2*. (**c**) Expression of eight RBEPM genes in benign tissue and primary and metastatic tumor tissues (GEO, GSE3325). $^*P < 0.05$, $^{**}P < 0.005$, $^{***}P < 0.0005$, two-tailed Student's *t* test; NS, not significant. (**d**) RBEPM genes are regulated by BAZ2A and EZH2 in PC3 but not RWPE1 cells. qRT-PCR showing the mRNA levels of RBEPMs in cells treated with siRNA to *BAZ2A* or *EZH2*. Data from two independent experiments were normalized to *ACTB* mRNA levels and to data for cells treated with control siRNA. Error bars, s.e.m. from three (PC3) and two (RWPE1) independent experiments.

regulated by EZH2, a proportion not expected by chance ($P = 2.2 \times 10^{-16}$, calculated by a combination of permutation and Fisher tests), indicating that BAZ2A and EZH2 regulate hundreds of genes in common in PC3 cells. In further support of an rDNA-independent role for BAZ2A in prostate cancer, abundant amounts of BAZ2A were present in the nucleoplasmatic fraction of PC3 cells (**Supplementary Fig. 4**), whereas all non-malignant mouse cells analyzed so far displayed an exclusive localization of BAZ2A within nucleoli, the nuclear compartment that contains rRNA genes (**Supplementary Fig. 4**). Gene set enrichment analysis (GSEA) uncovered a strong positive correlation with gene sets and pathways involved in metastasis (for example, extracellular matrix organization and collagen formation) and immune function (interferon and cytokine signaling) independently within both data sets ($q < 0.05$; **Supplementary Fig. 5** and **Supplementary Table 5**). Furthermore, the aging and senescence gene set that was recently found to be a signature for indolent prostate cancer[37] was negatively correlated with genes regulated by BAZ2A or EZH2 ($P < 0.01$ for both). In comparison to experiments in PC3 cells, knockdown of *BAZ2A* or *EZH2* in the non-malignant RWPE1 cell line resulted in an overlap of only 15% of genes, with only 16 of these genes having expression affected by both *BAZ2A* and *EZH2* knockdown in PC3 cells (**Fig. 3a**,**b** and **Supplementary Table 6**). Genes regulated by both BAZ2A and EZH2 in RWPE1 cells did not show any relevant gene ontology (GO) enrichment (**Supplementary Fig. 6**). Remarkably, the genes affected by *BAZ2A* depletion in PC3 and RWPE1 cells were implicated in distinct biological processes (**Supplementary Fig. 7**). Taken together, these data show that BAZ2A and EZH2 coordinate shared biological pathways in PC3 prostate cancer cells that are not present in non-malignant RWPE1 cells, suggesting a functional BAZ2A-EZH2 cooperation that is specific for metastatic prostate cancer cells.

To determine how the transcriptional repressors BAZ2A and EZH2 might cooperate to regulate genes with likely roles in prostate cancer metastasis, we identified 101 genes that were downregulated in metastatic tumors in comparison to normal prostate tissues or primary tumors[7,38] as well as upregulated upon *BAZ2A* or *EZH2* knockdown in PC3 cells. We termed these genes RBEPMs (repressed by BAZ2A and EZH2 in prostate cancer cells and repressed in metastatic prostate cancer tumors) (**Fig. 3c** and **Supplementary Table 3**). Upregulation of the nine RBEPMs (*AOX1*, *FBN1*, *FHL2*, *HOMER2*, *HOXA7*, *LAMB3*, *MKX*, *KLF6* and *ZNF185*) that showed the strongest downregulation in metastatic tumors (**Fig. 3c**) and had previously been reported to be hypermethylated and transcriptionally repressed in cancers[4,39–45] was validated in *BAZ2A* and *EZH2* knockdown cells (**Fig. 3d** and **Supplementary Fig. 8a**). Analysis of RWPE1 cells confirmed that these RBEPMs were predominantly not normally regulated by BAZ2A and EZH2 (**Fig. 3d** and **Supplementary Table 4**).

The substantial overlap of BAZ2A- and EZH2-regulated genes in PC3 cells prompted us to investigate the direct association and coordinated binding of BAZ2A and EZH2 at RBEPM promoters (**Fig. 3d**). Coimmunoprecipitation of Flag-HA-BAZ2A from the nuclear extracts of HEK293T cells showed an association with EZH2 (**Fig. 4a**). Chromatin immunoprecipitation (ChIP) analysis indicated

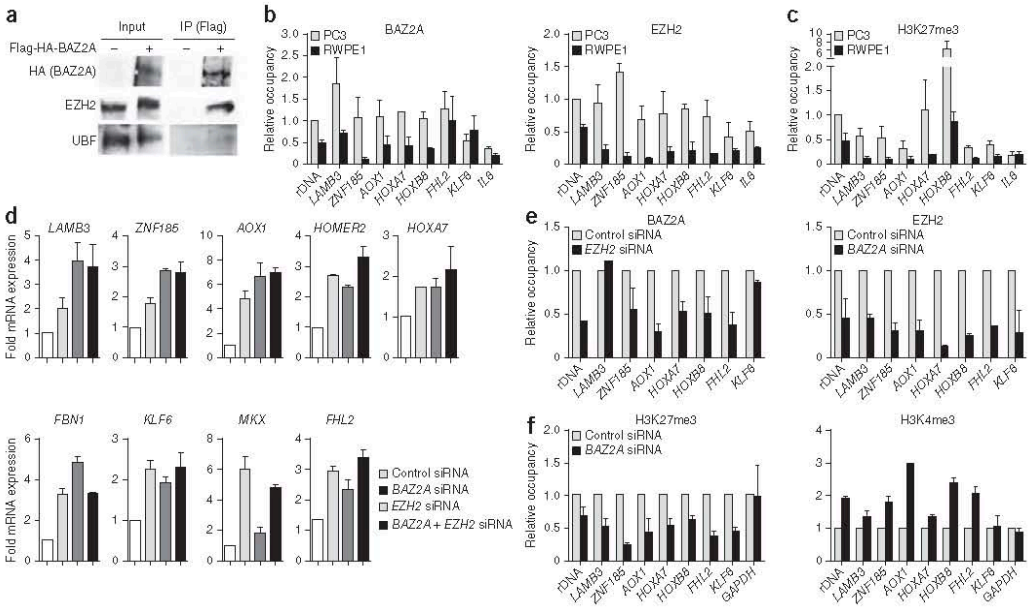

Figure 4 BAZ2A regulates aberrant epigenetic silencing in prostate cancer. (**a**) Flag-mediated immunoprecipitation of nuclear extracts from HEK293T cells expressing Flag-HA-BAZ2A. Immunoblots show the association of BAZ2A with EZH2. The specificity of immunoprecipitation was verified by the lack of immunoprecipitated UBF, which does not associate with BAZ2A. IP, immunoprecipitation. (**b**,**c**) BAZ2A and EZH2 levels (**b**) and H3K27me3 marks (**c**) are enriched at RBEPM gene promoters in PC3 cells. ChIP assays show associations with RBEPM promoters in PC3 and RWPE1 cells. Values are shown relative to input and to rDNA promoter sequences in PC3 cells. Error bars, s.e.m. from two independent experiments. (**d**) BAZ2A and EZH2 repress the transcription of RBEPM genes via a shared pathway. qRT-PCR of RBEPM transcripts from PC3 cells treated with siRNA to *BAZ2A*, *EZH2* or both. Error bars, s.e.m. from two independent experiments. (**e**) Recruitment of EZH2 to RBEPM promoters is interdependent with that of BAZ2A. ChIP analysis of the association of BAZ2A or EZH2 with RBEPM promoters in PC3 cells depleted of *EZH2* or *BAZ2A*, respectively. Data are shown relative to input and data for control cells. Error bars, s.e.m. from two independent experiments. (**f**) BAZ2A regulates H3K27me3 and H3K4me3 levels at RBEPMs in PC3 cells. ChIP of the indicated histone modifications. Data are shown relative to input and data for control cells. Error bars, s.e.m. from two independent experiments.

that BAZ2A and EZH2 were generally more associated with RBEPM and rDNA promoters in PC3 cells than in RWPE1 cells (**Fig. 4b**). Consistent with the BAZ2A and EZH2 binding profiles, H3K27me3 levels at RBEPM and rDNA promoter sequences were higher in PC3 cells than in RWPE1 cells, underscoring the role of histone repressive marks in transcriptional silencing at RBEPMs in prostate cancer cells (**Fig. 4c**). A lack of evident additive RBEPM activation upon combined depletion suggests that BAZ2A and EZH2 repress the transcription of RBEPM genes via a shared pathway (**Fig. 4d** and **Supplementary Fig. 8b**). Accordingly, all RBEPMs showed decreased association with EZH2 upon *BAZ2A* depletion (**Fig. 4e** and **Supplementary Fig. 8c**). Similar results were obtained for BAZ2A binding with the majority of RBEPMs (with the exception of *LAMB3* and *KLF6*) in PC3 cells in the absence of *EZH2*, indicating that the recruitment of EZH2 to RBEPM promoters is codependent on BAZ2A. Remarkably, depletion of *BAZ2A* decreased H3K27me3 levels and increased the association of the active histone mark H3K4me3 (trimethylation of histone H3 at lysine 4) with RBEPM and rDNA promoter sequences (**Fig. 4f**). Taken together, the results show the essential role of BAZ2A in coordinating EZH2 recruitment and the establishment of H3K27 methylation at genes frequently repressed in metastatic prostate cancer. The data indicate that BAZ2A acts as epigenetic regulator for the transcriptional repression of genes that are implicated in aggressive prostate cancer.

Tumors with high BAZ2A expression display a CpG island hypermethylator phenotype

Because BAZ2A is known to interact with DNA methyltransferases and this association is required to establish epigenetic silencing at rDNA in all cells[17], we next investigated whether the upregulation of BAZ2A was associated with altered DNA methylation in prostate tumors. As we determined that BAZ2A was primarily regulated post-transcriptionally, we analyzed BAZ2A protein levels in prostate tumors and normal tissues using immunohistochemistry on a tissue microarray (TMA) of 384 samples. BAZ2A immunostaining was variable between prostate tumor specimens in comparison to normal prostate epithelium, with strong and weak staining in 21% and 25% of samples, respectively. We selected 22 tumors with high BAZ2A protein levels and 13 tumors with low BAZ2A protein levels for DNA methylation analysis using the Illumina Infinium HumanMethylation450 (450K) array. Samples were also selected to have >70% tumor content, which was confirmed to not appreciably differ between samples with high and low BAZ2A expression by observing between the groups consistent hypermethylation of *GSTP1* (ref. 46) and *APC*[47], genes known to

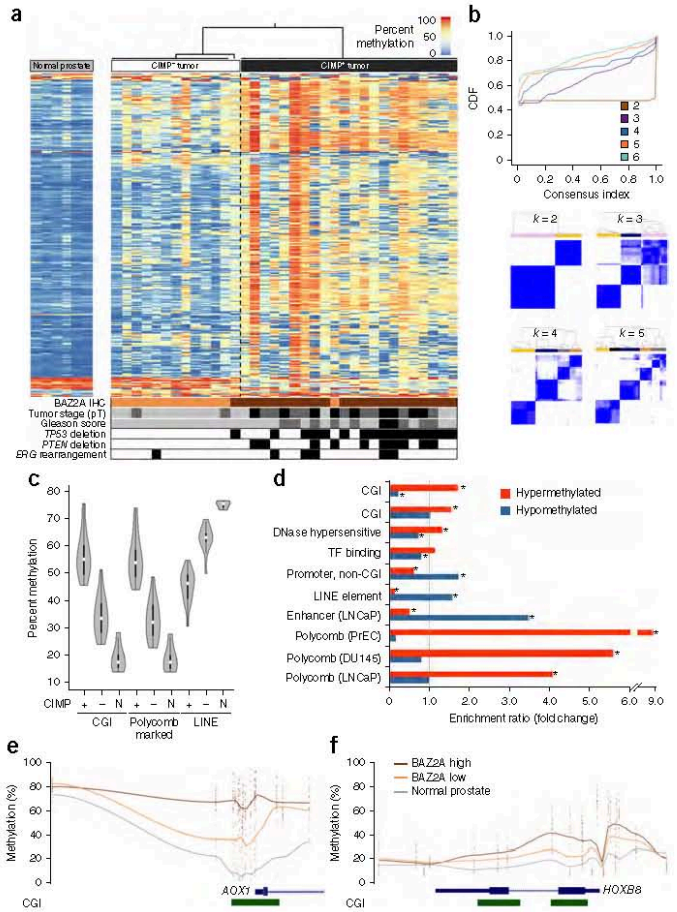

Figure 5 Epigenetic remodeling in prostate tumors overexpressing BAZ2A. (**a**) A heat map of the DNA methylation values of the 3,000 most variable CpG sites from 450K array analysis. Hierarchical clustering of tumors identifies two DNA methylation subtypes displaying relatively high and low levels of methylation (termed CIMP$^+$ and CIMP$^-$, respectively). Tumors displaying high and low levels of BAZ2A from immunohistochemical (IHC) evaluation are represented by dark and light brown color, respectively. Increasing tumor stage (pT2, pT3a and pT3b) and Gleason score (3+4, 4+3 and ≥4+4) are illustrated by an increase in shading intensity from light gray to dark gray to black for the corresponding indicators. The presence of *TP53* and *PTEN* deletions, as well as *ERG* rearrangements, is indicated. (**b**) Top, cumulative distribution function (CDF) for class numbers ranging from two to six. Bottom, consensus clustering heat maps of the consensus matrices for class numbers ranging from two to five. (**c**) DNA methylation levels of CGIs, Polycomb-marked regions and LINE elements in CIMP$^+$ and CIMP$^-$ tumors and in normal tissue (N) show methylation features consistent with previously defined CIMP phenotypes (white dots indicate the median, boxes indicate the interquartile range). (**d**) Enrichment and/or depletion of genomic features in tumors with high versus low BAZ2A expression. Annotations of enhancer and Polycomb features were derived from ChIP sequencing profiles for LNCaP, DU145 and PrEC cells. (TF, transcription factor; PrEC, prostate epithelial cells). *$P < 0.001$. (**e**,**f**) DNA methylation profiles of the promoter regions of the RBEPM genes *AOX1* (**e**) and *HOXB8* (**f**) in tumor subtypes with high and low BAZ2A expression versus normal prostate tissue.

be hypermethylated in early disease stages (**Supplementary Fig. 9a**). Genome-wide analysis showed that the methylation of 32,707 CpGs was significantly altered (by more than ±20%; $q < 0.05$) in comparison to 6 normal prostate samples, with 24,497 and 8,210 CpGs hyper- and hypomethylated, respectively (**Fig. 5a**). Unsupervised clustering of the 3,000 most variable of these CpGs identified 2 distinct DNA methylation subtypes. A statistical evaluation showed an optimal number of two distinct methylation subtypes (**Fig. 5b**). To validate this finding, we independently interrogated TCGA prostate cancer data using the same approach of separating samples into those with high versus low BAZ2A expression (on the basis of available RNA expression data) and identifying *de novo* the 3,000 most variable probes (**Supplementary Fig. 10**). Ninety percent of the most variable CpGs were common to both analyses and furthermore identified two distinct methylation subgroups. One of the subtypes was characterized by a higher degree of hypermethylation of CpG islands (CGIs) and sites associated with Polycomb repression (as defined in LNCaP cells[48]) while simultaneously demonstrating hypomethylation of repetitive elements (such as long interspersed nuclear elements, LINEs) (**Fig. 5c**). The pattern present in this subtype is reminiscent of a CGI hypermethylator phenotype (CIMP) observed in other cancers[49–51], as well as globally in prostate cancer[5,52]. We observed a striking correlation between BAZ2A expression levels and the CIMP subtype, with 21 of 22 CIMP-positive samples displaying high BAZ2A levels and 12 of 13 normal-like samples exhibiting low BAZ2A levels. We also observed a similar association of the CIMP subtype with high BAZ2A expression in the analysis of TCGA data (**Supplementary Fig. 10**). Comparing tumors with high and low BAZ2A expression, in the subtype with high expression, 6,155 CpGs were hypermethylated and 1,679 CpGs were hypomethylated (difference in methylation of greater than ±20%). Hypermethylated CpGs were enriched in transcription factor binding and DNase-hypersensitive sites in addition to CGIs and CGI shore regions (**Fig. 5d**). Hypermethylation in tumors with high BAZ2A levels was strongly enriched in Polycomb-silenced regions (as defined in DU145 and LNCaP cells or primary prostate epithelial cells). Thus, elevated BAZ2A levels are associated with widespread epigenetic remodeling that includes functional regions, such as promoter and enhancer regions, and with Polycomb-associated domains. Considering our findings connecting BAZ2A with EZH2 and H3K27me3 in PC3 prostate cancer cells, the observation of greater hypermethylation of H3K27me3-marked regions suggests that high BAZ2A overexpression might be involved in the

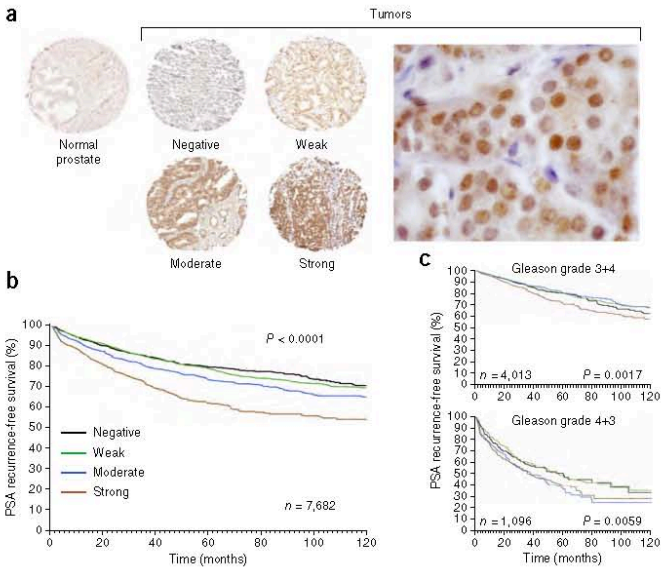

Figure 6 TMA and clinical evaluation of BAZ2A levels in 7,682 prostate tumor specimens. (**a**) Representative examples of TMA histological sections showing normal prostate and the negative, weak, moderate and strong BAZ2A staining classifications. Enhanced magnification (400x) of a representative tumor sample is shown (right). (**b**) Kaplan-Maier analysis of the time to postoperative PSA recurrence versus BAZ2A levels in all prostate tumors. *P* values were obtained by log-rank test (BAZ2A negative, $n = 1,998$; BAZ2A weak, $n = 2,809$; BAZ2A moderate, $n = 1,419$; BAZ2A strong, $n = 1,456$). (**c**) Cases were subdivided by Gleason grade to assess the capacity of BAZ2A levels to predict the frequency of postoperative PSA recurrence. Cases classified as low risk (3+4; top) and intermediate risk (4+3; bottom) display an increased likelihood of recurrence with increasing BAZ2A levels. Gleason grade 3+4: BAZ2A negative, $n = 1,036$; BAZ2A weak, $n = 1,461$; BAZ2A moderate, $n = 777$; BAZ2A strong, $n = 739$. Gleason grade 4+3: BAZ2A negative, $n = 211$; BAZ2A weak, $n = 353$; BAZ2A moderate, $n = 213$; BAZ2A strong, $n = 319$.

establishment of abnormal methylation patterns in prostate tumors. Tumors with high BAZ2A levels were also associated with advanced tumor stages and higher Gleason scores.

BAZ2A-associated alterations to DNA methylation were found to involve numerous genes and pathways that are known to be associated with prostate cancer in general (**Supplementary Table 7**), including hypermethylation of prostate cancer–relevant gene promoters and miRNAs known to inhibit androgen receptor expression[53–58] (**Supplementary Fig. 9b**,**c**). In comparison to the genes that become derepressed following *BAZ2A* knockdown in PC3 cells, 352 genes (35%) were found to have elevated levels of DNA methylation in tumors with high versus low BAZ2A expression, a number greater than expected by chance ($P = 0.0029$). There were 27 genes that were hypermethylated in tumors with high BAZ2A levels and upregulated upon both *BAZ2A* or *EZH2* knockdown in PC3 cells (**Fig. 5e**,**f**). Next, we performed GSEA on genes with differential promoter methylation in tumors with high and low BAZ2A levels (**Supplementary Fig. 11** and **Supplementary Tables 7** and **8**). Several cellular pathways and functions that are relevant to cancer development were found to be significantly enriched (FDR $q < 0.05$), including cell growth (cell cycle and transcription pathways) and genome stability (chromosome and telomere maintenance pathways). These gene sets were also identified for the genes showing differential expression with *BAZ2A* knockdown in PC3 cells (**Supplementary Fig. 5**). Moreover, hypermethylated genes in tumors with high BAZ2A levels and genes derepressed upon *BAZ2A* depletion in PC3 cells showed identical GO terms (**Supplementary Fig. 12**). Taken together, the data support a functional role for BAZ2A in DNA hypermethylation in prostate cancer tumors (**Supplementary Fig. 12**).

BAZ2A levels predict PSA recurrence in individuals with prostate cancer

We investigated the potential clinical relevance of BAZ2A in prostate cancer using a large TMA. This analysis included 7,682 informative samples for which clinical follow-up data were available. Case characteristics and clinical data are displayed in **Supplementary Table 9**. BAZ2A immunostaining in tumor samples was categorized as negative (26.1%), weak (36.7%), moderate (18.5%) or strong (19.0%) (as in **Fig. 5**; examples shown in **Fig. 6a**). We observed nuclear localization of BAZ2A, including increased staining in nucleoli (**Fig. 6a** and **Supplementary Fig. 13**). Strong BAZ2A staining was highly associated with advanced prostate tumor stage, high Gleason grade, the presence of lymph node metastasis, high preoperative PSA levels and positive surgical margin when considering all tumors or following subgrouping by *ERG* rearrangement status ($P < 0.0001$ for each; **Supplementary Table 10a–c**). The time to postoperative PSA recurrence was significantly shorter in the group with strong BAZ2A expression ($P < 0.0001$; **Fig. 6b**). Using Cox regression multivariate analysis to determine the relative dependence of recurrence on several prognostic and surgical parameters, the level of BAZ2A was determined to be independently predictive of PSA recurrence in multiple scenarios ($P < 0.0001$; **Supplementary Table 11a–c**). The independent predictive power of BAZ2A was further upheld following subdivision of the cases by *ERG* rearrangement status ($P < 0.0001$; **Supplementary Fig. 14**). Notably, to answer the question of whether BAZ2A levels could be used as a marker to aid in preoperative therapy decision-making for low- and intermediate-risk cases, we subdivided the cases by Gleason score and compared the frequency of postoperative PSA recurrence. BAZ2A levels were significantly predictive of PSA recurrence in cases with a Gleason score of 3+4 (low-intermediate risk; $n = 4,013$, $P = 0.0017$) or 4+3 (high-intermediate risk; $n = 1,096$, $P = 0.0059$) (**Fig. 6c**). BAZ2A levels did not show significant predictive ability in cases with a Gleason score of ≤3+3 (indolent prostate cancer; $n = 1,690$), likely owing to the occurrence of relatively very few events in this group, nor in very high-risk cases (Gleason score of ≥4+4; $n = 322$) (**Supplementary Fig. 14**). These results demonstrate a clear association of BAZ2A levels in prostate cancer tumor samples with PSA recurrence that is independent of standard prognostic and surgical parameters and can distinguish cases that

are ore likely to recur in the most uncertain group of individuals at intermediate risk.

DISCUSSION

Alterations involving epigenetic regulators are now recognized as key events governing the tumor cell phenotype by affecting the expression of genes critical to cancer. This work identified a new aberrant epigenetic signature (CIMP) that distinguishes prostate cancer tumors with high and low BAZ2A expression. Elevated BAZ2A levels associate with poor prognosis and disease recurrence, and tumors with high BAZ2A expression contain a specific set of hypermethylated genes implicated in several pathways relevant to cancer. We provide multiple lines of evidence that support the role of BAZ2A in the establishment of epigenetic alterations in cases with poor prognosis. Through the combined analysis of metastatic prostate cancer cell lines and tumor samples from patients, we found that the role of BAZ2A in prostate cancer goes beyond the epigenetic control of the rDNA locus. Using prostate cancer cell lines, we show that BAZ2A regulates genes (i) frequently repressed in metastatic prostate cancer and (ii) hypermethylated in prostate cancer cases with poor prognosis. The analysis of hypermethylated sequences in tumors with high BAZ2A expression identified an enrichment of sites associated with Polycomb repression that is in agreement with the results from the prostate cancer cell line describing the repression activity of BAZ2A in concert with Polycomb-based silencing. Furthermore, genes regulated by BAZ2A in prostate cancer cell lines and hypermethylated in tumors with high BAZ2A levels involve similar pathways and cancer-related processes. A role for BAZ2A in establishing epigenetic alterations that might favor the aggressive prostate cancer phenotype is also supported by the phenotypic analysis in prostate cancer cell lines showing an impact of BAZ2A on cancer-specific features such as proliferation, migration and invasion. Future studies will aim to define how and at which time point in prostate cancer progression BAZ2A exerts its oncogenic effect. Notably, we showed that high expression of BAZ2A in prostate cancer is likely caused by post-transcriptional regulation, supporting the idea that the disruption of epigenetic pathways is likely to have an important role in this disease.

Lethality in prostate cancer is linked to the evolution of a metastatic phenotype. PSA recurrence following radical prostatectomy signifies that tumor cells gained the ability to invade surrounding tissues and/or metastasize before surgery. Our results suggest that high BAZ2A levels in the primary tumor indicate a higher probability of metastasis, linking molecular findings with recurrence in clinical samples. We have shown BAZ2A levels to be an independent prognostic marker of recurrence, especially in low- and intermediate-risk cases, as assessed by Gleason score. Intermediate-risk cases are a subcohort with the most uncertainty in deciding the right balance between active surveillance and immediate definite therapy to avoid overtreatment. Screening of BAZ2A levels in biopsies might be a valuable biomarker to distinguish prostate cancer that may progress, aiding in the therapy decision-making for this important patient subgroup. Additionally, as an increasing number of epigenetic regulators, including members of the bromodomain-containing protein class, are currently being found to be dysregulated across many cancer types[59], BAZ2A, which contains a bromodomain required for its silencing function at rDNA[60], might represent a promising therapeutic target for metastatic prostate cancer.

URLs. TCGA Data Portal, https://tcga-data.nci.nih.gov/tcga/dataAccessMatrix.htm; Database for Annotation, Visualization and Integrated Discovery (DAVID), http://david.abcc.ncifcrf.gov/; miRGator v3.0, http://mirgator.kobic.re.kr/; Gene Set Enrichment Analysis (GSEA), http://www.broadinstitute.org/gsea/.

METHODS

Methods and any associated references are available in the online version of the paper.

Accession codes. The 450K array data can be found at the European Genome-phenome Archive (EGA) under accession EGAS00001000568.

Note: Any Supplementary Information and Source Data files are available in the online version of the paper.

ACKNOWLEDGMENTS

We acknowledge the entire team of the German ICGC Project on Early Onset Prostate Cancer. We thank M. Lupien, C. Schmidt, D. Wuttig, O. Bogatyrova, A. Postępska-Igielska and N. Schmitt for assistance with experiments and data. This project was supported by the German Federal Ministry of Education and Science in the Program for Medical Genome Research including the EOPC project within ICGC (PKZ; 01KU1001A, 01KU1001B, 01KU1001C, 01KU1001D and 01GS0890), by Krebsforschung Schweiz (KFS; 02732-02-2011), by the Swiss National Science Foundation (SNF; 310003A-135801 and 31003A-152854), by Swiss Life, by a Müller Molecular Life Science fellowship and by Mäxi Stiftung. We acknowledge assistance provided by the Genomics and Proteomics Core Facility at the German Cancer Research Center. In particular, we acknowledge the excellent technical support of M. Schick.

AUTHOR CONTRIBUTIONS

L.G., S.C.F., C.C.O., R. Simon, K.G., C.Y.G., D.B., M.P., C.B., M.W. and R.K. designed the experiments and performed experimental work. L.G., R.E., C.C.O., R. Simon, Z.G., R.K., M.D.R., M.S. and K.G. performed data analysis. R.K., G.S. and H.S. provided clinical samples or data. L.G., S.C.F., C.C.O., R. Simon, C.P., G.S., R.E. and R. Santoro prepared the manuscript and figures. M.-L.Y., B.B., J.K., T.S., G.S., R.E., H.S., C.P. and R. Santoro provided project leadership. All authors contributed to the final manuscript.

COMPETING FINANCIAL INTERESTS

The authors declare no competing financial interests.

1. Grasso, C.S. *et al.* The mutational landscape of lethal castration-resistant prostate cancer. *Nature* **487**, 239–243 (2012).
2. Weischenfeldt, J. *et al.* Integrative genomic analyses reveal an androgen-driven somatic alteration landscape in early-onset prostate cancer. *Cancer Cell* **23**, 159–170 (2013).
3. Plass, C. *et al.* Mutations in regulators of the epigenome and their connections to global chromatin patterns in cancer. *Nat. Rev. Genet.* **14**, 765–780 (2013).
4. Kim, J.H. *et al.* Deep sequencing reveals distinct patterns of DNA methylation in prostate cancer. *Genome Res.* **21**, 1028–1041 (2011).
5. Kron, K. *et al.* Altered DNA methylation landscapes of polycomb-repressed loci are associated with prostate cancer progression and *ERG* oncogene expression in prostate cancer. *Clin. Cancer Res.* **19**, 3450–3461 (2013).
6. Aryee, M.J. *et al.* DNA methylation alterations exhibit intraindividual stability and interindividual heterogeneity in prostate cancer metastases. *Sci. Transl. Med.* **5**, 169ra10 (2013).
7. Varambally, S. *et al.* The polycomb group protein EZH2 is involved in progression of prostate cancer. *Nature* **419**, 624–629 (2002).
8. Bracken, A.P. *et al. EZH2* is downstream of the pRB-E2F pathway, essential for proliferation and amplified in cancer. *EMBO J.* **22**, 5323–5335 (2003).
9. Hinz, S. *et al.* Expression of the polycomb group protein EZH2 and its relation to outcome in patients with urothelial carcinoma of the bladder. *J. Cancer Res. Clin. Oncol.* **134**, 331–336 (2008).
10. Bachmann, I.M. *et al.* EZH2 expression is associated with high proliferation rate and aggressive tumor subgroups in cutaneous melanoma and cancers of the endometrium, prostate, and breast. *J. Clin. Oncol.* **24**, 268–273 (2006).
11. Kleer, C.G. *et al.* EZH2 is a marker of aggressive breast cancer and promotes neoplastic transformation of breast epithelial cells. *Proc. Natl. Acad. Sci. USA* **100**, 11606–11611 (2003).
12. Crea, F., Paolicchi, E., Marquez, V.E. & Danesi, R. Polycomb genes and cancer: time for clinical application? *Crit. Rev. Oncol. Hematol.* **83**, 184–193 (2012).
13. Tsang, D.P. & Cheng, A.S. Epigenetic regulation of signaling pathways in cancer: role of the histone methyltransferase EZH2. *J. Gastroenterol. Hepatol.* **26**, 19–27 (2011).

14. Richly, H., Aloia, L. & Di Croce, L. Roles of the Polycomb group proteins in stem cells and cancer. *Cell Death Dis.* **2**, e204 (2011).
15. Cancer Genome Atlas Research Network. Comprehensive genomic characterization defines human glioblastoma genes and core pathways. *Nature* **455**, 1061–1068 (2008).
16. Brase, J.C. *et al. TMPRSS2-ERG*–specific transcriptional modulation is associated with prostate cancer biomarkers and TGF-β signaling. *BMC Cancer* **11**, 507 (2011).
17. Santoro, R., Li, J. & Grummt, I. The nucleolar remodeling complex NoRC mediates heterochromatin formation and silencing of ribosomal gene transcription. *Nat. Genet.* **32**, 393–396 (2002).
18. Zhou, Y., Santoro, R. & Grummt, I. The chromatin remodeling complex NoRC targets HDAC1 to the ribosomal gene promoter and represses RNA polymerase I transcription. *EMBO J.* **21**, 4632–4640 (2002).
19. Guetg, C., Scheifele, F., Rosenthal, F., Hottiger, M.O. & Santoro, R. Inheritance of silent rDNA chromatin is mediated by PARP1 via noncoding RNA. *Mol. Cell* **45**, 790–800 (2012).
20. Hein, N., Hannan, K.M., George, A.J., Sanij, E. & Hannan, R.D. The nucleolus: an emerging target for cancer therapy. *Trends Mol. Med.* **19**, 643–654 (2013).
21. Bywater, M.J. *et al.* Inhibition of RNA polymerase I as a therapeutic strategy to promote cancer–specific activation of p53. *Cancer Cell* **22**, 51–65 (2012).
22. Cho, S. *et al.* MiRGator v3.0: a microRNA portal for deep sequencing, expression profiling and mRNA targeting. *Nucleic Acids Res.* **41**, D252–D257 (2013).
23. Dong, Y.J. *et al.* MiR-133a inhibits colorectal cancer cell growth by direct targeting E3 ubiquitin ligase RFFL and activating p53-p21CIP1/WAF1 pathway. *Gastroenterology* **142**, S185 (2012).
24. Uchida, Y. *et al.* MiR-133a induces apoptosis through direct regulation of GSTP1 in bladder cancer cell lines. *Urol. Oncol.* **31**, 115–123 (2013).
25. Ji, F. *et al.* MicroRNA-133a, downregulated in osteosarcoma, suppresses proliferation and promotes apoptosis by targeting Bcl-xL and Mcl-1. *Bone* **56**, 220–226 (2013).
26. Tao, J. *et al.* MicroRNA-133 inhibits cell proliferation, migration and invasion in prostate cancer cells by targeting the epidermal growth factor receptor. *Oncol. Rep.* **27**, 1967–1975 (2012).
27. Kojima, S. *et al.* Tumor suppressors miR-1 and miR-133a target the oncogenic function of purine nucleoside phosphorylase (*PNP*) in prostate cancer. *Eur. Urol. Suppl.* **106**, 405–413 (2012).
28. Li, J., Santoro, R., Koberna, K. & Grummt, I. The chromatin remodeling complex NoRC controls replication timing of rRNA genes. *EMBO J.* **24**, 120–127 (2005).
29. Santoro, R., Lienemann, P. & Fussenegger, M. Epigenetic engineering of ribosomal RNA genes enhances protein production. *PLoS ONE* **4**, e6653 (2009).
30. Guetg, C. *et al.* The NoRC complex mediates the heterochromatin formation and stability of silent rRNA genes and centromeric repeats. *EMBO J.* **29**, 2135–2146 (2010).
31. Grummt, I. Life on a planet of its own: regulation of RNA polymerase I transcription in the nucleolus. *Genes Dev.* **17**, 1691–1702 (2003).
32. Li, H., Chen, X., Calhoun-Davis, T., Claypool, K. & Tang, D.G. PC3 human prostate carcinoma cell holoclones contain self-renewing tumor-initiating cells. *Cancer Res.* **68**, 1820–1825 (2008).
33. Sheng, X. *et al.* Isolation and enrichment of PC-3 prostate cancer stem-like cells using MACS and serum-free medium. *Oncol. Lett.* **5**, 787–792 (2013).
34. Zhang, K. & Waxman, D.J. PC3 prostate tumor–initiating cells with molecular profile FAM65B^{high}/MFI2^{low}/LEF1^{low} increase tumor angiogenesis. *Mol. Cancer* **9**, 319 (2010).
35. Doherty, R.E., Haywood-Small, S.L., Sisley, K. & Cross, N.A. Aldehyde dehydrogenase activity selects for the holoclone phenotype in prostate cancer cells. *Biochem. Biophys. Res. Commun.* **414**, 801–807 (2011).
36. Collins, A.T., Berry, P.A., Hyde, C., Stower, M.J. & Maitland, N.J. Prospective identification of tumorigenic prostate cancer stem cells. *Cancer Res.* **65**, 10946–10951 (2005).
37. Irshad, S. *et al.* A molecular signature predictive of indolent prostate cancer. *Sci. Transl. Med.* **5**, 202ra122 (2013).
38. Yu, Y.P. *et al.* Gene expression alterations in prostate cancer predicting tumor aggression and preceding development of malignancy. *J. Clin. Oncol.* **22**, 2790–2799 (2004).
39. Wang, Y. *et al.* Survey of differentially methylated promoters in prostate cancer cell lines. *Neoplasia* **7**, 748–760 (2005).
40. Mori, Y. *et al.* Novel candidate colorectal cancer biomarkers identified by methylation microarray-based scanning. *Endocr. Relat. Cancer* **18**, 465–478 (2011).
41. Kinoshita, M., Nakagawa, T., Shimizu, A. & Katsuoka, Y. Differently regulated androgen receptor transcriptional complex in prostate cancer compared with normal prostate. *Int. J. Urol.* **12**, 390–397 (2005).
42. Novak, P. *et al.* Epigenetic inactivation of the *HOXA* gene cluster in breast cancer. *Cancer Res.* **66**, 10664–10670 (2006).
43. Zhang, J.S., Gong, A. & Young, C.Y. ZNF185, an actin-cytoskeleton-associated growth inhibitory LIM protein in prostate cancer. *Oncogene* **26**, 111–122 (2007).
44. Cheng, X.F. *et al.* Growth inhibitory effect of Kruppel-like factor 6 on human prostatic carcinoma and renal carcinoma cell lines. *Tohoku J. Exp. Med.* **216**, 35–45 (2008).
45. Wang, N. *et al.* Screening and identification of distant metastasis-related differentially expressed genes in human squamous cell lung carcinoma. *Anat. Rec. (Hoboken)* **295**, 748–757 (2012).
46. Maksimovic, J., Gordon, L. & Oshlack, A. SWAN: subset-quantile within array normalization for Illumina Infinium HumanMethylation450 BeadChips. *Genome Biol.* **13**, R44 (2012).
47. Lee, W.H. *et al.* Cytidine methylation of regulatory sequences near the π-class glutathione S-transferase gene accompanies human prostatic carcinogenesis. *Proc. Natl. Acad. Sci. USA* **91**, 11733–11737 (1994).
48. Yu, J. *et al.* An integrated network of androgen receptor, polycomb, and *TMPRSS2-ERG* gene fusions in prostate cancer progression. *Cancer Cell* **17**, 443–454 (2010).
49. Issa, J.P. CpG island methylator phenotype in cancer. *Nat. Rev. Cancer* **4**, 988–993 (2004).
50. Zouridis, H. *et al.* Methylation subtypes and large-scale epigenetic alterations in gastric cancer. *Sci. Transl. Med.* **4**, 156ra140 (2012).
51. McCabe, M.T., Lee, E.K. & Vertino, P.M. A multifactorial signature of DNA sequence and polycomb binding predicts aberrant CpG island methylation. *Cancer Res.* **69**, 282–291 (2009).
52. Cho, N.Y. *et al.* Hypermethylation of CpG island loci and hypomethylation of LINE-1 and Alu repeats in prostate adenocarcinoma and their relationship to clinicopathological features. *J. Pathol.* **211**, 269–277 (2007).
53. Shyr, C.R. *et al.* Tumor suppressor PAX6 functions as androgen receptor co-repressor to inhibit prostate cancer growth. *Prostate* **70**, 190–199 (2010).
54. Nguyen, A.H. *et al.* Gata3 antagonizes cancer progression in *Pten*-deficient prostates. *Hum. Mol. Genet.* **22**, 2400–2410 (2013).
55. Kypta, R.M. & Waxman, J. Wnt/β-catenin signalling in prostate cancer. *Nat. Rev. Urol.* **9**, 418–428 (2012).
56. Kashat, M. *et al.* Inactivation of AR and Notch-1 signaling by miR-34a attenuates prostate cancer aggressiveness. *Am. J. Transl. Res.* **4**, 432–442 (2012).
57. Östling, P. *et al.* Systematic analysis of microRNAs targeting the androgen receptor in prostate cancer cells. *Cancer Res.* **71**, 1956–1967 (2011).
58. Shi, X.B. *et al.* Tumor suppressive miR-124 targets androgen receptor and inhibits proliferation of prostate cancer cells. *Oncogene* **32**, 4130–4138 (2013).
59. Dawson, M.A., Kouzarides, T. & Huntly, B.J. Targeting epigenetic readers in cancer. *N. Engl. J. Med.* **367**, 647–657 (2012).
60. Zhou, Y. & Grummt, I. The PHD finger/bromodomain of NoRC interacts with acetylated histone H4K16 and is sufficient for rDNA silencing. *Curr. Biol.* **15**, 1434–1438 (2005).

ONLINE METHODS

Gene expression analysis. Analysis of gene expression was performed using publically available TCGA level 3 gene expression data downloaded from the TCGA Data Portal (RNASeqV2 data). Analysis was restricted to patients with matched tumor and normal samples. RSEM ratio values (RSEM(tumor)/RSEM(matched normal)) were used to quantify mRNA expression levels[61]. Statistical evaluation was performed by paired *t* test. Expression data from Brase *et al.* were downloaded from the GEO database (GSE54516). Genes showing altered expression (FDR $q < 0.05$; displayed in **Supplementary Table 1**) were ranked according to the degree of expression difference in each data set. Data used for the measurement of *BAZ2A* and *EZH2* expression in metastatic samples were downloaded from the GEO database (GSE3325 and GSE6919). For the investigation of potential mechanisms of BAZ2A downregulation, data from 12 prostate cancer samples were obtained from the European Genome-phenome Archive (hosted at the European Bioinformatics Institute; accession EGAS00001000400), which includes whole-genome sequencing, mate-pair genome sequencing, methylcytosine immunoprecipitation (MCIp) sequencing, RNA sequencing and miRNA sequencing data[2]. MiRNA targeting prediction was performed using miRGator[22]. Low-abundance miRNAs were filtered out by including only miRNAs with a coverage of at least 1,000 reads in normal and prostate cancer samples. Validation of miR-133a expression was performed on samples from Brase *et al.* using quantitative PCR. Statistical significance was evaluated by *t* test.

Cell culture. All the indicated cell lines were purchased from the American Type Culture Collection. PC3 cells were cultured in RPMI 1640 medium and Ham's F12 medium (1:1; Gibco) containing 10% FBS (Gibco) and 1% penicillin-streptomycin (Gibco). RWPE1 cells were cultured in Keratinocyte-SFM medium (Gibco) supplemented with human recombinant epidermal growth factor 1-53 (EGF 1-53) and bovine pituitary extract (BPE) and 1% penicillin-streptomycin. DU 145, LNCaP and BPH1 cells were cultured in RPMI 1640 medium containing 10% FBS and 1% penicillin-streptomycin. All cells were regularly tested for mycoplasma contamination.

Evaluation of miRNA targeting. Luciferase assays were performed in HEK293T cells grown in DMEM. Cells grown in 384-well plates were transfected with 5 nM miRNA mimics (Qiagen) or non-targeting control (AllStar Negative Control, Qiagen) using DharmaFECT1 (Thermo Fisher Scientific). *BAZ2A* 3′ UTR fragments of 300–1,609 bp in length were cloned into the pMIR-Report vector (Ambion) 3′ to the firefly luciferase gene. The predicted miR-133a binding site was mutated using the QuikChange Site-Directed Mutagenesis kit (Stratagene). After 24 h, 0.3 ng of each pMIR-Report-BAZ2A 3′ UTR construct was mixed with 10 ng of the TK-*Renilla* plasmid (Promega) and was transfected into cells using TransIT-LT1 transfection reagent (Mirus Bio) with six replicates per construct. The readout was assessed 48 h after reporter transfection, as previously described[62]. Firefly luciferase activity was normalized to *Renilla* luciferase activity, and the average of technical replicates was calculated. Each experiment was performed in triplicate.

siRNA and shRNA transfections. Cells were seeded at a density of 12,000 cells/cm^2 and transfected with the indicated siRNAs using Lipofectamine RNAiMAX (Invitrogen) in Opti-MEM I Reduced-Serum Medium (Gibco). To achieve high siRNA transfection efficiencies, we performed reverse transfection in PC3 and DU145 cells and forward transfection in RWPE1 and LNCaP cells. Knockdown was analyzed 3–4 d after transfection by qRT-PCR or protein blot. Sequences encoding control shRNA and shRNA to *BAZ2A* were cloned into lentiviral vectors. Lentiviruses were generated in HEK293 cells and used to transduce 1×10^6 PC3 cells seeded on a 10-cm dish. Stable clones were selected with puromycin (0.4 µg/ml; Gibco).

RNA isolation, reverse transcription and quantitative RT-PCR. RNA was purified with TRIzol reagent (Invitrogen) according to the manufacturer's protocol. RNA (1 µg) was reverse transcribed using random hexamers. qRT-PCR was performed on a Rotor-Gene RG-3000 A (Corbett Research) using the SensiMix SYBR Hi-ROX Mix (Bioline). Relative transcription levels were determined by normalizing to *GAPDH* or *ACTB* mRNA levels. The statistical significance (*P* value) of the difference in expression levels for a gene was calculated using a two-sample paired *t* test. Sequences for the primer used in qRT-PCR are listed in **Supplementary Table 12**.

Cell proliferation assays. Twenty-four hours after transfection with the relevant siRNA or miRNA, cells (1×10^5) were seeded in 6-well plates. On each following day, cells from two distinct wells were counted using a cell counter (CASY, model TT, Roche). For WST1 assays, 1 d after siRNA transfections, 3×10^3 (PC3) or 4×10^3 (RWPE1) cells were seeded in each well of a 96-well plate. Cell proliferation and viability were determined every following day by the addition of Cell Proliferation Reagent WST-1 (Roche) according to the manufacturer's instructions.

Immunofluorescence. Cells were grown on coverslips coated with 0.01% poly-L-lysine (Sigma-Aldrich) and permeabilized with 0.05% Triton X-100 in 20 mM Tris-HCl (pH 8), 5 mM $MgCl_2$, 0.5 mM EDTA and 25% glycerol. After washing with PBS, cells were fixed with cold methanol (7 min) and stained with antibodies to BAZ2A (Diagenode, CS-090-100; 1:40 dilution) and UBF (Santa Cruz Biotechnology, sc-13125; 1:40 dilution) and with Hoechst 33258 (Sigma-Aldrich). Immunofluorescent images were digitally recorded with a Leica DMI 6000 B microscope.

Cell synchronization and FACS analysis. Cells were synchronized at G1/S through treatment with 2 mM thymidine (Sigma-Aldrich) for 14 h, released for 9 h and then treated for 14 h with 400 µM L-mimosine (Sigma-Aldrich). After being released from the L-mimosine block (here referred to as $t = 0$ h), cells at the indicated time points were trypsinized, washed with PBS, fixed with ice-cold ethanol at −20 °C and stained with propidium iodide (20 µg/ml). Cell cycle analysis was performed by flow cytometry on a CyAn ADP Analyzer (Beckman Coulter).

Colony formation assays. Cells were seeded in 6-well plates at a concentration of 500 cells/well and grown for 8 d. The colony formation potential of each clone expressing control shRNA or shRNA to *BAZ2A* was determined in triplicate using three six-well plates. Cells were stained with crystal violet (0.5% crystal violet in 20% methanol) for 3 min, destained by washing three times with 2 ml of water and air dried.

Boyden chamber invasion assays. Twenty-four hours after transfection, cells were starved for 24 h in growth medium containing 1% FBS. Boyden chamber invasion assays were performed according to the manufacturer's protocol. Briefly, 40,000 cells were subjected to Matrigel-coated cell inserts (BD Biosciences, 354480) in starvation medium (0% FBS). Growth medium containing 10% FBS was used as a chemoattractant for 18 h. Invaded cells were fixed with 100% methanol and visualized using Hoechst 33258 (Sigma-Aldrich). Membranes were mounted to glass slides, and cell numbers were quantified using a DMI6000 B microscope (Leica).

Scratch wound healing assays. siRNA-treated PC3 cells were seeded in triplicate in six-well plates and grown until confluent. Identical scratches were generated with a 1,000-µl plastic pipette tip. Any cellular debris was removed by medium replacement. After 24 h, closure of the scratch by migrating cells was analyzed with an Olympus CKX31 microscope.

Senescence and apoptosis assays. Cellular senescence was analyzed with the Senescence β-Galactosidase Staining kit (Cell Signaling) according to the manufacturer's protocol. Apoptosis was investigated using the FITC Annexin V Apoptosis Detection Kit I (BD Biosciences) following the manufacturer's instructions, and subsequent FACS analysis was performed on a CyAn ADP Analyzer (Beckman Coulter).

PC3 and RWPE1 gene expression microarrays. Three (PC3 cells) or two (RWPE1 cells) independent knockdown experiments were performed for gene expression microarray analysis. RNA was isolated using the NucleoSpin RNA II kit (Macherey-Nagel) followed by on-column DNase digestion to remove any contaminating genomic DNA. Total RNA (100 ng) was reverse transcribed to double-stranded cDNA, which was linearly amplified and labeled with Cy3. After quantification using the NanoDrop spectrophotometer (Witec) and quality

assessment with the Agilent 2100 Bioanalyzer (Agilent Technologies), 1.6 µg of Cy3-labeled cRNA was hybridized to SurePrint G3 Human Exon 4x180K microarrays (Agilent Technologies) according to the manufacturer's protocol. Arrays were scanned with an Agilent G2565CA Microarray Scanner System (Scan Control Software 8.5, Agilent Technologies). Raw intensity data were obtained using Agilent's Feature Extraction Software version 10.7 for array image analysis and the calculation of spot intensity measurements. Data were analyzed with R Bioconductor. Between-array normalization was performed using quantile normalization. Differential expression was computed using the limma package. Heat maps were generated using the heatmap.2 function in the gplots package. Transcripts with a fold change of >1.5 or <0.66 ($\log_2$ ±0.58) in cells expressing *BAZ2A* or *EZH2* siRNA relative to control cells and $P < 0.05$ were considered to have a statistically significant difference in expression and were analyzed for GO enrichment using the Database for Annotation, Visualization and Integrated Discovery (DAVID) for the enrichment of GO terms.

Immunoprecipitation. Immunoprecipitation was performed by transfection of HEK293T cells with the expression vector pcDNA-Flag-HA-BAZ2A. Nuclear extracts were immunoprecipitated overnight at 4 °C using an immobilized antibody against Flag (Anti-FLAG M2 Affinity Gel, Sigma). Precipitates were washed three times with wash buffer (20 mM Tris-HCl (pH 7.8), 150 mM KCl, 5 mM $MgCl_2$, 0.2 mM EDTA, 10% glycerol, 0.1% Tween and 0.1 mM PMSF), separated on a 6% SDS-polyacrylamide gel and analyzed by immunoblotting.

Chromatin immunoprecipitation. ChIP analysis was performed as previously described[63]. Briefly, 1% formaldehyde was added to cultured cells to cross-link proteins to DNA. Isolated nuclei were then lysed in 300 µl of lysis buffer (50 mM Tris-HCl (pH 8.1), 10 mM EDTA and 1% SDS) and sonicated using a Bioruptor ultrasonic cell disruptor (Diagenode) to shear genomic DNA to an average fragment size of 200 bp. Chromatin (20 µg) was diluted tenfold with immunoprecipitation buffer (16.7 mM Tris-HCl (pH 8.1), 167 mM NaCl, 1.2 mM EDTA, 0.01% SDS and 1.1% Triton X-100) and then immunoprecipitated overnight with the indicated antibodies. After washing, elution and reversion of cross-links, the precipitated DNA was purified with phenol-chloroform, ethanol precipitated and quantified by quantitative PCR. Primer sequences and antibodies are listed in **Supplementary Tables 12** and **13**.

DNA methylation data analysis. Prostate tumor samples were selected histologically to have >70% tumor content. DNA was isolated from formalin-fixed paraffin-embedded material using the QIAamp DNA FFPE Tissue kit (Qiagen). DNA methylation analysis was performed using 450K BeadChip arrays (Illumina) according to the manufacturer's instructions. We extracted the raw methylation intensity data and performed subset quantile within-array normalization (SWAN)[46]. Probes with a detection *P* value of <0.01 were excluded from further analysis. The 5,000 most variable probes were selected for *k*-means consensus clustering by the ConsensusClusterPlus package with Spearman distance and average linkage over 1,000 resampling iterations with random restart. The optimal number of clusters was determined by the CDF and consensus clustering. Hierarchical clustering was then performed to visualize the methylation patterns within 35 samples. Gene set enrichment analysis was performed using GSEA tools (version 2-2.0.13) with Molecular Signatures Databases (MSigDB version 4.0) from the Broad Institute as previous described[64] with modifications. Statistical enrichment of the intersection of the gene lists for differential methylation and expression was performed using random permutation.

Tissue microarrays. Radical prostatectomy specimens were obtained from 11,152 patients undergoing surgery between 1992 and 2011 at the Department of Urology and the Martini Clinics at the University Medical Center Hamburg-Eppendorf. Follow-up data were available for a total of 9,628 patients, with a median follow-up of 36.8 months (range of 1 to 228 months; **Supplementary Table 9**). PSA values were measured quarterly during the first 3 years and then biannually following surgery, and recurrence was defined as a postoperative PSA value of 0.2 ng/ml and increasing at first appearance. All prostate specimens were analyzed according to a standard procedure, including complete embedding of the entire prostate for histological analysis[65]. The TMA manufacturing process was described earlier in detail[66]. All histological sections stained with hematoxylin and eosin from all prostatectomy specimens were reviewed for the purpose of this study, and the positions of tumors were marked on the slides. One 0.6-mm tissue core was punched from a preselected area of each tumor and transferred in a TMA. The punch site was selected to contain the highest possible fraction of tumor cells. The tissues were distributed among 24 TMA blocks, each containing 144 to 522 tumor samples. Presence or absence of cancer tissue was validated by immunohistochemical AMACR and 34BE12 analysis on adjacent TMA sections. For internal controls, each TMA block also contained various control tissues, including normal prostate tissue.

Immunohistochemistry. Freshly cut TMA sections were immunostained in a single day and as one experiment. Primary antibody specific for BAZ2A (polyclonal, rabbit, Abnova, PAB21919; 1:150 dilution) was applied, and slides were deparaffinized and exposed to heat-induced antigen retrieval for 5 min in an autoclave at 121 °C in pH 7.8 Tris-EDTA buffer. Bound antibody was visualized using the EnVision kit (Dako). All stainings were analyzed by a single, experienced individual (K.G.). BAZ2A expression was predominantly localized to the nucleus, with lower expression levels in the cytoplasm of the cells. Nuclear BAZ2A staining was evaluated according to the following scoring system. The staining intensity (0, 1+, 2+ and 3+) and fraction of positive tumor cells were recorded for each tissue spot. A final immunohistochemistry score was built from these parameters as previously described[67–69]. Negative scores indicated the complete absence of staining; weak scores indicated a staining intensity of 1+ in ≤70% of tumor cells or a staining intensity of 2+ in ≤30% of tumor cells; moderate scores indicated a staining intensity of 1+ in >70% of tumor cells, a staining intensity of 2+ in >30% but ≤70% of tumor cells or a staining intensity of 3+ in ≤30% of tumor cells; and strong scores indicated a staining intensity of 2+ in >70% of tumor cells or a staining intensity of 3+ in >30% of tumor cells. As cytoplasmic BAZ2A staining was rare and typically associated with high nuclear staining levels, it was thus not considered for analysis.

Statistical analysis. To calculate whether the proportion of genes regulated by both BAZ2A and EZH2 was expected by chance, we used a combination of permutation and Fisher tests to calculate *P* values. Briefly, the number of overlaps between BAZ2A- and EZH2-regulated genes was determined, and we then performed random permutation of EZH2-regulated genes and computed the overlap with BAZ2A-regulated genes using 1,000 iterations. From the permutation, the mean numbers of overlapped and non-overlapped genes were obtained. Fisher's exact test was used to evaluate the statistical difference from the expected pattern.

Multivariate analysis. Four multivariate analyses were performed evaluating the clinical relevance of BAZ2A expression in different scenarios (listed in **Supplementary Table 9**). Scenario 1 used all postoperatively available parameters, including clinical stage, nodal status, margin status, preoperative PSA value and Gleason grade obtained on the resected prostate. Scenario 2 used all postoperatively available parameters with the exception of nodal status. The rationale for this approach was that lymphadenectomy is not a routine procedure in the surgical therapy of prostate cancer and that excluding nodal status in multivariate analysis increases case number. The next two scenarios tried to better model the preoperative situation. Scenario 3 included BAZ2A expression, preoperative PSA value, clinical stage and the Gleason grade obtained on the prostatectomy specimen. Because postoperative Gleason grade varies from preoperative Gleason grade, another multivariate analysis was added as scenario 4. In this scenario, the preoperative Gleason grade obtained on the original diagnostic biopsy was combined with the preoperative PSA value, clinical stage and BAZ2A expression.

61. Li, B. & Dewey, C.N. RSEM: accurate transcript quantification from RNA-Seq data with or without a reference genome. *BMC Bioinformatics* **12**, 323 (2011).
62. Metzig, M. *et al.* An RNAi screen identifies USP2 as a factor required for TNF-α–induced NF-κB signaling. *Int. J. Cancer* **129**, 607–618 (2011).
63. Santoro, R. Analysis of chromatin composition of repetitive sequences: the ChIP-Chop assay. *Methods Mol. Biol.* **1094**, 319–328 (2014).
64. Subramanian, A., Kuehn, H., Gould, J., Tamayo, P. & Mesirov, J.P. GSEA-P: a desktop application for Gene Set Enrichment Analysis. *Bioinformatics* **23**, 3251–3253 (2007).

doi:10.1038/ng.3165

65. Schlomm, T. *et al.* Clinical significance of p53 alterations in surgically treated prostate cancers. *Mod. Pathol.* **21**, 1371–1378 (2008).
66. Mirlacher, M. & Simon, R. Recipient block TMA technique. *Methods Mol. Biol.* **664**, 37–44 (2010).
67. Minner, S. *et al.* High level PSMA expression is associated with early PSA recurrence in surgically treated prostate cancer. *Prostate* **71**, 281–288 (2011).
68. Grupp, K. *et al.* Cysteine-rich secretory protein 3 overexpression is linked to a subset of *PTEN*-deleted *ERG* fusion–positive prostate cancers with early biochemical recurrence. *Mod. Pathol.* **26**, 733–742 (2013).
69. Muller, J. *et al.* Loss of pSer2448-mTOR expression is linked to adverse prognosis and tumor progression in *ERG*-fusion-positive cancers. *Int. J. Cancer* **132**, 1333–1340 (2013).

doi:10.1038/ng.3165 NATURE GENETICS

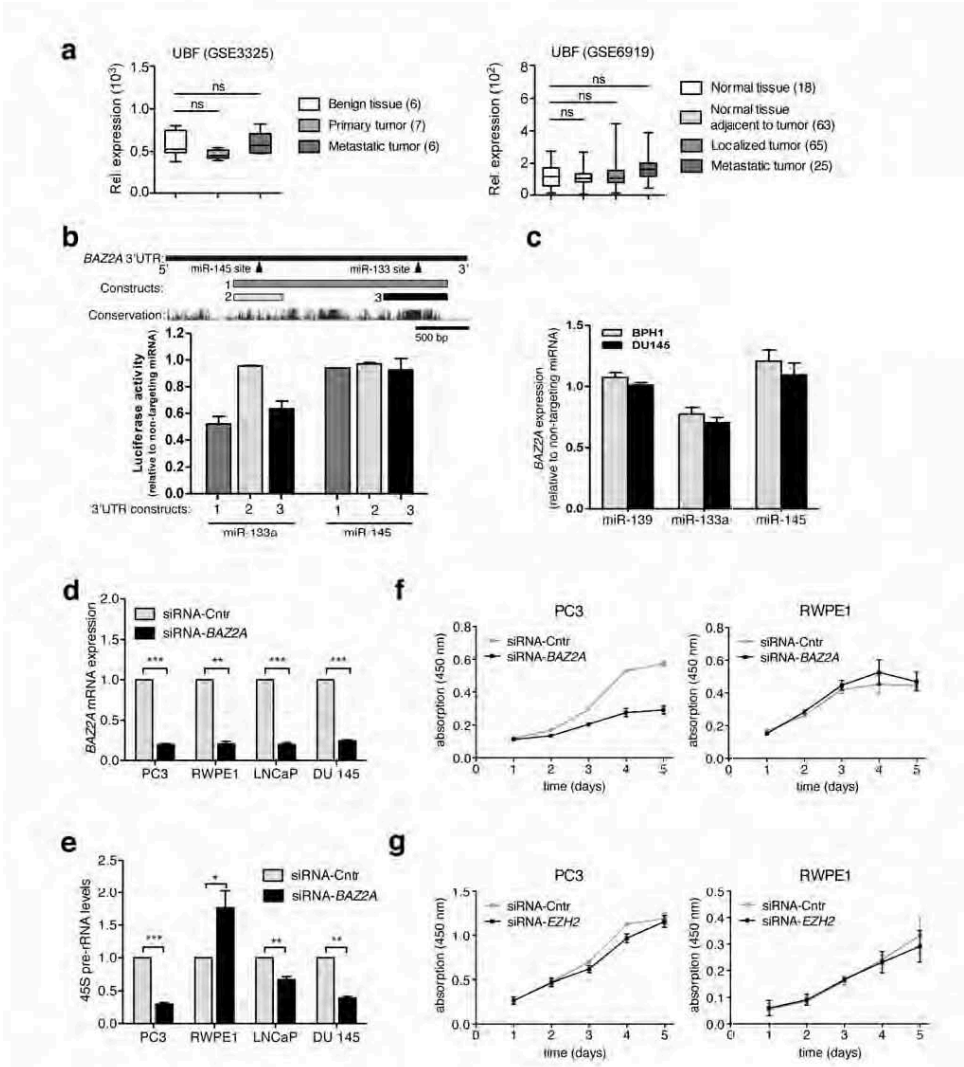

Supplementary Figure 1

Overexpression of BAZ2A via downregulation of miR-133a influences cell proliferation in prostate cancer.

Related to **Figure 1**. (**a**) Related to **Figure 1b**. Expression profiles of the upstream binding factor UBF from data sets GSE3325 and GSE6919. (**b**) Related to **Figure 1d**. Luciferase assays evaluating the direct interaction of miRNAs with the *BAZ2A* 3' UTR. miR-133a specifically interacts with a distal conserved site in the 3' UTR, while another miRNA, miR-145, although predicted to target the 3' UTR, does not interact. (**c**) Related to **Figure 1e**. Overexpression of miR-133a results in the downregulation of *BAZ2A* in the BPH1 and DU145 prostate cell lines in comparison to other miRNAs, miR-139 and miR-145, used as negative controls. Expression was measured

Nature Genetics: doi:10.1038/ng.3165

by three independent primer-probe pairs relative to the average of *GAPDH*, *ACTB* and *HPRT*. Each experiment was performed in triplicate for each cell line. (**d**) Related to **Figure 1f**. qRT-PCR showing the efficiency of *BAZ2A* knockdown of the indicated cell lines after treatment with siRNA-*BAZ2A*. (**e**) Related to **Figure 1f**. qRT-PCR showing 45S pre-rRNA transcript levels for the indicated cells after treatment with siRNA-*BAZ2A*. Data represent the average of three to four independent experiments. (**f**) Related to **Figure 1f**. Cell viability measured by WST1 assay of PC3 and RWPE1 cells treated with siRNA-*BAZ2A*. Data represent the average of two independent experiments. (**g**) Related to **Figure 1g**. WST1 assay of PC3 and RWPE1 cells treated with siRNA-*EZH2*. Data represent the average of two independent experiments.

Nature Genetics: doi:10.1038/ng.3165

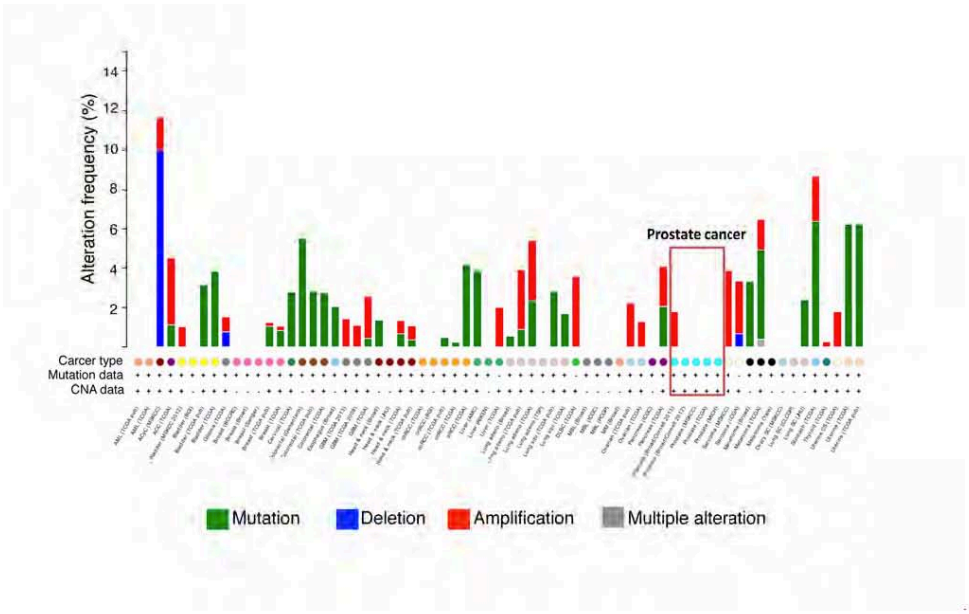

Supplementary Figure 2

Interrogation of the rate of genetic alterations in the *BAZ2A* locus.

Related to **Figure 1**. Histogram showing the frequency of mutations and copy number alterations in the *BAZ2A* locus using all publically available TCGA data sets, including 69 cancer studies obtained from the cBio database. Highlighted are the five prostate cancer studies, which show an overall lack of genetic aberrations. Only 1 case showed amplification in a total of 514 prostate adenocarcinoma samples investigated, and 0 cases showed aberrations in 61 metastatic samples (green bars, mutation; red bars, amplification; blue bars, deletion; gray bars, multiple deletions).

Nature Genetics: doi:10.1038/ng.3165

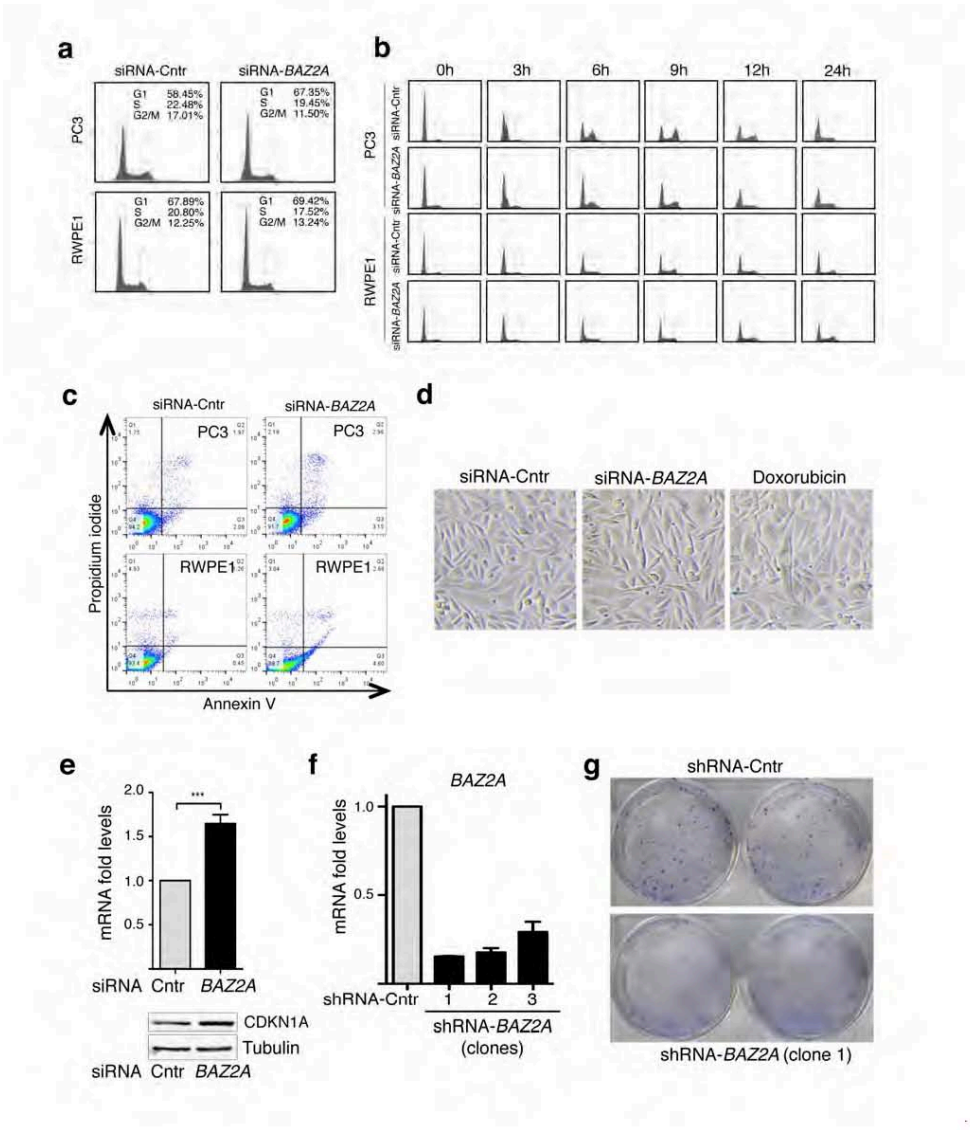

Supplementary Figure 3

BAZ2A influences the cell cycle progression of prostate cancer cells.

Related to **Figure 2**. (**a**) Depletion of *BAZ2A* does not induce apoptosis. PC3 and RWPE1 cells were labeled with Annexin V–AlexaFluor 647 and propidium iodide. (**b**) Depletion of *BAZ2A* does not induce senescence. *In vitro* senescence analysis was performed by measuring β-gal activity in PC3 cells depleted of *BAZ2A* by siRNA. Treatment with doxorubin served as a positive control

Nature Genetics: doi:10.1038/ng.3165

for staining. (**c**) Flow cytometry analysis of PC3 and RWPE1 cells depleted of *BAZ2A* by siRNA treatment. Images are representative of two independent experiments. (**d**) Flow cytometry analysis of PC3 and RWPE1 cells synchronized at G1/S and at the indicated time points after release into S phase. Images are representative of two independent experiments. (**e**) Expression of CDKN1A is upregulated upon knockdown of *BAZ2A* in PC3 cells. Top, qRT-PCR showing *BAZ2A* mRNA levels. Upregulation of *CDKN1A* was also consistent with microarray data for PC3 cells ($\log_2$ fold change = 0.66, $P = 0.005$ upon siRNA-*BAZ2A* treatment; $\log_2$ fold change = 0.84, $P = 0.001$ upon siRNA-*EZH2* treatment; **Supplementary Table 3**). No changes were detected in RWPE1 cells upon siRNA-*BAZ2A* treatment (**Supplementary Table 4**). Bottom, CDKN1A immunoblots of PC3 cells depleted of *BAZ2A* by siRNA. (**f**) Related to **Figure 2f**. qRT-PCR showing reduction in *BAZ2A* expression in PC3 cell lines stably expressing shRNA-*BAZ2A*. Data were normalized to *GAPDH* mRNA levels. (**g**) Related to **Figure 2f**. Clonogenic assay of PC3 cells expressing shRNA-*BAZ2A*. Cells (500) were cultured in a 6-well plate for 8 d. Crystal violet staining showed the presence of dense (shRNA-Control) and dispersed (shRNA-*BAZ2A*) cell colonies. Images are representative of three independent experiments.

Nature Genetics: doi:10.1038/ng.3165

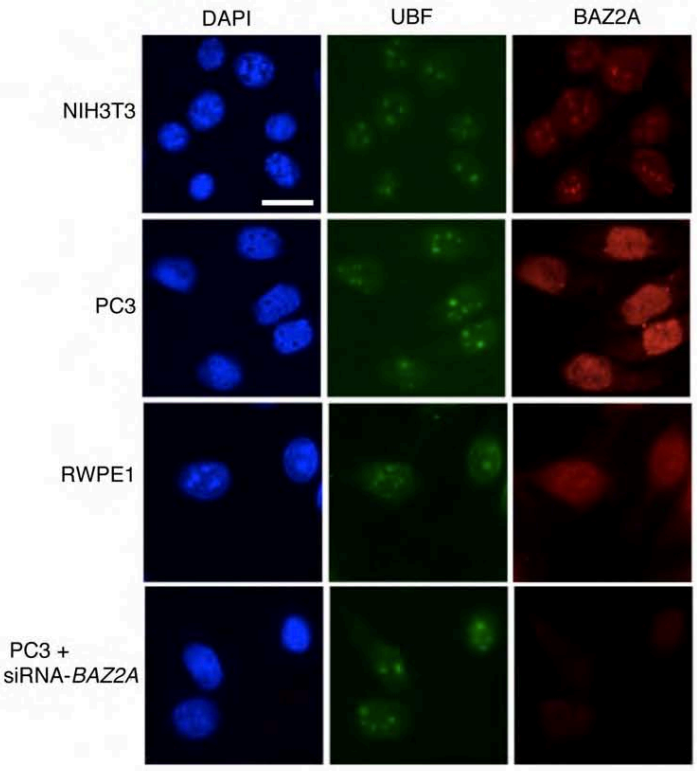

Supplementary Figure 4

A nucleoplasmatic BAZ2A fraction characterizes PC3 and RWPE1 cells.

Related to **Figure 3**. Immunofluorescence analysis of BAZ2A in mouse NIH3T3 cells and human PC3 and RWPE1 cells. Signal for UBF was used to visualize nucleoli. Whereas in mouse fibroblast cells BAZ2A is mainly localized within nucleoli, both PC3 and RWPE1 cells show an abundant nucleoplasmatic fraction. The specificity of the antibody to BAZ2A was verified by the lack of signal in PC3 cells depleted of *BAZ2A* by siRNA-*BAZ2A* treatment.

Nature Genetics: doi:10.1038/ng.3165

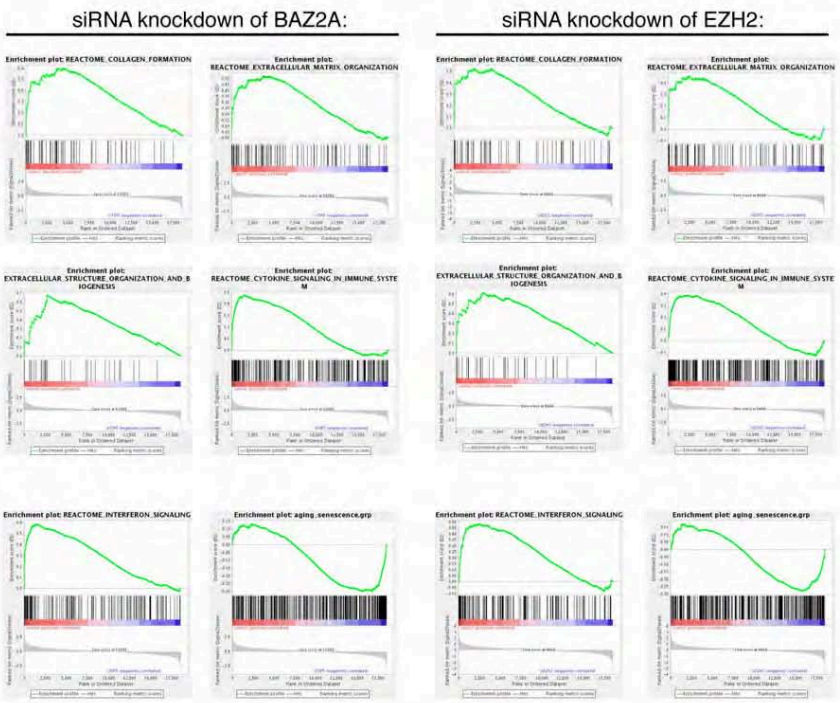

Supplementary Figure 5

Gene set enrichment analysis following knockdown of *BAZ2A* or *EZH2* in PC3 cells.

Related to **Figure 3**. Significant gene sets were chosen for display to highlight the regulation of similar prostate cancer–relevant pathways by BAZ2A and EZH2. For a complete list of significant gene sets, see **Supplementary Table 5**.

Nature Genetics: doi:10.1038/ng.3165

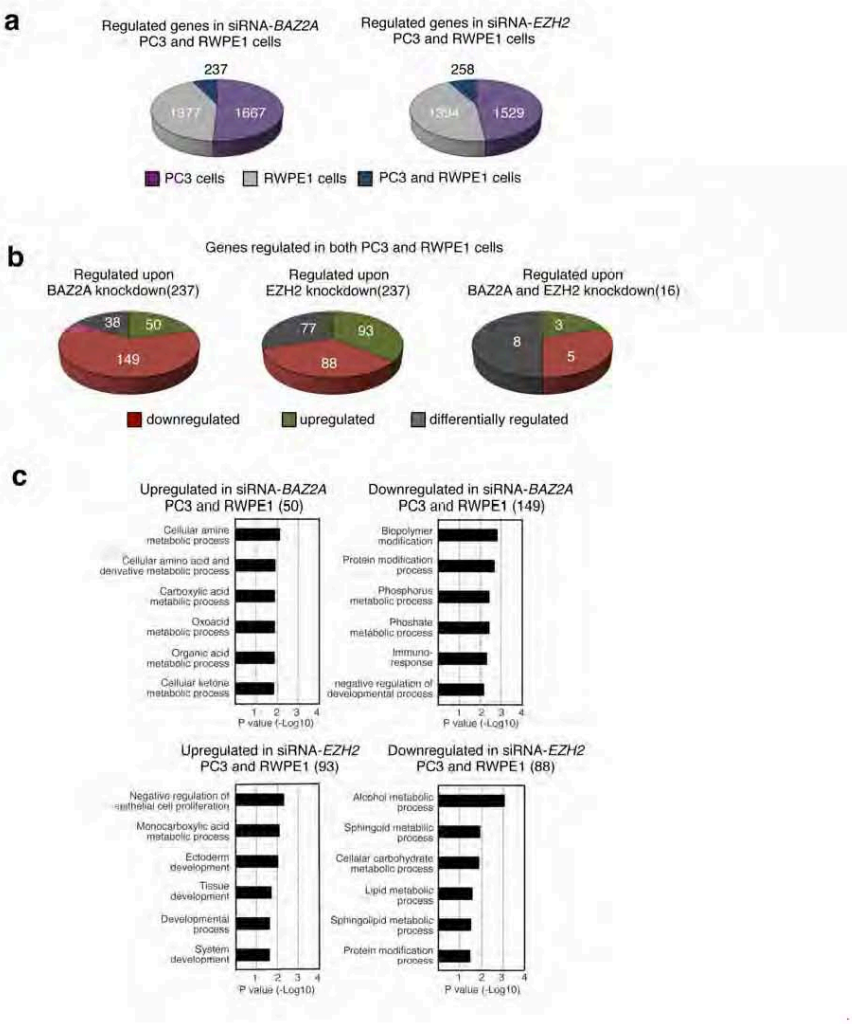

Supplementary Figure 6

Genes regulated by BAZ2A and EZH2 in both PC3 and RWPE1 cells do not act on relevant common biological processes. Related to **Figure 3**. (**a**) Venn diagrams showing genes regulated in both PC3 and RWPE1 cells upon knockdown of *BAZ2A* and *EZH2*. (**b**) Diagrams showing the effects on expression of genes regulated by BAZ2A, EZH2 or both BAZ2A and EZH2 in PC3 and RWPE1 cells. (**c**) Top six biological process gene ontology (GO) terms as determined using the Database for Annotation, Visualization and Integrated Discovery (DAVID) for genes up- and downregulated upon *BAZ2A* and *EZH2* knockdown in PC3 and RWPE1 cells. The data determined that genes common in PC3 and RWPE1 cells do not display any relevant biological pathways.

Nature Genetics: doi:10.1038/ng.3165

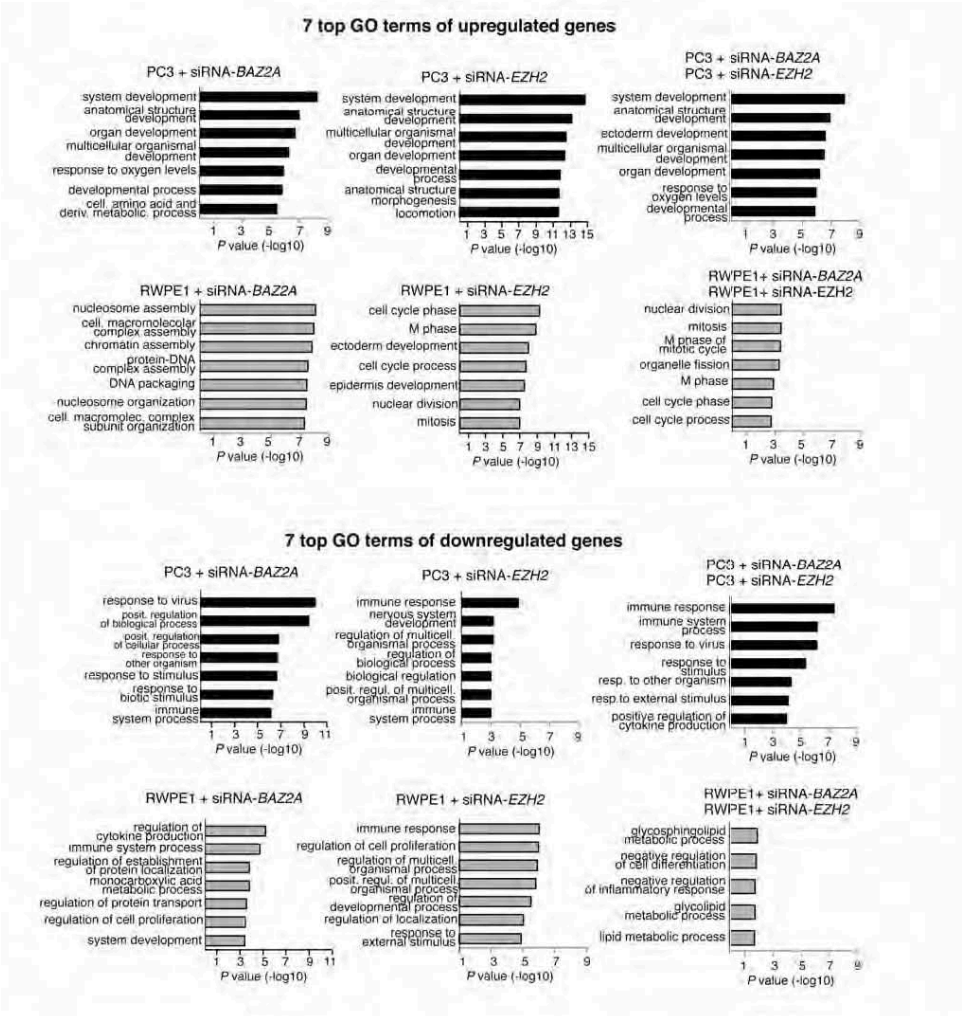

Supplementary Figure 7

BAZ2A- and EZH2-regulated genes show a substantial overlap of biological pathways in PC3 but not in RWPE1 cells.

Related to **Figure 3**. The top seven biological process gene ontology (GO) terms in PC3 and RWPE1 cells as determined using DAVID.

Nature Genetics: doi:10.1038/ng.3165

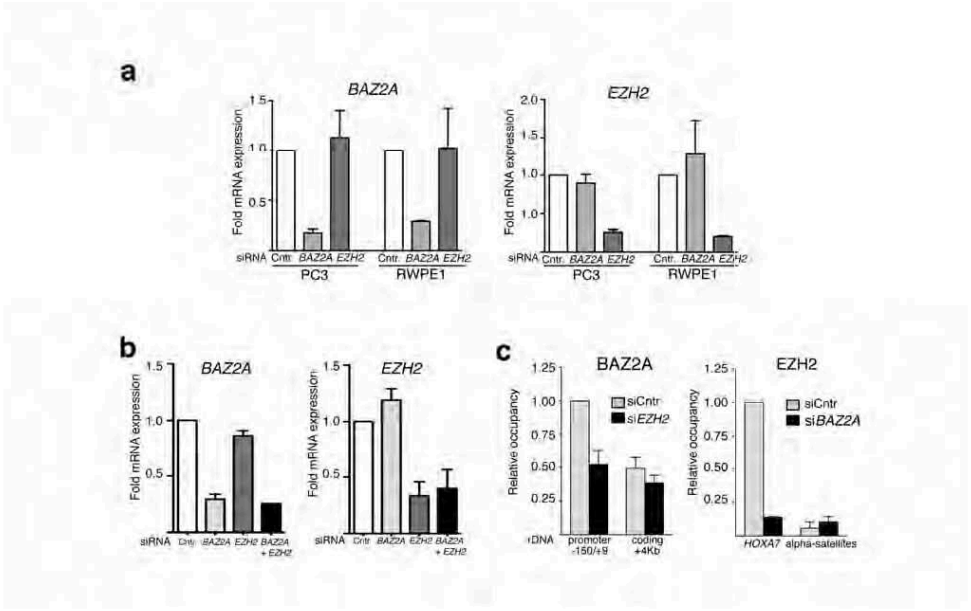

Supplementary Figure 8

BAZ2A and EZH2 coordinate gene repression in prostate cancer cells.

Related to **Figure 4**. (**a**) Related to **Figure 3d**. Knockdown efficiency of *BAZ2A* and *EZH2* in PC3 and RWPE1 cells. Data were normalized to *GAPDH* mRNA levels. (**b**) Related to **Figure 4d**. Knockdown efficiency of *BAZ2A* and *EZH2* in PC3 cells. Data were normalized to GAPDH mRNA levels. (**c**) Related to **Figure 4b,e**. Specificity of the described ChIP assay. The association of BAZ2A with the rDNA promoter is greater than with the rDNA coding region. EZH2 does not associate with α-satellites. Data are normalized to input and to association with the rDNA promoter (left) and the *HOXA7* promoter (right) in PC3 cells treated with siRNA-Control.

Nature Genetics: doi:10.1038/ng.3165

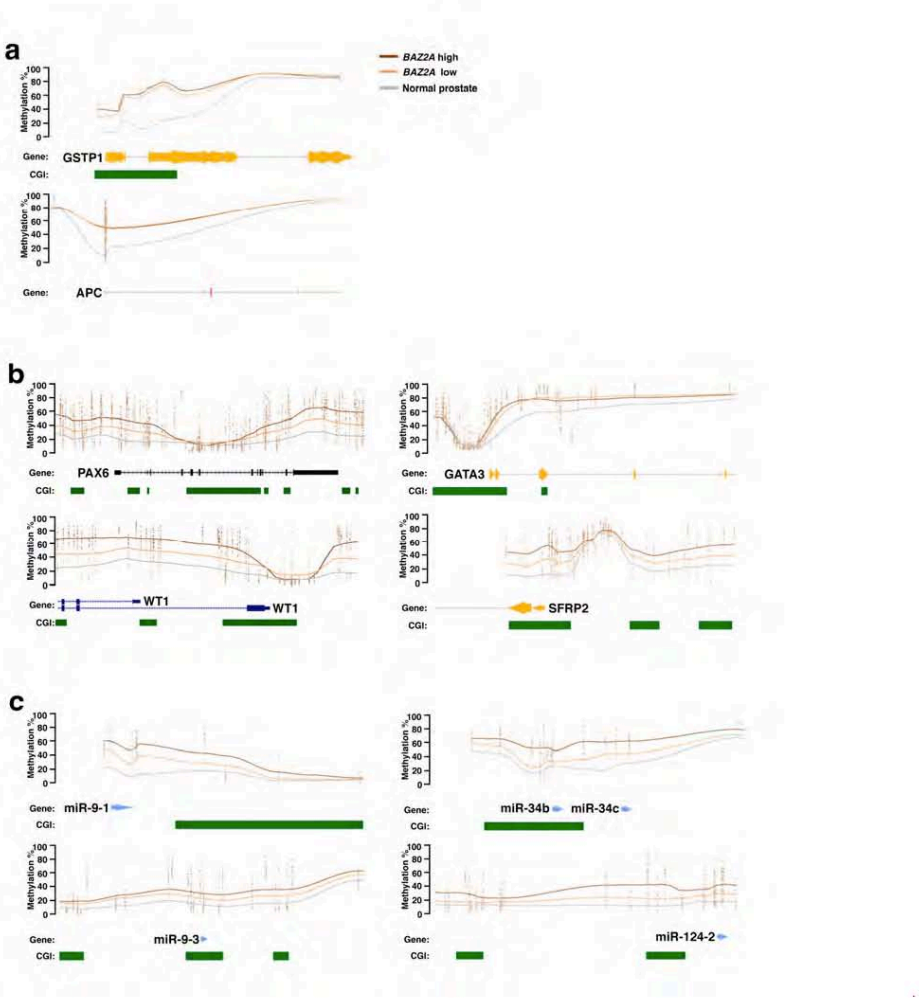

Supplementary Figure 9

Levels of DNA methylation found at the promoters of prostate cancer–relevant genes selected from 450k analysis.

Related to **Figure 5**. (**a**) *GSTP1* and *APC* are consistently hypermethylated in all prostate tumor samples relative to normal samples, demonstrating that tumor content does not appreciably differ among tumor samples. (**b**) Hypermethylation of the known tumor suppressors *WT1* (*Int. J. Oncol.* **24**, 461–471, 2004), *PAX6* (ref.), *GATA3* (ref.) and *SFRP2* (ref.) occurs primarily in the CIMP$^+$/BAZ2A-high subtype. (**c**) Hypermethylation of miRNAs 9-1, 9-3, 124-2, 34b and 34c, known to regulate androgen receptor expression, also occurs primarily in the CIMP$^+$/BAZ2A-high subtype.

Nature Genetics: doi:10.1038/ng.3165

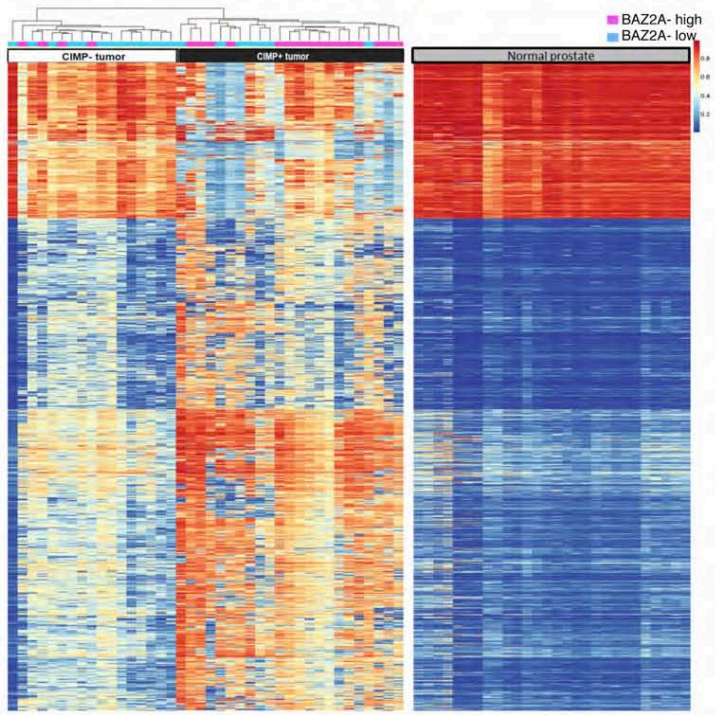

Supplementary Figure 10

Validation of global DNA methylation subtypes and association with BAZ2A expression in TCGA data.
Related to **Figure 5**. 450k DNA methylation prostate cancer profiles downloaded from the TCGA database were separated into the tumors with the 20 highest and lowest BAZ2A expression levels. Cluster analysis (using Euclidean distance measurement) of the top 3,000 most variable CpGs reveals 2 molecular subgroups, 1 that is similar to normal samples (normal-like subgroup) and 1 displaying profound hypermethylation (CIMP subgroup). High BAZ2A expression is associated with the CIMP subgroup. The heat map to the right shows normal prostate samples.

Nature Genetics: doi:10.1038/ng.3165

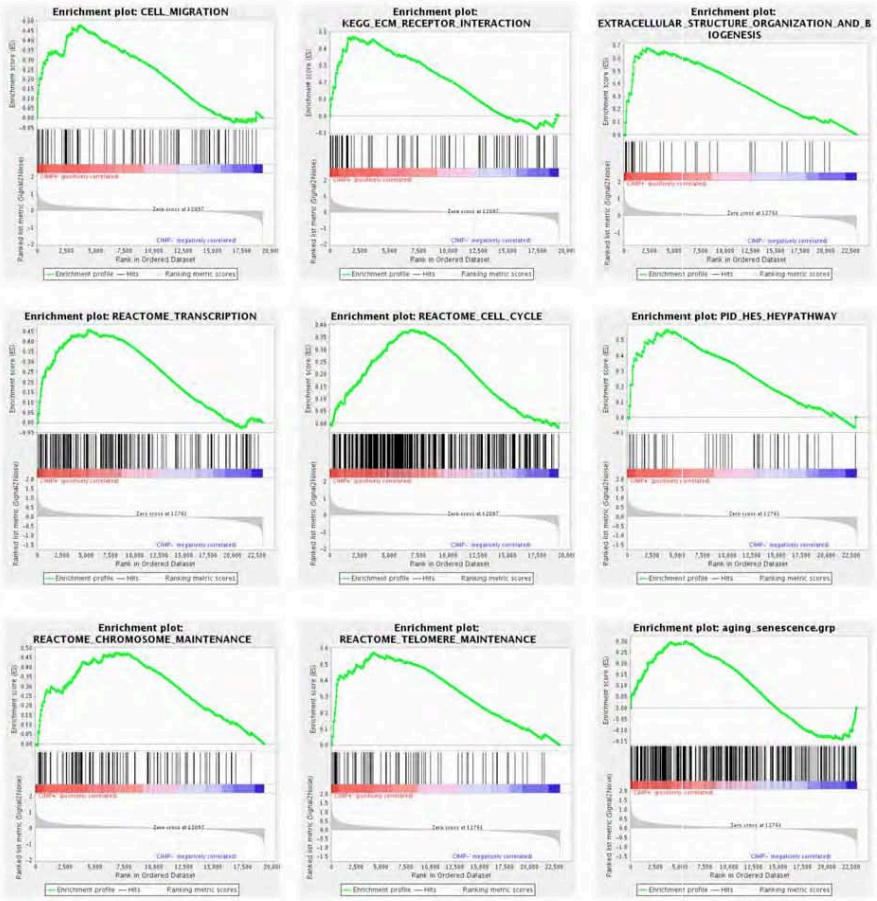

Supplementary Figure 11

Gene set enrichment analysis in BAZ2A-high tumors.
Related to **Figure 5**. Gene set enrichment analysis for prostate cancer–relevant pathways and gene ontology terms found to be significantly overrepresented (FDR $q < 0.05$) in BAZ2A-high/CIMP-like versus BAZ2A-low/normal-like tumors.

Nature Genetics: doi:10.1038/ng.3165

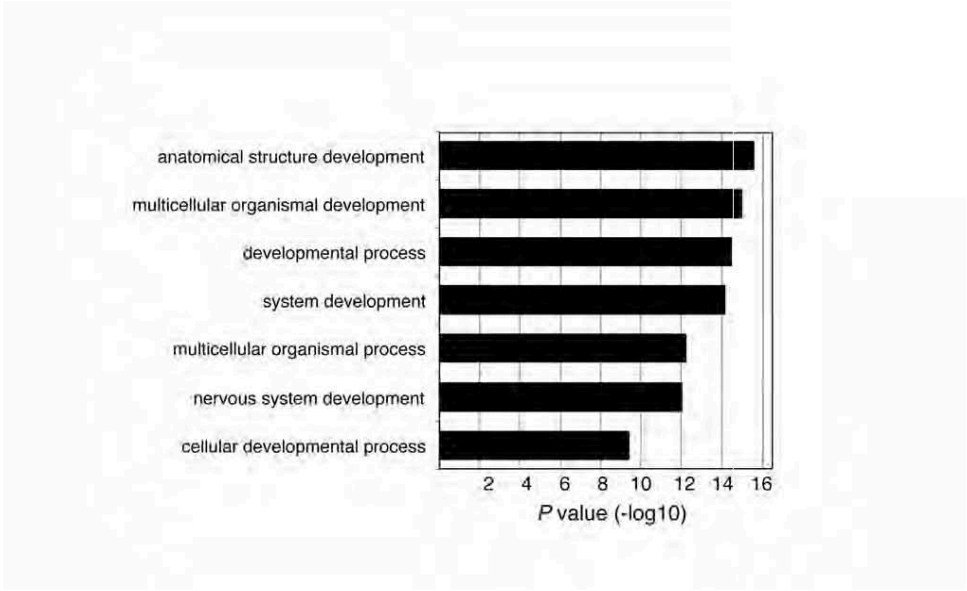

Supplementary Figure 12

Gene ontology analysis in BAZ2A-high tumors.
Related to **Figure 5**. Top seven biological process gene ontology (GO) terms of genes with hypermethylated promoters in BAZ2A-high versus BAZ2A-low tumors as determined using DAVID.

Nature Genetics: doi:10.1038/ng.3165

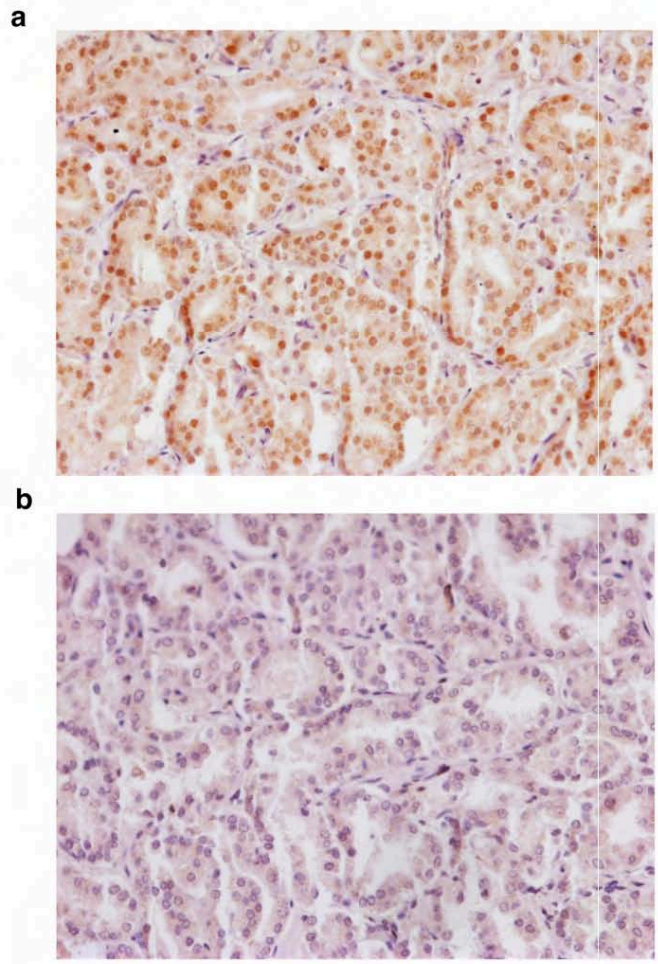

Supplementary Figure 13

BAZ2A staining of prostate tumor specimens.
Related to **Figure 6**. Wide-field micrographs of representative prostate tumor specimens showing positive (**a**) and negative (**b**) BAZ2A staining.

Nature Genetics: doi:10.1038/ng.3165

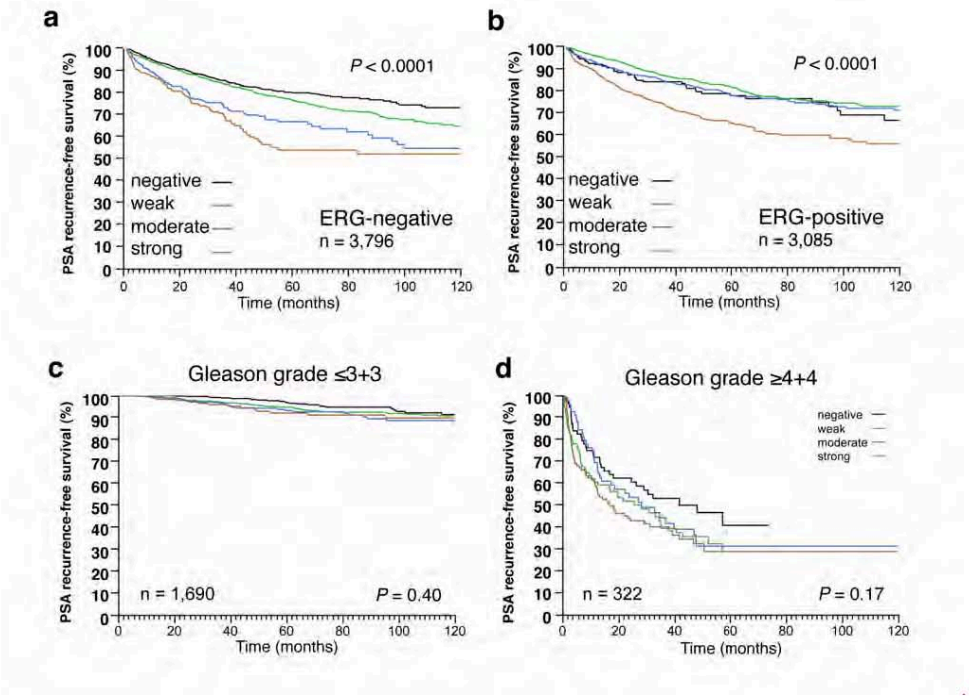

Supplementary Figure 14

PSA recurrence-free survival.
Related to **Figure 6**. PSA recurrence-free survival in (**a**) *ERG*-negative, (**b**) *ERG*-positive, (**c**) Gleason grade ≤3+3 (indolent prostate cancer) and (**d**) Gleason grade ≥4+4 (high-risk) patients.

Nature Genetics: doi:10.1038/ng.3165

Supplementary Note

German ICGC Project on Early Onset Prostate Cancer.
Members contributing to this work:

Roland Eils, Benedikt Brors:
[1]Division of Theoretical Bioinformatics, German Cancer Research Center (DKFZ), Heidelberg, Germany

Christoph Plass, Christopher Oakes, Lei Gu:
[2]Division of Epigenomics and Cancer Risk Factors, German Cancer Research Center (DKFZ), Heidelberg, Germany

Guido Sauter, Ronald Simon:
[5]Institute of Pathology, University Medical Center Hamburg-Eppendorf, Hamburg, Germany

Holger Sültmann, Rupert Kuner:
[9]Unit Cancer Genome Research, German Cancer Research Center (DKFZ) and National Center of Tumour Diseases, Heidelberg, Germany

Marie-Laure Yaspo:
[12]Max Planck Institute for Molecular Genetics, Berlin, Germany.

Jan Korbel:
[13]Genome Biology Unit, European Molecular Biology Laboratory (EMBL), Heidelberg, Germany

Thorsten Schlomm:
[14]Martini-Clinic, Prostate Cancer Center, University Medical Center Hamburg-Eppendorf, Hamburg, Germany

Nature Genetics: doi:10.1038/ng.3165

Supplementary Table 2: MiRNAs predicted to target *BAZ2A* and their expression in PCa.

miRNA	No. of prediction algorithms	Correlation value (miR-Gator)	Expression EOPCa (RPKM)	Fold change EOPCa (T/N)	*P*-value (corrected)
miR-133a	**5**	**1**	**12487**	**0.46**	**<0.01**
miR-125b	4	2	561413	0.35	<0.01
miR-99a	4	2	646877	0.52	<0.05
miR-99b	4	1	77822	0.57	*n.s.*
miR-100	4	3	448182	0.61	*n.s.*
miR-145	4	2	56057	0.70	*n.s.*
miR-214	4	2	5793	0.84	*n.s.*
miR-181a	4	1	30777	0.91	*n.s.*
miR-101	4	3	20506	2.23	*n.s.*

Nature Genetics: doi:10.1038/ng.3165

Supplementary Table 5a: The list of gene sets that are enriched following BAZ2A knockdown in PC3 cells using GSEA.

NAME	SIZE	ES	NES	Nominal p-value	FDR q-value
aging_senescence.grp	352	-0.30	-1.51	0.0000	0.0000
BIOCARTA_MPR_PATHWAY	33	-0.58	-2.03	0.0022	0.0137
BIOCARTA_PTDINS_PATHWAY	23	-0.68	-2.08	0.0000	0.0100
KEGG_AMINOACYL_TRNA_BIOSYNTHESIS	40	-0.64	-2.22	0.0000	0.0033
KEGG_LYSOSOME	121	-0.51	-2.27	0.0000	0.0000
KEGG_SNARE_INTERACTIONS_IN_VESICULAR_TRANSPORT	36	-0.60	-2.09	0.0000	0.0101
PID_INSULIN_PATHWAY	45	-0.54	-2.03	0.0000	0.0128
REACTOME_ACTIVATION_OF_CHAPERONE_GENES_BY_XBP1S	42	-0.55	-2.04	0.0000	0.0138
REACTOME_AMINO_ACID_SYNTHESIS_AND_INTERCONVERSION_TRANSAMINATION	16	-0.76	-2.19	0.0000	0.0033
REACTOME_CYTOSOLIC_TRNA_AMINOACYLATION	24	-0.68	-2.22	0.0000	0.0027
REACTOME_MITOCHONDRIAL_PROTEIN_IMPORT	49	-0.53	-2.01	0.0000	0.0140
REACTOME_SRP_DEPENDENT_COTRANSLATIONAL_PROTEIN_TARGETING_TO_MEMBRANE	108	-0.44	-1.90	0.0000	0.0488
REACTOME_TRANS_GOLGI_NETWORK_VESICLE_BUDDING	59	-0.50	-1.93	0.0000	0.0366
REACTOME_TRANSLATION	145	-0.48	-2.16	0.0000	0.0040
REACTOME_TRNA_AMINOACYLATION	42	-0.57	-2.08	0.0000	0.0089
REACTOME_UNFOLDED_PROTEIN_RESPONSE	73	-0.49	-2.00	0.0000	0.0157
REACTOME_INTERFERON_ALPHA_BETA_SIGNALING	59	0.76	2.82	0.0000	0.0000
REACTOME_INTERFERON_SIGNALING	150	0.59	2.55	0.0000	0.0000
PID_SYNDECAN_1_PATHWAY	46	0.54	1.97	0.0000	0.0159
REACTOME_CLASS_A1_RHODOPSIN_LIKE_RECEPTORS	296	0.41	1.92	0.0000	0.0293
REACTOME_COLLAGEN_FORMATION	58	0.60	2.22	0.0000	0.0010
REACTOME_COMPLEMENT_CASCADE	28	0.61	1.90	0.0000	0.0332
REACTOME_CYTOKINE_SIGNALING_IN_IMMUNE_SYSTEM	257	0.47	2.20	0.0000	0.0007
REACTOME_EXTRACELLULAR_MATRIX_ORGANIZATION	86	0.52	2.05	0.0000	0.0047
REACTOME_INTERFERON_GAMMA_SIGNALING	59	0.60	2.21	0.0000	0.0007
REACTOME_PEPTIDE_LIGAND_BINDING_RECEPTORS	183	0.43	1.90	0.0000	0.0314
REACTOME_REGULATION_OF_COMPLEMENT_CASCADE	13	0.75	1.97	0.0000	0.0148
GO_EXTRACELLULAR_STRUCTURE_ORGANIZATION_AND_BIOGENESIS	30	0.67	2.16	0.0000	0.0028
GO_LEUKOCYTE_DIFFERENTIATION	38	0.55	1.91	0.0000	0.0460
KEGG_ALANINE_ASPARTATE_AND_GLUTAMATE_METABOLISM	32	-0.55	-1.88	0.0000	0.0227
KEGG_NICOTINATE_AND_NICOTINAMIDE_METABOLISM	23	-0.59	-1.83	0.0086	0.0360
KEGG_VALINE_LEUCINE_AND_ISOLEUCINE_BIOSYNTHESIS	11	-0.69	-1.79	0.0061	0.0393
REACTOME_CHEMOKINE_RECEPTORS_BIND_CHEMOKINES	54	0.50	1.84	0.0000	0.0380
REACTOME_GOLGI_ASSOCIATED_VESICLE_BIOGENESIS	52	-0.49	-1.88	0.0022	0.0473
REACTOME_MAPK_TARGETS_NUCLEAR_EVENTS_MEDIATED_BY_MAP_KINASES	30	-0.55	-1.87	0.0064	0.0432
REACTOME_METABOLISM_OF_PROTEINS	419	-0.36	-1.88	0.0000	0.0440
REACTOME_NEGATIVE_REGULATORS_OF_RIG_I_MDA5_SIGNALING	30	0.56	1.81	0.0018	0.0483
REACTOME_RECYCLING_PATHWAY_OF_L1	26	-0.60	-1.90	0.0000	0.0412

ES, enrichment score; NES, normalized enrichment score; FDR, false-discovery rate

Nature Genetics: doi:10.1038/ng.3165

Supplementary Table 5b: The list of gene sets that are enriched following EZH2 knockdown in PC3 cells using GSEA.

NAME	SIZE	ES	NES	Nominal p-value	FDR q-value
aging_senescence.grp	352	-0.28	-1.33	0.0071	0.0071
REACTOME_GRB2_EVENTS_IN_ERBB2_SIGNALING	22	-0.79	-2.31	0.0000	0.0000
REACTOME_SHC1_EVENTS_IN_ERBB4_SIGNALING	20	-0.72	-2.07	0.0000	0.0213
REACTOME_TRIGLYCERIDE_BIOSYNTHESIS	38	-0.61	-2.02	0.0000	0.0363
REACTOME_SOS_MEDIATED_SIGNALLING	14	-0.76	-1.99	0.0000	0.0373
REACTOME_INTERFERON_ALPHA_BETA_SIGNALING	59	0.62	2.24	0.0000	0.0009
REACTOME_GENERIC_TRANSCRIPTION_PATHWAY	338	0.44	2.01	0.0000	0.0140
REACTOME_INTERFERON_SIGNALING	150	0.48	2.02	0.0000	0.0206
REACTOME_CHOLESTEROL_BIOSYNTHESIS	21	0.67	1.94	0.0038	0.0353
REACTOME_BASIGIN_INTERACTIONS	24	-0.63	-1.92	0.0000	0.0379
REACTOME_COLLAGEN_FORMATION	58	0.53	1.89	0.0000	0.0449
GO_T_CELL_DIFFERENTIATION	15	0.80	2.10	0.0000	0.0038
KEGG_TERPENOID_BACKBONE_BIOSYNTHESIS	15	0.70	1.85	0.0000	0.0372
REACTOME_EXTRACELLULAR_MATRIX_ORGANIZATION	86	0.46	1.75	0.0000	0.0000
REACTOME_CYTOKINE_SIGNALING_IN_IMMUNE_SYSTEM	257	0.39	1.73	0.0000	0.0000
GO_EXTRACELLULAR_STRUCTURE_ORGANIZATION_AND_BIOGENESIS	30	0.62	1.91	0.0019	0.0019

ES, enrichment score; NES, normalized enrichment score; FDR, false-discovery rate

Nature Genetics: doi:10.1038/ng.3165

Supplementary Table 8: List of enriched gene sets that show differential DNA methylation between BAZ2A-high versus low tumors using GSEA.

NAME	ES	Nominal p-value	FDR q-value
GO_SYNAPSE_ORGANIZATION_AND_BIOGENESIS	1.99	0.0000	0.0000
GO_SYNAPTOGENESIS	1.91	0.0000	0.0000
GO_REGULATION_OF_CELL_MIGRATION	1.83	0.0000	0.0000
GO_EXTRACELLULAR_STRUCTURE_ORGANIZATION_AND_BIOGENESIS	1.83	0.0000	0.0000
GO_BRAIN_DEVELOPMENT	1.83	0.0000	0.0000
GO_NERVOUS_SYSTEM_DEVELOPMENT	1.79	0.0000	0.0000
GO_NEGATIVE_REGULATION_OF_CELL_MIGRATION	1.79	0.0000	0.0000
GO_SYNAPTIC_TRANSMISSION	1.78	0.0000	0.0000
GO_TRANSMISSION_OF_NERVE_IMPULSE	1.74	0.0000	0.0000
GO_NEUROLOGICAL_SYSTEM_PROCESS	1.73	0.0000	0.0000
GO_AMINO_ACID_TRANSPORT	1.72	0.0000	0.0000
GO_CELL_MIGRATION	1.72	0.0000	0.0000
GO_CELL_CELL_SIGNALING	1.63	0.0000	0.0000
GO_G_PROTEIN_COUPLED_RECEPTOR_PROTEIN_SIGNALING_PATHWAY	1.60	0.0000	0.0000
GO_COLLAGEN_BINDING	1.80	0.0000	0.0000
GO_TRANSCRIPTION_FACTOR_ACTIVITY	1.59	0.0000	0.0000
REACTOME_RNA_POL_I_PROMOTER_OPENING	2.02	0.0000	0.0000
REACTOME_RNA_POL_I_TRANSCRIPTION	1.95	0.0000	0.0000
REACTOME_MEIOTIC_RECOMBINATION	1.83	0.0000	0.0000
REACTOME_AMYLOIDS	1.82	0.0000	0.0000
REACTOME_RNA_POL_I_RNA_POL_III_AND_MITOCHONDRIAL_TRANSCRIPTION	1.82	0.0000	0.0000
REACTOME_PACKAGING_OF_TELOMERE_ENDS	1.81	0.0000	0.0000
REACTOME_TELOMERE_MAINTENANCE	1.76	0.0000	0.0000
REACTOME_CHROMOSOME_MAINTENANCE	1.74	0.0000	0.0000
REACTOME_MEIOSIS	1.73	0.0000	0.0000
REACTOME_TRANSCRIPTION	1.71	0.0000	0.0000
REACTOME_DNA_REPLICATION	1.58	0.0000	0.0000
REACTOME_CELL_CYCLE	1.58	0.0000	0.0000
REACTOME_MITOTIC_M_M_G1_PHASES	1.49	0.0000	0.0000
KEGG_SYSTEMIC_LUPUS_ERYTHEMATOSUS	1.87	0.0000	0.0000
KEGG_NEUROACTIVE_LIGAND_RECEPTOR_INTERACTION	1.69	0.0000	0.0000
REACTOME_TRANSMISSION_ACROSS_CHEMICAL_SYNAPSES	1.51	0.0012	0.0213
REACTOME_MEIOTIC_SYNAPSIS	1.78	0.0013	0.0213
REACTOME_DEPOSITION_OF_NEW_CENPA_CONTAINING_NUCLEOSOMES_AT_THE_CENTROMERE	1.67	0.0013	0.0213
KEGG_BASAL_CELL_CARCINOMA	1.70	0.0014	0.0361
KEGG_AMYOTROPHIC_LATERAL_SCLEROSIS_ALS	1.70	0.0014	0.0361
KEGG_REGULATION_OF_ACTIN_CYTOSKELETON	1.46	0.0023	0.0479
REACTOME_CELL_CYCLE_MITOTIC	1.41	0.0033	0.0490
REACTOME_NEURONAL_SYSTEM	1.43	0.0034	0.0490
REACTOME_G_ALPHA_I_SIGNALLING_EVENTS	1.45	0.0036	0.0493

ES, enrichment score

Nature Genetics: doi:10.1038/ng.3165

Supplementary Table 9: Composition of the prostate prognosis tissue microarray containing 11,152 prostate cancer specimens.

	No. of patients	
	Study cohort on TMA, n=11,152 *	**Biochemical relapse rate in category, n=1,824 ****
Follow-up (mo)		
Mean	53	-
Median	37	-
Age (y)		
<50	318 (3%)	49 (18%)
50-60	2,768 (25%)	460 (19%)
60-70	6,548 (59%)	1,081 (19%)
>70	1,439 (13%)	232 (19%)
Pretreatment PSA (ng/ml)		
<4	1,407 (13%)	142 (11%)
4-10	6,735 (61%)	827 (14%)
10-20	2,159 (20%)	521 (28%)
>20	720 (7%)	309 (49%)
pT category (AJCC 2002)		
pT2	7,370 (66%)	570 (9%)
pT3a	2,409 (22%)	587 (28%)
pT3b	1,262 (11%)	618 (55%)
pT4	63 (1%)	49 (80%)
Gleason grade		
≤3+3	2,859 (26%)	193 (8%)
3+4	6,183 (56%)	849 (16%)
4+3	1,565 (14%)	573 (42%)
≥4+4	482 (4%)	208 (50%)
pN category		
pN0	6,117 (92%)	1,126 (21%)
pN+	561 (8%)	291 (59%)
Surgical margin		
negative	8,984 (82%)	1,146 (15%)
positive	1,970 (18%)	642 (37%)

* / ** numbers do not always add up to 11,152/1,824 in categories because of cases with missing data.
Abbreviation: AJCC, American Joint Committee on Cancer. *** p value not significant (ns) >0.05

Nature Genetics: doi:10.1038/ng.3165

Supplementary Table 10a: Associations between nuclear BAZ2A expression results and prostate cancer phenotype in all cancers.

Parameter	n Evaluable	IHC result				*P*
		Negative (%)	Weak (%)	Moderate (%)	Strong (%)	
All cancers	7682	26	37	18	19	
Tumor stage						< 0.0001
pT2	4872	29	38	18	15	
pT3a	1763	22	35	19	24	
pT3b	951	19	33	20	29	
pT4	59	24	31	17	29	
Gleason grade						< 0.0001
≤3+3	1791	32	43	15	11	
3+4	4340	26	36	20	19	
4+3	1163	20	33	19	29	
≥4+4	341	21	25	21	34	
Lymph node metastasis						< 0.0001
N0	4376	25	35	19	21	
N+	422	18	32	20	31	
Preoperative PSA level (ng/mL)						< 0.0001
<4	877	19	36	21	23	
4-10	4594	27	36	19	18	
10-20	1543	27	36	18	19	
>20	567	30	37	14	19	
Surgical mergin						0.0005
Negative	6051	26	37	19	18	
Positive	1488	24	35	18	23	

NOTE. Number do not always add up to 7682 in different categories because of cases with missing data

Nature Genetics: doi:10.1038/ng.3165

Supplementary Table 10b: Associations between nuclear BAZ2A expression results and prostate cancer phenotype in ERG-negative tumors.

Parameter	n Evaluable	IHC result				*P*
		Negative (%)	Weak (%)	Moderate (%)	Strong (%)	
All cancers	3786	37	37	13	11	
Tumor stage						< 0.0001
pT2	2508	42	38	12	8	
pT3a	780	36	37	15	12	
pT3b	459	27	37	14	23	
pT4	27	37	22	22	19	
Gleason grade						< 0.0001
≤3+3	825	48	40	8	4	
3+4	2127	39	38	14	9	
4+3	605	30	35	16	19	
≥4+4	213	27	28	20	26	
Lymph node metastasis						< 0.0001
N0	2206	37	38	14	12	
N+	200	26	30	19	27	
Preoperative PSA level (ng/mL)						0.0089
<4	367	32	38	14	16	
4-10	2246	39	38	13	10	
10-20	826	38	36	14	12	
>20	311	43	35	11	11	
Surgical mergin						0.018
Negative	2997	39	38	13	10	
Positive	720	38	37	12	14	

NOTE. Number do not always add up to 3786 in different categories because of cases with missing data

Nature Genetics: doi:10.1038/ng.3165

Supplementary Table 10c: Associations between nuclear BAZ2A expression results and prostate cancer phenotype in ERG-positive tumors.

Parameter	n Evaluable	IHC result				*P*
		Negative (%)	Weak (%)	Moderate (%)	Strong (%)	
All cancers	3085	9	35	26	30	
Tumor stage						< 0.0001
pT2	1801	10	37	27	26	
pT3a	841	9	34	23	34	
pT3b	402	7	30	27	37	
pT4	23	9	39	9	43	
Gleason grade						< 0.0001
≤3+3	686	11	45	26	19	
3+4	1806	10	34	27	29	
4+3	465	6	29	23	42	
≥4+4	104	6	17	23	54	
Lymph node metastasis						0.5818
N0	1767	9	33	26	33	
N+	186	8	31	24	38	
Preoperative PSA level (ng/mL)						0.0044
<4	401	6	34	28	32	
4-10	1870	10	33	27	29	
10-20	559	7	38	25	30	
>20	209	12	39	17	32	
Surgical mergin						0.059
Negative	2390	9	36	26	28	
Positive	637	8	33	25	34	

NOTE. Number do not always add up to 3085 in different categories because of cases with missing data

Nature Genetics: doi:10.1038/ng.3165

Supplementary Table 11a: Multivariate analysis of nuclear BAZ2A status in ERG-negative prostate cancer

Scenario	N evaluable	*P*							
		Preoperative PSA-level	pT stage	cT stage	Gleason grade prostatectomy	Biopsy Gleason grade	Lymph node metastasis	Surgical margin	BAZ2A expression on TMA
1	2034	0.0062	<0.0001	-	<0.0001	-	<0.0001	0.0034	0.0199
2	3230	<0.0001	<0.0001	-	<0.0001	-	-	0.0006	0.0006
3	3186	<0.0001	-	<0.0001	<0.0001	-	-	-	0.0007
4	3145	<0.0001	-	0.0003	-	<0.0001	-	-	0.0001

Supplementary Table 11b: Multivariate analysis of nuclear BAZ2A status in ERG-positive prostate cancer

Scenario	N evaluable	*P*							
		Preoperative PSA-level	pT stage	cT stage	Gleason grade prostatectomy	Biopsy Gleason grade	Lymph node metastasis	Surgical margin	BAZ2A expression on TMA
1	1673	0.0349	<0.0001	-	<0.0001	-	0.0077	0.0134	<0.0001
2	2655	0.0008	<0.0001	-	<0.0001	-	-	0.0039	<0.0001
3	2584	<0.0001	-	<0.0001	<0.0001	-	-	-	<0.0001
4	2537	<0.0001	-	<0.0001	-	<0.0001	-	-	<0.0001

Nature Genetics: doi:10.1038/ng.3165

Supplementary Table 12: List of primers used in this work

cDNA primers		
Name	**Forward/Reverse**	**Sequence**
BAZ2A	For	AAGATGTGTGGCTACAATGG
BAZ2A	Rev	TCTGCACCCATCAGCTCCG
EZH2	For	TACTTGTGGAGCCGCTGAC
EZH2	Rev	CTGCCACGTCAGATGGTG
rDNA promoter	For	CGATGGTGGCGTTTTTGG
rDNA promoter	Rev	GACAGGTCGCCAGAGGACAGC
rDNA 4kb	For	CGACGACCCATTCGAACGTCT
rDNA 4 kb	Rev	CTCTCCGGAATCGAACCCTGA
LAMB3	For	GCTTGTGGCCCTGAGGCTGG
LAMB3	Rev	TGGGCATTGAAGCCCCGCAG
ZNF185	For	AGCAGCCCCAGCGGATCTGA
ZNF185	Rev	GTCCTGCCAGGCCTCTCCGA
AOX1	For	CCGACAAGCCCAGCGACAGG
AOX1	Rev	GTGGCTGGACCAACGCCTCC
HOMER2	For	TTGACGCAGAGCGCAGCCAA
HOMER2	Rev	TGCAGTGCTGTGGTCAGCCG
HOXA7	For	CCTACGGCAACCTGCCCTGC
HOXA7	Rev	GCGCCTTTGGCGAGGTCACT
KLF6	For	ACCTCCGACCCCATTGGCGA
KLF6	Rev	AAGTCCCGCTGCGCACCTTC
FBN1	For	GCCTCAACACCCGTGGGAGC
FBN1	Rev	GCACTCGTCCTGGTTGGGGC
MKX	For	TCGGCCTGAGACACCGGAGG
MKX	Rev	CGTCATCTGCGAGCCGAGGG
FHL2	For	CCCATCACCACGGGAGGGGT
FHL2	Rev	CTGTGAGGAAGCCACGCCCC
CDKN1A	For	TGAGCCGCGACTGTGATG
CDKN1A	Rev	GTCTCGGTGACAAAGTCGAAGTT
GAPDH	For	TGCACCACCAACTGCTTAGC
GAPDH	Rev	GGCATGGACTGTGGTCATGAG
L28	For	GCAATTCCTTCCGCTACAAC
L28	Rev	TGTTCTTGCGGATCATGTGT
beta-ACTIN	For	ATCTGGCACCACACCTTCTACA
beta-ACTIN	Rev	TCACCGGAGTCCATCACGAT

Nature Genetics: doi:10.1038/ng.3165

ChIP primers		
Name	**Forward/Reverse**	**Sequence**
rDNA promoter	For	CGATGGTGGCGTTTTTGG
rDNA promoter	Rev	GACAGGTCGCCAGAGGACAGC
rDNA 4kb	For	CGACGACCCATTCGAACGTCT
rDNA 4 kb	Rev	CTCTCCGGAATCGAACCCTGA
LAMB3	For	AGGGCTAGTGTGCTCTAGGGGT
LAMB3	Rev	TGGGGTGATCCCCAGAAAGGACC
ZNF185	For	CAACGCTTGCCACCCCCGAT
ZNF185	Rev	TTGGTGCGGCCTCCAAGAGC
AOX1	For	GAACCAGCGCGGACACCACA
AOX1	Rev	GCTCACCTTGCGGCCGTTCA
HOXA7	For	CCTGTGAGGACTGCTGAGATTG
HOXA7	Rev	CCCCCAGATTTACACCAAACC
HOXB8	For	CCACAAAAAGTGTGTCGGCTTCGAG
HOXB8	Rev	TTCGCCGGCTCCTAGTCACCC
FHL2	For	AGGTTGCTGAAAAGCCAGGAGTCA
FHL2	Rev	AAGAGAGATTCGTTGCAATGGTGGC
KLF6	For	GCGCTCCGGGGAGACTTTCG
KLF6	Rev	GGGAGCACGTCCATGTCGGG
IL6	For	GGCACTGGCAGAAAACAACC
IL6	Rev	GCAAGTCTCCTCATTGAATCC
alpha-Satellite	For	CTGCACTACCTGAAGAGGAC
alpha-Satellite	Rev	GATGGTTCAACACTCTTACA
GAPDH	For	TACTAGCGGTTTTACGGGCG
GAPDH	Rev	TCGAACAGGAGGAGCAGAGAGCG

Nature Genetics: doi:10.1038/ng.3165

Supplementary Table 13: List of antibodies used in this work

Antibodies			
Name	**Manufacturer**	**Catalog number**	**Application (diluition)**
BAZ2A	Diagenode	CS-090-100	ChIP (1:25) IF (1:40)
BAZ2A	Abnova	PAB21919	TMA (1:150) WB (1:500)
EZH2	Cell Signaling	5246	ChIP (1:250)
UBF	Santa Cruz	sc-13125	IF (1:40)
H3K27me3	Millipore	17-622	ChIP (1:250)
H3K4me3	Millipore	07-473	ChIP (1:250)
HA	Santa Cruz	sc-7392	WB (1:1000)
CDKN1A	Santa Cruz	sc-397	WB (1:500)
Tubulin	Sigma-Aldrich	T6199	WB (1:1000)

Nature Genetics: doi:10.1038/ng.3165

Article

Cell Stem Cell

lncRNA Maturation to Initiate Heterochromatin Formation in the Nucleolus Is Required for Exit from Pluripotency in ESCs

Graphical Abstract

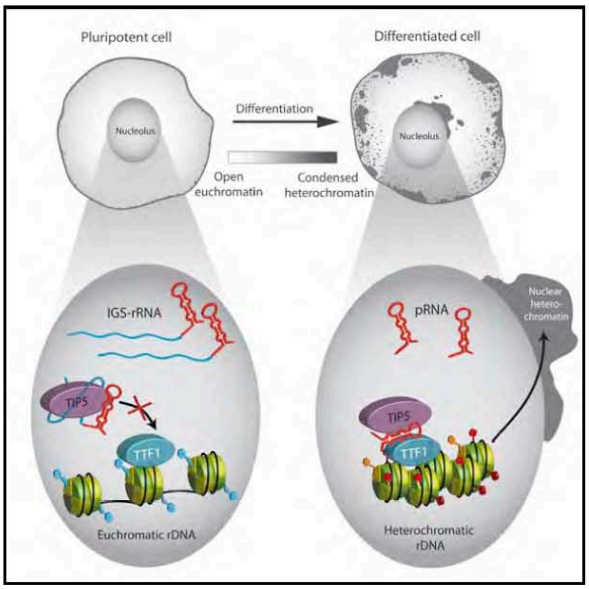

Highlights

rRNA genes (rDNA) acquire heterochromatin during ESC differentiation

Maturation of the lncRNA pRNA is required to establish rDNA heterochromatin

rDNA heterochromatin initiates heterochromatinization of ESC genomes

Inhibition of rDNA heterochromatin prevents ESC differentiation

Authors

Nataša Savić, Dominik Bär, ..., Paolo Cinelli, Raffaella Santoro

Correspondence

raffaella.santoro@vetbio.uzh.ch

In Brief

Savić et al. reveal that heterochromatin condensation in the nucleolus, where ribosomal genes are transcribed, triggers remodeling of the global open ESC chromatin into a highly condensed heterochromatic structure and that this mechanism is required for exit from pluripotency.

Savić et al., 2014, Cell Stem Cell 15, 720–734
December 4, 2014 ©2014 Elsevier Inc.
http://dx.doi.org/10.1016/j.stem.2014.10.005

CellPress

Cell Stem Cell
Article

lncRNA Maturation to Initiate Heterochromatin Formation in the Nucleolus Is Required for Exit from Pluripotency in ESCs

Nataša Savić,[1,2] Dominik Bär,[1] Sergio Leone,[1,2] Sandra C. Frommel,[1,2] Fabienne A. Weber,[2,3] Eva Vollenweider,[1,2] Elena Ferrari,[1] Urs Ziegler,[4] Andres Kaech,[4] Olga Shakhova,[5] Paolo Cinelli,[3,6,7] and Raffaella Santoro[1,6,*]
[1]Institute of Veterinary Biochemistry and Molecular Biology, University of Zurich, 8057 Zurich, Switzerland
[2]Molecular Life Science Program, Life Science Zurich Graduate School, University of Zurich, 8057 Zurich, Switzerland
[3]Institute of Laboratory Animal Science, University of Zurich, 8057 Zurich, Switzerland
[4]Center for Microscopy and Image Analysis, University of Zurich, 8057 Zurich, Switzerland
[5]Department of Oncology, University Hospital Zurich, 8952 Schlieren, Switzerland
[6]Center for Applied Biotechnology and Molecular Medicine, University of Zurich, 8057 Zurich, Switzerland
[7]Division of Trauma Surgery, Center for Clinical Research, University Hospital Zurich, 8091 Zurich, Switzerland
*Correspondence: raffaella.santoro@vetbio.uzh.ch
http://dx.doi.org/10.1016/j.stem.2014.10.005

SUMMARY

The open chromatin of embryonic stem cells (ESCs) condenses into repressive heterochromatin as cells exit the pluripotent state. How the 3D genome organization is orchestrated and implicated in pluripotency and lineage specification is not understood. Here, we find that maturation of the long noncoding RNA (lncRNA) pRNA is required for establishment of heterochromatin at ribosomal RNA genes, the genetic component of nucleoli, and this process is inactivated in pluripotent ESCs. By using mature pRNA to tether heterochromatin at nucleoli of ESCs, we find that localized heterochromatin condensation of ribosomal RNA genes initiates establishment of highly condensed chromatin structures outside of the nucleolus. Moreover, we reveal that formation of such highly condensed, transcriptionally repressed heterochromatin promotes transcriptional activation of differentiation genes and loss of pluripotency. Our findings unravel the nucleolus as an active regulator of chromatin plasticity and pluripotency and challenge current views on heterochromatin regulation and function in ESCs.

INTRODUCTION

The spatiotemporal organization of the genome has been recognized as an additional regulatory layer of chromatin, important for gene regulation and transcriptional competence (Gonzalez-Sandoval et al., 2013; Splinter and de Laat, 2011). Pluripotent stem cells such as embryonic stem cells (ESCs) are integral to the study of genome organization (Gorkin et al., 2014). Although ESCs organize their chromosomes into topological-associating domains that are largely invariant between cell types (Dixon et al., 2012; Nora et al., 2012), chromatin is generally less condensed and largely devoid of compact heterochromatin blocks compared to lineage-committed cells (Efroni et al., 2008; Jørgensen et al., 2007; Melcer et al., 2012; Meshorer et al., 2006). While ESC chromatin fibers occupy the entire nuclear volume, the highly compacted chromatin of differentiated cells is organized into discrete domains leading to large regions of the nucleus devoid of DNA (Fussner et al., 2010). Transcriptionally inactive chromatin in ESCs is unusually disorganized and tends to participate in fewer specific long-range interactions than in differentiated cells (de Wit et al., 2013). These results are consistent with a chromatin conformation that is particularly malleable and transcriptionally permissive in pluripotent cells and that may allow maintenance of a plastic state for the different transcriptional programs required for lineage specification (de Wit et al., 2013; Gaspar-Maia et al., 2011; Gorkin et al., 2014). Upon ESC differentiation, large-scale genome silencing takes place and ESC chromatin undergoes structural remodelling toward a highly condensed heterochromatic and transcriptionally repressed form (Bhattacharya et al., 2009; Meshorer and Misteli, 2006). These changes are also accompanied by alterations of nuclear architecture such as formation of large organized chromatin regions enriched in the heterochromatic and repressive histone modification H3K9 methylation (termed LOCKs) (Wen et al., 2009), maturation and compaction of constitutive heterochromatin (such as centric and pericentric repeats) and clustering of highly condensed heterochromatin either at the nucleolus or at the nuclear periphery (Aoto et al., 2006; Bártová et al., 2008a, 2008b; Efroni et al., 2008). However, how ESCs mediate the switch from a lower to a higher order chromatin structure remains elusive and calls for studies aimed at understanding the mechanism and function of this process.

An important component of nuclear architecture is the nucleolus, the compartment where transcription of hundreds of ribosomal RNA (rRNA) genes, rRNA processing, and ribosome subunit assembly take place (Moss and Stefanovsky, 2002). Clustering of highly condensed heterochromatin at nucleoli is a phenomenon known to occur in all somatic cells, yet neither the factors involved nor their physiological relevance is understood. Previous studies have however started to define a functional link between nuclear heterochromatin positioned in proximity to nucleoli and rRNA genes (rDNA), the genetic

component of the nucleolus. The nucleolar repressor factor TIP5 (TTF1-interacting protein 5, also known as BAZ2A) is required for heterochromatin formation of a fraction of rRNA genes through association with the long noncoding (lnc)RNA pRNA, DNA methyltransferases (DNMT1, DNMT3b), histone deacetylase HDAC1, and poly(ADP-ribose)-polymerase-1 (PARP1) (Guetg et al., 2012; Mayer et al., 2006; Santoro et al., 2002, 2010; Zhou et al., 2002). pRNA is a 250–300 nucleotide transcript corresponding to main rDNA promoter sequences and originates from processing of the 2 kb long IGS-rRNA (intergenic spacer rRNA) whose synthesis is driven by an alternative rDNA promoter located upstream of the main rDNA promoter (Mayer et al., 2006; Santoro et al., 2010). TIP5-pRNA interaction is necessary to form rDNA heterochromatin by mediating TIP5 nucleolar retention and association with rDNA and PARP1 (Guetg et al., 2012; Mayer et al., 2006). Depletion of TIP5 reduces silent epigenetic marks at rDNA and heterochromatic centric and pericentric repeats, and abrogates formation of condensed heterochromatic structures within and in proximity to the nucleolus (Guetg et al., 2010). Strikingly, this structural organization closely resembles the open chromatin of ESCs, prompting us to investigate if the chromatin state of the nucleolus regulates ESC chromatin plasticity and commitment to specific lineages.

RESULTS

Establishment of rDNA Heterochromatin Occurs during ESC Differentiation

We profiled the epigenetic state of the nucleolus, at rDNA, in ESCs and during differentiation into neural progenitor cells (NPCs) that are *Pax-6*, *Nestin*, and brain lipid-binding protein (*BLBP*) positive and do not express the pluripotency factor Nanog (Figure 1A; Figure S1A available online). Previous work showed that methylation of the two unique CpG dinucleotides at the mouse rDNA promoter distinguishes heterochromatic and silent rRNA genes from euchromatic, transcriptionally active rDNA (Santoro and Grummt, 2001). We quantified silent rDNA by measuring CpG methylation at rDNA promoter of ESCs, NPCs, and mouse somatic cells from brain tissue using HpaII digestion followed by qPCR, a method that accurately quantifies the amounts of silent rDNA (Santoro et al., 2002). Consistent with a previous bisulfite analysis (Schlesinger et al., 2009), rDNA promoter in ESCs displays very low meCpG levels, confirming the accuracy of our method. After 8 days of differentiation, a fraction of rRNA genes (25%–30%) acquired CpG methylation at levels comparable to brain tissue (Figure 1B). Similar results were obtained with a different ESC line and differentiation protocol (Figure S1B), indicating that rDNA is de novo methylated during early ESC differentiation. Consistent with these results, rDNA transcription levels were similar in NPCs and mouse fibroblast NIH 3T3 cells and lower than in ESCs (Figure 1C). Remarkably, rDNA methylation in induced pluripotent stem cells (iPSC) decreased to about one half when compared to the original fibroblasts (Figure 1D), implying a link between cell pluripotency and rDNA methylation levels. Upon differentiation, heterochromatin-related histone modifications H3K9me2, H3K9me3, and H3K27me3 increased at rDNA promoter and coding regions (Figure 1E; Figure S1C). In contrast, active histone modifications such as H3K4me2 and H3K4me3 were not greatly affected (Figure S1D). Consistent with previous reports, major and minor satellite repeats that compose centric and pericentric heterochromatin increased H3K9me3 levels during differentiation (Martens et al., 2005; Meshorer et al., 2006; Wong et al., 2009), whereas H3K9me2 occupancy was not greatly affected. These changes were accompanied by a reduction of major and minor satellite transcripts (Figure S1E), which are normally repressed in differentiated cells (Efroni et al., 2008). We conclude that formation of rDNA heterochromatin takes place during ESC-NPC transition and timely coincides with the switch to a higher condensed heterochromatic form of centric and pericentric repeats.

TIP5 Is Recruited to rDNA during ESC Differentiation

To determine how rDNA heterochromatin is established during ESC differentiation, we measured the association of upstream binding factor UBF, an essential rDNA transcription factor that exclusively binds to unmethylated, euchromatic rRNA genes, and of TIP5, which associates with methylated silent rDNA (Santoro and Grummt, 2001; Santoro et al., 2002). UBF occupancy at rDNA was lower in NPCs than in ESCs (Figure 1F), a further indication that the number of euchromatic active rRNA genes decreases during differentiation. In contrast, TIP5 binds to rDNA only in NPCs but not in ESCs (Figure 1F). Similarly, PARP1, previously shown to interact with TIP5 and implicated in the formation of rDNA heterochromatin (Guetg et al., 2012), increases its association with the rDNA promoter in NPCs. Thus, establishment of rDNA heterochromatin in ESC-NPC transcription is accompanied by a decrease in the association of factors specific to active genes and an increase in the binding of components of the rDNA silencing machinery.

TIP5 protein and mRNA levels were higher in ESCs than in NPCs (Figure 1G), implying that the lack of rDNA heterochromatin in ESC is independent of TIP5 amounts. We then analyzed the TIP5 cellular localization (Figure 1H; Figure S2). Consistent with previous results, TIP5 was exclusively localized within nucleoli of somatic MEFs, as indicated by the colocalization with the nucleolar protein UBF (Strohner et al., 2001). In contrast, the cellular localization of TIP5 in ESCs was predominantly nucleoplasmic and often excluded from the nucleoli. Upon differentiation, TIP5 was drastically reduced in the nucleoplasm and exclusively localized within the nucleoli of NPCs, showing a cellular localization that is characteristic of somatic cells (Figure 1H; Figure S2). We conclude that TIP5 association with rDNA is impaired in ESCs and its recruitment to rDNA is achieved upon ESC differentiation.

Processing of pRNA Mediates Formation of rDNA Heterochromatin

We reasoned that impairment of TIP5 binding to rDNA might be responsible for the lack of rDNA heterochromatin in ESCs. Previous studies implicated the lncRNA pRNA in TIP5 nucleolar retention and association with rDNA (Mayer et al., 2006). pRNA is a 250–300 nucleotide transcript corresponding to main rDNA promoter sequences and derives from processing of the 2 kb long IGS-rRNA (Mayer et al., 2006; Santoro et al., 2010) (Figure 2A). Measurements of pRNA sequences in ESCs and at different times of differentiation did not reveal remarkable differences between ESCs and NPCs (Figure 2B). However, this approach does not allow distinguishing between IGS-rRNA and mature pRNA.

Cell Stem Cell
The Nucleolus Regulates ESC Chromatin

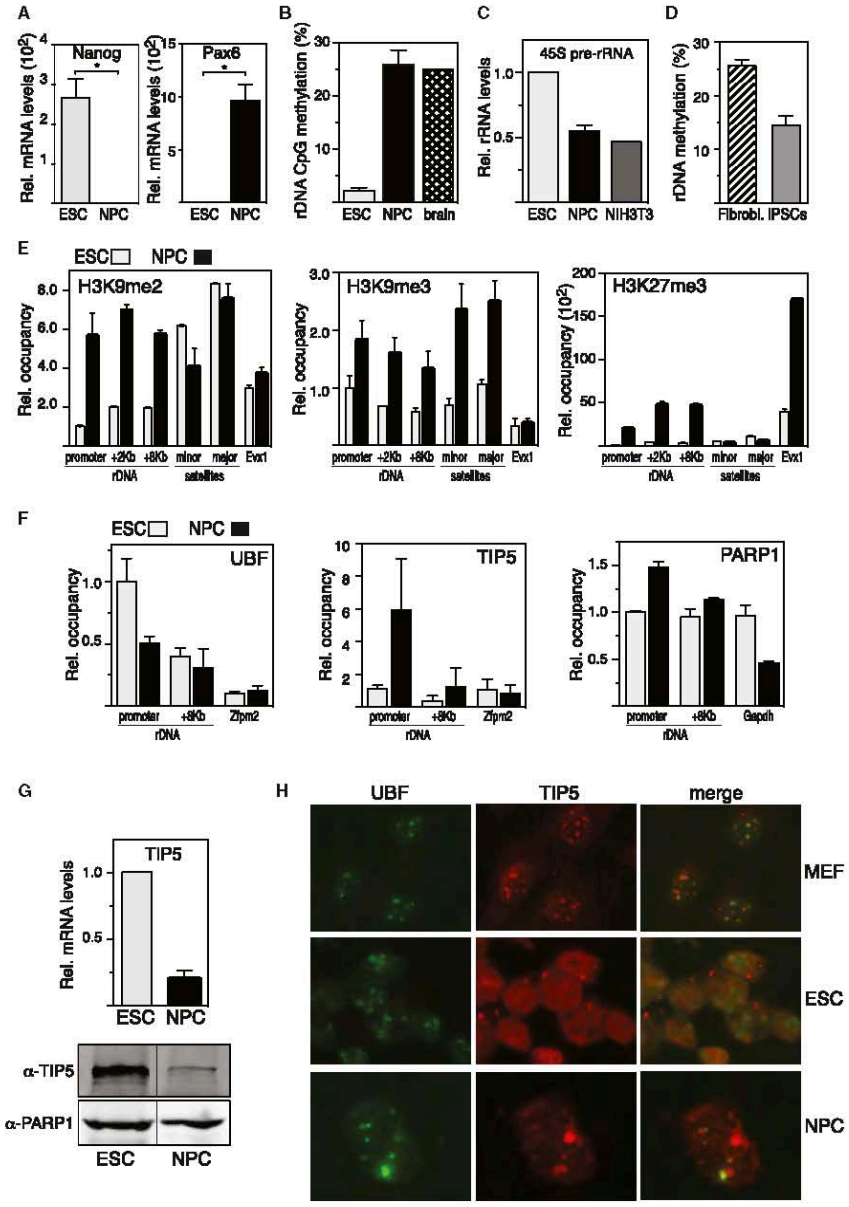

Figure 1. Establishment of rDNA Heterochromatin Occurs during ESC Differentiation and Correlates with the Recruitment of TIP5 to rDNA
(A) qRT-PCR. Nanog and Pax6 mRNA levels in ESCs and NPCs. Data were normalized to Rps12 mRNA.
(B) CpG methylation levels at rDNA promoter in ESCs, NPCs, and mouse brain tissues.

(legend continued on next page)

Quantification of 5′- and internal IGS-rRNA regions determined that unprocessed transcript levels were higher in ESCs than in NPCs (Figure 2B), suggesting that IGS-rRNA processing is less efficient in ESCs than in NPCs. To support these results, we measured ectopic IGS-rRNA and pRNA derived from an IGS-rRNA reporter gene plasmid that was transfected in NIH 3T3 cells, proficient for IGS-rRNA processing (Santoro et al., 2010), and in ESCs. Whereas ectopic IGS-rRNA was efficiently processed in NIH 3T3 cells (80%), maturation of pRNA was strongly reduced in ESCs (Figure 2C). Taken together, these results indicate that IGS-rRNA is not efficiently processed in ESCs and is thus less abundant in NPCs than in ESCs.

To test whether the lack of IGS-rRNA processing is the determinant that impairs formation of rDNA heterochromatin in ESCs, we transfected in vitro synthesized mature pRNA in ESCs and monitored TIP5 cellular localization, rDNA methylation, rDNA transcription, and H3K9me2 and H3K9me3 levels at rDNA (Figure 3). In ESCs transfected with pRNA, TIP5 decreased in the nucleoplasm and accumulated within nucleoli, as indicated by the colocalization with the nucleolar protein UBF (Figure 3A; Figure S3). Remarkably, the addition of pRNA in ESCs induced formation of heterochromatic rDNA as demonstrated by the reduction of rDNA transcription and the increase of both H3K9me2 and CpG methylation levels at the rDNA promoter (Figures 3B–3D; Figure S4). The modest increase in CpG methylation (from 1.7% to 4.4%) can also be attributed to the 2i conditions, recently described to lead to pronounced reduction in DNA methylation due to the downregulation of the de novo methyltransferases DNMT3a and DNMT3b (Leitch et al., 2013). Consistent with previous studies showing that TIP5 mediates dimethylation but not trimethylation of H3K9 at rRNA genes (Guetg et al., 2010; Santoro and Grummt, 2005), ectopic pRNA did not increase H3K9me3 levels at rDNA (Figure 3D; Figure S4). These results indicate that addition of pRNA in ESCs is sufficient to guide TIP5 to rDNA and to establish rDNA heterochromatin.

To determine how pRNA guides TIP5 to rDNA, we mutated pRNA sequences that were previously implicated in rDNA methylation and TIP5 association in somatic cells (Mayer et al., 2008; Schmitz et al., 2010). We mutated the T_0 element (pRNAΔT_0) that was previously described to form dsDNA:RNA triplex, a structure implicated in de novo rDNA methylation through recruitment of DNMT3b (Schmitz et al., 2010) and proposed as guiding module for TIP5 targeting to rDNA (Bierhoff et al., 2013). Similarly to wild-type pRNA, pRNAΔT_0 induced recruitment of TIP5 to nucleoli, promoted rDNA methylation and reduced rDNA transcription (Figures 3A–3C; Figure S3). Thus, pRNA-mediated nucleolar targeting of TIP5 and establishment of rDNA heterochromatin formation in ESCs is not mediated by rDNA:pRNA triplex. Accordingly, replacement of the 5′-pRNA region, including T_0 element, (hybrid, Control-pRNA) induced TIP5 nucleolar localization (Figure 3E; Figure S3). In contrast, replacement of 3′-pRNA sequences (hybrid, pRNA-Control), important for stem loop structure formation and the association with TIP5 in vitro (Mayer et al., 2008), impaired nucleolar localization of TIP5. Remarkably, point mutations that disrupt the stem loop structure (pRNA loop destroyed) were not efficient in recruiting TIP5 to the nucleoli whereas a compensatory mutation allowing hairpin formation did (pRNA loop recovered). Together, these results indicate that pRNA guides TIP5 to rDNA in *trans* through the hairpin structure and that addition of mature pRNA to ESCs is sufficient to establish rDNA heterochromatin. We conclude that the impairment of IGS-rRNA processing that abrogates formation of mature pRNA is the major determinant causing the euchromatic state of all rRNA genes in ESCs.

TIP5-TTF1 Association Is Mediated by pRNA and Impaired by IGS-rRNA

To determine why IGS-rRNA is unable to promote recruitment of TIP5 to rDNA, we determined whether TIP5 binds to IGS-rRNA using EMSA competition assays. Consistent with previous results, pRNA had a higher affinity for TIP5 compared to control RNA (Mayer et al., 2006) (Figure 4A). Surprisingly, TIP5 associates better with IGS-rRNA than with pRNA. To determine whether TIP5 preferentially associates with other IGS-rRNA sequences than pRNA, we analyzed TIP5 binding to IGS-rRNA sequences located upstream of the pRNA region. Spacer and enhancer RNA associate with TIP5 much less efficiently than pRNA (Figure S5A), suggesting that TIP5 binds to IGS-rRNA through the pRNA sequence and that upstream sequences might stabilize the complex through weak interactions. Together, these results indicate that TIP5 binds to IGS-rRNA and suggest that impairment of TIP5 recruitment to rDNA in ESCs might depend on the context of this interaction.

The requirement of the pRNA loop structure for nucleolar targeting of TIP5 (Figure 3) let us hypothesize that pRNA binding to TIP5 might favor the association with a docking protein for the recruitment to rDNA promoter and that IGS-rRNA might hinder this process. One important TIP5 interacting protein is the transcription terminator factor TTF1 (Németh et al., 2004; Strohner et al., 2001). TTF1 is a nucleolar protein that binds to terminator (T) elements, including the T_0 sequences at rDNA promoter, and is implicated in several rDNA regulatory processes (Evers and Grummt, 1995; Gerber et al., 1997; Längst et al., 1997). The association of TIP5 with TTF1 and its dependency on TTF1 for rDNA promoter binding proposed that TTF1 recruits TIP5 to rDNA (Németh et al., 2004; Santoro and Grummt, 2005; Strohner et al., 2001). However, whether and how pRNA is implicated in this process has so far not been investigated. TTF1 binds to RNA (Figure 4B), forming high-molecular-weight complexes. However, in contrast to TIP5, TTF1 did not display any

(C) qRT-PCR. rRNA transcription (45S pre-rRNA levels) in ESCs, NPCs, and NIH 3T3. Data were normalized to Rps12 mRNA.
(D) CpG methylation levels at rDNA promoter in mouse fibroblasts and iPSCs.
(E and F) ChIP. H3K9me2, H3K9me3 and H3K27me3, UBF, TIP5, and PARP1 occupancy. *Evx1*, *Zfpm2*, and *Gapdh* represent control genes. Data of two independent experiments were normalized to input and rDNA promoter value in ESCs.
(G) Tip5 mRNA (qRT-PCR) and protein levels (immunoblot) of ESCs and NPCs. Data were normalized to *Rps12* mRNA or PARP1 protein levels. Protein level titration was loaded and only the lanes with same protein amounts are shown.
(H) TIP5 cellular localization in MEFs, ESCs, and NPCs after 8 days of differentiation by immunofluorescence. Nucleoli are depicted by UBF signal.
All error bars represent the SD of two (when indicated) or three independent experiments. See also Figures S1 and S2.

Cell Stem Cell
The Nucleolus Regulates ESC Chromatin

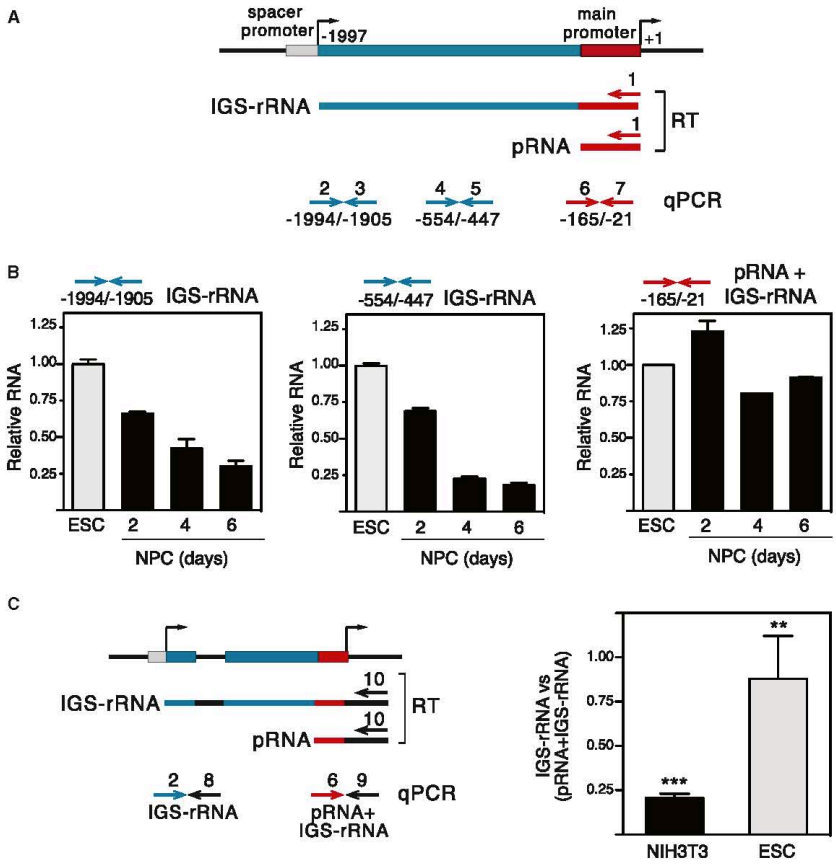

Figure 2. IGS-rRNA Is Not Efficiently Processed in ESCs

(A) Schema representing the mouse 5′-rDNA organization: Spacer promoter (gray), intergenic spacer region (blue), rDNA main promoter (red), and transcription start sites of IGS-rRNA (−1997) and 45S pre-rRNA (+1). Arrows represent primers used to perform RT (1; −20/−1) and to quantitatively amplify the indicated rDNA sequences (2–7).

(B) qRT-PCR. Levels IGS-rRNA and pRNA sequences of ESCs and NPCs (from days 2 to 6, from the beginning of differentiation). Data of two independent experiments were normalized to *Rps12* mRNA and to ESC values.

(C) Schema depicts the IGS-rRNA reporter plasmid. Black arrows represent primers used to perform RT (10) and to amplify plasmid sequences (8 and 9). Blue and red arrows (2 and 6) indicate primers hybridizing to rRNA sequences as described in (A). NIH 3T3 and ES cells were transfected with IGS-rRNA reporter plasmid. Data from three experiments are represented as values of amplifications with primers 2 and 8 (IGS-rRNA) normalized to amplifications with primers 6 and 9 (IGS-rRNA+pRNA).

preferential binding to pRNA sequences (Figure 4C). In ESCs, TTF1 is bound to rDNA promoter and is localized within nucleoli as in differentiated cells (Figures S5B and S5C). To determine whether the association of TIP5 with TTF1 is regulated by pRNA or IGS-rRNA, we performed pull-down assays using purified RNA-free His-tagged TTF1 (aa.1-210, containing TIP5-interacting region) and GST-tagged-TIP5 (aa. 332-723, comprising the RNA- and TTF1-interacting regions) (Mayer et al., 2006; Németh et al., 2004). Immobilized GST-$TIP5_{332–723}$ was incubated with no RNA, or with equivalent moles of RNAs and analyzed for the interaction with His-$TTF1_{1–210}$. In the absence of RNA and in the presence of RNA control, TIP5 and TTF1 did not associate (Figure 4D). In contrast, TIP5-pRNA complexes displayed a strong interaction with TTF1, indicating that pRNA is required for TIP5-TTF1 association. Remarkably, TIP5 bound to IGS-rRNA did not interact with TTF1. Consistent with the role of 3′-pRNA sequences in TIP5 nucleolar targeting, this region was sufficient for TIP5-TTF1 interaction while the 5′-pRNA

Cell Stem Cell
The Nucleolus Regulates ESC Chromatin

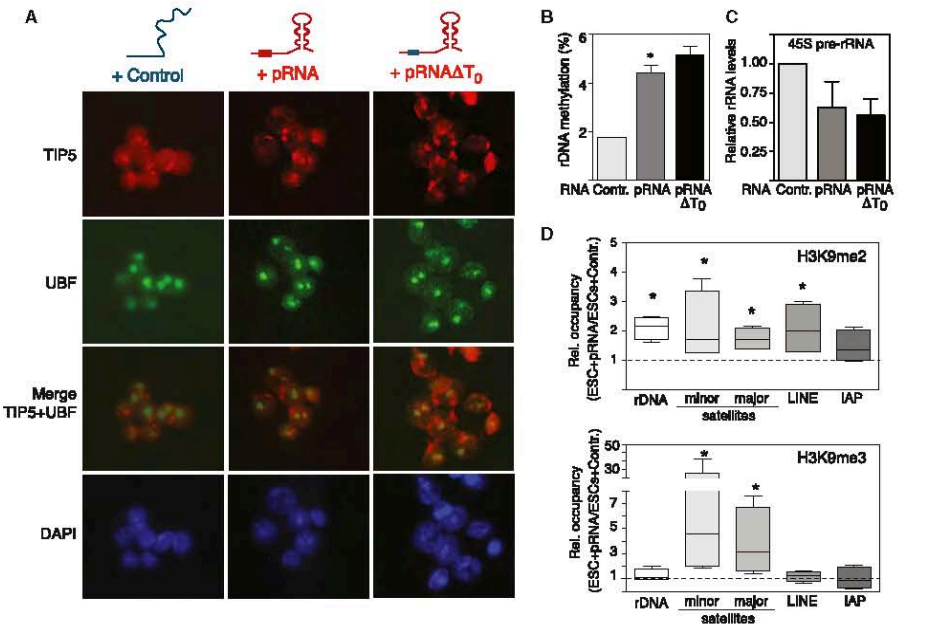

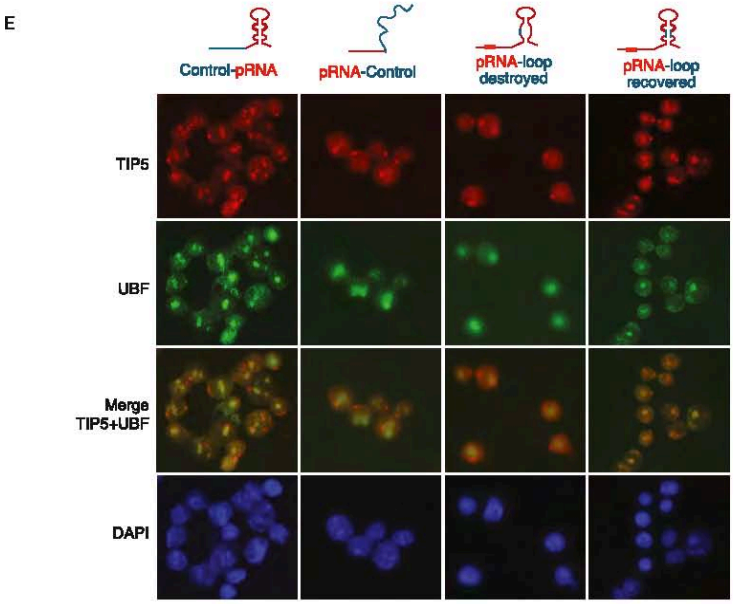

(legend on next page)

region was not. We conclude that pRNA mediates the association of TIP5 with TTF1 and that unprocessed IGS-rRNA prevents this interaction. Based on these results, we propose that the unprocessed IGS-rRNA in ESCs abolishes the interaction of TIP5 with TTF1, thus preventing TIP5 targeting to rDNA and nucleolar heterochromatin formation.

The Epigenetic State of Nucleolar Chromatin Affects ESC Chromatin and Pluripotency

Our previous studies showed that somatic cells depleted of TIP5 reduced silent epigenetic modifications at rDNA and at major and minor satellites and lack condensed heterochromatin adjacent to nucleoli (Guetg et al., 2010). Further structural alterations observed upon TIP5 knockdown, such as enlargement of nucleolar surfaces, reduction of nucleoli number, and formation of few decondensed DAPI-stained heterochromatic foci, resembled ESC chromatin organization (Figure 5A). To determine whether formation of rDNA heterochromatin affects the open chromatin of ESCs, we performed transmission electron microscopy to analyze and quantify the volume of heterochromatin associated to nucleoli in ESCs upon addition of pRNA (ESCs+pRNA) (Figure 5B; Figure S5D). Consistent with the loss of perinucleolar heterochromatin upon TIP5 knockdown in somatic cells (Guetg et al., 2010), ESCs+pRNA increased the amounts of condensed heterochromatin around nucleoli, displaying a structural organization like it is found in NPCs (Figure S5E). In line with these results, ESCs+pRNA increased H3K9me2 not only at rDNA, but also at major and minor repeats and at LINE elements while IAP transposons were not significantly affected (Figure 3D; Figure S4). H3K9me3 levels drastically increased at minor and major satellites while remaining unchanged at LINE L1 elements and IAP transposons and, as expected, at rDNA. Among the four performed experiments, we observed an inverse correlation between H3K9me2 and H3K9me3 levels at minor and major repeats (Figure S2), suggesting a two-step process that is initiated with H3K9me2 (the activity brought to rDNA by TIP5 (Santoro and Grummt, 2005)) and is further completed at major and minor satellite sequences with the establishment of H3K9me3. ESCs+pRNA increased the total amount of H3K9me2 to levels similar to those observed during ESC-NPC transition (Figure 5C). This result is in agreement with a previous work showing acquisition of large regions of H3K9 methylation during differentiation, which affects at least 30% of the genome (Wen et al., 2009). In contrast, the global H3K9me3 content was not altered in NPCs and ESCs+pRNA. Because terminally differentiated cells were previously described to contain elevated H3K9me3 levels (Hawkins et al., 2010), our results with NPCs most likely represent the epigenetic state at early differentiation time points. The elevated heterochromatic content of ESCs+pRNA was also accompanied by a reduction of minor satellites transcription as found during ESC differentiation (Figure S1E), whereas transcription of LINE and IAP elements was not greatly affected (Figure 5C). Taken together, these results suggest that tethering heterochromatin at rDNA via pRNA in ESCs initiates structural remodeling toward a highly condensed nuclear heterochromatin, a structure that ESCs normally acquire during differentiation.

We next addressed how the increased heterochromatic content mediated by pRNA affects ESC properties. ESCs+pRNA did not show alterations in important molecular features of the undifferentiated state such as cell proliferation, expression of the pluripotency genes *Oct4*, *Nanog*, and stage-specific embryonic antigen 1 (SSEA1), cell morphology, and alkaline phosphatase (AP) staining (Figures 6A–6D, and data not shown). To determine whether addition of pRNA affects pluripotency in vivo, we performed teratoma formation assays. ESCs+pRNA markedly decreased their capability to form teratoma compared to ESCs transfected with RNA control or with a pRNA mutant that is unable to recruit TIP5 to nucleoli (Figure 6E). Remarkably, teratomas derived from ESCs+pRNA showed a drastic reduced volume but displayed differentiation into all three germ layers (Figures S6A and S6B). Because ESCs were transiently transfected, we assume that teratomas obtained from ESCs+pRNA originated from untransfected cells, which is supported by the reduction in volume of these teratomas. To get insights into the loss of pluripotency, we analyzed transcription profiles of ESCs+pRNA and ESCs+RNA-control by RNaseq and found upregulation of 532 transcripts and downregulation of 509 transcripts in ESCs+pRNA (Table S1 available online). We carried out functional annotation analysis of transcripts whose levels were altered in ESCs+pRNA using DAVID tools (Huang et al., 2009) (Figure 6E; Table S1). The top eight gene ontology terms were all related to cell developmental and differentiation processes. Enrichment for these processes was particularly evident for transcripts upregulated in ESCs+pRNA, suggesting that addition of pRNA promotes expression of genes involved in cell differentiation and developmental processes. To exclude the possibility of pRNA off-target effects, we transfected a mutant pRNA unable to associate with TIP5 and analyzed transcription of *Btg3* and *Rdh10*, two genes upregulated in ESCs+pRNA and known to be implicated in neurogenesis and embryonic differentiation (Cammas et al., 2007; Yoshida et al., 1998). In contrast to pRNA, the pRNA mutant was unable to affect Btg3 and Rdh10 transcript levels (Figure S6C), indicating that upregulation of genes implicated in cell differentiation and the developmental processes is specifically mediated by a fully functional pRNA that is able to associate with TIP5, guide it to

Figure 3. Mature pRNA Is Required for the Establishment of rDNA Heterochromatin

(A) Mature pRNA induced recruitment of TIP5 to ESC nucleoli. Immunofluorescence with anti-TIP5 and anti-UBF antibodies in ESCs transfected with in vitro synthesized RNA control, pRNA, and pRNAΔT_0.

(B) Mature pRNA promotes rDNA promoter CpG methylation in ESCs. Error bars represent the SD of three independent experiments.

(C) Mature pRNA decreased rRNA synthesis in ESCs. rDNA transcription were measured by qRT-PCR and normalized to *Rps12* mRNA. Error bars indicate the SD of two independent experiments.

(D) Mature pRNA increased silent histone modifications at rDNA and centric-pericentric sequences of ESCs. Box-and-whisker plot of four independent ChIP experiments. Data are represented as bound over input in ESCs+pRNA normalized to values measured in ESCs+RNA control.

(E) pRNA loop structure mediates TIP5 recruitment to ESC nucleoli. Immunofluorescence with anti-TIP5 and anti-UBF antibodies of ESCs transfected with the indicated pRNA mutants.

See also Figure S3.

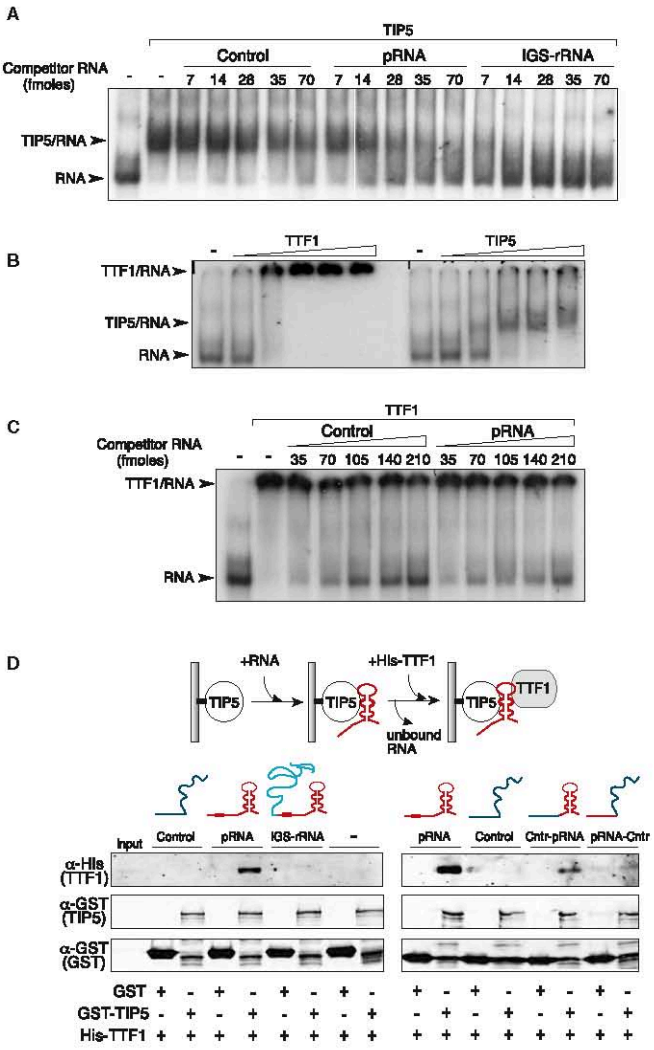

Figure 4. pRNA Mediates TIP5-TTF1 Interaction

(A) TIP5 binds to IGS-rRNA. Increasing equal moles of in vitro transcripts corresponding to control, pRNA, and IGS-rRNA sequences were used to compete for binding of $TIP5_{332-723}$ to radiolabelled run-off transcripts from pBluescript (MCS-RNA). RNA/protein complexes were analyzed by EMSA.

(B) TTF1 binds to RNA. Increasing equal moles of full-length TTF1 and $TIP5_{332-723}$ were analyzed for binding to radiolabeled MCS-RNA by EMSA.

(C) TTF1 does not show preferential binding to pRNA. Binding of full-length TTF1 to radiolabeled MCS-RNA was completed with increasing equal moles of RNA control and pRNA.

(D) TIP5-TTF1 interaction is mediated by pRNA and impaired by IGS-rRNA. Schema representing the GST-pull-down strategy used to analyze TIP5-TTF1 interaction in the presence of equivalent moles of RNAs. Pull-down assay. Bound proteins, GST, GST-TIP5, and His-TTF1, were detected with anti-GST and anti-His antibodies, respectively.

See also Figures S5A–S5C.

rDNA, and establish rDNA heterochromatin. Together, these results indicate that the elevated heterochromatic content induced by formation of nucleolar heterochromatin through pRNA impairs pluripotency and highlight the role of the nucleolus in the control of ESC chromatin plasticity that is required for the maintenance of the undifferentiated state.

To further explore the role of nucleolar chromatin in ESCs, we analyzed the differentiation capacity of cells depleted of TIP5. ESCs depleted of TIP5 by siRNA reduced TIP5 levels to 50% (Figures 7A and 7B). Upon TIP5 knockdown, ESCs proliferated less but displayed unaltered expression of *Oct4*, *Nanog*, and *Rex1*, exhibited the typical cell morphology of ESCs and were positive for AP staining (Figures 7B–7E). Similar results were obtained with other siRNA-TIP5 sequences (data not shown). To determine whether TIP5 depletion affects ESC differentiation, we treated an equal number of siRNA-control and -Tip5 treated ESCs with their respective siRNAs and induced monolayer differentiation upon withdrawal of 2i and LIF (Figure 7A). After 3 days, control cells displayed morphological structures typical of differentiated cells, whereas cells depleted of TIP5 underwent cell death and detached from the plate (Figures 7F–7H). The majority of the few siRNA-TIP5 cells that remained attached to plates showed ESC-like morphology and were positive for AP staining (Figures 7G and 7H; Figure S7). The effects observed with TIP5 depletion were specific for differentiated cells because ESCs double-treated with siRNA-Tip5 and cultured in 2i and LIF did not show any defect in viability (data not shown). These results indicate that TIP5 is required for ESC differentiation and suggest that the establishment of nucleolar heterochromatin is an event required for early differentiation.

DISCUSSION

The remodeling of the open and euchromatic genome structure of ESCs toward a highly condensed heterochromatic form

Cell Stem Cell
The Nucleolus Regulates ESC Chromatin

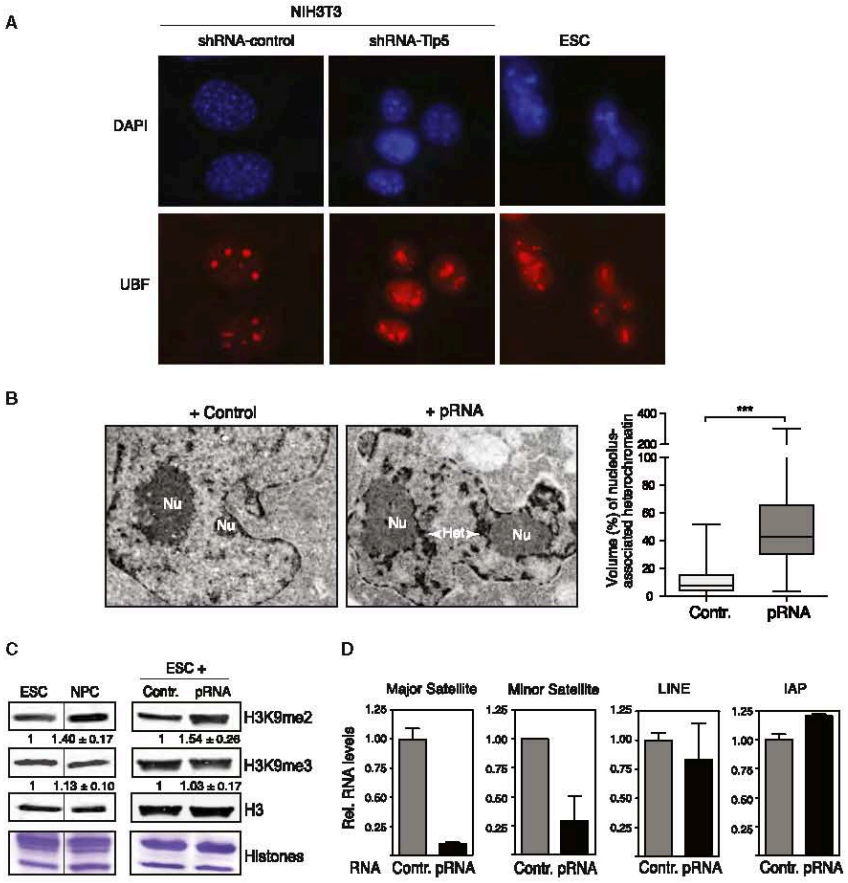

Figure 5. Mature pRNA Induces Global Remodelling toward Heterochromatic Structures

(A) Immunofluorescence showing heterochromatin (DAPI) and nucleoli (UBF) of NIH 3T3 cells stably expressing shRNA-control and -Tip5 sequences, and ESCs.

(B) Mature pRNA induced formation of condensed heterochromatin in ESCs. Transmission electron microscopy analysis. Representative images showing nucleolus-associated heterochromatin in ESCs+Control and ESCs+pRNA. The contrast procedure reveals in dark condensed heterochromatic structures (Het); 25–34 nucleoli of ESCs+RNA control and ESCs+pRNA of two independent experiments were selected at random. The volume of nucleolus-associated heterochromatin was expressed as a percentage of the volume of the nucleolus (Nu). Heteroscedastic two-tailed t test was used to compare the groups. See also Figures S5D and S5E.

(C) Immunoblot of H3K9me2, H3K9me3, and histone H3 of chromatin fractions of ESCs, NPCs, ESCs+RNA-control, and ESCs+pRNA. Values from three independent experiments were normalized to histone H3 levels. Protein level titration was loaded and only the lanes with same histone amounts are shown.

(D) qRT-PCR of major and minor satellite, LINE, and IAP retrotrasposon transcripts in ESCs+RNA-control and ESCs+pRNA. Values from two independent experiments were normalized to Rps12 mRNA.

characterizes the exit from pluripotency and the progression into differentiated states. ESC open chromatin correlates with a globally permissive transcriptional state contributing to the developmental plasticity and pluripotency of the ESC genome that has to have the ability to enter any distinct differentiation pathway (Gaspar-Maia et al., 2011). We determined here that the nucleolus is not only the place where ribosomes are produced, but it also plays a role in regulating genome architecture and pluripotency. Using mature pRNA as a mean to specifically tether heterochromatin at nucleoli of ESCs, we showed that the formation of heterochromatin at rRNA genes, the genetic component of nucleoli, has the ability to initiate the establishment of repressive chromatin structures at regions of the genome located outside of the nucleolus (Figure 7I). This process includes the formation of

Cell Stem Cell
The Nucleolus Regulates ESC Chromatin

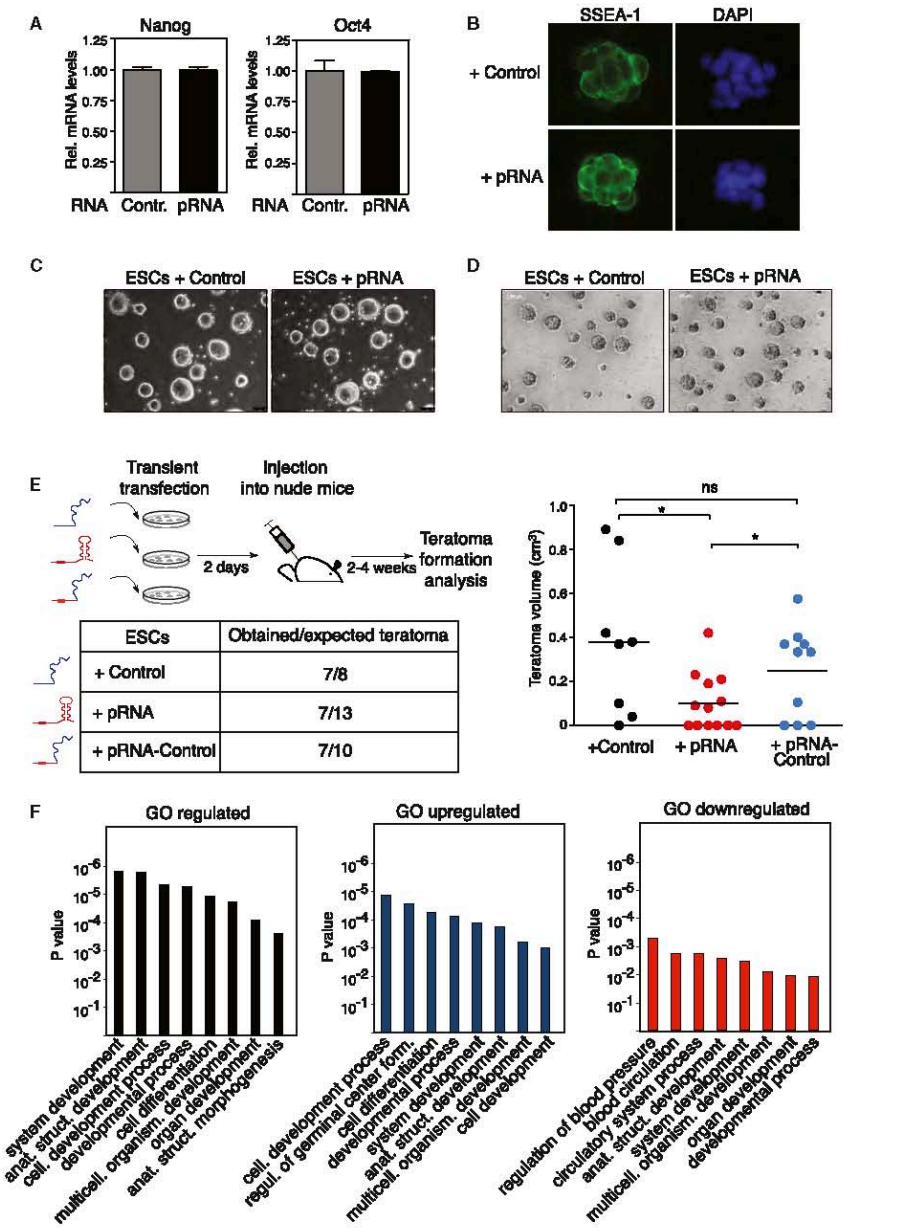

(legend on next page)

highly condensed heterochromatic structures clustering in proximity to nucleoli as found in differentiated cells. Such architectural remodeling is also evidenced by a global increase in H3K9me2, maturation of heterochromatin at repetitive sequences, and their transcriptional repression. These are characteristic features of the switch between pluripotency and differentiation. Although we cannot define which is the first event that globally initiates the formation of heterochromatin at the exit from pluripotency and entry into differentiation, our results place the nucleolus as an important regulator of this process. The establishment of rDNA heterochromatin during differentiation timely coincides with the formation of highly condensed heterochromatic structures and LOCKs (Meshorer and Misteli, 2006; Wen et al., 2009). This was particularly evident for the maturation of constitutive heterochromatin at major and minor satellite repeats, which displayed the same timing as rDNA for the acquisition of histone repressive marks and transcriptional repression upon ESC differentiation.

While showing some of the molecular outlines of the undifferentiated cells, pRNA-mediated heterochromatic ESCs transcribe genes implicated in differentiation processes and are no longer pluripotent. This observation highlights the role of the euchromatic organization in ESC identity and suggests that nucleolar chromatin is an important regulator of the pluripotent state. Likewise, impairing the formation of rDNA heterochromatin by TIP5 knockdown inhibits ESC differentiation, suggesting that the establishment of nucleolar heterochromatin is a necessary step for the switch from a lower to a higher order chromatin structure and lineage commitment.

How does the nucleolus influence heterochromatin formation? Due to the proximity of rDNA and centromeric sequences at rDNA-bearing chromosomes (Dev et al., 1977; Kurihara et al., 1994), the effect of rDNA heterochromatin on chromatin structures at major and minor repeats might in part be explained through spreading mechanisms. However, centromeres of chromosomes not containing rRNA genes also associate with the nucleolus at a frequency more than expected for a random distribution (Carvalho et al., 2001), indicating the existence of alternative mechanisms that establish heterochromatin at sequences that are further away from rDNA loci. In this case, the establishment of rDNA heterochromatin might allow the formation of a nucleolar/perinucleolar compartment enriched in chromatin repressor complexes that would be attractive for genomic regions that need to be repressed. Anchoring of heterochromatin at the nucleolus might have similar function like the ones described for the nuclear periphery that is responsible for the integrity of mammalian heterochromatin (Pinheiro et al., 2012; Towbin et al., 2012). Consistent with this, genomic regions localized at the lamina (LADs) were shown to relocate after cell division either at the lamina or at the nucleolus (Kind et al., 2013), suggesting interchangeable roles in establishing and maintaining heterochromatic states.

This study also provides evidence that rRNA genes do not only function in synthesizing rRNA. Silent rRNA repeats, present in all somatic cells, maintain their heterochromatic state independently of transcriptional activity, and are stably propagated throughout the cell cycle (Conconi et al., 1989). Our results indicated that the epigenetic state of rRNA genes contributes to nuclear architecture and cellular functions such as pluripotency and differentiation by controlling the balance between heterochromatin and euchromatin. Interestingly, rDNA deletions in *Drosophila* result in reduced heterochromatin elsewhere in the genome and the extent of the rDNA deletion correlates with the loss of silencing in much the same manner as mutations in known protein heterochromatin components (Paredes and Maggert, 2009).

Very little is understood about how specific lncRNAs selectively seek out interaction sites in the genome, the nature of lncRNA-chromatin interactions, and their possible functional roles (Rinn and Chang, 2012). This work underlined the role of lncRNA in targeting epigenetic regulatory processes at specific genomic loci leading to the establishment of chromatin conformation patterns that ultimately result in the fine control of genes. We show that the regulation of pRNA precursor IGS-rRNA processing is a key determinant for the control of the epigenetic state at rDNA and propose that the processing represents a mean of lncRNA regulation to modulate distinct functions of the same lncRNA. We determined that IGS-rRNA processing is a developmentally regulated process and that its impairment in ESCs prevents recruitment of TIP5 to rDNA and formation of rDNA heterochromatin. Although the mechanisms that impair IGS-rRNA processing in ESCs are yet to be determined, our results demonstrated that mature pRNA is necessary to establish rDNA heterochromatin. We showed that pRNA-mediated targeting of TIP5 occurs through DNA-protein recognition rules. Whereas IGS-rRNA abolishes the association of TIP5 with TTF1, pRNA promotes this interaction that serves to guide the complex to the rDNA promoter and to establish nucleolar heterochromatin. Thus, the same lncRNA can prevent or promote protein complex assembly and its processing controls the switch between these functions. Based on these results, it would not be surprising if processing emerges as a more general mechanism of lncRNA regulation.

In summary, our data underline the contribution of chromatin structure in ESC pluripotency and differentiation potential and indicate that the nucleolus is a key regulator of nuclear architecture and chromatin structure, which serves to control cell pluripotency and lineage commitment.

Figure 6. pRNA Impairs ESC Pluripotency

(A) Nanog and Oct4 mRNA levels in ESCs+RNA control and ESCs+pRNA (qRT-PCR). Values from two independent experiments were normalized to *Rps12* mRNA.

(B–D) (B) SSEA-1 immunostaining, (C) cell morphology, and (D) AP staining of ESCs+RNA control and ESCs+pRNA.

(E) ESCs+pRNA are not pluripotent. Efficiency of teratoma formation was assessed by the number of teratomas generated versus expected (injections) and by tumor volumes measured at the time when control animals were killed.

(F) Mature pRNA induced expression of genes implicated in cell differentiation and development. Top eight biological process gene ontology terms as determined using DAVID for genes regulated, and upregulated and downregulated in ESCs+pRNA.

See also Figure S6.

Cell Stem Cell
The Nucleolus Regulates ESC Chromatin

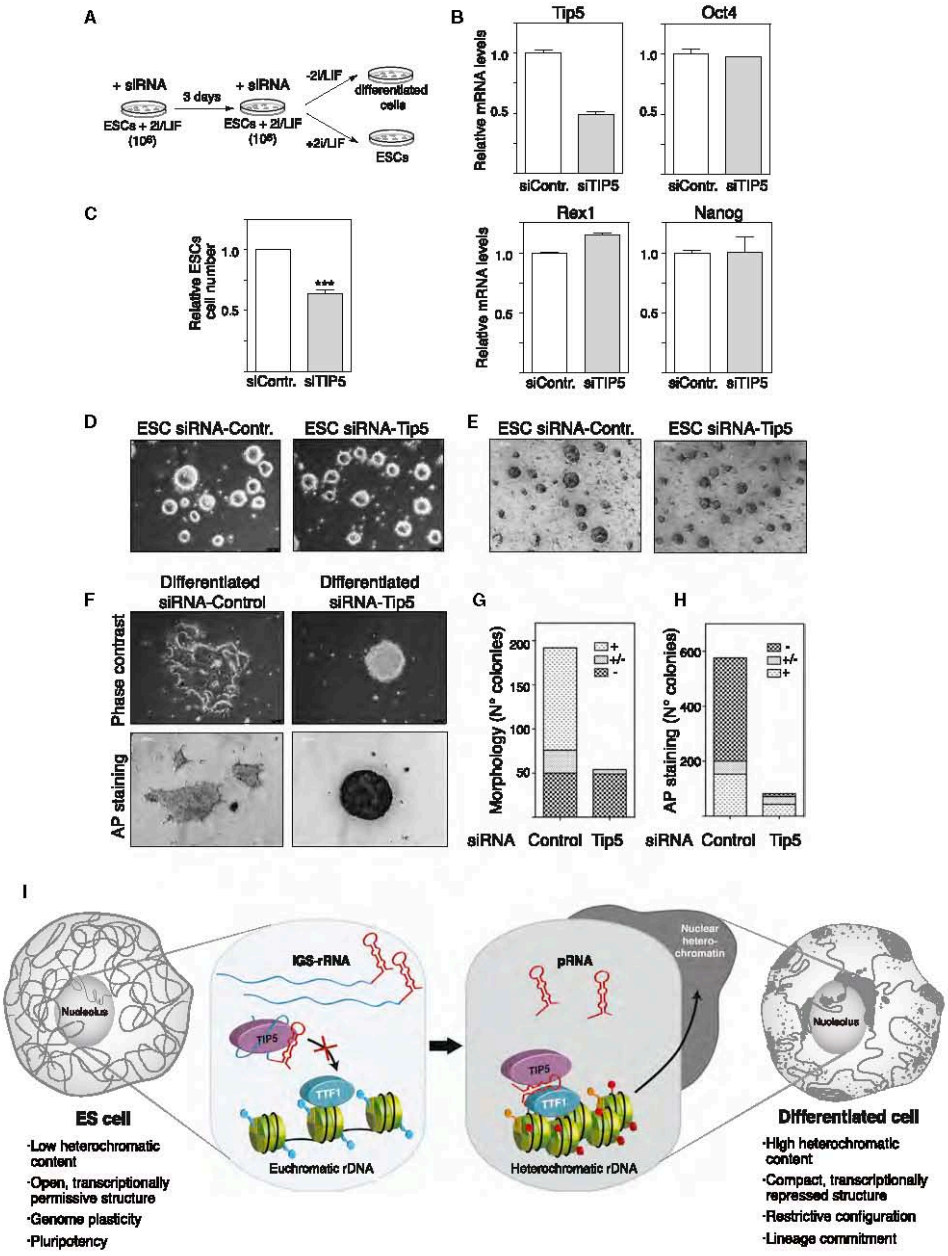

(legend on next page)

EXPERIMENTAL PROCEDURES

mESC Culture

One hundred twenty-nine mouse embryonic stem cells (E14 line) were cultured in N2B27 media (Dulbecco's modified Eagle's medium [DMEM] F12, neurobasal medium, N2/B27 supplements, 2 mM L-glutamine with Pen/Strep, β-Mercaptoethanol) supplemented with recombinant leukemia inhibitory factor, LIF (ESGRO, 1000 U/ml) and MEK and GSK3β inhibitors, 2i (Stemolecule CHIR99021 and PD0325901, 3 μM and 1 μM, respectively). Cells were seeded at a density of 50,000 cells/cm^2 in culture dishes (Corning CellBIND surface) treated with 0.1% gelatine without feeder layer. Propagation of cells was carried out every 2 days using Trypsin 0.5× for enzymatic cell dissociation.

mESC Differentiation

mESCs were differentiated to neural progenitor cells according to a previously established protocol (Bibel et al., 2004). In brief, differentiation used a suspension-based embryoid bodies formation (Bacteriological Petri Dishes, Bio-one with vents, Greiner). The neural differentiation media (DMEM, 10% fetal calf serum, 1× MEM NEAA, 2 mM L-glutamine with Pen/Strep, β-mercaptoethanol) was filtered through 0.22 μm filters and stored at 4°C. During the 8-day differentiation procedure, media was exchanged every 2 days. In the last 4 days of differentiation, the media was supplemented with 2 μM retinoic acid to generate neural precursors that are Pax-6-positive radial glial cells.

Immunocytochemistry

ESCs or differentiated cells were grown on gelatin-coated coverslips and permeabilized with 0.05% Triton X-100 in 20 mMTris-HCl (pH 8), 5 mM MgCl2, 0.5 mM EDTA, and 25% glycerol. After washing, cells were fixed with cold methanol (7 min) and stained with anti-TIP5 (Diagenode) and anti-UBF (SantaCruz) antibodies and DAPI (Molecular Probes), and immunofluorescent images were digitally recorded.

Transmission Electron Microscopy

Cells were first fixed with 2.5% glutaraldehyde, dehydrated in an ethanol series, transferred to methanol, and immersed into a freshly prepared mixture of methanol and acetic anhydride (5:1, v/v) at 25°C for 24 hr in the dark (Tandler and Solari, 1982; Testillano et al., 1991). Cells were then washed in pure methanol for 20 min, transferred in ethanol and embedded in Epon (Sigma). Ultrathin (50 nm) sections were contrasted with 5% aqueous uranyl acetate for 60 min at room temperature and examined with a CM100 transmission electron microscope (FEI).

The volume of nucleolus-associated heterochromatin was estimated using the Cavalieri-estimator (Gundersen et al., 1988; West, 2012). Volume estimates were performed for samples of 25 to 34 nucleoli selected at random from each electron microscopy sample of two independent experiments. Nucleoli were selected independent of their size or shape in the electron microscopy montages. The volume of nucleolus-associated heterochromatin was expressed as a percentage of the volume of the corresponding nucleolus. Due to unequal variances of heterochromatin volumes in control and experimental cells, a heteroscedastic two-tailed t test was used to compare the groups ($p = 7.6 \times 10^{-9}$).

EMSA

Radiolabeled MCS-RNA was synthesized by T7 RNA polymerase using pBluescript-KS(+)/EcoRI as template. After treatment with DNase I, transcripts were purified and 50,000 cpm of MCS-RNA were incubated for 15 min on ice with 40 ng recombinant TIP5 or TTF1 in EMSA buffer (20 mM Tris-HCl [pH 8.0], 5 mM MgCl2, 100 mM KCl, and 0.2 mM EDTA). Cold competitor RNA was added, and incubation was continued for 30 min. RNA-protein complexes were analyzed by electrophoresis on 6% (w/v) native polyacrylamide gels and depicted with autoradiography.

For detailed methods, list of antibodies, and tables of primers, see the Supplemental Experimental Procedures.

SUPPLEMENTAL INFORMATION

Supplemental Information includes Supplemental Experimental Procedures, seven figures, and one table and can be found with this article online at http://dx.doi.org/10.1016/j.stem.2014.10.005.

ACKNOWLEDGMENTS

The authors thank Ursula Luethi, Lutz Slomianka, and the Center for Microscopy and Image Analysis, University of Zurich for performing transmission electron microscopy analyses. This work was supported by the Swiss National Science Foundation (310003A-135801 and 31003A-152854 to R.S., 31003A-118361 to P.C., and 323530-133905 to F.A.W.), UBS-Promedica Stiftung (to R.S. and O.S.), Forschungskredit of the University of Zurich (to N.S. and E.V.), and the Mäxi Stiftung (to D.B. and R.S.).

Received: February 27, 2014
Revised: August 8, 2014
Accepted: October 16, 2014
Published: December 4, 2014

REFERENCES

Aoto, T., Saitoh, N., Ichimura, T., Niwa, H., and Nakao, M. (2006). Nuclear and chromatin reorganization in the MHC-Oct3/4 locus at developmental phases of embryonic stem cell differentiation. Dev. Biol. *298*, 354–367.

Bártová, E., Galiová, G., Krejcí, J., Harnicarová, A., Strasák, L., and Kozubek, S. (2008a). Epigenome and chromatin structure in human embryonic stem cells undergoing differentiation. Dev. Dyn. *237*, 3690–3702.

Bártová, E., Krejcí, J., Harnicarová, A., and Kozubek, S. (2008b). Differentiation of human embryonic stem cells induces condensation of chromosome territories and formation of heterochromatin protein 1 foci. Differentiation *76*, 24–32.

Bhattacharya, D., Talwar, S., Mazumder, A., and Shivashankar, G.V. (2009). Spatio-temporal plasticity in chromatin organization in mouse cell differentiation and during Drosophila embryogenesis. Biophys. J. *96*, 3832–3839.

Bibel, M., Richter, J., Schrenk, K., Tucker, K.L., Staiger, V., Korte, M., Goetz, M., and Barde, Y.A. (2004). Differentiation of mouse embryonic stem cells into a defined neuronal lineage. Nat. Neurosci. *7*, 1003–1009.

Figure 7. Depletion of TIP5 Impairs ESC Differentiation

(A) Schema showing the experimental strategy for TIP5 knockdown in ESCs.

(B) *Tip5*, *Oct4*, *Nanog*, and *Rex1* mRNA levels in ESCs depleted of TIP5.

(C) TIP5 knockdown affects ESC proliferation. Data represent relative cell numbers after 3 days of siRNA treatment.

(D and E) (D) Cell morphology and (E) AP staining of ESCs treated with siRNA-control and -*Tip5*.

(F–H) (F) Cell morphology and AP staining of cells after 3 days of differentiation. Quantifications are shown respectively in (G) differentiated (+), partially differentiated (+/−), and not differentiated (−); and (H) stained (+), partially stained (+/−), and not stained (−). See also Figure S7.

(I) Model showing the chromatin organization of the nucleus and nucleolus of ESCs (open, euchromatic) and differentiated cells (closed, heterochromatic). In ESCs, IGS-rRNA is not processed with consequent lack of mature pRNA. The unprocessed transcript impairs the association of TIP5 with TTF1, inhibiting TIP5 recruitment to rDNA and causing the euchromatic state of all rRNA genes. Upon differentiation, mature pRNA is produced and allows TIP5-TTF1 interaction that is productive for TIP5 targeting to rDNA and formation of heterochromatin at nucleoli. The arrow depicts the influence of rDNA heterochromatin in the formation of highly condensed and repressive chromatin structures at region outside the nucleolus. Establishment of compact heterochromatic structures abrogates genome plasticity of ESCs and set up a genome organization that favors cell lineage specification.

Bierhoff, H., Postepska-Igielska, A., and Grummt, I. (2013). Noisy silence: Non-coding RNA and heterochromatin formation at repetitive elements. Epigenetics *9*, 53–61.

Cammas, L., Romand, R., Fraulob, V., Mura, C., and Dolle, P. (2007). Expression of the murine retinol dehydrogenase 10 (Rdh10) gene correlates with many sites of retinoid signalling during embryogenesis and organ differentiation. Developmental dynamics *236*, 2899–2908.

Carvalho, C., Pereira, H.M., Ferreira, J., Pina, C., Mendonça, D., Rosa, A.C., and Carmo-Fonseca, M. (2001). Chromosomal G-dark bands determine the spatial organization of centromeric heterochromatin in the nucleus. Mol. Biol. Cell *12*, 3563–3572.

Conconi, A., Widmer, R.M., Koller, T., and Sogo, J.M. (1989). Two different chromatin structures coexist in ribosomal RNA genes throughout the cell cycle. Cell *57*, 753–761.

de Wit, E., Bouwman, B.A., Zhu, Y., Klous, P., Splinter, E., Verstegen, M.J., Krijger, P.H., Festuccia, N., Nora, E.P., Welling, M., et al. (2013). The pluripotent genome in three dimensions is shaped around pluripotency factors. Nature *501*, 227–231.

Dev, V.G., Tantravahi, R., Miller, D.A., and Miller, O.J. (1977). Nucleolus organizers in Mus musculus subspecies and in the RAG mouse cell line. Genetics *86*, 389–398.

Dixon, J.R., Selvaraj, S., Yue, F., Kim, A., Li, Y., Shen, Y., Hu, M., Liu, J.S., and Ren, B. (2012). Topological domains in mammalian genomes identified by analysis of chromatin interactions. Nature *485*, 376–380.

Efroni, S., Duttagupta, R., Cheng, J., Dehghani, H., Hoeppner, D.J., Dash, C., Bazett-Jones, D.P., Le Grice, S., McKay, R.D., Buetow, K.H., et al. (2008). Global transcription in pluripotent embryonic stem cells. Cell Stem Cell *2*, 437–447.

Evers, R., and Grummt, I. (1995). Molecular coevolution of mammalian ribosomal gene terminator sequences and the transcription termination factor TTF-I. Proc. Natl. Acad. Sci. USA *92*, 5827–5831.

Fussner, E., Ahmed, K., Dehghani, H., Strauss, M., and Bazett-Jones, D.P. (2010). Changes in chromatin fiber density as a marker for pluripotency. Cold Spring Harb. Symp. Quant. Biol. *75*, 245–249.

Gaspar-Maia, A., Alajem, A., Meshorer, E., and Ramalho-Santos, M. (2011). Open chromatin in pluripotency and reprogramming. Nat. Rev. Mol. Cell Biol. *12*, 36–47.

Gerber, J.K., Gögel, E., Berger, C., Wallisch, M., Müller, F., Grummt, I., and Grummt, F. (1997). Termination of mammalian rDNA replication: polar arrest of replication fork movement by transcription termination factor TTF-I. Cell *90*, 559–567.

Gonzalez-Sandoval, A., Towbin, B.D., and Gasser, S.M. (2013). The formation and sequestration of heterochromatin during development: delivered on 7 September 2012 at the 37th FEBS Congress in Sevilla, Spain. FEBS J. *280*, 3212–3219.

Gorkin, D.U., Leung, D., and Ren, B. (2014). The 3D genome in transcriptional regulation and pluripotency. Cell Stem Cell *14*, 762–775.

Guetg, C., Lienemann, P., Sirri, V., Grummt, I., Hernandez-Verdun, D., Hottiger, M.O., Fussenegger, M., and Santoro, R. (2010). The NoRC complex mediates the heterochromatin formation and stability of silent rRNA genes and centromeric repeats. EMBO J. *29*, 2135–2146.

Guetg, C., Scheifele, F., Rosenthal, F., Hottiger, M.O., and Santoro, R. (2012). Inheritance of silent rDNA chromatin is mediated by PARP1 via noncoding RNA. Mol. Cell *45*, 790–800.

Gundersen, H.J.G., Bendtsen, T.F., Korbo, L., Marcussen, N., Møller, A., Nielsen, K., Nyengaard, J.R., Pakkenberg, B., Sørensen, F.B., Vesterby, A., et al. (1988). Some new, simple and efficient stereological methods and their use in pathological research and diagnosis. APMIS *96*, 379–394.

Hawkins, R.D., Hon, G.C., Lee, L.K., Ngo, Q., Lister, R., Pelizzola, M., Edsall, L.E., Kuan, S., Luu, Y., Klugman, S., et al. (2010). Distinct epigenomic landscapes of pluripotent and lineage-committed human cells. Cell Stem Cell *6*, 479–491.

Huang, W., Sherman, B.T., and Lempicki, R.A. (2009). Systematic and integrative analysis of large gene lists using DAVID bioinformatics resources. Nat. Protoc. *4*, 44–57.

Jørgensen, H.F., Azuara, V., Amoils, S., Spivakov, M., Terry, A., Nesterova, T., Cobb, B.S., Ramsahoye, B., Merkenschlager, M., and Fisher, A.G. (2007). The impact of chromatin modifiers on the timing of locus replication in mouse embryonic stem cells. Genome Biol. *8*, R169.

Kind, J., Pagie, L., Ortabozkoyun, H., Boyle, S., de Vries, S.S., Janssen, H., Amendola, M., Nolen, L.D., Bickmore, W.A., and van Steensel, B. (2013). Single-cell dynamics of genome-nuclear lamina interactions. Cell *153*, 178–192.

Kurihara, Y., Suh, D.S., Suzuki, H., and Moriwaki, K. (1994). Chromosomal locations of Ag-NORs and clusters of ribosomal DNA in laboratory strains of mice. Mamm. Genome *5*, 225–228.

Längst, G., Blank, T.A., Becker, P.B., and Grummt, I. (1997). RNA polymerase I transcription on nucleosomal templates: the transcription termination factor TTF-I induces chromatin remodeling and relieves transcriptional repression. EMBO J. *16*, 760–768.

Leitch, H.G., McEwen, K.R., Turp, A., Encheva, V., Carroll, T., Grabole, N., Mansfield, W., Nashun, B., Knezovich, J.G., Smith, A., et al. (2013). Naive pluripotency is associated with global DNA hypomethylation. Nat. Struct. Mol. Biol. *20*, 311–316.

Martens, J.H., O'Sullivan, R.J., Braunschweig, U., Opravil, S., Radolf, M., Steinlein, P., and Jenuwein, T. (2005). The profile of repeat-associated histone lysine methylation states in the mouse epigenome. EMBO J. *24*, 800–812.

Mayer, C., Schmitz, K.M., Li, J., Grummt, I., and Santoro, R. (2006). Intergenic transcripts regulate the epigenetic state of rRNA genes. Mol. Cell *22*, 351–361.

Mayer, C., Neubert, M., and Grummt, I. (2008). The structure of NoRC-associated RNA is crucial for targeting the chromatin remodelling complex NoRC to the nucleolus. EMBO Rep. *9*, 774–780.

Melcer, S., Hezroni, H., Rand, E., Nissim-Rafinia, M., Skoultchi, A., Stewart, C.L., Bustin, M., and Meshorer, E. (2012). Histone modifications and lamin A regulate chromatin protein dynamics in early embryonic stem cell differentiation. Nat. Commun. *3*, 910.

Meshorer, E., and Misteli, T. (2006). Chromatin in pluripotent embryonic stem cells and differentiation. Nat. Rev. Mol. Cell Biol. *7*, 540–546.

Meshorer, E., Yellajoshula, D., George, E., Scambler, P.J., Brown, D.T., and Misteli, T. (2006). Hyperdynamic plasticity of chromatin proteins in pluripotent embryonic stem cells. Dev. Cell *10*, 105–116.

Moss, T., and Stefanovsky, V.Y. (2002). At the center of eukaryotic life. Cell *109*, 545–548.

Németh, A., Strohner, R., Grummt, I., and Längst, G. (2004). The chromatin remodeling complex NoRC and TTF-I cooperate in the regulation of the mammalian rRNA genes in vivo. Nucleic Acids Res. *32*, 4091–4099.

Nora, E.P., Lajoie, B.R., Schulz, E.G., Giorgetti, L., Okamoto, I., Servant, N., Piolot, T., van Berkum, N.L., Meisig, J., Sedat, J., et al. (2012). Spatial partitioning of the regulatory landscape of the X-inactivation centre. Nature *485*, 381–385.

Paredes, S., and Maggert, K.A. (2009). Ribosomal DNA contributes to global chromatin regulation. Proc. Natl. Acad. Sci. USA *106*, 17829–17834.

Pinheiro, I., Margueron, R., Shukeir, N., Eisold, M., Fritzsch, C., Richter, F.M., Mittler, G., Genoud, C., Goyama, S., Kurokawa, M., et al. (2012). Prdm3 and Prdm16 are H3K9me1 methyltransferases required for mammalian heterochromatin integrity. Cell *150*, 948–960.

Rinn, J.L., and Chang, H.Y. (2012). Genome regulation by long noncoding RNAs. Annu. Rev. Biochem. *81*, 145–166.

Santoro, R., and Grummt, I. (2001). Molecular mechanisms mediating methylation-dependent silencing of ribosomal gene transcription. Mol. Cell *8*, 719–725.

Santoro, R., and Grummt, I. (2005). Epigenetic mechanism of rRNA gene silencing: temporal order of NoRC-mediated histone modification, chromatin remodeling, and DNA methylation. Mol. Cell. Biol. *25*, 2539–2546.

Santoro, R., Li, J., and Grummt, I. (2002). The nucleolar remodeling complex NoRC mediates heterochromatin formation and silencing of ribosomal gene transcription. Nat. Genet. *32*, 393–396.

Santoro, R., Schmitz, K.M., Sandoval, J., and Grummt, I. (2010). Intergenic transcripts originating from a subclass of ribosomal DNA repeats silence ribosomal RNA genes in trans. EMBO Rep. *11*, 52–58.

Schlesinger, S., Selig, S., Bergman, Y., and Cedar, H. (2009). Allelic inactivation of rDNA loci. Genes Dev. *23*, 2437–2447.

Schmitz, K.M., Mayer, C., Postepska, A., and Grummt, I. (2010). Interaction of noncoding RNA with the rDNA promoter mediates recruitment of DNMT3b and silencing of rRNA genes. Genes Dev. *24*, 2264–2269.

Splinter, E., and de Laat, W. (2011). The complex transcription regulatory landscape of our genome: control in three dimensions. EMBO J. *30*, 4345–4355.

Strohner, R., Nemeth, A., Jansa, P., Hofmann-Rohrer, U., Santoro, R., Längst, G., and Grummt, I. (2001). NoRC—a novel member of mammalian ISWI-containing chromatin remodeling machines. EMBO J. *20*, 4892–4900.

Tandler, C.J., and Solari, A.J. (1982). Methanol-acetic anhydride: an efficient blocking agent for electron microscope cytochemistry. Its application to mouse testis and other tissues. Histochemistry *76*, 351–361.

Testillano, P.S., Sanchez-Pina, M.A., Olmedilla, A., Ollacarizqueta, M.A., Tandler, C.J., and Risueno, M.C. (1991). A specific ultrastructural method to reveal DNA: the NAMA-Ur. The journal of histochemistry and cytochemistry: official journal of the Histochemistry Society *39*, 1427–1438.

Towbin, B.D., González-Aguilera, C., Sack, R., Gaidatzis, D., Kalck, V., Meister, P., Askjaer, P., and Gasser, S.M. (2012). Step-wise methylation of histone H3K9 positions heterochromatin at the nuclear periphery. Cell *150*, 934–947.

Wen, B., Wu, H., Shinkai, Y., Irizarry, R.A., and Feinberg, A.P. (2009). Large histone H3 lysine 9 dimethylated chromatin blocks distinguish differentiated from embryonic stem cells. Nat. Genet. *41*, 246–250.

West, M.J. (2012). Estimating volume in biological structures. Cold Spring Harb Protoc. *2012*, 1129–1139.

Wong, L.H., Ren, H., Williams, E., McGhie, J., Ahn, S., Sim, M., Tam, A., Earle, E., Anderson, M.A., Mann, J., and Choo, K.H. (2009). Histone H3.3 incorporation provides a unique and functionally essential telomeric chromatin in embryonic stem cells. Genome Res. *19*, 404–414.

Yoshida, Y., Matsuda, S., Ikematsu, N., Kawamura-Tsuzuku, J., Inazawa, J., Umemori, H., and Yamamoto, T. (1998). ANA, a novel member of Tob/BTG1 family, is expressed in the ventricular zone of the developing central nervous system. Oncogene *16*, 2687–2693.

Zhou, Y., Santoro, R., and Grummt, I. (2002). The chromatin remodeling complex NoRC targets HDAC1 to the ribosomal gene promoter and represses RNA polymerase I transcription. EMBO J. *21*, 4632–4640.

Cell Stem Cell, Volume *15*
Supplemental Information

lncRNA Maturation to Initiate Heterochromatin Formation in the Nucleolus Is Required for Exit from Pluripotency in ESCs

Nataša Savić, Dominik Bär, Sergio Leone, Sandra C. Frommel, Fabienne A. Weber, Eva Vollenweider, Elena Ferrari, Urs Ziegler, Andres Kaech, Olga Shakhova, Paolo Cinelli, and Raffaella Santoro

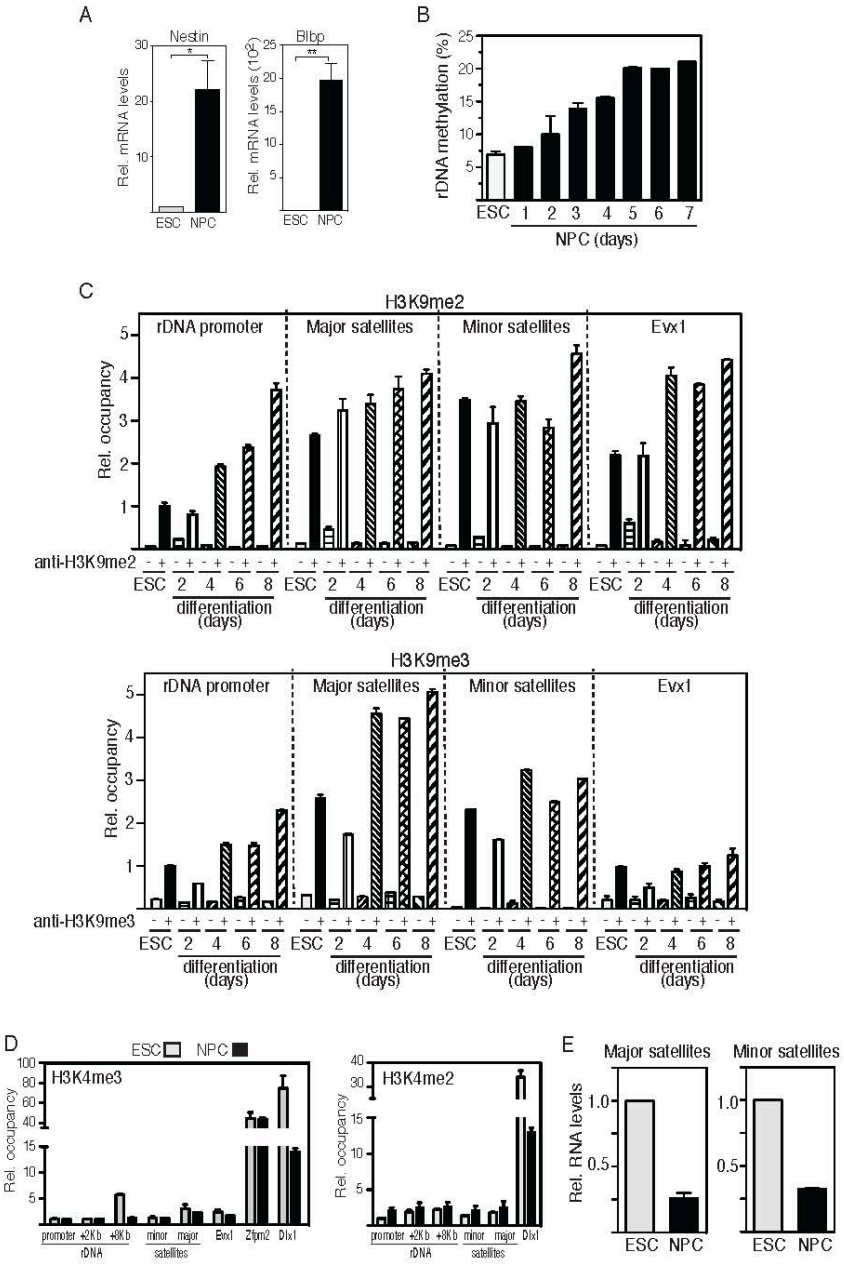
A
Nestin
Rel. mRNA levels
ESC NPC
Blbp
Rel. mRNA levels (10^2)
ESC NPC
B
rDNA methylation (%)
ESC 1 2 3 4 5 6 7
NPC (days)
C
H3K9me2
rDNA promoter
Major satellites
Minor satellites
Evx1
Rel. occupancy
anti-H3K9me2
ESC 2 4 6 8
differentiation (days)
H3K9me3
rDNA promoter
Major satellites
Minor satellites
Evx1
Rel. occupancy
anti-H3K9me3
ESC 2 4 6 8
differentiation (days)
D
ESC NPC
H3K4me3
Rel. occupancy
promoter +2Kb +8Kb minor major Evx1 Zfpm2 Dlx1
rDNA satellites
H3K4me2
Rel. occupancy
promoter +2Kb +8Kb minor major Dlx1
rDNA satellites
E
Major satellites
Minor satellites
Rel. RNA levels
ESC NPC
ESC NPC

Figure S1

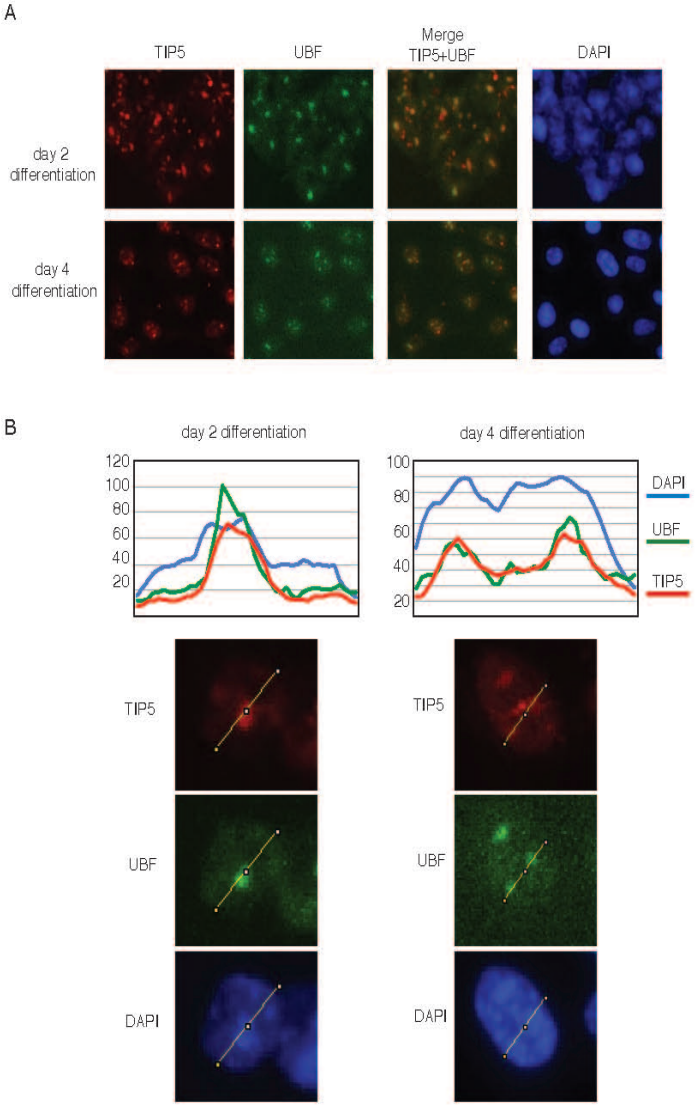
A
TIP5
UBF
Merge TIP5+UBF
DAPI
day 2 differentiation
day 4 differentiation
B
day 2 differentiation
day 4 differentiation
120
100
80
60
40
20
100
80
60
40
20
DAPI
UBF
TIP5
TIP5
UBF
DAPI
TIP5
UBF
DAPI

Figure S2

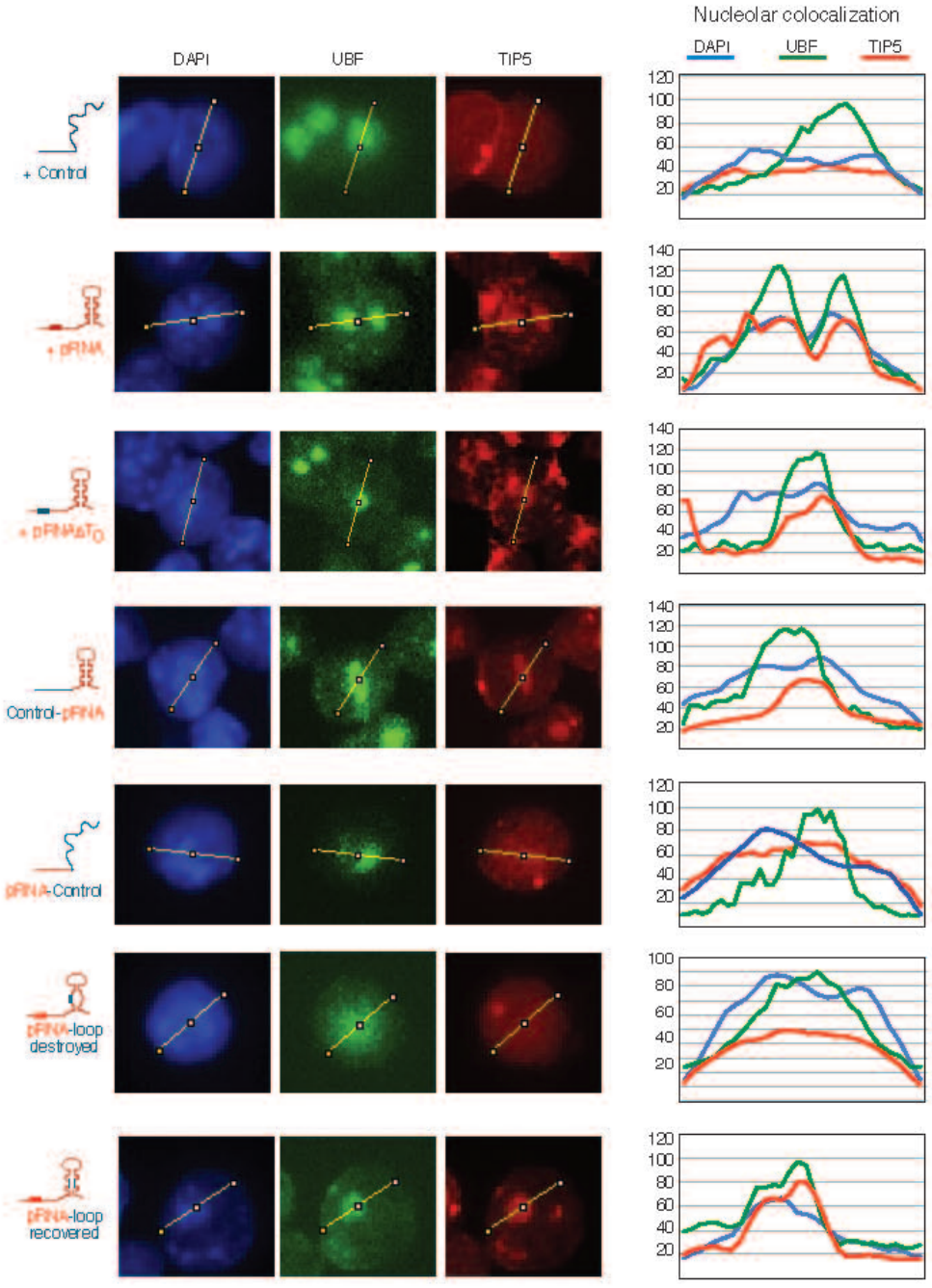
DAPI
UBF
TIP5
Nucleolar colocalization
DAPI
UBF
TIP5
+ Control
+ pRNA
+ pRNAΔT$_D$
Control-pRNA
pRNA-Control
pRNA-loop destroyed
pRNA-loop recovered
120
100
80
60
40
20
140
120
100
80
60
40
20
100
80
60
40
20

Figure S3

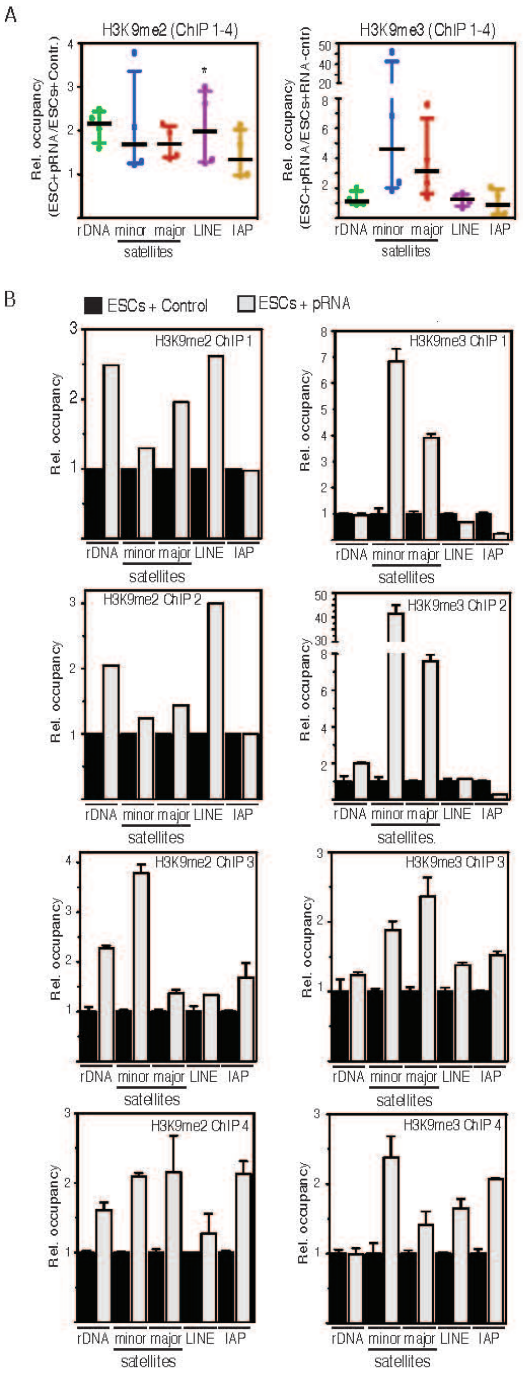
A
H3K9me2 (ChIP 1-4)
H3K9me3 (ChIP 1-4)
Rel. occupancy (ESC+pRNA/ESCs+Contr.)
Rel. occupancy (ESC+pRNA/ESCs+RNA-cntr)
rDNA minor major LINE IAP
satellites
B
ESCs + Control
ESCs + pRNA
H3K9me2 ChIP 1
H3K9me3 ChIP 1
H3K9me2 ChIP 2
H3K9me3 ChIP 2
H3K9me2 ChIP 3
H3K9me3 ChIP 3
H3K9me2 ChIP 4
H3K9me3 ChIP 4
Rel. occupancy

Figure S4

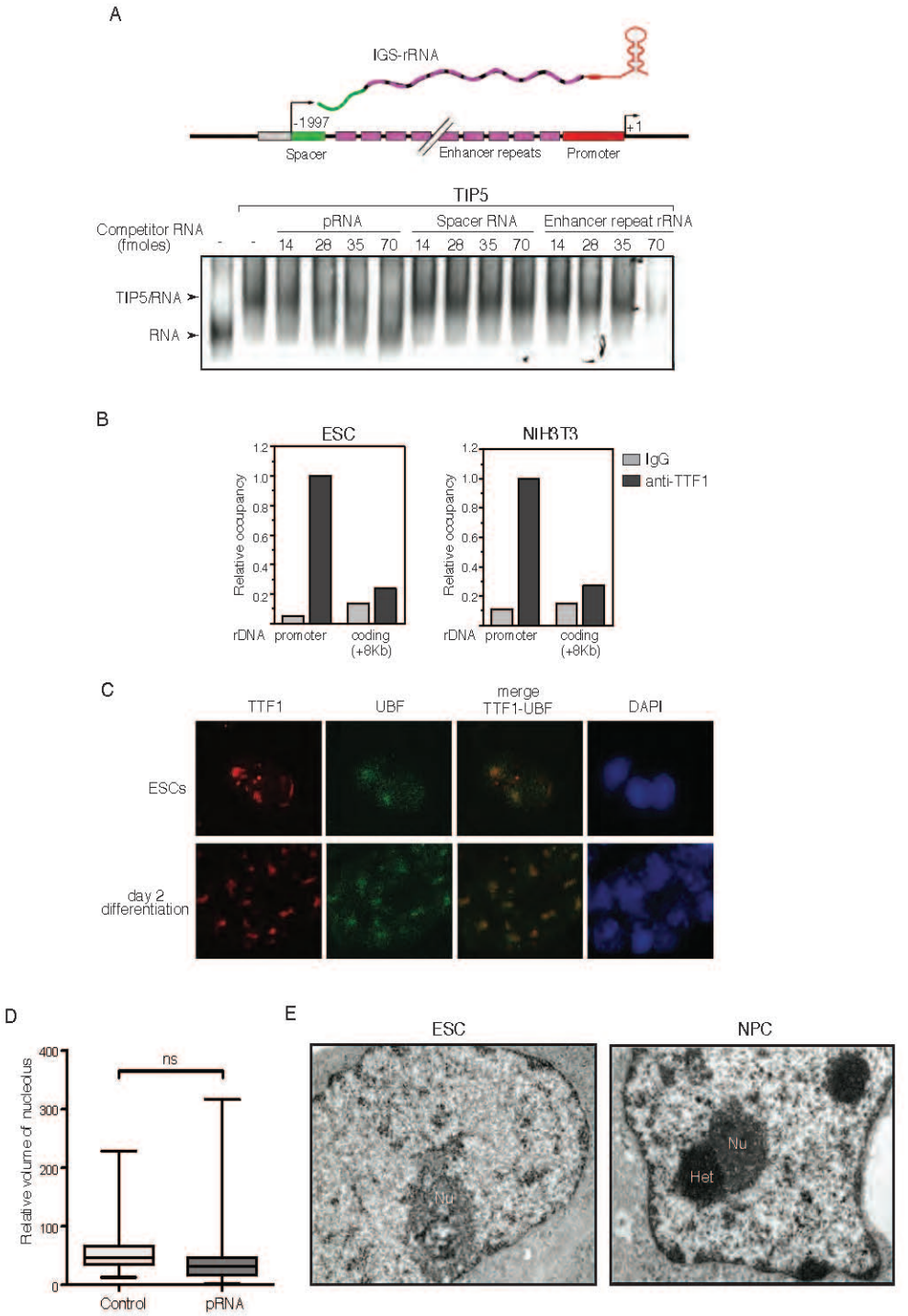
A
IGS-rRNA
-1997
+1
Spacer
Enhancer repeats
Promoter
TIP5
Competitor RNA (fmoles)
pRNA
Spacer RNA
Enhancer repeat rRNA
- - 14 28 35 70 14 28 35 70 14 28 35 70
TIP5/RNA
RNA
B
ESC
NIH3T3
IgG
anti-TTF1
Relative occupancy
rDNA promoter coding (+8Kb)
C
TTF1
UBF
merge TTF1-UBF
DAPI
ESCs
day 2 differentiation
D
Relative volume of nucleolus
ns
Control
pRNA
E
ESC
NPC
Nu
Het

Figure S5

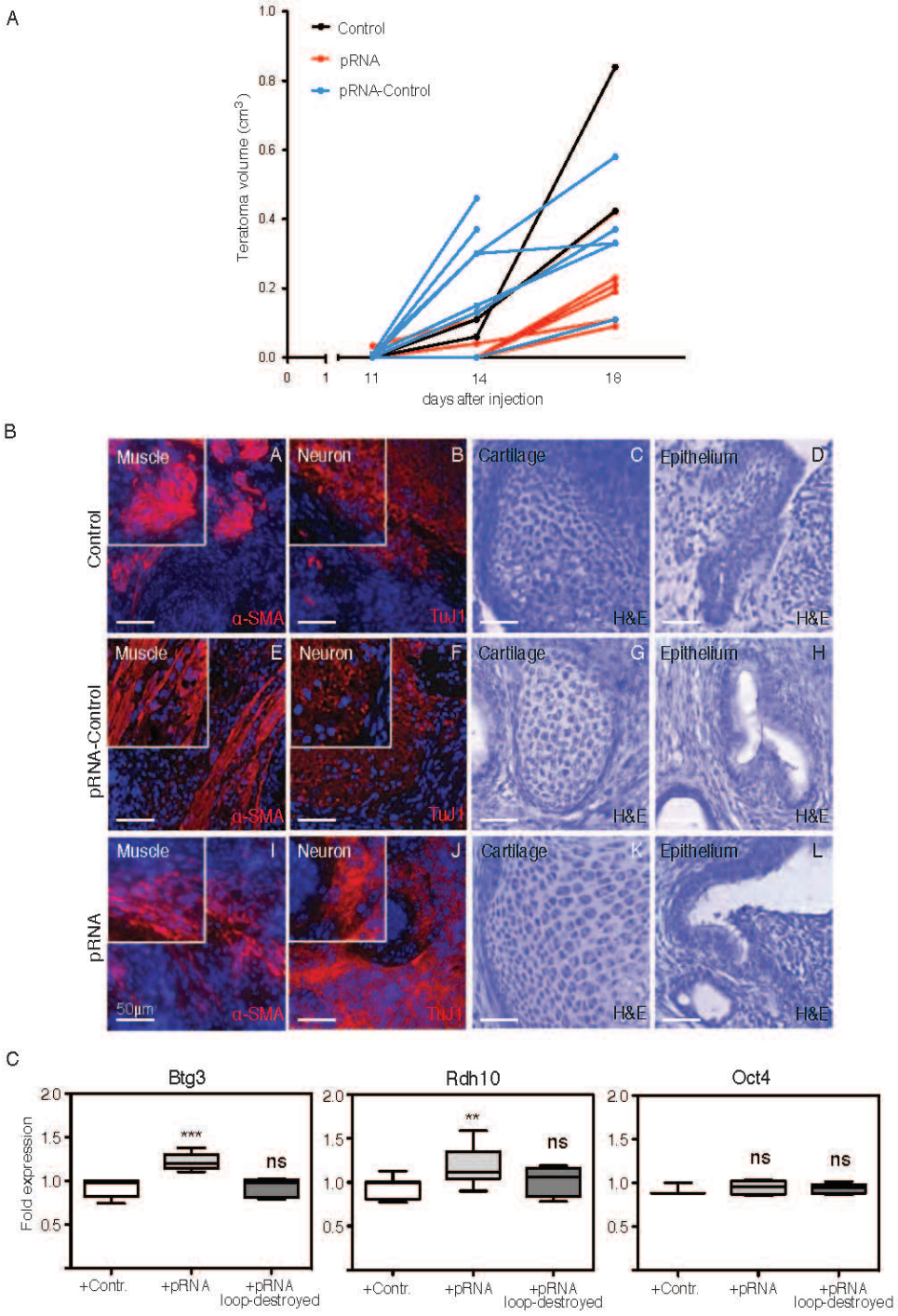
A
Control
pRNA
pRNA-Control
Teratoma volume (cm3)
days after injection
B
Control
pRNA-Control
pRNA
Muscle
Neuron
Cartilage
Epithelium
α-SMA
TuJ1
H&E
50µm
C
Btg3
Rdh10
Oct4
Fold expression
***
**
ns
+Contr.
+pRNA
+pRNA loop-destroyed

Figure S6

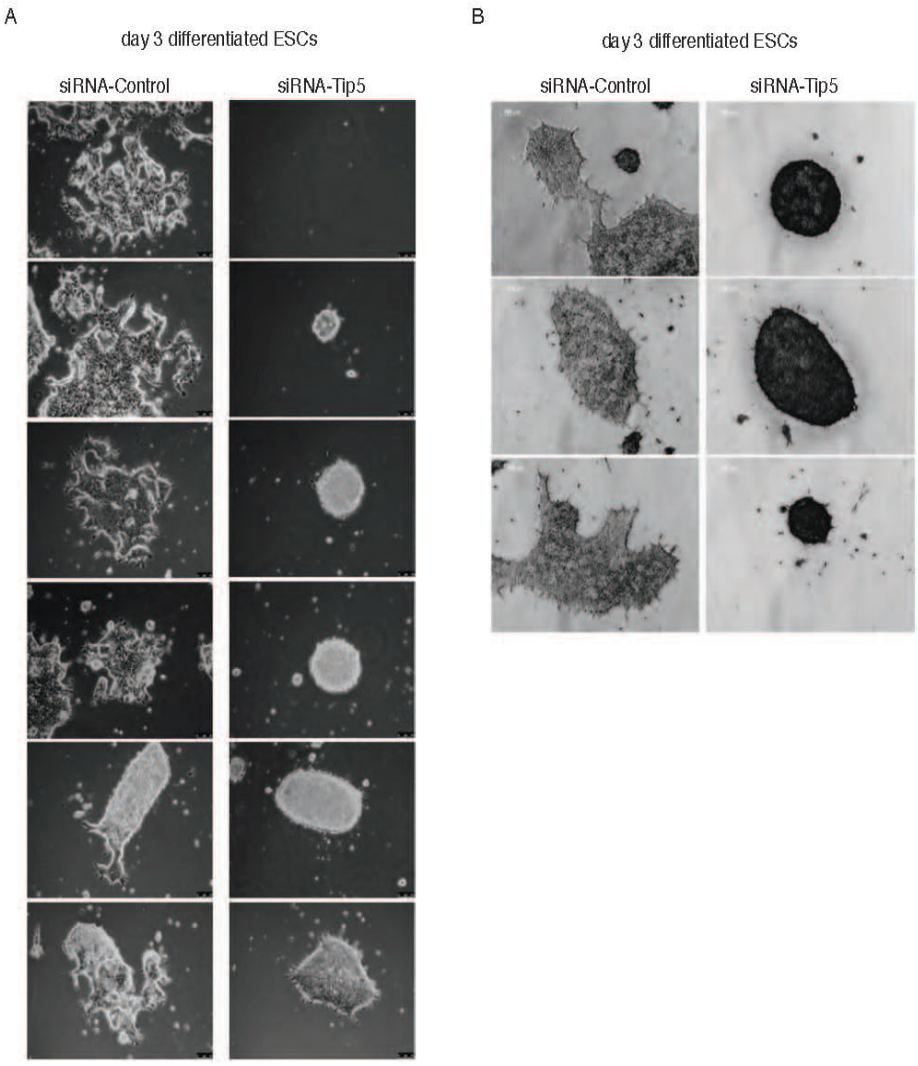
A
day 3 differentiated ESCs
siRNA-Control
siRNA-Tip5
B
day 3 differentiated ESCs
siRNA-Control
siRNA-Tip5

Figure S7

Supplemental Figure Legends

Figure S1. Establishment of rDNA heterochromatin occurs during ESC differentiation. Related to Figure 1.

(A) qRT-PCR. *Nestin* and *Blbp* (neural precursor markers) mRNA levels in ESCs and NPCs. Data were normalized to *Rps12* mRNA. Error bars indicate the SD of three independent experiments.

(B) CpG methylation levels at rDNA promoter in ESCs (JM8N4) and during 7 days of differentiation into NPCs. ESCs were cultivated on monolayer and differentiation was induced with N2B27 medium supplemented with RA. Error bars indicate the SD of two independent experiments.

(C) ChIP. H3K9me2 and H3K9me3 occupancy at rDNA promoter and coding sequences, major and minor satellites and control gene *Evx1* monitored during different time points (days) of differentiation. Data were normalized to input and rDNA promoter values in ESCs.

(D) ChIP. H3K4me2 and H3K4me3 occupancy in ESCs and NPCs. *Evx1*, *Zfpm2* and *Dlx1* represent control genes. Data were normalized to input and rDNA promoter values in ESCs.

(E) Major and minor satellite transcript levels in ESCs and NPCs were measured by qRT-PCR and normalized to *Rps12* mRNA. Error bars indicate the SD of two independent experiments.

Figure S2. Establishment of rDNA heterochromatin during ESC differentiation correlates with the recruitment of TIP5 to rDNA. Related to Figure 1.

(A) TIP5 localizes within nucleoli shortly after ESC differentiation. Immunofluorescence showing TIP5 nucleolar localization in ESCs after 2 and 4 days differentiation. Nucleoli are visualized by UBF signal.

(B) Quantification of TIP5, UBF and DAPI colocalization measured using Fiji image analysis software.

Figure S3. The stem-loop structure of pRNA is sufficient to target TIP5 to nucleoli. Related to Figure 3.

Quantification of nucleolar localization of TIP5 in ESCs transfected with RNA Control, pRNA, pRNA and pRNA mutants (pRNAΔT_0, Control-pRNA, pRNA-Control, pRNA-loop destroyed and pRNA-loop recovered). TIP5, UBF and DAPI signals were measured using Fiji image analysis software.

Figure S4. Mature pRNA increases H3K9me2 and H3K9me3 at rDNA and centric-pericentric heterochromatin in ESCs. Related to Figure 3.

(A) Scatter plot of the four ChIP experiments shown in Figure 3D.

(B) Results of the single four ChIP experiments showing an inverse correlation in the enrichment between H3K9me2 and H3K9me3 levels at minor and major repeats in ESCs+pRNA when compared to ESCs+RNA-control. Data are represented as bound over input in ESCs+pRNA normalized to values measured in ESCs+RNA-control.

Figure S5. Mature pRNA mediates TIP5-TTF1 interaction and induces global remodelling toward heterochromatic structures pRNA. Related to Figure 4 and 5.

(A) TIP5 binds to IGS-rRNA and it has a stronger affinity for pRNA sequences. Increasing equal moles of *in vitro* transcripts corresponding to pRNA, spacer promoter and enhancer repeat RNA were used to compete for binding of $TIP5_{332-723}$ to radiolabelled run-off transcripts from pBluescript (MCS-RNA). RNA/protein complexes were analyzed by EMSA.

(B) TTF1 binds to the rDNA promoter of ESCs. ChIP showing association of TTF1 with rDNA promoter in ESCs and NIH3T3 cells. Data of two independent experiments were normalized to input and rDNA promoter values. The low levels of TTF1 association with +8 Kb rDNA sequences (that do not contain T elements) demonstrated the specificity of the assay.

(C) TTF1 is localized within nucleoli of ESCs and differentiated cells. Immunofluorescence showing TTF1 nucleolar localization in ESCs and 2 days after differentiation. Nucleoli are visualized by UBF signal.

(D) Box-and-whisker plot of nucleoli size in ESCs+Control and ESCs+pRNA. 25 to 34 nucleoli of ESCs+RNA control and ESCs+pRNA of two independent experiments were selected at random

and independent of their size or shape in the EM montages. Volumes were estimated using the Cavalieri-estimator (Gundersen et al., 1988; West, 2012). Nucleoli volumes did not differ among control and ESCs+pRNA while heterochromatin associated to nucleoli did. The volume of nucleolus-associated heterochromatin was expressed as a percentage of the volume of the nucleolus (Nu) that was associated with and shown in main Figure 5B.

(E) Transmission electron microscopy analysis of ESCs and NPCs. The contrast procedure reveals in dark condensed heterochromatic structures (Het) and nucleoli (Nu).

Figure S6. pRNA impairs ESC pluripotency. Related to Figure 6.

(A) Kinetics of teratoma growth from the time of injection to euthanasia of control animals. In this experiment, tumors derived from ESCs+RNA-control (2), ESCs+pRNA (6) and ESCs+mutant pRNA-Control (7) were analysed.

(B) Histological analysis of teratomas derived from ESCs transfected with RNA-control, pRNA and mutant pRNA-Control revealed that ESCs differentiate into all three germ layers as shown by the presence of ectoderm (B, F, J), endoderm (C) and mesoderm (A,E,I). C,D,G,H,K,L haematoxylin staining. Immunostaining for bIII tubulin (TuJ1) (B,F,J), and smooth muscle actin (SMA) (A,E,I). Inserts show higher magnification. Scale bars, 50 μm.

(C) Box-and-whisker plot of three independent experiments showing mRNA levels of *Btg3*, *Rdh10* and *Oct4* measured in ESCs transfected with RNA-control, pRNA and mutant pRNA loop-destroyed. *Btg3* and *Rdh10* are known to be implicated in neurogenesis and embryonic differentiation (Cammas et al., 2007; Yoshida et al., 1998). Consistent with the results of Fig. 6A, *Oct4* mRNA levels remained unaffected in all three conditions.

Figure S7. Depletion of TIP5 impairs ESC differentiation. Related to Figure 7.

(A) Cell morphology and (B) AP staining of differentiated ESCs treated with siRNA-control and -*Tip5*.

Supplemental Table Legends

Supplemental Table S1. Related to Figure 6.

Total RNA of ESCs+RNA-Control and ESCs+pRNA from two biological replicates were purified and analyzed by RNA seq. The table includes the list of genes whose transcript levels were altered in ESCs+pRNA when compared to control cells (defined as regulated, upregulated and downregulated) and gene onthology analysis using DAVID tools.

Supplemental Experimental procedures

Reprogramming into iPSC

Reprogramming was performed as previously described (Weber et al., 2013). Breifly, mouse embryonic fibroblasts (MEF) were isolated from 14.5 day-pregnant C57BL/6 mice and cultured in DMEM supplemented with 10% FBS (PAA) and 1% L-glutamin/penicillin/streptomycin (10,000 U/ml penicillin G sodium; 10,000µg /ml streptomycin sulphate; 29.2mg/ml L-glutamine; 10mM sodium citrate in 0.14% NaCl, Gibco). The reprogramming of the MEFs was performed according to Yamanaka's protocol (Takahashi et al., 2007) using the pMXs retroviral vectors producing murine *Oct4*, *Sox2*, *Klf4* and *c-Myc* (Addgene, cat. nos. 13366, 13367, 13370 and 13375). Two days after infection, MEFs were cultured in DMEM containing 15% FBS, 1% L-glutamin/penicillin/streptomycin, 1x MEM non-essential amino acids (GIBCO) and 50 mM ß-mercaptoethanol (GIBCO) supplemented with 1000 U/ml ESGRO murine Leukemia inhibitory factor (LIF, Chemicon Int.). The iPSC cell line used for the experiment of Figure 1D has the ability to generate teratoma (data not shown).

Transfections

ESCs were seeded at a density of 20,000 cells/cm^2 and transfected with the indicated siRNAs (50 nM siRNA) or synthetic RNAs (1 mg/ml) using Lipofectamine® RNAiMAX (Life Techonlogies) in Opti-MEM® GlutaMAX™ (GIBCO) reduced-serum medium. Analysis of differentiated transfected ESCs was performed using consecutive transfections. Three days after the first transfection, equal amounts of ESCs (e.g. siRNA-control and siTIP5 treated cells) were again transfected and induced to differentiate in complete media (G-MEM, 10%FCS, Sodium Pyruvate 100mM, 1xMEM NEAA, L-Glutamine) by withdrawal of LIF and 2i. Efficiencies of siRNA-mediated depletions and synthetic RNA levels were monitored by qRT-PCR 3-4 days post-transfection.

In Vitro Transcription

The indicated pRNA and control sequences were cloned by PCR into pJET1/2 plasmids. pRNA : mrDNA from -232 to -1; Control-pRNA: control sequences at 5', mrDNA from -140 to -1 at 3';

pRNA-Control: mrDNA from -232 to -140 at 5', control sequences at 3' ; pRNA-loop destroyed: mrDNA from -232 to -1 sequences where GGG (-115/-113) were replaced with AAA; pRNA-loop recovered: mrDNA from -232 to -1 sequences where CCC (-60/-58) were replaced with TTT. All plasmids were verified by sequencing. Synthetic RNAs were synthesized using T7 polymerase and as substrate Xba I linearized pJET1/2 vectors containing the indicated sequences. After treatment with DNase I, transcripts were double purified using TRIzol reagent (Invitrogen) according to the manufacture's protocol.

Chromatin Immunoprecipitation

The chromatin immunoprecipitation (ChIP) protocol was previously described (Santoro, 2014). Briefly, formaldehyde 1% was added to cultured cells to cross-link proteins to DNA. Isolated nuclei were then lysed in 300µl lysis buffer (50 mM Tris-HCl [pH 8.1], 10 mM EDTA, 1% SDS) and sonicated using a Bioruptor ultrasonic cell disruptor to shear genomic DNA to an average fragment size of 200bp. 20 to 40 mg chromatin was diluted tenfold with IP buffer (16.7 mM Tris-HCl [pH 8.1]), 167 mM NaCl, 1.2 mM EDTA, 0.01% SDS, 1.1% Triton X-100) and than immunoprecipitated overnight with ChIP-grade antibodies. After elution and reversion of crosslinks, the precipitated DNA was purified with phenol/chloroform, ethanol precipitated and than quantified by qPCR. rDNA, major and minor satellite sequences were amplified with previously reported primers (Martens et al., 2005) (Martens et al., 2005; Santoro et al., 2002). Primers are listed in Table S2.

RNA Extraction, reverse transcription and quantitative PCR (RT-qPCR)

RNA was purified with Trizol reagent (Life Technologies) . Residual contaminating genomic DNA was removed with Ambion® TURBO™ DNase according to manufacture's instructions. RNA was primed with random hexamers and reverse-transcribed to first-strand cDNA. Reverse transcription of pRNA and IGS-rRNA was performed using DNA oligo -20/-1 Rev or random primers. qRT-PCR was performed with SensiMix SYBR Hi-ROX Mix (Bioline) on a Rotor-Gene Q (Qiagen). Amplification of samples without reverse transcriptase assured absence of DNA (data

not shown). The relative transcription levels were determined by normalizing to Rps12 mRNA levels. Statistical significance (P-values) of the difference in expression levels between genes was calculated using the two-sample paired t-test. Primer sequences used in qRT-PCR are listed in Table S2.

CpG methylation

rDNA CpG methylation was measured as previously described (Santoro, 2014; Santoro et al., 2002)). 2 μg genomic DNA were digested with HpaII (NEB) in the presence of 5 ng of unmethylated pBluescript KS(+) plasmid. rDNA CpG methylation levels were measured by quantitative amplification using primer pairs (-165/-145 Forw and -20/-1 Rev) that flank the restriction sites CCGG at -142 of rDNA promoter or primers that amplify neighbouring sequences lacking HpaII sites (+1/+20 Forw and +111/+130 Rev). Values were obtained using logarithmic dilutions of mouse genomic DNA as standard curve. CpG methylation levels were calculated as resistance to HpaII digestion by normalizing the amounts of rDNA amplified from -165 to -1 to the levels of amplicons from +1 to +130. To verify HpaII digestion efficiency, pBluescript KS(+) plasmid was analyzed by qPCR using one forward primer that is complementary to sequences upstream of the CCGG site of β-lactamase gene (at 2580) and two different reverse primers that map upstream and downstream the HpaII sites (see Table S2). All analyzed samples displayed 96-98% digestion efficiency.

GST-Pulldown

5 μg of GST-TIP5$_{235-741}$ were incubated with 15μl of GST beads (Glutathione Sepharose 4B, GE Healthcare) in AM100 buffer (100mM KCl, 20mM Tris-HCl pH 8.0, 5mM $MgCl_2$, 0.2mM EDTA, 1X Protease Inhibitor (Roche)) for 12-16 hours at 4°C. After two washes with EMSA buffer containing 3% Glycerol, bound GST-TIP5$_{235-741}$ was incubated with 25 nmoles of the indicated RNAs for 1h at 4°C. After a double wash with AM200 buffer (200mM KCl, 20mM Tris-HCl pH 8.0, 5mM $MgCl_2$, 0.2mM EDTA, 1X cOmplete Protease Inhibitor Cocktail (Roche)), bound GST-TIP5/RNA complexes were incubated with 0.5 μg of His-TTF1$_{1-210}$ for 2h at 4°C. Samples were then washed

three times with EBC buffer (250mM NaCl, 50mM Tris-HCl pH8.0, 0.5% NONIDET P-40, 5mM DTT, 1X cOmplete Protease Inhibitor Cocktail), run on a 12% SDS polyacrylamide gel and analyzed by Western blot with anti-GST and anti-RGS.HIS antibodies.

AP staining

Cells were fixed in 4% paraformaldehyde for 10min, washed with AP Buffer (100mM TrisCl pH 9.5, 100mM NaCl, 50mM MgCl2) and then incubated for 30 min in AP Buffer containing NBT (37 mg/ml) and 3.5µl BCIP (175 mg/ml). The staining was blocked with Tris-EDTA (Sigma) for 10min.

Whole-Transcriptome Shotgun Sequencing (RNA-Seq) and Data Analyses

Total RNA of ESCs+Control-RNA and ESCs+pRNA from two biological replicates were purified and analyzed by RNA seq. 100bp paired-end reads have been sequenced with illumina Hiseq. The reads were quality filtered and submitted to RSEM for expression quantitation (Li and Dewey, 2011). Expression counts were further analyzed with the glm method in the edgeR package to compute the significance of differential expression (Robinson et al., 2010).

Teratoma analysis

Teratoma samples were fixed in 4% buffered paraformaldehyde and embedded in paraffin. For immunostainings, 5 µm thickness paraffin sections were deparaffinized and rehydrated and subsequently subjected to the antigen retrieval (Citrate buffer pH 6.0 for 10 minutes at 110°C in rapid microwave histoprocessor, Milestone, USA). The following primary antibodies were used: anti-bIII tubulin (Sigma), anti-GFAP (DAKO) and anti-SMA (Sigma). Nuclei were stained with DAPI and slides were mounted with Fluorescent Mounting Medium (DAKO) to avoid bleaching. Images were captured with a Leica DMI 6000B Microscope and using LAS AF (Leica Application Suite Advanced Fluorescence) software. Animal experiments were performed in accordance with Swiss law and have been approved by the veterinary authorities of Zurich.

Antibodies

The following antibodies were used: anti-TIP5 (CS-090-100-Diagenode); anti-UBF (sc-13125), anti-GST (sc-459) and anti-PARP1 (sc-53643) from Santa Cruz; anti-H3K9me2 (17-648), anti-H3K9me3 (17-625), and anti-H3K27me3 (17-622) and anti-SSEA-1 from Millipore; anti-H3 (ab1791) from Abcam; anti-RGS.HIS (34610) from Qiagen. Anti-TTF1 antibody was produced with Genosphere.

List of primers

mouse rDNA CpG methylation primers		
Name	**For/Rev**	**Sequence**
rDNA promoter -165/-145	For	GACCAGTTGTTCCTTTGAGG
rDNA promoter -21/-1	Rev	ACCTATCTCCAGGTCCAATAG
rDNA coding +1/+20	For	ACTGACACGCTGTCCTTTCC
rDNA coding +111/+130	Rev	GACAGCTTCAGGCACCGCGA

mouse cDNA primers		
Name	**For/Rev**	**Sequence**
Tip5	For	AAGATGTGTGGCTACAATGG
Tip5	Rev	TCTGCACCCATCAGCTCCG
Nanog	For	AAGCAGAAGATGCGGACTGT
Nanog	Rev	ATCTGCTGGAGGCTGAGGTA
Pax6	For	GCACATGCAAACACACATGA
Pax6	Rev	ACTTGGACGGGAACTGACAC
Nestin	For	AGGCTGAGAACTCTCGCTTGC
Nestin	Rev	GGTGCTGGTCCTCTGGTATCC
Blbp	For	AGGTGGCAAAGTGGTGATCC
Blbp	Rev	TCCAACCGAACCACAGACTTAC
Minor satellites	For	CATGGAAAATGATAAAAACC
Minor satellites	Rev	CATCTAATATGTTCTACAGTGTGG
Major satellites	For	GACGACTTGAAAAATGACGAAATC
Major satellites	Rev	CATATTCCAGGTCCTTCAGTGTGC
rDNA spacer -1994/1975	For	GCAGACCGAGTTGCTGTAC
rDNA spacer -1922/1905	Rev	GGGTAGGACTTAAGCCTT
rDNA enhancer -554/-535	For	GAAGCCCTCTTGTCCCCGTC
rDNA enhancer -466/-447	Rev	GATCCAAAGCTCCAGCTGAC
rDNA promoter -165/-145	For	GACCAGTTGTTCCTTTGAGG
rDNA promoter -21/-1	Rev	ACCTATCTCCAGGTCCAATAG
45S pre-rRNA +550/570	For	CTCTTGTTCTGTGTCTGCC
45S pre-rRNA +745/765	Rev	GCCCGCTGGCAGAACGAGAAG
Line L1 ORF2	For	TTTGGGACACAATGAAAGCA
Line L1 ORF2	Rev	CTGCCGTCTACTCCTCTTGG
IAPgag	For	AGCAGGTGAAGCCACTG
IAPgag	Rev	CTTGCCACACTTAGAGC
Btg3	For	AAGGTCAGGCCTACAGATGC
Btg3	Rev	GGTCACCTTATCCAGAGCCC
Rdh10	For	GAAATCCTGCCCCCGTGTAA

Rdh10	Rev	TAGTGGTCCAGAAGTGTGCG
Oct-4	For	GGCGTTCGCTTTGGAAAGGTGTTC
Oct-4	Rev	CTCGAACCACATCCTTCTCT
Rex1	For	AGAAAGCAGGATCGCCTCAC
Rex1	Rev	AGGGAACTCGCTTCCAGAAC
Rps12	For	GAAGCTGCCAAAGCCTTAGA
Rps12	Rev	AACTGCAACCAACCACCTTC
Gapdh	For	TGCACCACCAACTGCTTAGC
Gapdh	Rev	GGCATGGACTGTGGTCATGAG

ChIP primers		
Name	**For/Rev**	**Sequence**
rDNA promoter -165/-145	For	GACCAGTTGTTCCTTTGAGG
rDNA promoter -21/-1	Rev	ACCTATCTCCAGGTCCAATAG
rDNA coding +2251/70	For	GCATCGGTGTGTCGGCATCG
rDNA coding +2346/65	Rev	CTGAGCAGTCCCACCACACC
rDNA coding +8124/145	For	GCGACCTCAGATCAGACGTGG
rDNA coding +8203/224	Rev	CTGTTCACTCGCCGTTACTGAG
Minor satellites	For	CATGGAAAATGATAAAAACC
Minor satellites	Rev	CATCTAATATGTTCTACAGTGTGG
Major satellites	For	GACGACTTGAAAAATGACGAAATC
Major satellites	Rev	CATATTCCAGGTCCTTCAGTGTGC
Evx1 TSS	For	TACACAGCATCTGGGGAGTG
Evx1 TSS	Rev	GTGTGCTGGGTTAAGGGAGA
Zfpm2 TSS	For	GGATGAAGTTCTCAGAGCTGGT
Zfpm2 TSS	Rev	GCGCGAACTTTTACACCTACTT
Dlx1 TSS	For	ATGTCTCCTTCTCCCATGTCC
Dlx1 TSS	Rev	ACTGCACGGAACTGATGTAGG
Gapdh promoter	For	GGTTGCTGTGTCACTACCGAAGAA
Gapdh promoter	Rev	AAATGGAGAAGTGTGGGTCTCCCT
Line L1 ORF2	For	TTTGGGACACAATGAAAGCA
Line L1 ORF2	Rev	CTGCCGTCTACTCCTCTTGG
IAPgag	For	AGCAGGTGAAGCCACTG
IAPgag	Rev	CTTGCCACACTTAGAGC

Supplemental References

Cammas, L., Romand, R., Fraulob, V., Mura, C., and Dolle, P. (2007). Expression of the murine retinol dehydrogenase 10 (Rdh10) gene correlates with many sites of retinoid signalling during embryogenesis and organ differentiation. Developmental dynamics : an official publication of the American Association of Anatomists *236*, 2899-2908.
Gundersen, H.J.G., Bendtsen, T.F., Korbo, L., Marcussen, N., Møller, A., Nielsen, K., Nyengaard, J.R., Pakkenberg, B., Sørensen, F.B., Vesterby, A., *et al.* (1988). Some new, simple and efficient stereological methods and their use in pathological research and diagnosis. Apmis *96*, 379-394.
Li, B., and Dewey, C.N. (2011). RSEM: accurate transcript quantification from RNA-Seq data with or without a reference genome. BMC Bioinformatics *12*, 323.
Martens, J.H., O'Sullivan, R.J., Braunschweig, U., Opravil, S., Radolf, M., Steinlein, P., and Jenuwein, T. (2005). The profile of repeat-associated histone lysine methylation states in the mouse epigenome. EMBO J *24*, 800-812.
Robinson, M.D., McCarthy, D.J., and Smyth, G.K. (2010). edgeR: a Bioconductor package for differential expression analysis of digital gene expression data. Bioinformatics *26*, 139-140.
Santoro, R. (2014). Analysis of chromatin composition of repetitive sequences: the ChIP-Chop assay. Methods Mol Biol *1094*, 319-328.
Santoro, R., Li, J., and Grummt, I. (2002). The nucleolar remodeling complex NoRC mediates heterochromatin formation and silencing of ribosomal gene transcription. Nat Genet *32*, 393-396.
Takahashi, K., Tanabe, K., Ohnuki, M., Narita, M., Ichisaka, T., Tomoda, K., and Yamanaka, S. (2007). Induction of pluripotent stem cells from adult human fibroblasts by defined factors. Cell *131*, 861-872.
Weber, F.A., Bartolomei, G., Hottiger, M.O., and Cinelli, P. (2013). Artd1/Parp1 regulates reprogramming by transcriptional regulation of Fgf4 via Sox2 ADP-ribosylation. Stem Cells *31*, 2364-2373.
West, M.J. (2012). Estimating volume in biological structures. Cold Spring Harb Protoc *2012*, 1129-1139.
Yoshida, Y., Matsuda, S., Ikematsu, N., Kawamura-Tsuzuku, J., Inazawa, J., Umemori, H., and Yamamoto, T. (1998). ANA, a novel member of Tob/BTG1 family, is expressed in the ventricular zone of the developing central nervous system. Oncogene *16*, 2687-2693.

nature COMMUNICATIONS

ARTICLE

Received 9 May 2014 | Accepted 4 Dec 2014 | Published 22 Jan 2015

DOI: 10.1038/ncomms7051

The epigenetic modifier EZH2 controls melanoma growth and metastasis through silencing of distinct tumour suppressors

Daniel Zingg[1], Julien Debbache[1,*], Simon M. Schaefer[1,*], Eylul Tuncer[1,*], Sandra C. Frommel[2], Phil Cheng[3], Natalia Arenas-Ramirez[4], Jessica Haeusel[1], Yudong Zhang[1], Mario Bonalli[1], Michael T. McCabe[5], Caretha L. Creasy[5], Mitchell P. Levesque[3], Onur Boyman[4], Raffaella Santoro[2], Olga Shakhova[1,6], Reinhard Dummer[3] & Lukas Sommer[1]

Increased activity of the epigenetic modifier EZH2 has been associated with different cancers. However, evidence for a functional role of EZH2 in tumorigenesis *in vivo* remains poor, in particular in metastasizing solid cancers. Here we reveal central roles of EZH2 in promoting growth and metastasis of cutaneous melanoma. In a melanoma mouse model, conditional *Ezh2* ablation as much as treatment with the preclinical EZH2 inhibitor GSK503 stabilizes the disease through inhibition of growth and virtually abolishes metastases formation without affecting normal melanocyte biology. Comparably, in human melanoma cells, EZH2 inactivation impairs proliferation and invasiveness, accompanied by re-expression of tumour suppressors connected to increased patient survival. These EZH2 target genes suppress either melanoma growth or metastasis *in vivo*, revealing the dual function of EZH2 in promoting tumour progression. Thus, EZH2-mediated epigenetic repression is highly relevant especially during advanced melanoma progression, which makes EZH2 a promising target for novel melanoma therapies.

[1] Cell and Developmental Biology, Institute of Anatomy, University of Zurich, Winterthurerstrasse 190, 8057 Zürich, Switzerland. [2] Institute of Veterinary Biochemistry and Molecular Biology, University of Zurich, Winterthurerstrasse 190, 8057 Zürich, Switzerland. [3] Department of Dermatology, University Hospital Zurich, Gloriastrasse 31, 8091 Zürich, Switzerland. [4] Department of Immunology, University Hospital Zurich, Gloriastrasse 30, 8091 Zürich, Switzerland. [5] Cancer Epigenetics Discovery Performance Unit, Cancer Research, Oncology R&D, GlaxoSmithKline, 1250 South Collegeville Road, Collegeville, Pennsylvania 19426, USA. [6] Department of Oncology, University Hospital Zurich, Rämistrasse 100, 8091 Zürich, Switzerland. * These authors contributed equally to this work. Correspondence and requests for materials should be addressed to L.S. (email: lukas.sommer@anatom.uzh.ch).

Melanoma is the most deadly skin cancer, with a yearly increasing incidence rate[1]. Its aggressiveness is based on the highly metastatic potential of melanoma cells, which can still not be efficiently targeted despite recent progress in melanoma therapies[2]. In fact, currently available drugs frequently induce resistance[3] and have even been shown to promote invasiveness and metastasis of resistant cells[4]. Thus, new treatments for metastatic melanoma need to be established.

Melanoma arises from melanocytes that originate during embryonic development from neural crest stem cells (NCSCs)[5]. In the embryo, neural crest cells delaminate from the neural tube by undergoing an epithelial-to-mesenchymal transition (EMT)[6], a process also implicated in early steps of tumour metastasis[7]. Upon EMT, neural crest cells adopt stem cell features and a remarkable migratory capacity, which allows the cells to disseminate through the embryonic tissue and to colonize distant sites, including the skin where they give rise to melanocytes[8]. Tumorigenesis from these cells is induced by acquired driver mutations, for instance in the *NRAS* or *BRAF* locus[9,10]. Moreover, genes known to regulate NCSCs and melanocyte development have been associated with melanoma formation. For instance, the small Rho GTPase Rac1 controls self-renewal and expansion of post migratory NCSCs[11], and activating mutations in *RAC1* drive melanoma formation[9,10]. Likewise, the transcription factor Sox10 promotes both NCSC maintenance and melanomagenesis in a murine melanoma model[12–14].

Apart from genetic factors, aberrant epigenetic control also frequently leads to developmental disorders[15] and has been connected to oncogenesis[16]. A prominent epigenetic modifier is enhancer of zeste homologue 2 (EZH2), which is a component of the polycomb repressive complex 2. EZH2 contains a SET domain, the catalytic subunit of histone methyltransferases, which catalyses trimethylation of lysine 27 in histone 3 (H3K27me3), and thus induces chromatin compaction and consequently prevents transcription of target genes[17,18]. During embryonic development and in tissue-specific stem cells, EZH2-mediated transcriptional repression often targets lineage commitment or differentiation[17,19,20]. Therefore, in many systems, EZH2 activity supports stem cell maintenance by repressing differentiation. In contrast, in NCSCs Ezh2 neither represses differentiation nor controls stem cell proliferation, but rather promotes the acquisition of a mesenchymal fate[21].

In a wide variety of cancers including melanoma, EZH2 expression is elevated and associated with poor survival[22–24]. In cancer, EZH2 function has predominantly been associated with proliferation and tumour growth, comparable to its role in embryonic and adult tissues[22]. Most of these data have been gathered by means of *in vitro* culture and tumour cell xenograft assays, while studies on the role of EZH2 in physiological *in vivo* models of tumorigenesis are sparse and only focus on hyperplastic transformation of normal cells rather than progression into metastatic disease[25–27].

In human melanoma cells, loss of EZH2 partially interfered with proliferation or invasion capacity, dependent on the cell line and the experimental set up used[28–30]. However, a study investigating EZH2 function in a physiological context of melanoma progression, from tumour initiation to metastatic disease, is still missing. In the present work, we identify essential roles of EZH2 for the initiation and progression of metastatic melanoma *in vivo* and reveal novel tumour suppressors regulated by EZH2. These tumour suppressors represent two distinct sets of target genes that are either involved in regulating proliferation or metastasis formation. Therefore, blocking EZH2 activity might represent a powerful strategy for the development of novel therapies interfering with distinct aspects of melanomagenesis.

Results

EZH2 is highly expressed in human and murine melanoma. Previously, high EZH2 expression has been described in biopsies of malignant melanoma in comparison to benign naevi[23,24]. To address whether changes in EZH2 expression affect cells of the melanocytic lineage rather than stromal cells in the tumour tissue, we performed co-staining of human cutaneous melanoma sections for EZH2 in combination with SOX10 or MART1-HMB45, all markers for the melanocytic lineage[14,31–33]. In agreement with previous studies[23,24], human primary melanomas and metastases displayed high EZH2 expression in cells of the melanocytic lineage compared with epidermal melanocytes and dermal naevus cells (Fig. 1a; Supplementary Fig. 1; Supplementary Table 1). To study the function of Ezh2 in an *in vivo* context of melanoma development, we took advantage of a mouse model of cutaneous melanoma. *Tyr::N-Ras^{Q61K} Ink4a$^{-/-}$* mice display dermal hyperplasia reminiscent of human congenital naevi and consistently develop metastatic melanoma within 6 months of age[14,34]. Similar to human patients, Ezh2 protein was strongly expressed in Sox10-positive cells of murine skin melanoma and distant metastases. In contrast, Sox10-expressing cells in hair follicle bulbs, the physiological location of melanocytes in murine trunk skin[35], and in dermal hyperplasia only showed marginal Ezh2 expression (Fig. 1b), consistent with the human data.

Increased EZH2 expression is linked to poor patient survival. To study the significance of high EZH2 expression for the survival of cutaneous melanoma patients, we established an EZH2 high and an EZH2 low patient group based on RNAseq and clinical data from The Cancer Genome Atlas (TCGA). These groups did not display obvious differences with respect to clinically relevant factors including *BRAF* and *NRAS* mutations (Fig. 1c). However, patients of the EZH2 high group showed a significantly shorter overall survival as compared with those of the EZH2 low group (Fig. 1d). Intriguingly, primary melanoma and lymph node metastases patients (stage I–III) of the EZH2 high group developed distant metastases (stage IV) significantly faster than EZH2 low-expressing stage I–III patients (Fig. 1e), implying a potential role of EZH2 in metastatic spread of melanoma.

Apart from expression levels, mutations affecting EZH2 activity have been implicated in malignancies, predominantly of the haematopoietic system[36]. We analyzed the occurrence of *EZH2* somatic mutations in cutaneous melanoma in comparison to nine different cancer types using TCGA and four further data sets[9,10,37,38]. In this analysis, cutaneous melanoma showed the highest non-synonymous *EZH2* mutation frequency besides primary lymphomas (including follicular and diffuse large B-cell lymphomas). In particular, cutaneous melanoma was the only solid cancer with non-synonymous mutations affecting tyrosine 646 (Y646*) in the SET domain of EZH2 (Fig. 2a,b) (EZH2^{Y646*} based on current NCBI protein reference sequence NP_004447.2; earlier referred as EZH2^{Y641*} based on NP_001190176.1). Previously, *EZH2^{Y646*}* mutations were reported to be widely present in primary lymphoma and to lead to increased EZH2 activity resulting in aberrant H3K27me3 (ref. 36). To associate *EZH2* non-synonymous mutations present in melanoma patients with EZH2 function, we overexpressed selected *EZH2* mutations *in vitro*. However, except *EZH2^{Y646*}*, none of the mutations analyzed induced an increase in global H3K27me3 (Fig. 2c,d). Further functional studies are necessary to uncover properties of these mutations that might allow a functional link to cutaneous melanomagenesis.

Ezh2 function is dispensable for homeostasis of melanocytes. Because EZH2 was highly expressed in human and murine

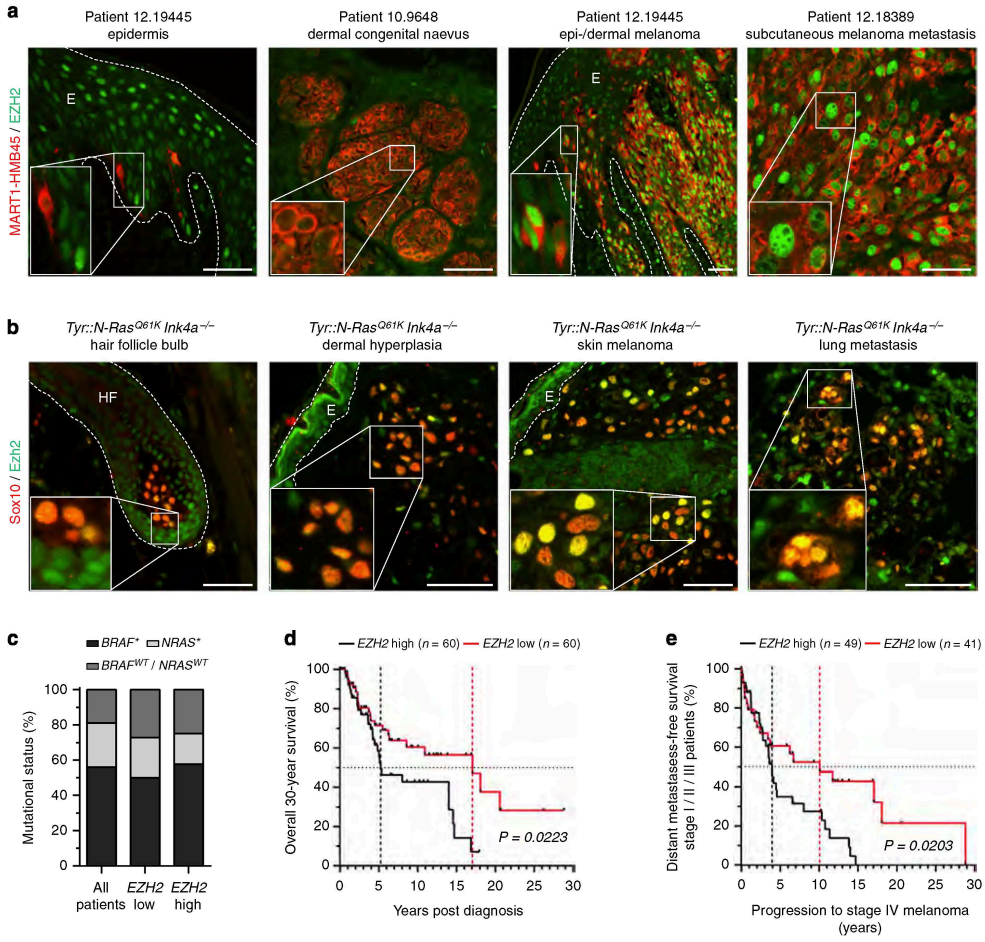

Figure 1 | EZH2 is upregulated in melanoma and correlates with adverse patient survival. (**a**) Immunofluorescent staining for HMB45-MART1 and EZH2 on human epidermis, congenital naevus, primary melanoma and subcutaneous melanoma metastasis sections from biopsies described in (Supplementary Table 1). (**b**) Immunofluorescent staining for Sox10 and Ezh2 on skin and lung sections of melanoma-developing *Tyr::N-Ras*^{Q61K} *Ink4a*$^{-/-}$ mice. (**c**) *BRAF* and *NRAS* mutational status of melanoma specimens included in *EZH2* TCGA analysis. All patients, $n=274$; *EZH2* low, $n=60$; *EZH2* high, $n=60$. (**d**) Kaplan–Meier curves comparing overall survival of melanoma specimens (stage I–IV) with respect to *EZH2* transcript levels based on TCGA. (**e**) Kaplan–Meier curves comparing distant metastases-free survival of stage I–III melanoma specimens (primary melanoma/lymph node metastases) with respect to *EZH2* transcript levels based on TCGA. E, epidermis; *EZH2* low/high, bottom and top 60 patients with respect to *EZH2* transcript levels; HF, hair follicle. *P* values calculated with log-rank (Mantel–Cox) test. Scale bars, 50 μm.

melanoma and linked to poor patient survival, we studied its function *in vivo*. To this end, mice carrying floxed alleles of the *Ezh2* locus[19] were used to conditionally delete *Ezh2* in the melanocytic lineage by tamoxifen (TM)-induced activation of Cre-recombinase (*Tyr::Cre*^{ERT2})[39]. Inclusion of a Cre-reporter allele (*R26R::LacZ*)[40] allowed fate mapping of recombined cells *in vivo*. To address a potential role of Ezh2 in maintaining normal melanocytic function, *Ezh2* was conditionally depleted in tumour-free *Tyr::Cre*^{ERT2} *Ezh2*$^{lox/lox}$ *R26R::LacZ* mice (Fig. 3a). TM was applied to 1-month-old animals, and mice were monitored for hair greying (Fig. 3b). Hair greying is the phenotype predominantly arising upon interference with homeostasis of melanocyte stem cells in the bulge[31,41], the permanent niche of epithelial and melanocyte stem cells in hair follicles[35,42]. However, hair pigmentation remained normal up to 1 year after *Ezh2* depletion (Fig. 3c). Importantly, *Ezh2* was efficiently and durably ablated in melanocytes of trunk skin hair follicles, leading to a concomitant loss of H3K27me3 (Fig. 3d,e).

***N-Ras*^{Q61K}-expressing naevus cells are Ezh2 independent**. This unforeseen independence of the normal melanocyte lineage from Ezh2-mediated gene repression prompted us to investigate a possible function of Ezh2 in maintaining benign naevus-like

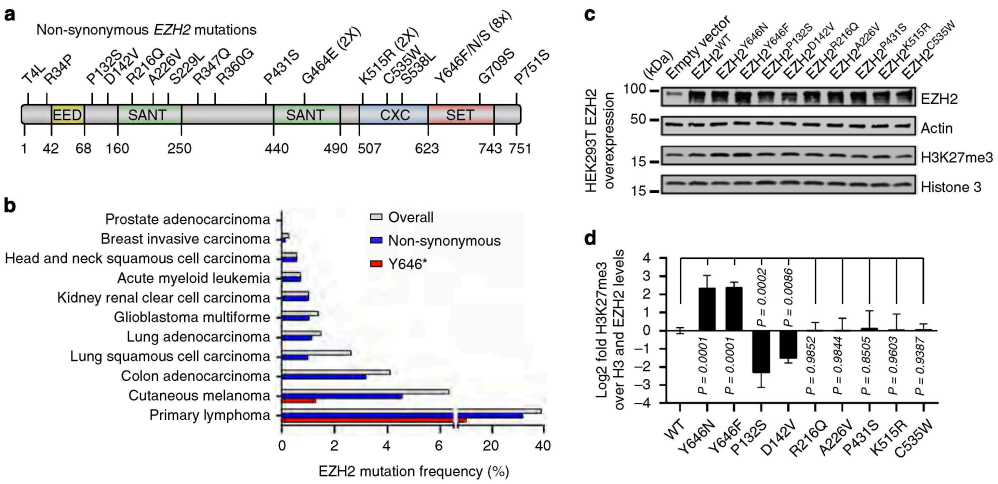

Figure 2 | *EZH2* is frequently mutated in human melanoma. (**a**) *EZH2* non-synonymous mutational landscape including $EZH2^{Y646*}$-activating mutations based on TCGA melanoma data set and three further data sets[9,10,37]. (**b**) *EZH2* mutation frequencies including Y646* in different cancers based on TCGA and two further data sets[9,38]. (**c**,**d**) Western blot for EZH2 protein and H3K27me3 on HEK293T cells overexpressing different *EZH2* mutations to quantify changes in H3K27me3. WT, wild type. Data are represented as mean ± s.e.m. of $n = 4$. *P* values calculated with analysis of variance and Fisher's least significant difference test.

dermal hyperplasia. Therefore, *Ezh2* was depleted in our genetic *Tyr::N-Ras*^{Q61K} *Ink4a*$^{-/-}$ *Tyr::Cre*^{ERT2} *Ezh2*$^{lox/lox}$ *R26R::LacZ* melanoma model (Fig. 4a,b; Supplementary Fig. 2a–c). As in tumour-free mice, conditional deletion of *Ezh2* in *Tyr::N-Ras*^{Q61K} *Ink4a*$^{-/-}$ animals had no effect on hair pigmentation (Fig. 4c; Supplementary Fig. 2d). Importantly, maintenance of benign dermal hyperplasia was also not affected (Supplementary Fig. 2d), despite efficient *Ezh2* depletion and subsequent loss of H3K27me3 (Supplementary Fig. 2e,f). Even when aged for up to 1 year after conditional knockout (cKO) of *Ezh2*, *Tyr::N-Ras*^{Q61K} mice with functional *Ink4a*^{wt} (wild type) loci did not show an overt reduction of recombined melanocytic cells in the dermis (Supplementary Fig. 2e). Accordingly, dermal hyperplasia grew to a similar size with a comparably low proliferation rate in both control and *Ezh2*-depleted mice (Fig. 4d,e). Thus, Ezh2-mediated gene repression is dispensable for both physiological homeostasis of normal melanocytes and maintenance of *N-Ras*^{Q61K}-transformed cells in dermal hyperplasia, independent of *Ink4a*-deficiency.

Ezh2 function is essential for melanoma initiation. To assess a possible role of Ezh2 in tumorigenesis, *Ezh2* was conditionally deleted in our murine melanoma model before appearance of cutaneous tumours (Fig. 4a,b; Supplementary Fig. 3a,b). While in control mice, many skin melanomas (Ø ≥ 2 mm) emerged after ~5 months, appearance of tumours was delayed in *Ezh2* cKO animals (Fig. 4c; Supplementary Fig. 3c) leading to an increased skin melanoma-free survival (Supplementary Fig. 3d). At day of sacrifice, the number of recombined skin melanomas was drastically reduced in *Ezh2* cKO mice compared with the total tumour load in controls (Fig. 4f; Supplementary Fig. 3e). In accordance with these data, melanoma-specific survival was significantly increased (Fig. 4g), independently of control type and sex of *Ezh2* cKO mice (Supplementary Fig. 3f).

Next, we addressed whether Ezh2 might also be implicated in melanoma progression after the onset of the disease. To this end, *Tyr::N-Ras*^{Q61K} *Ink4a*$^{-/-}$ *Tyr::Cre*^{ERT2} *Ezh2*$^{lox/lox}$ *R26R::LacZ* mice were individually monitored until appearance of skin melanomas (Fig. 5d; Supplementary Fig. 4f). *Ezh2* deletion was then induced by TM application (Fig. 5a,b; Supplementary Fig. 4a). High recombination efficiency became apparent 1 month post TM application (Supplementary Fig. 4b,c). Concomitantly, this also led to an efficient loss of Ezh2 protein and H3K27me3 in recombined tumour cells (Fig. 5c; Supplementary Fig. 4d,e). Frequent assessment of the animals showed a marked increase of new melanomas per week in control animals. In striking contrast, the tumour load was stabilized in *Ezh2* cKO mice, in which virtually no new skin melanomas were emerging (Fig. 5d; Supplementary Fig. 4f). Thus, early genetic interference with Ezh2 activity prevents progression of benign dermal hyperplasia into malignant cutaneous melanoma, while *Ezh2* depletion in established melanoma effectively stops emergence of further skin tumours.

Ezh2-targeted therapy interferes with melanoma progression. Our findings indicate that interference with EZH2 activity might be a valid strategy for therapy of advanced melanoma. To test this hypothesis, we treated mice with the preclinical EZH2 inhibitor GSK503, a small chemically optimized compound highly selective for the SET domain of EZH2 and exhibiting favourable pharmacokinetics in mice[27]. Independent of the genotype (wild type, *Ink4a*$^{-/-}$ or *Tyr::N-Ras*^{Q61K} *Ink4a*$^{-/-}$), mice suffered from a tolerable and reversible weight loss of ~10% and, in rare cases, from development of ascites after prolonged treatment with GSK503. To investigate the effect of pharmacological Ezh2 inhibition on tumour progression, *Tyr::N-Ras*^{Q61K} *Ink4a*$^{-/-}$ mice were individually monitored until skin melanomas were detectable (Fig. 5h; Supplementary Fig. 5c) and subsequently treated daily, either with vehicle or GSK503 for 35 consecutive days (Fig. 5e,f; Supplementary Fig. 5a). This procedure reduced H3K27me3 levels in tumour and stromal cells without affecting Ezh2 levels, confirming inhibition of the catalytic function of

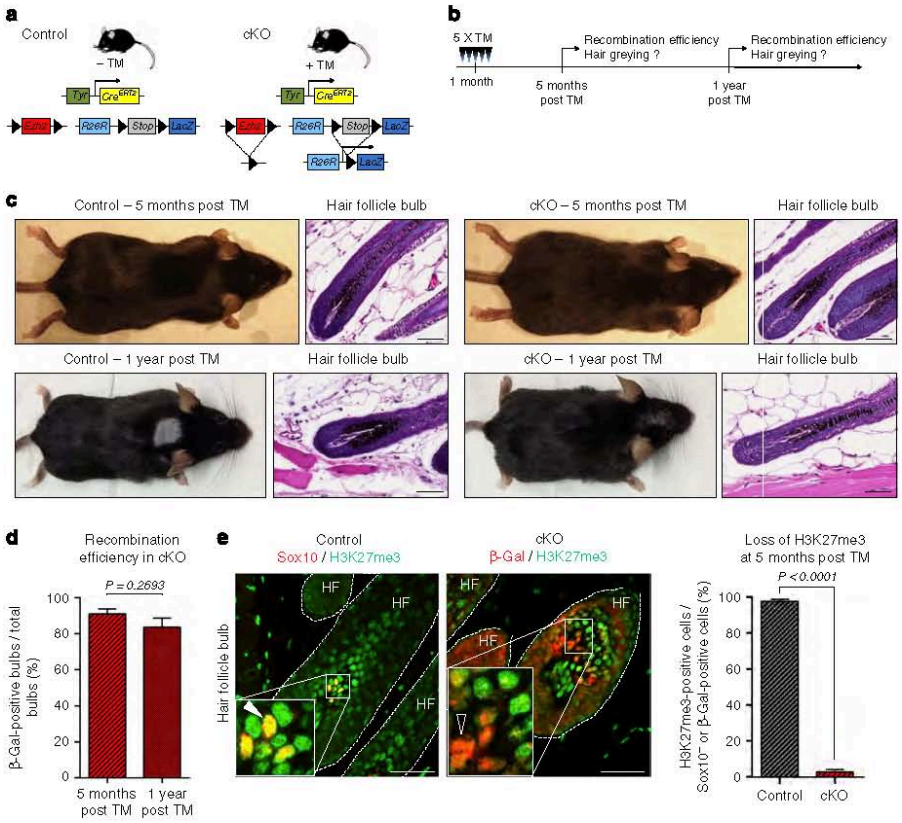

Figure 3 | Ezh2 is not required for normal melanocyte homeostasis. (**a**,**b**) Mouse genotypes (**a**) and strategy (**b**) used to analyze the effect of conditional *Ezh2* ablation in the melanocytic lineage of adult wild type mice. (**c**) Macroscopic pictures and H&E staining on trunk skin sections of control and cKO mice at 5 months and 1 year post conditional *Ezh2* ablation. (**d**) Immunofluorescent staining on trunk skin sections of wt mice for β-Gal to quantify recombination efficiencies (representative fields not shown). (**e**) Immunofluorescent staining on trunk skin sections of wt mice for Sox10 (control) or β-Gal (cKO) and H3K27me3 to quantify H3K27me3 depletion. White arrowhead, Sox10-positive cell considered H3K27me3 positive; white open arrowhead, β-Gal-positive cell considered H3K27me3 negative. H&E, haematoxylin and eosin; HF, hair follicle. Data are represented as mean ± s.e.m. of $n = 3$. *P* values calculated with unpaired Student's *t*-test. Scale bars, 50 μm.

Ezh2 (Fig. 5g, Supplementary Fig. 5b). Comparable to genetic ablation of *Ezh2*, GSK503 treatment drastically reduced the emergence of new skin melanomas over time after treatment start (Fig. 5h; Supplementary Fig. 5c).

EZH2 is required for growth of human and murine melanoma. Our findings demonstrate the requirement of Ezh2 for melanoma initiation. We hypothesized whether this might function through regulation of proliferation, since EZH2 has previously been associated with proliferation of human melanoma cells *in vitro*[28–30]. Interestingly, we observed a heterogeneity with respect to EZH2 expression in melanoma cells of both human biopsies as well as on *Tyr::N-Ras*^{Q61K} *Ink4a* $^{-/-}$ skin tumours and metastases, ranging from high EZH2 expression to almost background levels (Fig. 1a,b; Supplementary Fig. 1). EZH2 highly expressing cells significantly correlated with KI67-positive cells, implicating EZH2-regulated proliferation of melanoma at primary tumour and metastatic sites (Supplementary Fig. 6). To address the relevance of these findings for melanoma growth, we first blocked EZH2 activity in human melanoma cell cultures[43], either by RNA interference-mediated silencing (RNAi) or by chemical inhibition using GSK503. In agreement with our *in vivo* findings, RNAi effectively reduced EZH2, while GSK503 application did not affect EZH2 levels. Both approaches, however, led to a considerable loss of H3K27me3 (Supplementary Fig. 7a,b). Notably, neither RNAi nor prolonged GSK503 application for 8 days did affect cell survival (Supplementary Fig. 7c,d). However, suppressing EZH2 activity stimulated a G1 cell cycle arrest (Supplementary Fig. 7e,f) and slowed down cell growth in culture (Supplementary Fig. 7g,h).

To functionally study EZH2-regulated proliferation *in vivo*, we quantified proliferative cells in tumours of *Tyr::N-Ras*^{Q61K} *Ink4a* $^{-/-}$ mice, either after *Ezh2* cKO or GSK503 application (Fig. 6a,c). Both approaches led to a striking reduction of proliferative tumour cells (Fig. 6b,d). We next engrafted murine

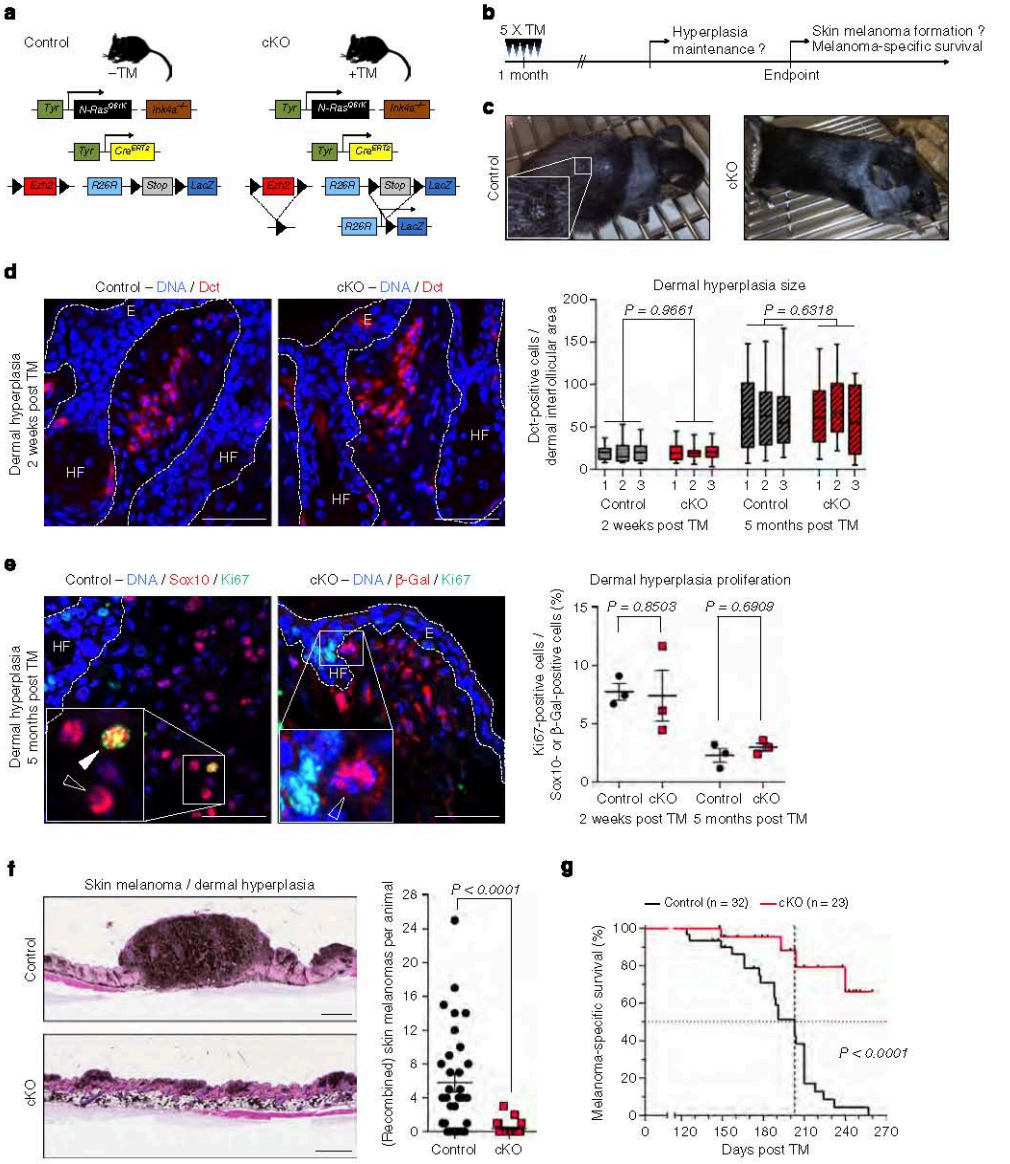

Figure 4 | *Ezh2* ablation in *Tyr::N-Ras^{Q61K} Ink4a$^{-/-}$* mice prevents skin melanoma formation. (**a**,**b**) Mouse genotypes (**a**) and strategy (**b**) used to analyze the effect of conditional *Ezh2* ablation on dermal hyperplasia and melanoma formation in *Tyr::N-Ras^{Q61K} Ink4a$^{-/-}$* mice. (**c**) Macroscopic pictures of a control and a cKO littermate at 5 months post *Ezh2* ablation. (**d**) Immunofluorescent staining for Dct on trunk skin sections 2 weeks after conditional *Ezh2* ablation to quantify dermal hyperplasia size. (**e**) Immunofluorescent staining for Sox10 (control) or β-Gal (cKO) and Ki67 on trunk skin sections 5 months after conditional *Ezh2* ablation to quantify proliferation rates. White arrowhead, Sox10-positive/Ki67-positive cell; white open arrowheads, Sox10- or β-Gal-positive/Ki67-negative cells. (**f**) H&E staining on trunk skin sections of control and cKO mice at day of sacrifice to quantify skin melanoma numbers. (**g**) Kaplan–Meier curves comparing melanoma-specific survival after conditional *Ezh2* ablation. For cKO mice, only recombined skin melanomas were taken into count as in (Supplementary Fig. 3e). E, epidermis; HF, hair follicle; H&E, haematoxylin and eosin. Data are represented as median ± 100% range of $n \geq 20$ interfollicular areas, three animals per group (**d**), mean ± s.e.m. of $n = 3$ (**e**), mean ± s.e.m. of $n = 32$ (control), $n = 23$ (cKO) (**f**). *P* values calculated with unpaired Student's *t*-test (**d**–**f**), log-rank (Mantel–Cox) test (**g**). Scale bars, 50 μm (**d**,**e**), 500 μm (**f**).

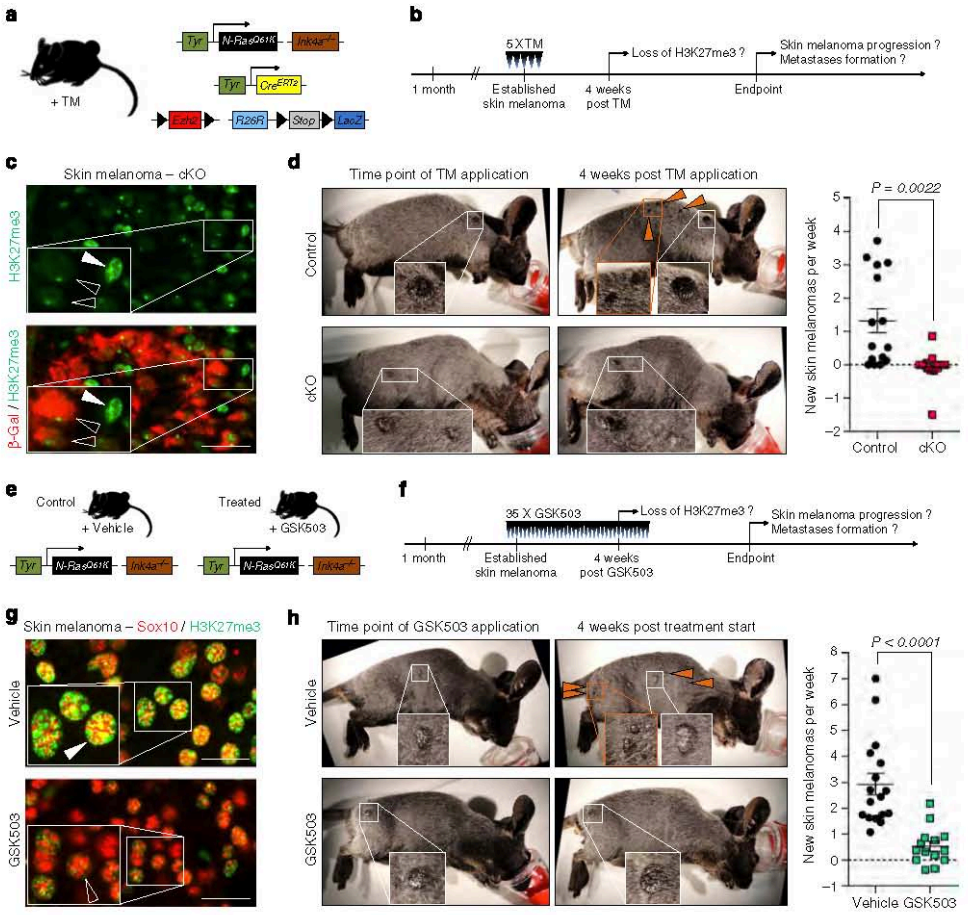

Figure 5 | Ezh2 inactivation in melanoma-bearing mice stabilizes the disease. (**a**,**b**) Mouse genotypes (**a**) and strategy (**b**) used to analyze the effect of conditional *Ezh2* ablation on melanoma progression in *Tyr::N-Ras*^{Q61K} *Ink4a*$^{-/-}$ mice. (**c**) Immunofluorescent staining for β-Gal and H3K27me3 on skin melanoma sections 4 weeks after conditional *Ezh2* ablation. White arrowhead, β-Gal-negative/H3K27me3-positive cell; white open arrowheads, β-Gal-positive/H3K27me3-negative cells. (**d**) Representative pictures of *Tyr::N-Ras*^{Q61K} *Ink4a*$^{-/-}$ mice at time point of *Ezh2* ablation and 4 weeks later to quantify formation of new skin melanomas per week. Orange arrowheads, new skin melanomas. (**e**,**f**) Mouse genotypes (**e**) and strategy (**f**) used to analyze the effect of temporary GSK503 treatment on *Tyr::N-Ras*^{Q61K} *Ink4a*$^{-/-}$ mice with established melanoma. (**g**) Immunofluorescent staining on skin melanoma sections for Sox10 and H3K27me3 4 weeks after treatment start with vehicle or GSK503. White arrowhead, Sox10-positive/H3K27me3-positive cell; white open arrowhead, Sox10-positive/H3K27me3-negative cell. (**h**) Representative pictures of *Tyr::N-Ras*^{Q61K} *Ink4a*$^{-/-}$ mice treated with vehicle or GSK503 at time point of treatment start and 4 weeks later to quantify formation of new skin melanomas per week. Orange arrowheads, new skin melanomas. H&E, haematoxylin and eosin. Data are represented as mean ± s.e.m. of $n = 15$ (control) $n = 13$ (cKO) (**d**), mean ± s.e.m. of $n = 17$ (vehicle) $n = 15$ (GSK503) (**h**). *P* values calculated with unpaired Student's *t*-test. Scale bars, 25 μm.

B16-F10 melanoma cells into *C57Bl/6* mice (Supplementary Fig. 8a). Depletion of Ezh2 function using RNAi or GSK503 significantly reduced global H3K27me3 levels *in vivo* (Supplementary Fig. 8b–e). Importantly, EZH2 inactivation led to an inhibition of tumour growth (Supplementary Fig. 8b,f). Finally, we engrafted *Tyr::N-Ras*^{Q61K} *Ink4a* $^{-/-}$ skin melanoma (RIM)-derived cells into athymic nude-*Foxn1*$^{nu/nu}$ mice (Fig. 6e). These RIM allografts were confirmed to express various melanocytic markers, reassuring their melanoma origin (Supplementary Fig. 8g,h). RIMs were first allowed to reach a considerable size for 15 to 25 days after transplantation (Fig. 6e,j; Supplementary Fig. 8k,n). Subsequent TM-induced *Ezh2* cKO in growing RIMs completely abolished Ezh2 protein and H3K27me3, while GSK503 application significantly reduced H3K27me3 (Fig. 6f–i). This was associated with an inhibition of further tumour growth in both cKO and GSK503-treated samples (Fig. 6f,j,k; Supplementary Fig. 8i–n), highlighting Ezh2 inactivation as an efficient strategy for blocking melanoma growth.

EZH2 inactivation prevents metastatic spread of melanoma. When depleting *Ezh2* in our melanoma model before appearance of skin melanoma (Supplementary Fig. 9a,b), we observed that control mice, apart from skin tumours, frequently developed Sox10-positive melanoma metastases. However, conditional loss of *Ezh2* almost fully prevented the generation of both lymph node and distant lung metastases, drastically increasing metastases-free survival (Supplementary Fig. 9c–e). Distant metastases likely arise

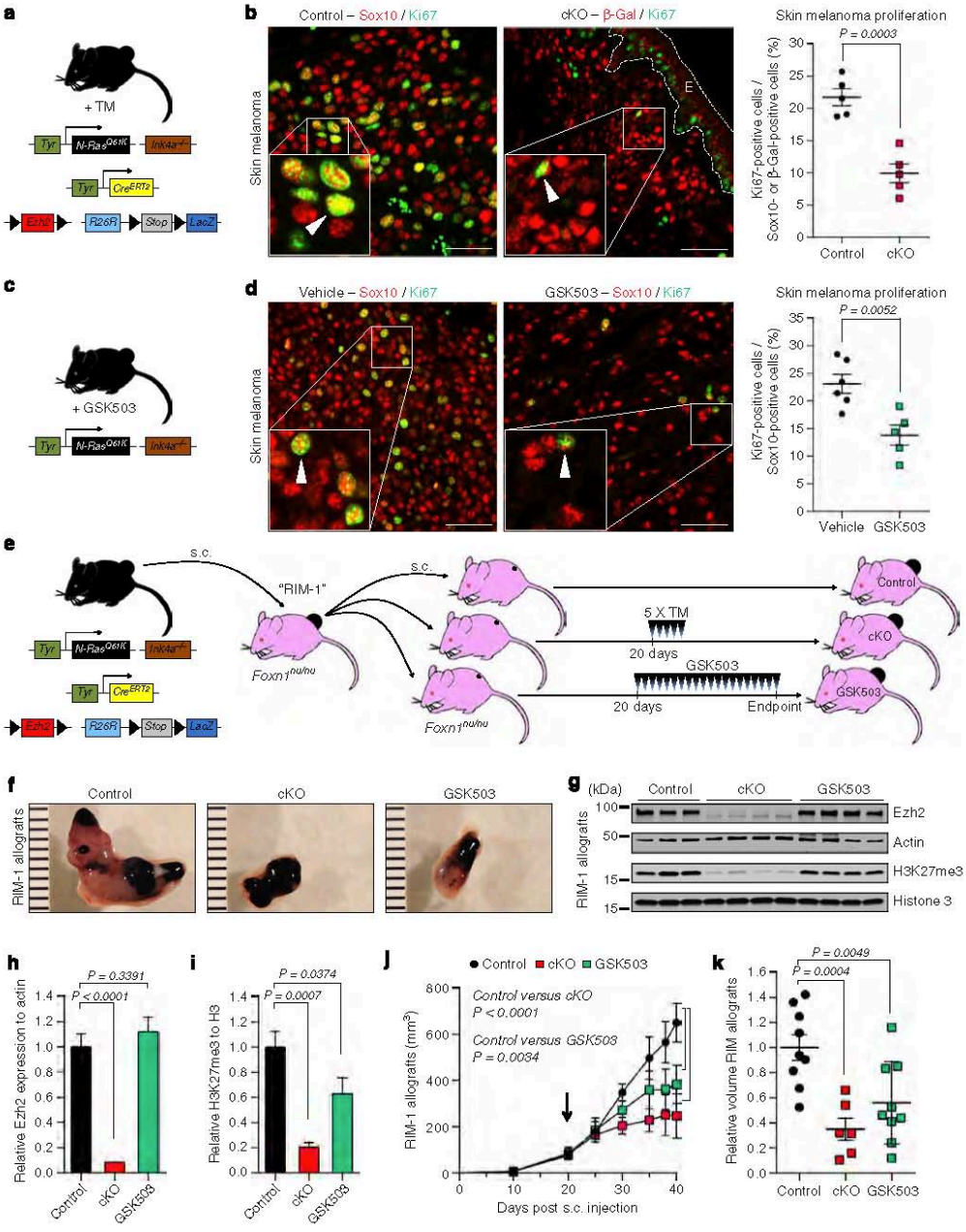

from primary skin melanomas. Thus, a lack of metastases was expected, since early *Ezh2* ablation also prevented emergence of skin tumours (Fig. 4). To functionally analyze metastatic spread from cutaneous melanoma, we inactivated Ezh2 function in *Tyr::N-Ras*^{Q61K} *Ink4a*$^{-/-}$ mice already bearing skin tumours (Fig. 7a–c). Strikingly, control animals consistently developed metastases, while *Ezh2* cKO mice exhibited a significant reduction in melanoma-positive lymph nodes (Fig. 7d) and a virtual absence of distant metastases in the lung (Fig. 7e). Consequently, *Ezh2* cKO mice displayed a highly increased melanoma-specific survival compared with controls (Fig. 7f). Likewise, GSK503-mediated Ezh2 inhibition counteracted formation of lymph node and lung metastases (Fig. 7g,h). Importantly, temporary inhibition of Ezh2 prolonged melanoma-specific survival compared with vehicle-treated animals, resulting in doubling of the median survival time (Fig. 7i).

Metastatic spread of a human primary melanoma is usually initialized by gain of invasive capacity, which allows a cell to evade from the primary tumour site[44]. Accordingly, both RNAi and drug-mediated inhibition of EZH2 significantly reduced the invasive capacity of human melanoma cultures measured in a Boyden Chamber assay (Fig. 7j; Supplementary Fig. 9f). Next, we used cell cultures derived from two distinct patients to perform a comparative global gene expression analysis of control versus EZH2-depleted melanoma cells (Supplementary Fig. 10). Cluster analysis of transcriptionally regulated genes indicated that reducing EZH2 levels affected expression of genes involved, among others, in cytoskeleton remodelling, extra cellular matrix remodelling and EMT (Fig. 7k). In support of these findings, we observed a gain of melanocyte markers including microphthalmia-associated transcription factor (Mitf) and a loss of NCSC/EMT genes when depleting Ezh2 in murine B16-F10 melanoma cells (Fig. 7l). Notably, an increase in MITF has previously been connected to loss of invasive capacity[45], while genes such as *TWIST1* and *ZEB1* are well-established drivers of NCSC delamination as much as of melanoma EMT and metastasis[6,46]. Finally, when inoculating B16-F10 cells intravenously into *C57Bl/6* mice, RNAi and importantly also GSK503 treatment drastically reduced lung nodule counts (Fig. 7m,n). In summary, EZH2 is crucial throughout several steps of melanoma metastasis, such as EMT and homing to distant sites. Therefore, targeting Ezh2 *in vivo* efficiently prevented metastasis formation in our melanoma model, and pharmacological EZH2 inhibition might represent a promising treatment strategy in preventing metastasis in patients.

EZH2 represses a set of genes connected to patient survival. To further characterize the transcriptional programmes controlled by EZH2 activity in melanoma, based on the gene expression arrays (Supplementary Fig. 10), we first defined genes significantly changed in both patient-derived cell cultures after EZH2 depletion (Fig. 8a). We next performed TCGA-based unbiased analyses to determine the clinical relevance of these EZH2-regulated genes. We correlated expression levels of each of these genes with disease outcome in patients using RNAseq and clinical data from TCGA. Strikingly, for 24% of all genes commonly upregulated upon *EZH2* silencing, high expression levels in patients were associated with improved survival, while only 5.3% correlated with poor survival (Fig. 8b; Supplementary Table 2). Furthermore, for 19.6% of all genes commonly downregulated after *EZH2* silencing, low expression levels in patients correlated with adverse survival (Fig. 8c). Thus, EZH2 activity predominantly suppresses a transcriptional programme beneficial for human patients and is associated with activation of a considerable fraction of genes linked to poor survival.

The genes upregulated upon *EZH2* silencing and associated with improved patient survival were, first, confirmed to be transcriptionally elevated after EZH2 depletion in human melanoma cell cultures. Indeed, messenger RNA of all 18 genes (24% in Fig. 8b) was significantly increased after EZH2 depletion (Fig. 8d; Supplementary Table 3). Second, chromatin immunoprecipitation (ChIP) assays for H3K27me3 were performed to determine whether these 18 genes are direct targets of EZH2-mediated histone methylation. Intriguingly, 17 out of these 18 analyzed genes exhibited promoter regions highly enriched for H3K27me3 in comparison to *GAPDH* promoter as negative control, indicating that these genes are targets of EZH2-dependent transcriptional repression (Fig. 8e; Supplementary Table 3).

EZH2 targets are functionally distinct suppressors of melanoma. To relate these EZH2 target genes (ETG) functionally to aspects of melanomagenesis, we performed functional screens in human melanoma cell cultures. We focussed on a potential rescue of, first, EZH2 depletion-induced G1 cell cycle arrest and, second, EZH2 depletion-induced loss of invasive capacity. Among the tested ETGs, deoxycytidine kinase (*DCK*), adenosylmethionine decarboxylase 1 *(AMD1)* and WD repeat domain 19 (*WDR19*) displayed promising features. We first established efficient RNAi-mediated silencing of these ETGs (Supplementary Fig. 11a). ETG silencing did not affect the efficiency of *EZH2* knockdown achieved by siEZH2 (Supplementary Fig. 11b). However, *EZH2* silencing-dependent upregulation of *DCK*, *AMD1* or *WDR19* was strongly counteracted with the double RNAi approach (Supplementary Fig. 11c). Interestingly, when simultaneously depleting EZH2 and DCK or WDR19, the G1 cell cycle arrest induced by *EZH2* silencing was significantly reverted (Fig. 8f; Supplementary Fig. 11d,f). Depletion of AMD1, however, was not sufficient to induce such a rescue (Supplementary Fig. 11d). In contrary, simultaneous depletion of EZH2 and AMD1 efficiently

Figure 6 | *Ezh2* ablation and GSK503 treatment prevents murine melanoma growth. (**a**) Mouse genotypes and strategy as in (Fig. 5b) used to analyze the effect of conditional *Ezh2* ablation on melanoma proliferation in *Tyr::N-Ras*^{Q61K} *Ink4a*$^{-/-}$ mice. (**b**) Immunofluorescent staining on skin melanoma sections for Sox10 (control) or β-Gal (cKO) and Ki67 4 weeks after conditional *Ezh2* ablation to quantify a proliferation rate. White arrowheads, Sox10- or β-Gal-positive/Ki67-positive cells. (**c**) Mouse genotypes and strategy as in (Fig. 5f) used to analyze the effect of temporary GSK503 treatment on melanoma proliferation in *Tyr::N-Ras*^{Q61K} *Ink4a*$^{-/-}$ mice. (**d**) Immunofluorescent staining on skin melanoma sections for Sox10 and Ki67 4 weeks after treatment start with vehicle or GSK503 to quantify a proliferation rate. White arrowheads, Sox10-positive/Ki67-positive cells. (**e**) Mouse genotypes and strategy used to s.c. engraft and expand *Tyr::N-Ras*^{Q61K} *Ink4a*$^{-/-}$ mice-derived melanoma cells in *Foxn1*$^{nu/nu}$ animals to analyze the effect of conditional *Ezh2* ablation and GSK503 treatment on melanoma growth. (**f**) Representative macroscopic pictures of control, cKO and GSK503-treated RIM-1 allografts. (**g–i**) Western blot for Ezh2 protein and H3K27me3 on lysed tumours from (**f**) to quantify loss of Ezh2 (**h**) and H3K27me3 (**i**). (**j,k**) Growth of control, cKO and GSK503-treated RIM-1 allografts (**j**) and relative tumour volume of all RIM allografts (**j**; Supplementary Fig. 8k,n) at endpoints (**k**). Black arrow, time point of TM application/start of GSK503 treatment. E, epidermis; s.c., subcutaneous. Data are represented as mean ± s.e.m. of $n=5$ (**b**), mean ± s.e.m. of $n=6$ (vehicle), $n=5$ (GSK503) (**d**), mean ± s.e.m. of $n=3$ (control), $n=4$ (cKO, GSK503) (**g–j**), mean ± s.e.m. of $n=9$ (control, GSK503), $n=6$ (cKO) (**k**). *P* values calculated with unpaired Student's *t*-test (**b**,**d**), analysis of variance and Fisher's least significant difference test (**h–k**). Scale bars, 50 μm (**b**,**d**), 1mm (**f**).

led to a regain of the invasive capacity that was lost upon silencing of *EZH2* alone (Fig. 8g; Supplementary Fig. 11e,g). *DCK* and *WDR19* silencing, however, had no effect on invasion of human melanoma cells (Supplementary Fig. 11e).

We then reconfirmed these genes as direct ETGs through a ChIP assay on control and EZH2-depleted cells. Indeed, upon RNAi targeting of *EZH2*, H3K27me3 mark was significantly reduced in promoter regions of *DCK*, *AMD1* and *WDR19* loci (Fig. 8h). Importantly, in both B16-F10 isografts and RIM-1 allografts (Fig. 6f; Supplementary Fig. 8b) *Dck*, *Amd1* and *Wdr19* were consistently upregulated upon Ezh2 inactivation through either cKO (or RNAi) or GSK503 treatment (Fig. 8i,j), identifying

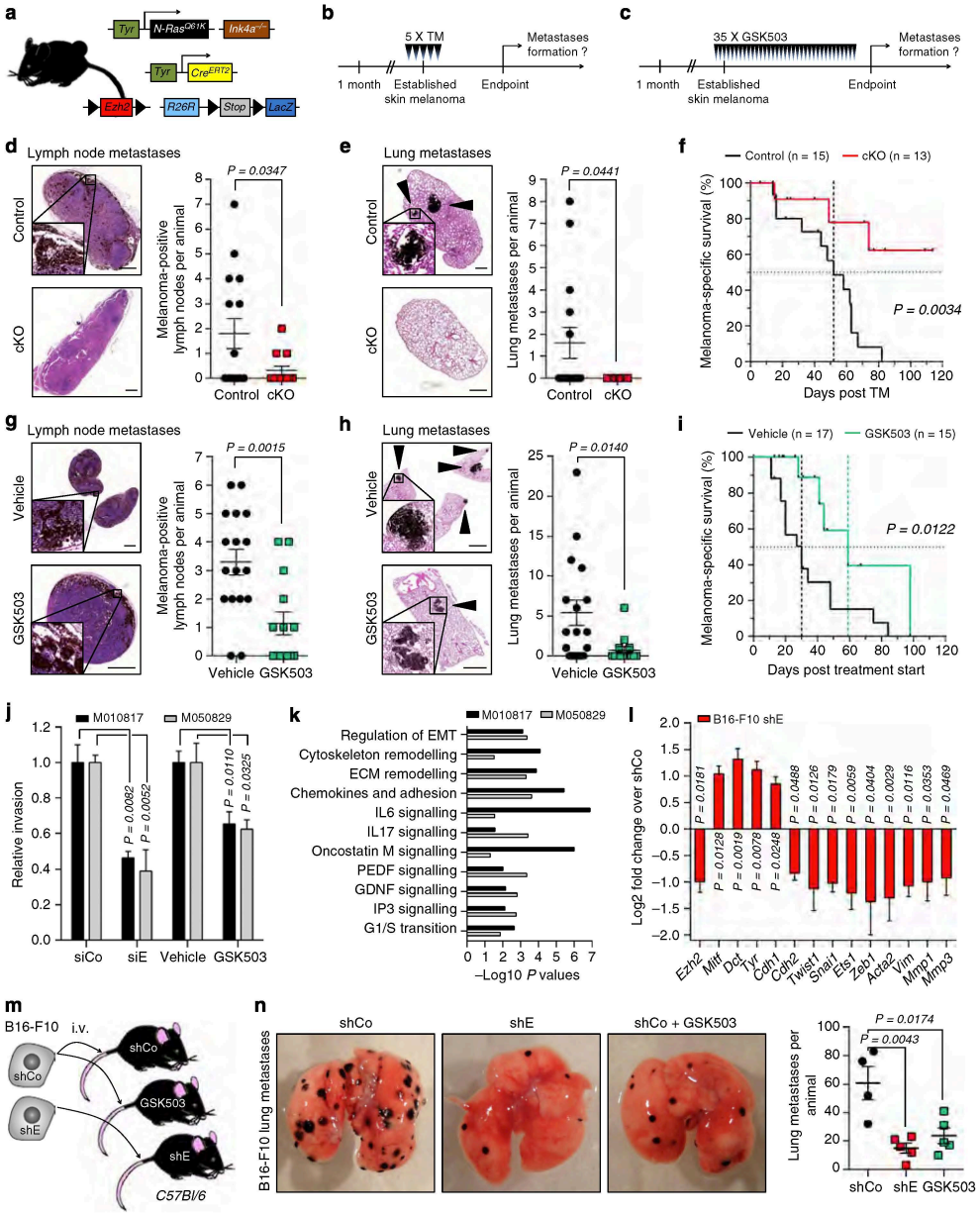

these ETGs as likely tumour suppressors *in vivo*. Thus, throughout melanomagenesis, EZH2 might dynamically repress diverse tumour suppressor genes to achieve either favourable growth or invasion kinetics.

AMD1 suppresses EMT and metastatic spread of melanoma. Interestingly, silencing of *AMD1* in human melanoma cultures induced an increase in invasion on its own (Fig. 8g; Supplementary Fig. 11e,g). Therefore, we further focused on the relevance of this tumour suppressor in preventing melanoma EMT and metastasis. Based on TCGA, patients with low AMD1 expression displayed a significantly shorter overall survival as compared with those with high AMD1 expression (Fig. 9a). Further, stage I–III patients of the AMD1 low group showed a considerably reduced distant metastases-free survival (Fig. 9b). Comparably, low AMD1 expression correlated with more advanced vertical invasion of primary melanomas (Fig. 9c). Finally, depletion of AMD1 in human melanoma cells induced expression of NCSC/EMT-relevant genes including *SNAI1*, *TWIST1* and *ZEB1* (Fig. 9d). Similarly, when silencing *Amd1* in B16-F1 (Supplementary Fig. 11h), a murine melanoma cell line with negligible metastatic potential, a comparable EMT gene set was upregulated (Fig. 9e). Therefore, to functionally link loss of Amd1 to metastasis, we first intravenously transplanted *Amd1*-silenced B16-F1 cells into *C57Bl/6* mice (Fig. 9f). Strikingly, loss of Amd1 strongly induced nodule formation in the lung (Fig. 9g). Next, we depleted Amd1 in highly metastatic B16-F10 cells (Supplementary Fig. 11i). Comparable to B16-F1, *Amd1* silencing further enhanced the metastatic potential of B16-F10 cells. Most importantly, when inhibiting lung nodule formation through Ezh2 inactivation by GSK503 treatment, depletion of Amd1 was sufficient to significantly re-induce metastasis (Fig. 9h). Thus, during melanomagenesis EZH2 epigenetically represses the tumour suppressor AMD1 allowing metastatic spread, while EZH2-targeted therapy successfully counteracts disease progression.

Discussion

In this study, we demonstrate EZH2 to be a key player in promoting malignant melanoma progression in a genetic mouse model of cutaneous melanoma. Importantly, conditional deletion of *Ezh2* did not interfere with normal melanocyte function and benign dermal hyperplasia, underlining the particular roles of EZH2 in melanoma growth and progression to metastatic disease. In support of this, temporary pharmacological inhibition of Ezh2 counteracted growth and metastasis *in vivo*, and blocking EZH2 activity in human melanoma cells affected their growth as well as invasive capacity. In line with these findings, human melanoma patients showed particularly poor survival when EZH2 transcript levels were high or when a newly identified set of EZH2 target genes was expressed at low levels. Importantly, these target genes displayed tumour-suppressive functions affecting either melanoma growth or metastatic spread. Hence, EZH2 activity exhibits two functionally distinct roles in driving malignant melanoma progression that appear to be highly relevant for human patients.

In many tissues as much as in corresponding malignancies a central function of EZH2 is to sustain stem cell identity and proliferation by transcriptional repression of senescence and differentiation genes[17,22]. For instance, in normal and cancerous breast epithelial cells, EZH2 induces stemness features, while *in vivo* Ezh2 expression initializes hyperplasia in mammary glands[25,26]. In haematopoietic stem cells, Ezh2 prevents exhaustion of the stem cell pool in aged mice[20], and Ezh2 function is also essential for maturation of early B-cell progenitors and for B-cell germinal centre formation[27,47,48]. Activating $Ezh2^{Y646N}$ mutations induce B-cell germinal centre hyperplasia resulting in lymphoma[27], while in a model of acute myeloid leukaemia, Ezh2 is required for leukemogenicity[49].

In contrast, in NCSCs, the embryonic progenitors of melanocytes, Ezh2 regulates the acquisition of a mesenchymal fate rather than stem cell maintenance[21]. Similarly, in certain epithelial tumours EZH2 has been associated with EMT and cellular migration, rather than tumour cell growth[50,51]. Therefore, to elucidate the role of Ezh2 in a given cell type, the proper cellular and physiological context has to be considered. For melanoma, this is best achieved in transgenic mice, in which melanoma is initiated and spontaneously grows in an undisturbed environment without prior *ex vivo* manipulation of tumour cells[52]. Indeed, the function of EZH2 in selected melanoma cell lines has been controversial and linked to control of proliferation or *in vitro* migration[28–30]. Taking advantage of an inducible and cKO strategy that allows functional gene investigation at different stages of disease in an intact environment, we show that Ezh2 plays a dual role during melanomagenesis. Ezh2 is required for malignant tumour growth at initial stages of melanoma formation, but a striking effect of Ezh2 inactivation is also on metastatic spread of melanoma. The process of melanoma metastasis is thought to be triggered by acquisition of mesenchymal features[44]. Thus, the role of Ezh2 in melanoma *in vivo* appears to be analogous, at least in part, to its function in embryonic neural crest development.

A few previous *in vivo* studies have also taken advantage of the cKO technique in genetic mouse models of melanoma, although most reports on gene function in melanoma are based on cell culture and xenotransplantation assays. However, up to date,

Figure 7 | EZH2 is required for metastatic progression of human and murine melanoma. (**a**–**c**) Mouse genotypes (**a**) and strategies (**b**,**c**) used to analyze the effect of conditional *Ezh2* ablation (**b**) and GSK503 treatment (**c**) on metastatic spread of *Tyr::N-Ras*^{Q61K} *Ink4a*$^{-/-}$ skin melanoma. (**d**,**e**) Metastases count at day of sacrifice in lymph nodes (**d**) and lung (**e**) of control and cKO animals using macroscopic pictures, H&E staining and Sox10 staining on sections. Macroscopic pictures and Sox10 staining performed as in (Supplementary Fig. 9). Black arrowheads, lung metastases. (**f**) Kaplan–Meier curves comparing melanoma-specific survival after conditional *Ezh2* ablation. (**g**,**h**) Metastases count at day of sacrifice in lymph nodes (**g**) and lung (**h**) of vehicle- and GSK503-treated animals using macroscopic pictures, H&E staining and Sox10 staining on sections. Macroscopic pictures and Sox10 staining performed as in (Supplementary Fig. 9). Black arrowheads, lung metastases. (**i**) Kaplan–Meier curves comparing melanoma-specific survival during and after GSK503 treatment. (**j**) Quantification of relative invasive capacity of M010817 and M050829 following EZH2 depletion with siE or EZH2 inhibition using GSK503. (**k**) −Log10 *P* values based on gene ontology analysis using gene signatures of M010817 and M050829 after EZH2 depletion with siE (Supplementary Fig. 10). (**l**) Reverse transcription–qPCR for melanocyte and EMT genes on B16-F10 after Ezh2 depletion with shE. (**m**) Mouse genotypes and strategy used to i.v. engraft B16-F10 cells following *Ezh2* silencing using shE to analyze the effect of Ezh2 depletion and GSK503 treatment on metastases formation. (**n**) Representative macroscopic pictures of lungs from vehicle and GSK503-treated (from day 1 on until endpoint) animals to quantify lung metastases after i.v. engraftment of shCo and shE B16-F10 cells. ECM, extra cellular matrix; H&E, haematoxylin and eosin; i.v., intravenous. Data are represented as mean ± s.e.m. of $n=15$ (control) $n=13$ (cKO) (**d**,**e**), mean ± s.e.m. of $n=17$ (vehicle) $n=15$ (GSK503) (**g**,**h**), mean ± s.e.m. of $n=4$ (**j**), mean ± s.e.m. of $n=3$ (**l**), mean ± s.e.m. of $n=4$ (shCo) $n=5$ (shE, GSK503) (**n**). *P* values calculated with unpaired Student's *t*-test (**d**,**e**,**g**,**h**,**j**), log-rank (Mantel–Cox) test (**f**,**i**), analysis of variance and Fisher's least significant difference test (**l**,**n**). Scale bars, 500 μm (**d**,**e**), 1mm (**g**,**h**).

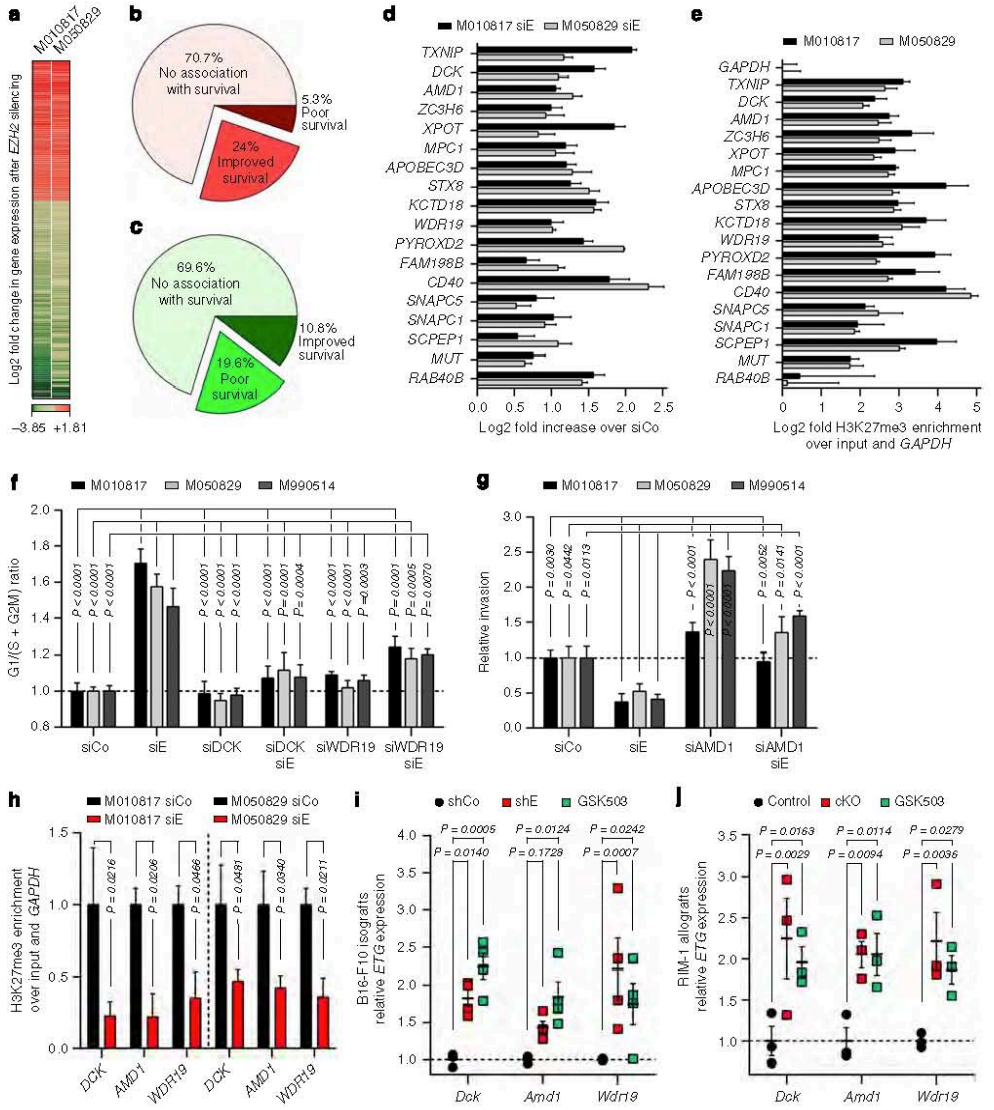

Figure 8 | EZH2 target genes are functionally involved in melanomagenesis. (**a**) Gene expression signature of M010817 and M050829 after EZH2 depletion using siE. Average log2 fold change values of three siE replicates compared with three siCo replicates in (Supplementary Fig. 10) and significantly changed in both cell lines are shown. (**b**,**c**) Summary of TCGA-based unbiased analyses of genes upregulated (**b**; Supplementary Table 2) or downregulated (**c**) in (**a**). For upregulated genes in (**a**), specimens with high RNAseq reads for the corresponding genes were compared with specimens with low RNAseq reads. For downregulated genes in (**a**), specimens with low RNAseq reads for the corresponding genes were compared with specimens with high RNAseq reads. (**d**) Reverse transcription–qPCR (RT–qPCR) for genes associated with improved survival in (**b**) on M010817 and M050829 after EZH2 depletion using siE (relative to *GAPDH*). (**e**) H3K27me3 ChIP and subsequent qPCR for promoters of genes associated with improved survival in (**b**) on untreated M010817 and M050829. (**f**) Quantification of G1/(S + G2M) ratio of M010817, M050829 and M990514 after depletion of EZH2 and DCK/WDR19 using siE and siDCK/siWDR19. (**g**) Quantification of relative invasive capacity of M010817, M050829 and M990514 after depletion of EZH2 and AMD1 using siE and siAMD1. (**h**) H3K27me3 ChIP and subsequent qPCR for gene promoters of selected ETGs on M010817 and M050829 after EZH2 depletion using siE. (**i**) RT–qPCR for selected ETGs on lysed shCo, shE and GSK503-treated B16-F10 tumours from (Supplementary Fig. 8b). (**j**) RT–qPCR for selected ETGs on lysed control, cKO and GSK503-treated RIM-1 tumours from (Fig. 6f). Data are represented as mean ± s.e.m. of $n = 3$ (**d**,**f**–**h**,**j**), mean ± s.e.m. of $n = 4$ (**e**), mean ± s.e.m. of $n = 3$ (shCo), $n = 4$ (shE, GSK503) (**i**). *P* values calculated with analysis of variance and Fisher's least significant difference test.

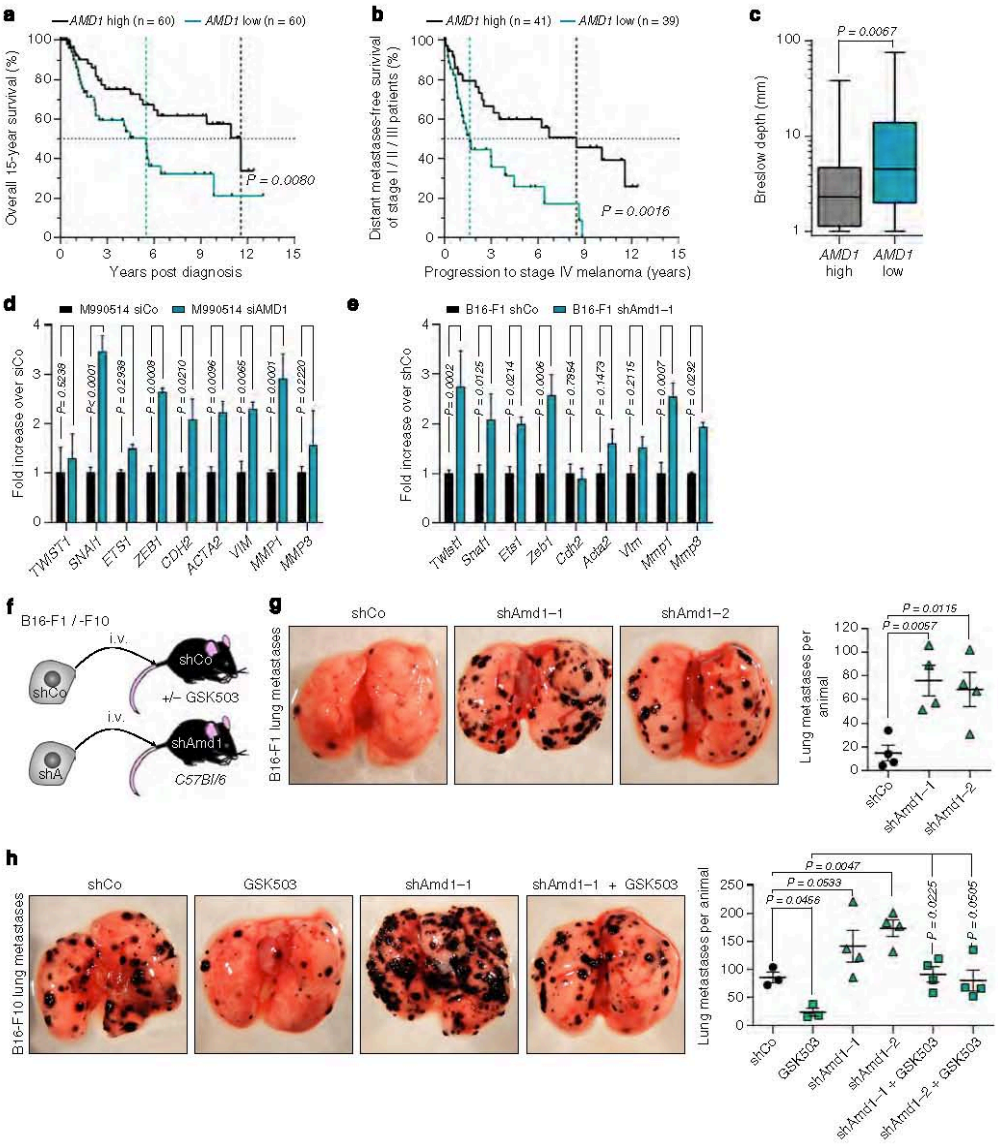

Figure 9 | The EZH2 target gene *AMD1* is a tumour suppressor that prevents melanoma metastasis. (**a**) Kaplan–Meier curves comparing overall survival of melanoma specimens (stage I–IV) with respect to *AMD1* transcript levels based on TCGA. (**b**) Kaplan–Meier curves comparing distant metastases-free survival of stage I–III melanoma specimens (primary melanoma/lymph node metastases) with respect to *AMD1* transcript levels based on TCGA. (**c**) Breslow depths of melanoma specimens' primary melanomas with respect to *AMD1* transcript levels based on TCGA. (**d**) Reverse transcription–qPCR (RT–qPCR) for EMT genes on M990514 after AMD1 depletion with siAMD1. (**e**) RT–qPCR for EMT genes on B16-F1 after Amd1 depletion with shAmd1. (**f**) Mouse genotypes and strategies used to i.v. engraft B16-F1/B16-F10 cells following *Amd1* silencing using shAmd1 to analyze the effect of Amd1 depletion and GSK503 treatment on metastases formation. (**g**) Representative macroscopic pictures of lungs from *C57Bl/6* animals after i.v. engraftment of shCo and shAmd1 B16-F1 cells to quantify lung metastases. (**h**) Representative macroscopic pictures of lungs from vehicle and GSK503-treated (from day 1 on until endpoint) animals to quantify lung metastases after i.v. engraftment of shCo and shAmd1 B16-F10 cells. *AMD1* low/high, bottom and top 60 patients with respect to *AMD1* transcript levels; i.v., intravenous; shA, shAmd1. Data are represented as median ± 100% range of $n = 48$ (*AMD1* high), $n = 43$ (*AMD1* low) (**c**), mean ± s.e.m. of $n = 3$ (**d**,**e**), mean ± s.e.m. of $n = 4$ (**g**,**h**), $n = 3$ (shCo, GSK503 in **h**). *P* values calculated with log-rank (Mantel–Cox) test (**a**,**b**), unpaired Student's *t*-test (**c**), analysis of variance and Fisher's least significant difference test (**d**,**e**,**g**,**h**).

genes shown to be involved in melanoma formation turned out to be also important for normal melanocytes and benign hyperplasia cells[14,31,41,53]. In contrast, Ezh2 plays a unique tumour-specific role in melanoma and is not required for normal melanocyte function, in accordance with the strong upregulation of its expression during malignant melanoma progression. Thus, unlike in many other cancers and their tissues of origin, EZH2 function appears to be of no relevance for the cells from which melanoma arises from. Based on TCGA and two further datasets[9,38], cutaneous melanoma is the only solid cancer with recurring *EZH2*^{Y646*} gain-of-function mutations. It will be of interest to investigate whether *EZH2*^{WT} and especially *EZH2*^{Y646*} operate as *de novo* oncogenic drivers of metastasizing melanoma.

Since EZH2 acts as a transcriptional repressor[17], genes upregulated on *EZH2* silencing are likely candidates for being direct targets of EZH2-mediated H3K27me3. In agreement with this, promoters of genes selected based on our TCGA analyses were indeed confirmed to be enriched in H3K27me3. Of note, these selected ETGs are not only potential indicators of improved patient survival, but have also been linked to characteristics relevant for tumour progression. For instance, loss of *DCK* was correlated with resistance to cytarabine and decitabine treatments of different cancers[54]. *AMD1*, another gene upregulated upon *EZH2* silencing, is involved in the biosynthesis of the non-canonical amino acid hypusine, and has recently been identified as part of a metabolic tumour suppressor network in lymphoma[55,56]. Finally, *WDR19* is a component of the intraflagellar transport machinery and has been associated with good prognosis in prostate cancer[57,58]. While epigenetic repression of *DCK* and *WDR19* supported melanoma cell growth, repression of *AMD1* induced EMT and metastasis of melanoma cells. Interestingly, alterations in biosynthesis networks, such as amino acid and nucleotide metabolism, have recently been demonstrated to be essential for EMT and metastasis[59]. Likewise, EZH2-mediated repression of AMD1-linked hypusine biosynthesis might thus contribute to EMT and metastatic spread of cutaneous melanoma. In the future, an unbiased screen for further EZH2-target genes might provide additional candidate factors possibly involved in melanoma disease progression.

Dependent on the mutational landscape, levels of oxidative and metabolic stress and the stromal context, the set of aberrantly silenced tumour suppressor genes might be assembled differently in a given melanoma and at a given time point. However, EZH2 itself represents a central node in the control of melanoma progression through epigenetic regulation of such genes. In support of this, pharmacological inhibition of Ezh2 using the preclinical drug GSK503 in melanoma-bearing mice efficiently counteracted metastatic melanoma progression, resulting in a doubled survival time. Further, GSK503 also prevented metastasis formation of transplanted melanoma cells through, at least partly, *Amd1* de-repression. Melanoma patients die of metastatic disease and not of primary tumour growth[1]. Therefore, novel therapeutic strategies effectively interfering with metastatic spread are required. Recently, several chromatin-modifying drugs have been successfully applied in preclinical cancer models and are likely to be taken forward to clinical trials[60]. Accordingly, our study reveals that EZH2 inhibition might be a promising strategy for future therapies of human melanoma patients.

Methods

Human biopsies. Human biopsies were isolated and genotyped as described[43]. Usage of naevus and melanoma biopsies as well as melanoma-derived cell cultures was approved by the official ethical authorities of Canton of Zurich, Switzerland. Written informed consent was obtained from all subjects and approved by the local institutional review boards (EK647 and EK800).

Mice. *Tyr::N-Ras*^{Q61K} animals and *Ink4a*-defficient mice have previously been described[14,34,61]. The *Tyr::Cre*^{ERT2} line[14,31,39], *Ezh2*^{lox} animals[19,21] and *R26R::LacZ* mice[40] have been analyzed elsewhere. Mouse genotyping was performed according to a standard DNA isolation protocol[62], followed by PCR using a Taq PCR Core Kit (201225, Qiagen) and primers indicated in (Supplementary Table 4). Genetic background of (*Tyr::N-Ras*^{Q61K} *Ink4a*$^{-/-}$) *Tyr::Cre*^{ERT2} *Ezh2*$^{lox/lox}$ *R26R::LacZ* mice was mixed, while background of *Tyr::N-Ras*^{Q61K} *Ink4a*$^{-/-}$ animals was Black 6. Mice were born with the expected ratio of Mendelian inheritance, and no changes in gender ratios were observed. Transgenic mice used were of both genders and were subjected to experiments either at the age of 1 month or on tumour development (5 to 7 months). Melanoma-developing mice were frequently monitored and killed at an endpoint defined by adverse clinical symptoms, such as multiple skin tumours ($\varnothing > 5$ mm), weight loss ($\Delta m > 15\%$) or hunched back. Three-month-old female *C57Bl/6J* and athymic nude-*Foxn1*$^{nu/nu}$ mice were purchased (Charles River Laboratories). Mice engrafted subcutaneously with melanoma cells were killed at an endpoint defined by tumour volume ($V > 1{,}000\,mm^3$). Tumour volume was calculated as follows:

$V = 2/3 \times \pi \times ((a+b)/4))^3$, where a (mm) was the length and b (mm) was the width of the tumour. Mice engrafted intravenously with melanoma cells were killed 12 days post engraftment. All animal experiments have been approved by the veterinary authorities of Canton of Zurich, Switzerland, and were performed in accordance with Swiss law and the GlaxoSmithKline policy on the Care, Welfare and Treatment of Animals.

***In vivo* TM and GSK503 application.** To conditionally ablate *Ezh2*, (*Tyr::N-Ras*^{Q61K} *Ink4a*$^{-/-}$) *Tyr::Cre*^{ERT2} *Ezh2*$^{lox/lox}$ *R26R::LacZ* mice were subjected to treatment with TM (T5648, Sigma-Aldrich), which was diluted (10 mg ml^{-1}) in ethanol and sunflower oil (1:9). Conditional ablation of *Ezh2* was achieved by daily intraperitoneal injections of 2 mg TM for 5 consecutive days. Mice were either 4 weeks old or at an age of 5 to 7 months, when first skin melanomas had become macroscopically detectable ($\varnothing \geq 2$ mm). To pharmacologically inhibit Ezh2 activity, *Tyr::N-Ras*^{Q61K} *Ink4a*$^{-/-}$, *Ink4a*$^{-/-}$ and *C57Bl/6* mice were subjected to treatment with GSK503 (ref. 27), which was diluted (15 mg ml^{-1}) in 20% Captisol solution (Cydex). Efficient Ezh2 inhibition was achieved by daily intraperitoneal injections of 150 mg kg^{-1} GSK503 over 35 consecutive days. *Ink4a*$^{-/-}$ and *C57Bl/6* mice were 5 months old. *Tyr::N-Ras*^{Q61K} *Ink4a*$^{-/-}$ animals were at an age of 5 to 7 months, when first skin melanomas had become macroscopically detectable ($\varnothing \geq 2$ mm). Mice were monitored during and after treatment to measure GSK503-induced reversible weight loss. Moreover, a few GSK503-treated animals developed ascites, independently of the genotype, and had to be excluded from the studies. *C57Bl/6* and *Foxn1*$^{nu/nu}$ mice engrafted with melanoma cells were subjected to TM and GSK503 treatment as described above.

Quantification of skin melanomas and metastases. When *Ezh2* ablation was done at 1 month, developing trunk skin lesions were considered as melanomas above a diameter of 2 mm ($\varnothing \geq 2$ mm). At day of sacrifice, a final skin melanoma count was established. In cKO mice, whole mount X-Gal staining was used to quantify recombined tumours and X-Gal-negative tumours were excluded from cKO melanoma count. To quantify metastases, accessory axillary, proper axillary, sciatic and subiliac lymph nodes (total of eight) as well as the lungs were subjected to further analyses. Lymph nodes were considered melanoma positive, when Sox10-positive cells were found on histological sections. Black dots on lung surface were counted and confirmed as melanoma metastases using Sox10 staining on histological sections. Melanoma-specific survival curves were based on presence of (recombined) skin melanomas and/or metastases. When *Ezh2* ablation or GSK503 treatment was done in established melanoma, newly forming skin melanomas ($\varnothing \geq 2$ mm) were counted weekly. At day of sacrifice, skin melanoma and metastases counts were established as described for early *Ezh2* ablation, except skin melanoma numbers were not based on recombination but solely on tumour numbers. Melanoma-specific survival curves were based on the presence of newly formed skin melanomas and/or metastases.

Isografting and allografting of murine melanoma cells. Skin melanomas from *Tyr::N-Ras*^{Q61K} *Ink4a*$^{-/-}$ (*Tyr::Cre*^{ERT2} *Ezh2*$^{lox/lox}$ *R26R::LacZ*) animals were dissociated into small pieces using forceps and scissors. Tissue was digested using 0.25 mg ml^{-1} Liberase DH Research Grade (05401054001, Roche) in RPMI 1640 (42401, Life Technologies) for 45 min at 37 °C followed by a treatment with 0.55 mg ml^{-1} Dispase II (17105, Life Technologies) and 0.2 mg ml^{-1} DNase I (10104159001, Roche) for 15 min at 37 °C. Single cells were separated from remaining tissue using a 70 μm cell strainer and engrafted subcutaneously into *Foxn1*$^{nu/nu}$ mice in PBS or cultured *in vitro* using growth medium as described below. *Foxn1*$^{nu/nu}$ mice were subcutaneously engrafted with either 500,000 RIM-1 cells, 500,000 RIM-2 cells or 1 Mio RIM-3 cells. *C57Bl/6* mice were either subcutaneously engrafted with 1 Mio B16-F10 cells or tail vein injected with 400,000 B16-F1 cells/100,000 B16-F10 cells.

Histological analysis and immunofluorescence. Human and mouse tissue samples were fixed in 4% buffered formaldehyde and embedded in paraffin, except for whole mount X-Gal staining. Therefore, mouse tissue samples were fixed in

formaldehyde for 20 min and subjected to X-Gal staining as described[14]. Human samples were processed into sections of 3 μm thickness, while mouse samples were processed into 5 μm sections. Slides were stained with haematoxylin and eosin according to standard protocols. Sections were subjected either to immunohistochemical analyses or to immunofluorescent analyses. Briefly, immunohistochemical stainings were performed using primary antibodies (Supplementary Table 5) in combination with the iVIEW DAB Detection Kit (760-091, Ventana) or the ChemMate Detection Kit (K5006, Dako) according to manufacturers' protocols. For immunofluorescence, protocols described elsewhere were applied[14]. Briefly, sections were deparaffinized and subjected to an antigen retrieval step using citrate buffer (S2369, Dako). Primary antibodies (Supplementary Table 5) were applied in blocking buffer (1% BSA in PBS and 0.05% Triton X-100) overnight at 4 °C and visualized using secondary antibodies (Supplementary Table 6) in blocking buffer for 1 h at room temperature. For visualization of β-Gal, a biotin α-chicken (1:300, AP194B, Merck Millipore) secondary antibody was combined with further signal amplification using horse radish peroxidase–streptavidin (1:300, 016-030-084, Jackson ImmunoResearch) and the TSA Plus Cy3 Kit (1:50, NEL744001KT, PerkinElmer) according to manufacturers' protocol. Subsequently, nuclei were stained with Hoechst 33342 (14533, Sigma-Aldrich) and slides were mounted with Fluorescent Mounting Medium (S3023, Dako). Immunohistochemical/fluorescent sections were analyzed using either a Mirax Midi Slide Scanner (Zeiss) or a DMI 6000B microscope (Leica).

***EZH2* mutagenesis and mutation analysis**. *EZH2* mutations were chosen based on specimens in the Somatic Mutations data set for skin cutaneous melanoma as described below. Specimens showing non-synonymous mutations in the coding sequence of *EZH2* and for which clinical data was available were selected. A previously validated pRetro-X construct containing human $EZH2^{WT}$, $EZH2^{Y646N}$ or $EZH2^{Y646F}$ complementary DNA (cDNA) was used[27]. Further mutations were introduced into $EZH2^{WT}$ cDNA using a QuikChange II Site-Directed Mutagenesis Kit (200523, Agilent Technologies) according to manufacturer's protocol. For each mutation, 10 ng of template $EZH2^{WT}$ cDNA was used with the appropriate primers containing the corresponding sequence modification (Supplementary Table 7), and constructs were sequenced using three pairs of primers covering the *EZH2* sequence (Supplementary Table 8).

Cell cultures. Human melanoma cell cultures were characterized before[43], XB2 and Melan-a cell lines were previously described[63], and HEK293T, B16-F1 and B16-F10 cell lines were purchased (ATCC). All cells (including primary RIM cells) were cultured in growth medium, which was RPMI 1640 supplemented with 10% FCS (16140, Life Technologies), 4 mM L-Glutamine (25030, Life Technologies), penicillin–streptomycin (15070, Life Technologies) and Fungizone Antimycotic (15290, Life Technologies) as previously specified[14,43].

Cell transfections and GSK503 treatment. To overexpress $EZH2^{WT}$ and mutated *EZH2*, HEK293T cells were grown in growth medium devoid of antibiotics and transfected with 10 μg *EZH2*-expressing plasmids using 2.5 M $CaCl_2$ in HEPES buffer according to standard protocols, and cells were subjected to functional analyses after 36 h. To temporarily deplete EZH2, DCK, AMD1 and WDR19, human melanoma cells were transfected with small interfering RNAs (siRNA) indicated in (Supplementary Table 9). siRNA (25 nM) was applied in combination with jetPRIME siRNA Transfection Reagent (114-15, Polyplus Transfection) according to manufacturer's guidelines. Growth medium was exchanged after 24 h and cells were subjected to further assays after 72 h, unless specified. For all functional assays the most efficient siRNAs underlined in (Supplementary Table 9) were used. To stably deplete Ezh2 and Amd1, murine melanoma cells were transfected with small hairpin RNA-expressing plasmids indicated in (Supplementary Table 9). Plasmid (10 μg) was applied in combination with jetPEI DNA Transfection Reagent (101-10 N, Polyplus Transfection) according to manufacturer's guidelines. Transfected cells were selected using 1 $\mu g\,ml^{-1}$ puromycin (A11138-02, Life Technologies) for 1 week before subjection to further assays. Efficiency of shEzh2 was previously validated[51]. To pharmacologically inhibit EZH2, melanoma cells were treated either with vehicle (DMSO) or 1 μM GSK503. Cells were treated for 8 days before subjection to further assays. Drug was only replenished when cells were passaged during the 8-day period.

Cell growth and apoptosis assays. To establish growth curves, cell counts were measured daily starting 48 h after transfection. For cell cycle analysis, cells were 50% ethanol fixed and labelled with propidium iodide including RNase A (P10797, Life Technologies). To measure apoptosis, an Annexin V Apoptosis Detection Kit (559763, BD Biosciences) was used. Cell cycle and apoptotic cells were quantified using a BD FACSCanto II flow cytometer (BD Biosciences) and FlowJo software (Tree Star).

Boyden chamber invasion assay. After 24 h of transfection or 8 days of GSK503 treatment, cells were starved for 48 h in starvation medium containing all supplements except 1% FCS. Subsequent Boyden Chamber invasion assays were done according to manufacturer's protocol. Briefly, 150,000 cells were subjected to matrigel-coated well inserts (354480, BD Biosciences) in empty medium (0% FCS and 0% L-Glutamine). Growth medium was used as chemoattractant for 24 h. Transvaded cells were 4% buffered formaldehyde fixed and visualized using Hoechst 33342. Membranes were mounted to glass slides, and cell numbers were quantified using a DMI 6000B microscope and CellProfiler software[64].

Immunofluorescence on cells. Cells were grown on cover slips, 50% ethanol fixed and subjected to immunofluorescent labelling using primary antibodies (Supplementary Table 5) in blocking buffer (1% BSA in PBS) overnight at 4 °C and secondary antibodies (Supplementary Table 6) for 1 h at room temperature. Nuclei were stained with Hoechst 33342, and cells were recorded with a DMI 6000B microscope.

Protein isolation and Western blotting. Protein isolation and Western blotting was done as previously described[14], unless specified. Briefly, cells were lysed in RIPA buffer (89900, Thermo Scientific) containing Halt Phosphatase and Protease Inhibitor Cocktail (78420, 87786, Thermo Scientific), while tumour biopsies were homogenized in such buffer using a tissue homogeniser (Polytron). SDS–PAGE was carried out on 4–20% Mini-PROTEAN TGX Gels (456–1094, Bio Rad). Primary antibodies (Supplementary Table 5) were applied in Odyssey blocking buffer (927–40000, LI-COR Biosciences) overnight at 4 °C and visualized using secondary antibodies (Supplementary Table 6) in Odyssey blocking buffer for 45 min at room temperature. Blots were scanned and quantified with an Odyssey imaging system (LI-COR Biosciences). Quantified band intensities were normalized using either β-Actin or H3 as housekeeping protein. Full scans are shown in (Supplementary Fig. 12).

RNA isolation and reverse transcription–qPCR. RNA extraction and DNase treatment of samples was performed using the RNeasy Mini Kit (74104, Qiagen) and the RNase-Free DNase Set (79254, Qiagen) according to manufacturer's guidelines. Purified RNA was quantified using nanodrop and subjected to reverse transcriptase reaction using Maxima First Strand cDNA Synthesis Kit (K1641, Thermo Scientific) followed by an RNase H (EN0202, Thermo Scientific) digestion step according to manufacturer's recommendations. Real-time quantitative PCR (qPCR) was performed on a LightCycler 480 System (Roche) using LightCycler 480 SYBR Green I Master (4707516001, Roche). Primers used are indicated in (Supplementary Tables 10 and 11). Each sample was analyzed in technical triplicates, and relative quantified RNA was normalized using *USF1* or *GAPDH*, when specified, as housekeeping transcript.

Chromatin isolation and ChIP. Chromatin isolation and ChIP was done as previously described[65]. Briefly, an antibody against H3K27me3 (1:250, 9733, Cell Signaling Technology) and Dynabeads Protein A (10002D, Life Technologies) were used. Real-time qPCR was performed on a Rotor Gene RG-3000 A (Qiagen) using the SensiFAST Probe Hi-ROX Kit (BIO-82005, Bioline). Primers were designed to amplify genomic DNA from a region flanking the transcriptional starting site − 500 bp to + 100 bp devoid of local CpG islands using CpG island prediction[66]. Primers used are indicated in (Supplementary Table 12). Relative promoter enrichment was normalized to chromatin inputs and to *GAPDH* promoter as negative control.

Microarray analysis. Total RNA was isolated as described for reverse transcription–qPCR. Total RNA was amplified and biotin labelled using the MessageAmp II-Biotin Enhanced aRNA Amplification Kit (AM1791, Life Technologies). Biotin-labelled RNA was hybridized to Human Gene 2.1 ST Array (902136, Affymetrix) following the manufacturer's protocol. After hybridization, microarrays were washed and stained using a GeneChip Fluidics Station 450 (Affymetrix) and scanned with a GeneChip Scanner 7G (Affymetrix). Differential gene expression was determined by R package limma[67]. Gene ontology network analysis was performed with MetaCore (Thomson Reuters).

TCGA analysis. The RNAseq, somatic mutations and clinical data sets for skin cutaneous melanoma and the somatic mutations data sets for colon adenocarcinoma, lung squamous cell carcinoma, lung adenocarcinoma, glioblastoma multiforme, kidney renal clear cell carcinoma, acute myeloid leukaemia, head and neck squamous cell carcinoma, breast invasive carcinoma and prostate adenocarcinoma were downloaded on 29 September 2013 from TCGA (http://cancergenome.nih.gov/). Somatic mutation data was annotated using ANNOVAR[68]. Non-synonymous *EZH2* mutations were mapped to functional EZH2 domains based on previous reports[17,18]. Raw RNAseq reads were normalized with edgeR[69] and differential RNA expression was analyzed with voom from R package limma[67]. Specimens with top and bottom transcript levels for a gene of interest were used for analysis. Patient numbers were gradually increased from a minimum of top and bottom 7% (19 out of 274) to a maximum of top and bottom 25% (69 out of 274) to optimize potential segregation of Kaplan–Meier curves. This procedure was

performed for *EZH2* and all commonly differentially expressed genes form the microarray data sets (Fig. 8a) in an unbiased way.

Statistical analyses. Quantifications of immunofluorescent stainings were done on sections of at least three different mice. Therefore, at least 150 hair follicles or at least 300 label-positive cells were counted. Cell culture-based experiments were done at least in biological triplicates. *P* values for comparison of two groups were calculated with unpaired Student's *t*-test, except for paired data (follow-up measurements on the same mouse). Therefore, paired Student's *t*-test was applied. *P* values for comparison of multiple groups were calculated with analysis of variance and Fisher's least significant difference test. *P* values for comparison of Kaplan–Meier curves were calculated with log-rank (Mantel–Cox) test. $P<0.05$ was considered significant.

References

1. Siegel, R., Ma, J., Zou, Z. & Jemal, A. Cancer statistics, 2014. *CA Cancer J. Clin.* **64,** 9–29 (2014).
2. Braeuer, R. R. *et al.* Why is melanoma so metastatic? *Pigment Cell Melanoma Res.* **27,** 19–36 (2014).
3. Lito, P., Rosen, N. & Solit, D. B. Tumor adaptation and resistance to RAF inhibitors. *Nat. Med.* **19,** 1401–1409 (2013).
4. Sanchez-Laorden, B. *et al.* BRAF inhibitors induce metastasis in RAS mutant or inhibitor-resistant melanoma cells by reactivating MEK and ERK signaling. *Sci. Signal.* **7,** 1–12 (2014).
5. Shakhova, O. Neural crest stem cells in melanoma development. *Curr. Opin. Oncol.* **26,** 215–221 (2014).
6. Theveneau, E. & Mayor, R. Neural crest delamination and migration: from epithelium-to-mesenchyme transition to collective cell migration. *Dev. Biol.* **366,** 34–54 (2012).
7. Chaffer, C. L. & Weinberg, R. A. A perspective on cancer cell metastasis. *Science* **331,** 1559–1564 (2011).
8. Dupin, E. & Sommer, L. Neural crest progenitors and stem cells: from early development to adulthood. *Dev. Biol.* **366,** 83–95 (2012).
9. Hodis, E. *et al.* A landscape of driver mutations in melanoma. *Cell* **150,** 251–263 (2012).
10. Krauthammer, M. *et al.* Exome sequencing identifies recurrent somatic RAC1 mutations in melanoma. *Nat. Genet.* **44,** 1006–1014 (2012).
11. Fuchs, S. *et al.* Stage-specific control of neural crest stem cell proliferation by the small rho GTPases Cdc42 and Rac1. *Cell Stem Cell* **4,** 236–247 (2009).
12. Paratore, C., Goerich, D. E., Suter, U., Wegner, M. & Sommer, L. Survival and glial fate acquisition of neural crest cells are regulated by an interplay between the transcription factor Sox10 and extrinsic combinatorial signaling. *Development* **128,** 3949–3961 (2001).
13. Kim, J., Lo, L., Dormand, E. & Anderson, D. J. SOX10 maintains multipotency and inhibits neuronal differentiation of neural crest stem cells. *Neuron* **38,** 17–31 (2003).
14. Shakhova, O. *et al.* Sox10 promotes the formation and maintenance of giant congenital naevi and melanoma. *Nat. Cell Biol.* **14,** 882–890 (2012).
15. Reik, W. Stability and flexibility of epigenetic gene regulation in mammalian development. *Nature* **447,** 425–432 (2007).
16. Esteller, M. Epigenetics in cancer. *N. Engl. J. Med.* **358,** 1148–1159 (2008).
17. Margueron, R. & Reinberg, D. The Polycomb complex PRC2 and its mark in life. *Nature* **469,** 343–349 (2011).
18. Ciferri, C. *et al.* Molecular architecture of human polycomb repressive complex 2. *Elife* **1,** e00005 (2012).
19. Hirabayashi, Y. *et al.* Polycomb limits the neurogenic competence of neural precursor cells to promote astrogenic fate transition. *Neuron* **63,** 600–613 (2009).
20. Kamminga, L. M. *et al.* The Polycomb group gene Ezh2 prevents hematopoietic stem cell exhaustion. *Blood* **107,** 2170–2179 (2006).
21. Schwarz, D. *et al.* Ezh2 is required for neural crest-derived cartilage and bone formation. *Development* **141,** 867–877 (2014).
22. Sauvageau, M. & Sauvageau, G. Polycomb group proteins: multi-faceted regulators of somatic stem cells and cancer. *Cell Stem Cell* **7,** 299–313 (2010).
23. Bachmann, I. M. *et al.* EZH2 expression is associated with high proliferation rate and aggressive tumor subgroups in cutaneous melanoma and cancers of the endometrium, prostate, and breast. *J. Clin. Oncol.* **24,** 268–273 (2006).
24. McHugh, J. B., Fullen, D. R., Ma, L., Kleer, C. G. & Su, L. D. Expression of polycomb group protein EZH2 in nevi and melanoma. *J. Cutan. Pathol.* **34,** 597–600 (2007).
25. Li, X. *et al.* Targeted overexpression of EZH2 in the mammary gland disrupts ductal morphogenesis and causes epithelial hyperplasia. *Am. J. Pathol.* **175,** 1246–1254 (2009).
26. Gonzalez, M. E. *et al.* EZH2 expands breast stem cells through activation of NOTCH1 signaling. *Proc. Natl Acad. Sci. USA* **111,** 3098–3103 (2014).
27. Béguelin, W. *et al.* EZH2 is required for germinal center formation and somatic EZH2 mutations promote lymphoid transformation. *Cancer Cell* **23,** 677–692 (2013).
28. Pan, T. *et al.* EZH2-dependent suppression of a cellular senescence phenotype in melanoma cells by inhibition of p21/CDKN1A expression. *Mol. Cancer Res.* **9,** 418–429 (2011).
29. Luo, C. *et al.* MiR-137 inhibits the invasion of melanoma cells through downregulation of multiple oncogenic target genes. *J. Invest. Dermatol.* **133,** 768–775 (2012).
30. Luo, C. *et al.* MiR-101 inhibits melanoma cell invasion and proliferation by targeting MITF and EZH2. *Cancer Lett.* **341,** 240–247 (2013).
31. Harris, M. L. *et al.* A dual role for SOX10 in the maintenance of the postnatal melanocyte lineage and the differentiation of melanocyte stem cell progenitors. *PLoS Genet.* **9,** e1003644 (2013).
32. Busam, K. J. *et al.* Expression of melan-A (MART1) in benign melanocytic nevi and primary cutaneous malignant melanoma. *Am. J. Surg. Pathol.* **22,** 976–982 (1998).
33. Gown, A. M., Vogel, A. M., Hoak, D., Gough, P. & McNutt, M. A. Monoclonal antibodies specific for melanocytic tumors distinguish subpopulations of melanocytes. *Am. J. Pathol.* **123,** 195–203 (1986).
34. Ackermann, J. *et al.* Metastasizing melanoma formation caused by expression of activated N-RasQ61K on an INK4a-deficient background. *Cancer Res.* **65,** 4005–4011 (2005).
35. Nishimura, E. K. *et al.* Dominant role of the niche in melanocyte stem-cell fate determination. *Nature* **416,** 854–860 (2002).
36. Chung, Y. R., Schatoff, E. & Abdel-Wahab, O. Epigenetic alterations in hematopoietic malignancies. *Int. J. Hematol.* **96,** 413–427 (2012).
37. Alexandrov, L. B. *et al.* Signatures of mutational processes in human cancer. *Nature* **500,** 415–421 (2013).
38. McCabe, M. T. *et al.* Mutation of A677 in histone methyltransferase EZH2 in human B-cell lymphoma promotes hypertrimethylation of histone H3 on lysine 27 (H3K27). *Proc. Natl Acad. Sci. USA* **109,** 2989–2994 (2012).
39. Bosenberg, M. *et al.* Characterization of melanocyte-specific inducible Cre recombinase transgenic mice. *Genesis* **44,** 262–267 (2006).
40. Soriano, P. Generalized lacZ expression with the ROSA26 Cre reporter strain. *Nat. Genet.* **21,** 70–71 (1999).
41. Rabbani, P. *et al.* Coordinated activation of Wnt in epithelial and melanocyte stem cells initiates pigmented hair regeneration. *Cell* **145,** 941–955 (2011).
42. Cotsarelis, G., Sun, T. T. & Lavker, R. M. Label-retaining cells reside in the bulge area of pilosebaceous unit: implications for follicular stem cells, hair cycle, and skin carcinogenesis. *Cell* **61,** 1329–1337 (1990).
43. Zipser, M. C. *et al.* A proliferative melanoma cell phenotype is responsive to RAF/MEK inhibition independent of BRAF mutation status. *Pigment Cell Melanoma Res.* **24,** 326–333 (2011).
44. Gaggioli, C. & Sahai, E. Melanoma invasion—current knowledge and future directions. *Pigment Cell Res.* **20,** 161–172 (2007).
45. Sáez-Ayala, M. *et al.* Directed phenotype switching as an effective antimelanoma strategy. *Cancer Cell* **24,** 105–119 (2013).
46. Caramel, J. *et al.* A switch in the expression of embryonic EMT-inducers drives the development of malignant melanoma. *Cancer Cell* **24,** 466–480 (2013).
47. Su, I.-H. *et al.* Ezh2 controls B cell development through histone H3 methylation and Igh rearrangement. *Nat. Immunol.* **4,** 124–131 (2003).
48. Caganova, M. *et al.* Germinal center dysregulation by histone methyltransferase EZH2 promotes lymphomagenesis. *J. Clin. Invest.* **123,** 5009–5022 (2013).
49. Tanaka, S. *et al.* Ezh2 augments leukemogenicity by reinforcing differentiation blockage in acute myeloid leukemia. *Blood* **120,** 1107–1117 (2012).
50. Min, J. *et al.* An oncogene-tumor suppressor cascade drives metastatic prostate cancer by coordinately activating Ras and nuclear factor-kappaB. *Nat. Med.* **16,** 286–294 (2010).
51. Tiwari, N. *et al.* Sox4 is a master regulator of epithelial-mesenchymal transition by controlling ezh2 expression and epigenetic reprogramming. *Cancer Cell* **23,** 768–783 (2013).
52. Shakhova, O. & Sommer, L. Testing the cancer stem cell hypothesis in melanoma: the clinics will tell. *Cancer Lett.* **338,** 74–81 (2013).
53. Damsky, W. E. *et al.* β-catenin signaling controls metastasis in Braf-activated Pten-deficient melanomas. *Cancer Cell* **20,** 741–754 (2011).
54. Stegmann, A. P. *et al.* *In vitro*-induced resistance to the deoxycytidine analogues cytarabine (AraC) and 5-aza-2'-deoxycytidine (DAC) in a rat model for acute myeloid leukemia is mediated by mutations in the deoxycytidine kinase (dck) gene. *Ann. Hematol.* **71,** 41–47 (1995).
55. Park, M. H., Nishimura, K., Zanelli, C. F. & Valentini, S. R. Functional significance of eIF5A and its hypusine modification in eukaryotes. *Amino Acids* **38,** 491–500 (2010).
56. Scuoppo, C. *et al.* A tumour suppressor network relying on the polyamine-hypusine axis. *Nature* **487,** 244–248 (2012).
57. Efimenko, E. *et al.* Caenorhabditis elegans DYF-2, an orthologue of human WDR19, is a component of the intraflagellar transport machinery in sensory cilia. *Mol. Biol. Cell* **17,** 4801–4811 (2006).
58. Lin, B. *et al.* WDR19 expression is increased in prostate cancer compared with normal cells, but low-intensity expression in cancers is associated with shorter

time to biochemical failures and local recurrence. *Clin. Cancer Res.* **14,** 1397–1406 (2008).
59. Shaul, Y. D. *et al.* Dihydropyrimidine accumulation is required for the epithelial-mesenchymal transition. *Cell* **158,** 1094–1109 (2014).
60. Helin, K. & Dhanak, D. Chromatin proteins and modifications as drug targets. *Nature* **502,** 480–488 (2013).
61. Serrano, M. *et al.* Role of the INK4a locus in tumor suppression and cell mortality. *Cell* **85,** 27–37 (1996).
62. Laird, P. W. *et al.* Simplified mammalian DNA isolation procedure. *Nucleic Acids Res.* **19,** 4293 (1991).
63. Bennett, D. C., Cooper, P. J. & Hart, I. R. A line of non-tumorigenic mouse melanocytes, syngeneic with the B16 melanoma and requiring a tumour promoter for growth. *Int. J. Cancer* **39,** 414–418 (1987).
64. Carpenter, A. E. *et al.* CellProfiler: image analysis software for identifying and quantifying cell phenotypes. *Genome Biol.* **7,** R100 (2006).
65. Santoro, R. Analysis of chromatin composition of repetitive sequences: the ChIP-Chop assay. *Methods Mol. Biol.* **1094,** 319–328 (2014).
66. Li, L.-C. & Dahiya, R. MethPrimer: designing primers for methylation PCRs. *Bioinformatics* **18,** 1427–1431 (2002).
67. Smyth, G. K. *Bioinformatics and Computational Biology Solutions Using R and Bioconductor. Statistics for Biology and Health* Vol. 5, 397–420 (Springer, 2005).
68. Wang, K., Li, M. & Hakonarson, H. ANNOVAR: functional annotation of genetic variants from high-throughput sequencing data. *Nucleic Acids Res.* **38,** e164 (2010).
69. Robinson, M. D., McCarthy, D. J. & Smyth, G. K. edgeR: a Bioconductor package for differential expression analysis of digital gene expression data. *Bioinformatics* **26,** 139–140 (2010).

Acknowledgements

We thank Charlotte Burger, Ines Kleiber-Schaaf and Jil Dreier for assistance in histology; Annika Geminn for help with plasmid preparation; the Center for Microscopy and Image Analysis (ZMB) for help with slide scanning and the Functional Genomics Center Zurich (FGCZ) for assistance in microarray analysis. We thank F. Beermann (ISREC, EPFL, Switzerland), L. Chin (MD Anderson Cancer Center, USA), H. Koseki (RIKEN Center for Integrative Medical Sciences, Japan), M. Serrano (Centro Nacional de Investigaciones Oncologicas, Spain) and P. Soriano (Icahn School of Medicine at Mount Sinai, USA) for providing *Tyr::N-Ras*^{Q61K}, *Tyr::Cre*^{ERT2}, *Ezh2*^{lox}, *Ink4a* $^{/}$ and *R26R::LacZ* mice. We thank D. Bennett (St. Georges University of London, UK) for providing XB2 and Melan-a cells; A. Melnick (Weill Cornell Medical College, USA) for providing EZH2 over-expression plasmids; G. Christofori (Department of Biomedicine, University of Basel, Switzerland) for providing an shEzh2-expressing plasmid and V. Hearing (NCI, NIH, USA) for providing Tyrp1 antibody. We acknowledge the advice by the Cancer Biology PhD Program of the University of Zurich (http://www.cnz.uzh.ch/phdprogram.html). This work was supported by the Swiss National Science Foundation, the National Research Program (NRP-63) 'Stem Cells and Regenerative Medicine', the Swiss Cancer League, the Sassella Foundation and the University Research Priority Program (URPP) 'Translational Cancer Research'.

Author contributions

D.Z., R.S., O.S. and L.S. designed the experiments; D.Z., J.D., S.M.S., E.T., S.C.F., P.C., N.A.-R., J.H., Y.Z. and M.B. performed the experiments; and D.Z., J.D., S.M.S., S.C.F., P.C. and L.S. analyzed the data. M.P.L. and R.D. provided human naevus and melanoma samples. N.A.-R. and O.B. provided expertise in engrafting murine melanoma cells. M.T.M and C.L.C. provided GSK503. D.Z. and L.S. wrote the manuscript.

Additional information

Accession codes. Microarray data have been deposited in the NCBI Gene Expression Omnibus (GEO) archive under the accession code GSE63165.

Supplementary Information accompanies this paper at http://www.nature.com/naturecommunications

Competing financial interests: The authors declare no competing financial interests.

Reprints and permission information is available online at http://npg.nature.com/reprintsandpermissions/

How to cite this article: Zingg, D. *et al.* The epigenetic modifier EZH2 controls melanoma growth and metastasis through silencing of distinct tumour suppressors. *Nat. Commun.* 6:6051 doi: 10.1038/ncomms7051 (2015).

Supplementary Information

The epigenetic modifier EZH2 controls melanoma growth and metastasis through silencing of distinct tumour suppressors

Daniel Zingg[1], Julien Debbache[1,*], Simon M. Schaefer[1,*], Eylul Tuncer[1,*], Sandra C. Frommel[2], Phil Cheng[3], Natalia Arenas-Ramirez[4], Jessica Haeusel[1], Yudong Zhang[1], Mario Bonalli[1], Michael T. McCabe[5], Caretha L. Creasy[5], Mitchell P. Levesque[3], Onur Boyman[4], Raffaella Santoro[2], Olga Shakhova[1,6], Reinhard Dummer[3], and Lukas Sommer[1]

- Supplementary Figures 1 – 12

- Supplementary Tables 1 – 12

- Supplementary References

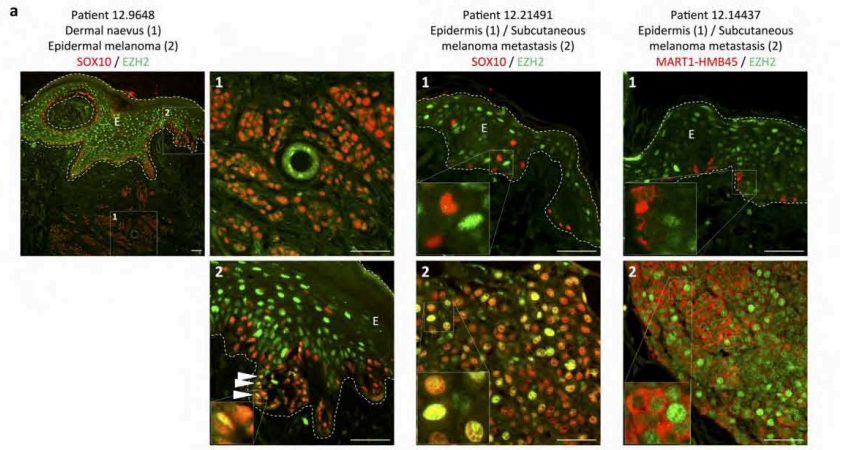

Supplementary Figure 1. EZH2 is highly expressed in human melanoma. (**a**) Representative collection of samples analysed for EZH2 expression. Immunofluorescent staining for SOX10 or MART1-HMB45 and EZH2 was used to define high EZH2 expression in melanocytic cells of malignant melanoma biopsies, as summarized in (**Supplementary Table 1**). White arrowheads, SOX10-positive cells highly expressing EZH2. E, epidermis. Scale bars, 50μm.

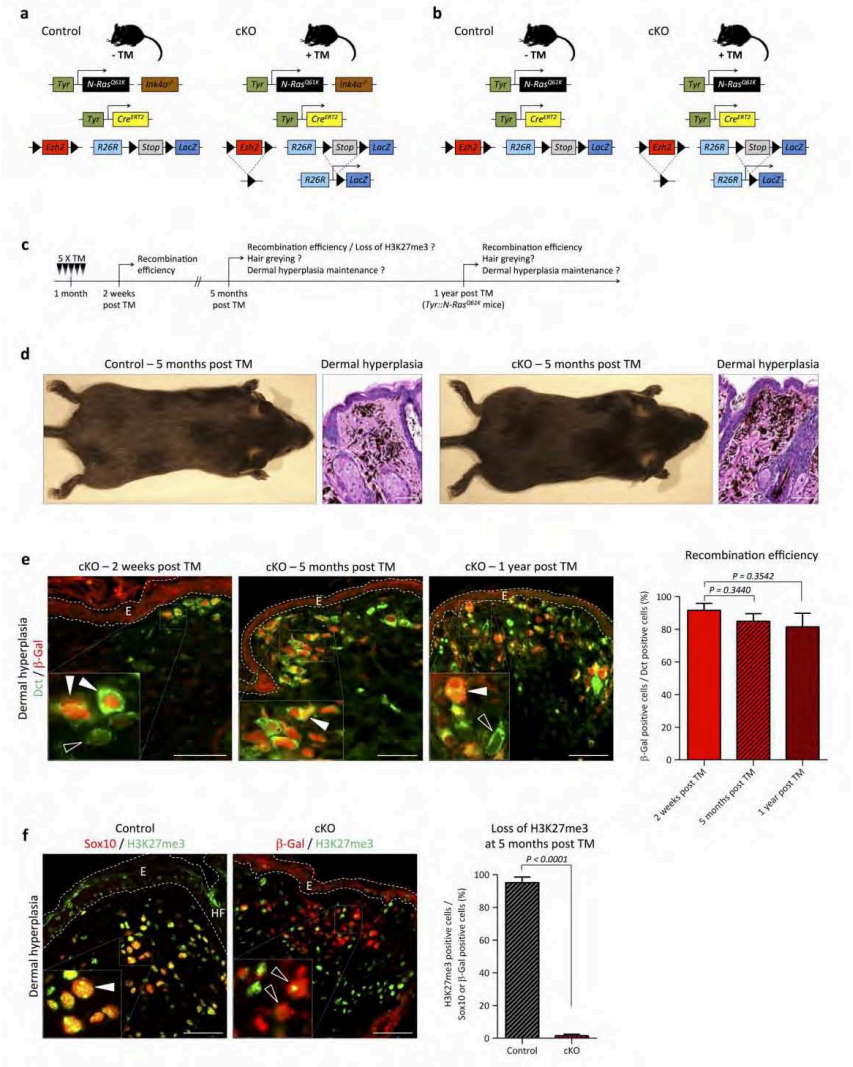

Supplementary Figure 2. Ezh2 is not required for maintenance of dermal hyperplasia. (**a** - **c**) Mouse genotypes (**a**, **b**) and strategy (**c**) used to analyse the effect of conditional *Ezh2* ablation in the melanocytic lineage of adult *Tyr::N-Ras*^{Q61K} (*Ink4a*$^{-/-}$) mice. (**d**) Macroscopic pictures and H&E staining on trunk skin sections of control and cKO mice at 5 months post conditional *Ezh2* ablation. (**e**) Immunofluorescent staining on trunk skin sections of *Tyr::N-Ras*^{Q61K} (*Ink4a*$^{-/-}$) mice for Dct and β-Gal in order to quantify recombination efficiencies. White arrowheads, Dct-positive cells considered β-Gal-positive; White open arrowheads, Dct-positive cells considered β-Gal-negative. (**f**) Immunofluorescent staining on trunk skin sections of *Tyr::N-Ras*^{Q61K} *Ink4a*$^{-/-}$ mice for Sox10 (control) or β-Gal (cKO) and

H3K27me3 in order to quantify H3K27me3 depletion. White arrowhead, Sox10-positive cell considered H3K27me3-positive; White open arrowheads, β-Gal-positive cells considered H3K27me3-negative. cKO, conditional *Ezh2* knockout; E, epidermis; H&E, haematoxylin and eosin; HF, hair follicle; TM, tamoxifen. Data are mean ± s.e.m. of n = 3. *P*-values calculated with ANOVA and Fisher's LSD-test (**e**), unpaired Student's t-test (**f**). Scale bars, 50μm.

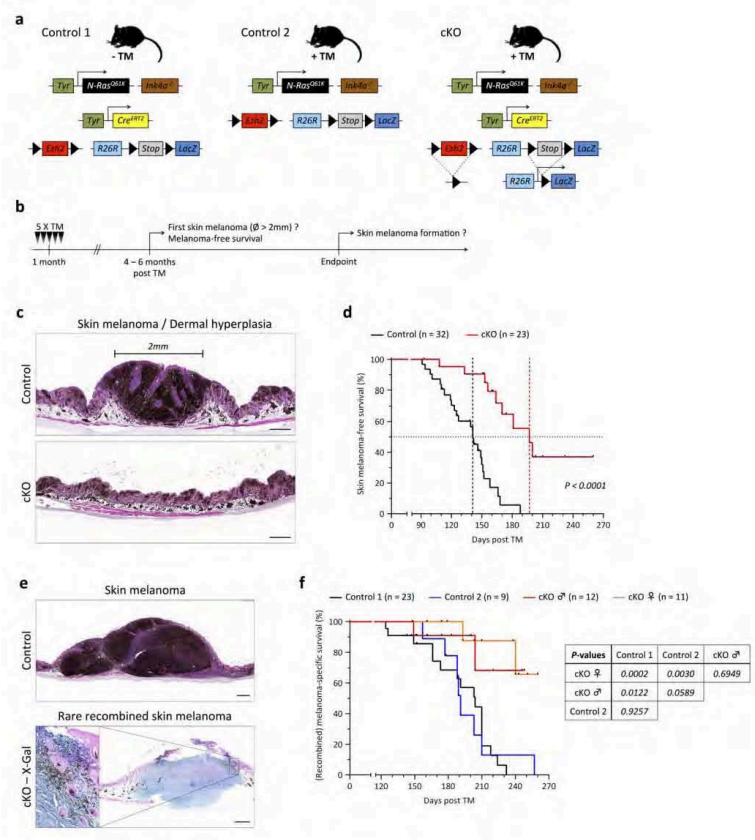

Supplementary Figure 3. Ezh2 is required for skin melanoma formation. (**a**, **b**) Mouse genotypes (**a**) and strategy (**b**) used to analyse the effect of conditional *Ezh2* ablation in the melanocytic lineage of adult *Tyr::N-Ras*^{Q61K} *Ink4a*$^{-/-}$ mice. (**c**) H&E staining on skin sections of a control and a cKO litter mate at 5 months post *Ezh2* ablation. (**d**) Kaplan-Meier curves comparing skin melanoma-free survival (skin melanoma = lesion Ø ≥ 2mm) of control and cKO mice taking into count all skin melanomas (recombined and non-recombined). (**e**) H&E staining on a melanoma section of a control animal and a section of whole mount X-Gal stained tumour of a cKO animal in order to quantify (recombined) tumour load in (**Fig. 4f**). (**f**) Kaplan-Meier curves comparing melanoma-specific survival of different controls and male versus female cKO mice. cKO, conditional *Ezh2* knockout; H&E, haematoxylin and eosin; TM, tamoxifen. *P*-values calculated with Log-rank (Mantel-Cox) test. Scale bars, 500µm.

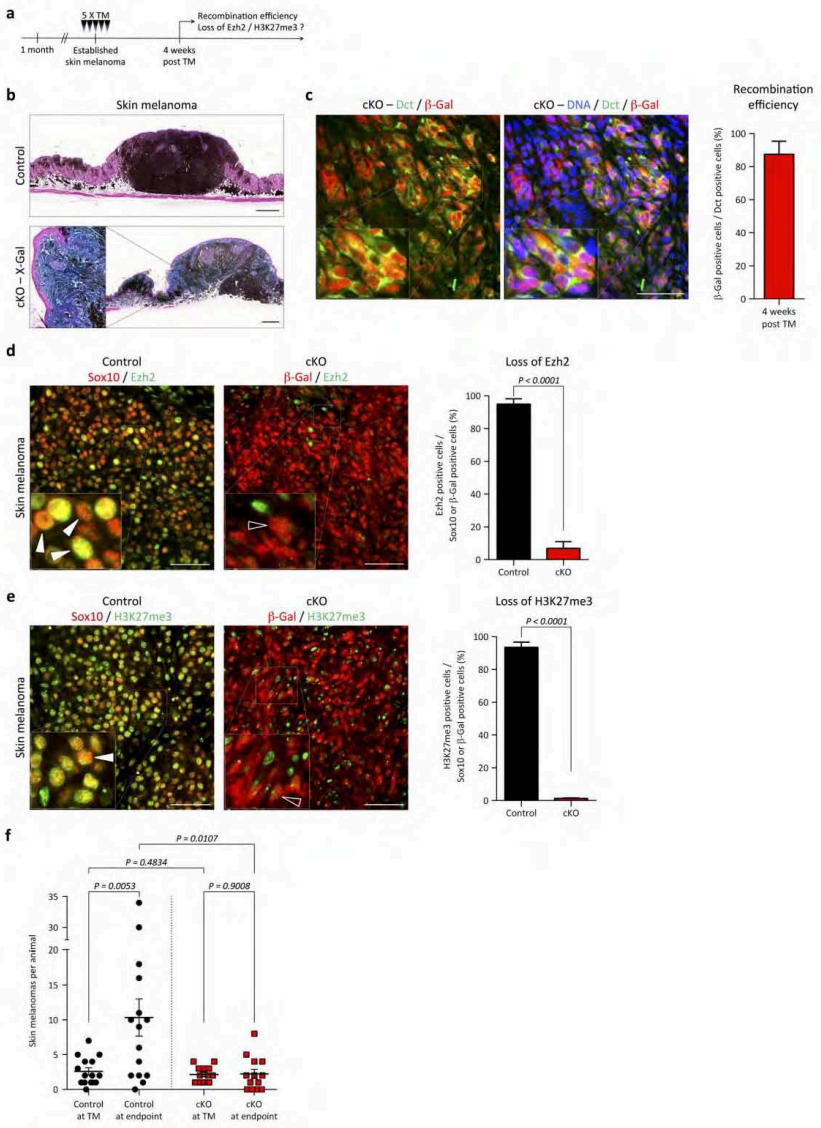

Supplementary Figure 4. ***Ezh2*** **ablation stabilises skin melanoma progression.** (**a**) Mouse genotypes as in (**Fig. 5a**) and strategy used to analyse the effects of conditional *Ezh2* ablation on skin melanoma progression in melanoma-bearing *Tyr::N-Ras*^{Q61K} *Ink4a*$^{-/-}$ mice. (**b**) H&E staining on skin melanoma sections and sections of whole mount X-Gal stained tumours 4 weeks after conditional *Ezh2* ablation. (**c**) Immunofluorescent staining on skin melanoma sections for Dct and β-Gal 4 weeks post conditional *Ezh2* ablation in order to quantify a recombination efficiency. (**d**, **e**) Immunofluorescent

staining on skin melanoma sections for Sox10 (control) or β-Gal (cKO) and Ezh2 (**d**) or H3K27me3 (**e**) 4 weeks post conditional *Ezh2* ablation in order to quantify Ezh2 and subsequent H3K27me3 depletion in melanoma cells. White arrowheads, Sox10-positive cells considered Ezh2- or H3K27me3-positive; White open arrowheads, β-Gal-positive cells considered Ezh2- or H3K27me3-negative. (**f**) Skin melanoma count at time point of *Ezh2* ablation and at day of sacrifice. cKO, conditional *Ezh2* knockout; H&E, hematoxylin and eosin; TM, tamoxifen. Data are mean ± s.e.m. of n = 3 (**c** - **e**), mean ± s.e.m. of n = 15 (Control), n = 13 (cKO) (**f**). *P*-values calculated with unpaired Student's t-test, paired Student's t-test for "Control at TM" versus "Control at endpoint", "cKO at TM" versus "cKO at endpoint" in (**f**). Scale bars, 500μm (**b**), 50μm (**c** - **e**).

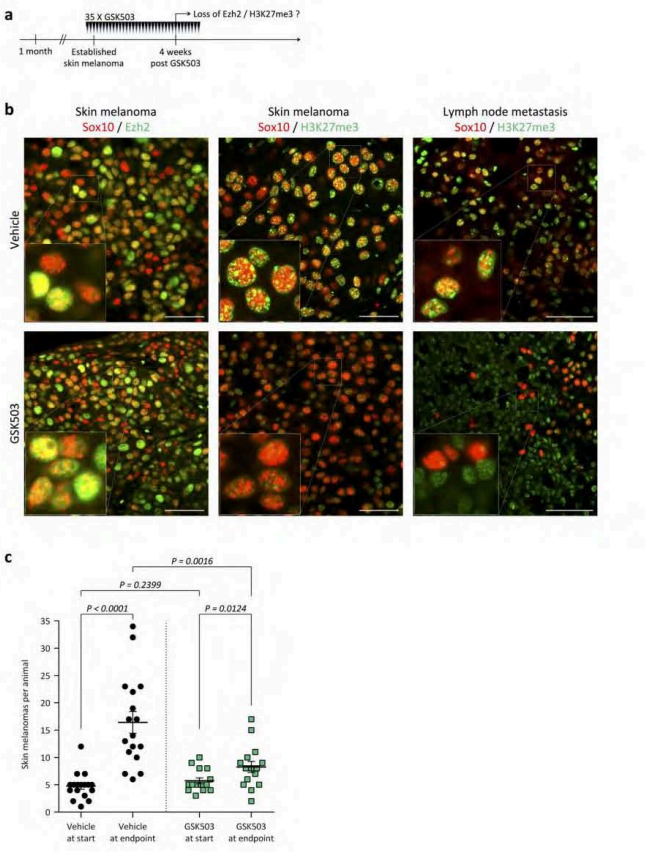

Supplementary Figure 5. Temporary GSK503 treatment stabilises skin melanoma progression. (**a**) Mouse genotypes as in (**Fig. 5e**) and strategy used to analyse the effect of temporary GSK503 treatment on skin melanoma progression in melanoma-bearing *Tyr::N-Ras*^{Q61K} *Ink4a*$^{-/-}$ mice. (**b**) Immunofluorescent staining on skin melanoma and lymph node sections for Sox10 and Ezh2 or H3K27me3 4 weeks after treatment start with vehicle or GSK503. (**c**) Skin melanoma count at time point of GSK503 treatment start and at day of sacrifice. Data are mean ± s.e.m. of n = 17 (Vehicle), n = 15 (GSK503). *P*-values calculated with unpaired Student's t-test, paired Student's t-test for "Vehicle at start" versus "Vehicle at endpoint", "GSK503 at start" versus "GSK503 at endpoint". Scale bars, 50μm.

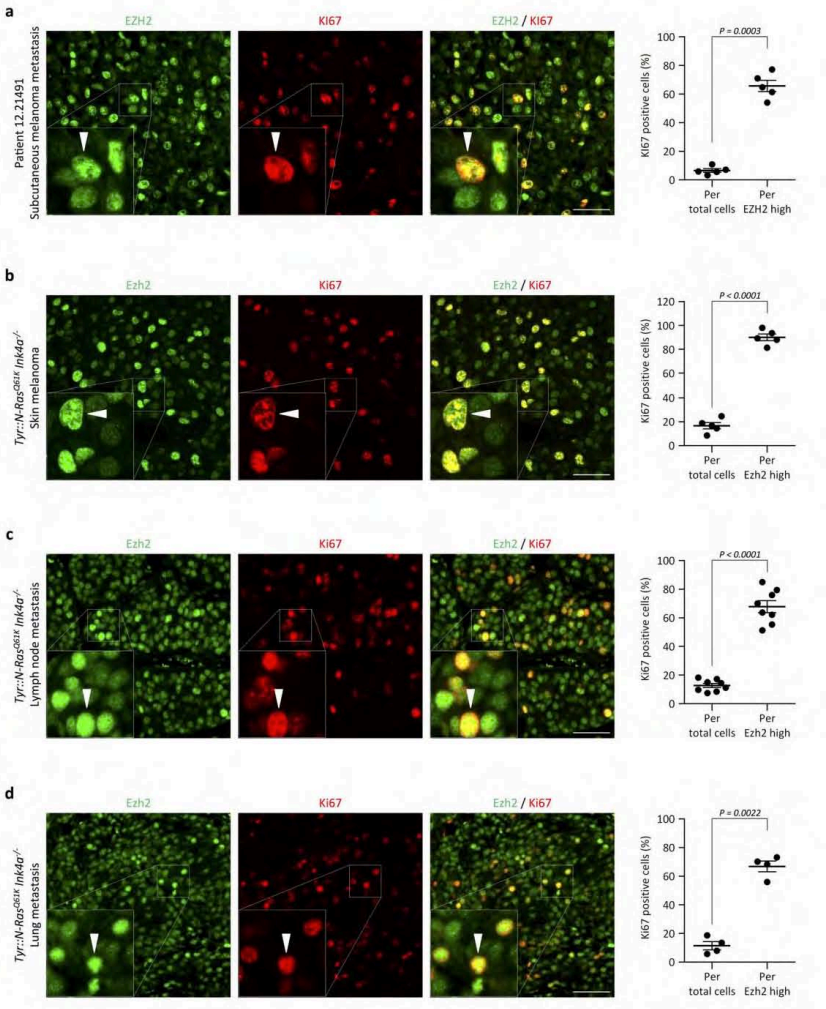

Supplementary Figure 6. Heterogeneous high EZH2 expression correlates with KI67 positivity. (**a** - **d**) Immunofluorescent staining on human melanoma metastases sections (**a**) and melanoma sections of *Tyr::N-Ras*^{Q61K} *Ink4a*$^{-/-}$ mice (**b** - **d**) for EZH2 and KI67 in order to quantify a correlation between high EZH2 expression and KI67 positivity. White arrowheads, EZH2-high cells considered KI67-positive. Data are mean ± s.e.m. of n = 5 (**a**, **b**), mean ± s.e.m. of n = 8 (**c**), mean ± s.e.m. of n = 4 (**d**). *P*-values calculated with unpaired Student's t-test. Scale bars, 50μm.

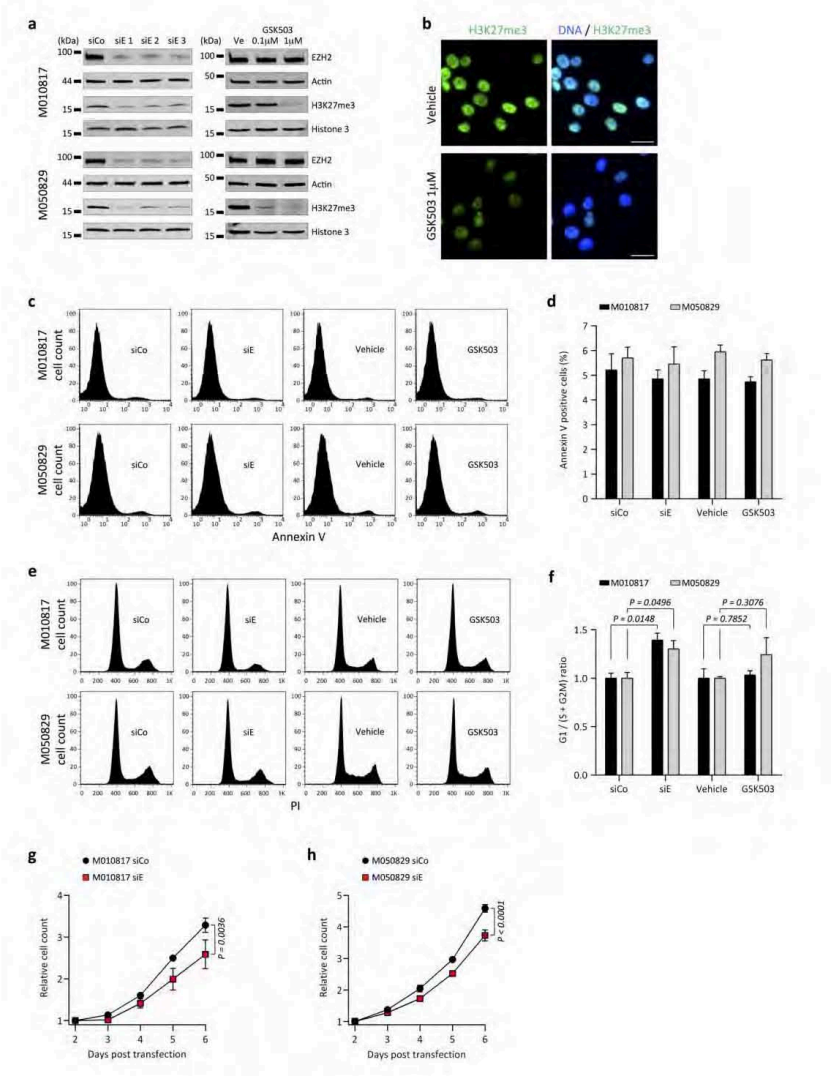

Supplementary Figure 7. EZH2 inactivation in human melanoma cells interferes with cell growth. (**a**) Western blot for EZH2 protein and H3K27me3 on whole cell lysates from 2 melanoma cell cultures (M010817, M050829) after EZH2 depletion with 3 different siEs or EZH2 inhibition using GSK503. (**b**) Immunofluorescent staining on M010817 for H3K27me3 after GSK503 treatment. (**c**, **d**) FACS analysis of M010817 and M050829 for Annexin V positivity after EZH2 depletion with siE or EZH2 inhibition using GSK503 in order to quantify induced apoptosis. (**e**, **f**) Cell cycle profiles of M010817 and M050829 using PI after EZH2 depletion with siE or EZH2 inhibition using GSK503 in order to quantify a G1 / (S + G2M) ratio. (**g**, **h**) Growth of M010817 (**g**) and M050829 (**h**) after EZH2

depletion with siE. PI, propidium iodide; Ve, vehicle. Data are mean ± s.e.m. of n = 3. *P*-values calculated with unpaired Student's t-test (**f**), ANOVA and Fisher's LSD-test (**g**, **h**). Scale bars, 25µm.

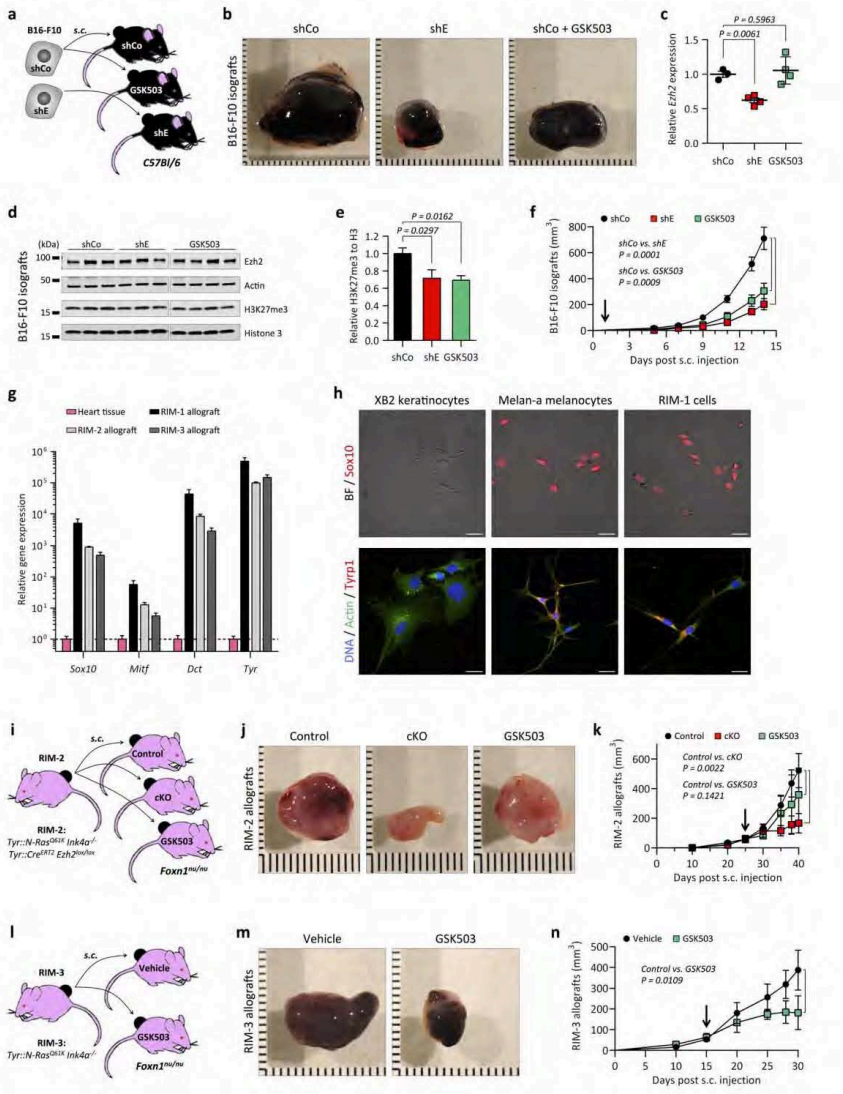

Supplementary Figure 8. Ezh2 inactivation interferes with growth of murine melanoma. (**a**) Mouse genotypes and strategy used to s.c. engraft B16-F10 cells following *Ezh2* silencing with shE in order to analyse the effect of Ezh2 depletion and GSK503 treatment on melanoma growth. (**b**) Representative macroscopic pictures of shCo, shE, and GSK503-treated B16-F10 isografts. (**c**) RT-qPCR for *Ezh2* on lysed shCo, shE, and GSK503-treated B16-F10 tumours from (**b**). (**d**, **e**) Western blot for Ezh2 protein and H3K27me3 on lysed shCo, shE, and GSK503-treated B16-F10 tumours from (**b**) in order to quantify loss of H3K27me3. (**f**) Growth of shCo, shE, and GSK503-treated B16-F10 isografts (**b**). Black arrow, GSK503 treatment start. (**g**) RT-qPCR for melanocytic lineage genes on

lysed heart tissue, RIM-1, RIM-2, and RIM-3 tumours. (**h**) Immunofluorescent staining on XB2, Melan-a, and RIM-1 cells for Sox10 and Tyrp1. (**i**, **l**) Mouse genotypes and strategies used to s.c. engraft and expand *Tyr::N-Ras*^{Q61K} *Ink4a*$^{-/-}$ mice-derived melanoma cells in *Foxn1*$^{nu/nu}$ animals in order to analyse the effect of conditional *Ezh2* ablation and GSK503 treatment on melanoma growth. (**j**, **k**) Representative macroscopic pictures (**j**) and growth (**k**) of control, cKO, and GSK503-treated RIM-2 allografts. Black arrow, time point of TM application / start of GSK503 treatment. (**m**, **n**) Representative macroscopic pictures (**m**) and growth (**n**) of vehicle- and GSK503-treated RIM-3 allografts. Black arrow, GSK503 treatment start. BF, bright field; cKO, conditional *Ezh2* knockout; H3, histone 3; RIM, *Tyr::N-Ras*^{Q61K} *Ink4a*$^{-/-}$ melanoma; s.c., subcutaneous; TM, tamoxifen. Data are mean ± s.e.m. of n = 3 (shCo), n = 4 (shE, GSK503) (**c**), mean ± s.e.m. of n = 3 (shCo, shE), n = 4 (GSK503) (**d**, **e**), mean ± s.e.m. of n = 3 (**g**, **k**, **n**). *P*-values calculated with ANOVA and Fisher's LSD-test. Scale bars, 1mm (**b**, **j**, **m**), 25µm (**h**).

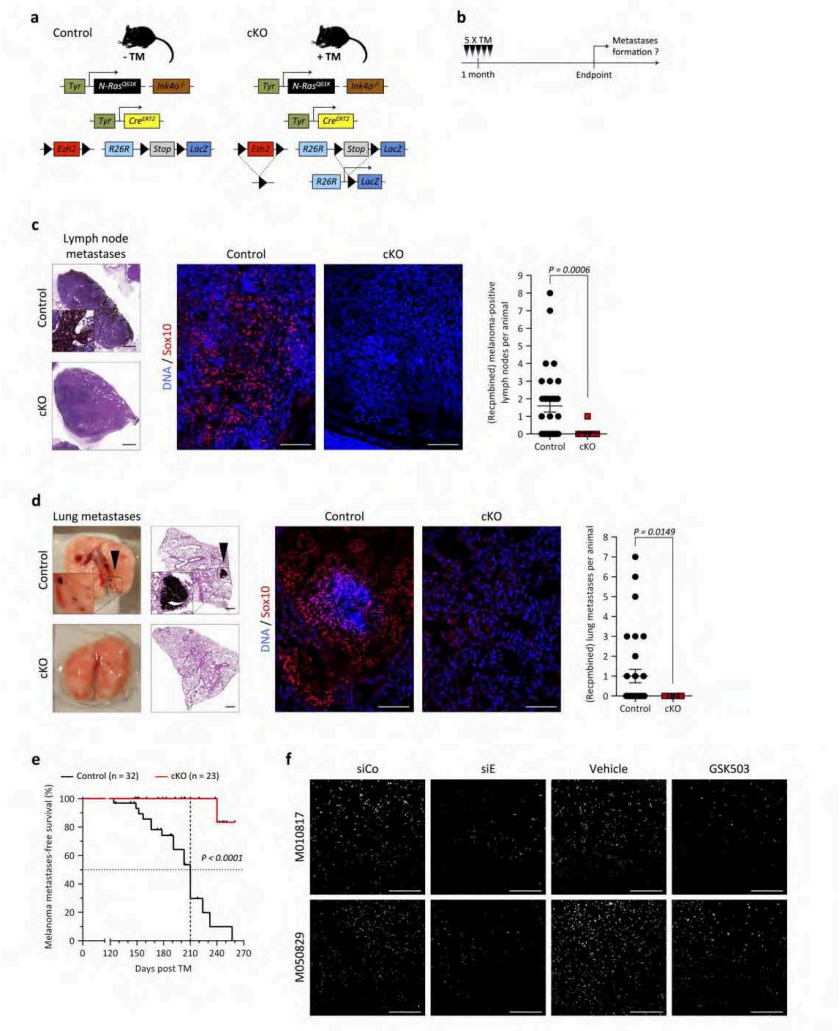

Supplementary Figure 9. *Ezh2* ablation before onset of melanomagenesis prevents metastases formation. (**a**, **b**) Mouse genotypes (**a**) and strategy (**b**) used to analyse the effect of conditional *Ezh2* ablation on metastases formation in *Tyr::N-Ras*^{Q61K} *Ink4a*$^{-/-}$ mice. (**c**, **d**) Metastases count at day of sacrifice in lymph nodes (**c**) and lung (**d**) of control and cKO animals using macroscopic pictures, H&E staining, and Sox10 staining on sections. Black arrowheads, lung metastases. (**e**) Kaplan-Meier curves comparing melanoma metastases-free survival after conditional *Ezh2* ablation. (**f**) Immunofluorescence fields of transvaded M010817 and M050829 cells after a Boyden Chamber assay using Hoechst 33342, representative of quantifications in (**Fig. 7j**). White, DNA. cKO, conditional *Ezh2* knockout; TM, tamoxifen. Data are mean ± s.e.m. of n = 32 (Control), n = 23 (cKO). *P*-values calculated with unpaired

Student's t-test (**c**, **d**), Log-rank (Mantel-Cox) test (**e**). Scale bars, 500μm (**c**, **d**), 100μm (immunofluorescence in **c**, **d**), 250μm (**f**).

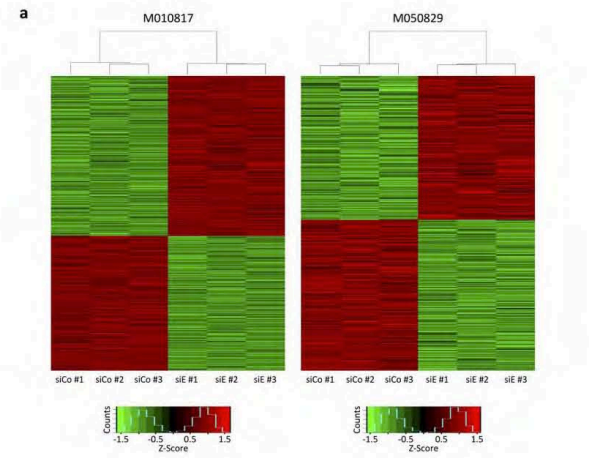

Supplementary Figure 10. Gene expression array heat maps. (**a**) Heat maps of differentially expressed genes in M010817 and M050829 after EZH2 depletion with siE showing normalized expression values of 3 biological replicates.

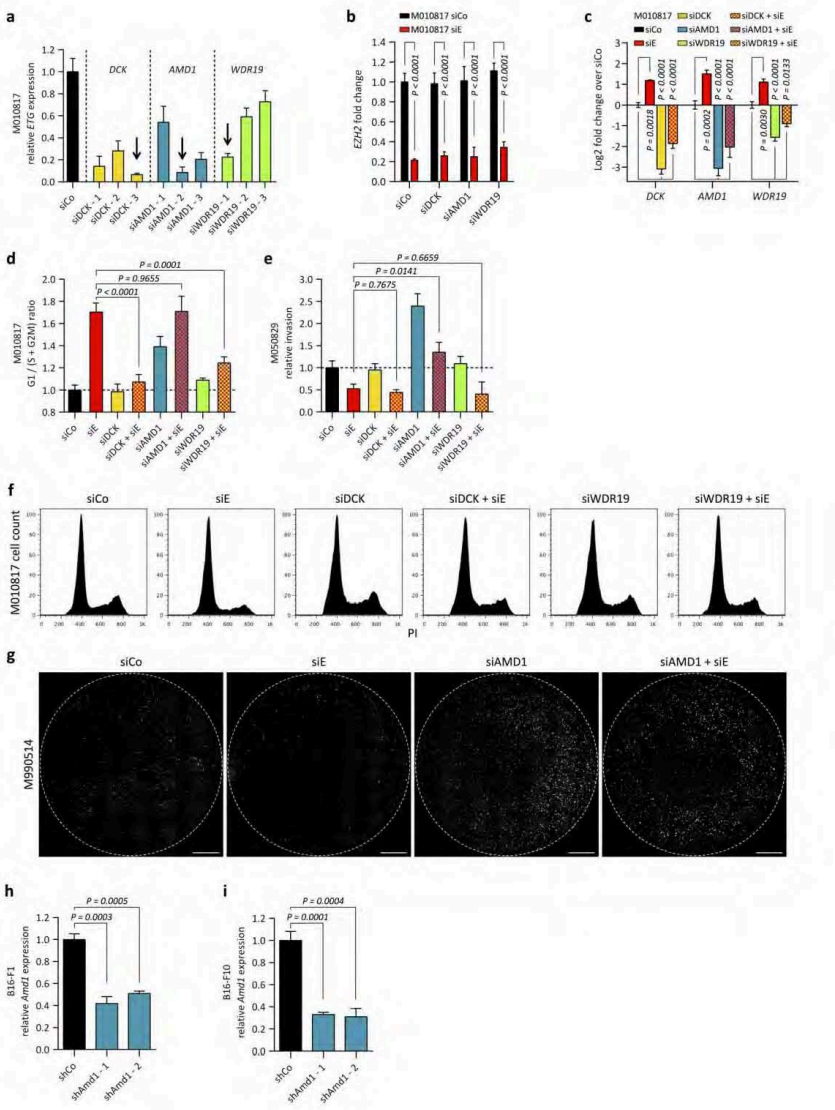

Supplementary Figure 11. Depletion of ETGs rescues EZH2 inactivation phenotypes. (**a**) RT-qPCR for selected ETGs on M010817 after DCK, AMD1, or WDR19 depletion with siRNAs targeting these genes. Black arrows, siRNAs chosen for further experiments. (**b**) RT-qPCR for *EZH2* on M010817 after EZH2 and DCK / AMD1 / WDR19 depletion with siE and siDCK / siAMD1 / siWDR19. (**c**) RT-qPCR for selected ETGs on M010817 after EZH2 and DCK / AMD1 / WDR19 depletion with siE and siDCK / siAMD1 / siWDR19. (**d**) Quantification of G1 / (S + G2M) ratio of M010817 after depletion of EZH2 and DCK / AMD1 / WDR19 using siE and siDCK / siAMD1 /

siWDR19. (**e**) Quantification of relative invasive capacity of M050829 after depletion of EZH2 and DCK / AMD1 / WDR19 using siE and siDCK / siAMD1 / siWDR19. (**f**) Cell cycle profiles of M010817 using PI, representative of quantifications in (**Fig. 8f**). (**g**) Immunofluorescence fields of transvaded M990514 cells after a Boyden Chamber assay using Hoechst 33342, representative of quantifications in (**Fig. 8g**). White, DNA. (**h**, **i**) RT-qPCR for *Amd1* on B16-F1 (**h**) and B16-F10 (**i**) after Amd1 depletion with shAmd1. ETG, EZH2 target gene; PI, propidium iodide. Data are mean ± s.e.m. of n = 3. *P*-values calculated with unpaired Student's t-test (**b**), ANOVA and Fisher's LSD-test (**c** - **e**, **h**, **i**). Scale bars, 1mm.

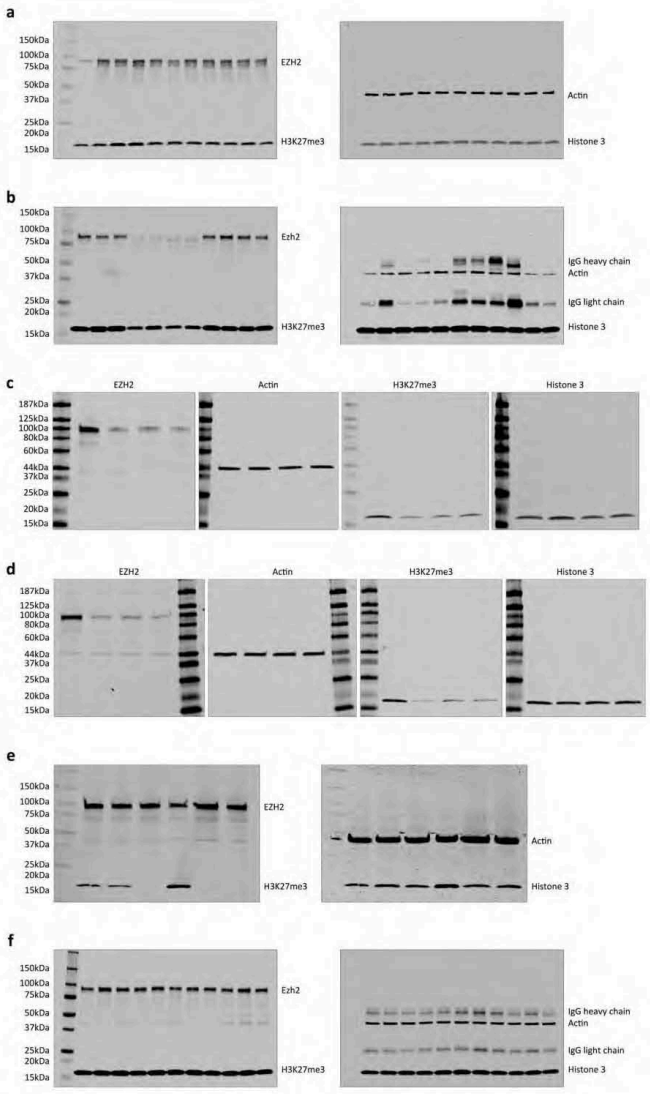

Supplementary Figure 12. Full scans of western blots. (**a**) Full scans corresponding to (**Fig. 2c**). (**b**) Full scans corresponding to (**Fig. 6g**). (**c - e**) Full scans of M010817 (**c**) and M050829 (**d**) after siE (**c**, **d**) or GSK503 (**e**) corresponding to (**Supplementary Fig. 7a**). (**f**) Full scans corresponding to (**Supplementary Fig. 8d**).

Supplementary Table 1. Clinical data for human melanoma biopsies

Patient ID	Sex	Age	AJCC	Naevus / Melanoma type	*BRAF**	*NRAS**	MART1	HMB45	EZH2 high
12.9648	M	48	0	Dermal naevus	n.d.	n.d.	+	-	no
12.9648	M	48	I	Epidermal melanoma	n.d.	n.d.	+	+	yes
12.6190	F	61	0	Dermal naevus	V600E	--	+	-	no
10.9640	M	36	0	Congenital naevus	--	Q61K	+	-	no
12.13497	M	76	II	Epidermal melanoma	V600E	--	+	+	yes
1219445	M	55	IIIA	Epi- / dermal melanoma	--	Q61K	+	+	yes
12.18389	F	65	IV	Subcutaneous metastasis	V600E	--	+	+	yes
12.14437	F	n.a.	IIIC	Subcutaneous metastasis	--	Q61R	+	+	yes
12.21491	F	84	IIIB	Subcutaneous metastasis	--	Q61R	+	+	yes

Immunohistochemical staining for MART1 and HMB45 was used to distinguish benign from malignant melanoma lesions[1,2]. n.a., not available; n.d., not defined.

Supplementary Table 2. Association of high gene expression with survival

Gene	Association with patient survival	Gene	Association with patient survival
TXNIP	improved	*MXRA7*	NS
WDTC1	NS	*DIS3L*	NS
ACO2	poor	*NFIC*	NS
DCK	improved	*APOBEC3D*	improved
TMEM143	NS	*AGPAT2*	poor
WDR34	poor	*KREMEN1*	NS
CAMKK2	NS	*SNAPC5*	improved
ZDHHC1	NS	*GNG7*	NS
ZC3H6	improved	*EIF2C4*	NS
XPOT	improved	*IL17RC*	NS
MPC1	improved	*MSRB2*	NS
CNN2	NS	*FAM198B*	improved
QPRT	NS	*SNAPC1*	improved
TCFL5	NS	*TMEM129*	NS
LAMTOR1	NS	*CDC42EP4*	NS
HIBADH	NS	*HDAC5*	NS
DDR2	NS	*NNT*	NS
HSBP1L1	NS	*CD40*	improved
ECSIT	NS	*DNAJC4*	NS
MCAT	NS	*SAYSD1*	NS
DCAKD	NS	*STX8*	improved
CYP27A1	NS	*SWAP70*	NS
CRYL1	NS	*MUT*	improved
XYLT2	NS	*SCPEP1*	improved
TMEM161A	NS	*RETSAT*	poor
REEP6	NS	*PYROXD2*	improved
RBFOX2	NS	*HDHD2*	NS
R3HDM2	NS	*TGS1*	NS
KCTD18	improved	*WBP1L*	NS
BCAS3	NS	*APOOL*	NS
NFIA	NS	*MCOLN3*	NS
FAM210B	NS	*ANKRD44*	NS
ADAM10	NS	*ST6GALNAC2*	NS
WDR19	improved	*TMEM140*	NS
AMD1	improved	*UBE3B*	NS
STARD5	NS	*GAS2L3*	NS
IER5	NS	*RAB40B*	improved
CTSF	NS		

improved, improved survival for specimens with high RNAseq reads for a specific gene compared to specimens with low RNAseq reads; poor, poor survival for specimens with high RNAseq reads for a specific gene compared to specimens with low RNAseq reads; NS, no significant difference between the high and the low group.

Supplementary Table 3. P-values related to Figure 8d, e

Figure 6d	*P*-values		Figure 6e	*P*-values	
Gene	M010817	M050829	Gene	M010817	M050829
TXNIP	*< 0.0001*	*0.0047*	*TXNIP*	*0.0003*	*0.0030*
DCK	*0.0009*	*0.0029*	***DCK***	*0.0051*	*0.0039*
AMD1	*0.0080*	*0.0017*	***AMD1***	*0.0012*	*0.0045*
ZC3H6	*0.0052*	*0.0329*	*ZC3H6*	*0.0189*	*0.0036*
XPOT	*0.0041*	*0.0288*	*XPOT*	*0.0195*	*0.0022*
MPC1	*0.0056*	*0.0177*	*MPC1*	*0.0018*	*0.0016*
APOBEC3D	*0.0075*	*0.0125*	*APOBEC3D*	*0.0114*	*0.0012*
STX8	*0.0065*	*0.0039*	*STX8*	*0.0088*	*0.0011*
KCTD18	*0.0016*	*0.0002*	*KCTD18*	*0.0102*	*0.0080*
WDR19	*0.0065*	*0.0001*	***WDR19***	*0.0078*	*0.0021*
PYROXD2	*0.0012*	*0.0007*	*PYROXD2*	*0.0040*	*0.0064*
FAM198B	*0.0272*	*0.0006*	*FAM198B*	*0.0238*	*0.0028*
CD40	*0.0046*	*0.0007*	*CD40*	*0.0066*	*0.0002*
SNAPC5	*0.0374*	*0.0539*	*SNAPC5*	*0.0025*	*0.0420*
SNAPC1	*0.0162*	*0.0071*	*SNAPC1*	*0.0914*	*0.0068*
SCPEP1	*0.0706*	*0.0058*	*SCPEP1*	*0.0083*	*0.0014*
MUT	*0.0133*	*0.0033*	*MUT*	*0.0039*	*0.0156*
RAB40B	*0.0008*	*0.0013*	*RAB40B*	*0.8299*	*0.9101*

Supplementary Table 4. Mouse genotyping primers

Allele	Forward sequence	Reverse sequence
Cre	CTATCCAGCAACATTTGGGCCAGC	CCAGGTTACGGATATAGTTCATGAC
Ezh2^{wt}	AAGGCTGTGTACAGGAAACAATC	AGTACTCCAGAGGTACTGAAGTTTG
Ezh2^{lox}	AAGGCTGTGTACAGGAAACAATC	TCACCTTAATATGCGAAGTGGAC
Ink4a^{wt}	ATGATGATGGGCAACGTTC	CAAATATCGCACGATGTC
Ink4a^{knockout}	CTATCAGGACATAGCGTTGG	AGTGAGAGTTTGGGGACAGAG
LacZ	GGTCGGCTTACGGCGGTGATTT	AGCGGCGTCAGCAGTTGTTTTT
N-Ras^{Q61K}	GATCCCACCATAGAGGATT	CTGGCGTATTTCTCTTACC

Supplementary Table 5. Primary antibodies

Anitgen	Specificity	Company	Serial number	Applications / Dilutions
β-Actin	human / mouse	Sigma-Aldrich	A5316	WB, 1:10'000 / IF, 1:1'000
DCT	human / mouse	Santa Cruz Biotechnology	sc-10451	IF, 1:200
EZH2	human / mouse	Cell Signaling Technology	3147	WB, 1:1'000 / IF, 1:200
β-Gal	mouse	Abcam	ab9361	IF, 1:1'000
Histone 3	human / mouse	Cell Signaling Technology	3638	WB, 1:1'000
H3K27me3	human / mouse	Cell Signaling Technology	9733	WB, 1:1'000 / IF, 1:500
HMB45	human	Dako	IS052	IHC, 1:50
KI67	human	Abcam	ab156956	IF, 1:50
Ki67	mouse	BioLegend	652402	IF, 1:100
MART1	human	Novocastra	PA0233	IHC, 1:50
MART1-HMB45	human	Abcam	ab732	IF, 1:200
SOX10	human / mouse	Santa Cruz Biotechnology	sc-17342	IF, 1:100
Tyrp1	mouse	V. Hearing lab, NIH [3]	αPEP1	IF, 1:500

Supplementary Table 6. Secondary antibodies

Fluorophore	Specificity	Company	Serial number	Applications / Dilutions
Alexa488	goat	Jackson ImmunoResearch	705-545-147	IF, 1:500
Alexa488	rabbit	Jackson ImmunoResearch	711-545-152	IF, 1:500
Alexa488	rat	Jackson ImmunoResearch	712-545-153	IF, 1:500
Alexa546	mouse	Life Technologies	A-11030	IF, 1:500
Cy3	goat	Jackson ImmunoResearch	705-165-147	IF, 1:500
Cy3	rat	Jackson ImmunoResearch	712-165-153	IF, 1:500
IRDye-800CW	mouse	LI-COR Biosciences	926-32212	WB, 1:10'000
IRDye-680LT	rabbit	LI-COR Biosciences	926-68023	WB, 1:10'000

Supplementary Table 7. Human *EZH2* mutagenesis primers

EZH2 mutation		Sequence
$EZH2^{F132S}$	forward	CTAAAACTTCATCTCCCATATAAGAAATGTTATGTAAAACAGTTTCATCTTC
$EZH2^{F132S}$	reverse	GAAGATGAAACTGTTTTACATAACATTTCTTATATGGGAGATGAAGTTTTAG
$EZH2^{D142V}$	forward	TAGTTCTTCAATGAAAGTACCAACCTGATCTAAAACTTCATCTCC
$EZH2^{D142V}$	reverse	GGAGATGAAGTTTTAGATCAGGTTGGTACTTTCATTGAAGAACTA
$EZH2^{R216Q}$	forward	TCAAAAATTTTATCAGAAGGAAATTTTTGAGGTGGGCGGCTTTCTTTATCATC
$EZH2^{R216Q}$	reverse	GATGATAAAGAAAGCCGCCCACCTCAAAAATTTCCTTCTGATAAAATTTTTGA
$EZH2^{A226V}$	forward	CTTATCTGGAAACATTGAGGAAATGACTTCAAAAATTTTATCAGAAGGAAAT
$EZH2^{A226V}$	reverse	ATTTCCTTCTGATAAAATTTTTGAAGTCATTTCCTCAATGTTTCCAGATAAG
$EZH2^{P431S}$	forward	CCACATTCTCAGGAGATTCAATATTTGGCTTCATCTTTATTGGT
$EZH2^{P431S}$	reverse	ACCAATAAAGATGAAGCCAAATATTGAATCTCCTGAGAATGTGG
$EZH2^{K515R}$	forward	GAGGAGCCGTCCCTTTTCAGCTGTATCTTTCTGCAG
$EZH2^{K515R}$	reverse	CTGCAGAAAGATACAGCTGAAAAGGGACGGCTCCTC
$EZH2^{C535W}$	forward	GGCACGAACTGTCCCAAGGCTGCCGTG
$EZH2^{C535W}$	reverse	CACGGCAGCCTTGGGACAGTTCGTGCC

Supplementary Table 8. Human *EZH2* sequencing primers

Gene location	Forward sequence	Reverse sequence
EZH2 N-term	TGTTCGGTGACCAGTGACTT	TTTGGTCCATCTATGTTGGGG
EZH2 middle	ATACAGACAGTGATAGGGAAGCA	CATCCCGGAAAGCGGTTTTG
EZH2 C-term	CAAGAACTGCAGTATTCAGCG	CCGACATACTTCAGGGCATC

Supplementary Table 9. RNAi constructs

Target gene	si/shRNA name	Specificity	Company	Serial numbers
none	siCo	human	Life Technologies	12935-112
EZH2	siE	human	Life Technologies	HSS176653, HSS176652, HSS103462
DCK	siDCK	human	Life Technologies	HSS141795, HSS175996, HSS175997
AMD1	siAMD1	human	Life Technologies	HSS100444, HSS178141, HSS178142
WDR19	siWDR19	human	Life Technologies	HSS126737, HSS126738, HSS184043
none	shCo	mouse	Sigma-Aldrich	SHC002
Ezh2	shE	mouse	Sigma-Aldrich	TRCN0000039040
none	shCo	mouse	GE Healthcare	RHS4346
Amd1	shAmd1	mouse	GE Healthcare	V2LMM_71494, V2LMM_72222

Supplementary Table 10. Mouse RT-qPCR primers

Gene	Forward sequence	Reverse sequence
Acta2	TGACAGAGGCACCACTGAAC	AGAGGCATAGAGGGACAGCA
Amd1	TGTGGAAGTCTTCAAGCCAGG	CGAAGAAAGCACTGTGCGAC
Cdh1	CTGCTGCCACCAGATGATGA	CTGTGCAGCTGGCTCAAATC
Cdh2	GCGCCATCATCGCTATCCTT	TCCCGCCGTTTCATCCATAC
Dck	AAGCTGGCTCCTTCATCGGA	TAACATCCAGTGTGAGGACGG
Dct	CCTGAATGGGACCAATGCCT	AGGCATCTGTGGAAGGGTTG
Ets1	GCCAACCCTACCTACCCAGA	GAGGGAGGAACACACTGAGC
Ezh2	GTGACCACAGGATAGGCATCT	CAAGGGATTTCCATTTCTCG
Mitf	CCCCAAGTCAAATGATCCAG	GCAACTTCCGGATGTAGTCC
Mmp1	GAACACGGGGAAGACCCTCT	TTCCTCTTCTATGAGGCGGGG
Mmp3	GACTCAAGGGTGGATGCTGT	CCAACTGCGAAGATCCACTG
Snai1	GTGGAAAGGCCTTCTCTAGGC	GGTTGGAGCGGTCAGCAAAA
Sox10	GAAGAAGGCTCCCCCATGTC	GCTCTGTCTTTGGGGTGGTT
Twist1	CGGCCAGGTACATCGACTTC	TGCAGCTTGCCATCTTGGAG
Tyr	GTACTTGGGAGGTCGTCACC	GTCCCTCAGGTGTTCCATCG
Usf1	CAGGGCTCAGAGGCACTACT	GCTCCCTCCCTGCAATACTT
Vim	GCGAGGAGAGCAGGATTTCT	TGAGTGGGTGTCAACCAGAG
Wdr19	ACCACCCCATGTCCATTCTG	CGTCTTTCAACATGTGTCGGC
Zeb1	GATCCAGCCAAACGGAAACC	TGGCGTGGAGTCAGAGTCAT

Supplementary Table 11. Human RT-qPCR primers

Gene	Forward sequence	Reverse sequence
ACTA2	GGCAAGTGATCACCATCGGA	GTGGTTTCATGGATGCCAGC
AMD1	CCAGGAAAATTTGTGACCACCT	ACTCTGGCAATCAAGACGCT
APOBEC3D	AAGCACCACTCAGCTGTCTTC	CCAGGTGACCTCGTAGTTTGT
CD40	AGTCAGTGCTGTTCTTTGTGC	TTCGCTTTCACCGCAAGGA
CDH2	ACAGTGGCCACCTACAAAGG	CCGAGATGGGGTTGATAATG
DCK	AAAGCTGGCTCCTGCATAGG	TCCAGTGTTAAGATAGGCACCTC
ETS1	GATAGTTGTGATCGCCTCACC	GTCCTCTGAGTCGAAGCTGTC
EZH2	CCCTGACCTCTGTCTTACTTGTGGA	ACGTCAGATGGTGCCAGCAATA
FAM198B	AGCGAAAGCATGACCCAAGG	CCGTAAGTGCTGGCTCTTCAA
GAPDH	ACCCAGAAGACTGTGGATGG	TCTAGACGGCAGGTCAGGTC
KCTD18	TGCGTCACATGGCTCCAAT	CTGAGGCCGAGTTCTTGACTT
MMP1	TTGTGGCCAGAAAACAGAAA	TTCGGGGAGAAGTGATGTTC
MMP3	CAATTTCATGAGCAGCAACG	AGGGATTAATGGAGATGCCC
MPC1	ATCAGTGGGCGGATGACATT	GGCATGCAAACAGAAGCCAG
MUT	ACTTAACTCCCTTGGACGGC	CGAGTCCCAGGACCAAATACA
PYROXD2	AGCAGGAGAGAGACGCTTATG	TGAGGATGTCTCTGCCAACC
RAB40B	ATGGGATGGACCGGCTCT	TTAAGGCAATGGGGAGCGG
SCPEP1	AGCATTGTGGACGAGTTGCT	ACTTCAGTTTCCGCACCCAG
SNAI1	CCTCCCTGTCAGATGAGGAC	CCAGGCTGAGGTATTCCTTG
SNAPC1	TGAAAGGGCAGAATCATTAGCG	TTGACTTGCCCTTGACCAGA
SNAPC5	GAAGAGGGGATGAGATGCTGTC	CAGCTCCAGGGTTGTTTGGT
STX8	TCGCCAAAAACAAATGGGGC	TGTTTACCCGCCTGGTTTCA
TWIST1	GTCCGCAGTCTTACGAGGAG	CCAGCTTGAGGGTCTGAATC
TXNIP	TATCCTGGGCTGCAACATCC	TCTGCTGCCAATTACCAGGG
USF1	TACTACCCAGGGCTCAGAGG	TCCCTGCAGTACTTCTTGTGG
VIM	GAGAACTTTGCCGTTGAAGC	GCTTCCTGTAGGTGGCAATC
WDR19	TGATGAGGCCTGAATACCGC	AATGGACATGGAGTCGTGGC
XPOT	GACCTGGCAGATGCACAAAC	GCAAGGAGGGCAGGTATTCT
ZC3H6	ATGAGTCCCTGCAAAACCCAG	TGGGCAAATTCACCATGCCA
ZEB1	GCACAACCAAGTGCAGAAGA	CATTTGCAGATTGAGGCTGA

Supplementary Table 12. Human ChIP primers

Promoter	Forward sequence	Reverse sequence
AMD1	ACAGCTGGAACAATCCGCAG	CGTGAGACTAGCGAACAACCA
APOBEC3D	TTTGCAATTGCCTTGGGTCC	GCCCTGGGACGCTTTATCTT
CD40	GAGTTGTTTTTGCCCCGACC	CTGCCCCCACAAAAATCAGC
DCK	CAGCCTGGCTCTCTAAGTGG	CATCTGGGGAGAAGGCACTG
FAM198B	CCCTGTCCCCTTTCTGTCTTC	TGTCCTAGCACAAAGGCAGG
GAPDH	TACTAGCGGTTTTACGGGCG	TCGAACAGGAGGAGCAGAGAGCG
KCTD18	AGTGACCTTGGACAATCGCA	CACACGGTAGAGAAGGCCAG
MPC1	GAGAGGGTGCGCTTGTCAG	CACTGTCACCGGCTCTCTAC
MUT	CGCGCCCAAACATTCGTAAA	AGGGTTAGATGCCCGTTTCC
PYROXD2	GCATGGAGTTGGAGCAGAGT	CAGAGTGGAGCTCGAAAGGG
RAB40B	AACTGGACCGACCCCGA	GAACTCGCTCCCACGGTC
SCPEP1	TGGTCTGAGTGCTTCCGTTC	CGGGGAAACCTCATTGACCA
SNAPC1	AGACCTAAAACCGCTCGTGA	TTGCTTTCACCCAGAGTGCT
SNAPC5	AGGTATTGACCAGCAGCCTC	CTGGCTTTGTCATGCCTGTG
STX8	TACAGAGAGGTCTTGCAGCG	CTGCGGACAGTACACTGGAG
TXNIP	AAGGAGTGCTTGTGGAGATCG	TACGCCGCTGGTTACACTAAG
WDR19	CTCCTCCCTTCTACCCCAGA	GGAGGCAGGATGGGCTAAAT
XPOT	CTGCTGTACTCGGGACACTT	GGATTCACGAATCAGGATGACG
ZC3H6	AAACTGCATGGCAAGCTATTTTCC	AAGGCGGCTGTAGAGTCCTTA

Supplementary References

1. Busam, K. J. *et al*. Expression of melan-A (MART1) in benign melanocytic nevi and primary cutaneous malignant melanoma. *Am. J. Surg. Pathol*. **22,** 976–982 (1998).

2. Gown, A. M., Vogel, A. M., Hoak, D., Gough, F. & McNutt, M. A. Monoclonal antibodies specific for melanocytic tumors distinguish subpopulations of melanocytes. *Am J Pathol* **123,** 195–203 (1986).

3. Kobayashi, T. & Hearing, V. J. Direct interaction of tyrosinase with Tyrp1 to form heterodimeric complexes in vivo. *J Cell Sci* **120,** 4261–4268 (2007).

Cheng et al. Genome Biology (2015) 16:42
DOI 10.1186/s13059-015-0594-4

Genome Biology

RESEARCH Open Access

Methylation-dependent *SOX9* expression mediates invasion in human melanoma cells and is a negative prognostic factor in advanced melanoma

Phil F Cheng[1], Olga Shakhova[3], Daniel S Widmer[1], Ossia M Eichhoff[1], Daniel Zingg[3], Sandra C Frommel[4], Benedetta Belloni[1], Marieke IG Raaijmakers[1], Simone M Goldinger[1], Raffaella Santoro[4], Silvio Hemmi[2], Lukas Sommer[3], Reinhard Dummer[1] and Mitchell P Levesque[1*]

Abstract

Background: Melanoma is the most fatal skin cancer displaying a high degree of molecular heterogeneity. Phenotype switching is a mechanism that contributes to melanoma heterogeneity by altering transcription profiles for the transition between states of proliferation/differentiation and invasion/stemness. As phenotype switching is reversible, epigenetic mechanisms, like DNA methylation, could contribute to the changes in gene expression.

Results: Integrative analysis of methylation and gene expression datasets of five proliferative and five invasion melanoma cell cultures reveal two distinct clusters. *SOX9* is methylated and lowly expressed in the highly proliferative group. *SOX9* overexpression results in decreased proliferation but increased invasion *in vitro*. In a B16 mouse model, sox9 overexpression increases the number of lung metastases. Transcriptional analysis of *SOX9*-overexpressing melanoma cells reveals enrichment in epithelial to mesenchymal transition (EMT) pathways. Survival analysis of The Cancer Genome Atlas melanoma dataset shows that metastatic patients with high expression levels of *SOX9* have significantly worse survival rates. Additional survival analysis on the targets of *SOX9* reveals that most SOX9 downregulated genes have survival benefit for metastatic patients.

Conclusions: Our genome-wide DNA methylation and gene expression study of 10 early passage melanoma cell cultures reveals two phenotypically distinct groups. One of the genes regulated by DNA methylation between the two groups is *SOX9*. *SOX9* induces melanoma cell invasion and metastasis and decreases patient survival. A number of genes downregulated by *SOX9* have a negative impact on patient survival. In conclusion, *SOX9* is an important gene involved in melanoma invasion and negatively impacts melanoma patient survival.

Background

Melanoma is an aggressive skin cancer that originates from melanocytes, that is, pigment cells that reside in the basal layer of the epidermis and are derived from the neural crest during early development [1]. It is the most life-threatening neoplasm of the skin and is considered a major health problem due to rising incidence and mortality rates [2,3]. Melanoma is a tumor with a high degree of heterogeneity and this phenotypic heterogeneity is reversible [4-7]. In addition to being a challenge for basic research, melanoma plasticity is a major hurdle for successful treatment [8]. Investigating the molecular basis of phenotypic heterogeneity is crucial to better understand melanoma progression and should provide useful insights for the development of more effective therapies.

In an effort to elucidate the molecular mechanisms of melanoma progression, significant differences have been detected between melanoma cells from the same lesion [4,6,9]. We and others have found that melanoma cells generally express two distinct gene expression signatures, that these signatures correlate with *in vitro* characteristics and these phenotypes are reversible depending on their cellular microenvironments [10-12]. One signature is characterized by the upregulation of several melanocytic genes like *MITF*, *TYR*, and *DCT*. These melanoma cells

* Correspondence: mitchellpaul.levesque@usz.ch
[1]Department of Dermatology, Faculty of Medicine, University Hospital Zürich, and University of Zürich, Wagistrasse 14, CH-8952 Zürich, Switzerland
Full list of author information is available at the end of the article

are highly proliferative and weakly invasive *in vitro* and so are named the proliferative phenotype. The other signature is characterized by the upregulation of many mesenchymal genes such as *WNT5A*, *TGF*β, and *FGF2*. In contrast to the proliferative cells, these cells are highly invasive but have a low proliferative capacity *in vitro* and are thus named the invasive phenotype. Meta-analysis of all available melanoma microarray datasets available on the NCBI GEO database confirmed these two gene signatures in 86% of the 536 melanomas [13]. Immunohistochemical analyses of MITF and WNT5A, markers of the proliferative and invasive phenotype, respectively, of human primary and metastatic melanomas displayed an anti-correlative staining pattern confirming that these phenotypes exist *in vivo* [14]. Together these findings culminated in the phenotype switching model for melanoma progression, in which melanoma cells respond to changing micro-environmental signals, such as hypoxia, by reprogramming their gene expression patterns to switch between states of proliferation and invasion [9,15]. Thus, phenotype switching has important implications in melanoma progression. Invasive phenotype cells characterized by low MITF expression, have stem-like properties [16], including the ability to initiate tumors with high efficiency [17]. Consequently, tumors comprise a mix of MITF positive and negative melanoma cells [18].

DNA methylation provides a stable and heritable gene regulatory mechanism for which melanoma cells could alter the expression of many genes [19]. Aberrant DNA methylation is a mechanism known to cause tumorigenesis [20]. Tumor suppressor genes become silenced by hypermethylation of their promoter region, thus promoting tumorigenesis. Global hypomethylation has been observed in many cancers, including melanoma, to decrease with progression of the disease [21-23]. DNMT3a and DNMT3b, the *de novo* DNA methyltransferases, were shown to have increased expression in metastatic melanomas compared to primary melanomas [24]. Another group showed that DNMT3a is required for melanoma development and metastasis in a melanoma mouse model [25]. Several signaling pathways have been shown to be deregulated as a result of aberrant DNMT-dependent methylation in melanoma, which include MAPK, WNT, PI3K, pRB, and pathways in cell cycle, apoptosis, invasion, and metastasis [26]. Progressive global DNA hypomethylation has been observed in malignant melanocyte transformation, and surprisingly transformation was blocked in the presence of 5-Aza-2-deoxycytidine (decitabine, Aza), a DNMT inhibitor [22]. It would suggest that targeted hypomethylation is required for malignant transformation and not overall global hypomethylation caused by Aza treatment. This is supported by our observation that treating proliferative melanoma cells with Aza had no measureable effect on their invasive abilities (data not shown). 5-Aza-2-deoxycytidine treatment of various melanoma cell lines was shown to increase SOX9 expression and induce expression of p27 and p21 [27]. SOX9 is a transcription factor involved in neural crest specification [28] and SOX9 overexpression in melanoma cell lines have been shown to induce cell cycle arrest in a p21 dependent manner [29]. Taken together, it would suggest that DNA methylation has a crucial role in malignant transformation and progression by altering the landscape of the methylome to promote tumor progression, and SOX9 is one of the targets of DNA methylation that induces cell cycle arrest.

In this study, we examine the expression of the DNMTs between the proliferative and invasive melanoma cell cultures and describe the differential melanoma methylome by MeDIP-chip. We confirm that SOX9 expression is regulated by DNA methylation and has a role in cell cycle regulation, invasion *in vitro* and *in vivo* and could be a prognostic marker for overall survival in metastatic melanoma patients.

Results

Proliferative melanoma cells have higher levels of global DNA-methylation

We have previously established melanocytic markers like MLANA to distinguish between the proliferative and invasive phenotype on a cohort of primary melanoma cell cultures (Additional file 1: Figure S1) [11,30]. To investigate if methylation differences exist between the proliferative and invasive melanoma phenotypes, we compared five proliferative (M000921, M010817, M080423, M980513, and M050829) and five invasive (M990115, M010119, M080201, M080307, and M080310) melanoma cell cultures for expression of *de novo* DNA methyltransferases DNMT1, 3a, and 3b (Figure 1A). We observed that the invasive phenotype melanoma cell cultures had about 51.1% less expression of DNMT1 as compared to the proliferative phenotype melanoma cell cultures (Figure 1A). DNMT3b had about 50% less protein expression in the proliferative melanoma cell cultures compared to the invasive melanoma cell cultures (Figure 1A). However, DNMT3a was not differentially expressed between the proliferative and invasive phenotype (Figure 1A). Global methylation analysis by methyl-cytosine ELISA showed that the invasive phenotype cells have significantly less DNA methylation in their genome compared to the proliferative phenotype cells, 13.0% to 20.9%, respectively (Figure 1B). This raises the possibility that differential methylation exists between the proliferative and invasive phenotype.

A 73-gene signature is significantly differentially methylated and expressed in proliferative melanoma cells

The difference in global methylation levels and protein expression of DNMT1 and DNMT3b prompted us to

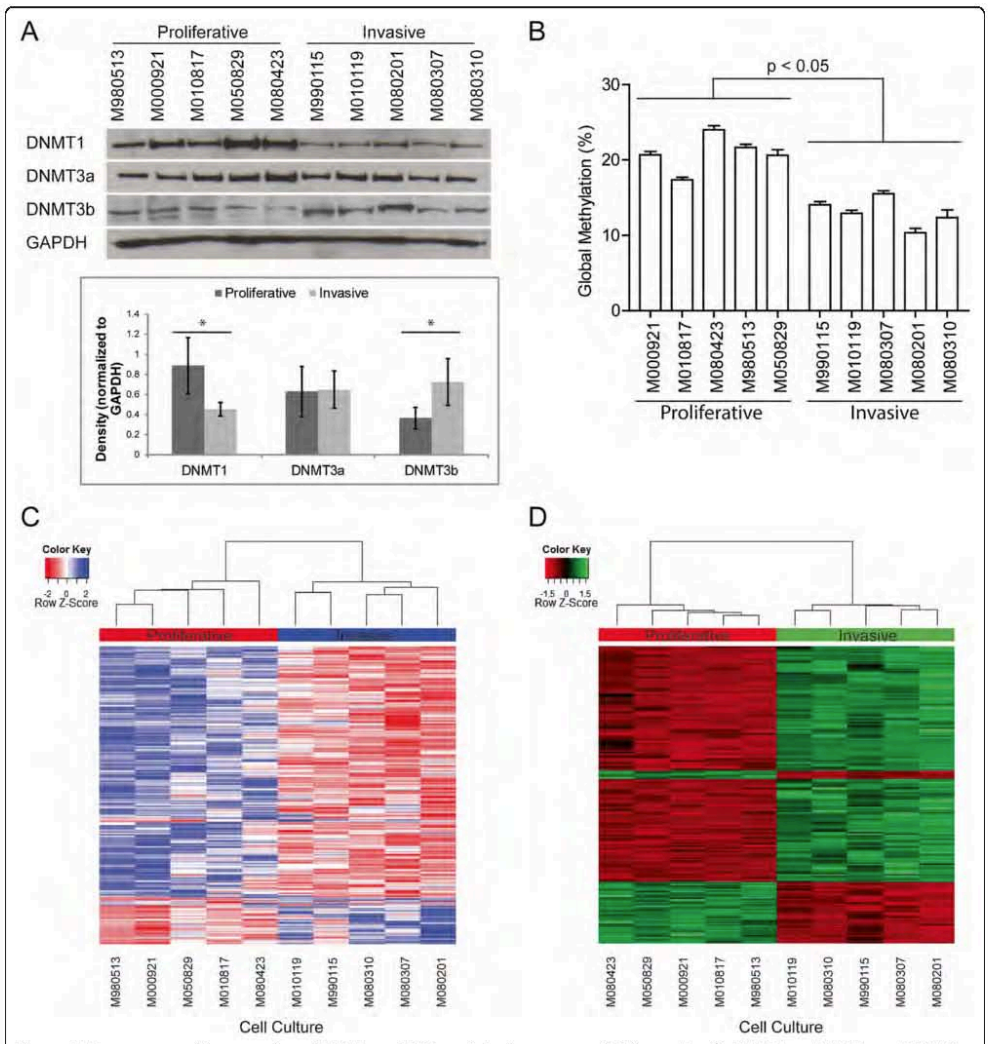

Figure 1 Phenotype specific expression of DNMTs and DNA methylation patterns. (A) Western blot for DNMT1 and DNMT3a and DNMT3b on five proliferative phenotype and five invasive phenotype cell lysates. GAPDH was used as a loading control. Optical density of each band was measured and normalized to GAPDH intensity. **(B)** Global methylation analysis by ELISA for methyl-cytosine on five proliferative cell cultures and five invasive cell cultures. There was a significant difference ($P < 0.05$, Student's t-test) in global methylation between the proliferative and invasive phenotype melanoma cells. **(C)** Heat map representing the 406 gene promoters differentially methylated between the proliferative and invasive phenotype cultures. **(D)** Heat map representing the top 250 genes differentially expressed between the proliferative and invasive phenotype.

investigate the methylation profiles of the proliferative and invasive phenotype melanoma cells. To determine which CpG islands were differentially methylated between the proliferative and invasive phenotypes, we immunoprecipitated methylated DNA from five proliferative and five invasive melanoma cell cultures by MeDIP [31] followed by hybridization to Nimblegen Human DNA Methylation 3x720K CpG Island Plus RefSeq Promoter Arrays. This array contains 720,000 probes for 22,532 promoter regions and 27,728 CpG islands. We calculated the differential

methylation levels between the five proliferative and five invasive melanoma cells with a sliding window ANOVA test with the R package DMR supplied from Nimblegen. We found 406 gene promoters to be significantly and differentially methylated between the proliferative and invasive phenotypes (Figure 1C). A total of 320 promoter regions were hypermethylated in the proliferative phenotype and 86 promoter regions were hypermethylated in the invasive phenotype. The greater number of hypermethylated regions in the proliferative phenotype would be consistent with the global methylation data.

Gene expression data for the 10 melanoma cell cultures previously generated by us [13] were reanalyzed for differential gene expression between the proliferative and invasive phenotypes using the R package limma [32]. A total of 1,750 genes were differentially expressed between the proliferative and invasive phenotype (fold change >2, FDR corrected P <0.05) (Figure 1D). We then analyzed the relationship between the promoter methylation status and mRNA expression levels for all genes in both datasets. Genes were filtered for a peak score >2 for methylation, fold change >2 for gene expression and an FDR-corrected P value <0.05. A total of 73 genes showed both significant differential DNA methylation and significant differential expression between the proliferative and invasive phenotype (Additional file 2: Table S1). Sixty-two genes from the proliferative phenotype had hypermethylated promoters and low RNA expression and 11 genes in the invasive phenotype had hypermethylated promoters and low RNA expression as compared to the proliferative phenotype. This suggests that methylation has a role in regulating a portion of the genes differentially expressed between the proliferative and invasive phenotype. We hypothesized that the 73 genes with both differential DNA methylation and mRNA expression between the proliferative and invasive melanoma cells were likely to be true targets of epigenetic regulation in melanoma. To determine which groups of genes were functionally important, we performed pathway analysis of the 73 genes on MetaCore. We looked for enrichment of pathways under GO processes, process networks, and Pathway maps (Additional file 3: Table S2). Interestingly, we observed significant enrichment in pathways involved in EMT, melanoma, and cell differentiation. We decided to focus on *SOX9* for validation due to its known function in melanocyte differentiation and melanoma progression [29,33,34].

Sox9 expression is silenced in proliferative melanoma cells through promoter DNA methylation

From the methylation array, the area that had the most enrichment for methylation was about 2 kb upstream of the *SOX9* transcriptional start site thus we validated the CpG island located there via sequencing of bisulfite-treated genomic DNA in the 10 melanoma cell cultures (Figure 2A). There are three predicted transcription factor binding sites in that upstream promoter region of *SOX9* for *MEF2*, *E2F*, and *HNF3B*. We analyzed the DNA methylation status of a cluster of 17 CpGs across a 283-bp region and 15 CpGs across a 256-bp region of a CpG island, located approximately −2,500 bp to −2,000 bp upstream of the *SOX9* transcriptional start site. The majority of CpGs in both regions of the *SOX9* promoter were consistently methylated in the proliferative phenotype melanoma cell cultures and consistently unmethylated in the invasive phenotype melanoma cell cultures.

To confirm that promoter DNA hypermethylation correlated with transcriptional silencing of SOX9, we assessed mRNA levels using real-time RT-PCR in the 10 melanoma cell cultures. *SOX9* mRNA was expressed robustly in the invasive phenotype melanoma cell cultures compared to the proliferative phenotype melanoma cell cultures (P <0.05) (Figure 2B). Protein expression of *SOX9* was detected in all invasive phenotype melanoma cell lysates, but little to no expression of *SOX9* was seen in the proliferative phenotype melanoma cell lysates (Figure 2C). To validate that *SOX9* is indeed regulated by DNA methylation, we treated the five proliferative phenotype melanoma cell cultures with 5 μM 5-Aza-2′-deoxycytidine (a DNMT inhibitor) for 72 h. Re-expression of *SOX9* was detected by western blot (Figure 2D). Thus, *SOX9* expression is regulated by DNA methylation between the proliferative and invasive phenotype.

SOX9 mediates proliferation and invasion in melanoma cell cultures

SOX9 is expressed in the invasive phenotype and we have previously described the greater invasive potential of invasive versus proliferative phenotype melanoma cells [30,35]. We hypothesized that some of the differentially expressed genes could have a role in generating this invasive capacity, thus we wanted to see if *SOX9* would have a role in invasion. SOX9 was knocked down with siRNA, and then the invasive ability of two invasive phenotype melanoma cell cultures was measured: M080201 and M080310. Treatment with two independent siRNAs for *SOX9* achieved about 70% knockdown of *SOX9* mRNA in M080201 and M080310 (Figure 3A). The invasive capacity of M080201 and M080310 decreased significantly (P <0.05) from 30% to 11.5% and from 64.8% to 36.6%, respectively, after 48 h treatment with siRNA targeting *SOX9* (Figure 3B and C). Proliferation was unaltered from *SOX9* knockdown (data not shown).

Consistent with this observation, we overexpressed *SOX9* in proliferative phenotype melanoma cell cultures (that is, M010817 and M980513) by lentiviral transfection (Figure 3D). Overexpression of *SOX9* was previously shown to drive melanoma cells into cell cycle arrest [29].

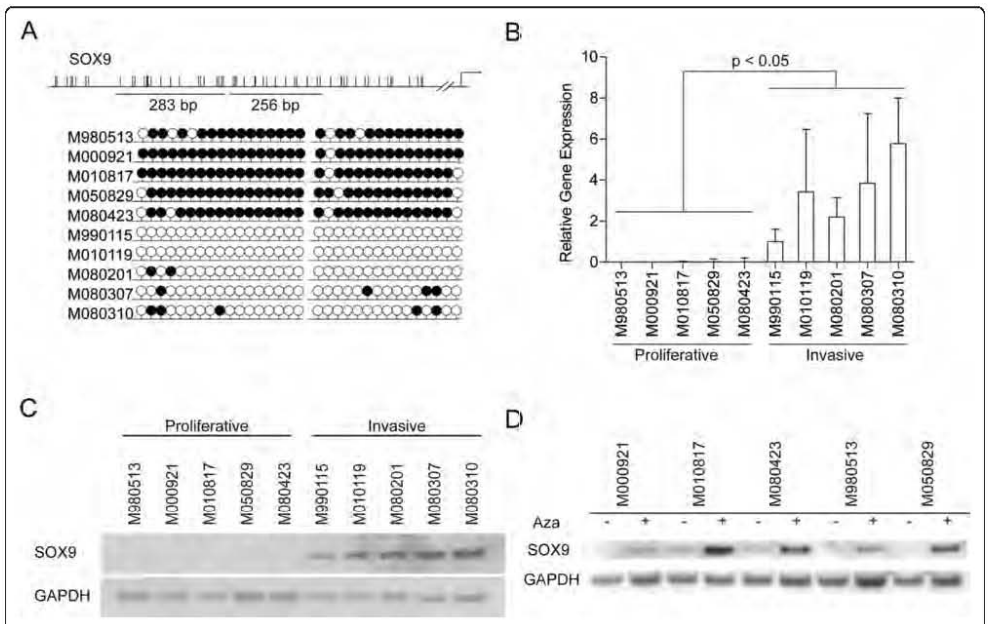

Figure 2 Validation of SOX9 methylation. (A) Lollipop diagrams of bisulphite sequencing of SOX9 promoter. Black lollipops are methylated CpGs; white lollipops are unmethylated CpGs. A minimum of five clones were sequenced for each cell culture. **(B)** mRNA expression of SOX9 normalized to the housekeeping gene RPL28 across 10 melanoma cell cultures. Results are presented as mean +/− s.d., n 3. Statistical significance of differential expression between the proliferative and invasive phenotype cell cultures was determined by Student's t-test. **(C)** Western blot for SOX9 in 10 melanoma cell cultures. GAPDH served as loading control. **(D)** Western blot for SOX9 of five proliferative melanoma cell cultures treated with 5-aza-2-deoxycytidine (Aza).

We measured proliferation and cell cycle progression by EdU and PI staining, respectively, and observed the cells transfected with vector have 50.5% in G1 phase, 37% in S phase, and 12.5% in G2/M phase, whereas the cells overexpressing SOX9 have 64.8% in G1 phase, 17.7% in S phase, and 17.5% in G2/M phase (P <0.05) (Figure 3E and F). The invasive capacity of M010817 and M980513 were significantly increased from 0.95% to 9.0% (P <0.05) and from 0.67% to 4.8% (P <0.05) from *SOX9* overexpression (Figure 3G and H). In concordance with previously published data on *SOX9* in melanoma, we also see G1/G0 arrest when SOX9 is overexpressed along with increased invasion.

SOX9 induces a partial invasive phenotype in proliferative melanoma cells

To determine the effect of *SOX9* overexpression on the proliferative phenotype, we performed microarray analysis of M010817 cells overexpressing *SOX9*. We detected 643 genes downregulated at least two-fold and 450 genes upregulated at least two-fold (P <0.05 (Figure 4A, Additional file 4: Table S3). We overlapped the gene signature from the SOX9 overexpression microarray with the gene signature from the 10 melanoma cell culture microarray to ask if *SOX9* induced genes are enriched in the invasive phenotype. There were 98 genes that were upregulated and 55 genes that were downregulated in both the *SOX9* overexpression and invasive phenotype gene sets. Hypergeometric distribution of the overlap of the *SOX9* microarray with 10 melanoma cell culture array was significant (P <0.001) (Figure 4B). Thus, *SOX9* apparently regulates about 10% of the genes that define the invasive phenotype gene set. This suggests that *SOX9* activation contributes to the invasive phenotype but other factors are also required for the full transition.

In vivo function of SOX9 overexpression

To examine the effects of SOX9 *in vivo*, we utilized the B16F1 mouse melanoma cells which do not express sox9 and are known not to metastasis in a tail vein injection assay. We transfected murine sox9 transiently into the B16F1 cells and monitored its expression over 288 h. Expression of sox9 decreases over time but protein is still detectable at 288 h (Figure 5A). To assess the *in vivo*

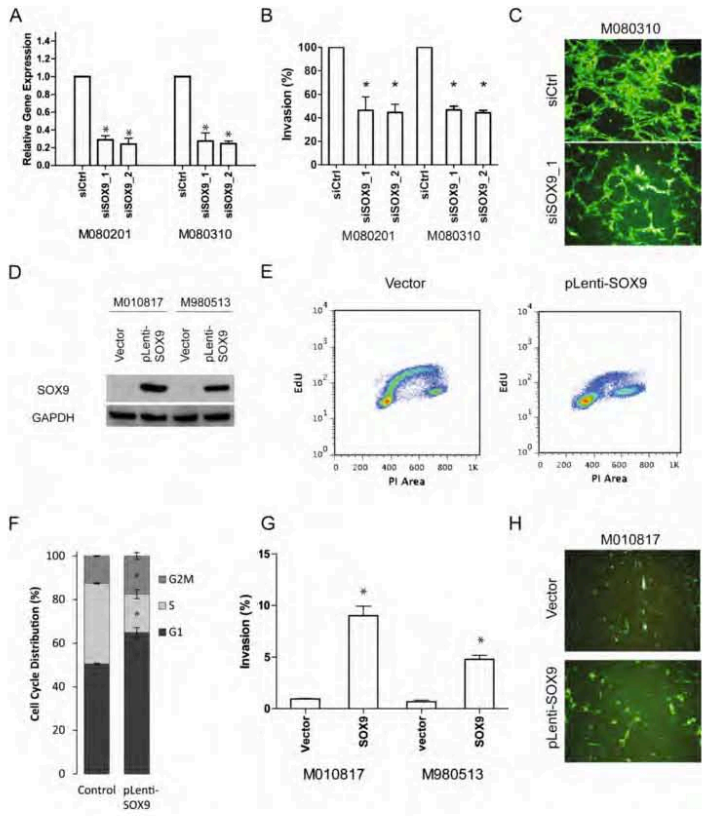

Figure 3 SOX9 mediates invasion and cell cycle arrest. (A) SOX9 knockdown by siRNA in two melanoma cell cultures M080201 and M080310. **(B)** Boyden chamber assay for siSOX9 knockdown in M080201 and M080310. **(C)** Representative picture of the Boyden chamber assay for knockdown of SOX9 in M080310. Top panel shows M080310 cells treated with control siRNA (siCtrl). Bottom panel shows M080310 cells treated with siSOX9_1. **(D)** SOX9 overexpression by lentiviral expression in proliferative phenotype melanoma cell cultures M010817 and M980513. **(E)** Proliferation assay by EdU pulse in cell cultures transfected with empty vector and pLenti-SOX9. **(F)** Cell cycle analysis by PI staining for cell cultures transfected with empty vector and pLenti-SOX9 (top and bottom left panels). Quantitation of cell cycle analysis (* $P < 0.05$, right panel). **(G)** Boyden chamber assay for SOX9 overexpressing melanoma cell cultures M010817 and M980513 (* $P < 0.05$). **(H)** Representative picture of the Boyden chamber assay for SOX9 overexpression in M010817. Top panel shows M010817 transfected with empty vector. Bottom panel shows M010817 transfected with SOX9.

metastatic potential of sox9, C57BL/6 J mice were intravenously injected with B16F1 cells transfected with sox9 and empty vector (Figure 5B). Twelve days after injection, the mice were sacrificed and the lungs were analyzed for tumor nodules. B16F1 cells expressing sox9 had significantly more metastases compared to control, $P < 0.05$.

Validation with TCGA melanoma dataset

The Cancer Genome Atlas (TCGA) has a melanoma dataset available for public access which contains over 300 tissue samples with RNAseq, DNA methylation, and clinical data. To validate our claim that *SOX9* is regulated by DNA methylation, we performed a correlation analysis of *SOX9* expression to *SOX9* promoter methylation using the data from the TCGA database. Three consecutive probes cg10471574, cg21049501, and cg06234051 in the *SOX9* promoter region have an anti-correlative association with the expression of *SOX9*, r = –0.58, –0.61, and –0.71 respectively (Figure 6A). Since high DNA methylation of *SOX9* is correlated with low *SOX9* expression it provides strong evidence that DNA methylation regulates *SOX9* expression *in vivo*.

The melanoma dataset contains 68 primary samples and 268 metastatic samples. The 268 metastatic samples

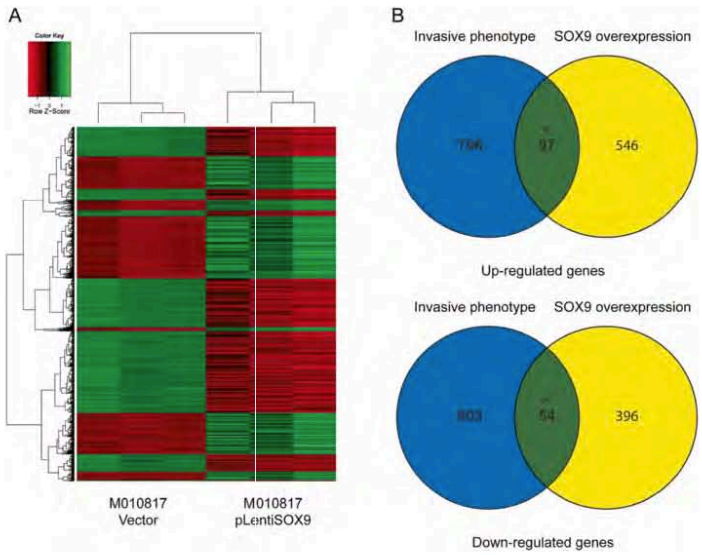

Figure 4 Microarray analysis of SOX9 overexpression. (A) Heat map of M010817 cells overexpressing SOX9. **(B)** Overlap of upregulated genes and downregulated genes between the SOX9 microarray and 10 melanoma cell culture microarray.

are comprised with 172 lymph node tumors, 59 regional cutaneous or subcutaneous metastases, and 37 distant metastases. Due to the diversity of this dataset we analyzed the primary and metastatic samples individually. We segregated the population into thirds by *SOX9* expression. We compared the upper and lower thirds for our analysis labelling them *SOX9* high and *SOX9* low. In both primary and metastatic datasets, the *SOX9* high group had at least three times more expression than the *SOX9* low group. We interrogated clinically relevant factors such as TNM staging, age, gender, and tumor type between the *SOX9* high and *SOX9* low group in the primary and metastatic datasets (Table 1, Additional file 5: Table S4). All parameters were statistically insignificant as tested by the Chi-squared test and t-test for age in the primary melanoma dataset. Only two clinical parameters were significant in the metastatic dataset. T1 was significant 2 vs. 11 ($P = 0.013$) in the *SOX9* low versus *SOX9* high, respectively. N0 was also significant 26 vs. 44 ($P = 0.031$) in the *SOX9* low versus *SOX9* high, respectively.

We next tested if the genes differentially expressed between the *SOX9* high and *SOX9* low patients in the primary and metastatic datasets were the same in our *SOX9* overexpression microarray. A total of 21 genes were differentially expressed between the *SOX9* high and *SOX9* low groups in the primary dataset with a minimum fold change of 2 and FDR corrected P value <0.05 (Additional file 6: Table S5). No genes from this set overlapped with the SOX9 microarray. A total of 427 genes were differentially expressed between the *SOX9* high and *SOX9* low groups in the metastatic dataset with a minimum fold change of 2 and FDR corrected P value <0.05 (Figure 6B, Additional file 7: Table S6). A total of 31 genes overlapped with the SOX9 microarray. Although the overlap was small, hypergeometric distribution of this overlap was significant (P <0.05). To examine the pathways in which, *SOX9* might play a role *in vivo*, we performed pathway analysis on the 427 genes. We saw significant enrichment of many EMT pathway processes such as 'Regulation of epithelial-to-mesenchymal transition (EMT)', 'TGF-beta dependent induction of EMT via SMADs', and 'Melanocyte development and pigmentation' (Figure 7A).

We interrogated if *SOX9* has a role in overall patient survival in all patients regardless of primary or metastatic disease. There was a significant difference in 10-year survival rates between the *SOX9* high and *SOX9* low groups. *SOX9* high patients had a median survival rate of 3.9 years whereas the *SOX9* low patients had a median survival time of 5.8 years (P <0.05) (Figure 7B). Cox multivariate analysis was carried out to identify if age, gender, TNM stage, and tumor type were significant contributing factors for 10-year survival of *SOX9* high and *SOX9* low patients. *SOX9* expression (hazard ratio 2.343; 95% confidence interval (CI) 1.402-3.915; $P = 0.001$; SOX9

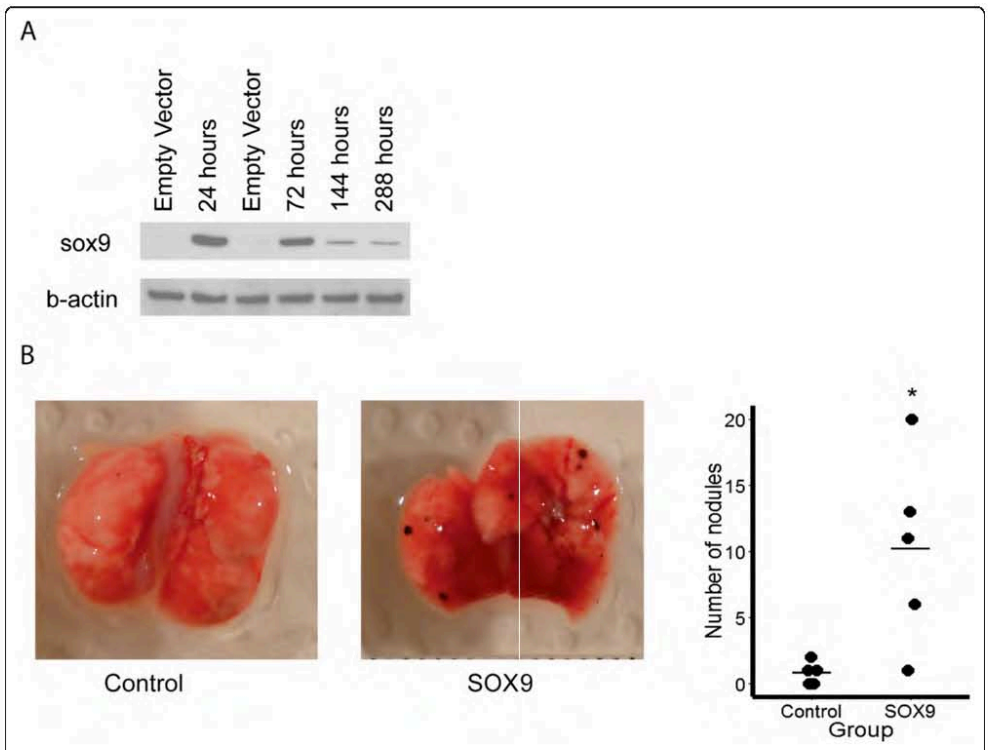

Figure 5 ***In vivo*** **function of sox9 overexpression. (A)** Western blot analysis of transient sox9 overexpression in B16F1 up to 12 days. **(B)** Representative pictures of B16F1 cells intravenously injected into C57BL/6 J mice 12 days after injection (n 5 mice per group). Quantification (right graph). * $P < 0.05$ Mann–Whitney U test.

high vs. SOX9 low) and T4 stage (hazard ratio 2.145; 95% CI 1.01-4.557; $P = 0.047$; T4 vs. T0) were significant (Table 2). We also segregated the patients into primary, lymph node, metastasis and regional/distant metastasis and reassessed survival based on SOX9 expression. We saw that SOX9 expression in primary tumors had no effect on patient survival. However, the cohort of patients with high SOX9 expression in lymph nodes had significantly lower survival ($P = 0.03$), as in the regional/distant metastasis cohort ($P = 0.01$) (Figure 7C).

We tested all 31 overlapping genes for survival benefit in the metastatic dataset (Additional file 8: Table S7). Twelve of the genes of this set were upregulated and 19 were downregulated when SOX9 expression was high. Most of the genes, 92% (11/12), that were upregulated when SOX9 expression is high had no influence on patient survival, only one gene 7% (1/12) was associated with improved survival (Figure 7D). This suggests that the genes upregulated by SOX9 are not direct factors for patient survival. Interestingly, 58% (11/19) of the genes downregulated when SOX9 expression is high were associated with improved survival and the other 42% (8/19) had no influence on patient survival (Figure 7D). This suggests that SOX9 represses a group of genes important for patient survival. Taken together, high SOX9 expression leads to poor survival possibly due to the downregulation of several genes that influence patient survival.

SOX9 binds to the promoter regions of its target genes

Using the SOX9 binding motif to screen for potential binding sites on the promoter regions from the 31 overlapping targets of the SOX9 microarray and the TCGA melanoma dataset, we found 19 of the 31 genes had a potential SOX9 binding site within a 3 kb region upstream from the TSS. To determine whether SOX9 directly binds to the promoter regions of these genes, we performed ChIP analysis using SOX9 antibodies on

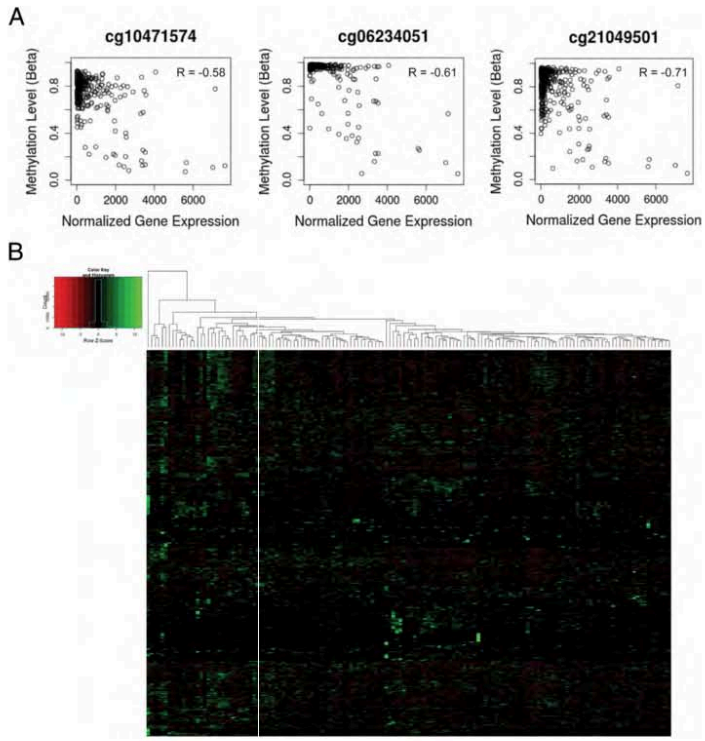

Figure 6 Validation of SOX9 methylation in TCGA and correlation with clinical features. (A) Correlation plots of RNAseq reads to b-values of methylation for SOX9. Three methylation probes of SOX9 are shown here to have significant anti-correlation of gene expression and DNA methylation. **(B)** Heatmap of the 427 genes differentially expressed between the SOX9 high and SOX9 low metastatic melanoma samples.

M010817-SOX9 cells and measured SOX9 occupancy at promoter regions of TMEM158, TBX3, and FYB, for which we could design specific primers for qPCR (Figure 7E). The specificity of this assay was demonstrated by the enrichment of three known SOX9 target sequences, COL2A1 intron 1 [36], p21 [29], and SOX10 [37]), as compared to a non-target gene (IP10). We observed a specific association of SOX9 with TMEM158, TBX3, and FYB, suggesting that TMEM158, TBX3, and FYB are direct targets of SOX9 in melanoma.

Discussion

Phenotypic, genetic, and epigenetic heterogeneity is a common feature in human melanomas [4,5,14,38]. Tumor subpopulations can be transient and have been seen to switch between phenotypic states *in vivo* [4,6,9,12,39]. We have previously described two subpopulations in melanoma, the proliferative phenotype and the invasive phenotype, which are defined by specific gene signatures, *in vitro* characteristics, and response to drug treatment [11,13,30,35,40]. Briefly, proliferative phenotype melanoma cells are distinguished by a high proliferative capacity and low invasive capacity and the invasive phenotype melanoma cells are distinguished by a low proliferative capacity and high invasive capacity. In this study, we found specific DNA methylation signatures for the proliferative and invasive melanoma phenotypes. We observed the invasive phenotype melanoma cell cultures had modest decrease of 5% in global methylation compared to the proliferative phenotype melanoma cell cultures. This may be due to decreased DNMT1 protein expression in the invasive phenotype melanoma cells. Global methylation levels have been observed to decrease as a cancerous lesion progresses from a benign tumor to metastasis [22,41], and we observed our invasive phenotype melanoma cell cultures had decreased DNA methylation levels and were more invasive than the proliferative phenotype melanoma cell cultures, suggesting the invasive cell

Table 1 Clinical parameters of metastatic melanoma patients

Clinical parameter	SOX9 low	SOX9 high	p value	
T0	15	13	0.706	
T1	2	11	0.013	*
T2	17	17	1	
T3	20	13	0.223	
T4	16	16	1	
N0	26	44	0.031	*
N1	16	9	0.162	
N2	15	9	0.221	
N3	12	9	0.513	
NX	1	0	1	
M0	67	64	0.793	
M1	2	6	0.157	
Female	29	25	0.586	
Male	45	49	0.68	
Lymph node	48	49	0.919	
Regional cutaneous or subcutaneous metastasis	17	14	0.59	
Distant metastasis	9	11	0.655	
Age	57	59.9	0.213[a]	

TNM stage, gender, and tumor location between the SOX9 high and SOX9 low patients were evaluated by the Chi-squared test.
[a]Age was evaluated by Student's t-test.
*$P < 0.05$.

cultures have progressed further in malignancy. Differential expression of the *de novo* DNA methyltransferase DNMT3b was also seen between the proliferative and invasive phenotype. These data are consistent with a model in which DNMT1 and DNMT3b have phenotype specificity and contribute to transcriptional heterogeneity by altering the methylation landscape of a melanoma cell in the context of melanoma phenotype switching. Pathway analysis of the 73 gene signature from the DNA methylation and gene expression array lead to the discovery of many transcription networks involved in development. These transcription factors were found to be hypomethylated and highly expressed in the invasive phenotype, which would suggest the invasive melanoma cell cultures may revert to a dedifferentiated state.

A number of other studies that have looked at genome-wide DNA methylation in melanoma have indicated that several tumor suppressors are silenced by DNA methylation compared to normal melanocytes [42-44] and compared to benign nevi [45]. Also, a recent study investigating 5-hydroxymethylation (5-hmC) in melanoma found a global decrease of 5-hmC was necessary for melanoma formation [46]. The results from these studies indicate aberrant DNA methylation is an important process in melanoma development and progression. In our work, we looked at the differences in DNA methylation landscape between 10 primary melanoma cell cultures and uncovered two distinct populations, as previously demonstrated by gene expression microarray analysis from our group [13]. Surprisingly, the targets we found to be differentially methylated between the two phenotypes do not overlap with the targets found to be differentially methylated between normal melanocytes and melanoma, and benign nevi and melanoma. We did not detect any differential methylation in validated methylation gene sets such as *COL1A2*, *NPM2*, *HSPB6*, *DDIT4L*, and *MTIG* from Koga *et al.* [43] or *UCHL1*, *COL1A2*, *THBS1*, and *TNFRSF10D* from Bonazzi *et al.* [42]. As those studies were comparing the methylation state of normal melanocytes to melanoma and in this study we compare within melanoma phenotypes, this might indicate that a different set of pathways are activated or silenced by DNA methylation in melanoma progression compared to melanoma initiation. In either case, it is clear that epigenetic modifications such as DNA methylation play an important role in melanoma initiation as well as progression, and embryonic developmental program reactivation may be one of the critical outcomes of this modulatory activity.

In our study, a subset of our melanoma cell cultures had lower SOX9 expression due to a hypermethylated promoter and the other subset with high SOX9 expression had a hypomethylated promoter. We confirmed that SOX9 is regulated by DNA methylation by treating low SOX9 expressing cells with 5-aza-2-deoxycytidine treatment and saw re-expression of SOX9. To determine if the regulation of SOX9 by DNA methylation is a common mechanism in melanoma or just seen within our melanoma cell cultures, we interrogated the melanoma TCGA dataset for SOX9 and found that SOX9 gene expression and DNA methylation are anti-correlated at three consecutive methylation probes in 293 samples. This provides strong evidence that specific DNA methylation is the molecular mechanism that regulates SOX9 expression in melanoma. Alcazar *et al.* demonstrated that after decitabine treatment of A375 and B16 melanoma cells, the promoter of SOX9 becomes hypomethylated and SOX9 is re-expressed with induction of p27 and p21 for cell cycle arrest [27]. Passeron *et al.* also observed that SOX9 was downregulated in some melanoma cell lines and induction of SOX9 expression in these melanoma cell lines resulted in lower proliferation due to upregulation of p21 [29]. We also overexpressed SOX9 in low SOX9 melanoma cell cultures and observed G1/S cell arrest, which is consistent with the study from Passeron *et al.* Although the proliferation rate is reduced, the invasive capacity of these SOX9 overexpressing cells is increased, which phenocopies the endogenous SOX9 expressing

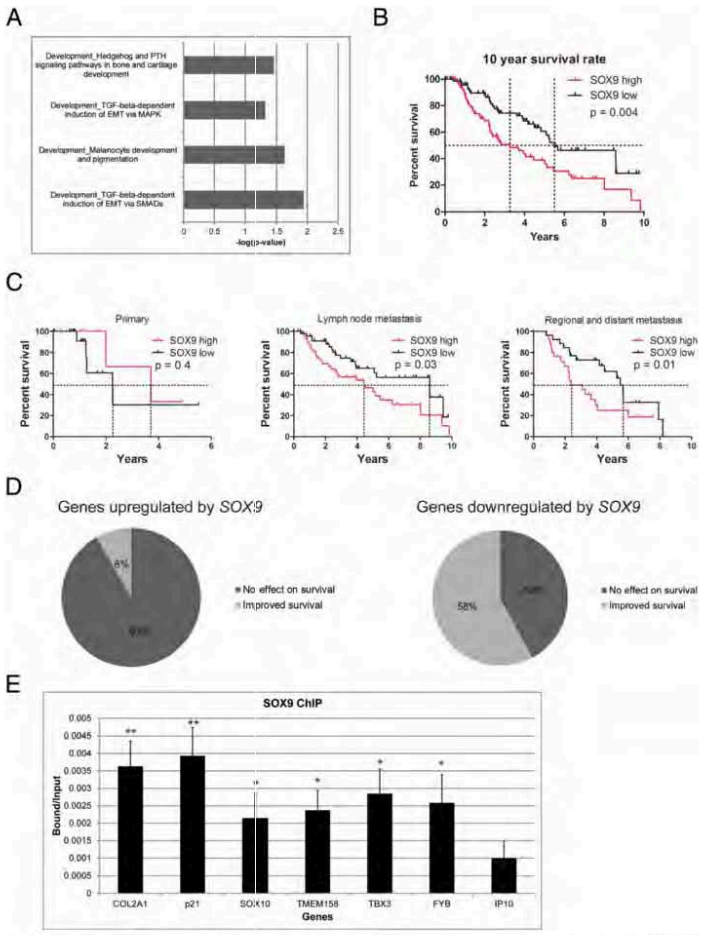

Figure 7 TCGA analysis of SOX9. (A) Pathway analysis from MetaCore for SOX9 reveals many pathways involved in EMT. **(B)** Median survival time for patients with high SOX9 expression is 3.9 years (n 74). Median survival time for patients with low SOX9 expression is 5.8 years (n 74). The difference in survival is significant (P <0.05). **(C)** Survival analysis for high and low SOX9 expression segregated into primary, lymph node, and metastatic cohorts. **(D)** Pie charts displaying the number of SOX9 target genes that have a contribution to patient survival. **(E)** ChIP analysis for SOX9 binding targets. Enrichment of the promoter regions for TMEM158, TBX3, and FYB were similar to positive controls COL2A1, p21, and SOX10 and greater than negative control IP10. Data are shown as bound vs. input. Error bars indicate standard error of the mean of three independent experiments. IgG controls not shown on graph because they were below detection limit.

cells. Conversely, knockdown of SOX9 in the invasive phenotype melanoma cells reduced the invasive capacity of the cells. Microarray analysis of SOX9 overexpression revealed an EMT-like transcriptional signature and had 10% overlap with invasive phenotype gene signature which supports the notion that SOX9 is a factor that contributes to the invasive phenotype. *In vivo*, sox9 expression in B16F1 cells increases their metastatic potential causing more tumor lung nodules in the tail vein injection assay. Taken together, SOX9 is a gene that is regulated by DNA methylation and functionally, SOX9 mediates cell cycle progression, invasion, and metastasis in melanoma.

TCGA is a great resource for clinical and next-generation sequencing data on human tumors. We

Table 2 Multivariate cox regression on metastatic melanoma patients

Covariate	HR	Lower 95%	Upper 95%	p-value
SOX9 (SOX9 low = 0, SOX9 high =1)	2.343	1.402	3.915	0.001***
Age	0.995	0.977	1.103	0.59
Gender (female = 0, male =1)	0.756	0.457	1.25	0.276
T0 (used as reference)				
T1	0.431	0.117	1.598	0.208
T2	0.943	0.416	2.138	0.888
T3	1.022	0.489	2.132	0.955
T4	2.145	1.01	4.557	0.047*
N0 (used as reference)				
N1	1.673	0.813	3.446	0.162
N2	1.365	0.673	2.771	0.388
N3	1.322	0.574	3.044	0.512
M0 (used as reference)				
M1	2.023	0.672	6.09	0.21
Lymph Node (used as reference)				
Regional Cutaneous or Subcutaneous Metastasis	0.844	0.452	1.577	0.595
Distant Metastasis	1.83	0.957	3.499	0.068

SOX9 expression, age, gender, TNM stage, and tumor location were evaluated in a multivariate cox regression model. Hazard ratio (HR) and the 95% CIs are displayed for each covariate.
*P <0.05.
***P <0.001.

took advantage of the melanoma dataset and demonstrated that *SOX9* expression levels have a significant impact on survival of metastatic melanoma patients but *SOX9* did not have a significant impact on survival in patients with primary melanomas. This could suggest that *SOX9* is required for progression of primary melanoma into metastasis and metastatic tumors with high SOX9 are more aggressive to the patient. There were no clinical metrics that could distinguish SOX9 high or low in primary melanoma. Only T1 and N0 stage in metastatic melanomas were significant between SOX9 high and low. Survival analysis of metastatic patients with high SOX9 expression versus low SOX9 expression revealed a significant difference in the overall 10-year survival rates. Patients with high-SOX9 expressing tumors had a 2.3 times increased risk of death compared to patients with low SOX9 expressing tumors. Based on these findings and the invasive properties of high SOX9 expressing melanomas, it would suggest that SOX9 expression in melanomas could push the tumor toward more aggressive metastasis. Thus, SOX9 could potentially be a prognostic marker for metastatic melanoma.

We performed differential gene expression analysis on the RNAseq dataset where we defined the SOX9 high group as having a minimum of three-fold greater expression than the SOX9 low group. We only saw an overlap of 31 genes between both datasets; however, the overlap was significant as determined by hypergeometric distribution. The contribution of heterogeneity in the melanoma TCGA patient population would be one of the largest factors for the difference in gene signatures between our SOX9 microarray and TCGA RNAseq data. Nonetheless, the significant overlap of genes narrow down the potential targets of SOX9. To confirm that the targets of SOX9 have prognostic value for the patients, we performed survival analysis on all 31 genes. Surprisingly, 58% (11/19) of the genes downregulated by SOX9 were associated with improved survival, which strongly suggests SOX9 represses a set of genes that decrease tumor malignancy. Genes that were upregulated by SOX9 expression had little impact on patient survival which implies that SOX9 expression alone is sufficient to drive disease progression. From this list of 31 genes, 19 of them had a potential SOX9 binding site in its promoter. We could validate TMEM158, TBX3, and FYB as direct targets of SOX9 binding by chromatin immunoprecipitation. FYB is downregulated when SOX9 levels are high suggesting a repressive effect of SOX9 on this gene. FYB is required for inflammatory cytokine production [47] but no known link has been established with melanoma. TMEM158 is upregulated by SOX9 but no clear role has been established for the gene in melanoma. TBX3 is also upregulated by SOX9 and TBX3 is known to cause increased invasiveness in melanoma [48,49], suggesting TBX3 could be an effector gene that drives the invasive phenotype we see in SOX9 high cells and in patients.

Conclusion

In conclusion, we found SOX9 to be regulated by DNA methylation, and high SOX9 expression leads to poor survival in melanoma patients due to the activation of EMT-like genes and the downregulation of potential tumor suppressor genes in melanoma cells. This was confirmed *in vivo*, and new direct targets of SOX9 that may mediate its function in tumor progression were identified by transcriptional profiling and chromatin-immunoprecipitation. Future therapies targeting SOX9 could be beneficial for patients to prevent progression and especially when combined with therapies targeting cells of the proliferative phenotype. Further investigation would be required to determine if SOX9 would have early prognostic value for tumor malignancy.

Materials and methods

Cell culture

Melanoma cell cultures were established from surplus material from primary cutaneous melanoma and melanoma metastases removed by surgery [50]. Written informed consent was approved by the local IRB (EK647 and EK800). Clinical diagnosis was confirmed by histology and immunohistochemistry. Melanoma cells were released from tissue biopsies and grown as previously described [51]. Melanoma cell cultures were maintained in RPMI (Invitrogen, Carlsbad, CA, USA) supplemented with 5 mM glutamine, 1 mM sodium pyruvate, and 10% heat-inactivated fetal calf serum, and cultured at 37°C and 5% CO_2. As RNA was extract previously from these cell cultures for gene expression array analysis, all cell cultures used for experiments in this paper were within five passages of the RNA isolation time point.

5-methylcytosine relative content analyses

Global DNA methylation level was evaluated by MethylFlash Methylated DNA Quantification Kit (Epigentek, Farmingdale, NY, USA) as per manufacturer's instructions.

MeDIP assay and analysis

The MeDIP assay was performed as described [31]. A monoclonal antibody to 5-Methylcytidine (BI-MECY-100, Eurogentec, Belgium) was used for immunoprecipitation. The immunoprecipated DNA and sonicated input DNA were differentially labeled with fluorescent dyes (Cy3 and Cy5, respectively) and hybridized to Human DNA Methylation 3x720K CpG Island Plus RefSeq Promoter Arrays (Roche Nimblegen, Madison, WI, USA). Acquisition and analysis was performed using Nimblescan 2.5 and R package DMR provided by Nimblegen. All data have been deposited into NCBI GEO GSE57971.

Gene expression analysis

Gene expression datasets were obtained from NCBI GEO GSE33728 [13], and analysis was performed by R using the limma package. *P* values were adjusted by FDR multiple hypothesis test correction.

Bisulphite sequencing

Genomic DNA was extracted from primary melanoma cell cultures and subjected to bisulfite (BS) modification (EZ DNA Methylation Gold Kit, Zymo Research, Irvine, CA, USA). To validate the DNA methylation status of individual DNA molecules, we cloned bisulfite-converted PCR fragments into the pCR2.1 vector using the TOPO-TA cloning kit (Invitrogen, Carlsbad, CA, USA). Individual colonies were screened for the insert, and the region of interest was sequenced using M13 primers. A minimum of five clones were sequenced for each region of interest. Lollipop diagrams were generated using BiQ Analyzer [52]. Primers used for bisulphite PCR are shown in Table 3.

Treatment with decitabine

Decitabine (5-Aza-2′-deoxycytidine, Sigma Chemical (Aza)) was dissolved in DMSO as a 10 mM stock solution, aliquoted, and kept at −20°C. Primary melanoma cell cultures were seeded in Petri dishes (approximately 5,000 cells/cm^2) in RPMI untreated or treated with Aza (5 μM) for 72 h, with fresh drug-supplemented medium every 24 h.

mRNA expression analysis

Total RNA was isolated using Trizol according to manufacturer's instructions (Invitrogen). In total, 1 μg aliquots of RNA were reverse transcribed with Reverse Transcription System (Promega) according to the manufacturer's instructions. Data collection and analysis were performed by ABI Viia7 Fast Real-Time PCR Systems (Applied Biosystems). Gene expression values of averaged triplicate reactions were normalized to *RPL28* expression levels. RPL28 primers are as follows: 5′-GCAATTGG TTCCGCTACAAC-3′ and 5′-TGTTCTTGCGGATCAT GTGT-3′. The primers for RT-PCR were purchased from QIAGEN: SOX9 (Hs_SOX9_1_SG).

Western blot

Cells were washed twice with cold phosphate-buffered saline (PBS) and lysed at 4°C in lysis buffer containing 20 mM Tris–HCl (pH 7.5), 1% Triton X-100 (Sigma-Aldrich, St Louis, MO, USA), 137 mM NaCl, 10% glycerol, and protease and phosphatase inhibitors (Roche, Basel, Switzerland). Proteins were separated by SDS-PAGE using the NuPAGE SDS-PAGE Gel System (Invitrogen) under reducing conditions. A total of 15 μg of protein was mixed with 9 μL of NuPage LDS sample buffer (4×) (Invitrogen, NP0007), 3.6 μL of NUPAGE Sample Reducing (Invitrogen, NP0009) and filled up to 36 μL with RIPA buffer. This mixture was incubated at 85°C for 10 min while shaking at 900 rpm. Samples were loaded on NuPage precast gels (Invitrogen). Membranes were probed with the following antibodies: SOX9 (GTX109661, GeneTex, Hsinchu City, Taiwan); DNMT1 (ab13537, Abcam, Cambridge, UK); DNMT3a (ab2850, Abcam, Cambridge, UK); DNMT3b (ab16049,

Table 3 Primers for bisulphite sequencing

Gene	Primer	Tm
SOX9_1	F: 5′-GGATTGGGGTTTTTTATTTTT-3′	59°C
	R: 5′-TTCAATTTTCTTCCCTTTCCT-3′	
SOX9_2	F: 5′-AGGTTATTAGGGTAGATTGGAGG-3′	59°C
	R: 5′5AAATACATATCCCATCACAACC-3′	

Abcam, Cambridge, UK); GAPDH (ab9483, Abcam, Cambridge, UK);

siRNA knockdown

Silencing RNA (siRNA) transfection of melanoma cells was carried out using INTERFERin transfection solution according to the manufacturer's protocol (Polyplus-transfection, Illkirch, France). Cells were transfected with 5 nM of siRNA (Qiagen) for 72 h before RNA or protein was extracted. As control siRNA, the All-Star negative siRNA sequence (Qiagen) was used, and gene-specific siRNAs targeting siSOX9 (SI00007595, SI00007609) were obtained from Qiagen.

SOX9 lentiviral transfection

Lentiviral particles containing plasmids expressing full-length SOX9 cDNA or eGFP were transfected into melanoma cells for 48 h. Media supplemented with 4 ng/mL blasticidin was used for selection. After 1 week of selection, protein lysate was extracted and analyzed for SOX9 expression. Plasmids for eGFP and SOX9 were a kind gift from Dr. Thierry Passeron [29].

SOX9 transient transfection

Empty vector or vector containing murine sox9 (a kind gift from Prof. Lukas Sommer) was transfected into B16F1 cells with jetPEI (Polyplus, France) according to manufacturer's protocol. Protein was isolated at 24 h, 72 h, 144 h, and 288 h after transfection and analyzed for sox9 expression by western blot.

Microarray and pathway analysis

Gene expression of eGFP and SOX9 transfected cells were analyzed using the Affymetrix Human Genome U133 Plus 2.0 Array at the Functional Genomics Center Zurich (FGCZ). Differential gene expression was determined by R package limma [53]. Pathway analysis was performed using MetaCore (GeneGo Inc., New York, USA).

Proliferation and cell cycle analysis

For cell cycle analysis, the Click-iT EdU Alexa Fluor 647 Flow Cytometry Assay Kit (Invitrogen) was used. Cells were labelled with PI according to the manufacturer's protocol and the DNA content was measured using a BD FACSCanto II flow cytometer (BD Biosciences) and BD FACSDiva software (BD Biosciences). Cell cycle analysis was performed in triplicate.

Boyden chamber invasion assay

Cells were seeded on FluoroBlok 24-multiwell Insert System (351157, BD Biosciences) and Biocoat Tumor Invasion System (354165, BD Biosciences). The invasion assay was performed as per manufacturer's instructions. Migrated and invaded cells were labeled with Calcein AM fluorescent dye (354216, BD Biosciences) and fluorescence was measured with Tecan GENios (Tecan, Männendorf, Switzerland) using 485 nm excitation and 535 nm emission. Relative invasion was calculated as the ratio of the fluorescence of invading cells of the Biocoat Tumor Invasion System divided by the fluorescence of migrating cells of the FluoroBlok 24-multiwell Insert System. Boyden chamber assays were performed in triplicate.

Viability assay

Cells were seeded in 24-well microplates at a density of 2×10^4 cells, and cell growth was determined with a standard colorimetric assay measuring 3-(4,5-dimethylthiazol-2-yl)-2,5 diphenyltetrazolium bromide (MTT) (Sigma-Aldrich, St Louis, MO, USA) reactivity after 72 h. MTT assays were performed in triplicate.

Chromatin immunoprecipitation

ChIP analysis was performed as previously described [54]. The Sox9 antibody was from Santa Cruz Biotechnology (sc-20095, Santa Cruz Biotechnology). Primer sequences were designed around SOX9 binding motifs [55,56] from the transcription start site (TSS) to 3 KB upstream of the TSS. Primers for p21, COL2A1, TMEM158, TBX3, FYB, SOX10, and IP10 are shown in Table 4.

In vivo metastasis

B16F1 cells were transfected with empty vector or vector containing murine sox9. 2×10^5 cells were injected intravenously into C57BL/6 J mice, five mice per group (Harlan Laboratories). After 12 days mice were sacrificed and lungs were examined for metastasis. Statistics were performed using the Mann–Whitney U test. All animal experiments have been approved by the veterinary authorities of Canton

Table 4 Primers for ChIP

Genes	Primer
COL2A1-F	ATCCTCCTTTGTGAGGCTTGTT
COL2A1-R	AGTACGAGAGAACCCACTGGAC
p21-F	TGATGTGCCACAGTTCACAA
p21-R	TCCTGCCAGTTTTCCTGTTC
TMEM158-F	TCTGCTGTGTTGGAGCCATT
TMEM158-R	GTCTCGCCTTAGTGCTACCG
TBX3-F	CTCGCCCCTTTCTTTCCCTT
TBX3-R	GGGGGTGTTATGAGCCAACA
FYB-F	CTCACATTGCATGGGGACG
FYB-R	ATGGGCTTATCACCGGAAGG
SOX10-F	CCTCTGCCTCGTGTGACTAC
SOX10-R	TCCTGTCTGGAGTGGGCTG-
IP10-F	GGGAAATTCCGTAACTTGGA
IP10-R	AAGCCATTTTCCCTCCCTAA

of Zurich, Switzerland, and were performed in accordance with Swiss law.

TCGA analysis

The SKCM DNA methylation, RNA-seq, and clinical dataset were downloaded on 28 July 2014 for analysis. Normalized reads from the level 3 RNA-seq data were used for analysis. The dataset was segregated into primary tumors and metastatic tumors for analysis. Chi-squared test was performed on the clinical parameters between the SOX9 high and low groups. Differential expression was analyzed with voom from the limma package [53]. Log rank test and Cox proportional hazard ratio were analyzed by the survival R package [57]. DNA methylation β-values were calculated by minfi [58]. Correlation was calculated by Spearman's rank correlation coefficient.

Additional files

Additional file 1: Figure S1. MLANA expression between the proliferative and invasive phenotype. Ten melanoma cell cultures were divided into the proliferative and invasive phenotype by expression of MLANA. GAPDH was used as loading control.

Additional file 2: Table S1. 73 genes with anti-correlative methylation and gene expression. Analysis of the methylation and expression profiles of the ten melanoma cell cultures produced this list of significant genes with a peak score greater than 2 from the MeDIP methylation array and with a fold change greater than 1 from the gene expression microarray.

Additional file 3: Table S2. Pathway analysis of 73 gene signature. Genes were uploaded to Metacore and analyzed for significant pathway enrichment in GO Processes, Process Networks and Pathway Maps.

Additional file 4: Table S3. Differential gene analysis of SOX9 overexpression. Limma output table for differentially expressed genes between SOX9 overexpression and control M010817 melanoma cells.

Additional file 5: Table S4. Clinical parameters of primary melanoma patients. TNM stage, gender, and tumor location between the SOX9 high and SOX9 low patients were evaluated by the Chi-squared test. Age was evaluated by Student's t-test. * represents $p < 0.05$.

Additional file 6: Table S5. Differential gene analysis of SOX9 high and low primary melanoma patients. Limma output table for SOX9 high primary melanoma patients versus SOX9 low primary melanoma patients.

Additional file 7: Table S6. Differential gene analysis of SOX9 high and low metastatic melanoma patients. Limma output table for SOX9 high metastatic melanoma patients versus SOX9 low metastatic melanoma patients.

Additional file 8: Table S7. Overlap of SOX9 overexpression and metastatic melanoma patients. List of genes overlapping from M010817 melanoma cells overexpressing SOX9 and SOX9 high metastatic melanoma patients.

Competing interests

The authors declare that they have no competing interests.

Authors' contributions

PFC, OS, DSW, DZ, SCF, BB, MIGR, OME, and SMG performed the experiments. PFC, OS, DSW, DZ, and SCF analyzed the data. PFC, RS, RD, and MPL contributed to the overall design of the study and directed research. PFC, SH, LS, RD, and MPL drafted the manuscript. All authors read and approved the final manuscript.

Acknowledgements

This work was financially supported by the Georg und Bertha Schwyzer-Winiker Stiftung (RD), the Forschungskredit FK-13-042 (PFC), the Swiss Cancer League and the Swiss National Science Foundation (LS, MPL), the Promedica Foundation (OS), and the Verein für Hautkrebsforschung (MPL). The University Research Priority Program (URPP) in translational cancer research at the University of Zürich provided cell lines used in this work. We thank the Cancer Biology PhD Program of the University/ETH Zürich for support and advice. We would also like to thank The Cancer Genome Atlas (TCGA) for providing important clinical and genomic data. Finally, all research on human materials was done according to Swiss law and following the Declaration of Helsinki on medical research. Consenting patients contributed surplus melanoma biopsy material according to IRB approval numbers (Ek.647/800), and cell lines were generated following IRB KEK-ZH-Nr.2014-0425.

Author details

[1]Department of Dermatology, Faculty of Medicine, University Hospital Zürich, and University of Zürich, Wagistrasse 14, CH-8952 Zürich, Switzerland. [2]Faculty of Mathematics and Natural Sciences, Institute of Molecular Life Sciences, University of Zürich, Zürich, Switzerland. [3]Cell and Developmental Biology, Institute of Anatomy, University of Zürich, Zürich, Switzerland. [4]Institute of Veterinary Biochemistry and Molecular Biology, University of Zürich, Zürich, Switzerland.

Received: 14 October 2014 Accepted: 23 January 2015
Published online: 22 February 2015

References

1. Dupin E, Le Douarin NM. Development of melanocyte precursors from the vertebrate neural crest. Oncogene. 2003;22:3016–23.
2. Garbe C, Leiter U. Melanoma epidemiology and trends. Clin Dermatol. 2009;27:3–9.
3. MacKie RM, Hauschild A, Eggermont AM. Epidemiology of invasive cutaneous melanoma. Ann Oncol. 2009;20:vi1–7.
4. Quintana E, Shackleton M, Foster HR, Fullen DR, Sabel MS, Johnson TM, et al. Phenotypic heterogeneity among tumorigenic melanoma cells from patients that is reversible and not hierarchically organized. Cancer Cell. 2010;18:510–23.
5. Perego M, Tortoreto M, Tragni G, Mariani L, Deho P, Carbone A, et al. Heterogeneous phenotype of human melanoma cells with in vitro and in vivo features of tumor-initiating cells. J Invest Dermatol. 2010;130:1877–86.
6. Roesch A, Fukunaga-Kalabis M, Schmidt EC, Zabierowski SE, Brafford PA, Vultur A, et al. A temporarily distinct subpopulation of slow-cycling melanoma cells is required for continuous tumor growth. Cell. 2010;141:583–94.
7. Landsberg J, Kohlmeyer J, Renn M, Bald T, Rogava M, Cron M, et al. Melanomas resist T-cell therapy through inflammation-induced reversible dedifferentiation. Nature. 2012;490:412–6.
8. Romano E, Schwartz GK, Chapman PB, Wolchock JD, Carvajal RD. Treatment implications of the emerging molecular classification system for melanoma. Lancet Oncol. 2011;12:913–22.
9. Hoek KS, Goding CR. Cancer stem cells versus phenotype-switching in melanoma. Pigment Cell Melanoma Res. 2010;23:746–59.
10. Freedman JA, Tyler DS, Nevins JR, Augustine CK. Use of gene expression and pathway signatures to characterize the complexity of human melanoma. Am J Pathol. 2011;178:2513–22.
11. Hoek KS, Schlegel NC, Brafford P, Sucker A, Ugurel S, Kumar R, et al. Metastatic potential of melanomas defined by specific gene expression profiles with no BRAF signature. Pigment Cell Res. 2006;19:290–302.
12. Hendrix MJ, Seftor EA, Seftor RE, Kasemeier-Kulesa J, Kulesa PM, Postovit LM. Reprogramming metastatic tumour cells with embryonic microenvironments. Nat Rev Cancer. 2007;7:246–55.
13. Widmer DS, Cheng PF, Eichhoff OM, Belloni BC, Zipser MC, Schlegel NC, et al. Systematic classification of melanoma cells by phenotype-specific gene expression mapping. Pigment Cell Melanoma Res. 2012;25:343–53.
14. Eichhoff OM, Zipser MC, Xu M, Weeraratna AT, Mihic D, Dummer R, et al. The immunohistochemistry of invasive and proliferative phenotype switching in melanoma: a case report. Melanoma Res. 2010;20:349–55.
15. Widmer DS, Hoek KS, Cheng PF, Eichhoff OM, Biedermann T, Raaijmakers MI, et al. Hypoxia contributes to melanoma heterogeneity by triggering HIF1alpha-dependent phenotype switching. J Invest Dermatol. 2013;133:2436–43.
16. Carreira S, Goodall J, Denat L, Rodriguez M, Nuciforo P, Hoek KS, et al. Mitf regulation of Dia1 controls melanoma proliferation and invasiveness. Genes Dev. 2006;20:3426–39.

17. Cheli Y, Giuliano S, Botton T, Rocchi S, Hofman V, Hofman P, et al. Mitf is the key molecular switch between mouse or human melanoma initiating cells and their differentiated progeny. Oncogene. 2011;30:2307–18.
18. Goodall J, Carreira S, Denat L, Kobi D, Davidson I, Nuciforo P, et al. Brn-2 represses microphthalmia-associated transcription factor expression and marks a distinct subpopulation of microphthalmia-associated transcription factor-negative melanoma cells. Cancer Res. 2008;68:7788–94.
19. Plass C. Cancer epigenomics. Hum Mol Genet. 2002;11:2479–88.
20. Baylin SB, Jones PA. A decade of exploring the cancer epigenome - biological and translational implications. Nat Rev Cancer. 2011;11:726–34.
21. Hansen KD, Timp W, Bravo HC, Sabunciyan S, Langmead B, McDonald OG, et al. Increased methylation variation in epigenetic domains across cancer types. Nat Genet. 2011;43:768–75.
22. Molognoni F, Cruz AT, Meliso FM, Morais AS, Souza CF, Xander P, et al. Epigenetic reprogramming as a key contributor to melanocyte malignant transformation. Epigenetics. 2011;6:450–64.
23. Sigalotti L, Coral S, Nardi G, Spessotto A, Cortini E, Cattarossi I, et al. Promoter methylation controls the expression of MAGE2, 3 and 4 genes in human cutaneous melanoma. J Immunother. 2002;25:16–26.
24. Nguyen T, Kuo C, Nicholl MB, Sim MS, Turner RR, Morton DL, et al. Downregulation of microRNA-29c is associated with hypermethylation of tumor-related genes and disease outcome in cutaneous melanoma. Epigenetics. 2011;6:388–94.
25. Deng T, Kuang Y, Wang L, Li J, Wang Z, Fei J. An essential role for DNA methyltransferase 3a in melanoma tumorigenesis. Biochem Biophys Res Commun. 2009;387:611–6.
26. Schinke C, Mo Y, Yu Y, Amiri K, Sosman J, Greally J, et al. Aberrant DNA methylation in malignant melanoma. Melanoma Res. 2010;20:253–65.
27. Alcazar O, Achberger S, Aldrich W, Hu Z, Negrotto S, Saunthararajah Y, et al. Epigenetic regulation by decitabine of melanoma differentiation in vitro and in vivo. Int J Cancer. 2012;131:18–29.
28. Cheung M, Briscoe J. Neural crest development is regulated by the transcription factor Sox9. Development. 2003;130:5681–93.
29. Passeron T, Valencia JC, Namiki T, Vieira WD, Passeron H, Miyamura Y, et al. Upregulation of SOX9 inhibits the growth of human and mouse melanomas and restores their sensitivity to retinoic acid. J Clin Invest. 2009;119:954–63.
30. Hoek KS, Eichhoff OM, Schlegel NC, Dobbeling U, Kobert N, Schaerer L, et al. In vivo switching of human melanoma cells between proliferative and invasive states. Cancer Res. 2008;68:650–6.
31. Weber M, Davies JJ, Wittig D, Oakeley EJ, Haase M, Lam WL, et al. Chromosome-wide and promoter-specific analyses identify sites of differential DNA methylation in normal and transformed human cells. Nat Genet. 2005;37:853–62.
32. Smyth GK. Linear models and empirical bayes methods for assessing differential expression in microarray experiments. Stat Appl Genet Mol Biol. 2004;3:Article3.
33. Passeron T, Valencia JC, Bertolotto C, Hoashi T, Le Pape E, Takahashi K, et al. SOX9 is a key player in ultraviolet B-induced melanocyte differentiation and pigmentation. Proc Natl Acad Sci U S A. 2007;104:13984–9.
34. Cook AL, Smith AG, Smit DJ, Leonard JH, Sturm RA. Co-expression of SOX9 and SOX10 during melanocytic differentiation in vitro. Exp Cell Res. 2005;308:222–35.
35. Eichhoff OM, Weeraratna A, Zipser MC, Denat L, Widmer DS, Xu M, et al. Differential LEF1 and TCF4 expression is involved in melanoma cell phenotype switching. Pigment Cell Melanoma Res. 2011;24:631–42.
36. Bell DM, Leung KK, Wheatley SC, Ng LJ, Zhou S, Ling KW, et al. SOX9 directly regulates the type-II collagen gene. Nat Genet. 1997;16:174–8.
37. Shakhova O, Cheng P, Mishra PJ, Zingg D, Schaefer SM, Debbache J, et al. Antagonistic cross-regulation between Sox9 and Sox10 controls an anti-tumorigenic program in Melanoma. PLoS Genet. 2015;11:e1004877.
38. Mihic-Probst D, Ikenberg K, Tinguely M, Schraml P, Behnke S, Seifert B, et al. Tumor cell plasticity and angiogenesis in human melanomas. PLoS One. 2012;7:e33571.
39. Hendrix MJ, Seftor EA, Hess AR, Seftor RE. Molecular plasticity of human melanoma cells. Oncogene. 2003;22:3070–5.
40. Zipser MC, Eichhoff OM, Widmer DS, Schlegel NC, Schoenewolf NL, Stuart D, et al. A proliferative melanoma cell phenotype is responsive to RAF/MEK inhibition independent of BRAF mutation status. Pigment Cell Melanoma Res. 2011;24:326–33.
41. Fraga MF, Herranz M, Espada J, Ballestar E, Paz MF, Ropero S, et al. A mouse skin multistage carcinogenesis model reflects the aberrant DNA methylation patterns of human tumors. Cancer Res. 2004;64:5527–34.
42. Bonazzi VF, Nancarrow DJ, Stark MS, Moser RJ, Boyle GM, Aoude LG, et al. Cross-platform array screening identifies COL1A2, THBS1, TNFRSF10D and UCHL1 as genes frequently silenced by methylation in melanoma. PLoS One. 2011;6:e26121.
43. Koga Y, Pelizzola M, Cheng E, Krauthammer M, Sznol M, Ariyan S, et al. Genome-wide screen of promoter methylation identifies novel markers in melanoma. Genome Res. 2009;19:1462–70.
44. Muthusamy V, Duraisamy S, Bradbury CM, Hobbs C, Curley DP, Nelson B, et al. Epigenetic silencing of novel tumor suppressors in malignant melanoma. Cancer Res. 2006;66:11187–93.
45. Conway K, Edmiston SN, Khondker ZS, Groben PA, Zhou X, Chu H, et al. DNA-methylation profiling distinguishes malignant melanomas from benign nevi. Pigment Cell Melanoma Res. 2011;24:352–60.
46. Lian CG, Xu Y, Ceol C, Wu F, Larson A, Dresser K, et al. Loss of 5-hydroxymethylcytosine is an epigenetic hallmark of melanoma. Cell. 2012;150:1135–46.
47. Rajasekaran K, Kumar P, Schuldt KM, Peterson EJ, Vanhaesebroeck B, Dixit V, et al. Signaling by Fyn-ADAP via the Carma1-Bcl-10-MAP3K7 signalosome exclusively regulates inflammatory cytokine production in NK cells. Nat Immunol. 2013;14:1127–36.
48. Peres J, Prince S. The T-box transcription factor, TBX3, is sufficient to promote melanoma formation and invasion. Mol Cancer. 2013;12:117.
49. Rodriguez M, Aladowicz E, Lanfrancone L, Goding CR. Tbx3 represses E-cadherin expression and enhances melanoma invasiveness. Cancer Res. 2008;68:7872–81.
50. Raaijmakers MIG, Widmer DS, Maudrich M, Koch T, Langer A, Flace A, et al. A new live cell biobank workflow efficiently recovers heterogeneous melanoma cells from native biopsies. Exp Dermatol. 2015.
51. Geertsen RC, Hofbauer GF, Yue FY, Manolio S, Burg G, Dummer R. Higher frequency of selective losses of HLA-A and -B allospecificities in metastasis than in primary melanoma lesions. J Invest Dermatol. 1998;111:497–502.
52. Bock C, Reither S, Mikeska T, Paulsen M, Walter J, Lengauer T. BiQ Analyzer: visualization and quality control for DNA methylation data from bisulfite sequencing. Bioinformatics. 2005;21:4067–8.
53. Smyth GK. Limma: linear models for microarray data. New York: Springer; 2005.
54. Santoro R. Analysis of chromatin composition of repetitive sequences: the ChIP-Chop assay. Methods Mol Biol. 2014;1094:319–28.
55. Kadaja M, Keyes BE, Lin M, Pasolli HA, Genander M, Polak L, et al. SOX9: a stem cell transcriptional regulator of secreted niche signaling factors. Genes Dev. 2014;28:328–41.
56. Mathelier A, Zhao X, Zhang AW, Parcy F, Worsley-Hunt R, Arenillas DJ, et al. JASPAR 2014: an extensively expanded and updated open-access database of transcription factor binding profiles. Nucleic Acids Res. 2014;42:D142–7.
57. Therneau TM: A Package for Survival Analysis in S. In R package version 237–4; 2013.
58. Aryee MJ, Jaffe AE, Corrada-Bravo H, Ladd-Acosta C, Feinberg AP, Hansen KD, et al. Minfi: a flexible and comprehensive Bioconductor package for the analysis of Infinium DNA methylation microarrays. Bioinformatics. 2014;30:1363–9.

Supplemental Figure 1

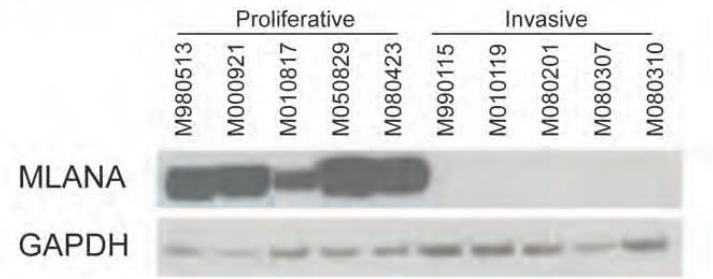

Bachmann et al. Molecular Cancer 2014, 13:125
http://www.molecular-cancer.com/content/13/1/125

MOLECULAR CANCER

RESEARCH Open Access

DTX3L and ARTD9 inhibit IRF1 expression and mediate in cooperation with ARTD8 survival and proliferation of metastatic prostate cancer cells

Samia B Bachmann[1], Sandra C Frommel[1,2], Rosalba Camicia[1,3], Hans C Winkler[1,4], Raffaella Santoro[1] and Paul O Hassa[1*]

Abstract

Background: Prostate cancer (PCa) is one of the leading causes of cancer-related mortality and morbidity in the aging male population and represents the most frequently diagnosed malignancy in men around the world. The Deltex (DTX)-3-like E3 ubiquitin ligase (DTX3L), also known as B-lymphoma and BAL-associated protein (BBAP), was originally identified as a binding partner of the diphtheria-toxin-like macrodomain containing ADP-ribosyltransferase-9 (ARTD9), also known as BAL1 and PARP9. We have previously demonstrated that ARTD9 acts as a novel oncogenic survival factor in high-risk, chemo-resistant, diffuse large B cell lymphoma (DLBCL). The mono-ADP-ribosyltransferase ARTD8, also known as PARP14 functions as a STAT6-specific co-regulator of IL4-mediated proliferation and survival in B cells.

Methods: Co-expression of DTX3L, ARTD8, ARTD9 and STAT1 was analyzed in the metastatic PCa (mPCa) cell lines PC3, DU145, LNCaP and in the normal prostate luminal epithelial cell lines HPE and RWPE1. Effects on cell proliferation, survival and cell migration were determined in PC3, DU145 and/or LNCaP cells depleted of DTX3L, ARTD8, ARTD9, STAT1 and/or IRF1 compared to their proficient control cells, respectively. In further experiments, real-time RT-PCR, Western blot, immunofluorescence and co-immunoprecipitations were conducted to evaluate the physical and functional interactions between DTX3L, ARTD8 and ARTD9.

Results: Here we could identify DTX3L, ARTD9 and ARTD8 as novel oncogenic survival factors in mPCa cells. Our studies revealed that DTX3L forms a complex with ARTD8 and mediates together with ARTD8 and ARTD9 proliferation, chemo-resistance and survival of mPCa cells. In addition, DTX3L, ARTD8 and ARTD9 form complexes with each other. Our study provides first evidence that the enzymatic activity of ARTD8 is required for survival of mPCa cells. DTX3L and ARTD9 act together as repressors of the tumor suppressor IRF1 in mPCa cells. Furthermore, the present study shows that DTX3L together with STAT1 and STAT3 is implicated in cell migration of mPCa cells.

Conclusions: Our data strongly indicate that a crosstalk between STAT1, DTX3L and ARTD-like mono-ADP-ribosyltransferases mediates proliferation and survival of mPCa cells. The present study further suggests that the combined targeted inhibition of STAT1, ARTD8, ARTD9 and/or DTX3L could increase the efficacy of chemotherapy or radiation treatment in prostate and other high-risk tumor types with an increased STAT1 signaling.

Keywords: Metastatic prostate cancer, Mono-ADP-ribosyltransferase, ARTD9/PARP9, ARTD8/PARP14, E3 ubiquitin ligase, DTX3L/BBAP, Proliferation, Survival, Migration, STAT1, STAT3

* Correspondence: hassa@vetbio.uzh.ch
[1]Institute of Veterinary Biochemistry and Molecular Biology, University of Zurich, Winterthurerstrasse 190, 8057 Zurich, Switzerland
Full list of author information is available at the end of the article

Introduction

Prostate cancer (PCa) is a clinically and molecularly heterogeneous disease that is characterized by its aggressive metastasization [1-3]. PCa is one of the leading causes of cancer-related mortality and morbidity in the aging male population and represents the most frequently diagnosed malignancy in men around the world [1,2]. Patients diagnosed with PCa and *de novo* metastatic tumors are generally treated with androgen deprivation therapy (ADT) since the growth of PCa is originally androgen-dependent [1,2]. However, ADT is primarily palliative, nearly all patients will eventually develop the androgen-independent and highly metastatic forms of PCa termed castration-resistant PCa (CRPC) [1,2]. Docetaxel-based chemotherapy remains the first-line treatment for men diagnosed with CRPC providing modest survival and palliative benefits [1,2,4]. Unfortunately, chemotherapy resistance develops in more than half of all CRPC patients and remains the major obstacle in treatment of CRPC [1,2,4]. Attempts to improve survival of cancer patients largely depend on strategies to target the tumor cell resistance. A common feature of PCa is the dependence on nuclear factor kappa B and the activated signal transducer and activators of transcription (STAT). Several studies have shown that STAT3 and STAT5 are required for cell growth, proliferation, survival, invasion and metastasis of many PCa subtypes [1,2,5-10]. In addition, STAT1 has been recently identified as a proto-oncogene product in a variety of cancers, including metastatic PCa (mPCa) [11-23]. A recent study has shown that 29% of clinical human mPCa's analyzed, constitutively expressed STAT1 and IFN-stimulated genes *in vivo* [12]. STAT1 has been initially suggested to act exclusively as a suppressor of tumorigenesis, by activating growth-inhibitory and pro-apoptotic signaling in tumor cells, mainly mediated by interferon response factor (IRF)-1 [24-27].

IFNγ/STAT1 signaling is mediated through activation of IFNγ receptor and Janus kinases (JAK) 1 and 2 that lead to tyrosine phosphorylation of STAT1 on Y701, homodimerization and translocation of STAT1 to the nucleus where it induces the transcription of IFNγ-stimulated genes, including the tumor suppressor IRF1 [28]. Phosphorylation on Y701 enhances the phosphorylation on S727 in the transactivation domain of STAT1α [29-31].

Several studies have demonstrated that chemotherapeutic agents, such as doxorubicin, docetaxel or anthracyclines enhance the expression of STAT1 and its activation in chemo-resistant cancer cells [11,12,14,32]. STAT1 has been shown to be required for the observed P-glycoprotein-independent chemo-resistance towards docetaxel [15]. Several mechanisms have been reported to mediate docetaxel resistance in metastatic CRPC, such as those mediated by the P-glycoprotein/ABC multidrug transporter family [33-35], the STAT1-AKT1-clusterin axis with its pro-survival functions [15,36] and via constitutive activation of the CXCR4, ERK1/2 and c-Myc signaling loop [37]. STAT1 has therefore been suggested as a potential target for chemo-sensitization of aggressive tumors that constitutively overexpress IFNγ/STAT1-dependent pathways [12].

We have previously demonstrated that the ADP-ribosyltransferase-9 (ARTD9), also known as B-aggressive lymphoma protein (BAL1) and PARP9, acts as a novel oncogenic survival factor in high-risk, chemo-resistant, host response (HR) sub-types of diffuse large B-Cell lymphoma (HR-DLBCL) and as a crucial negative and positive co-regulator of IFNγ/STAT1-signaling [23]. ARTD9 is an inactive mono-ADP-ribosyltransferase belonging to the intracellular Diphteria toxin-like glutamate/aspartate-specific mono- and polymerizing-ADP-ribosyltransferase (ARTD) family (also known as PARPs) [38] that also includes the active mono-ADP-ribosyltransferase ARTD8 (also known as PARP14) [38-41]. Like ARTD9, ARTD8 contains several evolutionary conserved macrodomains, which have been recently shown to act as binding modules for free and protein-linked mono- or poly-ADP-ribose [42-44]. ARTD9 counteracts the IFNγ-dependent anti-proliferative and pro-apoptotic IFNγ-STAT1-IRF1-p53 axis and induces an oncogenic switch in high-risk HR-DLBCL that transforms STAT1 from a tumor suppressor to a proto-oncogene [23]. As a consequence, ARTD9 mediates proliferation, survival and chemo-resistance in HR-DLBCL [23]. ARTD8 has been shown to mediate survival in c-Myc-driven Burkitt lymphoma-like tumors *in vivo* and in multiple myeloma *in vitro* [39,45,46]. ARTD8 functions as a STAT6-specific co-regulator of IL4-mediated gene expression and is suggested to be involved in mediating IL4-induced proliferation and protection of B cells against apoptosis following irradiation or growth factor withdrawal [39-41].

The Deltex (DTX)-3-like E3 ubiquitin ligase (DTX3L), also known as B-lymphoma and BAL-associated protein (BBAP), was originally identified as a binding partner of ARTD9 [47-49]. DTX3L is overexpressed in subtypes of high-risk chemotherapy-resistant aggressive HR-DLBCL with an active host inflammatory response and tightly associated with intrinsic IFNγ signaling and constitutive activity of STAT1 [23,47,48]. Recent studies have provided first evidence that DTX3L and ARTD9 are also overexpressed in a variety of solid cancers, such as Ewing tumor or cervical carcinomas [46,48-52]. The *DTX3L* and *ARTD9* genes are located in a head-to-head orientation on chromosome 3q21 and share the same bidirectional IFNγ-responsive promoter [48]. DTX3L monoubiquitinates histone H4 lysine 91 and has been suggested to protect cells exposed to DNA damaging agents [53]. Targeted inhibition of DTX3L has been therefore suggested to increase the efficacy of DNA-damaging chemotherapeutic agents or

radiation treatment [53]. However, the role of DTX3L in PCa, especially in the context of STAT1-signaling, has not been investigated.

In this study we identify DTX3L, ARTD8 and ARTD9 as novel oncogenic survival factors in androgen-independent CRPC-like mPCa cells. We demonstrate that DTX3L mediates together with ARTD8 and ARTD9 proliferation, chemo-resistance and survival in mPCa cells, indicating a functional and physical crosstalk between DTX3L and macrodomain-containing mono-ADP-ribosyltransferases in mPCa.

Results and discussion

DTX3L, ARTD8 and ARTD9 are constitutively overexpressed in mPCa associated with increased IFNγ/STAT1-signaling

The *DTX3L* gene and all three genes encoding macrodomain containing ARTD proteins (ARTD7-9) are located in the same evolutionary conserved gene cluster [48]. In order to investigate whether constitutive overexpression of DTX3L, ARTD8 and ARTD9 is associated with mPCa we analyzed their expression levels in the PCa cell lines PC3, DU145 and LNCaP [54-59], and in the normal prostate luminal epithelial cell lines HPE and RWPE1. PC3 and DU145 cells are androgen-refractory mPCa cell lines and are commonly used as CRPC models [60-62]. PC3 and DU145 cells have a high and moderate tumorigenic potential, respectively [58-62], and are highly invasive compared to the poorly tumorigenic LNCaP cells [62-65]. Contrary to the LNCaP cells, the PC3 and DU145 cells have been previously described to display enhanced basal levels of STAT1 activity and to express high levels of IL6 [15,66]. Both, PC3 and DU145 cells have been recently described to have an autocrine IL6 loop while LNCaP cells do not have any detectable IL6 secretion [66]. Our immunoblot analysis of DTX3L, ARTD8 and ARTD9, STAT1 and pSTAT1, revealed that DTX3L, ARTD8 and ARTD9 are constitutively overexpressed in the mPCa cell lines PC3 and DU145 but not in the JAK1-negative [67,68] LNCaP cells or in HPE and RWPE1 cells (Figure 1A).

We have previously demonstrated that overexpression of DTX3L and ARTD9 is tightly associated with intrinsic IFNγ-signaling and constitutively active STAT1 in HR-DLBCL [23]. We therefore examined whether constitutive overexpression of endogenous DTX3L, ARTD9 and ARTD8 is associated with STAT1 or alternatively with another STAT signaling pathway in mPCa cells. Our immunoblot analysis of DTX3L, ARTD8, ARTD9, STAT1, pSTAT1, STAT2, pSTAT2, STAT3α, STAT3αβ, pSTAT3α, STAT5, pSTAT5, STAT6 and pSTAT6 expression revealed that constitutive overexpression of DTX3L, ARTD8 and ARTD9 is indeed associated with enhanced STAT1 (pSTAT1-S727)-signaling and an autocrine IL6 loop [66] (Figure 1B-D and Additional file 1: Figure S1A-C). ARTD8 and ARTD9 were absent in LNCaP cells (Figure 1A, B and Additional file 1: Figure S1A, C). Subsequent experiments revealed that the expression of both DTX3L and ARTD9 but not of ARTD8 is dependent on JAK1 (Additional file 1: Figure S1D). A recent study has provided first evidence that expression of ARTD9 and DTX3L is induced by IL6 and strongly associated with an autocrine IL6-signaling loop in mPCa cells [66]. IL6 mainly activates STAT3, however under certain conditions, STAT1 can also be activated by IL6, [69-72]. Subsequent control experiments revealed that depletion of STAT3 in PC3 cells inhibits the expression of ARTD9 and DTX3L (Additional file 1: Figure S1E). Thus, constitutive overexpression of DTX3L and ARTD9 is likely mediated through an IL6/JAK1-STAT1:STAT3-signaling pathway in PC3 and DU145 cells in the absence of IFNγ, while further up-regulated through an IFNγ/JAK1-STAT1:STAT1-mediated signaling pathway. DTX3L was still expressed in LNCaP cells, though to a much lesser extend (Figure 1A, B Additional file 1: Figure S1A), suggesting that DTX3L can be regulated in a cell type-specific manner, independently of ARTD9, IFNγ/STAT1 and IL6/STAT3 signaling in mPCa cells.

Both, PC3 and DU145 cells showed high basal levels of transcriptionally active pSTAT1α(pS727) in the nucleus (Figure 1B, C, Additional file 1: Figure S1B and Additional file 2: Figure S2A), while PC3 cells showed enhanced basal levels of activated STAT1α/β(pY701) (Figure 1A-C and Additional file 1: Figure S1B, C). The JAK1-negative LNCaP cell line only shows low basal levels of transcriptionally active pSTAT1α(pS727) but did not show any enhanced basal levels of activated STAT1α/β(pY701) (Figure 1B and Additional file 2: Figure S2B). Phosphorylation on S727 in the transactivation domain of STAT1α can also occur independently of STAT1 tyrosine phosphorylation [73], indicating that heterodimerization with other (constitutively) tyrosine phosphorylated STATs such as STAT3 may be required for nuclear translocation of STAT1 in absence of phosphorylation on Y701 [69,74]. However, basal levels of constitutively active STAT1 in PC3 and DU145 cells are not comparable with those previously observed in the P-glycoprotein independent STAT1-AKT1-clusterin mediated docetaxel-resistant residual cell lines PC3-DR and DU145-DR [15,33,36,75-77]. The basal levels of active STAT1 (pSTAT1α-S727 and pSTAT1α/β-Y701) observed in PC3-DR or DU145-DR are highly similar to those previously observed in chemo-resistant HR-DLBCL cell lines such as SUDHL7 [23].

We have previously demonstrated that ARTD9 inhibits the transcriptional activation of tumor suppressor IRF1 in HR-DLBCL [23]. We therefore tested whether the expression of IRF1 is negatively correlated with the expression of DTX3L and ARTD9 in mPCa. Indeed, the tumor suppressor IRF1 is constitutively up-regulated in absence of DTX3L and ARTD9 in LNCaP cells, while down-regulated in presence of DTX3L and ARTD9 in PC3 and

Bachmann et al. Molecular Cancer 2014, 13:125
http://www.molecular-cancer.com/content/13/1/125

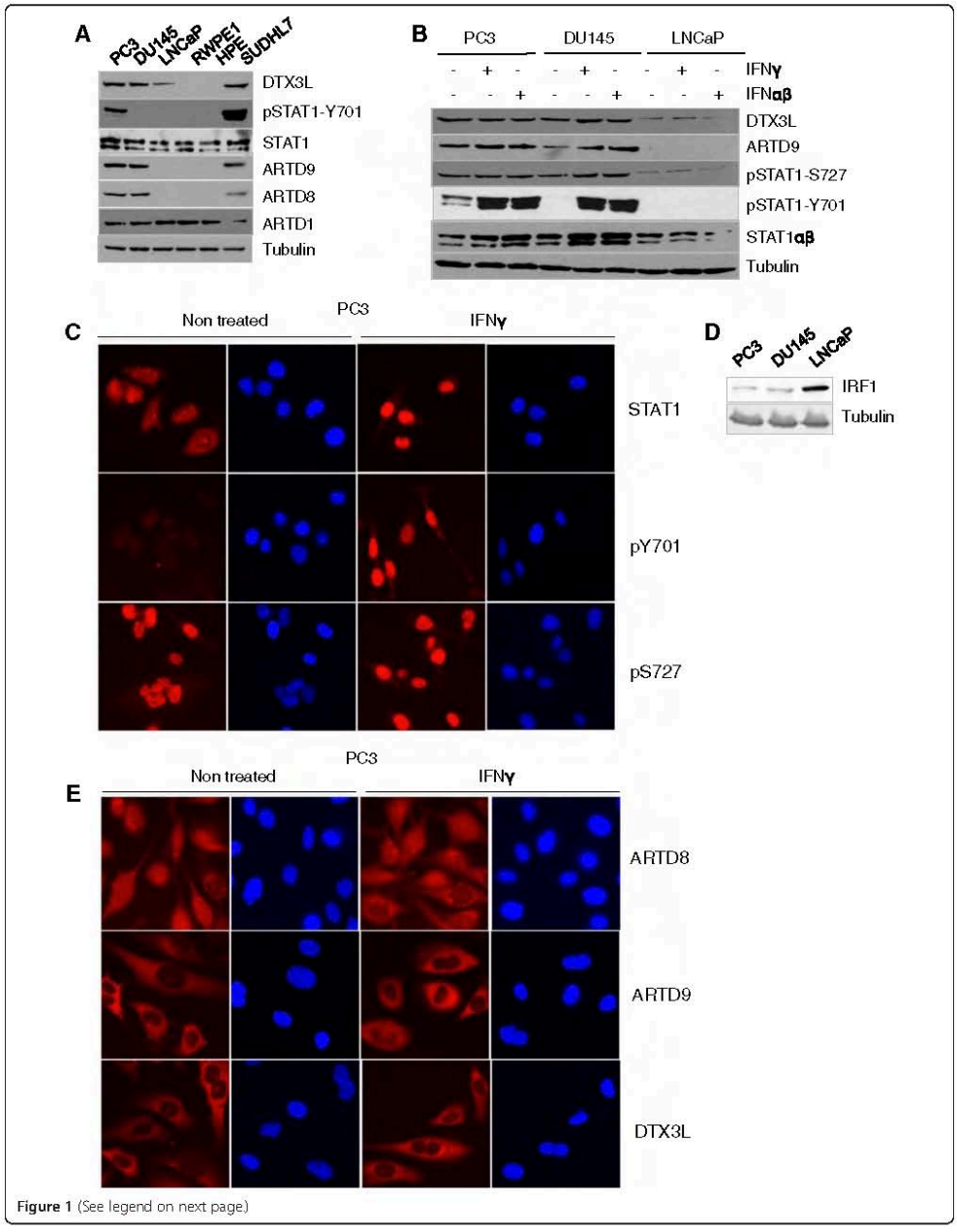

Figure 1 (See legend on next page.)

(See figure on previous page.)
Figure 1 DTX3L is constitutively overexpressed together with ARTD8 and ARTD9 in mPCa associated with increased IFNγ/STAT1 signaling. (A) Immunoblot analyses of untreated p53-negative, mPCa cell lines PC3 and DU145, androgen-sensitive and JAK1-negative LNCaP cell line and of the immortalized normal prostate luminal epithelial cell lines HPE and RWPE1. The HR-DLBCL-SUDHL7 cell line constitutively expressing DTX3L, ARTD9 and ARTD8 [23] was used as a positive control. Whole cell extracts were separated by SDS PAGE, blotted and subsequently probed with antibodies for DTX3L, ARTD1, ARTD8 and ARTD9 pSTAT1(Y701) and tubulin. **(B)** Immunoblot analyses of STAT1-signaling in p53-negative mPCa cell lines PC3 and DU145 and in the androgen-sensitive and JAK1-negative LNCaP cell line treated with or without IFNγ or IFNαβ. PC3, DU145 and LNCaP cells were treated with or without IFNγ (200 U/ml) or IFNαβ (50 U/ml each) for 2 h and then whole cell extracts separated by SDS PAGE and subsequently probed with antibodies for DTX3L, ARTD9, STAT1, pSTAT1(Y701), pSTAT1(S727) and tubulin. The immunoblots are representative of at least three independent experiments. **(C)** Immunofluorescence microscopy analyses and sub-cellular localization of endogenous STAT1, pSTAT1-(pY701) and pSTAT1-(pS727) in PC3 cells, in presence or absence of 1000 U/ml IFNγ. Original magnification × 400. Images are representative of at least three independent experiments. **(D)** Immunoblot analyses of basal expression levels of IRF1 in PC3, DU145 and LNCaP cell lines. Whole cell extracts were separated by SDS PAGE and subsequently probed with antibodies for IRF1 and tubulin. The immunoblot is representative of at least three independent experiments. **(E)** Immunofluorescence microscopy analyses and sub-cellular localization of endogenous DTX3L, ARTD8 and ARDT9 in PC3 cells, in presence or absence of 1000 U/ml IFNγ. Original magnification × 400. Images are representative of at least three independent experiments.

DU145 cells (Figure 1D and Additional file 2: Figure S2C). These observations suggest that DTX3L and ARTD9 might act together as transcriptional repressors of the *IRF1* gene in mPCa cells.

In agreement with previous studies in HR-DLBCL [23,48], DTX3L and ARTD9 were mainly localized in the cytoplasm whereas only small subfractions show nuclear localization (Figure 1E). Conversely, ARTD8 was evenly distributed in the nucleus and cytoplasm in these cells (Figure 1E). DTX3L is a nucleocytoplasmic shuttling protein and complex formation between DTX3L and ARTD9 in the nucleus has been suggested to facilitate the nuclear export of ARTD9 by DTX3L [48]. However, our subsequent siRNA-knockdown experiments revealed that endogenous DTX3L does not facilitate the nuclear export of ARTD9 in PC3 cells. ARTD9 was mainly localized in the cytoplasm in both PC3-siMock and PC3-siDTX3L cells (Additional file 3: Figure S3A, B and Additional file 4: Figure S4A, B). The same pattern was observed for DTX3L in PC3-siMock and PC3-siARTD9 cells (Additional file 3: Figure S3A, C and Additional file 4: Figure S4A, C), strongly indicating that the nuclear shuttling of ARTD9 is mainly regulated by other factors, and thus, the previously observed nuclear export of ectopically overexpressed fluorescent protein-tagged-ARTD9 by ectopically overexpressed fluorescent protein-tagged-DTX3L [48] most likely represents a mechanism highly specific to the cell type and stimuli.

Crosstalk among DTX3L, ARTD8 and ARTD9 mediates proliferation in mPCa cells

In order to investigate whether a crosstalk among DTX3L, ARTD8 and ARTD9 mediates proliferation in mPCa cells we first analyzed the proliferation of cells depleted of DTX3L, ARTD8 or ARTD9 using siRNA (Additional file 5: Figure S5A, B) in presence or absence of IFNγ. IFNγ is known to inhibit the proliferation of p53-negative, androgen-refractory mPCa cells [78,79]. These experiments revealed that knockdown of DTX3L or ARTD9 in PC3 cells strongly inhibits proliferation when compared to control cells (Figure 2A, B), whereas knockdown of ARTD8 only showed a minor effect on proliferation (Figure 2C). As expected, knockdown of DTX3L or ARTD9 in LNCaP cells did not affect cell growth in LNCaP cells (data not shown). We next analyzed the effect on proliferation upon double knockdown of ARTD8/DTX3L, ARTD9/DTX3L or ARTD8/ARTD9 in PC3 cells. These analyses revealed that ARTD8 acts synergistically or additively together with DTX3L and ARTD9 in proliferation, strongly suggesting a functional crosstalk between ARTD8, DTX3L and ARTD9 (Figure 2D, E). No significant additional effects on proliferation were observed in siDTX3L/siARTD9 double knockdown cells indicating that DTX3L and ARTD9 regulate the same signaling pathway(s) in proliferation (Figure 2F).

DTX3L was originally identified as an ADP-ribosylation independent binding partner of ARTD9, interacting with the catalytic domain of ARTD9 [47]. Moreover, a recent study suggested that DTX3L interacts through ARTD9 with ARTD1 (also known as PARP1) in a DNA damage and poly-ADP-ribosylation-dependent manner [80]. We therefore investigated whether DTX3L forms endogenous complexes with ARTD8 under normal physiological conditions. Indeed, our co-immunoprecipitation studies in PC3 cells revealed that endogenous DTX3L forms strong complexes with ARTD8 and ARTD9 (Figure 2G, J and Additional file 5: Figure S5C, D). However, endogenous DTX3L barely interacted with ARTD1 under normal physiological conditions (Figure 2G). No interaction was observed with ARTD2 (also known as PARP2) (Figure 2G). Subsequent co-immunoprecipitation experiments with endogenous ARTD8, ARTD9 and other ARTDs in PC3 cells revealed that endogenous ARTD9 strongly interacts with ARTD8 (Figure 2H, I and Additional file 5: Figure S5D, F) and also interacts to a lesser extent with other active mono-ADP-ribosyltransferases (Additional file 5: Figure S5E). ARTD9 only interacted weakly with ARTD1 (Figure 2H), whereas no interaction was observed with ARTD2 (Figure 2H). These experiments

Bachmann et al. Molecular Cancer 2014, 13:125
http://www.molecular-cancer.com/content/13/1/125

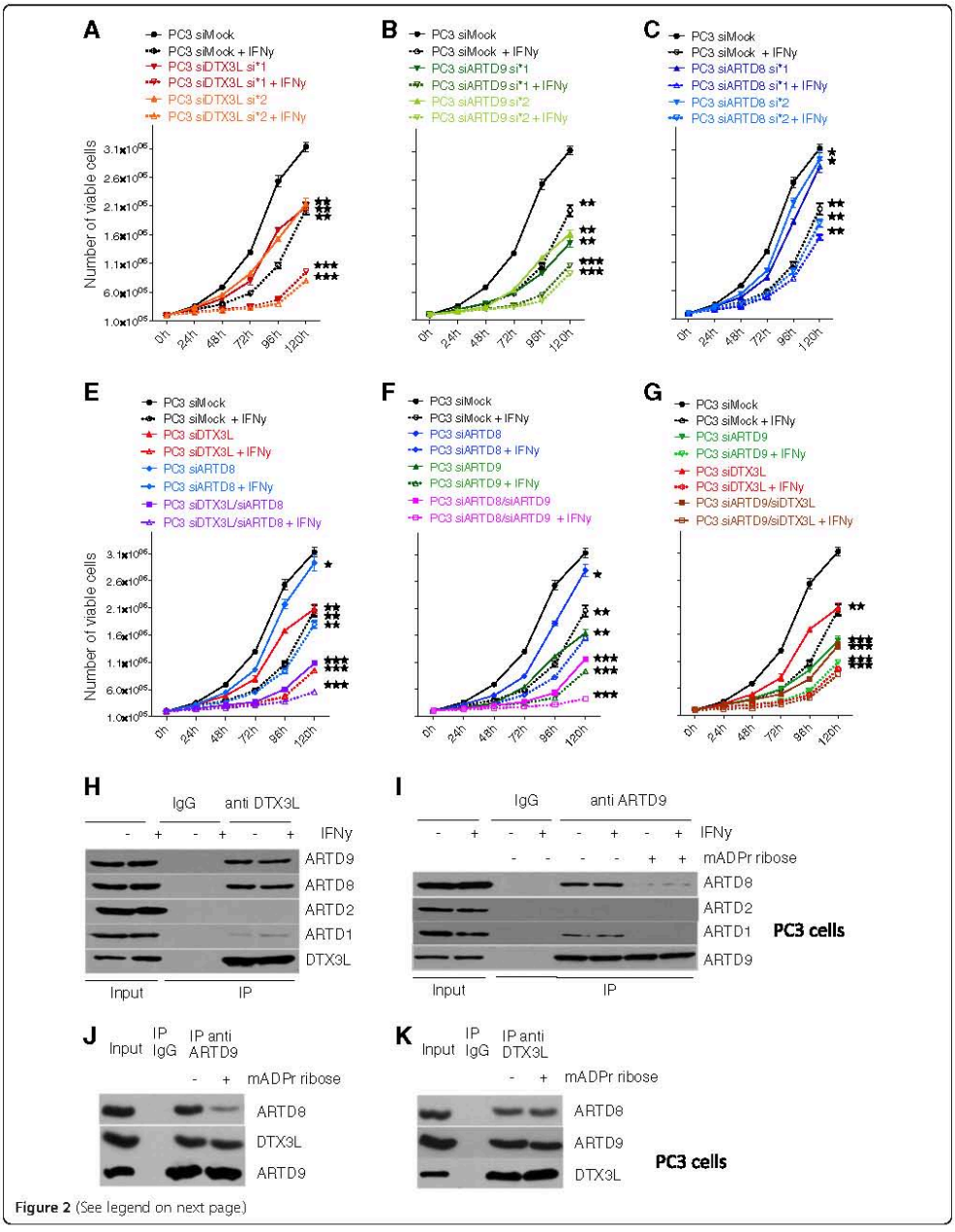

Figure 2 (See legend on next page)

(See figure on previous page.)
Figure 2 Crosstalk among DTX3L, ARTD8 and ARTD9 mediates proliferation in PC3 cells. (A-F) Cell proliferation analyses of PC3-siMock, PC3-siDTX3L, PC3-siARTD8, PC3-siARTD9 single knockdown cells **(A-C)** and PC3-siDTX3L/siARTD8, PC3 siDTX3L/siARTD9 or PC3-siARTD9/siARTD8 double knockdown cells **(D-F)** in presence or absence of IFNγ (200 U/ml) was assessed by the trypan blue exclusion assay. Relative cell proliferation and cell numbers are presented as mean from three independent experiments performed in triplicates. All error bars represent the SE. Statistical analysis was performed using the Student's t test. *$P < 0.05$, **$P < 0.001$ and ***$P < 0.0001$. **(G)** Co-immunoprecipitation analyses of endogenous DTX3L and ARTD family members in PC3 cells. PC3 cells were stimulated for 1 h with or without IFNγ (200 U/ml) and endogenous DTX3L complexes were then co-immunoprecipitated, separated on SDS PAGE, blotted and subsequently probed with antibodies for DTX3L, ARTD1 (positive control), ARTD2, ARTD8 and ARTD9. **(H)** Interaction of endogenous ARDT9 and ARTD1 or ARTD8 is mediated by (mono)-ADP-ribosylation. PC3 cells were stimulated for 1 h with IFNγ (200 U/ml) and endogenous ARTD9-ARTDx complexes subsequently co-immunoprecipitated in presence or absence of 5 mM mono-ADP-ribose using an anti-ARTD9 antibody. Complexes were then separated on SDS PAGE, blotted and subsequently probed with antibodies against endogenous ARTD1 (positive control), ARTD2, ARTD8 and ARTD9. **(I, J)** Interaction between endogenous DTX3L and ARTD8 or ARTD9 is independent of (mono)-ADP-ribosylation. Endogenous DTX3L-ARTD8/9 complexes were co-immunoprecipitated from extracts of PC3 cells in presence or absence of 5 mM mono-ADP-ribose using either an anti-ARTD9 **(I)** or an anti-DTX3L **(J)** antibody. Complexes were then separated on SDS PAGE, blotted and subsequently probed with antibodies against endogenous ARTD8, ARTD9 and DTX3L.

revealed that the observed interactions between ARTD9 and active mono-ADP-ribosyltransferases are mediated by (mono)-ADP-ribosylation (Figure 2H, I and Additional file 5: Figure S5D, E) and thus very likely mediated through their macrodomains. Several studies have demonstrated that the interaction between macrodomain-containing ARTDs and (mono)-ADP-ribosylated proteins, including active mono-ARTD enzymes, such as ARTD8 and ARTD10 (also known as PARP10), is mediated through their macrodomains [44,80,81]. Conversely, the observed interaction between DTX3L and ARTD8 or ARTD9 is not dependent on ADP-ribosylation ([47], Figure 2J and Additional file 5: Figure S5D), indicating that DTX3L could form different (mono)-ADP-ribosylation dependent and (mono)-ADP-ribosylation independent complexes with ARTD8 and ARTD9. Given that ARTD8 does not function as a coactivator for STAT1 [40] it is very likely that different DTX3L-ARTDx complexes simultaneously exist and do act in distinct signaling pathways.

Crosstalk among DTX3L, ARTD8 and ARTD9 mediates chemo-resistance and survival in mPCa cells in an ADP-ribosylation-dependent manner

In order to strengthen our previous observation in DLBCL [23], we subsequently analyzed the chemo-resistance and survival in PC3 cells depleted of either DTX3L, ARTD8 or ARTD9 in the presence or absence of IFNγ and/or docetaxel. Indeed we found that DTX3L, ARTD8 and ARTD9 mediate survival and chemo-resistance in mPCa cells (Figure 3A and Additional file 6: Figure S6A-F). To address whether there is a functional crosstalk between DTX3L, ARTD8 and ARTD9 in mediating survival and chemo-resistance, we performed double knockdown studies in PC3 cells. Interestingly, upon simultaneous depletion of ARTD8/DTX3L, ARTD9/DTX3L and ARTD8/ARTD9, IFNγ could enhance the sensitivity towards docetaxel in the absence of DTX3L or ARTD9. These results strongly suggest that both DTX3L and ARTD9, but not ARTD8, counteract the IFNγ-dependent anti-proliferative and pro-apoptotic IFNγ-STAT1-IRF1 axis [23] (Figure 3B). No significant additional effects on survival and chemo-resistance were observed in siDTX3L/siARTD9 double knockdown cells indicating that DTX3L and ARTD9 regulate the same signaling pathways in survival and chemo-resistance (Figure 3B). Together, these results indicate that there is a functional crosstalk between DTX3L, ARTD8 and ARTD9 in survival and chemo-resistance in mPCa cells. ARTD8 does not influence STAT1 signaling directly but through other mechanisms. A recent study in mice has provided first evidence that ARTD8 functions as a STAT6-specific co-regulator of IL4-mediated gene expression and is involved in IL4-induced proliferation and protection of B cells against apoptosis following irradiation or growth factor withdrawal [39]. Although no clear correlation between STAT6 expression or activity and ARTD8 could be observed in mPCa cell lines, it is very likely that ARTD8 might act together with DTX3L as a STAT6-specific survival factor in mPCa cells. STAT6 has been recently shown to act as a survival factor and to enhance mPCa progression [82]. Alternatively, ARTD8 might act together with DTX3L independently of STAT6 signaling in these cell lines.

Our finding of a (mono)-ADP-ribosylation-dependent interaction between ARTD8 and ARTD9 strongly suggests that the enzymatic activity of mono-ADP-ribosyl transferases is required for this interaction. Thus, we analyzed the effects of the enzymatic activity of ARTD8 or other ARTDs on survival and proliferation of mPCa cells. A recent study suggested that ARTD9 and ARTD1 physically and functionally interact and together mediate survival in response to genotoxic stress [80]. In order to test this hypothesis we treated ARTD8- or ARTD9-depleted PC3 cells in presence or absence of docetaxel with the ARTD1/2-specific inhibitors Olaparib and Veliparib [83-86] or with the more ARTD7/8-specific inhibitors DPQ and TIQ-A [83-85]. ARTD8- or ARTD9-depleted cells treated with Olaparib and Veliparib only showed a minor increase in cell death when compared to control cells. (Figure 3C).

Bachmann et al. Molecular Cancer 2014, 13:125
http://www.molecular-cancer.com/content/13/1/125

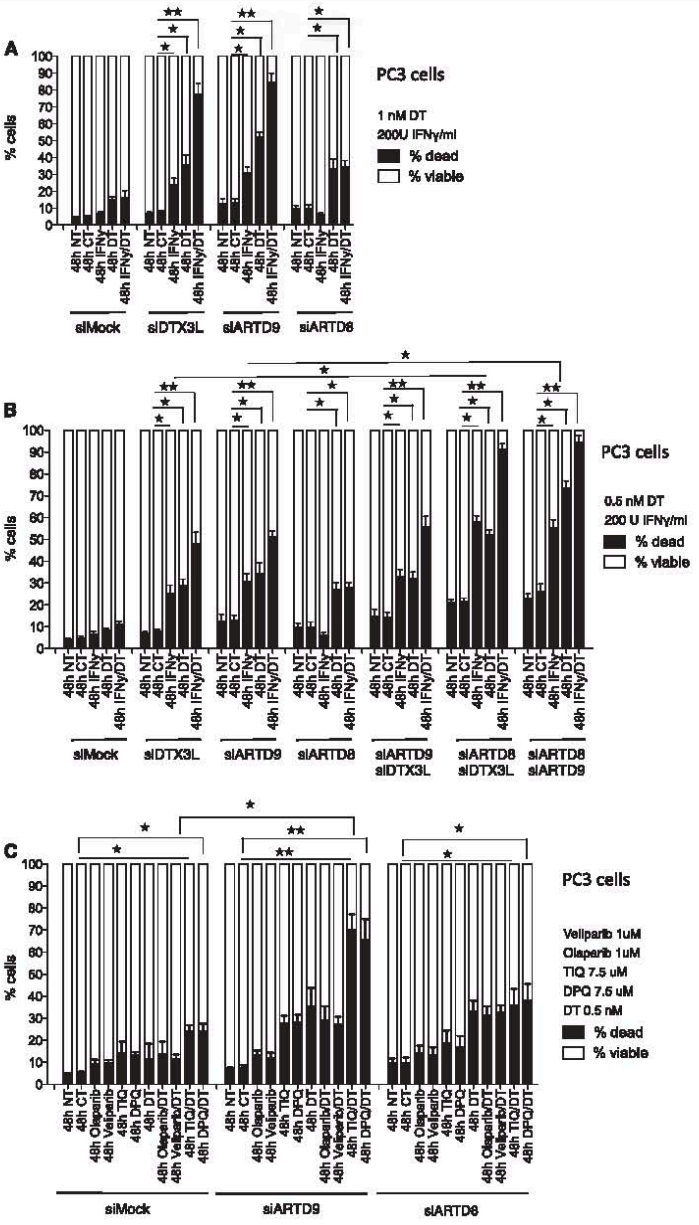

Figure 3 (See legend on next page.)

(See figure on previous page.)
Figure 3 Crosstalk among DTX3L, ARTD8 and ARTD9 mediates chemo-resistance and survival in PC3 cells and is dependent on ADP-ribosylation. (A) Cell viability analyses of PC3-siMock, PC3-siDTX3L, PC3-siARTD8 and PC3-siARTD9 single knockdown cells were assessed by the trypan blue exclusion assay. Cells were treated as indicated with IFNγ and/or docetaxel (DT) and counted after 48 h, NT: not treated, CT: control treatment (solvent). Values represent the means of three independent experiments, and the error bars represent the SE. Statistical analysis was performed using the Student's t test. *$P < 0.05$, **$P < 0.001$ and ***$P < 0.0001$ **(B)** Cell viability analyses of PC3-siMock, PC3-siDTX3L/siARTD8, PC3-siDTX3L/siARTD9 or PC3-si ARTD9/siARTD8 double knockdown cells were assessed by the trypan blue exclusion assay. Cells were treated as indicated with IFNγ and/or docetaxel (DT) and counted after 48 h, NT: not treated, CT: control treatment (solvent). Values represent the means of three independent experiments, and the error bars represent the SE. Statistical analysis was performed using the Student's t test. *$P < 0.05$, **$P < 0.001$ and ***$P < 0.0001$. **(C)** Cell viability analyses of PC3-siMock, PC3-siDTX3L, PC3-siARTD8 and PC3-siARTD9 single knockdown cells treated in presence or absence of docetaxel (DT) (0.5 nM) with the ARTD1/2-specific inhibitors Olaparib (1 μM) and Veliparib (1 μM) or with the more ARTD7/8-specific inhibitors DPQ (7.5 μM) and TIQ-A (7.5 μM) were assessed by the trypan blue exclusion assay. Values represent the means of three independent experiments performed in triplicate, and the error bars represent the SE. Statistical analysis was performed using the Student's t test. *$P < 0.05$, **$P < 0.001$ and ***$P < 0.0001$.

Remarkably, treatment with DPQ and TIQ-A strongly increased cell death in ARTD9-depleted cells when compared to control cells (Figure 3C). Conversely, in ARTD8-depleted cells we did not observe an increase in cell death upon DPQ and TIQ-A treatment when compared to control cells (Figure 3C), indicating that one of the definitive targets of DPQ and TIQ-A is the enzymatic activity of ARTD8. Moreover, we did not observe any functional crosstalk between ARTD1 and ARTD8 or ARTD9 n PC3 cells under the tested conditions (Figure 3C). In line with these observations, overexpression of active ARTD8 wild type in PC3 cells enhanced survival in siMock cells and rescued the effects on cell survival in siARTD8 knockdown cells. In contrast, overexpression of a catalytically inactive ARTD8 mutant form in ARTD8-depleted PC3 cells did not increase cell survival in siMock cells or siARTD8 knockdown cells (Additional file 6: Figure S6G). These results strongly suggest that the enzymatic activity of ARTD8 is required for the survival of mPCa cells.

DTX3L and ARTD9 mediate proliferation, chemo-resistance and survival in mPCa cells in a STAT1-dependent manner

Several studies strongly suggest that STAT1α activates anti-proliferative and pro-apoptotic genes (i.e. mediated through the IFNγ-STAT1-IRF1-p53 axis) while concomitantly activating anti-apoptotic-pro-survival pathways (i.e. mediated through the STAT1-IRF2/BCL2-axes) [23,87,88]. In addition, overexpression of STAT1β, the antagonistic isoform of STAT1α, increases the growth rate of cells and their resistance to drug-induced apoptosis and cell cycle arrest by repressing STAT1α target genes such as p21 and IRF1 [87]. Our previous study has demonstrated that ARTD9-mediated cell proliferation, chemo-resistance and cell survival in HR-DLBCL is dependent on STAT1 [23].

In order to examine whether depletion of STAT1 might inhibit the pro-apoptotic and/or anti-proliferative IFNγ-STAT1-IRF1-axis in absence of DTX3L or ARTD9 we next analyzed cell proliferation (Figure 4A-C) and cell survival (Figure 4D) defects in PC3 cells simultaneously depleted of DTX3L/STAT1, ARTD8/STAT1 and ARTD9/STAT1. Indeed, depletion of STAT1 did not further inhibit cell proliferation, chemo-resistance and cell survival in the absence of ARTD9 or DTX3L, when compared to the single knockdown cells (Figure 4A, B, D). However, the observed proliferation defects and the increase in cell death upon depletion of DTX3L or ARTD9 could not be fully rescued by simultaneous depletion of DTX3L/STAT1 and ARTD9/STAT1, when compared to single knockdown and control cells (Figure 4A-D). However, depletion of STAT1 alone strongly affected cell proliferation (Figure 4A, B), chemo-resistance and cell survival (Figure 4D), indicating that STAT1 itself is required for cell proliferation, chemo-resistance and cell survival. Conversely, cell proliferation and survival of ARTD8-depleted cells is even more inhibited upon additional depletion of STAT1 (Figure 4C, D), clearly indicating that STAT1 and ARTD8 do not act together in the same signaling pathway. Given that depletion of STAT1 alone strongly affected cell proliferation and survival, but did not further inhibit cell proliferation and survival in the absence of ARTD9 or DTX3L (Figure 4A, B), indicates that DTX3L and ARTD9 together with STAT1 act in the same signaling pathways.

Taken together these results suggest that both DTX3L and ARTD9 mediate cell proliferation, survival and chemo-resistance of mPCa cells in a STAT1-dependent manner whereas ARTD8 enhances survival and chemo-resistance independently of STAT1 (Figure 4A-D).

DTX3L and ARTD9 repress expression of the tumor suppressor IRF1 in PCa cells

ARTD9 can bind to the *IRF1*-promoter and together with STAT1β inhibits the transcription of the *IRF1* gene, thereby counteracting the IFNγ-dependent anti-proliferative and pro-apoptotic IFNγ-STAT1-IRF1-p53 axis in high-risk HR-DLBCL [23]. We therefore investigated whether DTX3L and/or ARTD9 function as transcriptional repressors of IRF1 and regulate STAT1 signaling in PCa cells. Our current study demonstrates that DTX3L and ARTD9 act together as repressors of the tumor suppressor IRF1

Bachmann *et al. Molecular Cancer* 2014, **13**:125
http://www.molecular-cancer.com/content/13/1/125

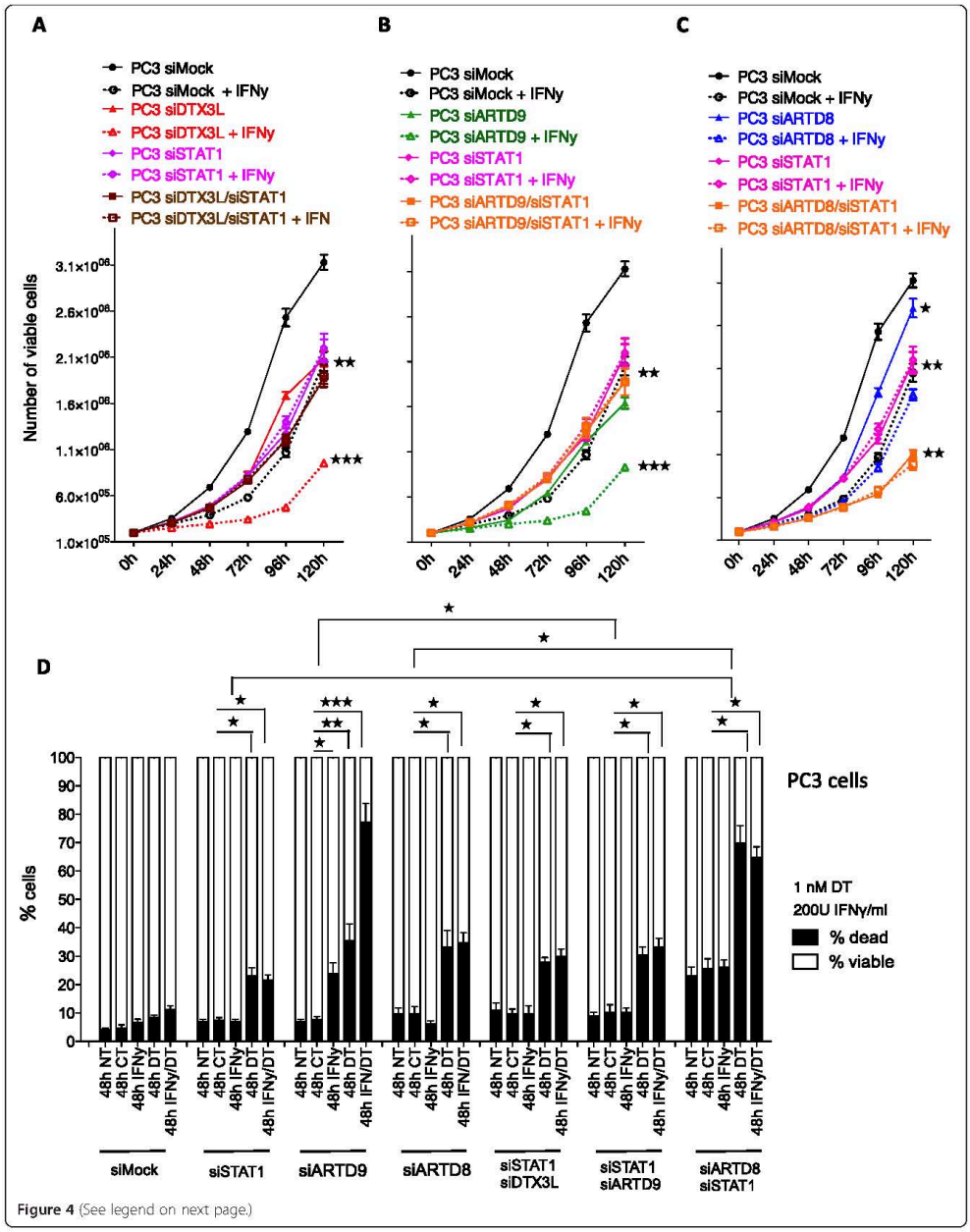

Figure 4 (See legend on next page.)

(See figure on previous page.)
Figure 4 DTX3L- and ARTD9-mediated proliferation, chemo-resistance and survival in PC3 cells is dependent on STAT1. (A-C) Cell proliferation analyses of PC3-siMock, PC3-siSTAT1, PC3-siSTAT1/siDTX3L **(A)**, PC3-siSTAT1/siARTD8 **(B)**, or PC3-siSTAT1/siARTD9 **(C)**, double knockdown cells in presence or absence of IFNγ (200 U/ml) were assessed by the trypan blue exclusion assay. Relative cell proliferation and cell numbers are presented as mean from three independent experiments performed in triplicate, the error bars represent the SE. Statistical analysis was performed using the Student's t test. *$P < 0.05$, **$P < 0.001$ and ***$P < 0.0001$. **(D)** Cell viability analyses of a PC3-siMock, PC3-siSTAT1 single knockdown, and PC3-siSTAT1/siDTX3L PC3-siSTAT1/siARTD8 or PC3-siSTAT1/siARTD9 double knockdown cells were assessed by the trypan blue exclusion assay. Cells were treated as indicated with IFNγ and/or docetaxel (DT), NT: not treated, CT: control treatment (solvent). Values represent the means of three independent experiments performed in triplicates, and the error bars represent the SE. Statistical analysis was performed using the Student's t test. *$P < 0.05$, **$P < 0.001$ and ***$P < 0.0001$.

in mPCa. The basal IRF1 protein and mRNA expression levels were strongly increased in PC3 cells depleted of DTX3L or ARTD9 in absence of IFNγ (Figure 5A-C and Additional file 7: Figure S7C). The IRF1 protein and mRNA expression was further increased in PC3 cells depleted of DTX3L or ARTD9 upon IFNγ treatment (Figure 5A-C and Additional file 7: Figure S7C). Subsequent *IRF1*-promoter-driven luciferase reporter assays in PC3 cells showed that overexpression of DTX3L or ARTD9 together with STAT1β down-regulates the *IRF1*-promoter-driven luciferase reporter (Additional file 7: Figure S7D-F). Moreover, co-overexpression of all three proteins together (DTX3L, ARTD9 and STAT1β) synergistically down-regulated the *IRF1*-promoter-driven luciferase reporter (Additional file 7: Figure S7G). Together, these results suggest that ARTD9 and DTX3L cooperate and act as transcriptional repressors by forming a ternary complex with STAT1β. It remains to be investigated whether DTX3L might monoubiquitinate histone H4 lysine 91 on the *IRF1*-promoter and thereby inhibits the transcription of the *IRF1* gene. In addition, our knockdown experiments demonstrate that DTX3L and ARTD9 positively regulate the expression of each other on their own gene expression level, though to a different extent (Figure 5A, B, D). Depletion of DTX3L strongly inhibited the expression of ARTD9 whereas depletion of ARTD9 inhibited the expression of DTX3L to a minor extent. We have previously shown that ARTD9 can bind to its own bidirectional promoter [23]. Thus, DTX3L and ARTD9 positively regulate each other directly through their shared bidirectional promoter.

To confirm these observations, we next analyzed the effect of IRF1 on proliferation and cell survival by either depletion or overexpression of IRF1 in PCa cells. Exogenous overexpression of human IRF1 in PC3 cells (Additional file 8: Figure S8A) revealed that the presence of IRF1 indeed strongly inhibited proliferation of PC3 cells (Figure 5E). In line with this, knockdown of IRF1 enhanced the proliferation of PC3 (Figure 5F and Additional file 8: Figure S8B, C) and of LNCaP cells (Figure 5G and Additional file 8: Figure S8D), although to a lesser extent in the JAK1-negative LNCaP cell line (Figure 5G). Several studies suggest that phosphorylation and/or acetylation of IRF1 is required for full transcriptional activity of IRF1 [89-91]. Tyrosine phosphorylation and probably also acetylation of IRF1 appears to be dependent on active IFNγ/JAK1 signaling [89,91]. Subsequent survival assays with cells depleted of IRF1 revealed that IRF1 does not inhibit survival of mPCa cells (Additional file 8: Figure S8E), strongly indicating that other STAT1-dependent target genes are involved and/or required for the DTX3L/ARTD9-mediated effects on survival of mPCa cells. Future studies will be required in order to identify the target genes involved in these processes and elucidate the exact molecular mechanisms.

DTX3L interacts with the IFNGR complex and antagonistically regulates together with ARTD9 the phosphorylation of STAT1 on Y701 in mPCa cells

Since our previous studies showed that ARTD9 enhances phosphorylation of both isoforms of STAT1 on Y701 we tested whether DTX3L might function together with ARTD9 in regulating the phosphorylation of STAT1 on Y701 in mPCa cells. Surprisingly, these experiments revealed that DTX3L and ARTD9 antagonistically regulate the phosphorylation of both STAT1 isoforms STAT1α and STAT1β, on Y701 in mPCa cells. ARTD9 also stimulated phosphorylation of STAT1 on Y701 (Figure 6A, C) whereas DTX3L strongly inhibited phosphorylation of STAT1 on Y701 (Figure 6B, D). However, the observed effects of ARTD9 on STAT1 phosphorylation are less pronounced than previously observed in HR-DLBCL [23]. In contrast to their P-glycoprotein-independent chemo-resistant variants PC3-DR or DU145-DR [15,33,36,75-77] both PC3 and DU145 cells do not have high basal levels of constitutively tyrosine phosphorylated STAT1 (pSTAT1α(Y701) and pSTAT1β(Y701) and are sensitive towards docetaxel [15,33,36,75-77]. Thus, the siDTX3L- and siARTD9-mediated effects on STAT1-signaling are most likely much higher in the PC3-DR or DU145-DR cells [15] and are therefore more comparable with the effects observed in HR-DLBCL. Moreover, since DTX3L and ARTD9 regulate each other on their gene expression level (Figure 5A, B and D) the observed antagonistic effects are tightly balanced and might explain why the effects are not completely visible in the knockdown cells.

Our previous study has provided preliminary evidence that ARTD9 interacts with the IFNGR-receptor complex

Bachmann et al. Molecular Cancer 2014, 13:125
http://www.molecular-cancer.com/content/13/1/125

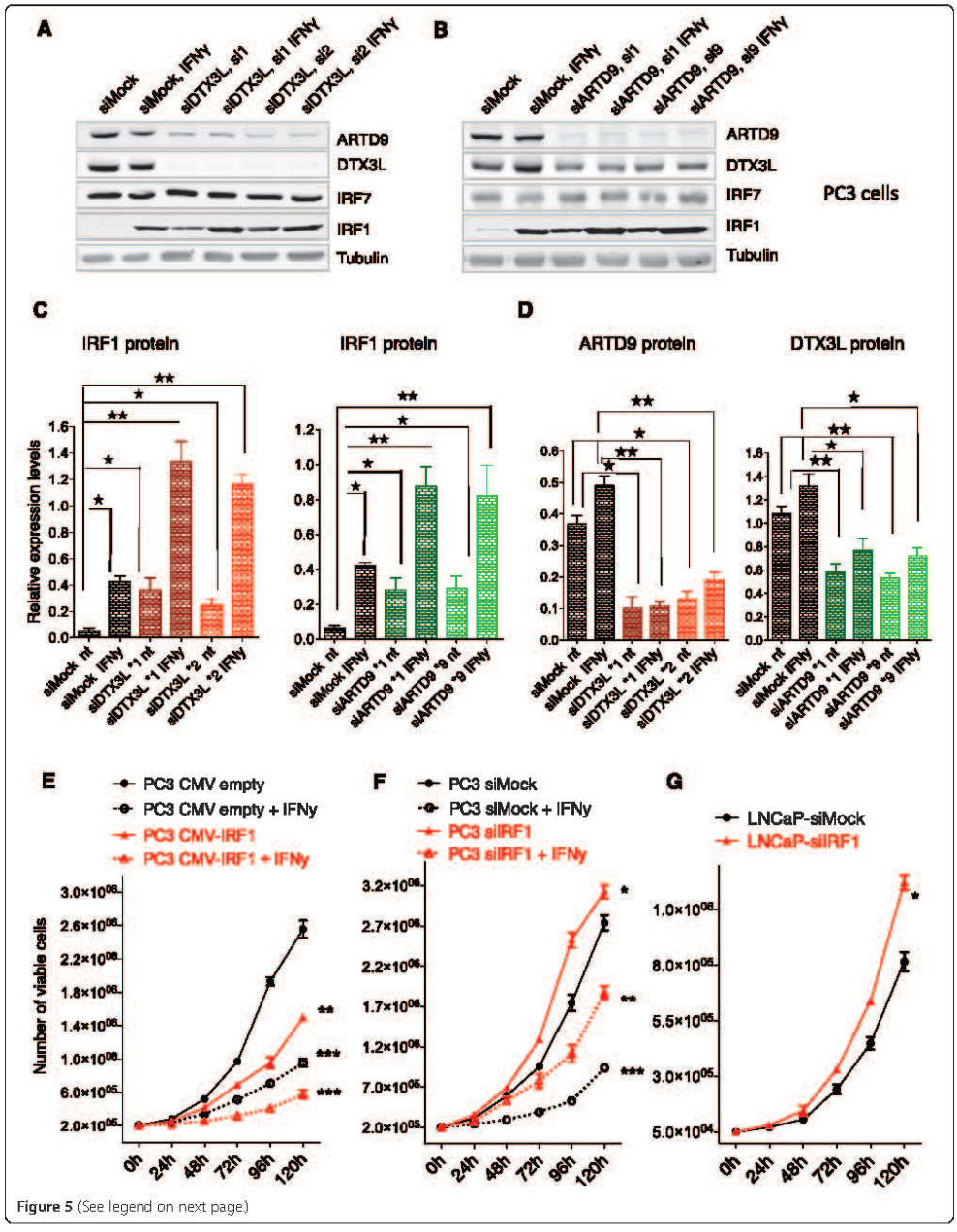

Figure 5 (See legend on next page.)

(See figure on previous page.)
Figure 5 DTX3L and ARTD9 repress tumor suppressor IRF1 expression in mPCa cells. (A and B) Immunoblot analyses of the tumor suppressor gene product IRF1. PC3-siMock, PC3-siDTX3L **(A)** or PC3-siARTD9 **(B)** single knockdown cells were treated with or without IFNγ (200 U/ml) for 6 h and then whole cell extracts separated by SDS PAGE, blotted and subsequently probed with antibodies for ARTD9, DTX3L, IRF1, IRF7 and tubulin. The immunoblots are representative of at least three independent experiments. **(C)** Quantification of IRF1 levels shown in Figure 5A, B. IRF1 levels were normalized to tubulin. Values represent the means of three independent experiments. **(D)** Quantification of ARTD9 and DTX3L protein levels in PC3-siMock, PC3-siDTX3L and PC3-siARTD9 single knockdown, respectively, as represented in Figure 5A, B. ARTD9 and DTX3L protein levels were normalized to tubulin. Values represent the means of three independent experiments. **(E)** Cell proliferation analyses of PC3-CMVprom-empty-control and PC3-CMVprom-IRF1 cells were assessed in presence or absence of IFNγ (100U/ml) by the trypan blue exclusion assay. Relative cell proliferation and cell numbers are presented as means of three independent experiments performed in triplicates. **(F)** Cell proliferation analyses of PC3-siMock, PC3-siIRF1 and PC3-siARTD9 single knockdown cells were assessed in presence or absence of IFNγ (200 U/ml) by the trypan blue exclusion assay. Relative cell proliferation and cell numbers are presented as means of three independent experiments performed in triplicate. **(G)** Cell proliferation analyses of LNCaP-siMock and LNCaP-siIRF1 single knockdown cells were assessed by the trypan blue exclusion assay. Relative cell proliferation and cell numbers are presented as means of two independent experiments performed in triplicate. All error bars shown in A to G represent the SE. Statistical analysis was performed using the Student's t test. $^{*}P < 0.05$, $^{**}P < 0.001$ and $^{***}P < 0.0001$.

and thereby stimulates directly or indirectly the kinase activity of JAK1/2 [23]. Indeed, our co-immunoprecipitation studies revealed that endogenous DTX3L interacts with activated STAT1-containing IFNGR-receptor complexes in the cytoplasm (Figure 6E, F) and forms together with ARTD9 complexes with STAT1 in the nucleus (Additional file 8: Figure S8F). No interaction with the tyrosine phosphatases PTPN1 and PTPN2, both known to dephosphorylate pSTAT1 on Y701 [92-94], was observed (Figure 6F). Our observations strongly suggest that DTX3L and ARTD9 might antagonistically regulate the JAK1/2 kinase activity and thereby antagonistically influence the nuclear activities of both STAT1α and STAT1β. Thus, DTX3L and ARTD9 seem to be required for the fine-tuning of STAT1-signaling, particularly in tumorigenesis. Moreover, since both DTX3L and ARTD9 are target genes of STAT1 [23,48] the suggested antagonistic and cooperative activities of DTX3L and ARTD9 may represent a general negative and positive feedback loop in STAT1-signaling. Due to the fact that ARTD9 and DTX3L are regulating each other on the level of gene expression it is quite difficult to experimentally address the exact molecular mechanisms underlying the proposed antagonism between them. The observed effect on STAT1 tyrosine phosphorylation might be regulated through (mono)-ubiquitinylation and/or mono-ADP-ribosylation. We have previously shown that the interactions between ARTD9 and STAT1α/β are mediated through macrodomains and dependent on ADP-ribosylation [23]. However, we did not find any direct evidence that STATs are mono-ADP-ribosylated *in vivo*. Thus, it remains to be investigated whether (mono)-ubiquitinylation and/or mono-ADP-ribosylation is involved in this process.

DTX3L mediates cell migration of mPCa cells in a STAT1 and/or STAT3-dependent manner

A recent study has provided first evidence that ARTD9 might be associated with lymphocyte migration and may promote the dissemination of malignant B cells in high-risk DLBCL *in vivo* [48,95]. Ectopic overexpression of ARTD9 in an ARTD9 and DTX3L-negative DLBCL cell line derived from low risk DLBCL tumor strongly enhanced the migration *in vitro* when compared to control cells [48]. In order to investigate whether endogenous DTX3L or ARTD9 are required for the migration of mPCa cells we analyzed the migration potential of PC3 cells depleted of DTX3L and ARTD9 using the classical scratch wound healing assay for adherent cell lines. Surprisingly, upon depletion of DTX3L, but not ARTD9 or ARTD8, cell migration was impaired in PC3 and DU145 cells (Figure 7A-C and Additional file 9: Figure S9A-F). These observations are in contrast to the previous study, which did not address the expression level of DTX3L in the ARTD9 ectopically overexpressing DLBCL cell line [48].

We next investigated whether the observed effects of DTX3L on migration of mPCa cells is dependent on STAT1. Besides its role in mediating tumor survival and growth, STAT3 plays a crucial role in tumor migration, invasion and metastasis [7,69] and recent studies provided preliminary evidence that STAT1 is involved in migration of mPCa cells [20,21]. In order to evaluate whether cell migration is also dependent on STAT1 we investigated the migration potential of cells depleted of STAT1 or both STAT1 and DTX3L. These experiments showed that the observed effect is indeed dependent on STAT1-signaling (Figure 7D, E and Additional file 10: Figure S10A, B, E). Migration of PC3 and DU145 cells was not further impaired upon double knockdown of STAT1 and DTX3L when compared to single depletion of DTX3L or STAT1, strongly indicating that DTX3L and STAT1 act together in the same pathway(s) (Figure 7D, E and Additional file 10: Figure S10A, B, E). Control experiments revealed that IRF1 does not affect migration of mPCa cells (Additional file 10: Figure S10D), suggesting that the IFNγ/IRF1 axis is not involved in cell migration. The fact that depletion of ARTD9 and IRF1 did not affect cell migration suggests that DTX3L acts in STAT1-signaling pathways in an ARDT9/IFNγ-independent

Bachmann et al. Molecular Cancer 2014, 13:125
http://www.molecular-cancer.com/content/13/1/125

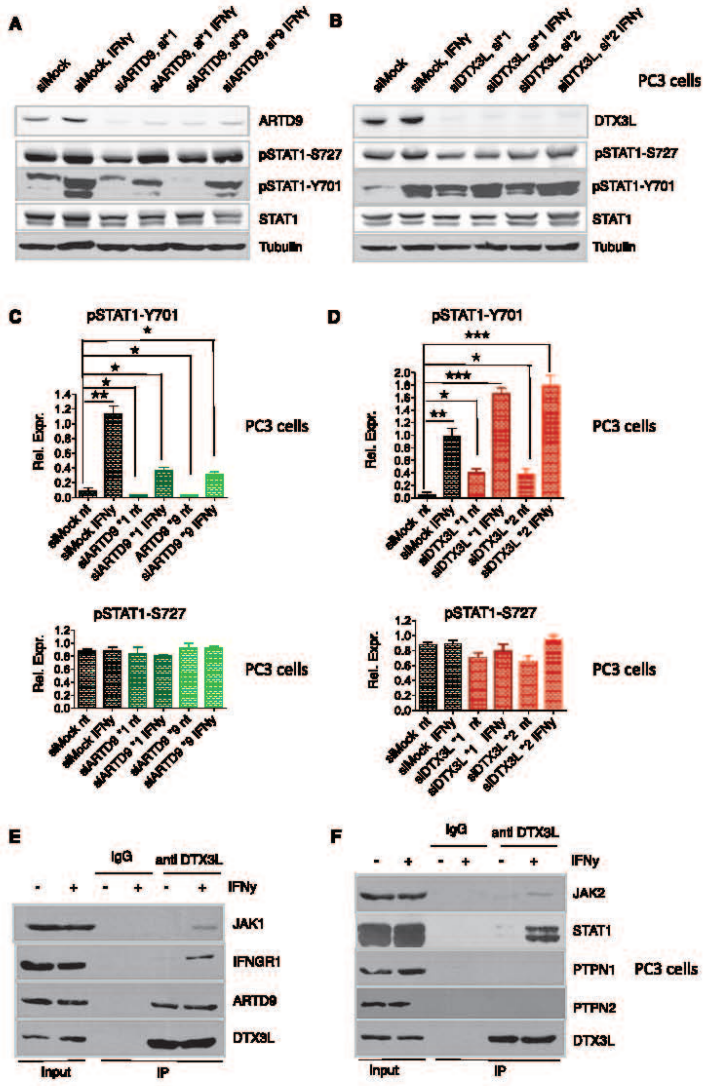

Figure 6 DTX3L interacts with the IFNGR complex and together with ARTD9 antagonistically regulates the phosphorylation of STAT1 on Y701 in PC3 cells. (A and B) Immunoblot analyses of STAT1-signaling in PC3-siMock, PC3-siDTX3L **(A)**, and PC3-siARTD9 **(B)** single knockdown cells. PC3-siMock, PC3-siDTX3L or PC3-siARTD9 single knockdown cells were treated with or without IFNγ (200 U/ml) for 2 h and then whole cell extracts separated by SDS PAGE, blotted and subsequently probed with antibodies for STAT1, pSTAT1(Y701), pSTAT1(S727) and tubulin. The immunoblots are representative of at least three independent experiments. **(C and D)** Quantification of pSTAT1(Y701) and pSTAT1(S727) levels shown in Figure 5A, B. pSTAT1(Y701) and pSTAT1(S727) levels were normalized to tubulin and STAT1. Values represent the mean of three independent experiments, and the error bar represents the SE. Statistical analysis was performed using the Student's t test. *$P < 0.05$, **$P < 0.001$ and ***$P < 0.0001$. **(E and F)** Co-immunoprecipitation analyses of endogenous DTX3L-IFNGR complexes in PC3 cells: Endogenous DTX3L/IFNGR complexes were co-immunoprecipitated using an anti-DTX3L antibody. Complexes were then separated on SDS PAGE, blotted and subsequently probed with antibodies against endogenous DTX3L, ARTD9, STAT1, IFNGR1, JAK1, JAK2, PTPN1 and PTPN2.

Bachmann et al. Molecular Cancer 2014, 13:125
http://www.molecular-cancer.com/content/13/1/125

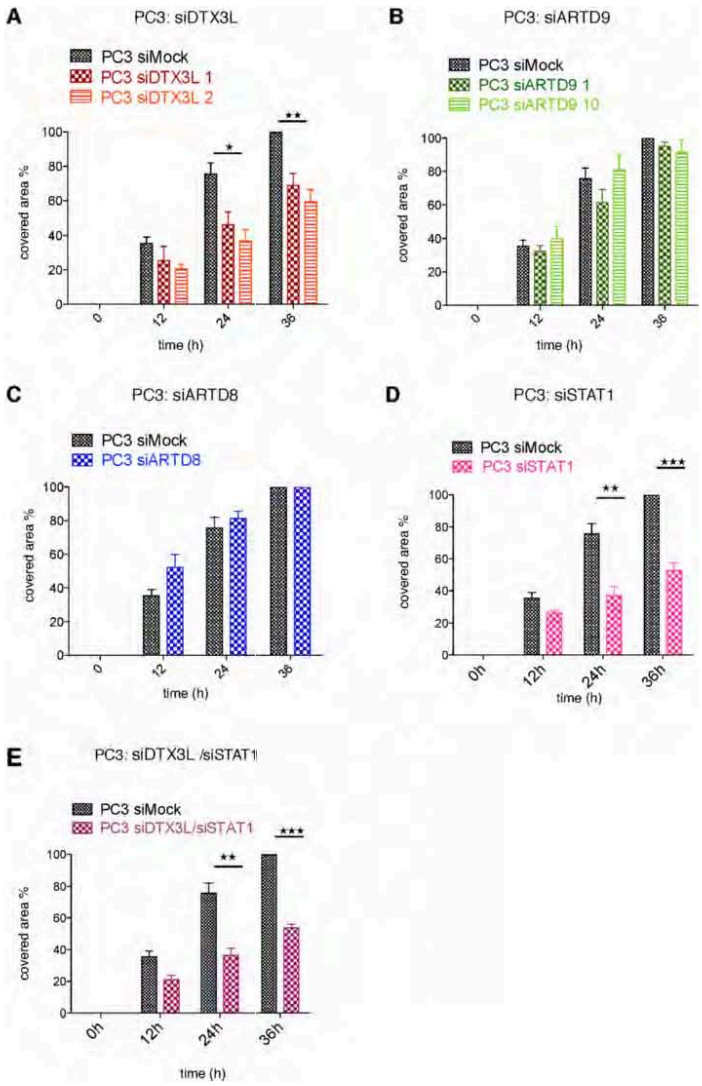

Figure 7 DTX3L but not ARTD9 or ARTD8 mediates together with STAT1 cell migration of PC3 cells. (A-E) PC3-siMock, PC3-siDTX3L **(A)**, PC3-siARTD9 **(B)**, PC3-siARTD8 **(C)**, PC3-siSTAT1 **(D)** single knockdown cells and PC3-siDTX3L/siSTAT1 **(E)** PC3-double knockdown cells were seeded into 6-well plates and treated as described in Material and Methods. At 0, 12, 24, and 36 h photographs were made and quantified as described in Material and Methods. Values represent the mean of three independent experiments and the error bars represent the SE. Statistical analysis was performed using the Student's t test. *$P < 0.05$, **$P < 0.001$ and ***$P < 0.0001$.

manner. The observed DTX3L-dependent effects on migration might be therefore mediated by the constitutive nuclear activity of pSTAT1α(pS727) homo- or heterodimers. Indeed, the observed impairment of cell migration upon DTX3L/STAT1 knockdown is in line with the cell migration analyzed upon depletion of STAT3 (Figure 8A and

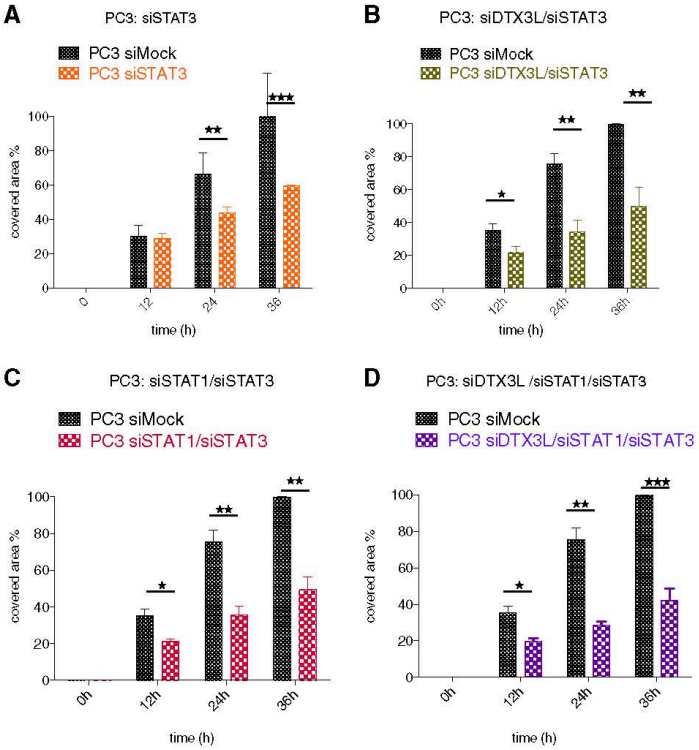

Figure 8 DTX3L-mediated cell migration of PC3 cells might also be dependent on STAT3. (A-F) PC3-siSTAT3 single knockdown cells **(A)**, PC3-siDTX3L/siSTAT3 **(B)**, PC3-siSTAT1/siSTAT3 **(C)** double knockdown cells and PC3-siDTX3L/siSTAT1/siSTAT3 **(D)** triple knockdown cells were seeded into 6-well plates and treated as described in Material and Methods. At 0, 12, 24, and 36 h photographs were made and quantified as described in Material and Methods. Values represent the mean of three independent experiments and the error bars represent the SE. Statistical analysis was performed using the Student's t test. *$P < 0.05$, **$P < 0.001$ and ***$P < 0.0001$.

Additional file 9: Figure S9F), which was used as positive control in this set of experiments. Subsequent control experiments revealed that the observed effect might be indeed also dependent on STAT3-signaling (Figure 8B-D and Additional file 10: Figure S10F-H). No further significant inhibition was observed neither in siSTAT1/siSTAT3, siDTX3L/siSTAT3 double knockdown cells nor in siDTX3L/siSTAT1/siSTAT3 triple knockdown cells when compared to siDTX3L, siSTAT1 or siSTAT3 single knockdown cells, strongly indicating that DTX3L, STAT1 and STAT3 act in the same pathway(s) (Figure 8B-D and Additional file 10: Figure S10F-H). DTX3L might function in a non-canonical STAT1:STAT3 heterodimer-mediated signaling pathway in migration of mPCa cells.

Together, our *in vitro* cell migration analyses strongly indicate that DTX3L together with STAT1 is crucial for proliferation and survival but might also be required together with STAT1 for the metastasization and dissemination of androgen-refractory mPCa cells *in vivo*.

Conclusions

We have identified the E3 ubiquitin ligase DTX3L and the macrodomain-containing mono-ADP-ribosyltransferases ARTD8 and ARTD9 as novel oncogenic survival factors in androgen-independent mPCa cells. Constitutive overexpression of DTX3L and ARTD9 is mediated through both IL6/JAK1-STAT1:STAT3- and IFNγ/JAK1-STAT1:STAT1-mediated signaling pathways (Figure 9A). Together with ARTD8 and ARTD9, DTX3L mediates proliferation, chemo-resistance and survival in mPCa cells (Figure 9B). Our study demonstrates that DTX3L and ARTD9 cooperate as repressors of the tumor suppressor IRF1 in mPCa cells (Figure 9C). However, since depletion of IRF1 does only positively affect proliferation but not cell survival, the

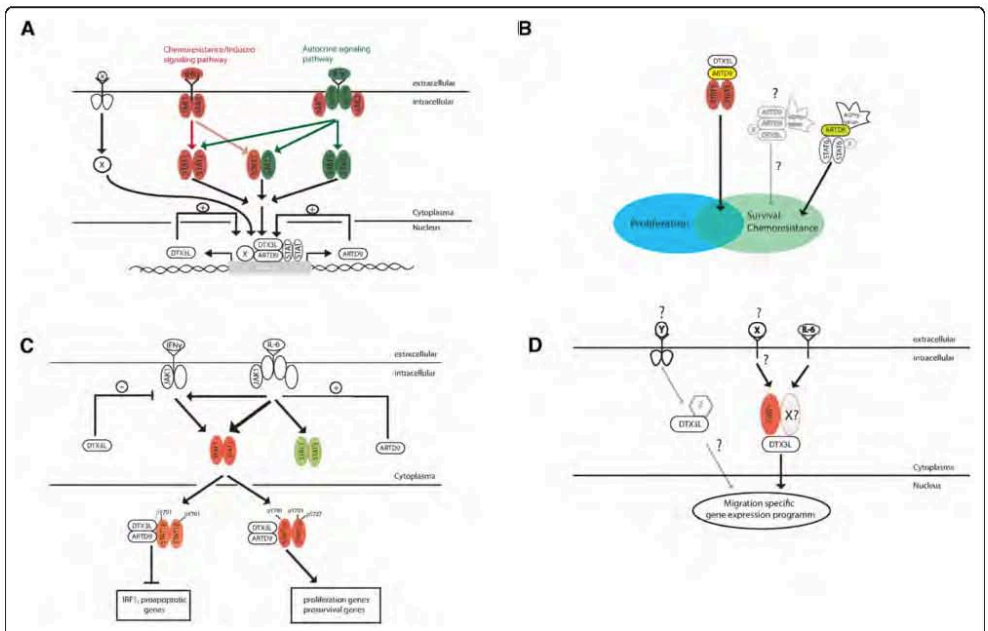

Figure 9 Proposed working models for the postulated crosstalk among DTX3L, ARTD8 and ARTD9 in chemotherapy-resistant mPCa cells. (A) Constitutively active IL6/STAT3-signaling and enhanced IFNGR-JAK1/2-STAT1- signaling in chemotherapy-resistant mPCa cells, including CRPC-like cells causes overexpression of DTX3L and ARTD9, which in turn, further stimulates their own expression through a positive feedback loop. **(B)** Crosstalk between DTX3L/ARTD9-STAT1 and ARTD8-STAT6-signaling pathways is required for proliferation and cell survival of chemotherapy-resistant mPCa cells, including CRPC-like cells. **(C)** Similar to the situation in HR-DLBCL, DTX3L and ARTD9, together with STAT1β repress the transcriptional activation of the tumor suppressor IRF1 and other anti-proliferative and pro-apoptotic genes while together with STAT1α both, DTX3L and ARTD9 might activate genes required for cell proliferation and survival of mPCa cells. **(D)** Overexpression of DTX3L but not ARTD8 or ARTD9 also mediates cell migration of mPCa cells, dependent on STAT1 and STAT3-signaling. DTX3L might form migration-specific, ARTD9-independent STAT1 homodimer or non-canonical STAT1/STAT3 heterodimer complexes.

DTX3L/ARTD9-mediated effects on survival observed in the mPCa cell lines used in this study are only partially dependent on IRF1 in these cells. Thus, the DTX3L/ARTD8 and DTX3L/ARTD9 target genes, which act together with IRF1 in mediating survival and/or proliferation, respectively, remain to be identified in future studies.

Our results suggest that both DTX3L and ARTD9 may influence the nuclear activities of both STAT1α and STAT1β by antagonistically regulating the tyrosine phosphorylation of STAT1 on Y701 and therefore being required for the fine-tuning of STAT1-signaling, particularly in tumorigenesis (Figure 9C). Conversely, both DTX3L and ARTD9 cooperate in the transcriptional repression of IRF1. Thus, the exact molecular mechanisms are much more complicated and remain to be elucidated in future studies.

In addition to their regulatory roles in STAT1-mediated chemo-resistance, both DTX3L and ARTD9 could also be directly involved in editing or inhibiting the IFNγ-dependent host immune response against tumor cells through the termination of IFNγ-mediated gene expression and the inhibition of the extrinsic IFNγ-induced anti-proliferative and pro-apoptotic STAT1-IRF1-X-axis. Alternatively, the observed crosstalk between DTX3L/ARTD9 and ARTD8 in absence of IFNγ strongly indicates that DTX3L/ARTD9 and ARTD8 act independently of IFNγ-mediated signaling in cell proliferation and survival.

Our data provide first evidence for a crosstalk between mono-ubiquitin-ligase(s) and mono-ADP-ribosyltransferases that mediates proliferation and survival in mPCa and thus suggest that these processes might be tightly regulated by mono-ADP-ribosylation and (mono)-ubiquitination. However, the potential (mono)-ubiquitinylation activity of DTX3L and the exact molecular mechanisms of ARTD8-mediated mono-ADP-ribosylation underlying the observed crosstalk remain to be addressed in future studies.

Our *in vitro* study suggests that DTX3L together with STAT1 might be required for the metastasis and

dissemination of metastatic CRPC cells *in vivo* (Figure 9D). Thus, further studies need to be carried out in order to determine whether simultaneous ectopic co-overexpression of ARTD9 together with wild type or enzymatic mutant forms of DTX3L and/or ARTD8 in xenograft prostate tumors confer docetaxel resistance and/or enhance metastasis *in vivo*.

Taken together, our study suggests that the combined targeted inhibition of STAT1, ARTD8, ARTD9 and/or DTX3L could increase the efficacy of chemotherapy or radiation treatment in prostate and other high-risk tumor types with an increased STAT1- and STAT3-signaling. For instance, the combination of classical therapeutic drugs with highly ARTD8 or DTX3L-specific inhibitors and drugs specifically targeting STAT1 or the macrodomains of ARTD9 might provide a novel therapeutic strategy to increase the sensitivity of PCa cells towards classical therapy, and thus pave the way to develop novel personalized therapeutic strategies for patients suffering from aggressive PCa.

Material and methods

Cell culture, transfections, luciferase reporter assays and generation of stable cell lines

The CRPC-like mPCa cell lines PC3 and DU145 [54,61] as well as the JAK1-negative, poorly tumorigenic cell line LNCaP [54,61,67,68] were all purchased from ATCC (American Type Culture Collection). They were cultured in 50% Ham's-F12 and 50% of RPMI-1640, Glutamax-I, 10 mmol/l HEPES with 10% FCS, and Penicillin and Streptomycin. Transfections of cells with plasmid DNA were performed with Fugene HD, Extreme gene 9 and HP transfection reagents (Roche Applied Science) according to the manufacturers' protocols. Transfections of siRNA oligos were performed with Lipofectamine RNAimax (Invitrogen) or Extreme gene siRNA reagents (Roche Applied Science) according to manufacturers' protocols. For complementation of PC3-siARTD8 knockdown cells with non-degradable cDNAs of active ARTD8 wild type or catalytically inactive ARTD8 mutant form, transfections of cells with cDNAs were performed 24 h after transfection of siRNA oligos. Cells were generally treated/pretreated with siRNA oligos for 36-48 h before the assays were performed.

Plasmids

Human *DTX3L* cDNA was amplified by PCR from a B-cell Lymphoma cDNA library and cloned into the corresponding expression vectors (*EF1a*-promoter driven) using BamHI-NotI respectively. The mouse *ARTD8* cDNA was a generous gift from Dr. M. Boothby (Vanderbilt University School of Medicine, Nashville, TN, USA) and cloned into the corresponding expression vectors (*EF1a*-promoter driven) using BamHI-NotI respectively. The enzymatically inactive ARTD8 mutant form containing two mutations in the evolutionary conserved catalytic triad motif (H-Y-I < – > Q-Y-T; aa 1698H-Q and aa1798I-T) [38,96] was generated by PCR and verified by sequencing. The siRNA oligos were purchased from Qiagen. The corresponding siRNA sequences are listed in Additional file 11: Table S1. Expression vectors for STAT1 and ARTD9 are described in [23]. Expression vectors for human IRF1 were purchased from Addgene. *hIRF1*-prom-luciferase reporter vectors were a nice gift from Dr. R. Pine (Public Health Research Institute, Newark, NJ, USA).

Reagents

Human recombinant interferons were all purchased from PeproTech or kindly provided by Dr. J. Pavlovic (Institute of Medical Virology, University of Zurich, Switzerland), docetaxel and doxorubicin were purchased from SIGMA. Tosyl-activated Dynabeads were purchased from Invitrogen. ADP-ribose was purchased from SIGMA.

Interaction assays, immunoblot analyses and immunofluorescence microscopy

Membrane, cytoplasmic, nuclear, and whole cell extracts were prepared as described in [23,97,98]. For immunoprecipitation membrane and cytoplasmic extract fractions were re-mixed. Co-immunoprecipitation assays were performed as described previously [23,97,98] using the following DTX3L and ARTD9 specific antibodies: rabbit anti-DTX3L antibody Cat.No.: D9644-01B), rabbit anti-DTX3L antibody (Bethyl Laboratories, Inc., Cat.No.: A300-833A,) and rabbit anti-ARTD9 antibody (Chemicon/EMD Millipore, Cat.No.: AB10619, Lot No.: LV1409682). All antibodies used for immunoprecipitation analysis were covalently coupled to tosyl-activated Dynabeads (Invitrogen) according to the manufacturers' protocols. Immunoblot analysis and immunofluorescence microscopy were performed as described in [23,97,98] using the following primary antibodies: Rabbit anti-DTX3L (US Biological, Cat. No.: D9644-01B), rabbit anti-DTX3L, (Bethyl Laboratories, Inc., Cat.No.: A300-833A), rabbit anti-ARTD9 (EMD Millipore, Cat.No.: AB10618), rabbit anti-ARTD9 antibody (EMD Millipore, Cat.No.: AB10619), mouse anti-ARTD2 (EMD Millipore, Cat.No.: MABE18), rabbit anti-ARTD3 (Aviva Systems Biology Corp., Cat.No.: OAAB03449), rabbit anti-ARTD10 (Aviva Systems Biology Corp., Cat.No.: ARP42810_P050), rabbit anti-ARTD12 (Aviva Systems Biology Corp., Cat.No.: OAAB03451), rabbit anti-ARTD11 (Abgent, Cat.No.: AP6297a), rabbit anti-ARTD13 (GeneTex, Cat.No.: N3C2), anti-STAT1α/β (RabMab, Epitomics, Cat.No.: 2728–1), anti-pSTAT1α/β(Y701) (RabMab, Epitomics, Cat.No.: 2825–1), anti-pSTAT1α (S727) (RabMab, Epitomics, Cat.No.: 3324–1), anti-STAT2 (RabMab, Epitomics, Cat.No.: 1513–1), anti-STAT3α (RabMab, Epitomics, Cat.No.: 3566–1), anti-pSTAT3α(S727)

(RabMab, Epitomics, Cat.No.: 2236–1), anti-STAT5 (RabMab, Epitomics, Cat.No.: 1289–1), anti-pSTAT5(S726) (RabMab, Epitomics, Cat.No.: 5734–1), anti-STAT6 (RabMab, Epitomics, Cat.No.: 1505–1), anti-PTPN1 (RabMab, Epitomics, Cat.No.: 3774–1), anti-PTPN2 (RabMab, Epitomics, Cat.No.: 5790–1), anti-pJAK1 (RabMab, Epitomics, Cat.No.: 6518–1), anti-JAK1 (RabMab, Epitomics, Cat.No.: 2856–1), anti-IFNGR1 (RabMab, Epitomics, Cat.No.: 5697–1), anti-IFNGR2 (RabMab, Epitomics, Cat.No.: 7932–1), anti-IRF1 (RabMab, Cell Signaling Technology, Cat.No.: 8478), anti-STAT3α/β (RabMab, Cell Signaling Technology, Cat.No.: 12640), rabbit anti-pSTAT2(Y690) (St. Cruz Biotechnology, Inc., Cat.No.: sc-21689-R), rabbit anti-pSTAT6(Y641) (St. Cruz Biotechnology, Inc., Cat.No.: sc-101808) and mouse anti-tubulin (SIGMA, Cat.No.: T5 618). The rabbit anti-ARTD8 antibody was a generous gift from Dr. Avraham Raz (Karmanos Cancer Institute, School of Medicine, Wayne State University, Detroit, Michigan 48201, USA [99]). Immunofluorescence analysis was performed with an automated inverted research microscope system (Leica DMI6000B, Leica Microsystem). Composite images were generated by Adobe Photoshop software. Quantification of immunoblots was performed using the GelEval software (FrogDance Software Inc.) and mean value ± SE was calculated and plotted into graphs using the GraphPad Prism 5 software (GraphPad Software, Inc.).

Survival and proliferation assays

Cell viability and proliferation was assessed by trypan blue exclusion assays as described in [23]. For the cell viability and proliferation assays cells were seeded at 0.2×10^6 cells/well (PC3 and DU145) and 0.1×10^5 cells/well (LNCaP) in 6 well dishes 8-12 h prior to initiation of treatment and then incubated for 24 h in the presence of PBS, DMSO (mock-treated), IFNγ (200 U/ml) or docataxel (0.5-1 nM), ARTD/PARP inhibitors Olaparib (1 μM), Veliparib (1 μM), DPQ or TIQ-A (7.5 μM). Relative cell viability/proliferation and cell numbers are presented as means from three (PC3 and DU145) or two (LNCaP) independent experiments performed in triplicates ± SE. All data were analyzed with Excel (Microsoft Inc.) and GraphPad Prism 5 software. Analyzed data were plotted into graphs using the GraphPad Prism 5 software (GraphPad Software, Inc.).

Gene expression analysis

Total RNA was isolated using Trizol (Invitrogen) or Tri-Reagent (MRC, Inc) according to manufacturer's protocols. RNA was subsequently reverse-transcribed using the 'High-capacity cDNA reverse transcription kit (Applied Biosystems) according to manufacturer's protocols. Real-time (RT) qPCR was performed using the Rotor-Gene 3000 (Corbett Life Science, now Qiagen) and SYBR Green kit (Bioline) according to manufacturer's protocols using the RT-qPCR primers listed in Additional file 12: Table S2. Mean value ± SE was calculated and blotted into graphs with GraphPad Prism 5 software (GraphPad Software). Q-RT-PCR Primer sequences are shown in Additional file 12: Table S2.

Luciferase reporter assays

Luciferase reporter assays were performed as previously described [97] and according to manufacturer's protocol (Promega) using the dual luciferase assay kit (Promega) and a TECAN infinite M200 luminometer (Tecan Systems). Briefly, PC3 cells were seeded in 6-well plates at 0.4×10^6 cells/well and co-transfected with an *IRF1*-promoter-driven luciferase reporter vector (500 ng DNA/ml) along with expression vectors for DTX3L, ARTD9 and/or STAT1α/β (800 ng DNA/ml) and with the control reporter plasmid, pRL-hTK (100 ng/ml) (*hTK*-prom-renilla–luciferase control), and subsequently treated with or without IFNγ (200 U/ml) for 4 h. *IRF1*-promoter-luciferase activities were normalized to the luciferase activities of the internal *hTK*-prom-renilla-luciferase control and presented as mean from five independent experiments performed in triplicates. Statistical analysis was performed using the Student's t test. $^*P < 0.05$, $^{**}P < 0.001$ and $^{***}P < 0.0001$. For siRNA knockdown experiments, PC3 cells were co-transfected in serious: first with mock-siRNA, STAT1-siRNA, DTX3L-siRNA or ARTD9-siRNA and subsequently (24 h later) with an *IRF1*-promoter-driven luciferase reporter vector (500 ng DNA/ml) along with expression vectors for DTX 3L, ARTD9 and/or STAT1α/β (800 ng DNA/ml) and with the control reporter plasmid, pRL-hTK (100 ng DNA/ml).

Scratch wound healing migration assay

DU145 or PC3 cells were seeded into 6-well plates (0.2×10^6 cells/well) and transfected with siRNA as indicated. After 24 h the cells were trypsinized and 400'000 cells were pooled into one well. After 24–36 h when cells reached confluency, identical scratches were made in parallel wells using a 1000 μl plastic pipette tip. Non-adherent cells were removed by two washes. The closure of the scratch was analyzed under the microscope and images were captured at 0, 12, 24, and 36 h after incubation. Photographs were made with a Leica DMI6000B automated inverted research microscope system (Leica Microsystems) at indicated time points. The size of the uncovered areas was measured with Adobe Photoshop software and converted into percentages. For analysis of the migration potential mean values of three independent experiments were analyzed. Mean value ± SE was calculated and plotted into graphs with GraphPad Prism 5 software (GraphPad Software, Inc.).

Statistical analysis

Continuous variables were summarized as mean and SE. Statistical evaluations (comparisons between control and

treated groups) were established by Student's T-test for unpaired data (for two comparisons). P values < 0.05 were considered statistically significant. All statistical evaluations were performed with GraphPad Prism 5 software (GraphPad Software, Inc.).

Availability of supporting data

"The data set(s) supporting the results of this article is (are) included within the article (and its additional file(s))".

Additional files

Additional file 1: Figure S1. Quantification of ARTD9, DTX3L, IRF1, STAT1 and pSTAT1 protein levels. **(A)** Quantification of ARTD9 and DTX3L protein levels in PC3, DU145 and LNCaP cells, represented in Figure 1B. ARTD9 and DTX3L protein levels were normalized to tubulin. **(B)** Quantification of pSTAT1-Y701 and pSTAT1-S727 protein levels in PC3, DU145 and LNCaP cells, represented in Figure 1B. pSTAT1-Y701 and pSTAT1-S727 protein levels were normalized to tubulin and STAT1. All values represent the means of three independent experiments, and the error bars represent the SE. Statistical analysis was performed using the Student's t test. *$P < 0.05$, **$P < 0.001$ and ***$P < 0.0001$. **(C)** Immunoblot analyses of STAT signaling in PC3, DU145 and LNCaP cells treated with or without IFNγ (200 U/ml) or IFNαβ (50 U/ml each). Whole cell extracts were separated by SDS PAGE and subsequently probed with antibodies for STAT1αβ, pSTAT1(Y701), STAT2, pSTAT2(Y690), STAT3α, STAT3αβ, pSTAT3α(S727), STAT5αβ, pSTAT5 (S726), STAT6 and pSTAT6(Y641) and tubulin. **(D)** Immunoblot analyses of ARTD8, ARTD9 and DTX3L levels in PC3-siMock and PC3-siJAK1 cells. Whole cell extracts were separated by SDS PAGE, blotted and subsequently probed with antibodies for JAK1, ARTD8, ARTD9, DTX3L and tubulin. (**D** right panel) Analysis of JAK1- siRNA knockdown efficiency in PC3 cells; JAK1 protein levels were normalized to tubulin. **(E)** Immunoblot analyses of ARTD9 and DTX3L protein levels in PC3-siMock and PC3-siSTAT3 cells. Whole cell extracts were separated by SDS PAGE, blotted and subsequently probed with antibodies for ARTD9, DTX3L and tubulin. All immunoblots are representative of at least three independent experiments. (**E** right panel) Analysis of STAT3-siRNA knockdown efficiency in PC3 cells; Total RNA was isolated from PC3-siMock, and PC3-siSTAT3 cells and STAT3 mRNA levels were measured by RT-qPCR, normalized against GAPDH and presented as mean from three independent experiments performed in triplicate ± SE.

Additional file 2: Figure S2. Sub-cellular localization of endogenous STAT1 in DU145 and LNCaP cells and quantification of IRF1 protein levels in PC3, DU145 and LNCaP cells. **(A)** Immunofluorescence microscopy analyses and sub-cellular localization of endogenous STAT1, pSTAT1-(pY701) and pSTAT1-(pS727) in DU145 cells, in presence or absence of 1000 U/ml IFNγ. Original magnification × 400. Images are representative of at least three independent experiments. **(B)** Immunofluorescence microscopy analyses and sub-cellular localization of endogenous STAT1, pSTAT1-(pY701) and pSTAT1-(pS727) in LNCaP cells. Original magnification × 400. Images are representative of at least three independent experiments. **(C)** Quantification of IRF1 protein levels in PC3, DU145 and LNCaP cells, as represented in Figure 1C. IRF1 levels were normalized to tubulin. Values represent the means of three independent experiments, and the error bars represent the SE. Statistical analysis was performed using the Student's t test. *$P < 0.05$, **$P < 0.001$ and ***$P < 0.0001$, according to the t-test analysis.

Additional file 3: Figure S3. Sub-cellular localization of endogenous DTX3L and ARTD9 in PC3-siARTD9 or -siDTX3L knockdown cells, respectively. **(A)** Immunofluorescence microscopy analyses and sub-cellular localization of endogenous DTX3L and ARTD9 in PC3-siMock **(A)**, PC3-siDTX3L **(B)** and PC3-siARTD9 **(C)** knockdown cells in absence or presence of IFNγ (200 U/ml). Original magnification × 400. Images are representative of at least three independent experiments.

Additional file 4: Figure S4. Co-staining of endogenous DTX3L and ARTD9 in PC3-siARTD9 or -siDTX3L knockdown cells, respectively. **(A)** Co-staining and immunofluorescence microscopy analyses of endogenous DTX3L and ARTD9 in PC3-siMock **(A)**, PC3-siDTX3L **(B)** and PC3-siARTD9 **(C)** knockdown cells in absence or presence of IFNγ (200 U/ml). Cells were co-stained using a mouse monoclonal anti-DTX3L antibody (red) together with a rabbit polyclonal anti-ARTD9 antibody (green). Original magnification × 400.

Additional file 5: Figure S5. Quantifications of ARTD8-, ARTD9- and DTX3L-siRNA knockdown efficiencies and analysis of ARTD8, ARTD9 and DTX3L containing complexes. **(A and B)** Analysis of ARTD8, ARTD9 and DTX3L-siRNA knockdown efficiency in PC3 cells. **(A)** Gene expression analysis of ARTD8, ARTD9 and DTX3L in PC3-siMock, PC3-siARTD8, PC3-siARTD9 and PC3-siDTX3L cells, respectively. ARTD8, ARTD9 and DTX3L mRNA levels were measured by RT-qPCR, normalized against GAPDH and presented as mean from three independent experiments performed in triplicate ± SE. **(B)** Quantification of ARTD8, ARTD9 and DTX3L protein levels in in PC3-siMock, PC3-siARTD8, PC3-siARTD9 and PC3-siDTX3L cells, respectively. ARTD8, ARTD9 and DTX3L levels were normalized to tubulin. Values represent the means of three independent experiments, and the error bars represent the SE. **(C)** Co-immunoprecipitation control analyses to confirm the specificity of the anti- DTX3L antibody. **(D)** Interactions of endogenous ARDT8 with ARTDs but not with DTX3L are mediated by (mono)-ADP-ribosylation. Endogenous ARTD8-ARTDx and ARTD8-DTX3L complexes from PC3 cell extracts were co-immunoprecipitated in presence or absence of 5 mM mono-ADP-ribose using epitope affinity purified anti-ARTD8 antibodies. Complexes were then separated on SDS PAGE, blotted and subsequently probed with antibodies against endogenous ARTD1, ARTD8, ARTD9, ARTD10 and DTX3L. ARTD1 was used as a positive control for ARTD8 and ARTD9 [80] and ARTD10 was used as a positive control for ARTD8 [44]. **(E)** Interactions of endogenous ARDT9 with ARTDs are mediated by (mono)-ADP-ribosylation. PC3 cells were stimulated for 1 h with IFNγ (200 U/ml) and endogenous ARTD9-ARTDx complexes subsequently co-immunoprecipitated in presence or absence of 5 mM mono-ADP-ribose using epitope affinity purified anti-ARTD9 antibodies. Complexes were then separated on SDS PAGE, blotted and subsequently probed with antibodies against endogenous ARTD9, ARTD10, ARTD12 (also known as PARP12) and ARTD13 (also known as PARP13, ZAPS/L). **(F)** Co-immunoprecipitation control analyses to confirm the specificity of the anti-ARTD9 antibody.

Additional file 6: Figure S6. Cell viability and proliferation analyses of siDTX3L, siARTD8 and siARTD9 single knockdown cells. **(A and B)** Cell viability analyses of PC3-siMock, PC3-siDTX3L cells silenced with si*1 or si*2 RNA oligos **(A)** and PC3-siARTD9 cells silenced with si*1 or si*9 RNA oligos **(B)** were assessed by the trypan blue exclusion assay. Cells were treated as indicated with IFNγ and/or docetaxel (DT) and counted after 48 h. Values represent the means of three independent experiments, and the error bars represent the SE. **(C and D)** Immunoblot analyses of ARTD9- and DTX3L-siRNA knockdown efficiencies in DU145 cells. Whole cell extracts were separated by SDS PAGE, blotted and subsequently probed with antibodies for ARTD9 **(C)**, DTX3L **(D)** and tubulin. **(E)** Cell proliferation analyses of DU145-siMock, DU145-siDTX3L and DU145-siARTD9 single knockdown cells in presence or absence of IFNγ (200 U/ml) was assessed by the trypan blue exclusion assay. **(F)** Cell viability analyses of DU145-siMock, DU145-siDTX3L and DU145-siARTD9 knockdown cells were assessed by the trypan blue exclusion assay. Cells were treated as indicated with IFNγ and/or docetaxel (DT) and counted after 48 h, NT: not treated, CT: control treatment (solvent). **(G)** Survival of PC3-siMock or PC3- siARTD8 knockdown cells, complemented with non-degradable mouse cDNAs of active ARTD8 wild type or catalytically inactive ARTD8 mutant form, respectively, were assessed by the trypan blue exclusion assay. Cells were treated as indicated with docetaxel (DT) and/or with the ARTD inhibitor TIQ, CT: control treatment (solvent), EV: empty vector control. All Values shown in **E** to **G** represent the means of three independent experiments performed in triplicates, and the error bars represent the SE. Statistical analysis was performed using the Student's t test. *$P < 0.05$, **$P < 0.001$ and ***$P < 0.0001$.

Additional file 7: Figure S7. Quantifications of STAT1-siRNA knockdown efficiencies and *IRF1* promoter analysis **(A and B)**. Analysis of STAT1-siRNA efficiency in PC3 cells. **(A)** Gene expression analysis of STAT1 in PC3-siMock and PC3-siSTAT1 knockdown cells; Total RNA was isolated from PC3-siMock and PC3-siSTAT1 knockdown cells and STAT1 mRNA levels were measured by RT-qPCR and normalized against GAPDH. **(B)** Quantification of STAT1 protein levels in PC3-siMock and PC3-siSTAT1 knockdown cells; STAT1 levels

were normalized to tubulin. **(C)** Gene expression analysis of IRF1 in PC3-siMock, PC3-siARTD9 and PC3-siDTX3L knockdown cells. Total RNA was isolated from PC3-siMock, PC3-siARTD9 and PC3-siDTX3L knockdown cells and IRF1 mRNA levels were measured by RT-qPCR and normalized against GAPDH. All Values shown in **A** to **C** represent the means of three independent experiments, and the error bars represent the SE. **(D)** DTX3L- iRNA and ARTD9-siRNA mediated activation of the *IRF1*-promoter driven luciferase in PC3 cells. PC3 cells were co-transfected in series with mock-siRNA, STAT1-siRNA, DTX3L-siRNA or ARTD9-siRNA and plasmids for an *IRF1*-promoter-driven luciferase reporter vector as described in Material and Methods and subsequently treated with or without IFNγ (200 U/ml) for 4 h. **(E-G)** DTX3L and ARTD9 together with STAT1β inhibit the *IRF1*-promoter driven luciferase in PC3 cells. PC3 cells were co-transfected with an *IRF1*-promoter-driven luciferase reporter vector along with expression vectors for DTX3L, ARTD9 and/or STAT1α/β and subsequently treated with or without IFNγ (200 U/ml) for 4 h. *IRF1*-promoter-luciferase activities shown in D to G are presented as mean from five independent experiments performed in triplicates. The error bar represents the SE. Statistical analysis was performed using the Student's t test. $*P < 0.05$, $**P < 0.001$ and $***P < 0.0001$.

Additional file 8: Figure S8. Quantifications of IRF1 protein levels, quantifications of IRF1-siRNA knockdown efficiencies and cell viability analysis of siIRF1 knockdown cells. **(A)** Immunoblot analyses of IRF1 protein levels in PC3-CMVprom-empty-control and PC3-CMVprom-IRF1 cells. Whole cell extracts of PC3-CMVprom-empty-control and PC3-CMVprom7 IRF1 cells were separated by SDS PAGE, blotted and probed with antibodies for IRF1 and tubulin. (**A** right panel) Quantification of IRF1 protein levels in PC3-CMVprom-empty-control and PC3-CMVprom-IRF1 cells; IRF1 levels were normalized to tubulin. **(B and C)** Analysis of IRF1- siRNA efficiency in PC3 cells. **(B)** Immunoblot analyses of IRF1 protein levels in PC3-siMock and PC3-siIRF1 cells. Whole cell extracts of PC3-siMock and PC3-siIRF1 cells were separated by SDS PAGE, blotted and probed with antibodies for IRF1 and tubulin. (**B** right panel) Quantification of IRF1 protein levels in PC3-simock and PC3-siIRF1 cells; IRF1 levels were normalized to tubulin. **(C)** Gene expression analysis of IRF1 in PC3-siMock and PC3-siIRF1 knockdown cells. IRF1 mRNA levels were measured by RT-qPCR and normalized against GAPDH. **(D)** Gene expression analysis of IRF1 in LNCaP-siMock and LNCaP-siIRF1 knockdown cells. IRF1 mRNA levels were measured by RT-qPCR and normalized against GAPDH. **(E)** Cell viability analyses of PC3-siMock, PC3-siIRF1, PC3-siARTD9 and PC3-siARTD9/siIRF1 cells were assessed by the trypan blue exclusion assay. Cells were treated as indicated with 50 ng/ml IFNγ and 0.25 μM doxorubicin **(D)** and counted after 48 h and 72 h, respectively, NT: not treated, CT: control treatment (solvent). All values shown in A to E represent the means of three independent experiments, and the error bars represent the SE. Statistical analysis was performed using the Student's t test. $*P < 0.05$, $**P < 0.001$ and $***P < 0.0001$. **(F)** Co-immunoprecipitation analyses of endogenous nuclear DTX3L/ARTD9/STAT1 complexes, respectively in PC3 cells. Endogenous STAT1, DTX3L or RTD9 complexes were co-immunoprecipitated from nuclear extracts using anti-ARTD9 antibodies and separated on SDS PAGE, blotted and probed with antibodies for STAT1, DTX3L and ARTD9.

Additional file 9: Figure S9. Photographs and quantification of cell migration in siARTD8, siARTD9 and siDTX3L single knockdown prostate cancer cells. **(A-D)** Photographs of cell migration in PC3 prostate cancer cells. PC3-siMock **(A)**, PC3-siDTX3L **(B)**, PC3-siARTD9 **(C)** and PC3-siARTD8 **(D)** single knockdown cells were seeded into 6-well plates and treated as described in Material and Methods. At 0, 12, 24, and 36 h photographs were made. **(E and F)** Quantification of cell migration in DU145 prostate cancer cells. DU145-siDTX3L **(E)** and DU145-siARTD9 **(F)** single knockdown cells were seeded into 6-well plates and treated as described in Material and Methods. At 0, 12, 24, and 36 h photographs were made and quantified as described in Material and Methods. Values represent the mean of three independent experiments and the error bars represent the SE. Statistical analysis was performed using the Student's t test. $*P < 0.05$, $**P < 0.001$ and $***P < 0.0001$.

Additional file 10: Figure S10. Photographs and quantification of cell migration in single, double and triple knockdown prostate cancer cells. **(A-C)** Photographs of cell migration in PC3 prostate cancer cells. PC3-siSTAT1 **(A)** PC3-siDTX3L/siSTAT1 **(B)** and PC3-siSTAT3 **(C)** single knockdown cells were seeded into 6-well plates and treated as described in Material and Methods. At 0, 12, 24, and 36 h photographs were made. **(D-F)** Quantification of cell migration in PC3 and DU145 prostate cancer cells. PC3-siIRF1 **(D)**, DU145-siSTAT1 **(E)** and DU145-siSTAT3 **(F)** single knockdown cells, DU145-siSTAT1/siSTAT3 **(G)** double knockdown cells and DU145-siDTX3L/siSTAT1/siSTAT3 (H) triple knockdown cells were seeded into 6-well plates and treated as described in Material and Methods. At 0, 12, 24, and 36 h photographs were made and quantified as described in Material and Methods. Values represent the mean of three independent experiments and the error bars represent the SE. Statistical analysis was performed using the Student's t test. $*P < 0.05$, $**P < 0.001$ and $***P < 0.0001$.

Additional file 11: Table S1. siRNA sequences.

Additional file 12: Table S2. qPCR Primer.

Competing interests
The authors declare no competing financial and non-financial interests.

Authors' contributions
Contribution: SBB, SCF, RC, HCW and POH designed the experiments and analyzed results. SBB, RC, HCW, SCF, RS and POH performed the research; SBB, SCF and POH wrote the paper. POH designed and supervised the research study. All the authors read and corrected the manuscript. All authors read and approved the final manuscript.

Acknowledgements
We are grateful to Drs. R. Pine (Public Health Research Institute, Newark, NJ, USA), J. Pavlovic (Institute of Medical Virology, University of Zurich, Switzerland), P. Richards and A.N. Tiaden (Competence Center for Applied Biotechnology and Molecular Medicine (CABMM)), University of Zurich, Switzerland), M. Boothby (Vanderbilt University School of Medicine, Nashville, TN USA), B. Lüscher (RWTH Aachen University, Aachen, Germany), A. Bradley (Wellcome Trust Sanger Institute, UK) and A. Raz (Wayne State University, Michigan USA) for providing cells, plasmids and reagents. We also thank all the members of the Institute of Veterinary Biochemistry and Molecular Biology (University of Zurich, Switzerland) and of the Competence Center for Applied Biotechnology and Molecular Medicine (CABMM)), University of Zurich, Switzerland) for reagents, helpful advice and discussions. This work was supported by the Swiss National Science Foundation (SNF-31003A_125190) (to P.O.H, R.C. and H.C.W), Novartis Foundation for medical-biological research (Nr. 10C63) (to P.O.H.) by the Oncosuisse Foundation (KFS-02732-02) (to S.C.F and R.S) and by the Kanton of Zurich (to P.O.H.).

Author details
[1]Institute of Veterinary Biochemistry and Molecular Biology, University of Zurich, Winterthurerstrasse 190, 8057 Zurich, Switzerland. [2]Molecular Life Science Program, Life Science Zurich Graduate School, University of Zurich, Winterthurerstrasse 190, 8057 Zurich, Switzerland. [3]Stem Cell Research Laboratory, NHS Blood and Transplant, Nuffield Division of Clinical Laboratory Sciences, Radcliffe Department of Medicine, University of Oxford, Oxford OX3 9DU, UK. [4]Institute of Pharmacology and Toxicology, Vetsuisse Faculty, University of Zurich, Winterthurerstrasse 260, 8057 Zurich, Switzerland.

Received: 12 February 2014 Accepted: 7 May 2014
Published: 27 May 2014

References
1. Shen MM, Abate-Shen C: **Molecular genetics of prostate cancer: new prospects for old challenges.** *Genes Dev* 2010, **24**(18):1967–2000.
2. Wegiel B, Evans S, Hellsten R, Otterbein LE, Bjartell A, Persson JL: **Molecular pathways in the progression of hormone-independent and metastatic prostate cancer.** *Curr Cancer Drug Targets* 2010, **10**(4):392–401.
3. Berger MF, Lawrence MS, Demichelis F, Drier Y, Cibulskis K, Sivachenko AY, Sboner A, Esgueva R, Pflueger D, Sougnez C, Onofrio R, Carter SL, Park K, Habegger L, Ambrogio L, Fennell T, Parkin M, Saksena G, Voet D, Ramos AH, Pugh TJ, Wilkinson J, Fisher S, Winckler W, Mahan S, Ardlie K, Baldwin J, Simons JW, Kitabayashi N, MacDonald TY, *et al*: **The genomic complexity of primary human prostate cancer.** *Nature* 2011, **470**(7333):214–220.
4. Cheng L, Montironi R, Bostwick DG, Lopez-Beltran A, Berney DM: **Staging of prostate cancer.** *Histopathology* 2012, **60**(1):87–117.
5. Rubin MA, Maher CA, Chinnaiyan AM: **Common gene rearrangements in prostate cancer.** *J Clin Oncol* 2011, **29**(27):3659–3668.

6. Ahonen TJ, Xie J, LeBaron MJ, Zhu J, Nurmi M, Alanen K, Rui H, Nevalainen MT: **Inhibition of transcription factor Stat5 induces cell death of human prostate cancer cells.** *J Biol Chem* 2003, **278**(29):27287–27292.
7. Abdulghani J, Gu L, Dagvadorj A, Lutz J, Leiby B, Bonuccelli G, Lisanti MP, Zellweger T, Alanen K, Mirtti T, Visakorpi T, Bubendorf L, Nevalainen MT: **Stat3 promotes metastatic progression of prostate cancer.** *Am J Pathol* 2008, **172**(6):1717–1728.
8. Battle TE, Frank DA: **The role of STATs in apoptosis.** *Curr Mol Med* 2002, **2**(4):381–392.
9. Gritsko T, Williams A, Turkson J, Kaneko S, Bowman T, Huang M, Nam S, Eweis I, Diaz N, Sullivan D, Yoder S, Enkemann S, Eschrich S, Lee JH, Bearn CA, Cheng J, Minton S, Muro-Cacho CA, Jove R: **Persistent activation of stat3 signaling induces survivin gene expression and confers resistance to apoptosis in human breast cancer cells.** *Clin Cancer Res* 2006, **12**(1):11–19.
10. Yu H, Jove R: **The STATs of cancer–new molecular targets come of age.** *Nat Rev Cancer* 2004, **4**(2):97–105.
11. Khodarev NN, Minn AJ, Efimova EV, Darga TE, Labay E, Beckett M, Mauceri HJ, Roizman B, Weichselbaum RR: **Signal transducer and activator of transcription 1 regulates both cytotoxic and prosurvival functions in tumor cells.** *Cancer Res* 2007, **67**(19):9214–9220.
12. Khodarev NN, Roizman B, Weichselbaum RR: **Molecular pathways: interferon/stat1 pathway: role in the tumor resistance to genotoxic stress and aggressive growth.** *Clin Cancer Res* 2012, **18**(11):3015–3021.
13. Tsai MH, Cook JA, Chandramouli GV, DeGraff W, Yan H, Zhao S, Coleman CN, Mitchell JB, Chuang EY: **Gene expression profiling of breast, prostate, and glioma cells following single versus fractionated doses of radiation.** *Cancer Res* 2007, **67**(8):3845–3852.
14. Weichselbaum RR, Ishwaran H, Yoon T, Nuyten DS, Baker SW, Khodarev N, Su AW, Shaikh AY, Roach P, Kreike B, Roizman B, Bergh J, Pawitan Y, van de Vijver MJ, Minn AJ: **An interferon-related gene signature for DNA damage resistance is a predictive marker for chemotherapy and radiation for breast cancer.** *Proc Natl Acad Sci U S A* 2008, **105**(47):18490–18495.
15. Patterson SG, Wei S, Chen X, Sallman DA, Gilvary DL, Zhong B, Pow-Sang J, Yeatman T, Djeu JY: **Novel role of Stat1 in the development of docetaxel resistance in prostate tumor cells.** *Oncogene* 2006, **25**(45):6113–6122.
16. Pitroda SP, Wakim BT, Sood RF, Beveridge MG, Beckett MA, MacDermed DM, Weichselbaum RR, Khodarev NN: **STAT1-dependent expression of energy metabolic pathways links tumour growth and radioresistance to the Warburg effect.** *BMC Med* 2009, **7**:68.
17. Cochet O, Frelin C, Peyron JF, Imbert V: **Constitutive activation of STAT proteins in the HDLM-2 and L540 Hodgkin lymphoma-derived cell lines supports cell survival.** *Cell Signal* 2006, **18**(4):449–455.
18. El-Hashemite N, Zhang H, Walker V, Hoffmeister KM, Kwiatkowski DJ: **Perturbed IFN-gamma-Jak-signal transducers and activators of transcription signaling in tuberous sclerosis mouse models: synergistic effects of rapamycin-IFN-gamma treatment.** *Cancer Res* 2004, **64**(10):3436–3443.
19. Legrand A, Vadrot N, Lardeux B, Bringuier AF, Guillot R, Feldmann G: **Study of the effects of interferon a on several human hepatoma cell lines: analysis of the signalling pathway of the cytokine and of its effects on apoptosis and cell proliferation.** *Liver Int* 2004, **24**(2):149–160.
20. Greenwood C, Metodieva G, Al-Janabi K, Lausen B, Alldridge L, Leng L, Bucala R, Fernandez N, Metodiev MV: **Stat1 and CD74 overexpression is co-dependent and linked to increased invasion and lymph node metastasis in triple-negative breast cancer.** *J Proteomics* 2012, **75**(10):3031–3040.
21. Sun Y, Cheng MK, Griffiths TR, Mellon JK, Kai B, Kriajevska M, Manson MM: **Inhibition of STAT signalling in bladder cancer by diindolylmethane: relevance to cell adhesion, migration and proliferation.** *Curr Cancer Drug Targets* 2013, **13**(1):57–68.
22. Magkou C, Giannopoulou I, Theohari I, Fytou A, Rafailidis P, Nomikos A, Papadimitriou C, Nakopoulou L: **Prognostic significance of phosphorylated STAT-1 expression in premenopausal and postmenopausal patients with invasive breast cancer.** *Histopathology* 2012, **60**(7):1125–1132.
23. Camicia R, Bachmann SB, Winkler HC, Beer M, Tinguely M, Haralambieva E, Hassa PO: **BAL1/ARTD9 represses the anti-proliferative and pro-apoptotic IFNgamma-STAT1-IRF1-p53 axis in diffuse large B-cell lymphoma.** *J Cell Sci* 2013, **126**(Pt 9):1969–1980.
24. Stephanou A, Latchman DS: **STAT-1: a novel regulator of apoptosis.** *Int J Exp Pathol* 2003, **84**(6):239–244.
25. Townsend PA, Scarabelli TM, Davidson SM, Knight RA, Latchman DS, Stephanou A: **STAT-1 interacts with p53 to enhance DNA damage-induced apoptosis.** *J Biol Chem* 2004, **279**(7):5811–5820.
26. Taniguchi T, Ogasawara K, Takaoka A, Tanaka N: **IRF family of transcription factors as regulators of host defense.** *Annu Rev Immunol* 2001, **19**:623–655.
27. Romeo G, Fiorucci G, Chiantore MV, Percario ZA, Vannucchi S, Affabris E: **IRF-1 as a negative regulator of cell proliferation.** *J Interferon Cytokine Res* 2002, **22**(1):39–47.
28. Dunn GP, Koebel CM, Schreiber RD: **Interferons, immunity and cancer immunoediting.** *Nat Rev Immunol* 2006, **6**(11):836–848.
29. Meyer T, Hendry L, Begitt A, John S, Vinkemeier U: **A single residue modulates tyrosine dephosphorylation, oligomerization, and nuclear accumulation of stat transcription factors.** *J Biol Chem* 2004, **279**(18):18998–19007.
30. Meyer T, Vinkemeier U: **Nucleocytoplasmic shuttling of STAT transcription factors.** *Eur J Biochem* 2004, **271**(23–24):4606–4612.
31. Lodige I, Marg A, Wiesner B, Malecova B, Oelgeschlager T, Vinkemeier U: **Nuclear export determines the cytokine sensitivity of STAT transcription factors.** *J Biol Chem* 2005, **280**(52):43087–43099.
32. Khodarev NN, Roach P, Pitroda SP, Golden DW, Bhayani M, Shao MY, Darga TE, Beveridge MG, Sood RF, Sutton HG, Beckett MA, Mauceri HJ, Posner MC, Weichselbaum RR: **STAT1 pathway mediates amplification of metastatic potential and resistance to therapy.** *PLoS One* 2009, **4**(6):e5821.
33. Huisman MT, Chhatta AA, van Tellingen O, Beijnen JH, Schinkel AH: **MRP2 (ABCC2) transports taxanes and confers paditaxel resistance and both processes are stimulated by probenecid.** *Int J Cancer* 2005, **116**(5):824–829.
34. van Brussel JP, van Steenbrugge GJ, Romijn JC, Schroder FH, Mickisch GH: **Chemosensitivity of prostate cancer cell lines and expression of multidrug resistance-related proteins.** *Eur J Cancer* 1999, **35**(4):664–671.
35. Zalcberg J, Hu XF, Slater A, Parisot J, El-Osta S, Kantharidis P, Chou ST, Parkin JD: **MRP1 not MDR1 gene expression is the predominant mechanism of acquired multidrug resistance in two prostate carcinoma cell lines.** *Prostate Cancer Prostatic Dis* 2000, **3**(2):66–75.
36. Zhong B, Sallman DA, Gilvary DL, Pernazza D, Sahakian E, Fritz D, Cheng JQ, Trougakos I, Wei S, Djeu JY: **Induction of clusterin by AKT–role in cytoprotection against docetaxel in prostate tumor cells.** *Mol Cancer Ther* 2010, **9**(6):1831–1841.
37. Hatano K, Yamaguchi S, Nimura K, Murakami K, Nagahara A, Fujita K, Uemura M, Nakai Y, Tsuchiya M, Nakayama M, Nonomura N, Kaneda Y: **Residual Prostate Cancer Cells after Docetaxel Therapy Increase the Tumorigenic Potential via Constitutive Signaling of CXCR4, ERK1/2 and c-Myc.** *Mol Cancer Res* 2013, **11**(9):1088–1100.
38. Hottiger MO, Hassa PO, Luscher B, Schuler H, Koch-Nolte F: **Toward a unified nomenclature for mammalian ADP-ribosyltransferases.** *Trends Biochem Sci* 2010, **35**(4):208–219.
39. Cho SH, Goenka S, Henttinen T, Gudapati P, Reinikainen A, Eischen CM, Lahesmaa R, Boothby M: **PARP-14, a member of the B aggressive lymphoma family, transduces survival signals in primary B cells.** *Blood* 2009, **113**(11):2416–2425.
40. Goenka S, Boothby M: **Selective potentiation of Stat-dependent gene expression by collaborator of Stat6 (CoaSt6), a transcriptional cofactor.** *Proc Natl Acad Sci U S A* 2006, **103**(11):4210–4215.
41. Goenka S, Cho SH, Boothby M: **Collaborator of Stat6 (CoaSt6)-associated poly(ADP-ribose) polymerase activity modulates Stat6-dependent gene transcription.** *J Biol Chem* 2007, **282**(26):18732–18739.
42. Timinszky G, Till S, Hassa PO, Hothorn M, Kustatscher G, Nijmeijer B, Colombelli J, Altmeyer M, Stelzer EH, Scheffzek K, Hottiger MO, Ladurner AG: **A macrodomain-containing histone rearranges chromatin upon sensing PARP1 activation.** *Nat Struct Mol Biol* 2009, **16**(9):923–929.
43. Moyle PM, Muir TW: **Method for the synthesis of mono-ADP-ribose conjugated peptides.** *J Am Chem Soc* 2010, **132**(45):15878–15880.
44. Forst AH, Karlberg T, Herzog N, Thorsell AG, Gross A, Feijs KL, Verheugd P, Kursula P, Nijmeijer B, Kremmer E, Kleine H, Ladurner AG, Schuler H, Luscher B: **Recognition of mono-ADP-ribosylated ARTD10 substrates by ARTD8 macrodomains.** *Structure* 2013, **21**(3):462–475.
45. Cho SH, Ahn AK, Bhargava P, Lee CH, Eischen CM, McGuinness O, Boothby M: **Glycolytic rate and lymphomagenesis depend on PARP14, an ADP ribosyltransferase of the B aggressive lymphoma (BAL) family.** *Proc Natl Acad Sci U S A* 2011, **108**(38):15972–15977.
46. Barbarulo A, Iansante V, Chaidos A, Naresh K, Rahemtulla A, Franzoso G, Karadimitris A, Haskard DO, Papa S, Bubici C: **Poly(ADP-ribose) polymerase family member 14 (PARP14) is a novel effector of the JNK2-dependent pro-survival signal in multiple myeloma.** *Oncogene* 2012, **32**(36):4231–4242.

47. Takeyama K, Aguiar RC, Gu L, He C, Freeman GJ, Kutok JL, Aster JC, Shipp MA: **The BAL-binding protein BBAP and related Deltex family members exhibit ubiquitin-protein isopeptide ligase activity.** *J Biol Chem* 2003, **278**(24):21930–21937.
48. Juszczynski P, Kutok JL, Li C, Mitra J, Aguiar RC, Shipp MA: **BAL1 and BBAP are regulated by a gamma interferon-responsive bidirectional promoter and are overexpressed in diffuse large B-cell lymphomas with a prominent inflammatory infiltrate.** *Mol Cell Biol* 2006, **26**(14):5348–5359.
49. Obiero J, Walker JR, Dhe-Paganon S: **Fold of the conserved DTC domain in Deltex proteins.** *Proteins* 2012, **80**(5):1495–1499.
50. Grunewald TG, Diebold I, Esposito I, Plehm S, Hauer K, Thiel U, da Silva-Buttkus P, Neff F, Unland R, Muller-Tidow C, Zobywalski C, Lohrig K, Lewandrowski U, Sickmann A: **Prazeres da Costa O, Gorlach A, Cossarizza A, Butt E, Richter GH, Burdach S: STEAP1 is associated with the invasive and oxidative stress phenotype of Ewing tumors.** *Mol Cancer Res* 2012, **10**(1):52–65.
51. Wilting SM, de Wilde J, Meijer CJ, Berkhof J, Yi Y, van Wieringen WN, Braakhuis BJ, Meijer GA, Ylstra B, Snijders PJ, Steenbergen RD: **Integrated genomic and transcriptional profiling identifies chromosomal loci with altered gene expression in cervical cancer.** *Genes Chromosomes Cancer* 2008, **47**(10):890–905.
52. Sun W, Gaykalova DA, Ochs MF, Mambo E, Arnaoutakis D, Liu Y, Loyo M, Agrawal N, Howard J, Li R, Ahn S, Fertig E, Sidransky D, Houghton J, Buddavarapu K, Sanford T, Choudhary A, Darden W, Adai A, Latham G, Bishop J, Sharma R, Westra WH, Hennessey P, Chung CH, Califano JA: **Activation of the NOTCH pathway in head and neck cancer.** *Cancer Res* 2014, **74**(4):1091–1104.
53. Yan Q, Dutt S, Xu R, Graves K, Juszczynski P, Manis JP, Shipp MA: **BBAP monoubiquitylates histone H4 at lysine 91 and selectively modulates the DNA damage response.** *Mol Cell* 2009, **36**(1):110–120.
54. Slack JK, Adams RB, Rovin JD, Bissonette EA, Stoker CE, Parsons JT: **Alterations in the focal adhesion kinase/Src signal transduction pathway correlate with increased migratory capacity of prostate carcinoma cells.** *Oncogene* 2001, **20**(10):1152–1163.
55. Wu HC, Hsieh JT, Gleave ME, Brown NM, Pathak S, Chung LW: **Derivation of androgen-independent human LNCaP prostatic cancer cell sublines: role of bone stromal cells.** *Int J Cancer* 1994, **57**(3):406–412.
56. Horoszewicz JS, Leong SS, Chu TM, Wajsman ZL, Friedman M, Papsidero L, Kim U, Chai LS, Kakati S, Arya SK, Sandberg AA: **The LNCaP cell line–a new model for studies on human prostatic carcinoma.** *Prog Clin Biol Res* 1980, **37**:115–132.
57. Horoszewicz JS, Leong SS, Kawinski E, Karr JP, Rosenthal H, Chu TM, Mirand EA, Murphy GP: **LNCaP model of human prostatic carcinoma.** *Cancer Res* 1983, **43**(4):1809–1818.
58. Kaighn ME, Narayan KS, Ohnuki Y, Lechner JF, Jones LW: **Establishment and characterization of a human prostatic carcinoma cell line (PC-3).** *Invest Urol* 1979, **17**(1):16–23.
59. Stone KR, Mickey DD, Wunderli H, Mickey GH, Paulson DF: **Isolation of a human prostate carcinoma cell line (DU 145).** *Int J Cancer* 1978, **21**(3):274–281.
60. Singh PP, Joshi S, Russell PJ, Verma ND, Wang X, Khatri A: **Molecular chemotherapy and chemotherapy: a new front against late-stage hormone-refractory prostate cancer.** *Clin Cancer Res* 2011, **17**(12):4006–4018.
61. Ranasinghe WK, Xiao L, Kovac S, Chang M, Michiels C, Bolton D, Shulkes A, Baldwin GS, Patel O: **The role of hypoxia-inducible factor 1alpha in determining the properties of castrate-resistant prostate cancers.** *PLoS One* 2013, **8**(1):e54251.
62. Hoosein NM, Boyd DD, Hollas WJ, Mazar A, Henkin J, Chung LW: **Involvement of urokinase and its receptor in the invasiveness of human prostatic carcinoma cell lines.** *Cancer Commun* 1991, **3**(8):255–264.
63. Tremblay L, Hauck W, Aprikian AG, Begin LR, Chapdelaine A, Chevalier S: **Focal adhesion kinase (pp125FAK) expression, activation and association with paxillin and p50CSK in human metastatic prostate carcinoma.** *Int J Cancer* 1996, **68**(2):164–171.
64. Tremblay L, Hauck W, Nguyen LT, Allard P, Landry F, Chapdelaine A, Chevalier S: **Regulation and activation of focal adhesion kinase and paxillin during the adhesion, proliferation, and differentiation of prostatic epithelial cells in vitro and in vivo.** *Mol Endocrinol* 1996, **10**(8):1010–1020.
65. Keer HN, Gaylis FD, Kozlowski JM, Kwaan HC, Bauer KD, Sinha AA, Wilson MJ: **Heterogeneity in plasminogen activator (PA) levels in human prostate cancer cell lines: increased PA activity correlates with biologically aggressive behavior.** *Prostate* 1991, **18**(3):201–214.
66. Erb HH, Langlechner RV, Moser PL, Handle F, Casneuf T, Verstraeten K, Schlick B, Schafer G, Hall B, Sasser K, Culig Z, Santer FR: **IL6 sensitizes prostate cancer to the antiproliferative effect of IFNalpha2 through IRF9.** *Endocr Relat Cancer* 2013, **20**(5):677–689.
67. Dunn GP, Sheehan KC, Old LJ, Schreiber RD: **IFN unresponsiveness in LNCaP cells due to the lack of JAK1 gene expression.** *Cancer Res* 2005, **65**(8):3447–3453.
68. Rossi MR, Hawthorn L, Platt J, Burkhardt T, Cowell JK, Ionov Y: **Identification of inactivating mutations in the JAK1, SYNJ2, and CLPTM1 genes in prostate cancer cells using inhibition of nonsense-mediated decay and microarray analysis.** *Cancer Genet Cytogenet* 2005, **161**(2):97–103.
69. Regis G, Pensa S, Boselli D, Novelli F, Poli V: **Ups and downs: the STAT1: STAT3 seesaw of Interferon and gp130 receptor signalling.** *Semin Cell Dev Biol* 2008, **19**(4):351–359.
70. Sikorski K, Czerwoniec A, Bujnicki JM, Wesoly J, Bluyssen HA: **STAT1 as a novel therapeutical target in pro-atherogenic signal integration of IFNgamma, TLR4 and IL-6 in vascular disease.** *Cytokine Growth Factor Rev* 2011, **22**(4):211–219.
71. Qing Y, Stark GR: **Alternative activation of STAT1 and STAT3 in response to interferon-gamma.** *J Biol Chem* 2004, **279**(40):41679–41685.
72. Schiavone D, Avalle L, Dewilde S, Poli V: **The immediate early genes Fos and Egr1 become STAT1 transcriptional targets in the absence of STAT3.** *FEBS Lett* 2011, **585**(15):2455–2460.
73. Decker T, Kovarik P: **Serine phosphorylation of STATs.** *Oncogene* 2000, **19**(21):2628–2637.
74. Stancato LF, David M, Carter-Su C, Larner AC, Pratt WB: **Preassociation of STAT1 with STAT2 and STAT3 in separate signalling complexes prior to cytokine stimulation.** *J Biol Chem* 1996, **271**(8):4134–4137.
75. Djeu JY, Wei S: **Clusterin and chemoresistance.** *Adv Cancer Res* 2009, **105**:77–92.
76. Epling-Burnette PK, Zhong B, Bai F, Jiang K, Bailey RD, Garcia R, Jove R, Djeu JY, Loughran TP Jr, Wei S: **Cooperative regulation of Mcl-1 by Janus kinase/stat and phosphatidylinositol 3-kinase contribute to granulocyte-macrophage colony-stimulating factor-delayed apoptosis in human neutrophils.** *J Immunol* 2001, **166**(12):7486–7495.
77. Sallman DA, Chen X, Zhong B, Gilvary DL, Zhou J, Wei S, Djeu JY: **Clusterin mediates TRAIL resistance in prostate tumor cells.** *Mol Cancer Ther* 2007, **6**(11):2938–2947.
78. Shou J, Soriano R, Hayward SW, Cunha GR, Williams PM, Gao WQ: **Expression profiling of a human cell line model of prostatic cancer reveals a direct involvement of interferon signaling in prostate tumor progression.** *Proc Natl Acad Sci U S A* 2002, **99**(5):2830–2835.
79. Sokoloff MH, Tso CL, Kaboo R, Taneja S, Pang S, de Kernion JB, Belldegrun AS: **In vitro modulation of tumor progression-associated properties of hormone refractory prostate carcinoma cell lines by cytokines.** *Cancer* 1996, **77**(9):1862–1872.
80. Yan Q, Xu R, Zhu L, Cheng X, Wang Z, Manis J, Shipp MA: **BAL1 and its partner E3 ligase, BBAP, link Poly(ADP-ribose) activation, ubiquitylation, and double-strand DNA repair independent of ATM, MDC1, and RNF8.** *Mol Cell Biol* 2013, **33**(4):845–857.
81. Feijs KL, Forst AH, Verheugd P, Luscher B: **Macrodomain-containing proteins: regulating new intracellular functions of mono(ADP-ribosyl)ation.** *Nat Rev Mol Cell Biol* 2013, **14**(7):443–451.
82. Das S, Roth CP, Wasson LM, Vishwanatha JK: **Signal transducer and activator of transcription-6 (STAT6) is a constitutively expressed survival factor in human prostate cancer.** *Prostate* 2007, **67**(14):1550–1564.
83. Andersson CD, Karlberg T, Ekblad T, Lindgren AE, Thorsell AG, Spjut S, Uciechowska U, Niemiec MS, Wittung-Stafshede P, Weigelt J, Elofsson M, Schuler H, Linusson A: **Discovery of ligands for ADP-ribosyltransferases via docking-based virtual screening.** *J Med Chem* 2012, **55**(17):7706–7718.
84. Wahlberg E, Karlberg T, Kouznetsova E, Markova N, Macchiarulo A, Thorsell AG, Pol E, Frostell A, Ekblad T, Oncu D, Kull B, Robertson GM, Pellicciari R, Schuler H, Weigelt J: **Family-wide chemical profiling and structural analysis of PARP and tankyrase inhibitors.** *Nat Biotechnol* 2012, **30**(3):283–288.
85. Ekblad T, Camaioni E, Schuler H, Macchiarulo A: **PARP inhibitors: polypharmacology versus selective inhibition.** *FEBS J* 2013, **280**(15):3563–3575.
86. Karlberg T, Hammarstrom M, Schutz P, Svensson L, Schuler H: **Crystal structure of the catalytic domain of human PARP2 in complex with PARP inhibitor ABT-888.** *Biochemistry* 2010, **49**(6):1056–1058.
87. Baran-Marszak F, Feuillard J, Najjar I, Le Clorennec C, Bechet JM, Dusanter-Fourt I, Bornkamm GW, Raphael M, Fagard R: **Differential roles of**

STAT1alpha and STAT1beta in fludarabine-induced cell cycle arrest and apoptosis in human B cells. *Blood* 2004, **104**(8):2475–2483.
88. Sanda T, Tyner JW, Gutierrez A, Ngo VN, Glover J, Chang BH, Yost A, Ma W, Fleischman AG, Zhou W, Yang Y, Kleppe M, Ahn Y, Tatarek J, Kelliher MA, Neuberg DS, Levine RL, Moriggl R, Muller M, Gray NS, Jamieson CH, Weng AP, Staudt LM, Druker BJ, Look AT: **TYK2-STAT1-BCL2 pathway dependence in T-cell acute lymphoblastic leukemia.** *Cancer Discov* 2013, **3**(5):564–577.
89. Yang H, Lee SM, Gao B, Zhang J, Fang D: **The histone deacetylase Sirtuin 1 deacetylates IRF1 and programs dendritic cells to control Th17 differentiation during autoimmune inflammation.** *J Biol Chem* 2013, **288**(52):37256–37266.
90. Sharf R, Meraro D, Azriel A, Thornton AM, Ozato K, Petricoin EF, Lamer AC, Schaper F, Hauser H, Levi BZ: **Phosphorylation events modulate the ability of interferon consensus sequence binding protein to interact with interferon regulatory factors and to bind DNA.** *J Biol Chem* 1997, **272**(15):9785–9792.
91. Lin R, Hiscott J: **A role for casein kinase II phosphorylation in the regulation of IRF-1 transcriptional activity.** *Mol Cell Biochem* 1999, **191**(1–2):169–180.
92. Shimizu T, Miyakawa Y, Oda A, Kizaki M, Ikeda Y: **STI571-resistant KT-1 cells are sensitive to interferon-alpha accompanied by the loss of T-cell protein tyrosine phosphatase and prolonged phosphorylation of Stat1.** *Exp Hematol* 2003, **31**(7):601–608.
93. ten Hoeve J, de Jesus I-SM, Fu Y, Zhu W, Tremblay M, David M, Shuai K: **Identification of a nuclear Stat1 protein tyrosine phosphatase.** *Mol Cell Biol* 2002, **22**(16):5662–5668.
94. Heinonen KM, Bourdeau A, Doody KM, Tremblay ML: **Protein tyrosine phosphatases PTP-1B and TC-PTP play nonredundant roles in macrophage development and IFN-gamma signaling.** *Proc Natl Acad Sci U S A* 2009, **106**(23):9368–9372.
95. Aguiar RC, Yakushijin Y, Kharbanda S, Salgia R, Fletcher JA, Shipp MA: **BAL is a novel risk-related gene in diffuse large B-cell lymphomas that enhances cellular migration.** *Blood* 2000, **96**(13):4328–4334.
96. Kleine H, Poreba E, Lesniewicz K, Hassa PO, Hottiger MO, Litchfield DW, Shilton BH, Luscher B: **Substrate-assisted catalysis by PARP10 limits its activity to mono-ADP-ribosylation.** *Mol Cell* 2008, **32**(1):57–69.
97. Hassa PO, Haenni SS, Buerki C, Meier NI, Lane WS, Owen H, Gersbach M, Imhof R, Hottiger MO: **Acetylation of poly(ADP-ribose) polymerase-1 by p300/CREB-binding protein regulates coactivation of NF-kappaB-dependent transcription.** *J Biol Chem* 2005, **280**(49):40450–40464.
98. Sen S, Roy K, Mukherjee S, Mukhopadhyay R, Roy S: **Restoration of IFNgammaR subunit assembly, IFNgamma signaling and parasite clearance in Leishmania donovani infected macrophages: role of membrane cholesterol.** *PLoS Pathog* 2011, **7**(9):e1002229.
99. Yanagawa T, Funasaka T, Tsutsumi S, Hu H, Watanabe H, Raz A: **Regulation of phosphoglucose isomerase/autocrine motility factor activities by the poly(ADP-ribose) polymerase family-14.** *Cancer Res* 2007, **67**(18):8682–8689.

doi:10.1186/1476-4598-13-125
Cite this article as: Bachmann *et al.*: DTX3L and ARTD9 inhibit IRF1 expression and mediate in cooperation with ARTD8 survival and proliferation of metastatic prostate cancer cells. *Molecular Cancer* 2014 **13**:125.

Bachmann S.B. et al., Suppl. Fig. 1

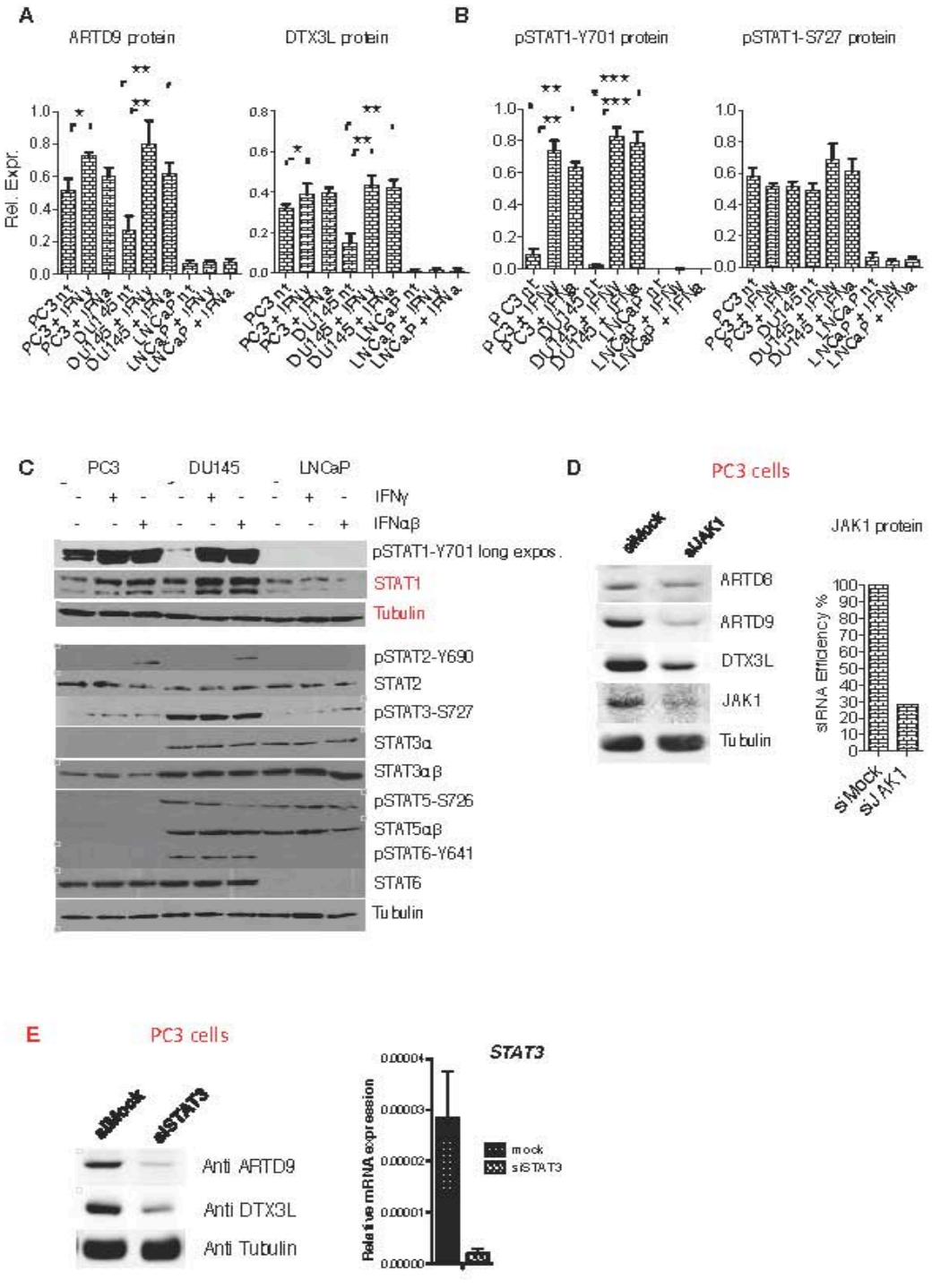

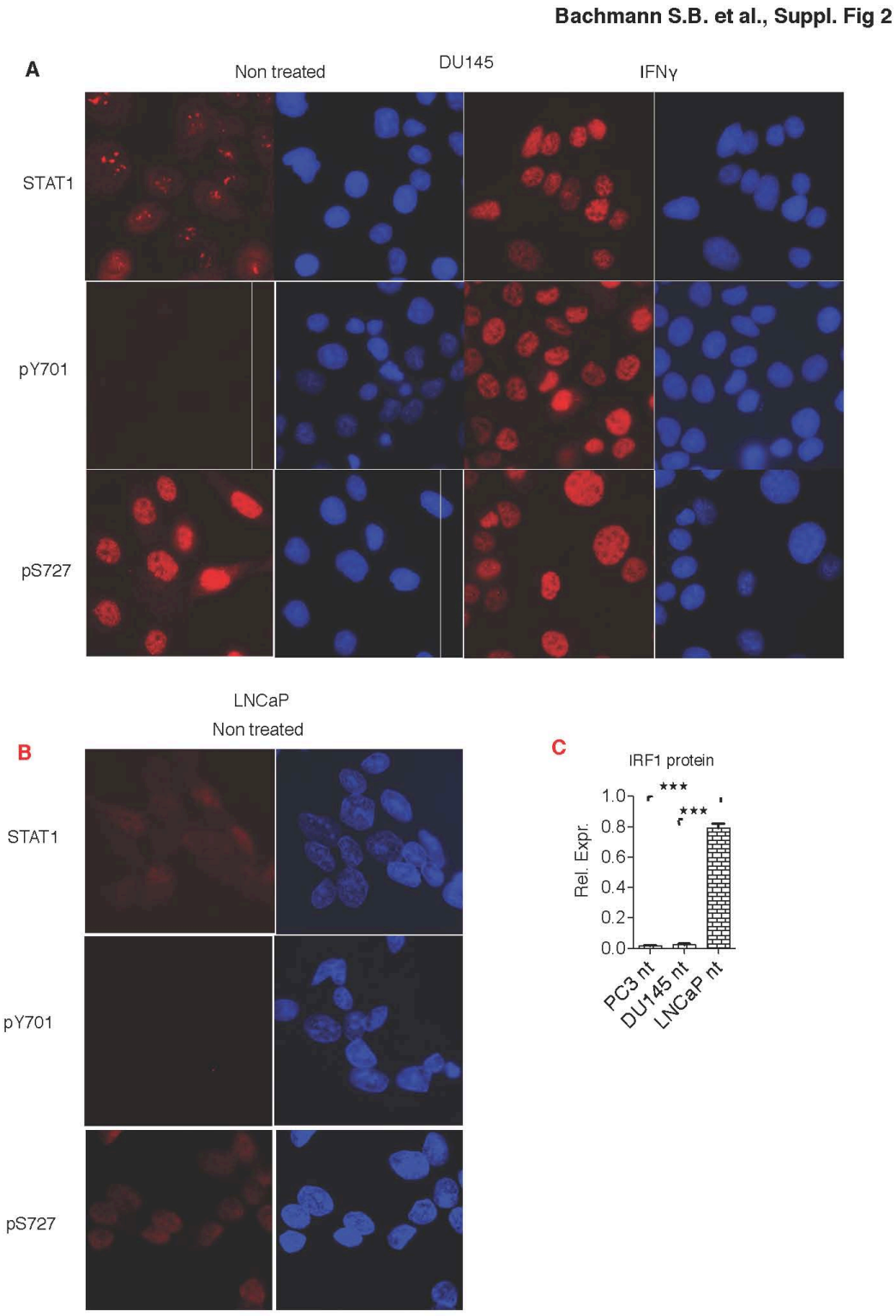
Bachmann S.B. et al., Suppl. Fig 2
A
Non treated
DU145
IFNγ
STAT1
pY701
pS727
LNCaP
Non treated
B
STAT1
pY701
pS727
C
IRF1 protein
Rel. Expr.
1.0
0.8
0.6
0.4
0.2
0.0
***
***
PC3 nt
DU145 nt
LNCaP nt

Bachmann S.B. et al., Suppl. Fig. 3

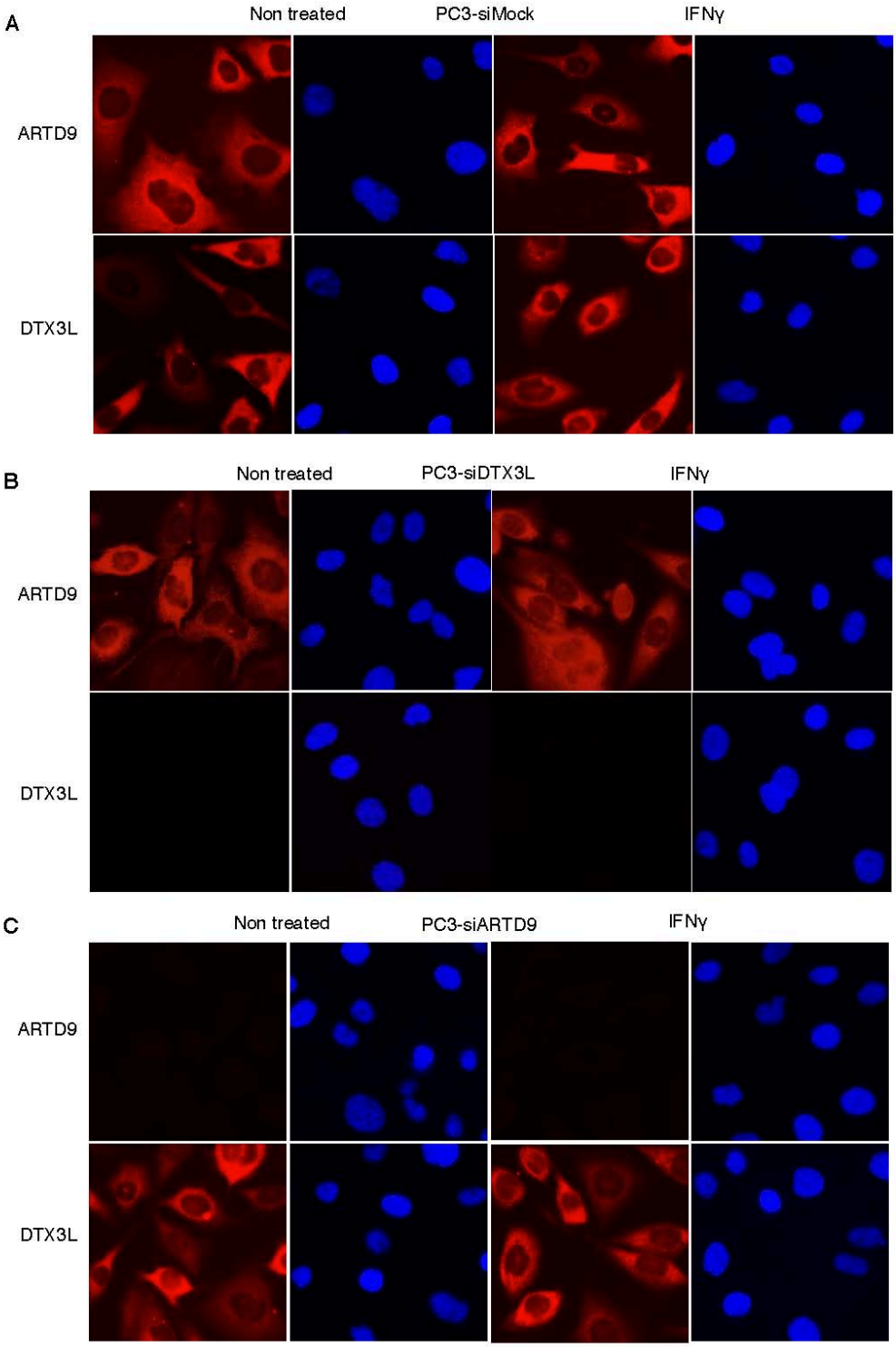

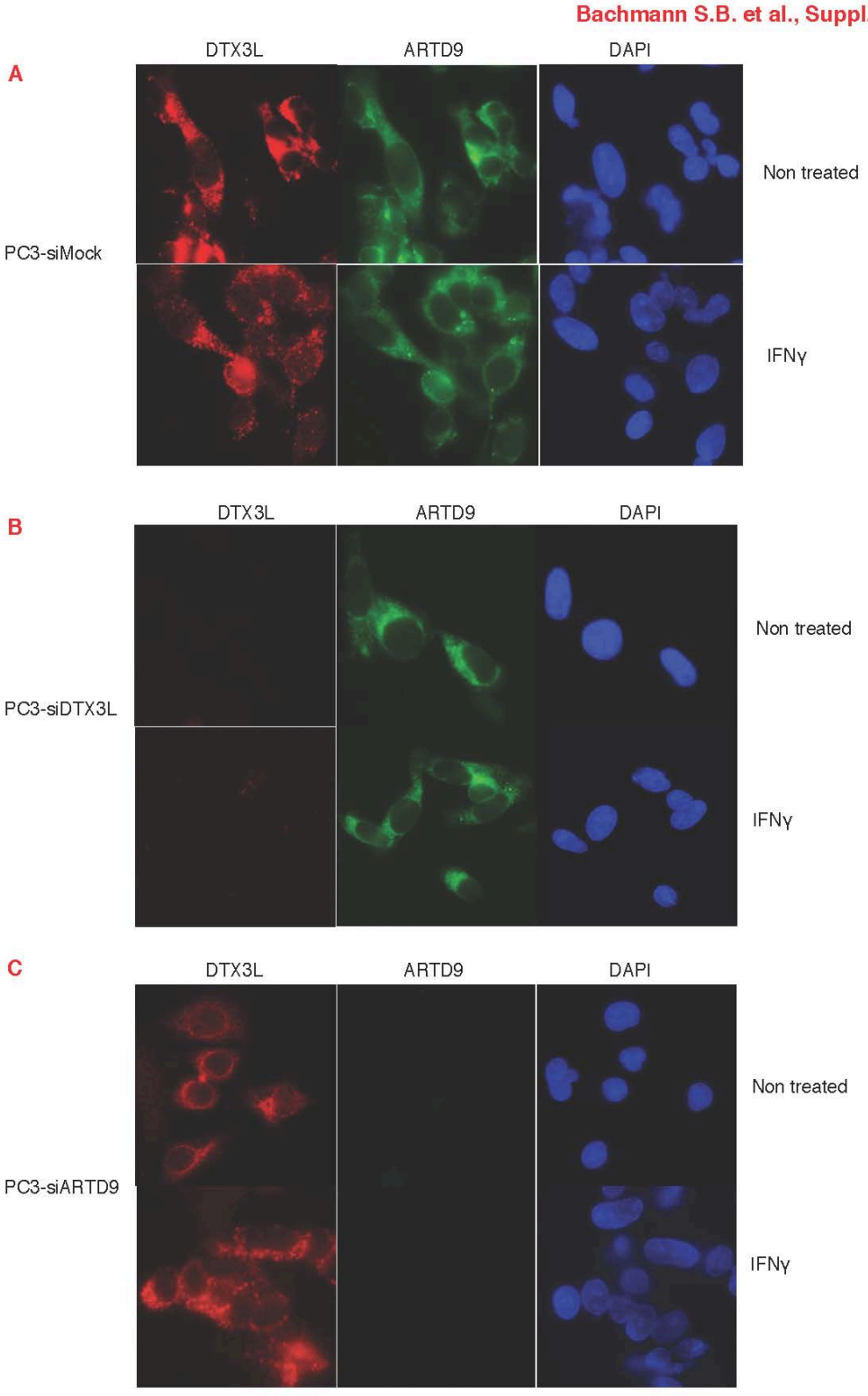
Bachmann S.B. et al., Suppl. Fig. 4
A
DTX3L
ARTD9
DAPI
PC3-siMock
Non treated
IFNγ
B
DTX3L
ARTD9
DAPI
PC3-siDTX3L
Non treated
IFNγ
C
DTX3L
ARTD9
DAPI
PC3-siARTD9
Non treated
IFNγ

Bachmann S.B. et al., Suppl.Fig. 5

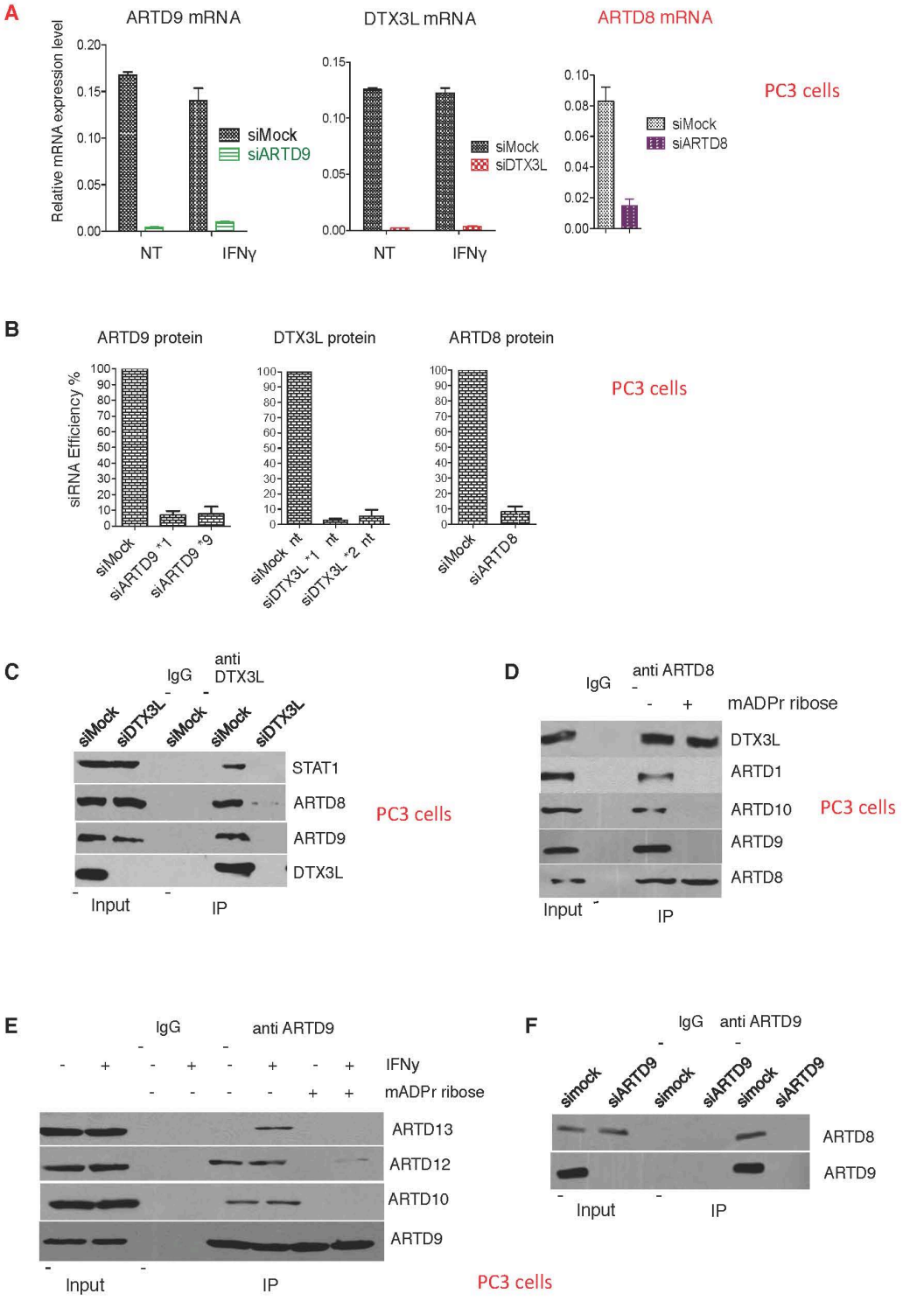

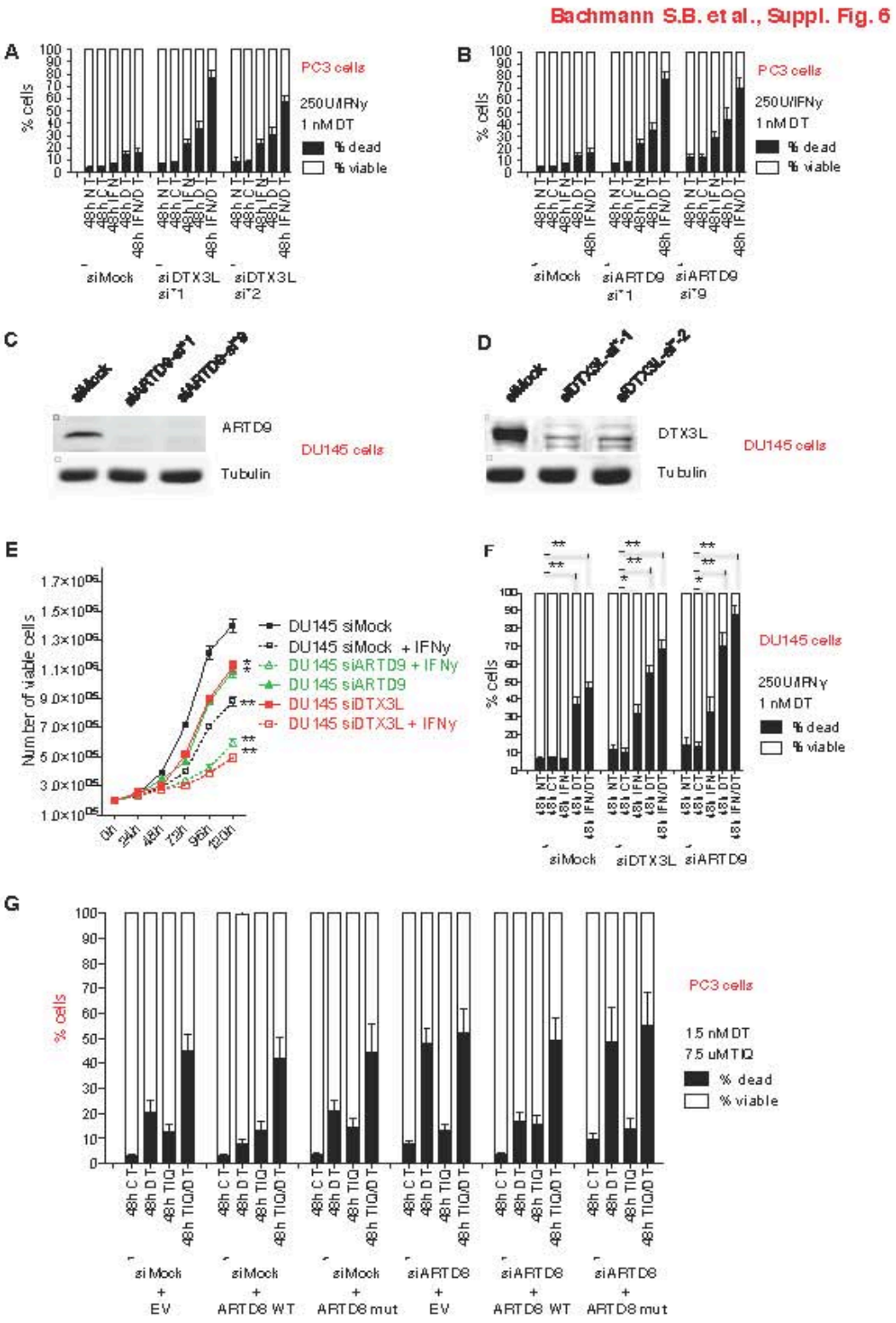
Bachmann S.B. et al., Suppl. Fig. 6
A
% cells
PC3 cells
250 U/IFNγ
1 nM DT
% dead
% viable
siMock
siDTX3L si#1
siDTX3L si#2
B
siMock
siARTD9 si#1
siARTD9 si#9
C
siMock
siARTD9-si#1
siARTD9-si#3
ARTD9
Tubulin
DU145 cells
D
siMock
siDTX3L-si#1
siDTX3L-si#2
DTX3L
Tubulin
DU145 cells
E
Number of viable cells
DU145 siMock
DU145 siMock + IFNγ
DU145 siARTD9 + IFNγ
DU145 siARTD9
DU145 siDTX3L
DU145 siDTX3L + IFNγ
F
DU145 cells
250 U/IFNγ
1 nM DT
% dead
% viable
siMock
siDTX3L
siARTD9
G
% cells
PC3 cells
1.5 nM DT
7.5 uM TIQ
% dead
% viable
siMock + EV
siMock + ARTD8 WT
siMock + ARTD8 mut
siARTD8 + EV
siARTD8 + ARTD8 WT
siARTD8 + ARTD8 mut

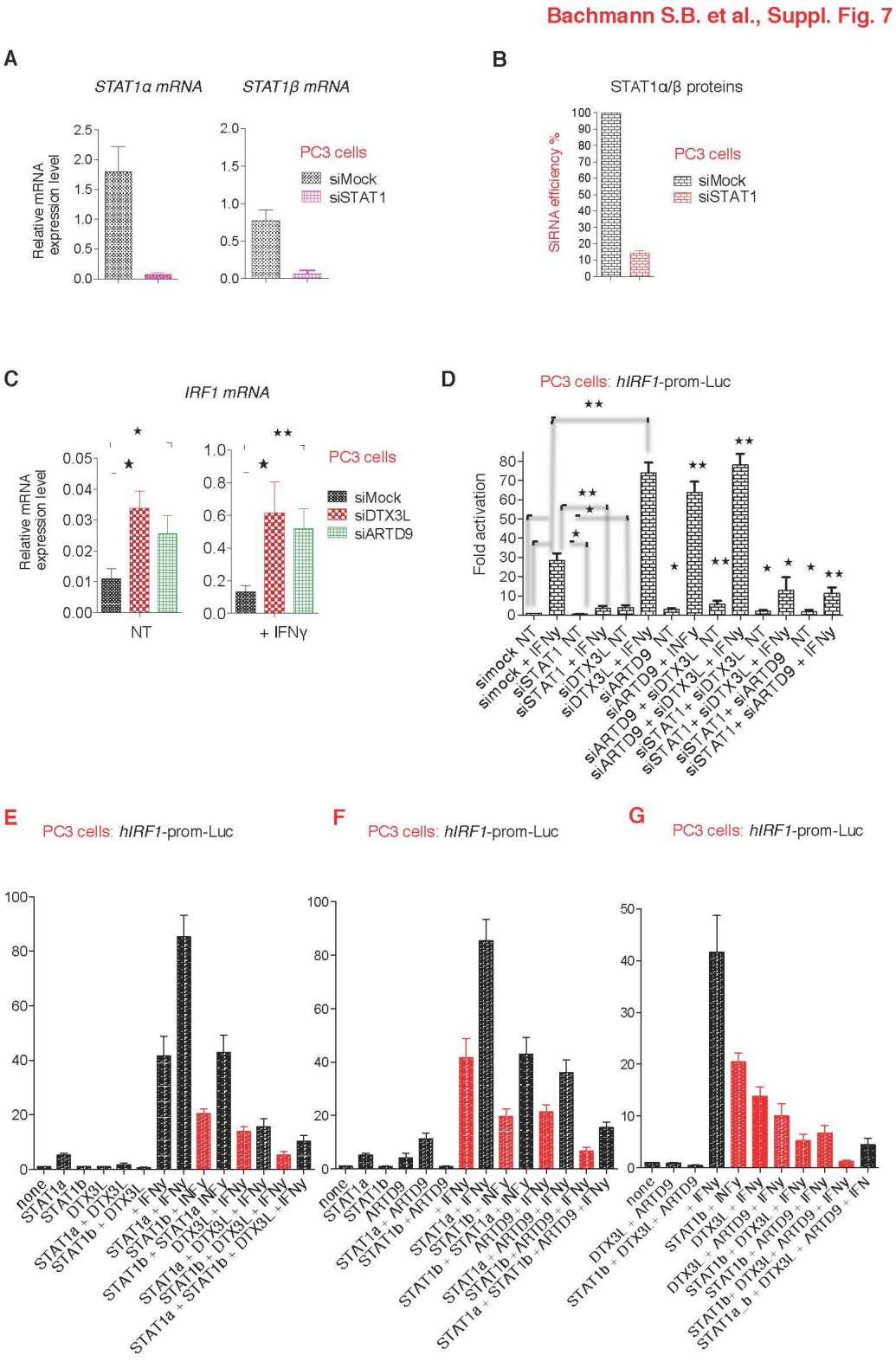
Bachmann S.B. et al., Suppl. Fig. 7
A
STAT1α mRNA
STAT1β mRNA
Relative mRNA expression level
PC3 cells
siMock
siSTAT1
B
STAT1α/β proteins
SiRNA efficiency %
PC3 cells
siMock
siSTAT1
C
IRF1 mRNA
Relative mRNA expression level
PC3 cells
siMock
siDTX3L
siARTD9
NT
+ IFNγ
D
PC3 cells: hIRF1-prom-Luc
Fold activation
simock NT
simock + IFNγ
siSTAT1 NT
siSTAT1 + IFNγ
siDTX3L NT
siDTX3L + IFNγ
siARTD9 NT
siARTD9 + INFγ
siARTD9 + siDTX3L NT
siARTD9 + siDTX3L + IFNγ
siSTAT1 + siDTX3L NT
siSTAT1 + siDTX3L + IFNγ
siSTAT1 + siARTD9 NT
siSTAT1 + siARTD9 + IFNγ
E
PC3 cells: hIRF1-prom-Luc
Fold activation
none
STAT1a
STAT1b
DTX3L
STAT1a + DTX3L
STAT1b + DTX3L
STAT1a + IFNγ
STAT1b + IFNγ
STAT1a + DTX3L + IFNγ
STAT1b + DTX3L + IFNγ
STAT1a + STAT1b + DTX3L + IFNγ
F
PC3 cells: hIRF1-prom-Luc
none
STAT1a
STAT1b
ARTD9
STAT1a + ARTD9
STAT1b + ARTD9
STAT1a + IFNγ
STAT1b + IFNγ
STAT1a + STAT1b + IFNγ
ARTD9 + IFNγ
STAT1a + ARTD9 + IFNγ
STAT1b + ARTD9 + IFNγ
STAT1a + STAT1b + ARTD9 + IFNγ
G
PC3 cells: hIRF1-prom-Luc
none
DTX3L + ARTD9
STAT1b + DTX3L + ARTD9
STAT1b + IFNγ
DTX3L + IFNγ
STAT1b + ARTD9 + IFNγ
DTX3L + ARTD9 + IFNγ
STAT1b + DTX3L + IFNγ
STAT1b + DTX3L + ARTD9 + IFNγ
STAT1a_b + DTX3L + ARTD9 + IFN

Bachmann S.B. et al., Suppl. Fig. 8

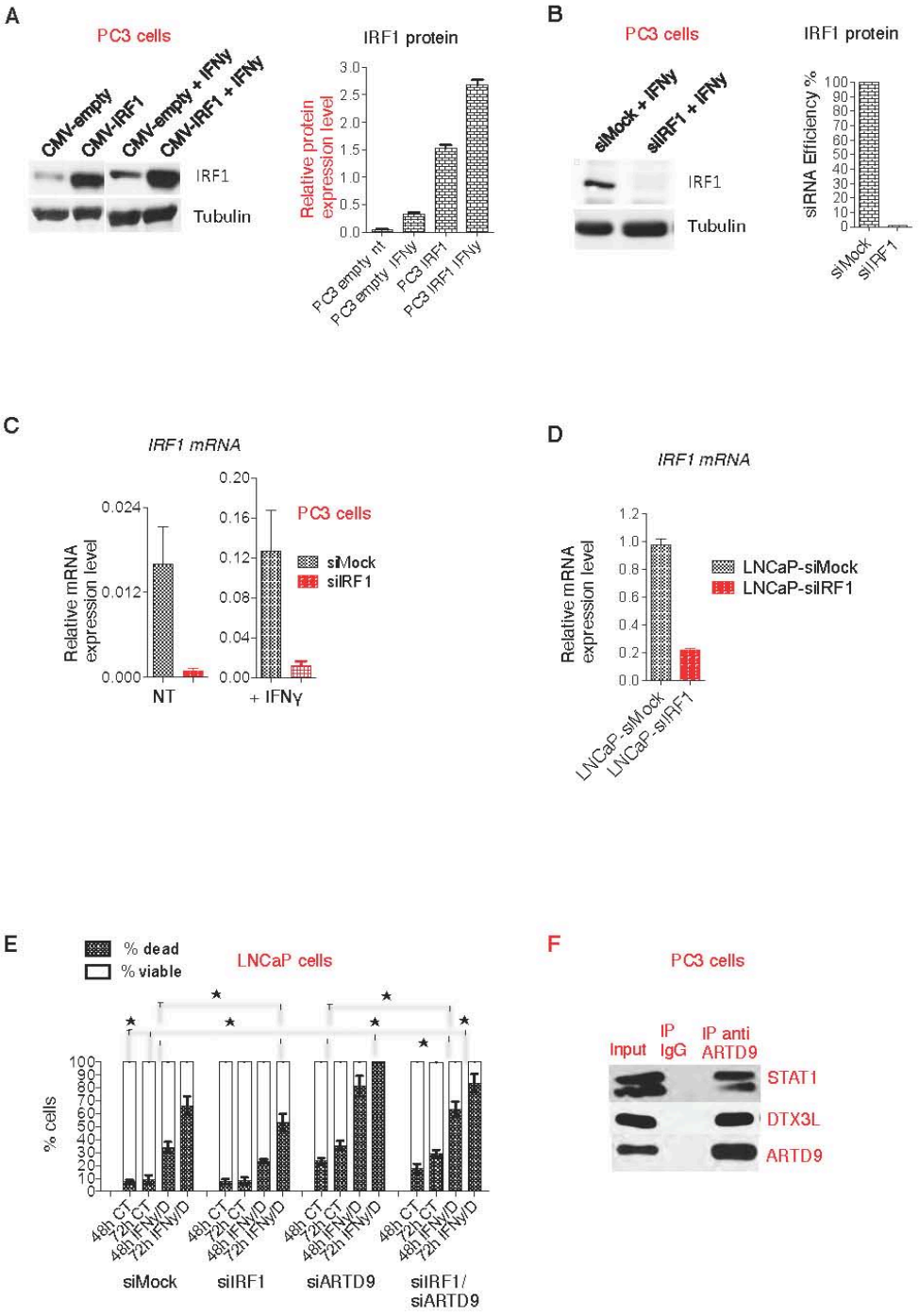

Bachmann S.B. et al., Suppl. Fig. 9

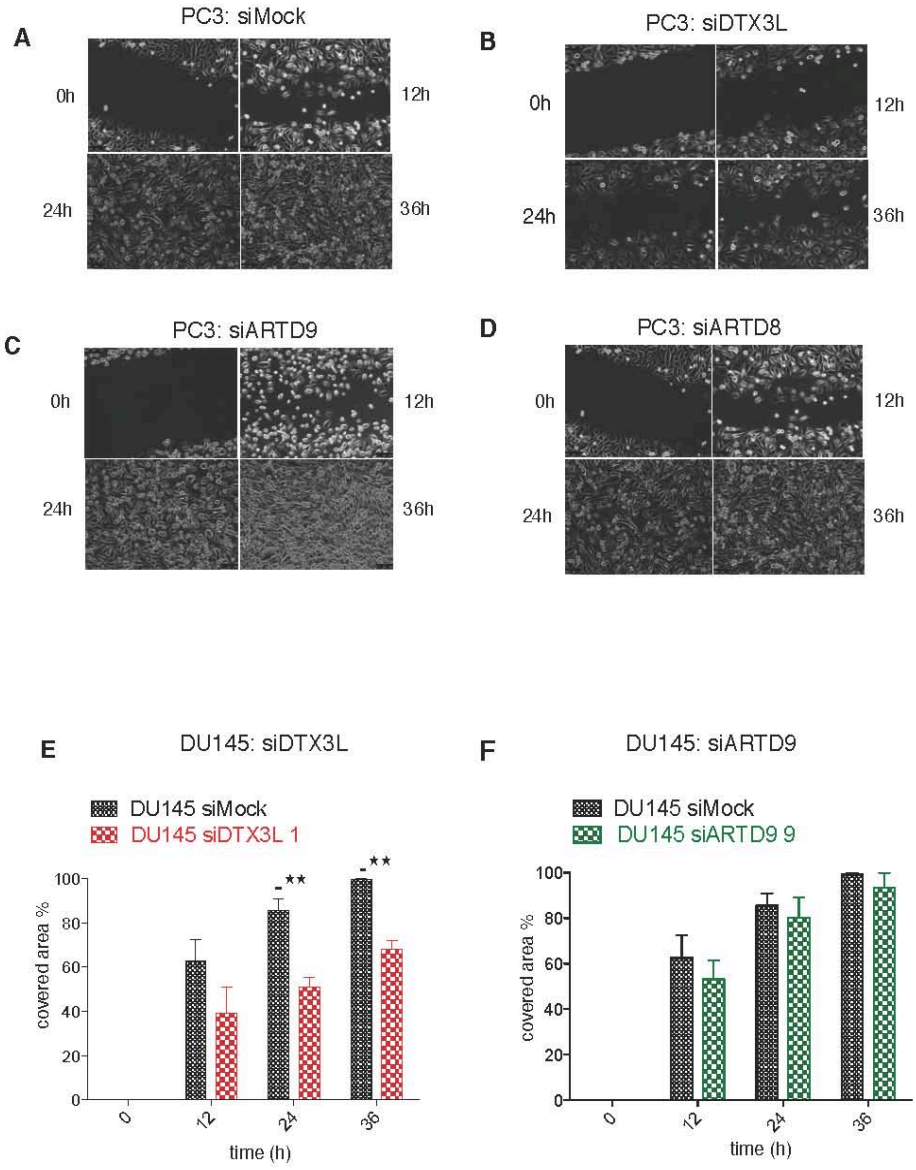

Bachmann S.B. et al., Suppl. Fig. 10

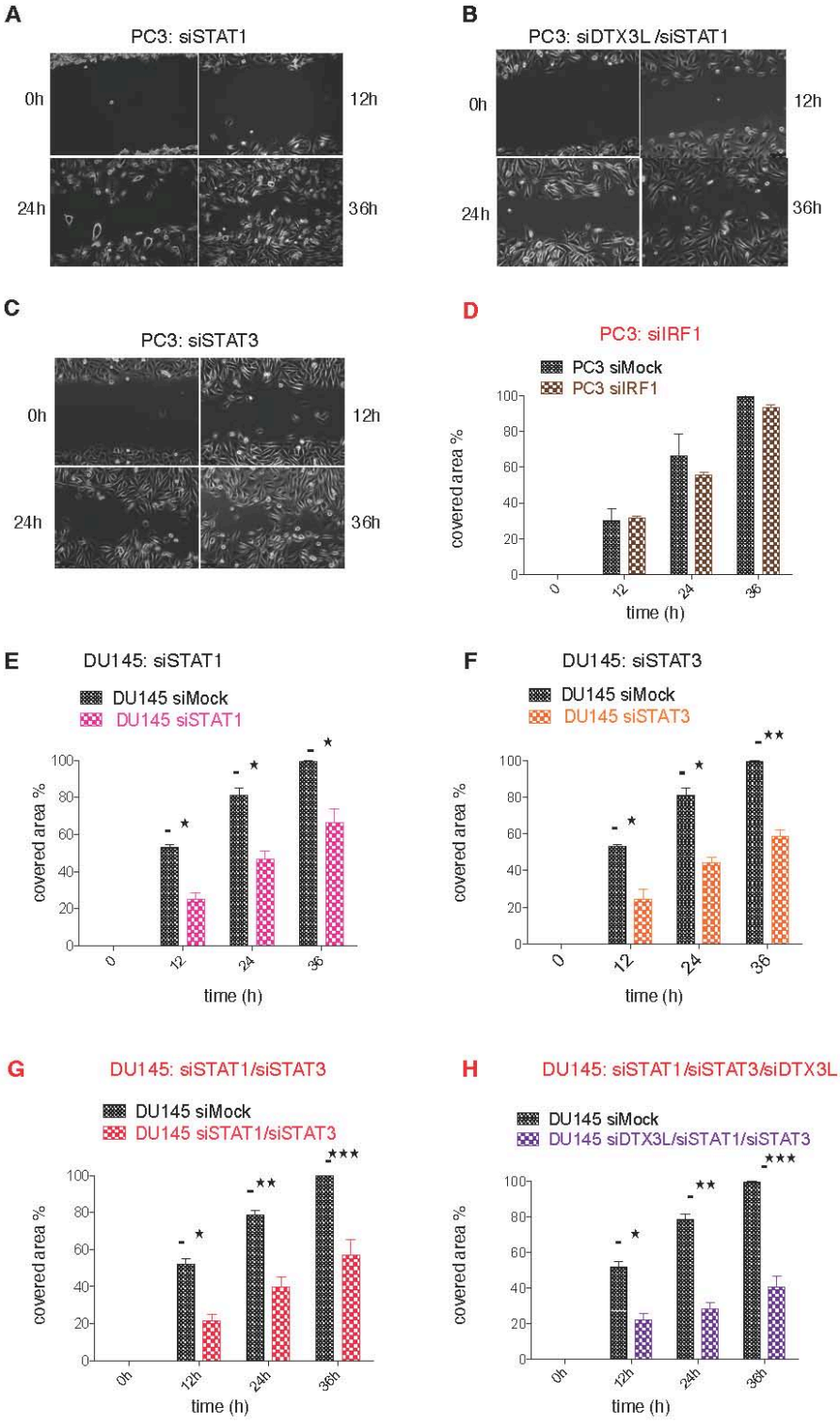

Table S1: siRNA sequences

siRNA	Targeting sequence
AllStar mock siRNA negative control	GGGUAUCGACGAUUACAAA
ARTD9-shRNA #-1	TGCAGGTTCTAAAGGTGGA
ARTD9-shRNA #-2	GGCAAAGTCAATTCTACAA
ARTD9-siRNA #-9	TTACCTTGGGTGAACTAAC
ARTD9-siRNA #-10	GGACAGAGTTAGAGATTGAAAC
STAT1-siRNA #-6 (validated by Qiagen)	CAGAAAGAGCTTGACAGTAAA
STAT1-siRNA #-7 (validated by Qiagen)	CCAGATGTCTATGATCATTTA
ARTD8-shRNA #-1	CTAGTGCAGATGTGTATAA
ARTD8-shRNA #-2	GGA AAG GGC TCA CTC ACA ATT
DTX3L-shRNA #-1	TCCAGGTTATGAGTCCTTTGGCA
DTX3L-shRNA #-2	GTTAGAGGTGGGTCCGAAATAA
DTX3L-shRNA #-3	GGCAAGCATTGGTAATAAATGGA
DTX3L-shRNA #-4	GCCCTGCCACAGTAATGCTATA
STAT3-siRNA #-7 (validated by Qiagen)	CAGCCTCTCTGCAGAATTCAA
STAT3-siRNA #-8 (validated by Qiagen)	CAGGCTGGTAATTTATATAAT
IRF1-siRNA #-1	CCAAGAACCAGAGAAAAGA
IRF1-siRNA #-2	AGACCAGAGCAGGAACAAG
JAK1-siRNA #-1 (validated by Qiagen)	CTGGGAATTCCAACCATCCAA
JAK1-siRNA #-6 (validated by Qiagen)	CACGGATAACATCAGCTTCAT

Table S2: qPCR Primer

Target gene (human)	FWD Primer	Rev Primer
ARTD8	GACTGTCGCTATGTGCTTCAC	GGACAAGCTCTCAGTGATCTCC
ARTD9	GGCAAAGAGGTCCAAGATGCTG	GCCTCACACATCTCTTCCACGT
DTX3L	CCAGGTTATGAGTCCTTTGGCAC	TGCAGTTCGCTGTATTCCAGGG
STAT1α	TGCTGTTACTTTCCCTGACATCA	GAGTAGCAGGAGGGAATCACAGAT
STAT1β	CGCAATTACAAAGTCATGGCTG	AGCAAGGCTGGCTTGAGGTTT
IRF1	AAAAGGAGCCAGATCCCAAGA	CATCCGGTACACTCGCACAG
STAT3	CATCATGGGCTTTATCAGTAAGGA	GTCAATGGTATTGCTGCAGGTCGT
GAPDH	GAAATCCCATCACCATCTTCC	GAGCCCCAGCCTTCTCCATG

4 Discussion

Alterations involving epigenetic regulators are now recognized as key events governing the tumor cell phenotype by affecting expression of genes critical to cancer. This work has identified a novel aberrant role for TIP5, an epigenetic regulator that was so far exclusively implicated in the epigenetic repression of rRNA genes. Elevated expression of TIP5 correlates with metastatic and advanced prostate cancer and serves as an independent predictor of PSA recurrence. This work has determined that TIP5 directly regulates a host of non-rRNA genes and interacts with EZH2 to maintain aberrant repression directly at the promoters of genes recurrently silenced in prostate cancer and other cancer metastasis. Finally, this study has shown that TIP5 overexpression is tightly associated with a tumor subtype displaying dramatic genome-wide hypermethylation. Thus, TIP5 is implicated in aberrant epigenetic profiles and gene silencing characterizing aggressive prostate cancer, and serves as a useful marker to elucidate and predict metastatic potential in prostate cancer.

This work has demonstrated that TIP5 is upregulated alongside EZH2 in prostate cancer. TIP5 and EZH2 physically interact with each other and cooperate to maintain silencing in prostate cancer cells at genes aberrantly repressed in metastatic tumors. Although TIP5 regulates the epigenetic state of rRNA genes in PC3 cells as in non-malignant cells, in cancer cells its function appears to go beyond the epigenetic control of the rDNA locus. Depletion of TIP5 in non-malignant cells induces loss of rDNA silencing with consequent upregulation of rRNA transcription and proliferation (this work and (Guetg et al., 2010; Santoro et al., 2009)) whereas the lack of TIP5 in prostate cancer cells reduces cell proliferation and viability, delays cell cycle progression, and impairs malignant-specific features of PC3 cells such as cell mobility/invasion and self-renewal. The distinction of TIP5 function is further supported by the strong divergence in processes related to TIP5-regulated genes between non-cancer and prostate cancer cells. The switch of TIP5 function and its key role in prostate cancer is also underscored by the substantial overlap of TIP5- and EZH2-regulated genes in PC3 cells that share common biological processes, including pathways involved in extracellular matrix structure organization and biogenesis, and collagen synthesis known to be important for prostate cancer metastasis (Hall, 2008; Banyard, 2007). Likewise, TIP5-high expressing tumors display hypermethylation of genes involved in these key pathways. In contrast, genes regulated by TIP5 and EZH2 in RWPE1 cells did not show any relevant common biological process

underscoring a functional TIP5/EZH2 cooperation, which is specific for prostate cancer cells.

Many EZH2 target genes in cancer are also EZH2 targets in embryonic stem cells (Yu et al., 2007) suggesting a strong association between PRC2 function in cancer and stem cells, which represent dedifferentiated and proliferative cell states. Hence, overexpression of EZH2 might cause a normal cell to dedifferentiate back to a stem cell–like state by epigenetically repressing cell fate-regulating and tumor suppressor genes resulting in tumor development (Jones and Baylin, 2007; Kondo et al., 2008; Sparmann and van Lohuizen, 2006).

Why does TIP5 have an oncogenic activity in prostate cancer? EZH2 upregulation can be detected in the vast majority of all tumors, whereas TIP5 upregulation is specific to some cancers and biased towards a more aggressive prostate cancer disease. These data support the possibility that TIP5 upregulation in combination with EZH2 causes additional gene silencing distinct from the silenced gene signature, which would be achieved separately, and this cooperation endows the tumor cells with an additionally aggressive phenotype. Alternatively, elevated levels of TIP5 might favor the recruitment to specific gene loci that would otherwise not be associated with TIP5 and, consequently, not be repressed. Future studies will decipher the nature of TIP5-binding sites in the genome of prostate cancer cells and the molecular features that dictate the recruitment.

The data of this work have shown that the upregulation of TIP5 is further associated with DNA hypermethylation in tumors which likely strengthens and/or stabilizes gene silencing. Remarkably, TIP5 was previously reported to establish epigenetic silencing at rRNA genes through recruitment of DNMTs (Guetg et al., 2012; Santoro et al., 2002), raising the possibility that similar silencing mechanisms might take place at non-rRNA genes in cancer. This is also supported by the observation that 35% (352) of genes upregulated upon TIP5 depletion in PC3 cells have elevated DNA methylation in TIP5-high expressing tumors. Although EZH2-mediated recruitment of DNMTs inducing *de novo* methylation in cancer was reported in an experimental model (Vire et al., 2006), the relation between H3K27me3 and DNA methylation remains to be clearly defined. Several studies in cancer cells have observed that many hypermethylated CpG islands actually contain low levels of H3K27me3 (Gal-Yam et al., 2008; Kondo et al., 2008) and knockdown of EZH2 did not alter DNA methylation profiles of candidate CpG islands (McGarvey et al., 2007). Although our analysis in tumors does not allow for a direct measurement of H3K27me3 and DNA methylation co-occupancy, the presence of a large portion of Polycomb group sites among hypermethylated genes in TIP5-high tumors supports a functional crosstalk between TIP5, EZH2 and DNA methylation. Re-

markably, among hypermethylated genes in TIP5-high tumors, 27 genes were upregulated by TIP5 and EZH2 depletion in PC3 cells and 82 by EZH2 alone.

Lethality in prostate cancer is linked to the evolution of a metastatic phenotype. PSA recurrence following radical prostatectomy reveals that tumor cells have gained the ability to invade the surrounding local tissue and/or metastasize prior to surgery. This work demonstrates a key role for TIP5 in the growth and invasiveness of metastatic prostate cancer cells and in the regulation of genes related to metastatic features. Our results suggest that high TIP5 levels in the primary tumor indicate a higher probability of metastasis, linking molecular findings with recurrence in clinical samples. TIP5 may be involved in endowing cells with these abilities and could represent a promising therapeutic target for metastatic prostate cancer. An increasing number of epigenetic regulatory genes, including members of the class of bromodomain-containing proteins, are currently found to be dysregulated across many cancer types (Dawson et al., 2012). These genes represent novel targets of a new generation of potential cancer therapeutics. Accordingly, the fact that TIP5 contains a bromodomain previously shown to be important for its silencing function at the rDNA locus (Zhou and Grummt, 2005) might open the possibility to develop compounds to inactivate TIP5 function in cancer.

This study shows that TIP5 levels can serve as an independent prognostic marker of recurrence, especially in low/intermediate risk cases as assessed by Gleason score. Low expression of FGFR1 and CDKN1A together with PMP22 has recently been proposed as a prognostic indicator for low Gleason score prostate tumors that failed surveillance (Irshad et al., 2013). Remarkably, this work has identified *FGFR1* and *CDKN1A* as genes upregulated upon knockdown of TIP5 and EZH2 in PC3 cells, underscoring the potential role of TIP5 in epigenetic alterations contributing to the aggressive prostate cancer phenotype. Intermediate risk cases are a patient sub-cohort where most uncertainty exists to balance between active surveillance or immediate definite therapy in order to avoid overtreatment. Screening of TIP5 levels in biopsies may be a valuable biomarker to distinguish prostate cancer that possesses the potential for disease progression, aiding in therapy decision-making for this important patient subgroup.

5 References

Abdullah, L. N., and Chow, E. K. (2013). Mechanisms of chemoresistance in cancer stem cells. Clin Transl Med *2*, 3.

Albany, C., Alva, A. S., Aparicio, A. M., Singal, R., Yellapragada, S., Sonpavde, G., and Hahn, N. M. (2011). Epigenetics in prostate cancer. Prostate cancer *2011*, 580318.

Albertsen, P. C., Hanley, J. A., and Fine, J. (2005). 20-year outcomes following conservative management of clinically localized prostate cancer. JAMA *293*, 2095-2101.

Allfrey, V. G., Faulkner, R., and Mirsky, A. E. (1964). Acetylation and Methylation of Histones and Their Possible Role in the Regulation of Rna Synthesis. Proc Natl Acad Sci U S A *51*, 786-794.

Ambs, S., Prueitt, R. L., Yi, M., Hudson, R. S., Howe, T. M., Petrocca, F., Wallace, T. A., Liu, C. G., Volinia, S., Calin, G. A.*, et al.* (2008). Genomic profiling of microRNA and messenger RNA reveals deregulated microRNA expression in prostate cancer. Cancer Res *68*, 6162-6170.

Arrowsmith, C. H., Bountra, C., Fish, P. V., Lee, K., and Schapira, M. (2012). Epigenetic protein families: a new frontier for drug discovery. Nature reviews Drug discovery *11*, 384-400.

Asangani, I. A., Dommeti, V. L., Wang, X., Malik, R., Cieslik, M., Yang, R., Escara-Wilke, J., Wilder-Romans, K., Dhanireddy, S., Engelke, C.*, et al.* (2014). Therapeutic targeting of BET bromodomain proteins in castration-resistant prostate cancer. Nature *510*, 278-282.

Babbio, F., Pistore, C., Curti, L., Castiglioni, I., Kunderfranco, P., Brino, L., Oudet, P., Seiler, R., Thalman, G. N., Roggero, E.*, et al.* (2012). The SRA protein UHRF1 promotes epigenetic crosstalks and is involved in prostate cancer progression. Oncogene *31*, 4878-4887.

Baca, S. C., and Garraway, L. A. (2012). The genomic landscape of prostate cancer. Frontiers in endocrinology *3*, 69.

Bachmann, I. M., Halvorsen, O. J., Collett, K., Stefansson, I. M., Straume, O., Haukaas, S. A., Salvesen, H. B., Otte, A. P., and Akslen, L. A. (2006). EZH2 expression is associated with high proliferation rate and aggressive tumor subgroups in cutaneous melanoma and cancers of the endometrium, prostate, and breast. J Clin Oncol *24*, 268-273.

Ball, P. (2003). Portrait of a molecule. Nature *421*, 421-422.

Ballestar, E., Paz, M. F., Valle, L., Wei, S., Fraga, M. F., Espada, J., Cigudosa, J. C., Huang, T. H., and Esteller, M. (2003). Methyl-CpG binding proteins identify novel sites of epigenetic inactivation in human cancer. Embo J *22*, 6335-6345.

Bannister, A. J., and Kouzarides, T. (2011). Regulation of chromatin by histone modifications. Cell research *21*, 381-395.

Barbieri, C. E., Baca, S. C., Lawrence, M. S., Demichelis, F., Blattner, M., Theurillat, J. P., White, T. A., Stojanov, P., Van Allen, E., Stransky, N.*, et al.* (2012). Exome sequencing identifies recurrent SPOP, FOXA1 and MED12 mutations in prostate cancer. Nat Genet *44*, 685-689.

Barski, A., Cuddapah, S., Cui, K., Roh, T. Y., Schones, D. E., Wang, Z., Wei, G., Chepelev, I., and Zhao, K. (2007). High-resolution profiling of histone methylations in the human genome. Cell *129*, 823-837.

Bartke, T., Vermeulen, M., Xhemalce, B., Robson, S. C., Mann, M., and Kouzarides, T. (2010). Nucleosome-interacting proteins regulated by DNA and histone methylation. Cell *143*, 470-484.

Basavapathruni, A., Olhava, E. J., Daigle, S. R., Therkelsen, C. A., Jin, L., Boriack-Sjodin, P. A., Allain, C. J., Klaus, C. R., Raimondi, A., Scott, M. P.*, et al.* (2014). Nonclinical pharmacokinetics and metabolism of EPZ-5676, a novel DOT1L histone methyltransferase inhibitor. Biopharmaceutics & drug disposition *35*, 237-252.

Basnet, H., Su, X. B., Tan, Y., Meisenhelder, J., Merkurjev, D., Ohgi, K. A., Hunter, T., Pillus, L., and Rosenfeld, M. G. (2014). Tyrosine phosphorylation of histone H2A by CK2 regulates transcriptional elongation. Nature *516*, 267-271.

Baylin, S. B., Esteller, M., Rountree, M. R., Bachman, K. E., Schuebel, K., and Herman, J. G. (2001). Aberrant patterns of DNA methylation, chromatin formation and gene expression in cancer. Human molecular genetics *10*, 687-692.

Baylin, S. B., Hoppener, J. W., de Bustros, A., Steenbergh, P. H., Lips, C. J., and Nelkin, B. D. (1986). DNA methylation patterns of the calcitonin gene in human lung cancers and lymphomas. Cancer Res *46*, 2917-2922.

Baylin, S. B., and Jones, P. A. (2011). A decade of exploring the cancer epigenome - biological and translational implications. Nat Rev Cancer *11*, 726-734.

Baylin, S. B., and Ohm, J. E. (2006). Epigenetic gene silencing in cancer - a mechanism for early oncogenic pathway addiction? Nat Rev Cancer *6*, 107-116.

Bell, O., Tiwari, V. K., Thoma, N. H., and Schubeler, D. (2011). Determinants and dynamics of genome accessibility. Nature reviews Genetics *12*, 554-564.

Bender, S., Tang, Y., Lindroth, A. M., Hovestadt, V., Jones, D. T., Kool, M., Zapatka, M., Northcott, P. A., Sturm, D., Wang, W.*, et al.* (2013). Reduced H3K27me3 and DNA hypomethylation are major drivers of gene expression in K27M mutant pediatric high-grade gliomas. Cancer Cell *24*, 660-672.

Berdasco, M., Ropero, S., Setien, F., Fraga, M. F., Lapunzina, P., Losson, R., Alaminos, M., Cheung, N. K., Rahman, N., and Esteller, M. (2009). Epigenetic inactivation of the Sotos overgrowth syndrome gene histone methyltransferase NSD1 in human neuroblastoma and glioma. Proc Natl Acad Sci U S A *106*, 21830-21835.

Berger, M. F., Lawrence, M. S., Demichelis, F., Drier, Y., Cibulskis, K., Sivachenko, A. Y., Sboner, A., Esgueva, R., Pflueger, D., Sougnez, C.*, et al.* (2011). The genomic complexity of primary human prostate cancer. Nature *470*, 214-220.

Bernardi, R., and Pandolfi, P. P. (2007). Structure, dynamics and functions of promyelocytic leukaemia nuclear bodies. Nature reviews Molecular cell biology *8*, 1006-1016.

Bernstein, E., and Allis, C. D. (2005). RNA meets chromatin. Genes & development *19*, 1635-1655.

Bernstein, E., Duncan, E. M., Masui, O., Gil, J., Heard, E., and Allis, C. D. (2006). Mouse polycomb proteins bind differentially to methylated histone H3 and RNA and are enriched in facultative heterochromatin. Mol Cell Biol *26*, 2560-2569.

Berry, W. L., and Janknecht, R. (2013). KDM4/JMJD2 histone demethylases: epigenetic regulators in cancer cells. Cancer Res *73*, 2936-2942.

Bestor, T. H., and Bourc'his, D. (2004). Transposon silencing and imprint establishment in mammalian germ cells. Cold Spring Harbor symposia on quantitative biology *69*, 381-387.

Bettstetter, M., Woenckhaus, M., Wild, P. J., Rummele, P., Blaszyk, H., Hartmann, A., Hofstadter, F., and Dietmaier, W. (2005). Elevated nuclear maspin expression is associated with microsatellite instability and high tumour grade in colorectal cancer. The Journal of pathology *205*, 606-614.

Bird, A. P., and Wolffe, A. P. (1999). Methylation-induced repression--belts, braces, and chromatin. Cell *99*, 451-454.

Bitler, B. G., Aird, K. M., Garipov, A., Li, H., Amatangelo, M., Kossenkov, A. V., Schultz, D. C., Liu, Q., Shih Ie, M., Conejo-Garcia, J. R.*, et al.* (2015). Synthetic lethality by targeting EZH2 methyltransferase activity in ARID1A-mutated cancers. Nat Med *21*, 231-238.

Bjerke, L., Mackay, A., Nandhabalan, M., Burford, A., Jury, A., Popov, S., Bax, D. A., Carvalho, D., Taylor, K. R., Vinci, M.*, et al.* (2013). Histone H3.3. mutations drive pediatric glioblastoma through upregulation of MYCN. Cancer discovery *3*, 512-519.

Bracken, A. P., and Helin, K. (2009). Polycomb group proteins: navigators of lineage pathways led astray in cancer. Nat Rev Cancer *9*, 773-784.

Brenner, C., Deplus, R., Didelot, C., Loriot, A., Vire, E., De Smet, C., Gutierrez, A., Danovi, D., Bernard, D., Boon, T.*, et al.* (2005). Myc represses transcription through recruitment of DNA methyltransferase corepressor. Embo J *24*, 336-346.

Brooks, J. D., Weinstein, M., Lin, X., Sun, Y., Pin, S. S., Bova, G. S., Epstein, J. I., Isaacs, W. B., and Nelson, W. G. (1998). CG island methylation changes near the GSTP1 gene in prostatic intraepithelial neoplasia. Cancer epidemiology, biomarkers & prevention : a publication of the American Association for Cancer Research, cosponsored by the American Society of Preventive Oncology *7*, 531-536.

Brothman, A. R., Swanson, G., Maxwell, T. M., Cui, J., Murphy, K. J., Herrick, J., Speights, V. O., Isaac, J., and Rohr, L. R. (2005). Global hypomethylation is common in prostate cancer cells: a quantitative predictor for clinical outcome? Cancer Genet Cytogenet *156*, 31-36.

Bryan, E. J., Jokubaitis, V. J., Chamberlain, N. L., Baxter, S. W., Dawson, E., Choong, D. Y., and Campbell, I. G. (2002). Mutation analysis of EP300 in colon, breast and ovarian carcinomas. International journal of cancer Journal international du cancer *102*, 137-141.

Bubendorf, L., Schopfer, A., Wagner, U., Sauter, G., Moch, H., Willi, N., Gasser, T. C., and Mihatsch, M. J. (2000). Metastatic patterns of prostate cancer: an autopsy study of 1,589 patients. Human pathology *31*, 578-583.

Cai, Y., Jin, J., Yao, T., Gottschalk, A. J., Swanson, S. K., Wu, S., Shi, Y., Washburn, M. P., Florens, L., Conaway, R. C., and Conaway, J. W. (2007). YY1 functions with INO80 to activate transcription. Nature structural & molecular biology *14*, 872-874.

Caligiuri, M. A., Strout, M. P., Oberkircher, A. R., Yu, F., de la Chapelle, A., and Bloomfield, C. D. (1997). The partial tandem duplication of ALL1 in acute myeloid leukemia with normal cytogenetics or trisomy 11 is restricted to one chromosome. Proc Natl Acad Sci U S A *94*, 3899-3902.

Cao, Q., Yu, J., Dhanasekaran, S. M., Kim, J. H., Mani, R. S., Tomlins, S. A., Mehra, R., Laxman, B., Cao, X., Kleer, C. G.*, et al.* (2008). Repression of E-cadherin by the polycomb group protein EZH2 in cancer. Oncogene *27*, 7274-7284.

Cao, R., Tsukada, Y., and Zhang, Y. (2005). Role of Bmi-1 and Ring1A in H2A ubiquitylation and Hox gene silencing. Mol Cell *20*, 845-854.

Cao, R., and Zhang, Y. (2004). SUZ12 is required for both the histone methyltransferase activity and the silencing function of the EED-EZH2 complex. Mol Cell *15*, 57-67.

Carapeti, M., Aguiar, R. C., Goldman, J. M., and Cross, N. C. (1998). A novel fusion between MOZ and the nuclear receptor coactivator TIF2 in acute myeloid leukemia. Blood *91*, 3127-3133.

Caretti, G., Di Padova, M., Micales, B., Lyons, G. E., and Sartorelli, V. (2004). The Polycomb Ezh2 methyltransferase regulates muscle gene expression and skeletal muscle differentiation. Genes & development *18*, 2627-2638.

Cedar, H., and Bergman, Y. (2009). Linking DNA methylation and histone modification: patterns and paradigms. Nature reviews Genetics *10*, 295-304.

Chen, F. J., Sun, M., Li, S. Q., Wu, Q. Q., Ji, L., Liu, Z. L., Zhou, G. Z., Cao, G., Jin, L., Xie, H. W.*, et al.* (2013). Upregulation of the long non-coding RNA HOTAIR promotes esophageal squamous cell carcinoma metastasis and poor prognosis. Mol Carcinog *52*, 908-915.

Chen, H., Tu, S. W., and Hsieh, J. T. (2005). Down-regulation of human DAB2IP gene expression mediated by polycomb Ezh2 complex and histone deacetylase in prostate cancer. J Biol Chem *280*, 22437-22444.

Chen, Y., Sawyers, C. L., and Scher, H. I. (2008). Targeting the androgen receptor pathway in prostate cancer. Current opinion in pharmacology *8*, 440-448.

Chi, P., Allis, C. D., and Wang, G. G. (2010). Covalent histone modifications--miswritten, misinterpreted and mis-erased in human cancers. Nat Rev Cancer *10*, 457-469.

Cimmino, L., Abdel-Wahab, O., Levine, R. L., and Aifantis, I. (2011). TET family proteins and their role in stem cell differentiation and transformation. Cell stem cell *9*, 193-204.

Collins, A. T., Berry, P. A., Hyde, C., Stower, M. J., and Maitland, N. J. (2005). Prospective identification of tumorigenic prostate cancer stem cells. Cancer Res *65*, 10946-10951.

Coolen, M. W., Stirzaker, C., Song, J. Z., Statham, A. L., Kassir, Z., Moreno, C. S., Young, A. N., Varma, V., Speed, T. P., Cowley, M.*, et al.* (2010). Consolidation of the cancer genome into domains of repressive chromatin by long-range epigenetic silencing (LRES) reduces transcriptional plasticity. Nature cell biology *12*, 235-246.

Cooperberg, M. R., Broering, J. M., Kantoff, P. W., and Carroll, P. R. (2007). Contemporary trends in low risk prostate cancer: risk assessment and treatment. The Journal of urology *178*, S14-19.

Cortazar, D., Kunz, C., Selfridge, J., Lettieri, T., Saito, Y., MacDougall, E., Wirz, A., Schuermann, D., Jacobs, A. L., Siegrist, F.*, et al.* (2011). Embryonic lethal phenotype reveals a function of TDG in maintaining epigenetic stability. Nature *470*, 419-423.

Cortellino, S., Xu, J., Sannai, M., Moore, R., Caretti, E., Cigliano, A., Le Coz, M., Devarajan, K., Wessels, A., Soprano, D.*, et al.* (2011). Thymine DNA glycosylase is essential for active DNA demethylation by linked deamination-base excision repair. Cell *146*, 67-79.

Costello, J. F., Fruhwald, M. C., Smiraglia, D. J., Rush, L. J., Robertson, G. P., Gao, X., Wright, F. A., Feramisco, J. D., Peltomaki, P., Lang, J. C.*, et al.* (2000). Aberrant CpG-island methylation has non-random and tumour-type-specific patterns. Nat Genet *24*, 132-138.

Creyghton, M. P., Markoulaki, S., Levine, S. S., Hanna, J., Lodato, M. A., Sha, K., Young, R. A., Jaenisch, R., and Boyer, L. A. (2008). H2AZ is enriched at polycomb complex target genes in ES cells and is necessary for lineage commitment. Cell *135*, 649-661.

Dai, Y., Rahmani, M., Dent, P., and Grant, S. (2005). Blockade of histone deacetylase inhibitor-induced RelA/p65 acetylation and NF-kappaB activation potentiates apoptosis in leukemia cells through a process mediated by oxidative damage, XIAP downregulation, and c-Jun N-terminal kinase 1 activation. Mol Cell Biol *25*, 5429-5444.

Daigle, S. R., Olhava, E. J., Therkelsen, C. A., Basavapathruni, A., Jin, L., Boriack-Sjodin, P. A., Allain, C. J., Klaus, C. R., Raimondi, A., Scott, M. P.*, et al.* (2013). Potent inhibition of DOT1L as treatment of MLL-fusion leukemia. Blood *122*, 1017-1025.

Daigle, S. R., Olhava, E. J., Therkelsen, C. A., Majer, C. R., Sneeringer, C. J., Song, J., Johnston, L. D., Scott, M. P., Smith, J. J., Xiao, Y.*, et al.* (2011). Selective killing of mixed lineage leukemia cells by a potent small-molecule DOT1L inhibitor. Cancer Cell *20*, 53-65.

Dalgliesh, G. L., Furge, K., Greenman, C., Chen, L., Bignell, G., Butler, A., Davies, H., Edkins, S., Hardy, C., Latimer, C.*, et al.* (2010). Systematic sequencing of renal carcinoma reveals inactivation of histone modifying genes. Nature *463*, 360-363.

Dawson, M. A., Bannister, A. J., Gottgens, B., Foster, S. D., Bartke, T., Green, A. R., and Kouzarides, T. (2009). JAK2 phosphorylates histone H3Y41 and excludes HP1alpha from chromatin. Nature *461*, 819-822.

Dawson, M. A., Kouzarides, T., and Huntly, B. J. (2012). Targeting epigenetic readers in cancer. N Engl J Med *367*, 647-657.

Dawson, M. A., Prinjha, R. K., Dittmann, A., Giotopoulos, G., Bantscheff, M., Chan, W. I., Robson, S. C., Chung, C. W., Hopf, C., Savitski, M. M.*, et al.* (2011). Inhibition of BET recruitment to chromatin as an effective treatment for MLL-fusion leukaemia. Nature *478*, 529-533.

Dean, M., Fojo, T., and Bates, S. (2005). Tumour stem cells and drug resistance. Nat Rev Cancer *5*, 275-284.

Deaton, A. M., and Bird, A. (2011). CpG islands and the regulation of transcription. Genes & development *25*, 1010-1022.

Delmore, J. E., Issa, G. C., Lemieux, M. E., Rahl, P. B., Shi, J., Jacobs, H. M., Kastritis, E., Gilpatrick, T., Paranal, R. M., Qi, J.*, et al.* (2011). BET bromodomain inhibition as a therapeutic strategy to target c-Myc. Cell *146*, 904-917.

Denisenko, O., Shnyreva, M., Suzuki, H., and Bomsztyk, K. (1998). Point mutations in the WD40 domain of Eed block its interaction with Ezh2. Mol Cell Biol *18*, 5634-5642.

Denmeade, S. R., and Isaacs, J. T. (2002). A history of prostate cancer treatment. Nat Rev Cancer *2*, 389-396.

Di Croce, L., Raker, V. A., Corsaro, M., Fazi, F., Fanelli, M., Faretta, M., Fuks, F., Lo Coco, F., Kouzarides, T., Nervi, C.*, et al.* (2002). Methyltransferase recruitment and DNA hypermethylation of target promoters by an oncogenic transcription factor. Science *295*, 1079-1082.

Dickinson, M., Ritchie, D., DeAngelo, D. J., Spencer, A., Ottmann, O. G., Fischer, T., Bhalla, K. N., Liu, A., Parker, K., Scott, J. W.*, et al.* (2009). Preliminary evidence of disease response to the pan deacetylase inhibitor panobinostat (LBH589) in refractory Hodgkin Lymphoma. Br J Haematol *147*, 97-101.

Dobosy, J. R., and Selker, E. U. (2001). Emerging connections between DNA methylation and histone acetylation. Cell Mol Life Sci *58*, 721-727.

Dohner, K., Tobis, K., Ulrich, R., Frohling, S., Benner, A., Schlenk, R. F., and Dohner, H. (2002). Prognostic significance of partial tandem duplications of the MLL gene in adult patients 16 to 60 years old with acute myeloid leukemia and normal cytogenetics: a study of the Acute Myeloid Leukemia Study Group Ulm. J Clin Oncol *20*, 3254-3261.

Doi, A., Park, I. H., Wen, B., Murakami, P., Aryee, M. J., Irizarry, R., Herb, B., Ladd-Acosta, C., Rho, J., Loewer, S.*, et al.* (2009). Differential methylation of tissue- and cancer-specific CpG island shores distinguishes human induced pluripotent stem cells, embryonic stem cells and fibroblasts. Nat Genet *41*, 1350-1353.

Dong, J. T. (2001). Chromosomal deletions and tumor suppressor genes in prostate cancer. Cancer metastasis reviews *20*, 173-193.

Donohoe, M. E., Zhang, X., McGinnis, L., Biggers, J., Li, E., and Shi, Y. (1999). Targeted disruption of mouse Yin Yang 1 transcription factor results in peri-implantation lethality. Mol Cell Biol *19*, 7237-7244.

Duncan, I. M. (1982). Polycomblike: a gene that appears to be required for the normal expression of the bithorax and antennapedia gene complexes of Drosophila melanogaster. Genetics *102*, 49-70.

Eggener, S. E., Scardino, P. T., Carroll, P. R., Zelefsky, M. J., Sartor, O., Hricak, H., Wheeler, T. M., Fine, S. W., Trachtenberg, J., Rubin, M. A., *et al.* (2007). Focal therapy for localized prostate cancer: a critical appraisal of rationale and modalities. The Journal of urology *178*, 2260-2267.

Egger, G., Liang, G., Aparicio, A., and Jones, P. A. (2004). Epigenetics in human disease and prospects for epigenetic therapy. Nature *429*, 457-463.

el-Deiry, W. S., Nelkin, B. D., Celano, P., Yen, R. W., Falco, J. P., Hamilton, S. R., and Baylin, S. B. (1991). High expression of the DNA methyltransferase gene characterizes human neoplastic cells and progression stages of colon cancer. Proc Natl Acad Sci U S A *88*, 3470-3474.

Ellinger, J., Bachmann, A., Goke, F., Behbahani, T. E., Baumann, C., Heukamp, L. C., Rogenhofer, S., and Muller, S. C. (2014). Alterations of global histone H3K9 and H3K27 methylation levels in bladder cancer. Urologia internationalis *93*, 113-118.

Ellinger, J., Kahl, P., von der Gathen, J., Rogenhofer, S., Heukamp, L. C., Gutgemann, I., Walter, B., Hofstadter, F., Buttner, R., Muller, S. C., *et al.* (2010). Global levels of histone modifications predict prostate cancer recurrence. Prostate *70*, 61-69.

Ellis, L., Pan, Y., Smyth, G. K., George, D. J., McCormack, C., Williams-Truax, R., Mita, M., Beck, J., Burris, H., Ryan, G., *et al.* (2008). Histone deacetylase inhibitor panobinostat induces clinical responses with associated alterations in gene expression profiles in cutaneous T-cell lymphoma. Clin Cancer Res *14*, 4500-4510.

Epstein, J. I. (2010). An update of the Gleason grading system. The Journal of urology *183*, 433-440.

Ernst, T., Chase, A. J., Score, J., Hidalgo-Curtis, C. E., Bryant, C., Jones, A. V., Waghorn, K., Zoi, K., Ross, F. M., Reiter, A., *et al.* (2010). Inactivating mutations of the histone methyltransferase gene EZH2 in myeloid disorders. Nat Genet *42*, 722-726.

Eskeland, R., Leeb, M., Grimes, G. R., Kress, C., Boyle, S., Sproul, D., Gilbert, N., Fan, Y., Skoultchi, A. I., Wutz, A., and Bickmore, W. A. (2010). Ring1B compacts chromatin structure and represses gene expression independent of histone ubiquitination. Mol Cell *38*, 452-464.

Espada, J., Ballestar, E., Santoro, R., Fraga, M. F., Villar-Garea, A., Nemeth, A., Lopez-Serra, L., Ropero, S., Aranda, A., Orozco, H., *et al.* (2007). Epigenetic disruption of ribosomal RNA genes and nucleolar architecture in DNA methyltransferase 1 (Dnmt1) deficient cells. Nucleic acids research *35*, 2191-2198.

Esteller, M. (2005). Aberrant DNA methylation as a cancer-inducing mechanism. Annual review of pharmacology and toxicology *45*, 629-656.

Esteller, M. (2007a). Cancer epigenomics: DNA methylomes and histone-modification maps. Nature reviews Genetics *8*, 286-298.

Esteller, M. (2007b). Epigenetic gene silencing in cancer: the DNA hypermethylome. Human molecular genetics *16 Spec No 1*, R50-59.

Esteller, M., Corn, P. G., Baylin, S. B., and Herman, J. G. (2001a). A gene hypermethylation profile of human cancer. Cancer Res *61*, 3225-3229.

Esteller, M., Fraga, M. F., Guo, M., Garcia-Foncillas, J., Hedenfalk, I., Godwin, A. K., Trojan, J., Vaurs-Barriere, C., Bignon, Y. J., Ramus, S., *et al.* (2001b). DNA methylation patterns in hereditary human cancers mimic sporadic tumorigenesis. Human molecular genetics *10*, 3001-3007.

Esteller, M., and Herman, J. G. (2004). Generating mutations but providing chemosensitivity: the role of O6-methylguanine DNA methyltransferase in human cancer. Oncogene *23*, 1-8.

Fahrner, J. A., Eguchi, S., Herman, J. G., and Baylin, S. B. (2002). Dependence of histone modifications and gene expression on DNA hypermethylation in cancer. Cancer Res *62*, 7213-7218.

Faust, C., Schumacher, A., Holdener, B., and Magnuson, T. (1995). The eed mutation disrupts anterior mesoderm production in mice. Development *121*, 273-285.

Feinberg, A. P., and Tycko, B. (2004). The history of cancer epigenetics. Nat Rev Cancer *4*, 143-153.

Felsenfeld, G., and Groudine, M. (2003). Controlling the double helix. Nature *421*, 448-453.

Fenaux, P. (2005). Inhibitors of DNA methylation: beyond myelodysplastic syndromes. Nature clinical practice Oncology *2 Suppl 1*, S36-44.

Feng, S., Jacobsen, S. E., and Reik, W. (2010). Epigenetic reprogramming in plant and animal development. Science *330*, 622-627.

Ferguson, A. D., Larsen, N. A., Howard, T., Pollard, H., Green, I., Grande, C., Cheung, T., Garcia-Arenas, R., Cowen, S., Wu, J.*, et al.* (2011). Structural basis of substrate methylation and inhibition of SMYD2. Structure *19*, 1262-1273.

Figueroa, M. E., Abdel-Wahab, O., Lu, C., Ward, P. S., Patel, J., Shih, A., Li, Y., Bhagwat, N., Vasanthakumar, A., Fernandez, H. F.*, et al.* (2010). Leukemic IDH1 and IDH2 mutations result in a hypermethylation phenotype, disrupt TET2 function, and impair hematopoietic differentiation. Cancer Cell *18*, 553-567.

Filippakopoulos, P., Qi, J., Picaud, S., Shen, Y., Smith, W. B., Fedorov, O., Morse, E. M., Keates, T., Hickman, T. T., Felletar, I.*, et al.* (2010). Selective inhibition of BET bromodomains. Nature *468*, 1067-1073.

Florl, A. R., Steinhoff, C., Muller, M., Seifert, H. H., Hader, C., Engers, R., Ackermann, R., and Schulz, W. A. (2004). Coordinate hypermethylation at specific genes in prostate carcinoma precedes LINE-1 hypomethylation. British journal of cancer *91*, 985-994.

Fraga, M. F., Ballestar, E., Villar-Garea, A., Boix-Chornet, M., Espada, J., Schotta, G., Bonaldi, T., Haydon, C., Ropero, S., Petrie, K.*, et al.* (2005). Loss of acetylation at Lys16 and trimethylation at Lys20 of histone H4 is a common hallmark of human cancer. Nat Genet *37*, 391-400.

Fraga, M. F., Herranz, M., Espada, J., Ballestar, E., Paz, M. F., Ropero, S., Erkek, E., Bozdogan, O., Peinado, H., Niveleau, A.*, et al.* (2004). A mouse skin multistage carcinogenesis model reflects the aberrant DNA methylation patterns of human tumors. Cancer Res *64*, 5527-5534.

Friedman, J. M., Liang, G., Liu, C. C., Wolff, E. M., Tsai, Y. C., Ye, W., Zhou, X., and Jones, P. A. (2009). The putative tumor suppressor microRNA-101 modulates the cancer epigenome by repressing the polycomb group protein EZH2. Cancer Res *69*, 2623-2629.

Frigola, J., Song, J., Stirzaker, C., Hinshelwood, R. A., Peinado, M. A., and Clark, S. J. (2006). Epigenetic remodeling in colorectal cancer results in coordinate gene suppression across an entire chromosome band. Nat Genet *38*, 540-549.

Fuks, F. (2005). DNA methylation and histone modifications: teaming up to silence genes. Curr Opin Genet Dev *15*, 490-495.

Futscher, B. W., O'Meara, M. M., Kim, C. J., Rennels, M. A., Lu, D., Gruman, L. M., Seftor, R. E., Hendrix, M. J., and Domann, F. E. (2004). Aberrant methylation of the maspin promoter is an early event in human breast cancer. Neoplasia *6*, 380-389.

Futscher, B. W., Oshiro, M. M., Wozniak, R. J., Holtan, N., Hanigan, C. L., Duan, H., and Domann, F. E. (2002). Role for DNA methylation in the control of cell type specific maspin expression. Nat Genet *31*, 175-179.

Gal-Yam, E. N., Egger, G., Iniguez, L., Holster, H., Einarsson, S., Zhang, X., Lin, J. C., Liang, G., Jones, P. A., and Tanay, A. (2008). Frequent switching of Polycomb repressive marks and DNA hypermethylation in the PC3 prostate cancer cell line. Proc Natl Acad Sci U S A *105*, 12979-12984.

Gallagher, W. M., Bergin, O. E., Rafferty, M., Kelly, Z. D., Nolan, I. M., Fox, E. J., Culhane, A. C., McArdle, L., Fraga, M. F., Hughes, L.*, et al.* (2005). Multiple markers for melanoma progression regulated by DNA methylation: insights from transcriptomic studies. Carcinogenesis *26*, 1856-1867.

Gao, H., Ouyang, X., Banach-Petrosky, W. A., Shen, M. M., and Abate-Shen, C. (2006). Emergence of androgen independence at early stages of prostate cancer progression in Nkx3.1; Pten mice. Cancer Res *66*, 7929-7933.

Gaudet, F., Hodgson, J. G., Eden, A., Jackson-Grusby, L., Dausman, J., Gray, J. W., Leonhardt, H., and Jaenisch, R. (2003). Induction of tumors in mice by genomic hypomethylation. Science *300*, 489-492.

Gazin, C., Wajapeyee, N., Gobeil, S., Virbasius, C. M., and Green, M. R. (2007). An elaborate pathway required for Ras-mediated epigenetic silencing. Nature *449*, 1073-1077.

Girault, I., Tozlu, S., Lidereau, R., and Bieche, I. (2003). Expression analysis of DNA methyltransferases 1, 3A, and 3B in sporadic breast carcinomas. Clin Cancer Res *9*, 4415-4422.

Goelz, S. E., Vogelstein, B., Hamilton, S. R., and Feinberg, A. P. (1985). Hypomethylation of DNA from benign and malignant human colon neoplasms. Science *228*, 187-190.

Goll, M. G., and Bestor, T. H. (2005). Eukaryotic cytosine methyltransferases. Annual review of biochemistry *74*, 481-514.

Gordon, S., Akopyan, G., Garban, H., and Bonavida, B. (2006). Transcription factor YY1: structure, function, and therapeutic implications in cancer biology. Oncogene *25*, 1125-1142.

Grasso, C. S., Wu, Y. M., Robinson, D. R., Cao, X., Dhanasekaran, S. M., Khan, A. P., Quist, M. J., Jing, X., Lonigro, R. J., Brenner, J. C.*, et al.* (2012). The mutational landscape of lethal castration-resistant prostate cancer. Nature *487*, 239-243.

Guetg, C., Lienemann, P., Sirri, V., Grummt, I., Hernandez-Verdun, D., Hottiger, M. O., Fussenegger, M., and Santoro, R. (2010). The NoRC complex mediates the heterochromatin formation and stability of silent rRNA genes and centromeric repeats. Embo J *29*, 2135-2146.

Guetg, C., and Santoro, R. (2012). Noncoding RNAs link PARP1 to heterochromatin. Cell Cycle *11*, 2217-2218.

Guetg, C., Scheifele, F., Rosenthal, F., Hottiger, M. O., and Santoro, R. (2012). Inheritance of silent rDNA chromatin is mediated by PARP1 via noncoding RNA. Mol Cell *45*, 790-800.

Gupta, R. A., Shah, N., Wang, K. C., Kim, J., Horlings, H. M., Wong, D. J., Tsai, M. C., Hung, T., Argani, P., Rinn, J. L.*, et al.* (2010). Long non-coding RNA HOTAIR reprograms chromatin state to promote cancer metastasis. Nature *464*, 1071-1076.

Hackett, J. A., Zylicz, J. J., and Surani, M. A. (2012). Parallel mechanisms of epigenetic reprogramming in the germline. Trends in genetics : TIG *28*, 164-174.

Hall, T. M. (2005). Multiple modes of RNA recognition by zinc finger proteins. Current opinion in structural biology *15*, 367-373.

Hamamoto, R., Furukawa, Y., Morita, M., Iimura, Y., Silva, F. P., Li, M., Yagyu, R., and Nakamura, Y. (2004). SMYD3 encodes a histone methyltransferase involved in the proliferation of cancer cells. Nature cell biology *6*, 731-740.

Hanahan, D., and Weinberg, R. A. (2000). The hallmarks of cancer. Cell *100*, 57-70.

Hargreaves, D. C., and Crabtree, G. R. (2011). ATP-dependent chromatin remodeling: genetics, genomics and mechanisms. Cell research *21*, 396-420.

Harikrishnan, K. N., Chow, M. Z., Baker, E. K., Pal, S., Bassal, S., Brasacchio, D., Wang, L., Craig, J. M., Jones, P. L., Sif, S., and El-Osta, A. (2005). Brahma links the SWI/SNF chromatin-remodeling complex with MeCP2-dependent transcriptional silencing. Nat Genet *37*, 254-264.

Haupt, Y., Alexander, W. S., Barri, G., Klinken, S. P., and Adams, J. M. (1991). Novel zinc finger gene implicated as myc collaborator by retrovirally accelerated lymphomagenesis in E mu-myc transgenic mice. Cell *65*, 753-763.

He, G., Wang, Q., Zhou, Y., Wu, X., Wang, L., Duru, N., Kong, X., Zhang, P., Wan, B., Sui, L.*, et al.* (2011a). YY1 is a novel potential therapeutic target for the treatment of HPV infection-induced cervical cancer by arsenic trioxide. International journal of gynecological cancer : official journal of the International Gynecological Cancer Society *21*, 1097-1104.

He, Y. F., Li, B. Z., Li, Z., Liu, P., Wang, Y., Tang, Q., Ding, J., Jia, Y., Chen, Z., Li, L.*, et al.* (2011b). Tet-mediated formation of 5-carboxylcytosine and its excision by TDG in mammalian DNA. Science *333*, 1303-1307.

Hennig, L., and Derkacheva, M. (2009). Diversity of Polycomb group complexes in plants: same rules, different players? Trends in genetics : TIG *25*, 414-423.

Herman, J. G., and Baylin, S. B. (2003). Gene silencing in cancer in association with promoter hypermethylation. The New England journal of medicine *349*, 2042-2054.

Hsu, P. Y., Hsu, H. K., Singer, G. A., Yan, P. S., Rodriguez, B. A., Liu, J. C., Weng, Y. I., Deatherage, D. E., Chen, Z., Pereira, J. S.*, et al.* (2010). Estrogen-mediated epigenetic repression of large chromosomal regions through DNA looping. Genome research *20*, 733-744.

Huntly, B. J., Shigematsu, H., Deguchi, K., Lee, B. H., Mizuno, S., Duclos, N., Rowan, R., Amaral, S., Curley, D., Williams, I. R.*, et al.* (2004). MOZ-TIF2, but not BCR-ABL, confers properties of leukemic stem cells to committed murine hematopoietic progenitors. Cancer Cell *6*, 587-596.

Iorio, M. V., Ferracin, M., Liu, C. G., Veronese, A., Spizzo, R., Sabbioni, S., Magri, E., Pedriali, M., Fabbri, M., Campiglio, M.*, et al.* (2005). MicroRNA gene expression deregulation in human breast cancer. Cancer Res *65*, 7065-7070.

Irizarry, R. A., Ladd-Acosta, C., Wen, B., Wu, Z., Montano, C., Onyango, P., Cui, H., Gabo, K., Rongione, M., Webster, M.*, et al.* (2009). The human colon cancer methylome shows similar hypo- and hypermethylation at conserved tissue-specific CpG island shores. Nat Genet *41*, 178-186.

Irshad, S., Bansal, M., Castillo-Martin, M., Zheng, T., Aytes, A., Wenske, S., Le Magnen, C., Guarnieri, P., Sumazin, P., Benson, M. C.*, et al.* (2013). A molecular signature predictive of indolent prostate cancer. Sci Transl Med *5*, 202ra122.

Issa, J. P. (2004). CpG island methylator phenotype in cancer. Nat Rev Cancer *4*, 988-993.

Ito, S., D'Alessio, A. C., Taranova, O. V., Hong, K., Sowers, L. C., and Zhang, Y. (2010). Role of Tet proteins in 5mC to 5hmC conversion, ES-cell self-renewal and inner cell mass specification. Nature *466*, 1129-1133.

Ito, S., Shen, L., Dai, Q., Wu, S. C., Collins, L. B., Swenberg, J. A., He, C., and Zhang, Y. (2011). Tet proteins can convert 5-methylcytosine to 5-formylcytosine and 5-carboxylcytosine. Science *333*, 1300-1303.

Ito, Y., Koessler, T., Ibrahim, A. E., Rai, S., Vowler, S. L., Abu-Amero, S., Silva, A. L., Maia, A. T., Huddleston, J. E., Uribe-Lewis, S.*, et al.* (2008). Somatically acquired hypomethylation of IGF2 in breast and colorectal cancer. Human molecular genetics *17*, 2633-2643.

Jacobs, J. J., Kieboom, K., Marino, S., DePinho, R. A., and van Lohuizen, M. (1999a). The oncogene and Polycomb-group gene bmi-1 regulates cell proliferation and senescence through the ink4a locus. Nature *397*, 164-168.

Jacobs, J. J., Scheijen, B., Voncken, J. W., Kieboom, K., Berns, A., and van Lohuizen, M. (1999b). Bmi-1 collaborates with c-Myc in tumorigenesis by inhibiting c-Myc-induced apoptosis via INK4a/ARF. Genes & development *13*, 2678-2690.

Jaenisch, R., and Bird, A. (2003). Epigenetic regulation of gene expression: how the genome integrates intrinsic and environmental signals. Nat Genet *33 Suppl*, 245-254.

Jemal, A., Bray, F., Center, M. M., Ferlay, J., Ward, E., and Forman, D. (2011). Global cancer statistics. CA: a cancer journal for clinicians *61*, 69-90.

Jenkins, T. G., and Carrell, D. T. (2012). Dynamic alterations in the paternal epigenetic landscape following fertilization. Frontiers in genetics *3*, 143.

Jenuwein, T., and Allis, C. D. (2001). Translating the histone code. Science *293*, 1074-1080.

Jeon, Y., and Lee, J. T. (2011). YY1 tethers Xist RNA to the inactive X nucleation center. Cell *146*, 119-133.

Jeronimo, C., Henrique, R., Hoque, M. O., Mambo, E., Ribeiro, F. R., Varzim, G., Oliveira, J., Teixeira, M. R., Lopes, C., and Sidransky, D. (2004). A quantitative promoter methylation profile of prostate cancer. Clin Cancer Res *10*, 8472-8478.

Ji, H., Ehrlich, L. I., Seita, J., Murakami, P., Doi, A., Lindau, P., Lee, H., Aryee, M. J., Irizarry, R. A., Kim, K.*, et al.* (2010). Comprehensive methylome map of lineage commitment from haematopoietic progenitors. Nature *467*, 338-342.

Jiao, J., Wang, S., Qiao, R., Vivanco, I., Watson, P. A., Sawyers, C. L., and Wu, H. (2007). Murine cell lines derived from Pten null prostate cancer show the critical role of PTEN in hormone refractory prostate cancer development. Cancer Res *67*, 6083-6091.

Jones, P. A. (1999). The DNA methylation paradox. Trends in genetics : TIG *15*, 34-37.

Jones, P. A., and Baylin, S. B. (2007). The epigenomics of cancer. Cell *128*, 683-692.

Jones, P. L., Veenstra, G. J., Wade, P. A., Vermaak, D., Kass, S. U., Landsberger, N., Strouboulis, J., and Wolffe, A. P. (1998). Methylated DNA and MeCP2 recruit histone deacetylase to repress transcription. Nat Genet *19*, 187-191.

Jones, S., Wang, T. L., Shih Ie, M., Mao, T. L., Nakayama, K., Roden, R., Glas, R., Slamon, D., Diaz, L. A., Jr., Vogelstein, B.*, et al.* (2010). Frequent mutations of chromatin remodeling gene ARID1A in ovarian clear cell carcinoma. Science *330*, 228-231.

Jürgens, G. (1985). A group of genes controlling the spatial expression of the bithorax complex in Drosophila. Nature *316*, 153 - 155.

Kahl, P., Gullotti, L., Heukamp, L. C., Wolf, S., Friedrichs, N., Vorreuther, R., Solleder, G., Bastian, P. J., Ellinger, J., Metzger, E.*, et al.* (2006). Androgen receptor coactivators lysine-specific histone demethylase 1 and four and a half LIM domain protein 2 predict risk of prostate cancer recurrence. Cancer Res *66*, 11341-11347.

Kalakonda, N., Fischle, W., Boccuni, P., Gurvich, N., Hoya-Arias, R., Zhao, X., Miyata, Y., Macgrogan, D., Zhang, J., Sims, J. K.*, et al.* (2008). Histone H4 lysine 20 monomethylation promotes transcriptional repression by L3MBTL1. Oncogene *27*, 4293-4304.

Kaneda, M., Okano, M., Hata, K., Sado, T., Tsujimoto, N., Li, E., and Sasaki, H. (2004). Essential role for de novo DNA methyltransferase Dnmt3a in paternal and maternal imprinting. Nature *429*, 900-903.

Kang, G. H., Lee, S., Lee, H. J., and Hwang, K. S. (2004). Aberrant CpG island hypermethylation of multiple genes in prostate cancer and prostatic intraepithelial neoplasia. The Journal of pathology *202*, 233-240.

Kangaspeska, S., Stride, B., Metivier, R., Polycarpou-Schwarz, M., Ibberson, D., Carmouche, R. P., Benes, V., Gannon, F., and Reid, G. (2008). Transient cyclical methylation of promoter DNA. Nature *452*, 112-115.

Kanhere, A., Viiri, K., Araujo, C. C., Rasaiyaah, J., Bouwman, R. D., Whyte, W. A., Pereira, C. F., Brookes, E., Walker, K., Bell, G. W.*, et al.* (2010). Short RNAs are transcribed from repressed polycomb target genes and interact with polycomb repressive complex-2. Mol Cell *38*, 675-688.

Kantarjian, H. M., Thomas, X. G., Dmoszynska, A., Wierzbowska, A., Mazur, G., Mayer, J., Gau, J. P., Chou, W. C., Buckstein, R., Cermak, J.*, et al.* (2012). Multicenter, randomized, open-label, phase III trial of decitabine versus patient choice, with physician advice, of either supportive care or low-dose cytarabine for the treatment of older patients with newly diagnosed acute myeloid leukemia. J Clin Oncol *30*, 2670-2677.

Kelly, T. K., De Carvalho, D. D., and Jones, P. A. (2010). Epigenetic modifications as therapeutic targets. Nature biotechnology *28*, 1069-1078.

Kelly, W. K., O'Connor, O. A., Krug, L. M., Chiao, J. H., Heaney, M., Curley, T., MacGregore-Cortelli, B., Tong, W., Secrist, J. P., Schwartz, L.*, et al.* (2005). Phase I study of an oral histone deacetylase inhibitor, suberoylanilide hydroxamic acid, in patients with advanced cancer. J Clin Oncol *23*, 3923-3931.

Keshet, I., Schlesinger, Y., Farkash, S., Rand, E., Hecht, M., Segal, E., Pikarski, E., Young, R. A., Niveleau, A., Cedar, H., and Simon, I. (2006). Evidence for an instructive mechanism of de novo methylation in cancer cells. Nat Genet *38*, 149-153.

Kim, H., Kang, K., and Kim, J. (2009). AEBP2 as a potential targeting protein for Polycomb Repression Complex PRC2. Nucleic acids research *37*, 2940-2950.

Kirmizis, A., Bartley, S. M., and Farnham, P. J. (2003). Identification of the polycomb group protein SU(Z)12 as a potential molecular target for human cancer therapy. Molecular cancer therapeutics *2*, 113-121.

Kleer, C. G., Cao, Q., Varambally, S., Shen, R., Ota, I., Tomlins, S. A., Ghosh, D., Sewalt, R. G., Otte, A. P., Hayes, D. F.*, et al.* (2003). EZH2 is a marker of aggressive breast cancer and promotes neoplastic transformation of breast epithelial cells. Proc Natl Acad Sci U S A *100*, 11606-11611.

Kohli, R. M., and Zhang, Y. (2013). TET enzymes, TDG and the dynamics of DNA demethylation. Nature *502*, 472-479.

Kondo, Y., Shen, L., Cheng, A. S., Ahmed, S., Boumber, Y., Charo, C., Yamochi, T., Urano, T., Furukawa, K., Kwabi-Addo, B.*, et al.* (2008). Gene silencing in cancer by histone H3 lysine 27 trimethylation independent of promoter DNA methylation. Nat Genet *40*, 741-750.

Kondo, Y., Shen, L., Suzuki, S., Kurokawa, T., Masuko, K., Tanaka, Y., Kato, H., Mizuno, Y., Yokoe, M., Sugauchi, F.*, et al.* (2007). Alterations of DNA methylation and histone modifications contribute to gene silencing in hepatocellular carcinomas. Hepatology research : the official journal of the Japan Society of Hepatology *37*, 974-983.

Kornberg, R. D. (1974). Chromatin structure: a repeating unit of histones and DNA. Science *184*, 868-871.

Kouzarides, T. (2007). Chromatin modifications and their function. Cell *128*, 693-705.

Kriaucionis, S., and Heintz, N. (2009). The nuclear DNA base 5-hydroxymethylcytosine is present in Purkinje neurons and the brain. Science *324*, 929-930.

Krivtsov, A. V., and Armstrong, S. A. (2007). MLL translocations, histone modifications and leukaemia stem-cell development. Nat Rev Cancer *7*, 823-833.

Krivtsov, A. V., Feng, Z., Lemieux, M. E., Faber, J., Vempati, S., Sinha, A. U., Xia, X., Jesneck, J., Bracken, A. P., Silverman, L. B.*, et al.* (2008). H3K79 methylation profiles define murine and human MLL-AF4 leukemias. Cancer Cell *14*, 355-368.

Ku, M., Koche, R. P., Rheinbay, E., Mendenhall, E. M., Endoh, M., Mikkelsen, T. S., Presser, A., Nusbaum, C., Xie, X., Chi, A. S., *et al.* (2008). Genomewide analysis of PRC1 and PRC2 occupancy identifies two classes of bivalent domains. PLoS genetics *4*, e1000242.

Kumar, A., White, T. A., MacKenzie, A. P., Clegg, N., Lee, C., Dumpit, R. F., Coleman, I., Ng, S. B., Salipante, S. J., Rieder, M. J., *et al.* (2011). Exome sequencing identifies a spectrum of mutation frequencies in advanced and lethal prostate cancers. Proc Natl Acad Sci U S A *108*, 17087-17092.

Landeira, D., Sauer, S., Poot, R., Dvorkina, M., Mazzarella, L., Jorgensen, H. F., Pereira, C. F., Leleu, M., Piccolo, F. M., Spivakov, M., *et al.* (2010). Jarid2 is a PRC2 component in embryonic stem cells required for multi-lineage differentiation and recruitment of PRC1 and RNA Polymerase II to developmental regulators. Nature cell biology *12*, 618-624.

Lapointe, J., Li, C., Giacomini, C. P., Salari, K., Huang, S., Wang, P., Ferrari, M., Hernandez-Boussard, T., Brooks, J. D., and Pollack, J. R. (2007). Genomic profiling reveals alternative genetic pathways of prostate tumorigenesis. Cancer Res *67*, 8504-8510.

Lapointe, J., Li, C., Higgins, J. P., van de Rijn, M., Bair, E., Montgomery, K., Ferrari, M., Egevad, L., Rayford, W., Bergerheim, U., *et al.* (2004). Gene expression profiling identifies clinically relevant subtypes of prostate cancer. Proc Natl Acad Sci U S A *101*, 811-816.

Lawrence, M. S., Stojanov, P., Mermel, C. H., Robinson, J. T., Garraway, L. A., Golub, T. R., Meyerson, M., Gabriel, S. B., Lander, E. S., and Getz, G. (2014). Discovery and saturation analysis of cancer genes across 21 tumour types. Nature *505*, 495-501.

Lee, T. I., Jenner, R. G., Boyer, L. A., Guenther, M. G., Levine, S. S., Kumar, R. M., Chevalier, B., Johnstone, S. E., Cole, M. F., Isono, K., *et al.* (2006). Control of developmental regulators by Polycomb in human embryonic stem cells. Cell *125*, 301-313.

Lee, W. H., Morton, R. A., Epstein, J. I., Brooks, J. D., Campbell, P. A., Bova, G. S., Hsieh, W. S., Isaacs, W. B., and Nelson, W. G. (1994). Cytidine methylation of regulatory sequences near the pi-class glutathione S-transferase gene accompanies human prostatic carcinogenesis. Proc Natl Acad Sci U S A *91*, 11733-11737.

Leite, K. R., Sousa-Canavez, J. M., Reis, S. T., Tomiyama, A. H., Camara-Lopes, L. H., Sanudo, A., Antunes, A. A., and Srougi, M. (2011). Change in expression of miR-let7c, miR-100, and miR-218 from high grade localized prostate cancer to metastasis. Urol Oncol *29*, 265-269.

Lewis, E. B. (1978). A gene complex controlling segmentation in Drosophila. Nature *276*, 565-570.

Lewis, P. (1949). Pc: Polycomb. Drosophila Information Service *21*.

Ley, T. J., Ding, L., Walter, M. J., McLellan, M. D., Lamprecht, T., Larson, D. E., Kandoth, C., Payton, J. E., Baty, J., Welch, J., *et al.* (2010). DNMT3A mutations in acute myeloid leukemia. The New England journal of medicine *363*, 2424-2433.

Li, E., Bestor, T. H., and Jaenisch, R. (1992). Targeted mutation of the DNA methyltransferase gene results in embryonic lethality. Cell *69*, 915-926.

Li, G., Margueron, R., Ku, M., Chambon, P., Bernstein, B. E., and Reinberg, D. (2010). Jarid2 and PRC2, partners in regulating gene expression. Genes & development *24*, 368-380.

Li, G., Zhang, W., Zeng, H., Chen, L., Wang, W., Liu, J., Zhang, Z., and Cai, Z. (2009). An integrative multi-platform analysis for discovering biomarkers of osteosarcoma. BMC Cancer *9*, 150.

Li, H., Ilin, S., Wang, W., Duncan, E. M., Wysocka, J., Allis, C. D., and Patel, D. J. (2006). Molecular basis for site-specific read-out of histone H3K4me3 by the BPTF PHD finger of NURF. Nature *442*, 91-95.

Li, J., Santoro, R., Koberna, K., and Grummt, I. (2005). The chromatin remodeling complex NoRC controls replication timing of rRNA genes. Embo J *24*, 120-127.

Liang, J., Prouty, L., Williams, B. J., Dayton, M. A., and Blanchard, K. L. (1998). Acute mixed lineage leukemia with an inv(8)(p11q13) resulting in fusion of the genes for MOZ and TIF2. Blood *92*, 2118-2122.

Lilja, H., Ulmert, D., and Vickers, A. J. (2008). Prostate-specific antigen and prostate cancer: prediction, detection and monitoring. Nat Rev Cancer *8*, 268-278.

Lin, J. C., Jeong, S., Liang, G., Takai, D., Fatemi, M., Tsai, Y. C., Egger, G., Gal-Yam, E. N., and Jones, P. A. (2007). Role of nucleosomal occupancy in the epigenetic silencing of the MLH1 CpG island. Cancer Cell *12*, 432-444.

Logothetis, C. J., and Lin, S. H. (2005). Osteoblasts in prostate cancer metastasis to bone. Nat Rev Cancer *5*, 21-28.

Lowe, S. W., and Sherr, C. J. (2003). Tumor suppression by Ink4a-Arf: progress and puzzles. Curr Opin Genet Dev *13*, 77-83.

Lu, C., Ward, P. S., Kapoor, G. S., Rohle, D., Turcan, S., Abdel-Wahab, O., Edwards, C. R., Khanin, R., Figueroa, M. E., Melnick, A.*, et al.* (2012). IDH mutation impairs histone demethylation and results in a block to cell differentiation. Nature *483*, 474-478.

Lubbert, M., Suciu, S., Baila, L., Ruter, B. H., Platzbecker, U., Giagounidis, A., Selleslag, D., Labar, B., Germing, U., Salih, H. R.*, et al.* (2011). Low-dose decitabine versus best supportive care in elderly patients with intermediate- or high-risk myelodysplastic syndrome (MDS) ineligible for intensive chemotherapy: final results of the randomized phase III study of the European Organisation for Research and Treatment of Cancer Leukemia Group and the German MDS Study Group. J Clin Oncol *29*, 1987-1996.

Luger, K., Mader, A. W., Richmond, R. K., Sargent, D. F., and Richmond, T. J. (1997). Crystal structure of the nucleosome core particle at 2.8 A resolution. Nature *389*, 251-260.

Lujambio, A., Calin, G. A., Villanueva, A., Ropero, S., Sanchez-Cespedes, M., Blanco, D., Montuenga, L. M., Rossi, S., Nicoloso, M. S., Faller, W. J.*, et al.* (2008). A microRNA DNA methylation signature for human cancer metastasis. Proc Natl Acad Sci U S A *105*, 13556-13561.

Lujambio, A., Ropero, S., Ballestar, E., Fraga, M. F., Cerrato, C., Setien, F., Casado, S., Suarez-Gauthier, A., Sanchez-Cespedes, M., Git, A.*, et al.* (2007). Genetic unmasking of an epigenetically silenced microRNA in human cancer cells. Cancer Res *67*, 1424-1429.

Mack, S. C., Witt, H., Piro, R. M., Gu, L., Zuyderduyn, S., Stutz, A. M., Wang, X., Gallo, M., Garzia, L., Zayne, K.*, et al.* (2014). Epigenomic alterations define lethal CIMP-positive ependymomas of infancy. Nature *506*, 445-450.

Malik, H. S., and Henikoff, S. (2003). Phylogenomics of the nucleosome. Nature structural biology *10*, 882-891.

Margueron, R., Li, G., Sarma, K., Blais, A., Zavadil, J., Woodcock, C. L., Dynlacht, B. D., and Reinberg, D. (2008). Ezh1 and Ezh2 maintain repressive chromatin through different mechanisms. Mol Cell *32*, 503-518.

Margueron, R., and Reinberg, D. (2011). The Polycomb complex PRC2 and its mark in life. Nature *469*, 343-349.

Maruyama, R., Toyooka, S., Toyooka, K. O., Virmani, A. K., Zochbauer-Muller, S., Farinas, A. J., Minna, J. D., McConnell, J., Frenkel, E. P., and Gazdar, A. F. (2002). Aberrant promoter methylation profile of prostate cancers and its relationship to clinicopathological features. Clin Cancer Res *8*, 514-519.

Marx, V. (2012). Epigenetics: Reading the second genomic code. Nature *491*, 143-147.

Mayer, C., Schmitz, K. M., Li, J., Grummt, I., and Santoro, R. (2006). Intergenic transcripts regulate the epigenetic state of rRNA genes. Mol Cell *22*, 351-361.

Mayer, W., Niveleau, A., Walter, J., Fundele, R., and Haaf, T. (2000). Demethylation of the zygotic paternal genome. Nature *403*, 501-502.

McCabe, M. T., Ott, H. M., Ganji, G., Korenchuk, S., Thompson, C., Van Aller, G. S., Liu, Y., Graves, A. P., Della Pietra, A., 3rd, Diaz, E.*, et al.* (2012). EZH2 inhibition as a therapeutic strategy for lymphoma with EZH2-activating mutations. Nature *492*, 108-112.

McCormack, M. P., and Rabbitts, T. H. (2004). Activation of the T-cell oncogene LMO2 after gene therapy for X-linked severe combined immunodeficiency. The New England journal of medicine *350*, 913-922.

McGarvey, K. M., Greene, E., Fahrner, J. A., Jenuwein, T., and Baylin, S. B. (2007). DNA methylation and complete transcriptional silencing of cancer genes persist after depletion of EZH2. Cancer research *67*, 5097-5102.

Melki, J. R., Warnecke, P., Vincent, P. C., and Clark, S. J. (1998). Increased DNA methyltransferase expression in leukaemia. Leukemia *12*, 311-316.

Mellinger, G. T., Gleason, D., and Bailar, J., 3rd (1967). The histology and prognosis of prostatic cancer. The Journal of urology *97*, 331-337.

Melo, S. A., Ropero, S., Moutinho, C., Aaltonen, L. A., Yamamoto, H., Calin, G. A., Rossi, S., Fernandez, A. F., Carneiro, F., Oliveira, C.*, et al.* (2009). A TARBP2 mutation in human cancer impairs microRNA processing and DICER1 function. Nat Genet *41*, 365-370.

Mertz, J. A., Conery, A. R., Bryant, B. M., Sandy, P., Balasubramanian, S., Mele, D. A., Bergeron, L., and Sims, R. J., 3rd (2011). Targeting MYC dependence in cancer by inhibiting BET bromodomains. Proc Natl Acad Sci U S A *108*, 16669-16674.

Metivier, R., Gallais, R., Tiffoche, C., Le Peron, C., Jurkowska, R. Z., Carmouche, R. P., Ibberson, D., Barath, P., Demay, F., Reid, G.*, et al.* (2008). Cyclical DNA methylation of a transcriptionally active promoter. Nature *452*, 45-50.

Metzger, E., Wissmann, M., Yin, N., Muller, J. M., Schneider, R., Peters, A. H., Gunther, T., Buettner, R., and Schule, R. (2005). LSD1 demethylates repressive histone marks to promote androgen-receptor-dependent transcription. Nature *437*, 436-439.

Michaelis, M., Michaelis, U. R., Fleming, I., Suhan, T., Cinatl, J., Blaheta, R. A., Hoffmann, K., Kotchetkov, R., Busse, R., Nau, H., and Cinatl, J., Jr. (2004). Valproic acid inhibits angiogenesis in vitro and in vivo. Molecular pharmacology *65*, 520-527.

Mikkelsen, T. S., Ku, M., Jaffe, D. B., Issac, B., Lieberman, E., Giannoukos, G., Alvarez, P., Brockman, W., Kim, T. K., Koche, R. P.*, et al.* (2007). Genome-wide maps of chromatin state in pluripotent and lineage-committed cells. Nature *448*, 553-560.

Min, J., Zaslavsky, A., Fedele, G., McLaughlin, S. K., Reczek, E. E., De Raedt, T., Guney, I., Strochlic, D. E., Macconaill, L. E., Beroukhim, R.*, et al.* (2010). An oncogene-tumor suppressor cascade drives metastatic prostate cancer by coordinately activating Ras and nuclear factor-kappaB. Nat Med *16*, 286-294.

Moore, S. D., Herrick, S. R., Ince, T. A., Kleinman, M. S., Dal Cin, P., Morton, C. C., and Quade, B. J. (2004). Uterine leiomyomata with t(10;17) disrupt the histone acetyltransferase MORF. Cancer Res *64*, 5570-5577.

Mulero-Navarro, S., and Esteller, M. (2008). Chromatin remodeling factor CHD5 is silenced by promoter CpG island hypermethylation in human cancer. Epigenetics *3*, 210-215.

Musselman, C. A., Lalonde, M. E., Cote, J., and Kutateladze, T. G. (2012). Perceiving the epigenetic landscape through histone readers. Nature structural & molecular biology *19*, 1218-1227.

Nan, X., Ng, H. H., Johnson, C. A., Laherty, C. D., Turner, B. M., Eisenman, R. N., and Bird, A. (1998). Transcriptional repression by the methyl-CpG-binding protein MeCP2 involves a histone deacetylase complex. Nature *393*, 386-389.

Nekrasov, M., Klymenko, T., Fraterman, S., Papp, B., Oktaba, K., Kocher, T., Cohen, A., Stunnenberg, H. G., Wilm, M., and Muller, J. (2007). Pcl-PRC2 is needed to generate high levels of H3-K27 trimethylation at Polycomb target genes. Embo J *26*, 4078-4088.

Nikoloski, G., Langemeijer, S. M., Kuiper, R. P., Knops, R., Massop, M., Tonnissen, E. R., van der Heijden, A., Scheele, T. N., Vandenberghe, P., de Witte, T.*, et al.* (2010). Somatic mutations of the histone methyltransferase gene EZH2 in myelodysplastic syndromes. Nat Genet *42*, 665-667.

Noonan, E. J., Place, R. F., Pookot, D., Basak, S., Whitson, J. M., Hirata, H., Giardina, C., and Dahiya, R. (2009). miR-449a targets HDAC-1 and induces growth arrest in prostate cancer. Oncogene *28*, 1714-1724.

Noushmehr, H., Weisenberger, D. J., Diefes, K., Phillips, H. S., Pujara, K., Berman, B. P., Pan, F., Pelloski, C. E., Sulman, E. P., Bhat, K. P.*, et al.* (2010). Identification of a CpG island methylator phenotype that defines a distinct subgroup of glioma. Cancer Cell *17*, 510-522.

O'Carroll, D., Erhardt, S., Pagani, M., Barton, S. C., Surani, M. A., and Jenuwein, T. (2001). The polycomb-group gene Ezh2 is required for early mouse development. Mol Cell Biol *21*, 4330-4336.

O'Connor, O. A., Heaney, M. L., Schwartz, L., Richardson, S., Willim, R., MacGregor-Cortelli, B., Curly, T., Moskowitz, C., Portlock, C., Horwitz, S.*, et al.* (2006). Clinical experience with intravenous and oral formulations of the novel histone deacetylase inhibitor suberoylanilide hydroxamic acid in patients with advanced hematologic malignancies. J Clin Oncol *24*, 166-173.

Oda, H., Okamoto, I., Murphy, N., Chu, J., Price, S. M., Shen, M. M., Torres-Padilla, M. E., Heard, E., and Reinberg, D. (2009). Monomethylation of histone H4-lysine 20 is involved in chromosome structure and stability and is essential for mouse development. Mol Cell Biol *29*, 2278-2295.

Oh, B. K., Kim, H., Park, H. J., Shim, Y. H., Choi, J., Park, C., and Park, Y. N. (2007). DNA methyltransferase expression and DNA methylation in human hepatocellular carcinoma and their clinicopathological correlation. International journal of molecular medicine *20*, 65-73.

Ohm, J. E., McGarvey, K. M., Yu, X., Cheng, L., Schuebel, K. E., Cope, L., Mohammad, H. P., Chen, W., Daniel, V. C., Yu, W.*, et al.* (2007). A stem cell-like chromatin pattern may predispose tumor suppressor genes to DNA hypermethylation and heritable silencing. Nat Genet *39*, 237-242.

Okada, Y., Feng, Q., Lin, Y., Jiang, Q., Li, Y., Coffield, V. M., Su, L., Xu, G., and Zhang, Y. (2005). hDOT1L links histone methylation to leukemogenesis. Cell *121*, 167-178.

Okano, M., Bell, D. W., Haber, D. A., and Li, E. (1999). DNA methyltransferases Dnmt3a and Dnmt3b are essential for de novo methylation and mammalian development. Cell *99*, 247-257.

Oswald, J., Engemann, S., Lane, N., Mayer, W., Olek, A., Fundele, R., Dean, W., Reik, W., and Walter, J. (2000). Active demethylation of the paternal genome in the mouse zygote. Current biology : CB *10*, 475-478.

Ozen, M., Creighton, C. J., Ozdemir, M., and Ittmann, M. (2008). Widespread deregulation of microRNA expression in human prostate cancer. Oncogene *27*, 1788-1793.

Palacios, D., Mozzetta, C., Consalvi, S., Caretti, G., Saccone, V., Proserpio, V., Marquez, V. E., Valente, S., Mai, A., Forcales, S. V.*, et al.* (2010). TNF/p38alpha/polycomb signaling to Pax7 locus in satellite cells links inflammation to the epigenetic control of muscle regeneration. Cell stem cell *7*, 455-469.

Palanisamy, N., Ateeq, B., Kalyana-Sundaram, S., Pflueger, D., Ramnarayanan, K., Shankar, S., Han, B., Cao, Q., Cao, X., Suleman, K.*, et al.* (2010). Rearrangements of the RAF kinase pathway in prostate cancer, gastric cancer and melanoma. Nat Med *16*, 793-798.

Panagopoulos, I., Strombeck, B., Isaksson, M., Heldrup, J., Olofsson, T., and Johansson, B. (2006). Fusion of ETV6 with an intronic sequence of the BAZ2A gene in a paediatric pre-B acute lymphoblastic leukaemia with a cryptic chromosome 12 rearrangement. Br J Haematol *133*, 270-275.

Pandey, R. R., Mondal, T., Mohammad, F., Enroth, S., Redrup, L., Komorowski, J., Nagano, T., Mancini-Dinardo, D., and Kanduri, C. (2008). Kcnq1ot1 antisense noncoding RNA mediates lineage-specific transcriptional silencing through chromatin-level regulation. Mol Cell *32*, 232-246.

Pasini, D., Bracken, A. P., Jensen, M. R., Lazzerini Denchi, E., and Helin, K. (2004). Suz12 is essential for mouse development and for EZH2 histone methyltransferase activity. Embo J *23*, 4061-4071.

Pasini, D., Cloos, P. A., Walfridsson, J., Olsson, L., Bukowski, J. P., Johansen, J. V., Bak, M., Tommerup, N., Rappsilber, J., and Helin, K. (2010). JARID2 regulates binding of the Polycomb repressive complex 2 to target genes in ES cells. Nature *464*, 306-310.

Patra, S. K., Patra, A., Zhao, H., and Dahiya, R. (2002). DNA methyltransferase and demethylase in human prostate cancer. Mol Carcinog *33*, 163-171.

Paz, M. F., Fraga, M. F., Avila, S., Guo, M., Pollan, M., Herman, J. G., and Esteller, M. (2003). A systematic profile of DNA methylation in human cancer cell lines. Cancer Res *63*, 1114-1121.

Peng, J. C., Valouev, A., Swigut, T., Zhang, J., Zhao, Y., Sidow, A., and Wysocka, J. (2009). Jarid2/Jumonji coordinates control of PRC2 enzymatic activity and target gene occupancy in pluripotent cells. Cell *139*, 1290-1302.

Perry, A. S., Loftus, B., Moroose, R., Lynch, T. H., Hollywood, D., Watson, R. W., Woodson, K., and Lawler, M. (2007). In silico mining identifies IGFBP3 as a novel target of methylation in prostate cancer. British journal of cancer *96*, 1587-1594.

Perry, A. S., Watson, R. W., Lawler, M., and Hollywood, D. (2010). The epigenome as a therapeutic target in prostate cancer. Nature reviews Urology *7*, 668-680.

Peters, A. H., O'Carroll, D., Scherthan, H., Mechtler, K., Sauer, S., Schofer, C., Weipoltshammer, K., Pagani, M., Lachner, M., Kohlmaier, A.*, et al.* (2001). Loss of the Suv39h histone methyltransferases impairs mammalian heterochromatin and genome stability. Cell *107*, 323-337.

Petrylak, D. P., Tangen, C. M., Hussain, M. H., Lara, P. N., Jr., Jones, J. A., Taplin, M. E., Burch, P. A., Berry, D., Moinpour, C., Kohli, M.*, et al.* (2004). Docetaxel and estramustine compared with mitoxantrone and prednisone for advanced refractory prostate cancer. The New England journal of medicine *351*, 1513-1520.

Plass, C., Pfister, S. M., Lindroth, A. M., Bogatyrova, O., Claus, R., and Lichter, P. (2013). Mutations in regulators of the epigenome and their connections to global chromatin patterns in cancer. Nature reviews Genetics *14*, 765-780.

Plath, K., Fang, J., Mlynarczyk-Evans, S. K., Cao, R., Worringer, K. A., Wang, H., de la Cruz, C. C., Otte, A. P., Panning, B., and Zhang, Y. (2003). Role of histone H3 lysine 27 methylation in X inactivation. Science *300*, 131-135.

Portela, A., and Esteller, M. (2010). Epigenetic modifications and human disease. Nature biotechnology *28*, 1057-1068.

Rajasekhar, V. K., and Begemann, M. (2007). Concise review: roles of polycomb group proteins in development and disease: a stem cell perspective. Stem cells *25*, 2498-2510.

Rakyan, V. K., Down, T. A., Balding, D. J., and Beck, S. (2011). Epigenome-wide association studies for common human diseases. Nature reviews Genetics *12*, 529-541.

Ramsahoye, B. H., Biniszkiewicz, D., Lyko, F., Clark, V., Bird, A. P., and Jaenisch, R. (2000). Non-CpG methylation is prevalent in embryonic stem cells and may be mediated by DNA methyltransferase 3a. Proc Natl Acad Sci U S A *97*, 5237-5242.

Rathkopf, D., Wong, B. Y., Ross, R. W., Anand, A., Tanaka, E., Woo, M. M., Hu, J., Dzik-Jurasz, A., Yang, W., and Scher, H. I. (2010). A phase I study of oral panobinostat alone and in combination with docetaxel in patients with castration-resistant prostate cancer. Cancer chemotherapy and pharmacology *66*, 181-189.

Razin, S. V., Iarovaia, O. V., Sjakste, N., Sjakste, T., Bagdoniene, L., Rynditch, A. V., Eivazova, E. R., Lipinski, M., and Vassetzky, Y. S. (2007). Chromatin domains and regulation of transcription. Journal of molecular biology *369*, 597-607.

Rich, J. N. (2007). Cancer stem cells in radiation resistance. Cancer Res *67*, 8980-8984.

Riising, E. M., Comet, I., Leblanc, B., Wu, X., Johansen, J. V., and Helin, K. (2014). Gene silencing triggers polycomb repressive complex 2 recruitment to CpG islands genome wide. Mol Cell *55*, 347-360.

Ringrose, L., and Paro, R. (2004). Epigenetic regulation of cellular memory by the Polycomb and Trithorax group proteins. Annual review of genetics *38*, 413-443.

Ringrose, L., and Paro, R. (2007). Polycomb/Trithorax response elements and epigenetic memory of cell identity. Development *134*, 223-232.

Rinn, J. L., Kertesz, M., Wang, J. K., Squazzo, S. L., Xu, X., Brugmann, S. A., Goodnough, L. H., Helms, J. A., Farnham, P. J., Segal, E., and Chang, H. Y. (2007). Functional demarcation of active and silent chromatin domains in human HOX loci by noncoding RNAs. Cell *129*, 1311-1323.

Rocchi, P., Tonelli, R., Camerin, C., Purgato, S., Fronza, R., Bianucci, F., Guerra, F., Pession, A., and Ferreri, A. M. (2005). p21Waf1/Cip1 is a common target induced by short-chain fatty acid HDAC inhibitors (valproic acid, tributyrin and sodium butyrate) in neuroblastoma cells. Oncology reports *13*, 1139-1144.

Ropero, S., Fraga, M. F., Ballestar, E., Hamelin, R., Yamamoto, H., Boix-Chornet, M., Caballero, R., Alaminos, M., Setien, F., Paz, M. F.*, et al.* (2006). A truncating mutation of HDAC2 in human cancers confers resistance to histone deacetylase inhibition. Nat Genet *38*, 566-569.

Rudek, M. A., Zhao, M., He, P., Hartke, C., Gilbert, J., Gore, S. D., Carducci, M. A., and Baker, S. D. (2005). Pharmacokinetics of 5-azacitidine administered with phenylbutyrate in patients with refractory solid tumors or hematologic malignancies. J Clin Oncol *23*, 3906-3911.

Russo, V., Riggs, A., and Martienssen, R. (1996). Epigenetic mechanisms of gene regulation, (Cold Spring Habor, NY: Cold Spring Habor Laboratory Press).

Ryan, R. J., and Bernstein, B. E. (2012). Molecular biology. Genetic events that shape the cancer epigenome. Science *336*, 1513-1514.

Saito, Y., Liang, G., Egger, G., Friedman, J. M., Chuang, J. C., Coetzee, G. A., and Jones, P. A. (2006). Specific activation of microRNA-127 with downregulation of the proto-oncogene BCL6 by chromatin-modifying drugs in human cancer cells. Cancer Cell *9*, 435-443.

Sakabe, K., Wang, Z., and Hart, G. W. (2010). Beta-N-acetylglucosamine (O-GlcNAc) is part of the histone code. Proc Natl Acad Sci U S A *107*, 19915-19920.

Santoro, R., and Grummt, I. (2005). Epigenetic mechanism of rRNA gene silencing: temporal order of NoRC-mediated histone modification, chromatin remodeling, and DNA methylation. Mol Cell Biol *25*, 2539-2546.

Santoro, R., Li, J., and Grummt, I. (2002). The nucleolar remodeling complex NoRC mediates heterochromatin formation and silencing of ribosomal gene transcription. Nat Genet *32*, 393-396.

Santoro, R., Lienemann, P., and Fussenegger, M. (2009). Epigenetic engineering of ribosomal RNA genes enhances protein production. PLoS One *4*, e6653.

Saramaki, O. R., Tammela, T. L., Martikainen, P. M., Vessella, R. L., and Visakorpi, T. (2006). The gene for polycomb group protein enhancer of zeste homolog 2 (EZH2) is amplified in late-stage prostate cancer. Genes, chromosomes & cancer *45*, 639-645.

Sarma, K., Margueron, R., Ivanov, A., Pirrotta, V., and Reinberg, D. (2008). Ezh2 requires PHF1 to efficiently catalyze H3 lysine 27 trimethylation in vivo. Mol Cell Biol *28*, 2718-2731.

Sarma, K., and Reinberg, D. (2005). Histone variants meet their match. Nature reviews Molecular cell biology *6*, 139-149.

Sartor, A. O., Hricak, H., Wheeler, T. M., Coleman, J., Penson, D. F., Carroll, P. R., Rubin, M. A., and Scardino, P. T. (2008). Evaluating localized prostate cancer and identifying candidates for focal therapy. Urology *72*, S12-24.

Sasaki, M., Tanaka, Y., Perinchery, G., Dharia, A., Kotcherguina, I., Fujimoto, S., and Dahiya, R. (2002). Methylation and inactivation of estrogen, progesterone, and androgen receptors in prostate cancer. Journal of the National Cancer Institute *94*, 384-390.

Satijn, D. P., Hamer, K. M., den Blaauwen, J., and Otte, A. P. (2001). The polycomb group protein EED interacts with YY1, and both proteins induce neural tissue in Xenopus embryos. Mol Cell Biol *21*, 1360-1369.

Savla, U., Benes, J., Zhang, J., and Jones, R. S. (2008). Recruitment of Drosophila Polycomb-group proteins by Polycomblike, a component of a novel protein complex in larvae. Development *135*, 813-817.

Schepeler, T., Reinert, J. T., Ostenfeld, M. S., Christensen, L. L., Silahtaroglu, A. N., Dyrskjot, L., Wiuf, C., Sorensen, F. J., Kruhoffer, M., Laurberg, S.*, et al.* (2008). Diagnostic and prognostic microRNAs in stage II colon cancer. Cancer Res *68*, 6416-6424.

Schlesinger, Y., Straussman, R., Keshet, I., Farkash, S., Hecht, M., Zimmerman, J., Eden, E., Yakhini, Z., Ben-Shushan, E., Reubinoff, B. E.*, et al.* (2007). Polycomb-mediated methylation on Lys27 of histone H3 pre-marks genes for de novo methylation in cancer. Nat Genet *39*, 232-236.

Schoeftner, S., Sengupta, A. K., Kubicek, S., Mechtler, K., Spahn, L., Koseki, H., Jenuwein, T., and Wutz, A. (2006). Recruitment of PRC1 function at the initiation of X inactivation independent of PRC2 and silencing. EMBO J *25*, 3110-3122.

Schotta, G., Lachner, M., Sarma, K., Ebert, A., Sengupta, R., Reuter, G., Reinberg, D., and Jenuwein, T. (2004). A silencing pathway to induce H3-K9 and H4-K20 trimethylation at constitutive heterochromatin. Genes & development *18*, 1251-1262.

Schuebel, K. E., Chen, W., Cope, L., Glockner, S. C., Suzuki, H., Yi, J. M., Chan, T. A., Van Neste, L., Van Criekinge, W., van den Bosch, S.*, et al.* (2007). Comparing the DNA hypermethylome with gene mutations in human colorectal cancer. PLoS genetics *3*, 1709-1723.

Schuettengruber, B., Chourrout, D., Vervoort, M., Leblanc, B., and Cavalli, G. (2007). Genome regulation by polycomb and trithorax proteins. Cell *128*, 735-745.

Schwartz, Y. B., and Pirrotta, V. (2007). Polycomb silencing mechanisms and the management of genomic programmes. Nature reviews Genetics *8*, 9-22.

Schwartzentruber, J., Korshunov, A., Liu, X. Y., Jones, D. T., Pfaff, E., Jacob, K., Sturm, D., Fontebasso, A. M., Quang, D. A., Tonjes, M.*, et al.* (2012). Driver mutations in histone H3.3 and chromatin remodelling genes in paediatric glioblastoma. Nature *482*, 226-231.

Seligson, D. B., Horvath, S., Shi, T., Yu, H., Tze, S., Grunstein, M., and Kurdistani, S. K. (2005). Global histone modification patterns predict risk of prostate cancer recurrence. Nature *435*, 1262-1266.

Shain, A. H., and Pollack, J. R. (2013). The spectrum of SWI/SNF mutations, ubiquitous in human cancers. PLoS One *8*, e55119.

Shen, H., Powers, N., Saini, N., Comstock, C. E., Sharma, A., Weaver, K., Revelo, M. P., Gerald, W., Williams, E., Jessen, W. J.*, et al.* (2008a). The SWI/SNF ATPase Brm is a gatekeeper of proliferative control in prostate cancer. Cancer Res *68*, 10154-10162.

Shen, M. M., and Abate-Shen, C. (2010). Molecular genetics of prostate cancer: new prospects for old challenges. Genes & development *24*, 1967-2000.

Shen, X., Kim, W., Fujiwara, Y., Simon, M. D., Liu, Y., Mysliwiec, M. R., Yuan, G. C., Lee, Y., and Orkin, S. H. (2009). Jumonji modulates polycomb activity and self-renewal versus differentiation of stem cells. Cell *139*, 1303-1314.

Shen, X., Liu, Y., Hsu, Y. J., Fujiwara, Y., Kim, J., Mao, X., Yuan, G. C., and Orkin, S. H. (2008b). EZH1 mediates methylation on histone H3 lysine 27 and complements EZH2 in maintaining stem cell identity and executing pluripotency. Mol Cell *32*, 491-502.

Sherr, C. J. (2001). The INK4a/ARF network in tumour suppression. Nature reviews Molecular cell biology *2*, 731-737.

Sheu, J. J., Choi, J. H., Yildiz, I., Tsai, F. J., Shaul, Y., Wang, T. L., and Shih Ie, M. (2008). The roles of human sucrose nonfermenting protein 2 homologue in the tumor-promoting functions of Rsf-1. Cancer Res *68*, 4050-4057.

Shi, Y. (2007). Histone lysine demethylases: emerging roles in development, physiology and disease. Nature reviews Genetics *8*, 829-833.

Simon, J. A., and Kingston, R. E. (2009). Mechanisms of polycomb gene silencing: knowns and unknowns. Nature reviews Molecular cell biology *10*, 697-708.

Simon, J. A., and Lange, C. A. (2008). Roles of the EZH2 histone methyltransferase in cancer epigenetics. Mutation research *647*, 21-29.

Sing, A., Pannell, D., Karaiskakis, A., Sturgeon, K., Djabali, M., Ellis, J., Lipshitz, H. D., and Cordes, S. P. (2009). A vertebrate Polycomb response element governs segmentation of the posterior hindbrain. Cell *138*, 885-897.

Singh, D., Febbo, P. G., Ross, K., Jackson, D. G., Manola, J., Ladd, C., Tamayo, P., Renshaw, A. A., D'Amico, A. V., Richie, J. P.*, et al.* (2002). Gene expression correlates of clinical prostate cancer behavior. Cancer Cell *1*, 203-209.

Smith, Z. D., and Meissner, A. (2013). DNA methylation: roles in mammalian development. Nature reviews Genetics *14*, 204-220.

Sparmann, A., and van Lohuizen, M. (2006). Polycomb silencers control cell fate, development and cancer. Nat Rev Cancer *6*, 846-856.

Sporn, J. C., Kustatscher, G., Hothorn, T., Collado, M., Serrano, M., Muley, T., Schnabel, P., and Ladurner, A. G. (2009). Histone macroH2A isoforms predict the risk of lung cancer recurrence. Oncogene *28*, 3423-3428.

Stiles, B., Groszer, M., Wang, S., Jiao, J., and Wu, H. (2004). PTENless means more. Developmental biology *273*, 175-184.

Stock, J. K., Giadrossi, S., Casanova, M., Brookes, E., Vidal, M., Koseki, H., Brockdorff, N., Fisher, A. G., and Pombo, A. (2007). Ring1-mediated ubiquitination of H2A restrains poised RNA polymerase II at bivalent genes in mouse ES cells. Nat Cell Biol *9*, 1428-1435.

Strahl, B. D., and Allis, C. D. (2000). The language of covalent histone modifications. Nature *403*, 41-45.

Strohner, R., Nemeth, A., Jansa, P., Hofmann-Rohrer, U., Santoro, R., Langst, G., and Grummt, I. (2001). NoRC--a novel member of mammalian ISWI-containing chromatin remodeling machines. Embo J *20*, 4892-4900.

Struhl, G. (1981). A gene product required for correct initiation of segmental determination in Drosophila. Nature *293*, 36-41.

Sturm, D., Witt, H., Hovestadt, V., Khuong-Quang, D. A., Jones, D. T. W., Konermann, C., Pfaff, E., Tonjes, M., Sill, M., Bender, S.*, et al.* (2012). Hotspot Mutations in H3F3A and IDH1 Define Distinct Epigenetic and Biological Subgroups of Glioblastoma. Cancer Cell *22*, 425-437.

Sui, G., Affar el, B., Shi, Y., Brignone, C., Wall, N. R., Yin, P., Donohoe, M., Luke, M. P., Calvo, D., and Grossman, S. R. (2004). Yin Yang 1 is a negative regulator of p53. Cell *117*, 859-872.

Tahiliani, M., Koh, K. P., Shen, Y., Pastor, W. A., Bandukwala, H., Brudno, Y., Agarwal, S., Iyer, L. M., Liu, D. R., Aravind, L., and Rao, A. (2009). Conversion of 5-methylcytosine to 5-hydroxymethylcytosine in mammalian DNA by MLL partner TET1. Science *324*, 930-935.

Tannock, I. F., de Wit, R., Berry, W. R., Horti, J., Pluzanska, A., Chi, K. N., Oudard, S., Theodore, C., James, N. D., Turesson, I.*, et al.* (2004). Docetaxel plus prednisone or mitoxantrone plus prednisone for advanced prostate cancer. The New England journal of medicine *351*, 1502-1512.

Taverna, S. D., Li, H., Ruthenburg, A. J., Allis, C. D., and Patel, D. J. (2007). How chromatin-binding modules interpret histone modifications: lessons from professional pocket pickers. Nature structural & molecular biology *14*, 1025-1040.

Taylor, B. S., Schultz, N., Hieronymus, H., Gopalan, A., Xiao, Y., Carver, B. S., Arora, V. K., Kaushik, P., Cerami, E., Reva, B.*, et al.* (2010). Integrative genomic profiling of human prostate cancer. Cancer Cell *18*, 11-22.

Thillainadesan, G., Chitilian, J. M., Isovic, M., Ablack, J. N., Mymryk, J. S., Tini, M., and Torchia, J. (2012). TGF-beta-dependent active demethylation and expression of the p15ink4b tumor suppressor are impaired by the ZNF217/CoREST complex. Mol Cell *46*, 636-649.

Tomlins, S. A., Laxman, B., Dhanasekaran, S. M., Helgeson, B. E., Cao, X., Morris, D. S., Menon, A., Jing, X., Cao, Q., Han, B.*, et al.* (2007a). Distinct classes of chromosomal rearrangements create oncogenic ETS gene fusions in prostate cancer. Nature *448*, 595-599.

Tomlins, S. A., Mehra, R., Rhodes, D. R., Cao, X., Wang, L., Dhanasekaran, S. M., Kalyana-Sundaram, S., Wei, J. T., Rubin, M. A., Pienta, K. J.*, et al.* (2007b). Integrative molecular concept modeling of prostate cancer progression. Nat Genet *39*, 41-51.

Tomlins, S. A., Rhodes, D. R., Perner, S., Dhanasekaran, S. M., Mehra, R., Sun, X. W., Varambally, S., Cao, X., Tchinda, J., Kuefer, R.*, et al.* (2005). Recurrent fusion of TMPRSS2 and ETS transcription factor genes in prostate cancer. Science *310*, 644-648.

Tomlins, S. A., Rhodes, D. R., Yu, J., Varambally, S., Mehra, R., Perner, S., Demichelis, F., Helgeson, B. E., Laxman, B., Morris, D. S.*, et al.* (2008). The role of SPINK1 in ETS rearrangement-negative prostate cancers. Cancer Cell *13*, 519-528.

Torchia, J., Rose, D. W., Inostroza, J., Kamei, Y., Westin, S., Glass, C. K., and Rosenfeld, M. G. (1997). The transcriptional co-activator p/CIP binds CBP and mediates nuclear-receptor function. Nature *387*, 677-684.

Toyota, M., Ahuja, N., Ohe-Toyota, M., Herman, J. G., Baylin, S. B., and Issa, J. P. (1999). CpG island methylator phenotype in colorectal cancer. Proc Natl Acad Sci U S A *96*, 8681-8686.

Trojer, P., Li, G., Sims, R. J., 3rd, Vaquero, A., Kalakonda, N., Boccuni, P., Lee, D., Erdjument-Bromage, H., Tempst, P., Nimer, S. D.*, et al.* (2007). L3MBTL1, a histone-methylation-dependent chromatin lock. Cell *129*, 915-928.

Trojer, P., and Reinberg, D. (2008). Beyond histone methyl-lysine binding: how malignant brain tumor (MBT) protein L3MBTL1 impacts chromatin structure. Cell Cycle *7*, 578-585.

True, L., Coleman, I., Hawley, S., Huang, C. Y., Gifford, D., Coleman, R., Beer, T. M., Gelmann, E., Datta, M., Mostaghel, E.*, et al.* (2006). A molecular correlate to the Gleason grading system for prostate adenocarcinoma. Proc Natl Acad Sci U S A *103*, 10991-10996.

van Haaften, G., Dalgliesh, G. L., Davies, H., Chen, L., Bignell, G., Greenman, C., Edkins, S., Hardy, C., O'Meara, S., Teague, J.*, et al.* (2009). Somatic mutations of the histone H3K27 demethylase gene UTX in human cancer. Nat Genet *41*, 521-523.

Van Holde, K. E., Allen, J. R., Tatchell, K., Weischet, W. O., and Lohr, D. (1980). DNA-histone interactions in nucleosomes. Biophysical journal *32*, 271-282.

van Lohuizen, M., Verbeek, S., Scheijen, B., Wientjens, E., van der Gulden, H., and Berns, A. (1991). Identification of cooperating oncogenes in E mu-myc transgenic mice by provirus tagging. Cell *65*, 737-752.

Varambally, S., Cao, Q., Mani, R. S., Shankar, S., Wang, X., Ateeq, B., Laxman, B., Cao, X., Jing, X., Ramnarayanan, K.*, et al.* (2008). Genomic loss of microRNA-101 leads to overexpression of histone methyltransferase EZH2 in cancer. Science *322*, 1695-1699.

Varambally, S., Dhanasekaran, S. M., Zhou, M., Barrette, T. R., Kumar-Sinha, C., Sanda, M. G., Ghosh, D., Pienta, K. J., Sewalt, R. G., Otte, A. P.*, et al.* (2002). The polycomb group protein EZH2 is involved in progression of prostate cancer. Nature *419*, 624-629.

Vella, P., Barozzi, I., Cuomo, A., Bonaldi, T., and Pasini, D. (2012). Yin Yang 1 extends the Myc-related transcription factors network in embryonic stem cells. Nucleic acids research *40*, 3403-3418.

Versteege, I., Sevenet, N., Lange, J., Rousseau-Merck, M. F., Ambros, P., Handgretinger, R., Aurias, A., and Delattre, O. (1998). Truncating mutations of hSNF5/INI1 in aggressive paediatric cancer. Nature *394*, 203-206.

Vire, E., Brenner, C., Deplus, R., Blanchon, L., Fraga, M., Didelot, C., Morey, L., Van Eynde, A., Bernard, D., Vanderwinden, J. M.*, et al.* (2006). The Polycomb group protein EZH2 directly controls DNA methylation. Nature *439*, 871-874.

Vivanco, I., and Sawyers, C. L. (2002). The phosphatidylinositol 3-Kinase AKT pathway in human cancer. Nat Rev Cancer *2*, 489-501.

Voncken, J. W., Roelen, B. A., Roefs, M., de Vries, S., Verhoeven, E., Marino, S., Deschamps, J., and van Lohuizen, M. (2003). Rnf2 (Ring1b) deficiency causes gastrulation arrest and cell cycle inhibition. Proc Natl Acad Sci U S A *100*, 2468-2473.

Voo, K. S., Carlone, D. L., Jacobsen, B. M., Flodin, A., and Skalnik, D. G. (2000). Cloning of a mammalian transcriptional activator that binds unmethylated CpG motifs and shares a CXXC domain with DNA methyltransferase, human trithorax, and methyl-CpG binding domain protein 1. Mol Cell Biol *20*, 2108-2121.

Wade, P. A. (2001). Methyl CpG-binding proteins and transcriptional repression. BioEssays : news and reviews in molecular, cellular and developmental biology *23*, 1131-1137.

Walker, E., Chang, W. Y., Hunkapiller, J., Cagney, G., Garcha, K., Torchia, J., Krogan, N. J., Reiter, J. F., and Stanford, W. L. (2010). Polycomb-like 2 associates with PRC2 and regulates transcriptional networks during mouse embryonic stem cell self-renewal and differentiation. Cell stem cell *6*, 153-166.

Wang, H., Wang, L., Erdjument-Bromage, H., Vidal, M., Tempst, P., Jones, R. S., and Zhang, Y. (2004a). Role of histone H2A ubiquitination in Polycomb silencing. Nature *431*, 873-878.

Wang, P., Lin, C., Smith, E. R., Guo, H., Sanderson, B. W., Wu, M., Gogol, M., Alexander, T., Seidel, C., Wiedemann, L. M.*, et al.* (2009). Global analysis of H3K4 methylation defines MLL family member targets and points to a role for MLL1-mediated H3K4 methylation in the regulation of transcriptional initiation by RNA polymerase II. Mol Cell Biol *29*, 6074-6085.

Wang, S., Gao, J., Lei, Q., Rozengurt, N., Pritchard, C., Jiao, J., Thomas, G. V., Li, G., Roy-Burman, P., Nelson, P. S.*, et al.* (2003). Prostate-specific deletion of the murine Pten tumor suppressor gene leads to metastatic prostate cancer. Cancer Cell *4*, 209-221.

Wang, Y., Fischle, W., Cheung, W., Jacobs, S., Khorasanizadeh, S., and Allis, C. D. (2004b). Beyond the double helix: writing and reading the histone code. Novartis Foundation symposium *259*, 3-17; discussion 17-21, 163-169.

Weikert, S., Christoph, F., Kollermann, J., Muller, M., Schrader, M., Miller, K., and Krause, H. (2005). Expression levels of the EZH2 polycomb transcriptional repressor correlate with aggressiveness and invasive potential of bladder carcinomas. International journal of molecular medicine *16*, 349-353.

Weisenberger, D. J., Siegmund, K. D., Campan, M., Young, J., Long, T. I., Faasse, M. A., Kang, G. H., Widschwendter, M., Weener, D., Buchanan, D.*, et al.* (2006). CpG island methylator phenotype underlies sporadic microsatellite instability and is tightly associated with BRAF mutation in colorectal cancer. Nat Genet *38*, 787-793.

Widschwendter, M., Fiegl, H., Egle, D., Mueller-Holzner, E., Spizzo, G., Marth, C., Weisenberger, D. J., Campan, M., Young, J., Jacobs, I., and Laird, P. W. (2007). Epigenetic stem cell signature in cancer. Nat Genet *39*, 157-158.

Wiegand, K. C., Shah, S. P., Al-Agha, O. M., Zhao, Y., Tse, K., Zeng, T., Senz, J., McConechy, M. K., Anglesio, M. S., Kalloger, S. E.*, et al.* (2010). ARID1A mutations in endometriosis-associated ovarian carcinomas. The New England journal of medicine *363*, 1532-1543.

Wilson, A. S., Power, B. E., and Molloy, P. L. (2007). DNA hypomethylation and human diseases. Biochimica et biophysica acta *1775*, 138-162.

Wilson, B. G., and Roberts, C. W. (2011). SWI/SNF nucleosome remodellers and cancer. Nat Rev Cancer *11*, 481-492.

Wolf, S. F., Jolly, D. J., Lunnen, K. D., Friedmann, T., and Migeon, B. R. (1984). Methylation of the hypoxanthine phosphoribosyltransferase locus on the human X chromosome: implications for X-chromosome inactivation. Proc Natl Acad Sci U S A *81*, 2806-2810.

Woo, C. J., Kharchenko, P. V., Daheron, L., Park, P. J., and Kingston, R. E. (2010). A region of the human HOXD cluster that confers polycomb-group responsiveness. Cell *140*, 99-110.

Wu, G., Broniscer, A., McEachron, T. A., Lu, C., Paugh, B. S., Becksfort, J., Qu, C., Ding, L., Huether, R., Parker, M.*, et al.* (2012). Somatic histone H3 alterations in pediatric diffuse intrinsic pontine gliomas and non-brainstem glioblastomas. Nat Genet *44*, 251-253.

Wu, H., Coskun, V., Tao, J., Xie, W., Ge, W., Yoshikawa, K., Li, E., Zhang, Y., and Sun, Y. E. (2010). Dnmt3a-dependent nonpromoter DNA methylation facilitates transcription of neurogenic genes. Science *329*, 444-448.

Wu, S., Shi, Y., Mulligan, P., Gay, F., Landry, J., Liu, H., Lu, J., Qi, H. H., Wang, W., Nickoloff, J. A., and Wu, C. (2007). A YY1-INO80 complex regulates genomic stability through homologous recombination-based repair. Nature structural & molecular biology *14*, 1165-1172.

Wu, S. C., and Zhang, Y. (2010). Active DNA demethylation: many roads lead to Rome. Nature reviews Molecular cell biology *11*, 607-620.

Wysocka, J., Swigut, T., Xiao, H., Milne, T. A., Kwon, S. Y., Landry, J., Kauer, M., Tackett, A. J., Chait, B. T., Badenhorst, P*., et al.* (2006). A PHD finger of NURF couples histone H3 lysine 4 trimethylation with chromatin remodelling. Nature *442*, 86-90.

Xi, H., Yu, Y., Fu, Y., Foley, J., Halees, A., and Weng, Z. (2007). Analysis of overrepresented motifs in human core promoters reveals dual regulatory roles of YY1. Genome research *17*, 798-806.

Xiao, Y. (2011). Enhancer of zeste homolog 2: A potential target for tumor therapy. The international journal of biochemistry & cell biology *43*, 474-477.

Xu, W., Yang, H., Liu, Y., Yang, Y., Wang, P., Kim, S. H., Ito, S., Yang, C., Xiao, M. T., Liu, L. X*., et al.* (2011). Oncometabolite 2-hydroxyglutarate is a competitive inhibitor of alpha-ketoglutarate-dependent dioxygenases. Cancer Cell *19*, 17-30.

Yamada, Y., Warren, A. J., Dobson, C., Forster, A., Pannell, R., and Rabbitts, T. H. (1998). The T cell leukemia LIM protein Lmo2 is necessary for adult mouse hematopoiesis. Proc Natl Acad Sci U S A *95*, 3890-3895.

Yamashita, K., Upadhyay, S., Osada, M., Hoque, M. O., Xiao, Y., Mori, M., Sato, F., Meltzer, S. J., and Sidransky, D. (2002). Pharmacologic unmasking of epigenetically silenced tumor suppressor genes in esophageal squamous cell carcinoma. Cancer Cell *2*, 485-495.

Yan, X. J., Xu, J., Gu, Z. H., Pan, C. M., Lu, G., Shen, Y., Shi, J. Y., Zhu, Y. M., Tang, L., Zhang, X. W*., et al.* (2011). Exome sequencing identifies somatic mutations of DNA methyltransferase gene DNMT3A in acute monocytic leukemia. Nat Genet *43*, 309-315.

Yanaihara, N., Caplen, N., Bowman, E., Seike, M., Kumamoto, K., Yi, M., Stephens, R. M., Okamoto, A., Yokota, J., Tanaka, T*., et al.* (2006). Unique microRNA molecular profiles in lung cancer diagnosis and prognosis. Cancer Cell *9*, 189-198.

Yang, Z. Q., Imoto, I., Fukuda, Y., Pimkhaokham, A., Shimada, Y., Imamura, M., Sugano, S., Nakamura, Y., and Inazawa, J. (2000). Identification of a novel gene, GASC1, within an amplicon at 9p23-24 frequently detected in esophageal cancer cell lines. Cancer Res *60*, 4735-4739.

Yap, K. L., Li, S., Munoz-Cabello, A. M., Raguz, S., Zeng, L., Mujtaba, S., Gil, J., Walsh, M. J., and Zhou, M. M. (2010). Molecular interplay of the noncoding RNA ANRIL and methylated histone H3 lysine 27 by polycomb CBX7 in transcriptional silencing of INK4a. Mol Cell *38*, 662-674.

Yegnasubramanian, S., Haffner, M. C., Zhang, Y., Gurel, B., Cornish, T. C., Wu, Z., Irizarry, R. A., Morgan, J., Hicks, J., DeWeese, T. L*., et al.* (2008). DNA hypomethylation arises later in prostate cancer progression than CpG island hypermethylation and contributes to metastatic tumor heterogeneity. Cancer Res *68*, 8954-8967.

Yegnasubramanian, S., Kowalski, J., Gonzalgo, M. L., Zahurak, M., Piantadosi, S., Walsh, P. C., Bova, G. S., De Marzo, A. M., Isaacs, W. B., and Nelson, W. G. (2004). Hypermethylation of CpG islands in primary and metastatic human prostate cancer. Cancer Res *64*, 1975-1986.

Yoo, C. B., and Jones, P. A. (2006). Epigenetic therapy of cancer: past, present and future. Nature reviews Drug discovery *5*, 37-50.

Yu, J., Rhodes, D. R., Tomlins, S. A., Cao, X., Chen, G., Mehra, R., Wang, X., Ghosh, D., Shah, R. B., Varambally, S*., et al.* (2007). A polycomb repression signature in metastatic prostate cancer predicts cancer outcome. Cancer Res *67*, 10657-10663.

Zgouras, D., Becker, U., Loitsch, S., and Stein, J. (2004). Modulation of angiogenesis-related protein synthesis by valproic acid. Biochemical and biophysical research communications *316*, 693-697.

Zhang, Y., Ng, H. H., Erdjument-Bromage, H., Tempst, P., Bird, A., and Reinberg, D. (1999). Analysis of the NuRD subunits reveals a histone deacetylase core complex and a connection with DNA methylation. Genes & development *13*, 1924-1935.

Zhang, Y., and Reinberg, D. (2001). Transcription regulation by histone methylation: interplay between different covalent modifications of the core histone tails. Genes & development *15*, 2343-2360.

Zhao, J., Ohsumi, T. K., Kung, J. T., Ogawa, Y., Grau, D. J., Sarma, K., Song, J. J., Kingston, R. E., Borowsky, M., and Lee, J. T. (2010). Genome-wide identification of polycomb-associated RNAs by RIP-seq. Mol Cell *40*, 939-953.

Zhao, J., Sun, B. K., Erwin, J. A., Song, J. J., and Lee, J. T. (2008). Polycomb proteins targeted by a short repeat RNA to the mouse X chromosome. Science *322*, 750-756.

Zhao, X. D., Han, X., Chew, J. L., Liu, J., Chiu, K. P., Choo, A., Orlov, Y. L., Sung, W. K., Shahab, A., Kuznetsov, V. A.*, et al.* (2007). Whole-genome mapping of histone H3 Lys4 and 27 trimethylations reveals distinct genomic compartments in human embryonic stem cells. Cell Stem Cell *1*, 286-298.

Zhou, Y., and Grummt, I. (2005). The PHD finger/bromodomain of NoRC interacts with acetylated histone H4K16 and is sufficient for rDNA silencing. Current biology : CB *15*, 1434-1438.

Zhou, Y., Santoro, R., and Grummt, I. (2002). The chromatin remodeling complex NoRC targets HDAC1 to the ribosomal gene promoter and represses RNA polymerase I transcription. Embo J *21*, 4632-4640.

Zhu, P., Martin, E., Mengwasser, J., Schlag, P., Janssen, K. P., and Gottlicher, M. (2004). Induction of HDAC2 expression upon loss of APC in colorectal tumorigenesis. Cancer Cell *5*, 455-463.

Ziemin-van der Poel, S., McCabe, N. R., Gill, H. J., Espinosa, R., 3rd, Patel, Y., Harden, A., Rubinelli, P., Smith, S. D., LeBeau, M. M., Rowley, J. D., and et al. (1991). Identification of a gene, MLL, that spans the breakpoint in 11q23 translocations associated with human leukemias. Proc Natl Acad Sci U S A *88*, 10735-10739.

Ziller, M. J., Muller, F., Liao, J., Zhang, Y., Gu, H., Bock, C., Boyle, P., Epstein, C. B., Bernstein, B. E., Lengauer, T.*, et al.* (2011). Genomic distribution and inter-sample variation of non-CpG methylation across human cell types. PLoS genetics *7*, e1002389.

6 Curriculum vitae

PERSONAL INFORMATION

Surname	Frommel
Name	Sandra Carina
Date of Birth	May 6, 1985
Hometown	Grenzach-Wyhlen
Nationality	German

EDUCATION

2011 – present	Doctoral Thesis in Molecular Biology (Dr. sc. nat./Ph.D.) Institute of Veterinary Biochemistry and Molecular Biology, University of Zurich, Switzerland
2009 – 2011	Master studies in Biology (M. Sc.) Technische Universität München, Germany
2006 – 2009	Bachelor studies in Biology (B. Sc.) Technische Universität München, Germany
2005 – 2006	Voluntary Year of Social Service German Red Cross, Rheinfelden (Baden), Germany
2002 – 2005	High school (Abitur) Biotechnologisches Gymnasium Lörrach, Germany
1996 – 2002	Middle school Realschule Efringen-Kirchen, Germany
1992 – 1996	Primary school Grundschule Istein, Germany

AWARDS

2015	1-year Fellowship from Sassella Stiftung, Zurich, Switzerland
2014	Best Poster Award, Symposium on Medical Epigenetics 2014, April 7-9, Freiburg i. B., Germany
2012	1-year Müller Fellowship, Molecular Life Sciences PhD Program, LSZGS Zurich, Switzerland

PUBLICATIONS

Haedke, U.R., Frommel, S.C., Hansen, F., Hahne, H., Kuster, B., Bogyo, M. & Verhelst, S.H. Phosphoramidates as novel activity-based probes for serine proteases. *ChemBioChem* (2014) **15**, 1106-1110.

Bachmann, S.B., Frommel, S.C., Camicia, R., Winkler, H.C., Santoro, R. & Hassa, P.O. DTX3L and ARTD9 inhibit IRF1 expression and mediate in cooperation with ARTD8 survival and proliferation of metastatic prostate cancer cells. *Molecular Cancer* (2014) 13:125.

Savić N., Bär D., Leone S., Frommel S.C., Weber F.A., Vollenweider E., Ferrari E., Ziegler U., Kaech A., Shakhova O., Cinelli P. & Santoro R. lncRNA maturation to initiate heterochromatin formation in the nucleolus is required for exit from pluripotency in ESCs. *Cell Stem Cell* (2014), 15(6):720-34.

Frommel S.C., Gu L., Oakes C.C., Simon R., Grupp K., Gerig C.Y., Bär D., Robinson M.D., Baer C., Weiss M., Gu Z., Schapira M., Kuner R., Sültmann H., Provenzano M.; ICGC Project on Early Onset Prostate Cancer, Yaspo M.L., Brors B., Korbel J., Schlomm T., Sauter G., Eils R., Plass C. & Santoro R. BAZ2A (TIP5) is involved in epigenetic alterations in prostate cancer and its overexpression predicts disease recurrence. *Nature Genetics* (2015) 47(1):22-30.

Zingg D., Debbache J., Schaefer S.M., Tuncer E., Frommel S.C., Cheng P., Arenas-Ramirez N., Haeusel J., Zhang Y., Bonalli M., McCabe M.T., Creasy C.L., Levesque M.P., Boyman O., Santoro R., Shakhova O., Dummer R. & Sommer L. The epigenetic modifier EZH2 controls melanoma growth and metastasis through silencing of distinct tumour suppressors. *Nature Communications* (2015) 6:6051.

Cheng P. F., Shakhova O., Widmer D.S., Eichhoff O.M., Zingg D., Frommel S.C., Belloni B., Raaijmakers M.I.G., Goldinger S.M., Santoro R., Hemmi S., Sommer L., Dummer R. & Levesque M.P. Methylation-dependent *SOX9* expression mediates invasion in human melanoma cells and is a negative prognostic factor in advanced melanoma. *Genome Biology* (2015), 16:42